UNIVERSITY
OF TASMANIA

INTEGRATION OF GEOTECHNICAL AND STRUCTURAL DATA FROM SAVAGE RIVER MINE, TASMANIA

by

Victoria Braniff (BSc Hons, MSc)

Submitted in fulfilment of the requirements for the degree of

Doctor of Philosophy

University of Tasmania

October, 2013

DECLARATION OF ORIGINALITY

This thesis contains no material which has been accepted for the award of any other degree or diploma in any tertiary institution and, to the best of my knowledge and belief, contains no copy or paraphrase of material previously published or written by another person, except where due reference is made in the text of this thesis.

Signature:  Date: 07/10/13

AUTHORITY OF ACCESS

This thesis is not to be made available for loan or copying for 24 months from the date this statement was signed; after that time limited copying is permitted in accordance with the Copyright Act 1968.

Signature:  Date: 07/10/13

ABSTRACT

Savage River Mine consists of a number of large open-cut workings in NW Tasmania, based on a group of magnetite lenses irregularly distributed within marble, schist and metabasic rocks of the Bowry Formation, Arthur Metamorphic Complex. The ore bodies strike NNE within host rocks that have a near vertical N-S striking schistosity.

Historically, the open-cuts have been subjected to small- to large-scale rock failure controlled by the geology and the groundwater regime. The majority of magnetite extraction since 2009 has been from North Pit, the largest and deepest of the open-cuts in the lease area. This research includes geotechnical engineering principles and techniques, and structural geology. The aim is to test whether any advantages can be found by correlating the results from these two fields. The project developed a structural model of three major fault bounded assemblages in North Pit and used this as a basis for predicting the geotechnical performance of future open pit designs. Historical failures have been used to inform the analysis of rock stability in North Pit. The nature of brittle and ductile movement on faults within North Pit was studied using the geotechnical data and conventional structural geology data.

Unfavourably orientated brittle features controlling pit wall stability have been identified, geographically located and described. Structure infill has a major impact on pit wall failure with hematite filled structures behaving as a release surface for the majority of recent failures. The terminology of such features in the geotechnical and geological fields has been discussed. Magnetism in the area and the safety issues involved in accessing pit faces has made conventional geotechnical and geological mapping techniques difficult. Therefore, research into alternative mapping methods e.g. photogrammetry, has been carried out. There was extensive use of drill core logging. The use of the geotechnical database to retrieve geological conclusions has been attempted and vice versa.

Two large-scale brittle faults bound the three rock assemblages in North Pit; the Eastern Contact Fault (ECF) and the Magnesite Fault. The highest grade ore is located immediately W of the near vertical N-S striking ECF. This causes inherent mining problems due to pit wall steepness and rock quality in the area directly affecting pit wall stability. A quartz, dolomite, talc and graphite rich damage zone is associated with the ECF, ranging from 7 m to 61 m wide along strike. The characteristics and extent of damage is discussed using structural, geological and geotechnical methods and data. Although more difficult to constrain, a zone of similar lithology is present 30 m W of the Magnesite Fault. It is vital that mine planning takes the nature and extent of the damage zone into account when planning the future expansion of North Pit.

Pit mapping indicates the presence of two generations of mylonite at the Savage River Mine; one showing a dip-slip, west-block-up movement regime and the other a strike-slip, sinistral movement regime. The foliation orientation is similar for both generations of mylonite (i.e. steeply dipping, N striking), however the older mylonites (Middle Cambrian) have a sub-horizontal stretching lineation. These mylonites contain biotite, and locally preserve hornblende and Na-Ca amphiboles typical of high P/T metamorphic rocks in Tasmania (e.g. ferrowinchite). Monazite dating indicates the dip slip mylonites either formed or were reactivated during the Devonian. The high P/T minerals were not found in these more widespread Devonian mylonite zones (low greenschist facies mineral assemblages). Neither of the suites of mylonitic rocks are recorded in the geotechnical database of the mine and the inability to recognise these rocks is a significant issue for the mine geology. Although the strike-slip samples show a stronger mylonitic fabric and includes the presence of ultramylonite, shear sense could also be determined within the dip-slip samples. It is likely that both generations are mylonites were active at low metamorphic grade.

ACKNOWLEDGEMENTS

First and foremost I'd like to extend my gratitude to Grange Resources who have funded this research. Having spent two years at Savage River Mine, not only has my geotechnical and geological understanding increased considerably but I have made life-long friends and memories. Mike Everitt, Ben Maynard, Bruce Hutchison, Roger Hill and Geoff Macqueen: thank you all for your guidance, knowledge, encouragement and support on the journey. The thesis definitely benefited with the knowledge of your experiences. Thank you to my Savage River 'family' including all the technical staff on the mine, especially Carol Steyn and Emily McPhee for the laughs (and a little core-shed dancing) along the way. Ivan Johnston and Cris Clarke: thanks for teaching me your ways of geotechnical core logging and for all the sound advice you offered in the early days of the research.

I would like to thank my supervisors: Dr Tony Webster, Dr Rob Scott and Professor Ron Berry. Thank you Tony, for providing the building blocks at the start of the thesis and for your unwavering support and encouragement along the way. I am grateful to Rob for the visits to Savage River Mine and teaching me the skills of a real structural geologist! Ron, thank you for dedicating large amounts of your valuable time to review the drafts of this thesis. I've enjoyed all the numerous discussions we've had, and your patience and support have been greatly appreciated in the final critical months. Many thanks to Professor Bruce Gemmell and Professor Jocelyn McPhie for your support and encouragement.

Many thanks to all the staff at CODES and the School of Earth Sciences who have provided so much assistance with this research. Sarah Gilbert, Sebastien Meffre and Jay Thompson; thank you all for your analytical assistance. Many thanks to Karsten Goemann and Sandrin Feig of the Central Science Laboratory for teaching me analytical methods I had not used and for your patience and help. Thank you Al Cuison for lapidary work and Keith Dobson for all computer assistance. I'd like to extend my gratitude to the geologists at Mineral Resources

Tasmania. In particular; Ralph Bottrill, Jafar Taheri and Geoff Green. Thank you for all the help and support you have offered throughout the course of the research. Your knowledge of the rocks in NW Tasmania, in particular the Savage River Mine area, has made this complex region that much easier to understand and for that I am truly grateful.

All the people I met at CODES and around Tasmania that became great friends, thank you for your encouragement and support. The Woodwards, the Dunstones, the Ageneaus, Selina, Dan, Janina, Frazer, Chris, Erin, Evan, Gisela, the Rinnes, Jeff, Francisco, Sean, Sam, Claire, Carlos, Helen, Karen and Izzy; thank you for the laughs, you are all wonderful. Special thanks to my structural partner in crime, Roisin, who just completely understood, supported and encouraged me throughout. Also to Rose. Who would have thought a brief encounter for post-it notes would have blossomed into such a great friendship? Thank you for your help with formatting at the end and for believing in me...and for never failing to make me smile.

Thank you to my two best friends, Mark and Hannah. You both have been my towers of strength. Hannah, I've honestly forgotten which one of us is meant to be Thelma and which one Louise but I don't think it matters, as long as we're on the road together. Mark, your unconditional love, patience and support grounds me every day. Thank you for sacrificing your own dreams so that I could fulfil mine. Whatever the future holds: how exciting, thrilling or scary, we will be there, experiencing it together. Always.

Many thanks to my wonderful sisters who I'm so proud of and to my baby niece, Polly; I can't wait to teach you the wonders of the Earth. But most of all, this thesis is dedicated to my parents, Kath and Alwyn Braniff. Thank you for encouraging me to seize every opportunity and for the constant support you offer when I do. Your contagious positive attitude, wise words and strength inspire me every day. Thank you for supporting my passion, believing in me and helping me live my dream. I hope I have made you proud. With you two at my wings, who knows where my final destination will be. All I know is that I can't wait to find out.

TABLE OF CONTENTS

CHAPTER 2

GEOLOGY AND DEFORMATIONAL HISTORY OF THE ARTHUR LINEAMENT AND SURROUNDING ROCKS

CHAPTER 3

BRITTLE DEFORMATION AND GEOTECHNICAL PROPERTIES

CHAPTER 4

FAULT STYLES

CHAPTER 5

DUCTILE DEFORMATION

APPENDICES

Appendix 1 A comparative analysis of the 3DM Analyst (Adam Technology) photogrammetry and the TerraLuma Unmanned Aerial Vehicle (UAV) technique at Savage River Mine, NW Tasmania

Appendix 2 XRF Methodology and raw data

Appendix 3 Pyrite chemistry

Appendix 4 Monazite Dating Methodology

DIGITAL APPENDICES (PROVIDED ON ACCOMPANYING CD)

Appendix 5 Drillhole logs; including collar and survey information and the geology and geotechnical log

Appendix 6 Geological map of North Pit

Appendix 7 Map of North Pit, South Lens and Centre Pits showing historical failure locations, 2009-2013 failures, regional faults, foliation and lithological trends

Appendix 8 Leapfrog™ Legend

Appendix 9 XRD Methodology and raw data

Appendix 10 Geotechnical Properties

Appendix 11 Rock-fall Register Database (2006 – 2012)

LIST OF FIGURES

Chapter 1

Chapter 2

Chapter 3

Chapter 4

Chapter 5

LIST OF TABLES

CHAPTER 1

INTRODUCTION

1.1 Preamble

1.1.1 Location and Access

Savage River Mine is located in NW Tasmania and consists of five large to very large open-cut workings based on a group of magnetite-rich lenses irregularly distributed within a series of highly metamorphosed rocks (Figure 1.1). The mine is situated within the Arthur Metamorphic Complex; a NE-trending, E-dipping Early Palaeozoic high strain metamorphic belt (Gee, 1967). The regional geology and deformational history is outlined in Chapter 2.

Savage River mine is currently owned by Grange Resources following a merger between Grange Resources and Australian Bulk Minerals (ABM) in January 2009.

Access to the mine is gained approximately 37km along the B23 Mount Road from Waratah, approximately 100km SW of Burnie. The mine itself is located within the Savage River National Park which covers an area of 17,980 hectares. This National Park is one of the protected areas within the Tarkine, a temperate rainforest spanning around 3800km² in the NW of Tasmania.

1.1.2 Geomorphology, Climate, Flora and Fauna

Savage River Mine is located at latitude of 41.49°S and longitude of 145.21°E, at an elevation of 100 – 350m a.s.l (courtesy of the Commonwealth of Australia, Bureau of Meteorology). The terrain is rugged, covered with dense vegetation (temperate rainforest) and mountainous. The area contains a rich diversity of flora including myrtle, sassafras and celery top pine as well as providing a valuable habitat for many species including Tasmanian devils, bats, wet forest birds and reptiles (courtesy of Parks and Wildlife Service Tasmania).

The climate is generally cool with high and persistent annual rainfall. The mean maximum temperature is 14.3°C with mean minimum temperature being 6.3°C. Mean annual rainfall is 1943.6 mm (courtesy of the Commonwealth of Australia, Bureau of Meteorology). The Savage River Mine and concentrating plant are both located within the Savage River valley, with the Savage River flowing through the mine site. The river discharges into the Pieman River and ultimately flows westwards to the coast.

1.2 Objectives of this study

The primary objective of this study is to develop a structural model of the Savage River rock package in North Pit that will allow the reasonable prediction of the geotechnical performance of planned and future open pit designs. This has involved the detailed geological and geotechnical mapping within the pit itself, examination of historical wall failures and historical drill core and the geotechnical logging of core from a drilling programme carried out in 2009-2010. Further objectives are to:

- Establish the geotechnical properties of each lithology. The use of 3DM photogrammetry software, core logging and in-pit mapping will assist with this task.
- Develop a classification scheme for the various forms of discontinuities seen in the rock masses at Savage River Mine based on the identification of various infilling minerals in discontinuities. Furthermore define if joint infilling impacts on wall failure and how.
- Identify the structures that have the greatest influence on pit wall stability.
- Establish the types of rock failure in North Pit. If rock failure modes are different within each assemblage define how and why.
- Design and implement new parameters within the current database system in the mine technical services department for the geotechnical logging of recent core and geotechnical in-pit mapping.

- Modify the existing fault models in North Pit and comment on if the presence of the faults affects pit wall stability.
- Document the sequence of ductile structural events that may have impacted on the ore bodies and wall rocks. Undertake mapping and microscopy to determine whether any overprinting relationships exist.
- Confirm whether there are any advantages and/or disadvantages to overlapping the two usually separate disciplines of geotechnical engineering and structural geology.

1.3 Deposit Geology and Previous Work

1.3.1 Exploration History

The Savage River Magnetite deposits were discovered in 1877 although the first shipment of pellets was not made until 1968, the location being seen as too isolated and the magnetite too low-grade (Centre for Tasmanian Historical Studies, 2006). The exploration team was led by surveyor Charles Sprent and Joe Savage, the latter giving his name to the Savage River. By 1968 the workforce was three hundred and seventy five so the Savage River Township was built to house the growing workforce. Magnetite mineralisation exposed in the banks of the Savage River were associated with small amounts of copper so early exploration efforts were aimed at finding economic concentrations of copper, gold and silver. During the 1890's, four adits were driven into the banks of the Savage River. Three were into one of the magnetite lenses and one was driven into a copper bearing sulphide gossan which is now located adjacent to the current main river crossing (MLEP, 2006). Twelvetrees (1900) records old company assays that indicated the presence of significant gold in these adits. Several small gold mines were worked on the Savage River Mine Lease separate from the magnetite deposits notably at Golden Ridge to the south of the lease. Taheri and Bottrill (2013) suggest that the deposit contains minor copper, gold and rare earths, but these minerals mostly post-date the main magnetite-forming event.

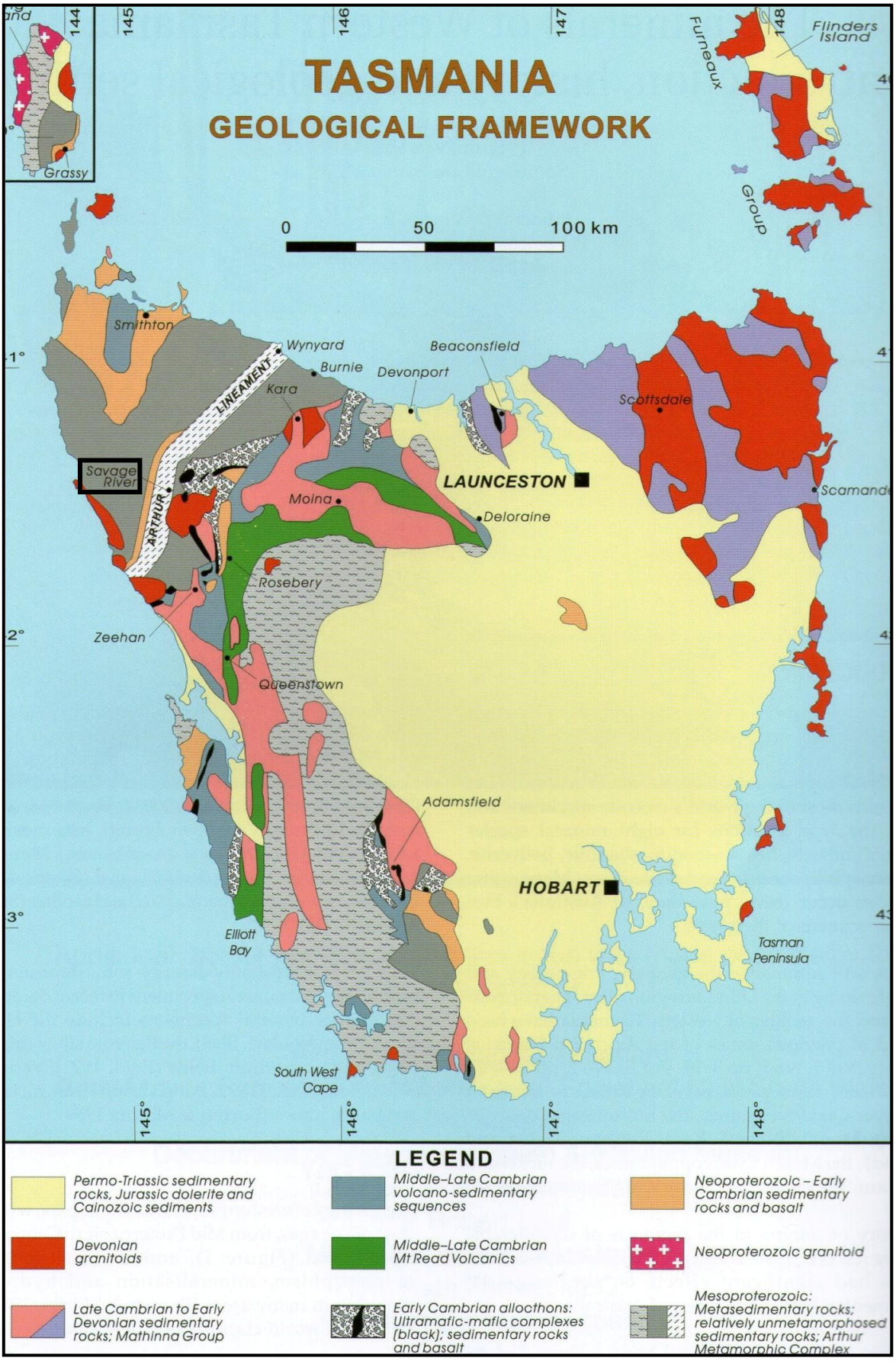

Figure 1.1. The Geology of Tasmania (modified after Bottrill and Baker, 2008). The location of Savage River Mine is highlighted.

The Hoskins Iron and Steel Company in 1926 tested the magnetite orebodies for their suitability as a source of iron for steel making. After sixteen trenches had been dug, the company concluded that the amount of pyrite within the magnetite meant the commodity was not suitable for this purpose. Airborne and ground magnetometer surveys were conducted in 1956 to test the extent of the magnetite deposits in the Savage River area. These surveys were followed by diamond drilling carried out between 1957 and 1959 by the Tasmania Department of Mines. Industrial and Mining Investigations Pty Ltd instigated further diamond drilling in 1961. The company also entered into an agreement with Pickands Mathers and Co. International, who conducted metallurgical investigations that proved the magnetite mineralisation could be developed as a source of iron for steel making. Pickands Mathers and Co. International were appointed managing agent for operations and the open cut mining of Centre Pit commenced in 1967. Australian Bulk Minerals bought the lease in 1997 and now the operation is managed by Grange Resources, following a merger with Australian Bulk Minerals in January 2009.

1.3.2 Mining Method

The mine comprises three principal open pits namely North Pit, Centre Pits and South Pit. All oriented north-south; they comprise a strike length of approximately 6km (Figure 1.2). The principal pits are separated by unmined zones of waste or low-grade material. Grange Resources' mine lease also extends south to an area called Long Plains where another magnetite anomaly exists unmined. The Savage River separates Centre Pit and North Pit. Based on site are a primary crusher and concentrator. Magnetic separation is used to separate gangue and ore. The gangue is transported to the tailings dam and the ore is pumped through a slurry pipeline 87 km north to Port Latta, on the NW coast of Tasmania, where the filtered concentrate is formed into pellets and awaits shipment to steel producers in Australia and Asia. The mine and dedicated port facilities currently produce approximately 2.4 million

tonnes per annum of pelletised iron ore.

North Pit is divided into Stage 1 and 2 (Figure 1.3). The 2009-2010 drilling programme defined the ore body in Stage 2, which is situated to the north of Stage 1. Pre-stripping and subsequent mining in Stage 2 commenced in 2009.

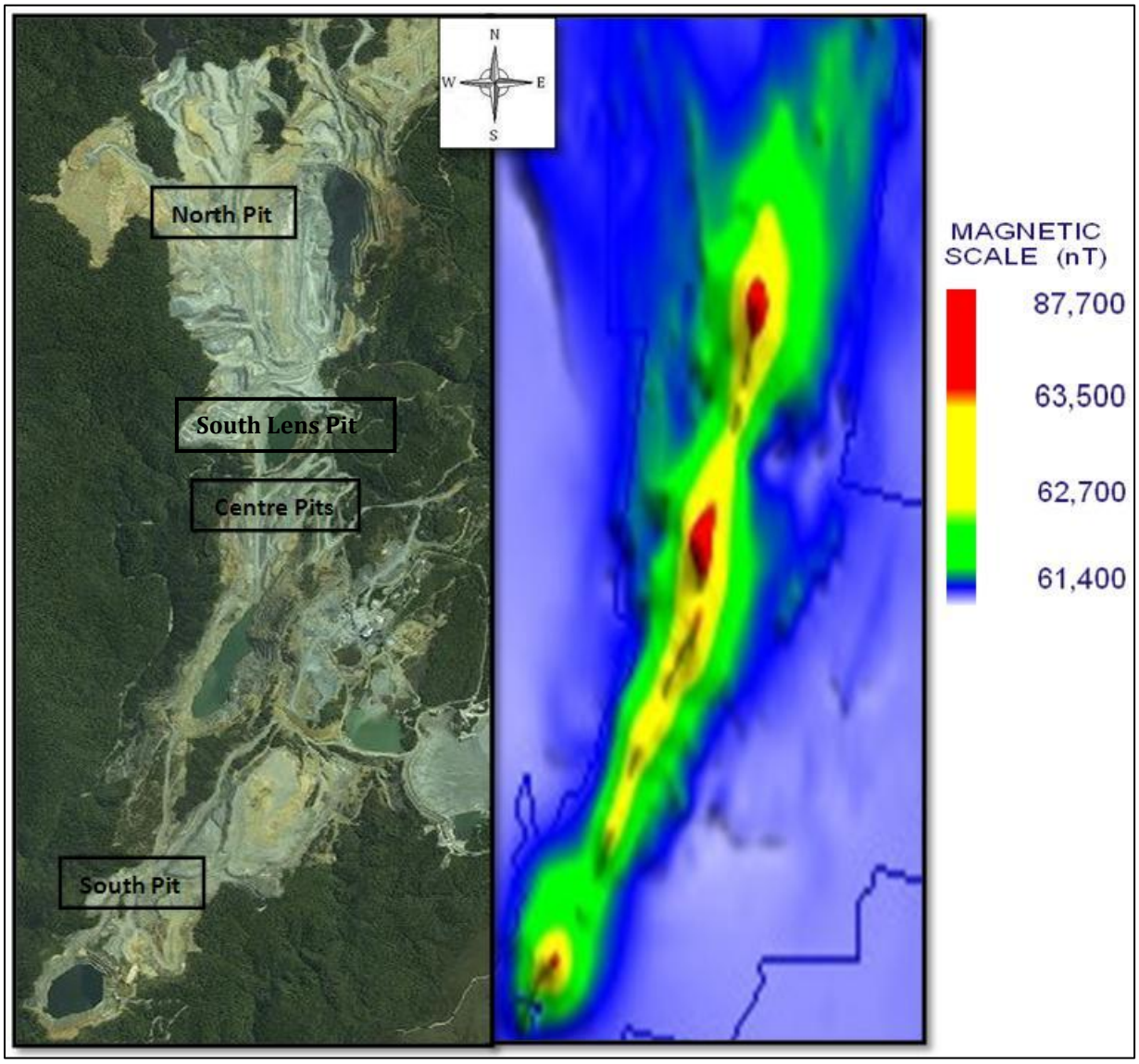

Figure 1.2. An aerial photograph taken in January 2009 (to the left) showing the open pits that make up Savage River Mine. This research only focuses on North Pit, which was the only operating pit up until 2012. The excavation of South Pit resumed in 2012. Plans to re-open Centre Pit South are currently underway, and this is likely in 2013. The total magnetic intensity in the area is shown to the right (modified from ABM internal report, 2009). Each open pit was excavated at areas of the highest (red colour) magnetic intensity.

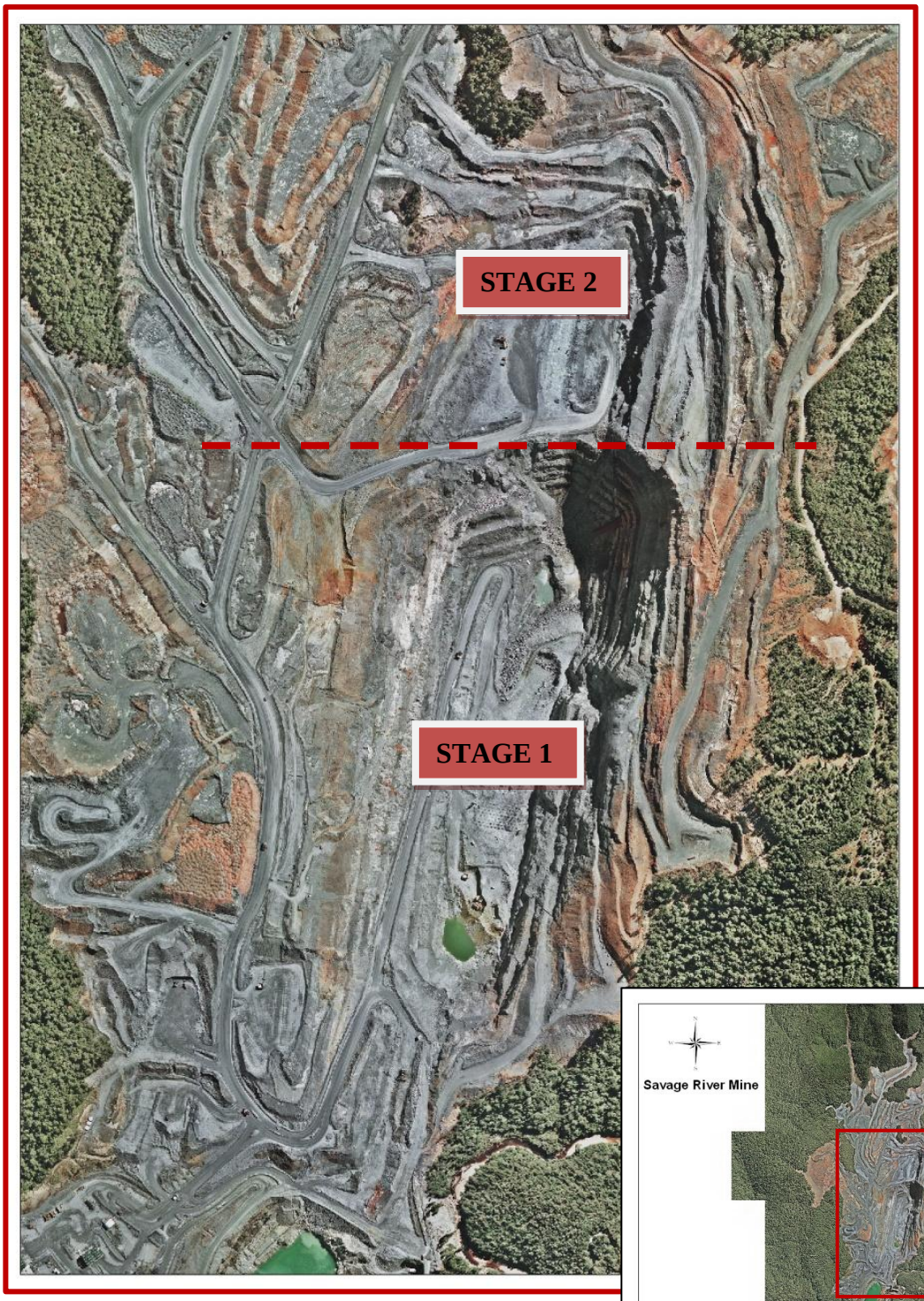

Figure 1.3. A plan view aerial photograph of North Pit taken in March 2012. Stages 1 and 2 are highlighted. The inset aerial photograph shows the Savage River Mine lease and the location of North Pit. In August 2012, Stage 1 was at a maximum depth of 310 m and Stage 2 a depth of 175 m.

1.3.3 Geological Mapping

In September 2006, Australian Bulk Minerals produced a series of reports for the Mine Life Extension Project (MLEP). This project was carried out to investigate the potential to extend the open pit mine life beyond the originally planned 2009 closure. All geological mapping of the magnetite orebodies and their host rocks were compiled. This part of the thesis relies heavily on Savage River Mine records such as maps and small reports prepared by consultant geologists and the Mine Life Extension Plan (MLEP) carried out in 2006.

All geological mapping of the open pits was carried out with an emphasis on distinguishing the individual lithologies using the Savage River Mine nomenclature outlined in Section 1.5. Several substantial rounds of exploration and geotechnical drilling were also carried out. Turner produced the current geological map of all the open pits in 2006. This included the compilation of previous mapping from South Lens Pit (Thornett, 1999), Centre Pit North and South (Turner, 2006), North Pit (Turner, 2006), South Pit (Turner, 2006) and Centre Pit Southern Extension (Urquhart, 1966). In addition to mapping, Turner (2006) used grade control data for the delineation of the main magnetite orebodies. Turner's 2006 mapping resulted in a brief report and a series of 1:1000 scale maps of North Pit, South Lens Pit, Centre Pit North and South, and South Deposit. Two regional, 1:5000 scale maps and a series of cross-sections from North Pit were also produced. For the purpose of the thesis, the main focus was on Turner's 2006 North Pit regional geology map and cross-sections (Figures 1.4 and 1.5 respectively). Four cross-sections were produced at Northing coordinates of 8940, 9540, 9940 and 9740 in reference to the Savage River Mine Grid. A full copy of Turner's 2006 North Pit regional geology map is provided in Appendix 6 (digital). These maps only encompass Stage 1 in North Pit. Although not as extensively mapped, the sequences of lithologies in Stage 2 are generally a continuation of Stage 1 as expected (McPhee, 2011). Certain structures were not visible in 2006, when the maps were compiled. These include the

Eastern Splay Fault in the southern sector of Stage 1 (Figure 1.6). Williams (2011) compiled a lithological model for North Pit required for geological resource modelling (domaining), geotechnical studies and future pit design. Unpublished, internal reports were used to compile a 2D (Figure 1.6) and 3D model of North Pit. Eight domains were designated relating to the separate units of the Bowry Formation subdivided by Turner (2006).

The Savage River magnetite orebodies are located within the Bowry Formation which stretches some 42 km south and south west from the mine to the coast (MLEP, Vol 2, 2006). The Oonah Formation outcrops to the east of North Pit, the Timbs Group to the north west and the Ahrberg Group to the west (MLEP, 2006). These units will be described fully in Chapter 2. Due to the lithological differences in structural/ metamorphic style, Turner (2006) subdivided the Bowry Formation within the mine lease into eight separate units. This nomenclature is used on the mine for defining the separate units of the Bowry Formation. From west to east (refer to Figure 1.4) these units are as follows:

Fulfords Creek Schist – This lithology outcrops to the north west of North Pit (Figure 1.4). Being quartz and muscovite rich it is commonly mapped as part of the Ahrberg Group. Taheri and Bottrill (2013) however suggest it is more similar in metamorphic grade and constitution to the upper parts of Oonah Formation.

Mega Ramp Schist - This lithology consists of chlorite-albite +/- pyrite +/- porphyroblastic albite (code MXC) and chlorite-muscovite-albite schist +/- porphyroblastic albite (code OXH). The lithology is thought to be of sedimentary origin due to minor intervals of muscovite schist and quartz schist. These schists are the most westerly unit in the Bowry Formation in the mine lease area. The Mega Ramp Schists pass eastwards with structural conformity into the Box Cut Carbonate Assemblage.

Box Cut Carbonate Assemblage - The Box Cut Carbonate Assemblage is located on the west of North Pit directly east of the Mega Ramp Schists. No equivalent unit is located on the

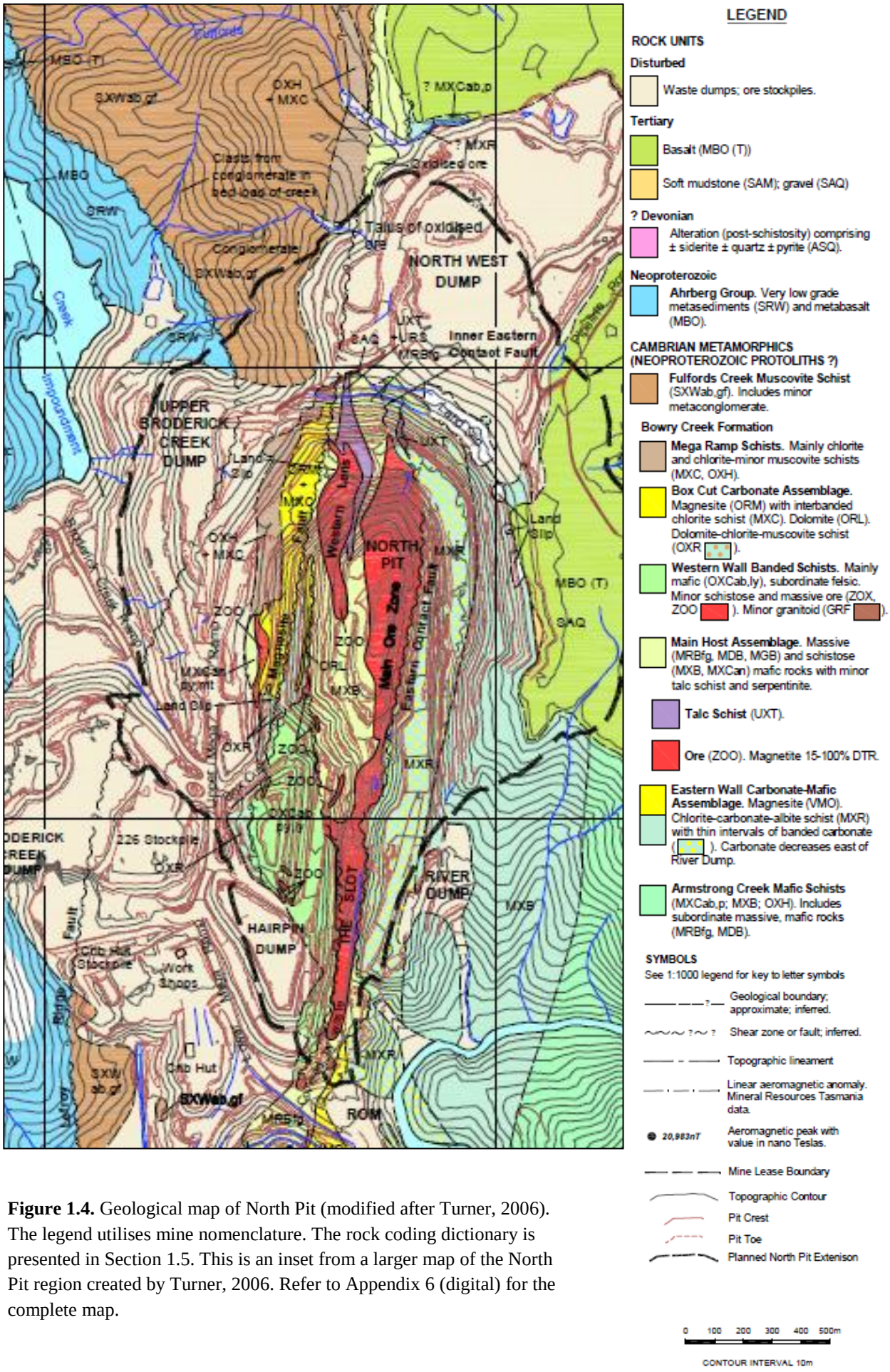

Figure 1.4. Geological map of North Pit (modified after Turner, 2006). The legend utilises mine nomenclature. The rock coding dictionary is presented in Section 1.5. This is an inset from a larger map of the North Pit region created by Turner, 2006. Refer to Appendix 6 (digital) for the complete map.

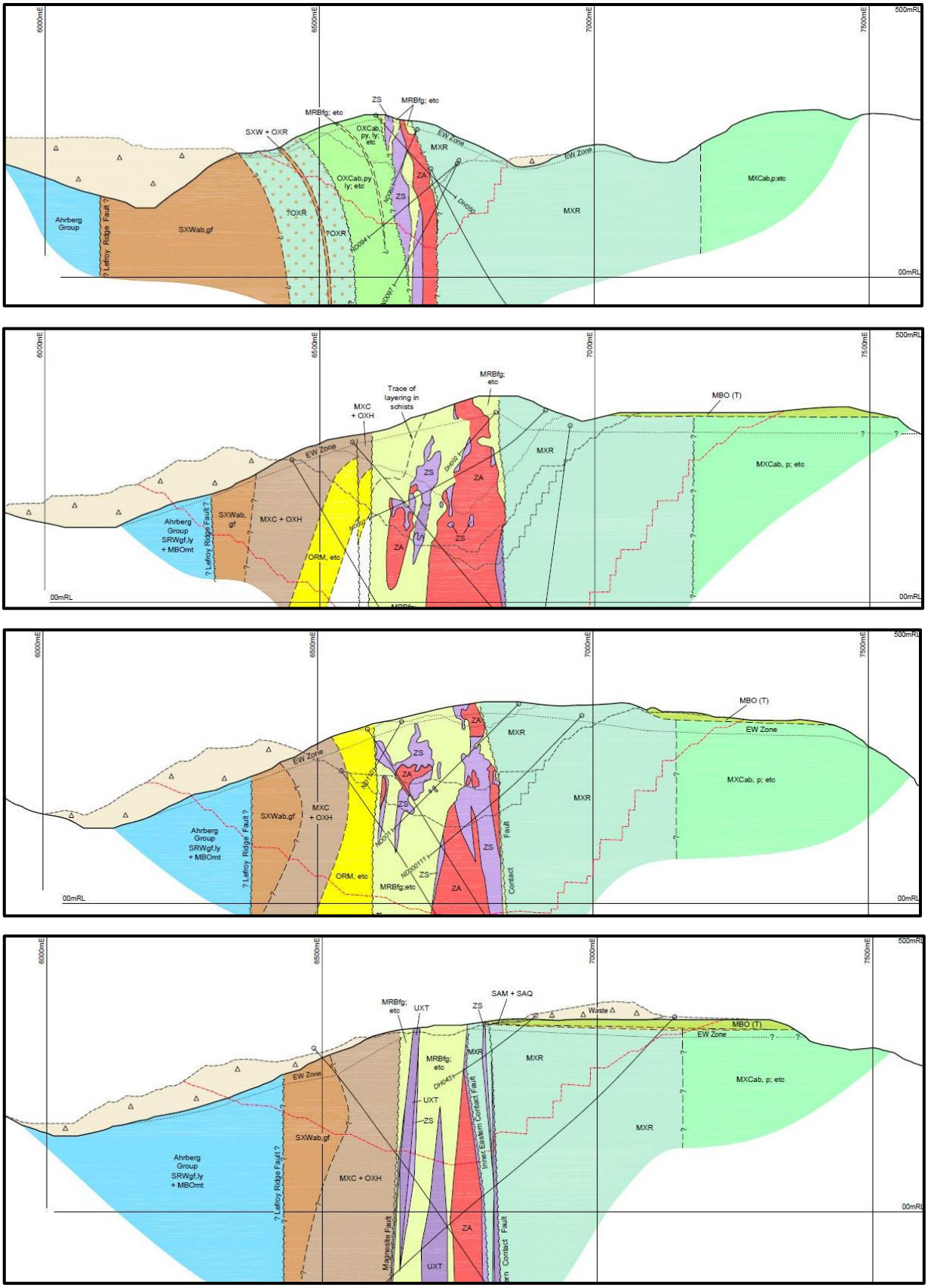

Figure 1.5. A series of four cross-sections in North Pit (modified from Turner, 2006). The sections move from the south (top section) to the north of North Pit (bottom section) at Northing coordinates; 8940, 9540, 9740 and 9940 respectively. The colours relate to the legend shown on the map on the previous page.

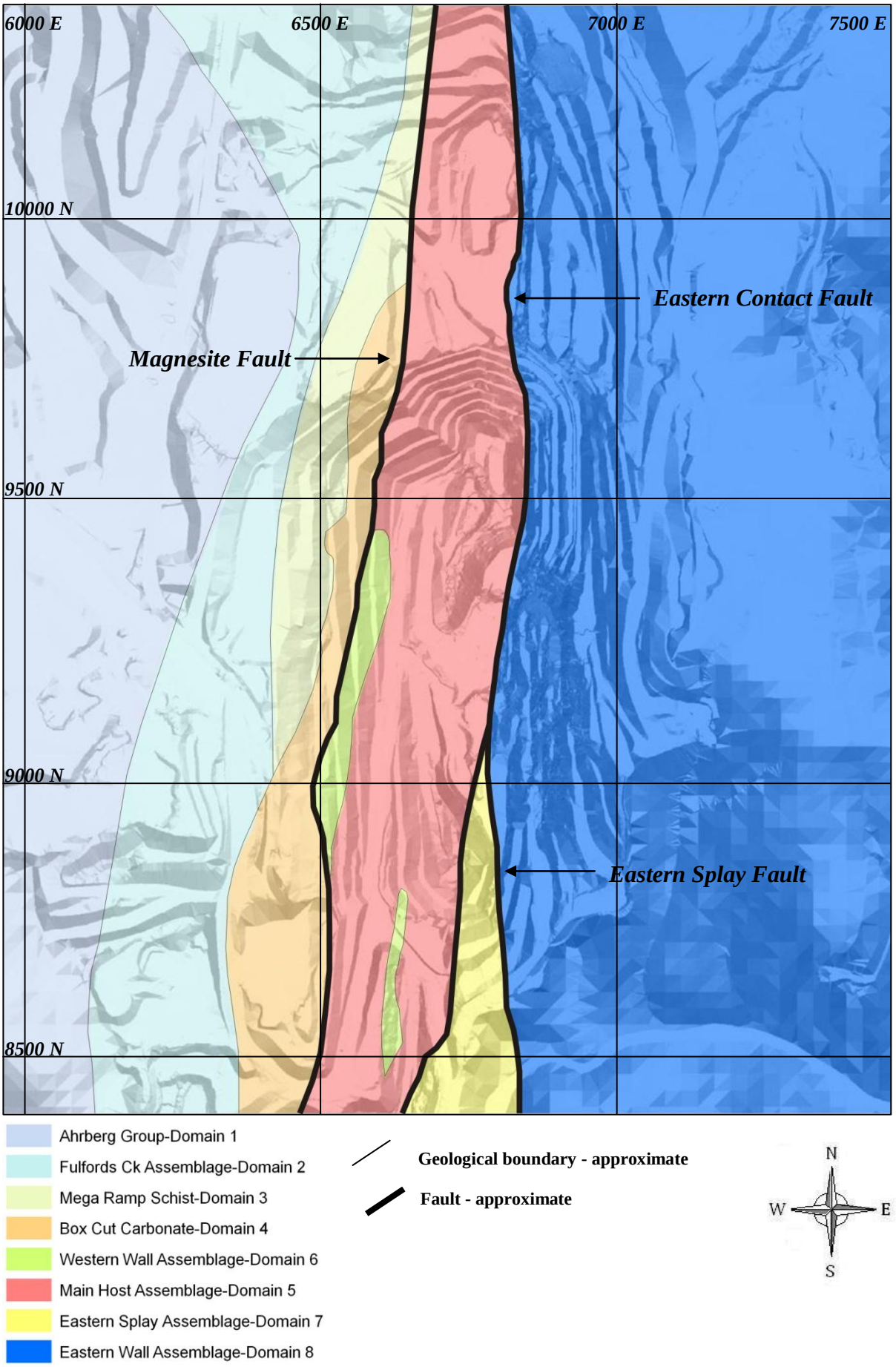

Figure 1.6. Map of North Pit indicating lithological domains. The nomenclature described by Turner (2006) has been used. Modified after Williams, 2011.

western walls of South Lens Pit, Centre Pit or South Deposit Pit. Turner (2006) describes the Box Cut Carbonate Assemblage as boudinaged, blocky, massive magnetite (code ORM) with interbanded chlorite schist (code MXC). Blocky, massive dolomite is also observed (code ORL) as well as thinly banded dolomite-chlorite-muscovite schist (code OXR) with lenses of muscovite schist, micaceous quartz schist and graphitic schist. This is indicative of a sedimentary origin.

Western Wall Banded Schist - Flaggy, mafic and subordinate felsic schists that display sub-planar, 1-20 mm metamorphic banding parallel to foliation characterise the unit. This fabric is attributed to metamorphic differentiation during mylonitic deformation, probably preceded or accompanied by albite alteration. Broader scale banding is also common and may reflect primary compositional variations. These flaggy schists are prone to toppling events and have been associated with major wall failure in Centre Pit. Other rock types in the Western Wall Banded Schists include widespread boudins and lenses of meta-dolerite and minor meta-gabbro.

Main Host Assemblage - The main host assemblage is dominated by massive mafic material notably meta-dolerite in the form of structurally concordant boudins or lenses within the meta-igneous rocks of this assemblage. Pillow lavas are observed in a restricted part of the upper eastern wall of Centre Pit as well as narrow, fine grained, cross cutting dolerite dykes on the eastern wall of the Centre Pit.

Magnetite Ore - The grade of the magnetite ore (code ZOO) ranges from 15- 100% DTR. Low grade ore ranges from 15-35% DTR and high grade ore is >35% DTR. The principal magnetite ore bodies range in thickness from 40 to 150 metres.

Three types of higher grade ore include:

- pyritic ore
- serpentinitic ore

- talc-carbonate ore

These range from being fine-grained to coarsely crystalline and they may be massive or layered. Accessory mineral phases include talc, tremolite, actinolite, chlorite, epidote, apatite and carbonate in varying amounts.

Low grade ore is disseminated and contains a high proportion of silicate minerals. The main North Deposit orebody (MOZ) and the orebody beneath the Savage River in Centre Pit North are the largest ore lenses in the Savage River Mining Lease. The boundaries of these bodies and the other ore bodies are steeply dipping. The MOZ becomes wider at depth and the mineralisation is massive and continuous. This is very different to that of the southern part of Centre Pit South where the mineralisation occurs as relatively thin lodes separated by barren silicate rocks. Other mineralisation in the area ranges between these extremes. The western lens located in North Pit, lies parallel to the north west of the MOZ. It is a highly sheared body of predominantly low-grade ore and has been exposed by mining. Exploratory drilling has failed to define a resource in this lens. Two other substantial magnetite deposits have been identified to the south of the mine lease area by using aeromagnetic surveys. One is located at Long Plains and the other is at Rocky River. Long Plains is of interest to Grange Resources and exploration of the deposit has commenced.

Talc Schist - Talc schist (code UXT) is found in the Main Host Assemblage and usually sufficiently mineralised to be classed as a low grade ore. On the northern wall of North Pit a substantial unit of weakly mineralised talc schist is visible. Other rock types associated with this schist include:

- Serpentine schist
- Chlorite-carbonate schist
- Minor massive serpentine

Other rocks may contain substantial amounts of quartz and muscovite mica and there is also magnetite and pyrite present.

Eastern Wall Carbonate-Mafic Assemblage - The eastern contact of the Main Host Assemblage is faulted. The fault is called the Eastern Contact Fault. At South Deposit, the same contact is not recognised as a fault. On the eastern side of the contact in most areas there is mafic chlorite schist that is distinctive in its high carbonate content. This schist contains boudins and lenses of massive, fine grained mafic rock. The carbonate in the schist is disseminated and also occurs in abundant small veinlets. There is also sparse to common thin structurally conformable intervals of banded carbonate in the mafic schist. These intervals of banded carbonate diminish eastwards in all areas, as does the overall carbonate content.

The carbonate includes magnesite, dolomite and calcite. Calcite appears to be the common disseminated carbonate and the common carbonate in the veinlets. Boudins and bands of cream magnesite and grey dolomite occur in the Main Host Assemblage in South Deposit Pit. A few of these bodies contain substantial disseminated magnetite. The carbonate rich mafic schist of the South Deposit Pit contains bands of graphitic phyllonite. These seams are up to 1m in thickness and represents intense shearing and dislocation. The eastern wall of the South Deposit Pit is strongly sheared and foliated and is prone to toppling events. However, the chlorite- carbonate schist on the eastern wall of North Pit is competent, has strong mineral alignment, blocky and parts on relatively regular discontinuities.

Armstrong Creek Mafic Schist - Turner (2006) describes this schist (MXCab, p; etc) as chlorite- albite characterised by 1-2mm, rounded, albite porphyroblasts and interbanded with meta dolerite (code MDB), chlorite- muscovite-albite schist +/- porphyroblastic albite (code OXH), mafic rocks including fine grained extrusive and intrusive types (code MRBfg) and the main host assemblage. East of the Eastern Wall Carbonate-Mafic Assemblage the carbonate content of the rock decreases and there is an increase in the proportion of strongly

foliated schist in this sequence. The contact between the Armstrong Creek Mafic Schist and the Eastern Wall Carbonate-Mafic Assemblage is strongly foliated chlorite schist where porphyroblastic albite becomes prominent. The mafic rocks are massive and moderately foliated to the east of the contact. The contact between the Armstrong Creek Mafic Schist and the Oonah Formation is structurally concordant (margins parallel to the foliation of the country rock). The pre-metamorphic contact was transitional due to the presence of inter banding of mafic and metasedimentary lithologies at the boundary to the east of South Deposit Pit. Further east of this exposure, meta-dolerite sills occur within the Oonah Formation (MLEP, Vol 1, 2006).

There are two major faults in North Pit; the Eastern Contact Fault (ECF) and the Magnesite Fault (Figures 1.4 – 1.6). The ECF is a consistently steeply dipping feature bounding the barren rocks of the east wall from the mineralised rocks of the Main Host Assemblage. The Magnesite Fault forms the western boundary of the Main Host Assemblage and the eastern boundary of the west wall rock units. These faults are analysed and described in Chapter 4.

For simplicity within this research, the North Pit has been divided into three assemblages; the East Wall Assemblage, the Main Host Assemblage (MHA) and the West Wall Assemblage (WWA). The only assemblage of the east wall is the Eastern Wall Carbonate-Mafic Assemblage. Due to lack of drilling and minimal outcrop, the Armstrong Creek Mafic Schist is not included as part of this rock package in the present study. The MHA includes the magnetite ore and talc schist. The WWA includes the Mega Ramp Schist unit, Box Cut Carbonate unit and the Western Wall Banded Schists.

1.3.4 Previous Geotechnical Evaluations and Historical Rock Failure Modes

There have been many significant failures that have impacted on mining activities particularly within North Pit and Centre Pits (Figure 1.7). Geotechnical consultants have carried out several major and minor geotechnical studies during the mine life. The most comprehensive

reports are those by Australian Rock Engineering (ARENCO, 1974) and Piteau and Associates, 1979, which were concentrated on the mining of Centre Pit South and Centre Pit North (MLEP, Vol 2, 2006). The ARENCO study was initiated following the occurrence of a series of slides over half of the length of the eastern wall of Centre Pit South. At the time, the slope height was only 80 m with the average overall slope angle of 34° (MLEP, Vol 2, 2006). Two modes of failure were investigated; rotational wedge failure and planar failure. The rotational wedge failure was facilitated by a series of cross-cutting faults on the east wall which occurred in the rocks of the Main Host Assemblage (MHA). During phase II of the project, a group of weak serpentine rich rocks had been identified in the east wall within the regions of the various slips. They had some evidence this lithology pinched out with depth so postulated that the final slopes could be steeper than that of 34°. On the west wall the presence of bedding dipping to the east at angles of 45° was reported with a joint set dipping at 35°-55° to the east. The occurrence of planar failure was hypothesized but later drilling confirmed that the rocks rolled over with depth and dipped westwards (MLEP, Vol 2, 2006). Piteau and Associates (1979) carried out a slope stability and design of open pit slopes study in Centre Pits North and South. The consultants carried out detailed slope stability analyses and the pit was divided into nine structural domains with forty-two separate design sectors, which in turn were assigned specific intermediate slope angles between haul roads. The failures they studied all occurred on the east wall which was within the MHA, not the East Wall Assemblage.

Within the Pickands Mather and Co. International mine life, there was a series of reports by Barrett, Fuller and Partners (between 1988 and 1992) on Centre Pit North and North Pit. The North Pit study was carried out when the pit was 100-120 m deep. Discontinuity mapping of the east wall was undertaken but several failures along the west wall prevented extensive mapping in the location. Direct shear tests, UCS, density and Young's Modulus were carried

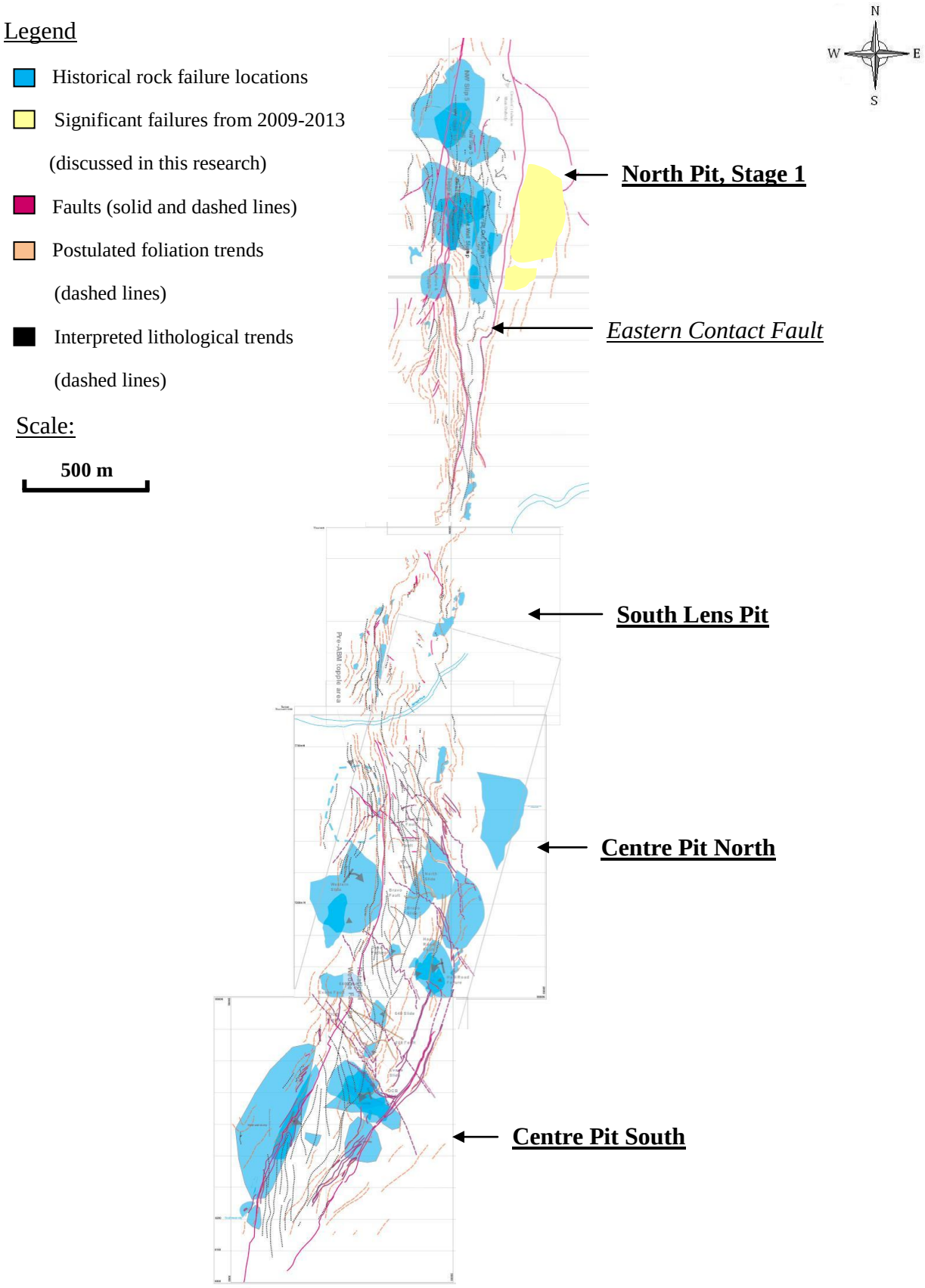

Figure 1.7. Map of North Pit, South Lens and Centre Pits showing historical failure locations, 2009-2013 failures, regional faults, foliation and lithological trends (modified after Webster, 2009). Significant failure areas were plotted by Webster and documented by Australian Bulk Minerals (2006), Thornett (1999) and Turner (2006). The historical failures occurred from 1974 to 2005. For the full resolution map see Appendix 7 (digital).

out and obtained from samples around the pit. Simple failure analyses were produced and recommendations made on overall slope angles, batter angles and heights for each rock package. An investigation into the mechanics of cable bolting as applied to slope stability in open pit mines was carried out from 1979 to 1982 with the completion of a PhD (Dight, 1982) from Monash University, Melbourne. The research looked at cable bolting as a means of creating more stable batters. After the research, cable bolts utilising high tensile strand were used but wide scale use of the technique was not adopted. Instead, the focus was on better blasting and excavation techniques (MLEP, Vol 2, 2006). ABM employed MinServe to carry out a feasibility study (ABM, 1996) prior to the commencement of mining. The study included a geotechnical assessment which essentially brought together previous geotechnical work although some drilling, geotechnical mapping and FLAC modelling of final slopes were undertaken. Samples were also tested for intact strength, shear strength and elastic properties.

Historical failure modes of the Savage River Mine open-pits include; toppling failures that develop slowly, rotational wedge failures (Centre Pits) that occur relatively slowly but continually develop as slopes are excavated downwards, circular failures that develop along folded structures or in weak materials, large-scale slumps and complex failures (MLEP, Vol 2, 2006). Complex failures were only observed in Centre Pit South. This research is solely based on the North Pit so only failure modes within this area will be discussed.

North Pit first opened in 1984 and a major geotechnical study was completed in 1990 (BFP, 1990). At that time, there were two toppling failures on the west wall which was only 30-40 m high at an overall slope angle of 40° to 45°. It was recommended that the future overall slope angle should be 37° (this is in fact the present slope angle). In 1996/97 ABM began operations in the southern end of North Pit and began the 37° cutback of the west wall. Several modes of failure were observed in the Western Banded Schist unit (MLEP, Vol 2, 2006). There was a large slump in chlorite schist and tension crack development including

localised failures on the upper benches. Reverse scarps were displayed 50-70 m behind the crest indicative of toppling movement. The material gradually slumped and the cracks opened leaving a scarp up to 400 mm in height. Slumping on undulating hematite coated discontinuities caused some mining disruptions, moving for approximately a month at a rate of 2-3 mm/day (MLEP, Vol 2, 2006).

BFP Consultants were employed by ABM in 1999 to analyse the west wall toppling and to advise remediation action. A joint proposal from BFP and M.A.Coulthard and Associates suggested UDEC modelling of the North Pit west wall. The intent was to try to numerically model the toppling phenomena taking into account the excavation sequences (BFP Consultants Pty. Ltd, 2000). UDEC is a distinct element programme, which allows discontinuum modelling of blocks and incorporates groundwater pressures acting within the rock mass (MLEP, Vol 2, 2006). The results showed that the installation of horizontal drain-holes, nominally at 50 m horizontal and 30 m vertical spacings can control toppling on the 37° intermediate angle slopes but only up to 90 m height. A wide ramp or berm was suggested when an 80–90 m high slope was reached.

Five circular failures occurred from 1999, all within the northwest area of North Pit. Basal surfaces of the two slips were structurally controlled by the foliation in schistose rocks of the MHA. The first failure developed on a 42° slope that was approximately 70 m high. This was a very slow moving failure. This slip was reactivated in late 1999 due to excavation initiating movement along undulating hematite coated discontinuities steeply dipping to the east. The third, fourth and fifth slips gradually occurred in the sheared Western Lens Ore body, directly behind the first and second slips (Figure 1.7).

Horizontal dewatering drain-holes have played a major role in controlling rock failures, especially toppling failures. These de-pressurise the walls decreasing the risk of rock failure. Other geotechnical monitoring techniques includes the use of an Automated Tracking System

(ATS) for monitoring prism movements. This has proven to be a very effective tool in monitoring and evaluating various pit wall movements. Since 2009, three major rock failures have occurred on the east wall of North Pit (refer to Chapter 3, Section 3.3.6). Due to the fast development of these failures, two Movement and Surveying Radars (MSR), supplied by Rock Australia™ (Reutech Mining), are currently being used on the mine. The radars continuously scan the east wall in Stage 1 and 2 and detect movement of less than a millimetre within a 50-2500 m range. The radars ensure a safer working environment through the reduction of risk and a degree of peace of mind when mining near suspect mine slopes. The radars have consistently proved that when mining in a deep open pit in an unstable geotechnical environment, pit wall monitoring is paramount. All monitoring techniques are utilised, with the additional use of risk based assessments and safe operating procedures. Many of the historical and present failures could have been avoided by more conservative slope designs. However, conservative slope designs are less economical and would have resulted in the premature closing of the mine.

In August 2012, Stage 1 of North Pit was at a maximum depth of 310 m and Stage 2 at 175 m depth. Currently, the overall slope angle of the west wall is 37° (due to the recommendation of previous consultant reports) and the slope angle of the east wall is 62°. Currently Stage 1 is temporarily closed, following major east wall rock failures. Magnetite from Stage 2 is currently the main ore supply, although mining has commenced in South Pit and a geotechnical evaluation and feasibility study on Centre Pit South is imminent and included in the 2013 budget.

1.3.5 Additional Previous Work – Ore Genesis

There have been several previous studies of the genesis of the ore bodies at Savage River Mine. Twelvetrees (1900) considered them to have formed by magmatic segregation in a mafic magma. This was argued however due to the unexplainably high concentrations of iron

in a magma resulting in Reid (1919), Hughes (1958) and Hall and Solomon (1962) reporting on other genetic suggestions. A hydrothermal replacement origin, relating to the Cambrian ultramafic complexes was suggested by Urquhart (1966), and Gee (1967) and Coleman (1975) suggested that the deposits were deformed by the late Proterozoic Penguin Orogeny. The suggestion of the deposits being volcanogenic or volcano-sedimentary was argued by Spiller (1974), Coleman (1975), Collins and Williams (1986) and Duncan and Weatherstone (1990). Matzat (1984) related the ore to Kiruna-style iron deposits whilst Thornett (1999) preferred a primary magmatic (cumulus) origin, considerably modified by metamorphic recrystallisation, remobilisation and resegregation. Bottrill et al., (1998), Bottrill (2006), Bottrill and Taheri (2007), and Bottrill and Taheri (2008) introduced the concept of the mineralisation being a highly deformed magnesian magnetite skarn. Webster (2009) used structural studies to confirm this analogy and to suggest that several phases of Cambrian and Devonian deformation are present, the late Cambrian event being more prevalent within the rocks. The most recent work of Taheri and Bottrill (2013) suggests that the magnetite ore carries the basic characteristics of the iron skarn facies of an IOCG deposit. They argue that there is no evidence for any significant orthomagmatic or exhalative mineralisation and that locally, the orebodies contain minor copper, gold and rare earths that post-date the main magnetite forming event.

1.4 Methods

1.4.1 Field Methods

Mapping within the currently operational North Pit on Savage River Mine is relatively opportunistic. Due to the instability of the walls, JHA's (Job Hazard Analysis) have to be compiled prior to mapping in any areas deemed unstable. A comprehensive assessment has to be undertaken prior to any mapping and an understanding of several factors has to be taken into account. These factors are primarily; the location of production work being carried out

and the proximity of the mapping in relation to this, the advice of the geotechnical engineers on site and the potential need for a spotter (a second person accompanying the geologist to stand back and observe the face for rilling and cracking, both diagnostic of a potential wall failure). Once these tasks have been completed, mapping can commence with caution. Bench scale mapping is mainly carried out (approximately 15m high and 50m width). The Savage River Mine surveying equipment namely the Trimble Rover R8 which uses GPS technology is used to retrieve mine-grid coordinates of any features of importance and the extremity of the mapping traverse. Scanline survey mapping was attempted and the Geological Strength Index (Hoek-Brown, 2000) was utilised in domaining rock masses.

3DM photogrammetry by Adam Technology™ was utilised in conjunction with in-pit mapping. Photogrammetry enables a three-dimensional digital terrain model to be created from different photographs incorporating the mining grid. These DTM's can then be analysed using 3DM Analyst™ and where planar discontinuities, foliation and faults can be digitised, features can be assigned to sets, the dip and dip directions can be obtained and subsequent stereonets are automatically produced. The resulting information can then be imported into mine planning software such as Surpac™ or Leapfrog™. A trial investigation into the TerraLuma Unmanned Aerial Vehicle technique was conducted which involved a camera mounted 'OktoKopter'. A comparative analysis of this technique and the standard photogrammetry technique is available in Appendix 1.

Geological and geotechnical data collected from drillcore logging is heavily relied upon in this research. Savage River Mine logging dictionaries and nomenclature were used (refer to Section 1.5) but some logging parameters were added for this research. A metal pivoting arm protractor was used to measure alpha angles of discontinuities and a wrap-around protractor method was used to measure beta angles in orientated core. A discussion into the methods of measurements is provided in Chapter 3, Section 3.8. Sample identification numbers provided

in this research correspond to the University of Tasmania cataloguing system.

1.4.2 Software Tools

The mine planning software Gemcom Surpac™ is currently used by the technical team at Savage River Mine. Several methods can be performed using Surpac™ including; drillhole data management, geological modelling, block modelling, geostatistics, mine design, mine planning and resource estimation. Although Surpac™ was used for the creation of geological structures from photogrammetry, the locating of structures and samples and for the retrieval of bearing and distance measurements in this research, Leapfrog™ (another 3D geology modelling programme) was used for the creation of cross-sections. These programmes are compatible, meaning data can be shared with ease. Leapfrog™ has subsequently become the main modelling programme used by on site geotechnical engineers for the observation of brittle structures and rock mass conditions throughout North Pit.

For further stereographical analysis the Rocscience programme DIPS™ was used for the presentation of structural measurements and for the manipulation of data used in back analysis of rock failure. Structural measurements are shown in dip/dip direction format unless specified.

1.5 Nomenclature

The geological and geotechnical nomenclature used in this thesis follows the nomenclature used on Savage River Mine (Figures 1.8 and 1.9 respectively). The geological codes were current as from November 2005 and the geotechnical codes as from July 2007. Other parameters have since been added to the logging dictionaries.

The geological codes used on the mine outline rock type, minerals, texture, colour and serpentinisation. A thorough logging dictionary such as this is vital due to the vast lithological changes within the mine. All lithologies mapped and/or logged are given at least a three letter

code such as ***MXR***; ***M*** – Mafic, ***X*** – Schist, ***R*** – Chlorite and carbonate = Mafic chlorite and carbonate schist. Abbreviations such as ***py*** can be added to the three letter code to indicate other major minerals present such as pyrite in this instance. Turner et al. in 2005 and 2006 used this logging dictionary whilst compiling the current geological map and cross sections of North Pit (Figure 1.4 and 1.5).

The geotechnical logging dictionary is solely for the use of logging drill core. It describes (using abbreviations) the structure being logged, rock strength and weathering. If the feature is a joint or fault, abbreviated minerals relating to infill, joint roughness, joint wall strength and joint alteration are all noted using the logging dictionary. All core logs are entered into the Access 2007 Savage River Mine Drillhole Database and Surpac™ is used for viewing the drillhole location, geology and geotechnical properties down-hole. Leapfrog™ however, is used in this research for the same purpose. The Leapfrog™ legend is provided in Appendix 8 (digital).

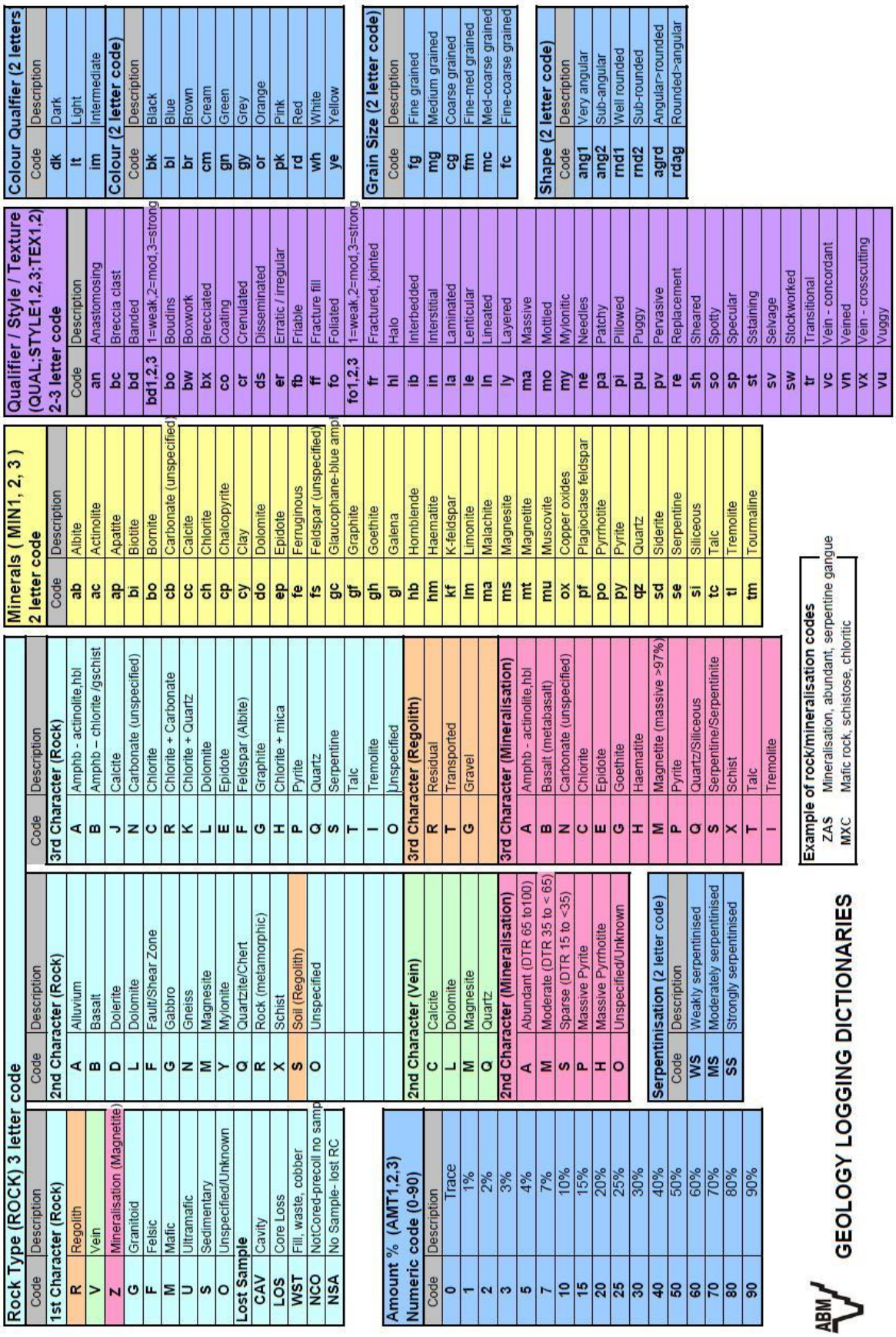

Figure 1.8. Geology logging dictionary employed at Savage River Mine (internal unpublished report ABM, 2005). Refer to Appendix 5 (digital) for borehole logs utilising this geology dictionary. These boreholes were logged by the author and used as raw data for this research.

Joint Type (j_type)		
Colour	Code	Description
	AX	axial plane - fold axis
orange	BO	boudin
blue	CF	contact - shear / fault
blue	CG	contact - gradational
blue	CS	contact - sharp
	FO	foliation - bedding / schistosity
	FO1,2,3	1=weak; 2=moderate; 3=strong
	FR	fractures - intense fractured zone
yellow	JC	joint - closed
yellow	JN	joint - open
	LN	lineation - linear feature
	MB	mineral banding
	MB1,2,3	1=weak; 2=moderate; 3=strong
red	SH	shear/fault
green	VN	vein - healed unless a joint contact

Joint Qualifier (j_qual)		Joint Fill Type (j_infill)	
Code	Description	Code	Description
BD	banded	ab	albite (feldspar)
BX	brecciated	ac	actinolite (green xtals)
BO	boudins	bx	breccia
BW	boxwork	cb	carbonate
FR	fractured / jointed	cc	calcite (pink/white)
FB	friable	cl	carbonate + chlorite
IB	interbedded	ch	chlorite
LA	laminated	cy	clay
MA	massive	ep	epidote
MO	mottled	gf	graphite
MY	mylonitic	hm	haematite
OS	offset (veins, joints,etc)	lm	limonite
PA	patchy	ms	magnesite
PU	puggy	mt	magnetite
SH	sheared	py	pyrite
SW	stockworked	qz	quartz
SO	spotty	tc	talc
VN	veined	tl	tremolite (white xtals)
VU	vuggy	se	serpentine

Rock Strength (Field Test)	
Code	Description
R6	Extremely strong (chip only)
R5	Very strong (fracture by many hits)
R4	Strong (fracture by >1 hit)
R3	Medium strong (fracture by 1 hit)
R2	Weak (scratch with difficulty)
R1	Very weak (scratch easily)
R0	Ext weak (scratch with thumbnail)

Joint Wall Strength (jws)	
Code	Description
1	wall = rock (default)
2	wall greater than rock
3	wall less than rock

Joint Roughness (j_rough)			
	Profile		
Roughness	Planar	Undulating	Stepped
Rough	PR	UR	SR
Smooth	PS	US	SS
Slickensided	PK	UK	SK

Recovery / RQD / Rock Strength / Fracture Frequency
measured for all one metre intervals as marked up

NOTE
intervals may be < or >1m due to litho change, geotech domain change, or core loss. Use 0.1m as the min cutoff for assigning a new interval. Use 0.5m as the max cutoff for taking a 'odd' interval up or down to the nearest metre eg.1.0-2.3m, 2.3-3.0m or 10.0-10.8m, 10.8-12.0m.
Recovery = core recovered in 1 metre interval (m)
When rec=0, make interval from coreblock to coreblock
RQD = Σ pieces core >10cm in 1 metre interval (m), only for recovered core ie if rec=0, rqd=0
Fracture Frequency = fracture count in 1 metre interval (MAX 40)
NOTE : only use / count natural breaks ie ***DO NOT*** include breaks that are drilling induced (end of run; core lifter; overdrilled); drillers (marked with an X); or handling (marked with an X).

Number of Joint Sets (j_num)	
Code	Count
0	None
0.5	Random
1	1 set
1.5	1 + random
2	2 sets
2.5	2 + random
3	3 sets
3.5	3 + random
4	4 sets +++
5	Crushed rock

Weathering				
Code	Description	Decompo	Staining	Rock Fabric
CW	residual soil	Total	Strong	Destroyed
HW	extremely weathered	Strong	Strong	Strongly obscured
MW	distinctly weathered	Slight	Strong	Visible
SW	slightly weathered	None	Slight	Preserved
UW	fresh	None	None	Preserved

Figure 1.9. Geotechnical logging dictionary employed at Savage River Mine for the logging of drillcore (internal unpublished report, ABM, 2007). Refer to Appendix 5 (digital) for borehole logs utilising this geotechnical logging dictionary. These boreholes were logged by the author and used as raw data for this research.

CHAPTER 2

GEOLOGY AND DEFORMATIONAL HISTORY OF THE ARTHUR LINEAMENT AND SURROUNDING ROCKS

2.1 Introduction

Savage River Mine magnetite ore bodies occur within the Arthur Metamorphic Complex. This is a Cambrian (510 +/- 10 Ma) high-strain metamorphic belt (Turner et al., 1998) up to 10 km wide and strikes NNE (Gee, 1967) across NW Tasmania from near Granville Harbour on the west coast to near Somerset on the North Coast. The complex runs through Savage River and Corinna, a distance of 110 km. A time-space diagram for the district is shown in Figure 2.1. Figure 2.2 shows how the lineament separates the weakly deformed Neoproterozoic Rocky Cape Group correlates (shelf siliciclastics) to the NW from the "low-strain" Burnie and Oonah Formations (turbidites) to the east (Holm and Berry, 2002). The lineament was multiply deformed during the Middle to Late Cambrian, Tyennan Orogeny and has subsequently undergone several episodes of less intense deformation in the Middle Devonian (Holm and Berry, 2002). Turner (1989) suggested that the name 'Arthur Metamorphic Complex' should be used as a stratigraphic term to describe the rocks within the lineament which is a tectonic term. Ambient seismic noise tomography research suggests that the Arthur Lineament continues to a depth of >8 km (Young et al., 2011).

2.2. Lithostratigraphy

The Arthur Metamorphic Complex was defined to include the most deformed parts of the Oonah Formation and the Ahrberg Group, and includes all the mineralised Bowry Formation and the "eastern" Ahrberg Group. Historically, the schistose meta-sedimentary and meta-igneous rocks of the "eastern" Ahrberg Group were called the Timbs Group (Turner et al.,

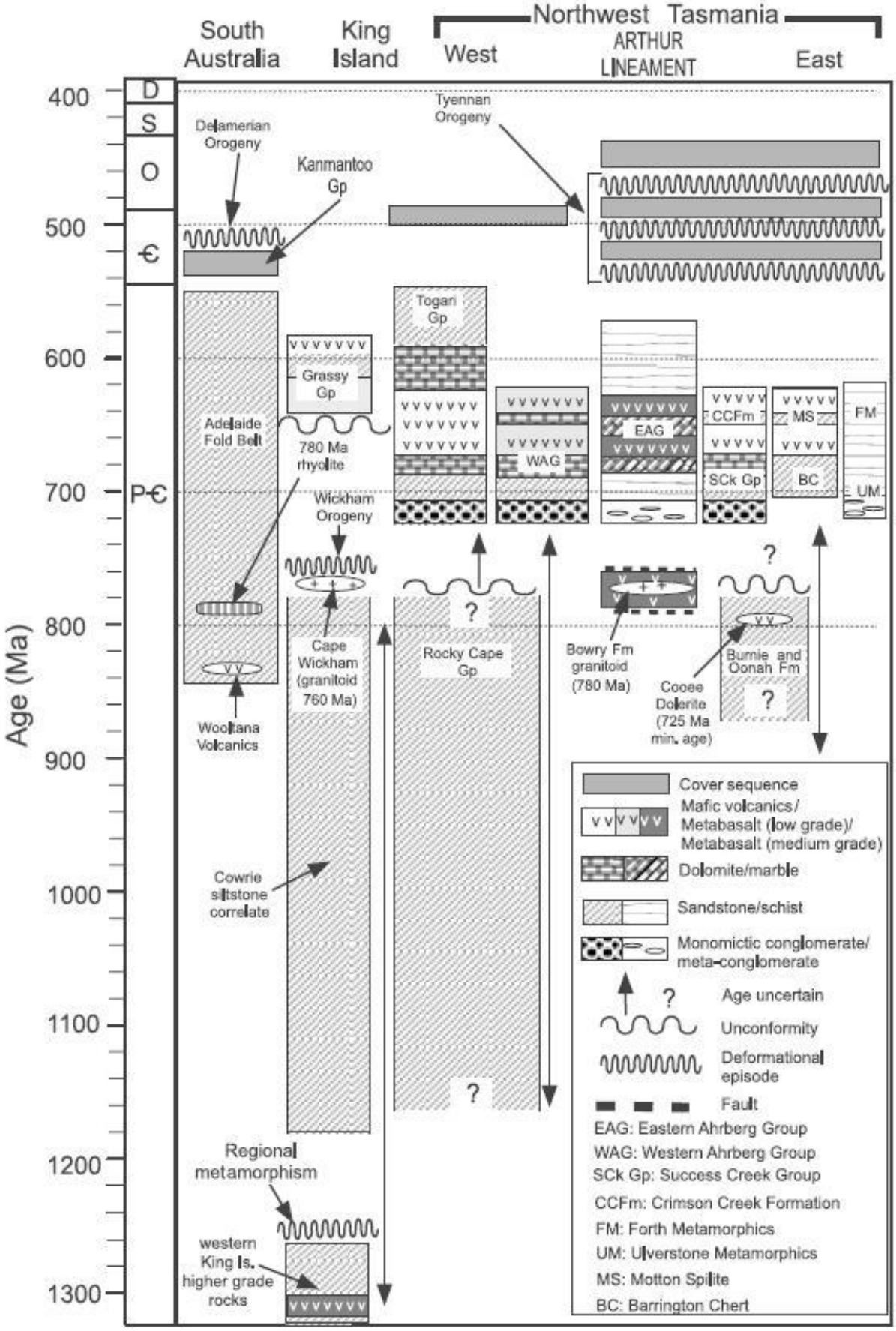

Figure 2.1. Space-time diagram displaying the tectonostratigraphy of NW Tasmania including the Arthur Lineament and surrounding units, King Island and South Australia. (Holm et al., 2002).

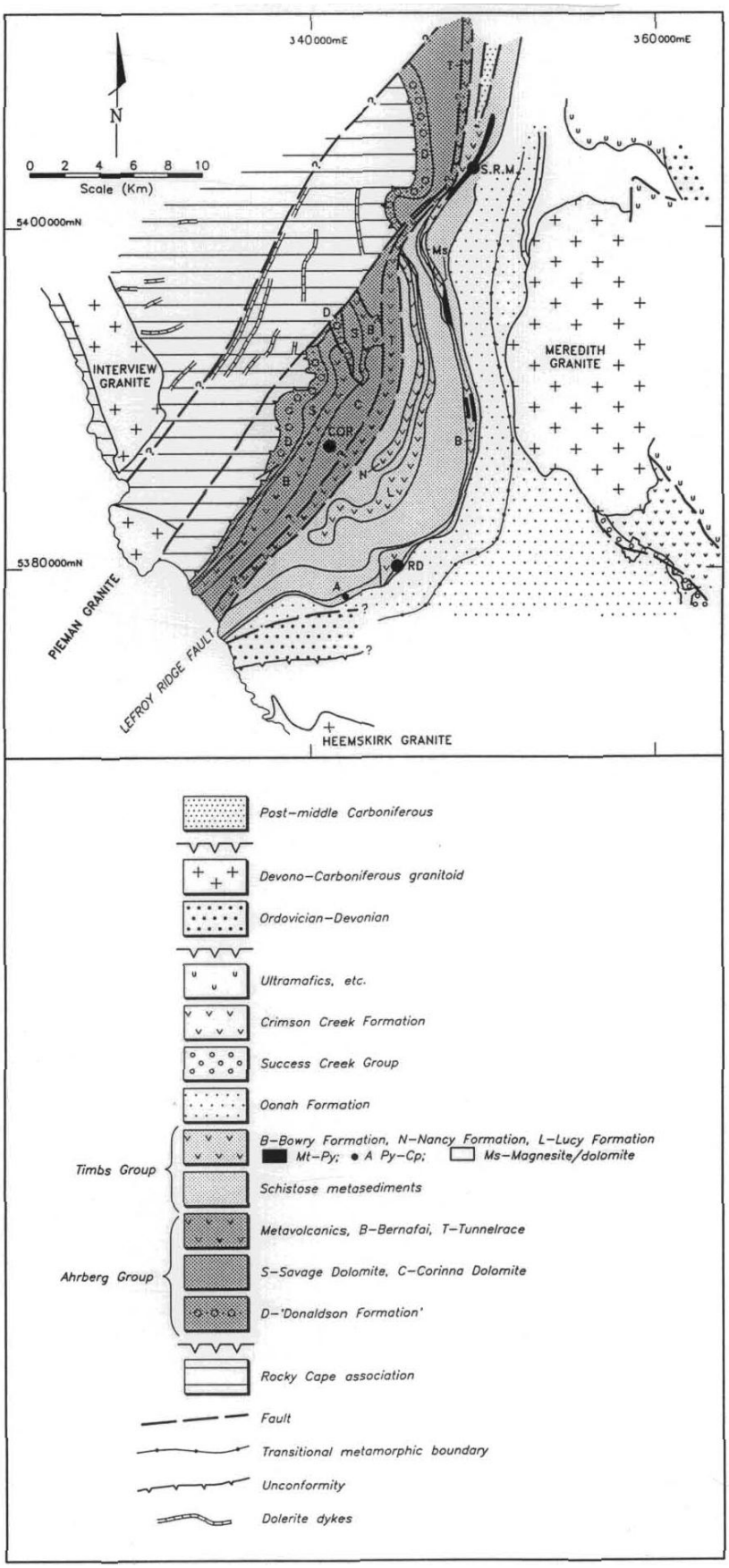

Figure 2.2. Geology of the Corinna District (Turner, 1991). COR = Corinna; SRM= Savage River Mine; A = Alpine locality; RD = Reece Dam. The Arthur Metamorphic Complex extends eastwards from the Lefroy Ridge fault to the transitional metamorphic boundary in the Oonah Formation.

1991 (Figure 2.2)). This was previously known as the Whyte Schist (Spry, 1964). Spry (1964) also observed the highly deformed turbiditic Burnie and Oonah Formations that lie to the east of the complex. The Bowry Formation which hosts the magnetite ores at Savage River lies to the east of the Ahrberg Group.

A large Late Devonian (340-360 Ma) granite batholith called the Meredith Granite (Figure 2.2) is exposed a few kilometres to the east of Savage River Mine. This generated some major tin mineralising events such as at the Mt Bischoff and Mt Cleveland tin deposits (Taheri and Bottrill, 2005). A similar Devonian batholith called the Interview Granite (Figure 2.2) lies 20-30 km to the west and also has some related tin-tungsten mineralisation (Taheri and Bottrill, 2013). A Devonian granite porphyry dyke intruding the Ahrberg Group, a few kilometres south west of Savage River has been dated at 380 Ma (Turner et al., 1998). There is no proven relationship between any of these Devonian intrusives and the mineralisation, alteration and metamorphism at Savage River Mine, but a 400 Ma U-Pb date on apatite in the ores suggests it must have had a sufficient heating effect to reset U-Pb apatite ages (Taheri and Bottrill, 2013).

2.2.1 Rocky Cape Group

The Rocky Cape Group lies to the west of the Arthur Lineament (Figure 2.3a and b) and was first described by Gee (1967). Gee (1967) describes four main lithologies within the Rocky Cape Group on the north coast in stratigraphic order starting at the top; *Jacob Quartzite* – supermature quartzarenite with silica cement, with abundant planar cross-bedding, *Irby Siltstone* – siltstone with minor black shale, dolomite, sub-greywacke and hematitic breccia, *Detention Subgroup* – supermature cross-bedded quartz sandstone with minor interbedded siltstone and *Cowrie Siltstone* – black pyritic shale with interbedded siltstone. The Burnie Formation, which lies to the east of the Arthur Lineament, was initially correlated to that of the Rocky Cape Group (Spry et al., 1962) and placed at the bottom of the Rocky Cape

sequence. This interpretation however was altered after Gee (1967) observed overturned beds and younging direction to the east within the Rocky Cape Group thus suggesting the Burnie Formation overlay the Rocky Cape Group. Holm (2002) described the Rocky Cape Group within the lower Pieman River area consisting of an upwards coarsening, eastward younging, siliciclastic shallow marine sequence. The minimum age of the Rocky Cape Group is 620 – 650 Ma based on K-Ar dating of slates taken from the Irby Siltstone (Adams et al., 1985). The maximum age of the Rocky Cape Group is 1200 Ma based on SHRIMP U-Pb dating of detrital zircons (Black et al., 1997).

2.2.2 Oonah Formation

The Oonah Formation outcrops immediately to the east of the mine lease. It is one of the oldest units in the immediate vicinity of Savage River Mine and is a unit shown on company geological maps (Turner, 2006). Mostly occurring to the east of the Bowry Formation (Holm and Berry, 2002), the unit has also been tentatively mapped to the west. Taheri and Bottrill (2013) argue that the mine unit namely the Fulfords Creek Schist could be part of the Oonah Formation. This unit outcrops to the west of the mine sequence (refer to Chapter 1, Section 1.3.3) and has previously been mapped by geologists as part of the Ahrberg Group which is the most westerly unit on the mine.

The turbiditic Oonah Formation is made up of relatively clean quartz sandstone, dolomite, chert and conglomerate (Turner, 1989; Seymour and Calver, 1995). The Oonah Formation has been sub-divided into two domains; low-strain and high-strain. The Oonah Formation undergoes a gradual transition in strain and texture westwards towards Savage River Mine (Figure 2.2). The texture changes from phyllitic to schistose (Holm, 2002). Morris (2012) sampled along the main road access to the mine from Waratah within the high-strain Oonah Formation for an illite crystallinity study. The results did not yield any metamorphic temperature gradients between samples with all illite crystallinity typical of sub-greenschist

grade (Morris, 2012).

The Burnie Formation which occurs further north to the east of the Arthur Lineament is a close correlate to the Oonah Formation (Gee, 1967). The Burnie Formation consists predominantly of sandy turbidite-facies quartzose wacke and slaty mudstone, intruded by minor altered mafic dykes and containing occasional basaltic pillow lavas (Holm, 2002). Turner et al. (1998) proposed that the Burnie and Oonah Formations and the Ahrberg Group were sourced from the Rocky Cape Group to the west, as a result of the Wickham Orogeny. The units that have been described within the Oonah Formation including the abundance of mudstone and siltstone units suggest a deep basinal depositional setting. The Oonah Formation displays much greater lithological variation than the Burnie Formation, suggesting a more complex depositional history. The higher proportion of sandstone and debris flows suggests the Oonah Formation was deposited closer to a continental margin than that of the Burnie Formation (Mueller, 1998).

2.2.3 Ahrberg Formation

The Ahrberg Formation was described by Turner et al., (1991) as pelitic sandstone with banded chert and thin oolitic carbonate interbeds. It includes the Bernafai and Tunnelrace Volcanics (Figure 2.3b), (Turner et al., 1991). Turner and Crawford (1993) suggested that the Bernafai Volcanics consists of basalt and sedimentary rocks of very low metamorphic grade whilst the Tunnelrace Volcanics contained abundant metamorphic hornblende indicative of a higher grade of metamorphism (Turner and Crawford, 1993). The Ahrberg Group was divided into fault-bounded eastern and western sectors by Holm and Berry (2002), based on structural and metamorphic differences. The eastern sector is an east-dipping package of meta-sedimentary and meta-igneous rocks (Holm, 2002). Turner et al., (1991) named the easternmost metabasalts-dominated unit in the Arthur Metamorphic Complex the Bowry Formation. The eastern Ahrberg Group starts with siliclastics and conglomerate, grading

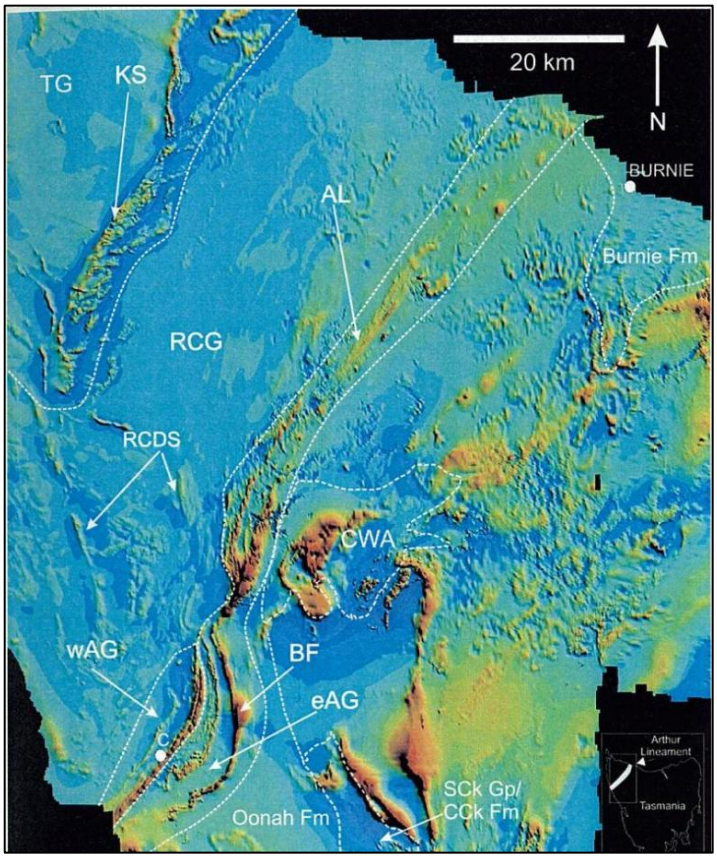

Figure 2.3a. Total magnetic intensity aeromagnetic image of NW Tasmania. Units in red are anomalously magnetic, whereas blue units have minimal magnetic component. AL – Arthur Lineament, RCG – Rocky Cape Group and correlates, eAG – eastern Ahrberg Group, wAG – western Ahrberg Group, RCDS – Rocky Cape Dyke Swarm, TG – Togari Group, KS – Kanunnah Subgroup, SCk Gp/ CCk Fm – Success Creek Group/ Crimson Creek Formation, CWA – Cleveland-Waratah Association and C – Corinna. Modified after Holm, 2002.

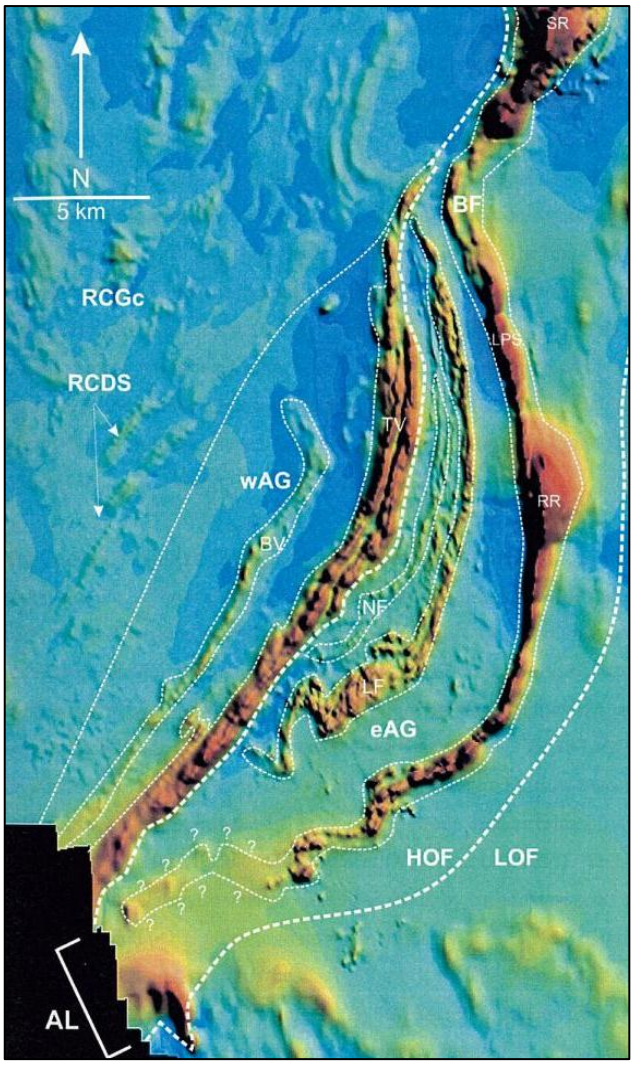

Figure 2.3b. Total magnetic intensity aeromagnetic image of NW Tasmania. Units in red are anomalously magnetic, whereas blue units have minimal magnetic component. AL – Arthur Lineament, eAG – eastern Ahrberg Group, wAG – western Ahrberg Group, HOF – high strain Oonah Formation, LOF – low strain Oonah Formation, BV – Bernafai Volcanics, TV – Tunnelrace Volcanics, NF- Nancy Formation, LF – Lucy Formation, BF – Bowry Formation, RR – Rocky River, SR – Savage River, LPS – Long Plains South, RCGc – Rocky Cape Group Correlates and RCDS – Rocky Cape Dyke Swarm. Modified after Holm, 2002.

upwards into a calcareous, psammopelite-dominated, shallow marine sequence (Holm, 2002). The contact between the eastern and western Ahrberg Formations is interpreted to be a major fault (Holm, 2002 (Figure 2.3a and b)). The western Ahrberg Formation is east facing and interpreted to represent a transgressing basinal sequence. The volcanic units of the western and eastern Ahrberg Group have rift tholeiitic chemistry (Brown, 1986; Turner, 1992; Crawford, 1992).

2.2.4 Bowry Formation

The Bowry Formation is easily distinguishable on the aeromagnetic imaging (Figure 2.3a) and contains the main ore bodies within the Arthur Lineament including magnetite at Savage River, Long Plains and Rocky River, magnesite at Long Plains and Savage River and gold and chalcopyrite at Rocky River. Geochronology by Turner et al., (1998) suggested that the Bowry Formation is older than the Ahrberg Group (pre-770 Ma). Taheri and Bottrill (2013) however indicate that the structure is complex and some units mapped of the Bowry Formation may be younger than 760 Ma and be correlates of the Ahrberg Group. The mafic rocks are mostly rift-type MORB-like tholeiites indicating that the sediments and volcanics may have been deposited in a rift basin (Taheri and Bottrill, 2013). Altered dykes appear to cross-cut the mineralisation and foliation in Savage River magnetite orebodies and may be Late Cambrian (Taheri and Bottrill, 2013).

2.3 Deformational history of the Arthur Lineament

The two main units of rock that dominate the Arthur Lineament, the Bowry Formation and the eastern Ahrberg Group, are more strongly metamorphosed and deformed than units surrounding the Arthur Lineament. This section describes the deformational history of the rocks within the Arthur Lineament. Table 2.1 summarises the results and conclusions of some important studies undertaken in the area.

Author(s)	Proposal
Spry (1957)	• Defined the Whyte Schist unit in the south of the area, from Corinna to Savage River.
Gee (1967)	• Defined the Keith Metamorphics separating the Rocky Cape Group and the Burnie Formation. • Attributed major deformation to the Precambrian Penguin Orogeny. • Suggested a correlation between the Whyte Schist in the south and the Keith Metamorphics in the north of the area, based on aeromagnetic imagery interpretation. • Proposed the name 'Arthur Lineament', for the narrow NE-trending belt of high strain metamorphic rocks.
Spiller (1974)	• Established that the metamorphic grade of exposed basement rocks in the Arthur Lineament ranged from upper greenschist to amphibolite facies.
Turner (1989)	• Lithological boundaries are sub-vertical to sub-parallel to the cleavage, suggesting tight to isoclinal folding. • Metamorphism was associated with first and second deformational phases. • The increase in strain in the Oonah Formation towards the west across the eastern boundary of the Arthur Lineament is gradational.
Turner et al., (1991)	• Defined the eastern and western sequences of the Whyte Schist in the southern part of the Arthur Lineament.
Holm (2002)	• Recognised three deformation events during the Cambrian (*CaD1*, *CaD2* and *CaD3*) and three in the Devonian (*DeD1*, *DeD4* and *DeD5*).
Holm and Berry (2002)	• *CaD1* produced a schistose axial-planar fabric and isoclinal folds synchronous with thrusting. • *CaD2* produced a coarser schistosity and tight to isoclinal folds. • *CaD3* folded the earlier foliations and produced west-dipping steep thrusts, creating the linear expression of the structure.

Table 2.1. Summary of significant studies on the geology and deformational history of the Arthur Lineament. Modified after Morris, 2012.

The most recent and comprehensive study of the structure of the Arthur Lineament was carried out by Holm (2002) and Holm and Berry (2002). Therefore the following sections rely heavily on this work. The nomenclature used is taken from Holm (2002) and relates to Cambrian (*CaD1*, *CaD2* and *CaD3*) and Devonian (*DeD1*, *DeD4* and *DeD5*) deformation. Table 2.2 summarises the characteristics of the deformational events.

2.3.1 Deformation CaD1

This is a well developed event, observed throughout the lineament. It is commonly overprinted by *CaD2*. *CaD1* produced mesoscopic to macroscopic, gently inclined to recumbent, isoclinal folds (*CaF1*). These folds were not observed in the low strain domains. They are interpreted to be widely developed in areas of high strain, in zones of weak *CaD2*. *CaD1* has produced a finely spaced to schistose, bedding-parallel axial planar foliation (*CaS1*) that varies in pervasiveness. In low *CaD1* strain zones to the east of the lineament, *CaS1* is finely spaced to phyllitic. In the low strain zone which is 3-7 km east of the lineament, the *CaS1* foliation dips steeply to the north west whereas S1/S0 intersection lineations plunge moderately to steeply to the north east. In the higher strain zones, 0-3 km east of the lineament, the *CaS1* foliation dips moderately to the north east whereas intersection lineations plunge gently to moderately to the north east.

2.3.2 Deformation CaD2

CaD1 and *CaD2* strain levels are high throughout the Arthur Lineament although locally the intensity varies. According to Holm (2002) the *CaD2* event is the dominant deformational episode within the Arthur Lineament. *CaD2* decreases in intensity gradually to the east of the lineament. *CaD2* produced recumbent, tight to isoclinal folds (*CaF2*) of varying scales. The mesoscopic folds were predominantly asymmetrical folds with attenuated long limbs. In the south, 3-7 km from the lineament the *CaF2* folds plunge moderately to the northeast and

CaS2 dips moderately to steeply to the east. Nearer to the lineament (1-3 km to the east of the lineament), *CaS2* is a smooth 2-3 mm spaced, parallel, phyllitic cleavage. Regionally, in the moderate to high strain areas, *CaS2* is the dominant foliation in both pelitic and psammitic layering. At the lineament's western boundary, there is a sharp decrease in intensity of *CaD2*, *CaS2* is less well developed, and the *CaF2* folds are less tight.

2.3.3 Deformation CaD3

The *CaD3* deformational event is not as strongly developed and *CaS3* is not as pervasive as *CaS1* and *CaS2*. This deformation featured east-west compression and is most prominent to the west of the lineament, within the western Ahrberg Group and the Rocky Cape Group. In the south of Holms' 2002 study, near Corinna, the structural overprint of the *CaD3* event is represented by gently south plunging; open to close *CaF3* folds, with gently dipping western limbs and steeply dipping to overturned eastern limbs. West dipping syn-*CaD3* thrusts were mapped by Holm in the Rocky Cape Group.

2.3.4 Devonian Deformation

Devonian age deformation, attributed to the Tabberabberan Orogeny, is widespread throughout western Tasmania and is interpreted to predate the widespread 350-374 Ma granitoid intrusion (Williams et al., 1989 and Black et al., 2004). Williams et al (1989) indicated the presence of two deformational events in the Savage River area that overprint the Cambrian deformation. Holms (2002) referred to the first event as DeD4 and the second as DeD5. In the south of the Holms' study area (near to Savage River); both DeD4 and DeD5 produced gently plunging meso- to macroscopic upright open folds (DeF4 and DeF5). The DeS4 is a smooth, 5-10 mm spaced parallel crenulation cleavage locally developed in DeF4 fold hinges. The DeS5 is a very weak, smooth, <10 mm spaced, parallel crenulation cleavage that is also locally developed (Holm, 2002). The trends of DeF4 (east-west) and DeF5 (ESE -

WNW) folds produced small scale dome and basin style fold interference patterns.

Period	Structure (S)	Folds (F)	Alteration? Comments
CaD1	Syn-*CaD1* Thrust Faults. Finely spaced to schistose axial planar foliation. *CaS1* – parallel quartz segregations common in high strain zones.	Macroscopic isoclinal folds – gently inclined to recumbent. Strongly attenuated limbs, associated with related shear zones.	Chlorite alteration in gabbro/dolerite. Formation of magnesite and serpentinite? Albitic alteration? *CaD1* commonly overprinted by *CaD2*.
***Ca*D2**	*CaD2* structures are pervasive throughout the Arthur Lineament and to the east. The *CaS2* foliation is a coarser schistosity that is the dominant foliation in both pelitic & psammitic layering throughout the region. Boudinage of *CaS1* quartz segregations.	Limbs of *CaF1* folds and syn-*CaD1* thrust faults are tight to isoclinally folded by *CaF2*.	Albitic alteration – preceded or accompanied *CaS2*. In areas where *CaS2* is strongly developed, *CaF1* and *CaS1* are overprinted and difficult to identify.
CaD3	Deformational event not as strongly developed. *CaD3* not as pervasive as *CaD1* and *CaD2*. Variably developed, upright to west-dipping, north-northeast striking cleavage, associated with *CaF3* is a smooth, 2–5 mm spaced, parallel cleavages with discrete transitions between cleavage domains & microlithons.	Gently south-plunging, open to close *CaF3* folds. *CaD3* featured east–west compression & produced west-dipping steep thrusts. Boudinage of competent beds. Competent beds are commonly boudinaged on the limbs of *CaF3* folds.	*CaD3* created the present linear expression of the Arthur Lineament.
DeD1	Several episodes of minor deformation are recognised in the Middle Devonian (*DeD1*, *DeD4* and *DeD5*). The interference of the north–south-trending *CaF3* and the east–west-trending *DeF1* results in localised dome-and-basin style folding (5–15m wavelength) and additional variability in the trend of the Arthur Lineament.	Sub-horizontal to gently plunging upright open folds that have produced a poorly developed axial-planar cleavage.	Devonian deformation was observed in region but is patchy in development.
DeD4	*DeD4* related faulting is brittle in style and occurs in localized zones of intense deformation.	Folds are minor, weakly developed, mesoscopic scale (1 metre wavelength) folds and rarely produce an axial planar fabric. Folds are open, mostly plunge to the east.	Open *DeF5* folds overprint *DeF4* and produce dome-and-basin interference patterns.
DeD5	The *DeS5* is a locally developed, very weak, smooth, 5–10 mm spaced, parallel crenulation cleavage. Minor examples of *DeS5*-parallel extensional quartz veins in *DeF5* fold hinge zones.	Minor *DeS5*-parallel extensional quartz veins, occur in the hinge zones of the *DeF5* folds.	Post-schistosity siderite + quartz + pyrite alteration. Carbonate veining/brecciation & alteration overprints the *CaS2* cleavage and intrafolial *CaF2*.

Table 2.2. Summary of the Cambrian and Devonian deformation events in the Savage River area outlined by Holm (2002).

2.3.5 Savage River Mine deformational history

Webster (2009) suggests that a clear succession of structural events can be recognised in the rocks of the Savage River Mine and Oonah Formation lying immediately adjacent to it. Webster (2009) describes the following sequence;

- Very early quartz segregations form (parallel to a foliation). Early isoclinal folds.
- Isoclinal folding and transposition at all scales, development of pervasive, near-vertical axial planar schistosity and establishment of the predominant 'grain' of the mine rocks. Destruction of most protolith features of the Main Host Assemblage and formation of schists in high strain Oonah Formation. Refolding, boudinaged and differentiation of very early quartz segregations in association with major cleavage development.
- Major faulting events (bounding faults of the Main Host Assemblage) with dissection of mine sequence; and minor folding.
- Macroscopic warping (refolding) of the dominant fabric of the mine area within broad, northwest trending belts leaving large parts of the deposit unaffected; reactivation of earlier faults; thrusting with minor displacements and associated minor drag folding; minor and widely-spaced zones of mesoscopic folding (crenulations); flat quartz vein development.

Webster (2009) suggests that although the full sequence of structural events defined by Holm and Berry (2002) elsewhere in the Arthur Lineament has not been defined on the Savage River Mine, the effects of most of the key deformations can be recognised. He indicates that the structural history is preserved within the Main Host Assemblage in the mine and within the rocks of the Oonah Formation metasediments. He argues that whereas the intense strain has destroyed most of the evidence of earlier deformations and protoliths in the Main Host Assemblage, the highly strained parts of the Oonah Formation have preserved that evidence

and provide the key to understanding the entire structural history of the mine.

2.4 Metamorphism

Since the 1960's, ideas on the metamorphic history of the rocks within the Arthur Lineament have changed considerably. Gee (1967) interpreted the pelitic schists and amphibolites that separate the Burnie Formation and the Rocky Cape Group to have been metamorphosed to low-mid greenschist facies. However, Green and Spiller (1977) placed maximum P-T conditions for magnetite rich rocks of the Savage River Mine between greenschist and glaucophane-lawsonite schist facies. Blue amphiboles were analysed from a number of areas within the Arthur Lineament (Turner and Bottrill, 2001) and a spread of compositions from sodic-calcic (winchite) to sodic (glaucophane) amphiboles were found. Turner and Bottrill (2001) suggested that the amphiboles are a product of prograde metamorphism at a maximum P-T of 700 MPa and 350°C. Holm (2002) recognised three main metamorphic events affecting the rocks of the Arthur Lineament. The first coincided with CaD1 although this has been extensively overprinted by two phases of metamorphism coinciding with CaD2. The earlier event described by Holm (2002) is a high pressure (>700 MPa or >25 km depth) low temperature event that produced high pressure amphiboles of blueschist facies. Turner (2005), states that the glaucophane series indicates that the rocks experienced a depth of burial of the order of 20 km. He argues that the low temperature greenschist assemblage is a retrogressive phase formed during uplift and accompanying deformation.

More recent work of Taheri and Bottrill (2013) argued that during the Early Cambrian, the Bowry Formation was subjected to subduction to about 20 km, with relatively high pressures locally forming blueschist facies although this is not seen within the magnetite ore at Savage River. During the rapid, extrusive emplacement of the Bowry Formation, later in the Early Cambrian, these high grade rocks experienced lower grades of metamorphism (greenschist facies), replacing most of the early formed skarn silicates and blueschist facies assemblages with assemblages of serpentine ± talc ± chlorite ± tremolite assemblages). Strong folding,

faulting, shearing, boudinaging and brecciation of magnetite layers and surrounding lithologies (as part of Bowry Formation) during and particularly after the emplacement, caused the current configuration of the near vertical magnetite ore lenses (Taheri and Bottrill, 2013).

2.5 Conclusions

The geological and deformational history of NW Tasmania can be summarised as follows; the early to middle Neoproterozoic of NW Tasmania was dominated by shallow water siliciclastics and siltstone – Rocky Cape Group and correlates in the west and turbidites (Burnie and Oonah Formations) in the east. An extensional phase in the Late Neoproterozoic ca. 550-650 Ma (Adams et al., 1985; Calver and Walter, 2000) produced the Rocky Cape dolerite dyke swarm, the extrusion of basalts and the deposition of associated volcanogenic sediments, carbonates and shallow marine siliciclastics (Ahrberg Group). An arc-continent collision in the Early to Middle Cambrian initiated the Tyennan Orogeny (510 ± 10 Ma) (Berry and Crawford, 1988; Crawford and Berry, 1992; Turner et al., 1998). This resulted in the emplacement of allochthons including the Bowry Formation. Movement indicators from the allochthonous mafic-ultramafic complexes indicate west-directed obduction. This supports the interpretation by Berry and Crawford (1988) of an east-dipping subduction zone. The Arthur Lineament was formed during the early stages of the Tyennan Orogeny. The subsequent deformation in the Middle Devonian as part of the Tabberabberan Orogeny (370 Ma) resulted in further faulting and dome-and-basin style folding. This Devonian deformation was closely followed by granitoid intrusion (332-367 Ma).

No geotechnical based studies have been carried out on the rocks specifically within the Arthur Lineament. Geotechnical reports have been completed for a variety of other mines near to the Arthur Lineament but the majority of these reports are closed file and could not be obtained for this research.

CHAPTER 3
BRITTLE DEFORMATION AND GEOTECHNICAL PROPERTIES

3.1 Introduction

This chapter describes the geotechnical and failure style of the three packages of rock of North Pit in Savage River Mine. The joint, vein and foliation styles of the East Wall Assemblage, Main Host Assemblage and West Wall Assemblage are discussed respectively. Structural and geological drill core logging and in-pit mapping techniques have provided the data used in this chapter. The geotechnical data used for the analysis of all assemblages were retrieved from the 2005-2007 resource drilling programmes, the 2008 geotechnical drilling programme and the 2009-2010 resource drilling programme. Photogrammetry and mapping data were also used. The 2009-2010 geological and structural data were logged by the author for this PhD. Although the other boreholes were reviewed and validated, the data was obtained by Grange Resources in-house Geologists and Geotechnical Engineers at the time of the drilling programmes. All orientation measurements, unless specified, are shown in dip/dip direction format.

3.2 Geotechnical drill core logging parameters

In order to obtain the maximum amount of useful data from each structural defect evident in the drill core, certain parameters were recorded. As well as the standard alpha and beta measurements in oriented core, measured parameters included; type of defect, infill thickness and material, surface roughness and decoration of the defect and rock strength. Geological Strength Index (GSI) was recorded for domaining the drillcore. This method however will be discussed in Chapter 4, Section 4.4.2. Vein thickness and the intensity of foliation were also recorded. Weak, moderate and strong foliations are indicated using the codes FO1, FO2 and

FO3 respectively.

3.2.1 Defect infilling and thickness

The nature of the infilling has a very significant impact on the strength of structural defects. Slope stability analysis and design relies heavily on the appropriate strength parameters allocated to defects from identified infillings. The thickness and the mechanical properties of the infilling material directly affect the shear strength of the defect. Discontinuities may contain infilling materials such as gouge in faults, silt in bedding planes, low-friction materials such as chlorite, graphite and serpentine in joints and stronger materials such as quartz or calcite in veins or healed joints. The presence of gouge or clay seams can decrease both stiffness and shear strength. Low-friction materials such as chlorite, graphite and serpentine can markedly decrease friction angles, while vein materials such as quartz can serve to increase shear strengths (Brady and Brown, 2004). Therefore, infill material and thickness were recorded in an attempt to highlight areas of increased and decreased shear strength.

3.2.2 Surface Roughness

The effect of surface roughness of a structural defect greatly affects the friction angle (the maximum angle before which one of the items will begin sliding). Rough, clean defects will increase the friction angle and smooth, clean defects will decrease the friction angle. Patton (1966) carried out a study demonstrating that the rougher the bedding plane traces in unstable limestone slopes, the steeper the slope. Therefore, surface roughness was recorded in an attempt to estimate friction angles. The ISRM (International Society for Rock Mechanics, 2007) suggested characterisation of defect roughness was used in this study (Figure 3.1).

3.2.3 Surface Decoration

Defect decoration was also recorded along with infilling and roughness. Decoration may include striations such as slickensides, slickenlines or slickenfibres. The shear strength of the defect will be affected by the direction of sliding, where the shear strength is much greater across the corrugations than along them (Karzulovic and Read, 2009). Therefore, defect decoration was recorded to assist with slope stability analysis.

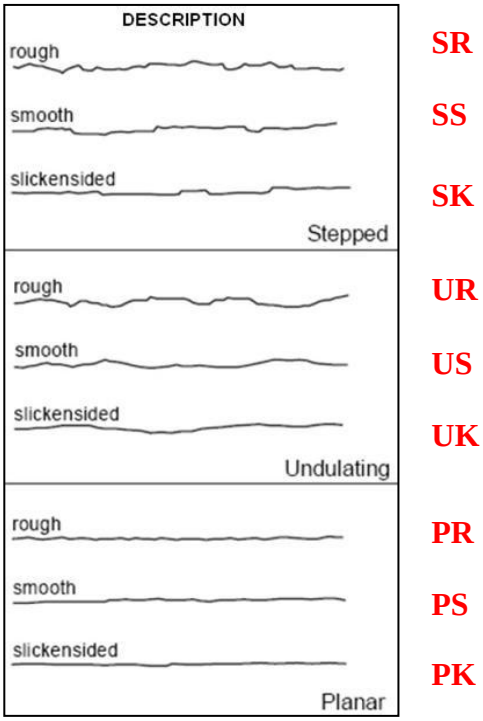

Figure 3.1 ISRM suggested characterisation of defect roughness. The red letters are abbreviated codes following Savage River Mine nomenclature.

3.2.4 Rock Strength

Field estimates of Uniaxial Compressive Strength (UCS) of drill core from the Savage River Mine were recorded. Brown (1981) produced a grading system whereby an estimate of UCS (MPa) and point load index (MPa) can be allocated to rock types using field estimates of strength (Table 3.1). From using this technique, strength estimates can be produced cheaply and quickly prior to laboratory testing.

Point load testing was performed generally every five metres down a drillhole. The point load strength index is an indirect estimate of the UCS of an intact rock. It was used in conjunction with the relatively subjective field estimates of strength. Although useful for hard rock, point load tests on rocks with a UCS below 25 MPa are likely to yield ambiguous results. Both these methods produce an intact rock strength result which is a very important parameter in slope stability analysis.

Grade*	Term	Uniaxial Comp. Strength (MPa)	Point Load Index (MPa)	Field estimate of strength	Examples
R6	Extremely Strong	> 250	>10	Specimen can only be chipped with a geological hammer	Fresh basalt, chert, diabase, gneiss, granite, quartzite
R5	Very strong	100 - 250	4 - 10	Specimen requires many blows of a geological hammer to fracture it	Amphibolite, sandstone, basalt, gabbro, gneiss, granodiorite, peridotite , rhyolite, tuff
R4	Strong	50 - 100	2 - 4	Specimen requires more than one blow of a geological hammer to fracture it	Limestone, marble, sandstone, schist
R3	Medium strong	25 - 50	1 - 2	Cannot be scraped or peeled with a pocket knife, specimen can be fractured with a single blow from a geological hammer	Concrete, phyllite, schist, siltstone
R2	Weak	5 - 25	**	Can be peeled with a pocket knife with difficulty, shallow indentation made by firm blow with point of a geological hammer	Chalk, claystone, potash, marl, siltstone, shale, rocksalt,
R1	Very weak	1 - 5	**	Crumbles under firm blows with point of a geological hammer, can be peeled by a pocket knife	Highly weathered or altered rock, shale
R0	Extremely Weak	0.25 - 1	**	Indented by thumbnail	Stiff fault gouge

Table 3.1 Field estimates of UCS of intact rock (Marinos and Hoek, 2000). * Grade according to Brown (1981).

3.2.5 Criteria and Terminology of geotechnical features

Discontinuities within rock assemblages generally control the mechanical behaviour of rock masses. Within North Pit, each assemblage contains discontinuities that form planes of weakness or surfaces of separation including joints, foliation, fractured veins and zones of shearing. These features generally control the strength, deformation and permeability of the rock mass. Within North Pit, most engineering problems relate to the type, orientation and persistence of discontinuities rather than to lithology and intact rock strength hence the adequate description of discontinuities is paramount. This section outlines the criteria employed during geotechnical logging to distinguish between the different types of discontinuity. The criterion is site specific and in places purely arbitrary.

Relatively planar fractures within the drillcore were logged as joints. Where a joint infill mineral is present, striations and/or polishing on the joint surface are evidence of movement along the joint. The gamma angle (γ) (Holcombe 2012) was added to the database for the purpose of this research, in order to record the orientation of striations within a plane. A fracture containing a mineral infill that is different to the minerals within the host rock is termed a joint. For example, fractures with a striated, polished hematite infill within mafic schist were classified as a hematite coated joint.

Veins (as classified in this project) are generally not as planar as joints and are mostly unbroken. Broken veins however are distinguished from infilled joints by the lack of striations on the fracture surface, the degree of planarity and the thickness. Thicker infills were taken as evidence for broken veins. If the fracture surface was fresh, it was taken as evidence that the break was of a mechanical nature. Also, discontinuities within rock core that are oriented similarly are joints of the same set. Veins are not necessarily consistently similar in orientation to other nearby veins with the same infill. This aids the logger when deciding on whether to classify a discontinuity as a joint or a broken vein. Although logged as a vein, a

comment is made that the feature is in fact broken and will act as a discontinuity.

The logger employed at the drill rig marks all natural joints and veins on the core. Fractures that have been broken in the transporting of the core at any stage through the process are also marked. This ensures that when the core is geotechnically logged, the logger can decide which fractures are related to the drilling process and which are natural. This technique is time efficient and the most reliable way of ensuring accurate geotechnical logging if the drill core is not logged at the drill rig. Although this technique is effective, each marked discontinuity including mechanical fractures have to be inspected. Mechanical fractures are distinguished from natural fractures by the fresh appearance of the fracture surface. They are usually very rough in appearance, with no infill or striations. Joints with no infill are distinguished from mechanical fractures by the very thin coating of silt they usually present. The surfaces are also slightly weathered ensuring a slight colour change in comparison to the host rock. For example, a joint with no infill within mafic schist presents a slightly brown/orange joint surface. A mechanical break within the same lithology will be a grey/green fresh surface.

Foliation is a penetrative planar fabric present in all assemblages in North Pit. The foliation is mostly defined by chlorite. Foliation intensity is variable throughout the assemblages and the intensity is mainly controlled by the lithology. Within areas of intense foliation, the planes are very weak causing breaks on foliation planes or 'foliation breaks'. Within less foliated areas, the cleavage is stronger and only banding or striping on the core is visible. The geotechnical properties of different intensities of foliation are recorded and a comment is made if the foliation is broken. Currently, the logging database at the mine accounts for foliation breaks within the logging dictionary (*FB* – foliation break). However at the time of this research, this option was unavailable so comments were made whenever a foliation break was encountered. Due to the weakness of some cleavage, it is impossible to deduce whether the feature is

broken in-situ or whether drilling methods and transportation has broken the planes. For ease within this research, foliation breaks were not differentiated from other recorded foliations. Only the intensity of foliation was reported.

Distinguishing between foliation breaks and joints with a chlorite infill was subjective. Chlorite filled joints tend to show signs of slight movement, presenting with irregular small areas of striations and/or polishing on the joint surface. Foliation breaks however, also have a polished appearance. The orientation of cleavage is also uniform in most lithologies so discontinuities cross-cutting the foliation or with a differing orientation were highlighted easily by the logger. Whilst care was exercised in the identification of discontinuities, the logging system employed is subjective; meaning a certain amount of misclassification remains within the data set. This error can be partly identified from the stereographic projections of each joint type. A large number of discontinuities termed joints are the same orientation as the local foliation. Some of these could be correct and there is a joint set orientated parallel to foliation, but it is also possible that a proportion of these joints are misclassified foliation breaks.

A shear zone or fault zone was recorded where gouge, breccia and very fractured or crushed rock was found. Core loss and a lack of oriented core within these areas are also indicative of shear or fault zones. The presence of graphitic and/or dolomitic lithologies within the core from North Pit also highlights major fault zones. Currently, the logging database at the mine accounts for fault zones and shears within the logging dictionary (*X* – Fault). However at the time of this research, this option was unavailable so comments were made whenever a fault or shear zone was encountered. No attempt was made in the geotechnical database to differentiate regional cleavage from mylonitic foliation.

3.3 Structural Style – East Wall carbonate-mafic Assemblage

3.3.1 Introduction

During the period of this research, there have been several rock failures at Savage River Mine. The majority of these failures have developed from the E Wall of North Pit, mainly due to unfavourably oriented joints as well as the pit design and specifically the slope angle of the E Wall. The next section characterises the geotechnical and failure style of this package of rock.

3.3.2 Joint Characteristics

Turner (2006) describes the carbonate-mafic assemblage of the E Wall exhibiting 'strong mineral alignment although the principal parting surfaces are sub planar joints'. Although the assemblage is a strong, competent rock mass, the defining feature of this rock mass is the large number of joints it contains. The uniaxial compressive strength of the rock mass was recorded at 125 MPa (Hutchison et al., 2000). The joints within this assemblage can exhibit extremely close (<10 mm) spacing as well as moderate (>500 mm) spacing (Bieniawski, 1979). Most joints are non-persistent terminating usually when a joint with a different orientation intercepts it. However, some joint surfaces are persistent and can be traced along the entire length of the E Wall.

Approximately 36% of all joints were recorded to contain a mineral infilling or coating on the joint plane. The main infill minerals are calcite and hematite but others include chlorite and pyrite. Four thousand joint orientations were recorded. Joint roughness measurements were also taken (refer to section 3.2.2 for explanation).

Of all E Wall joints logged, 20% exhibited a calcite infill. The calcite infilling the joint is of a varying thickness (Figure 3.2). Figure 3.3 shows that there is one main set of calcite coated joints; oriented at approximately 80°/270° but with dip directions varying from 235-285°. There is however another two minor sets; oriented at approximately 10°/090° and 45°/250°.

Although the majority of calcite coated joints are one of these three orientations there are a few joints with highly variable orientations. A manual methodology of defining sets was used.

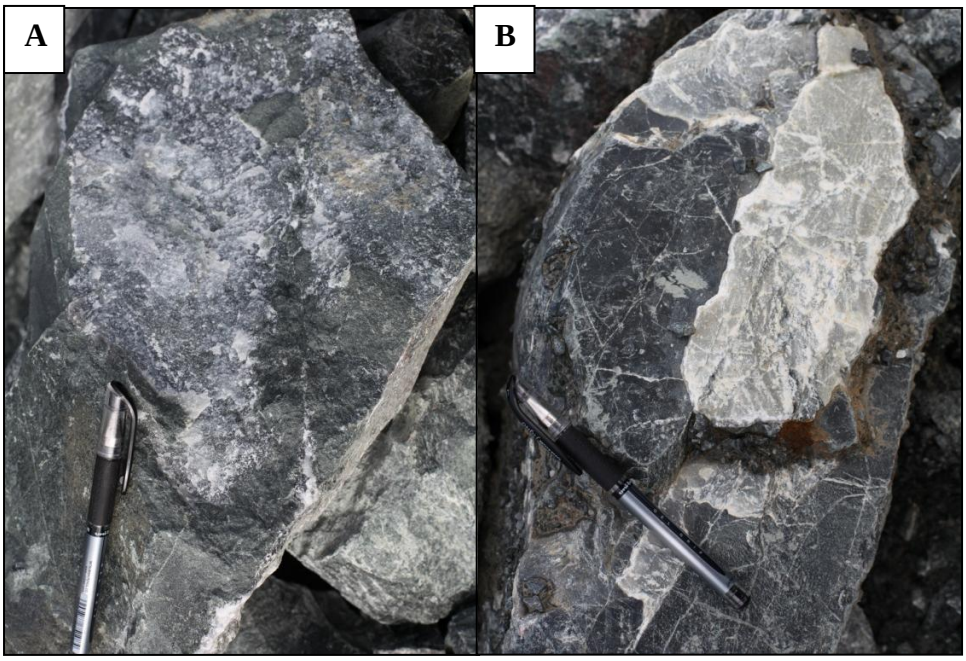

Figure 3.2. Examples of calcite coated joints from the E Wall of North Pit. **A** - Joint with <1 mm calcite coating and **B** - Joint with a thicker calcic infill.

The most common roughness profiles are of all calcite infilled joints are undulating, smooth (40%) and undulating, rough (23%). The rest have a mixture of planar, smooth; stepped, slickensided; undulating, slickensided; stepped, smooth; stepped, rough; planar, rough and planar, slickensided (Figure 3.4).

Barton (1973) and Barton and Choubrey (1977) produced a table showing typical value of the basic friction angle for some rock types. Amphibolite and gneiss/schistose rock types are the most similar to the E Wall carbonate-mafic assemblage of North Pit so these friction angles have been used as a guideline. Dry Amphibolite has a basic friction angle of 32° and gneiss/schistose rock types; 26-29°. The smooth profile of the majority of joints will decrease this figure but in turn the undulating nature will increase the friction angle. The friction angle will increase along the rough, undulating joints.

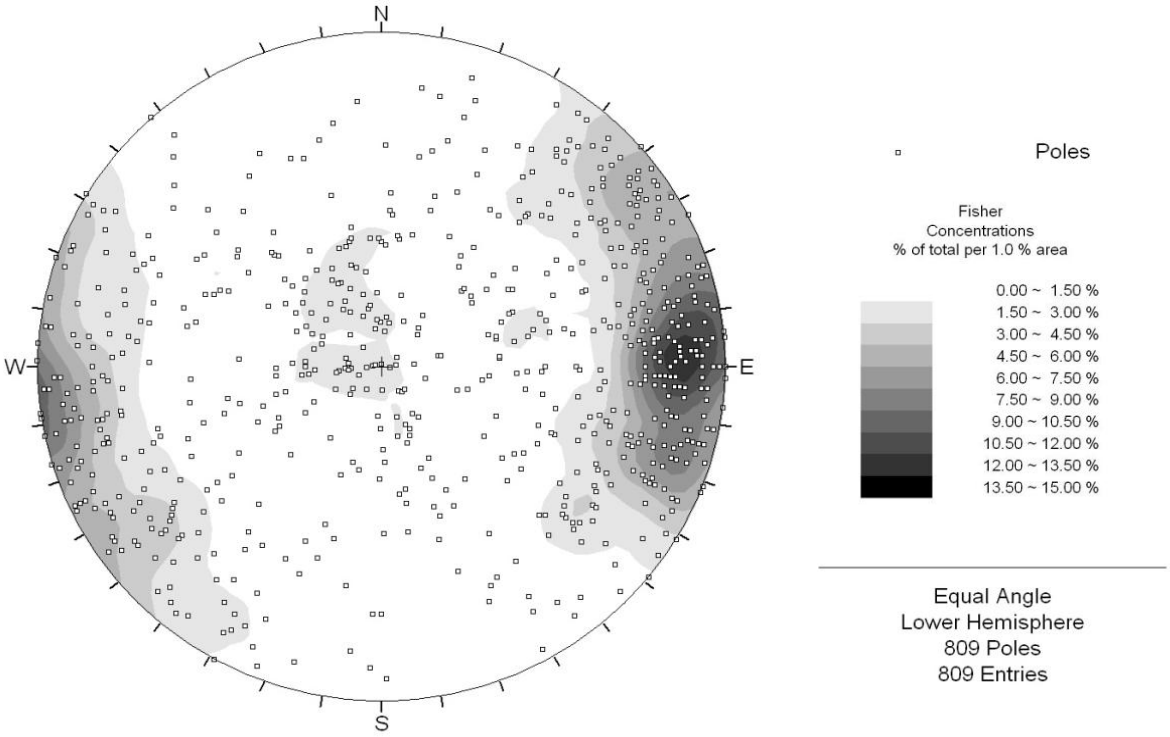

Figure 3.3. Contoured stereographic plot showing poles to 809 calcite coated joints on the E Wall of North Pit.

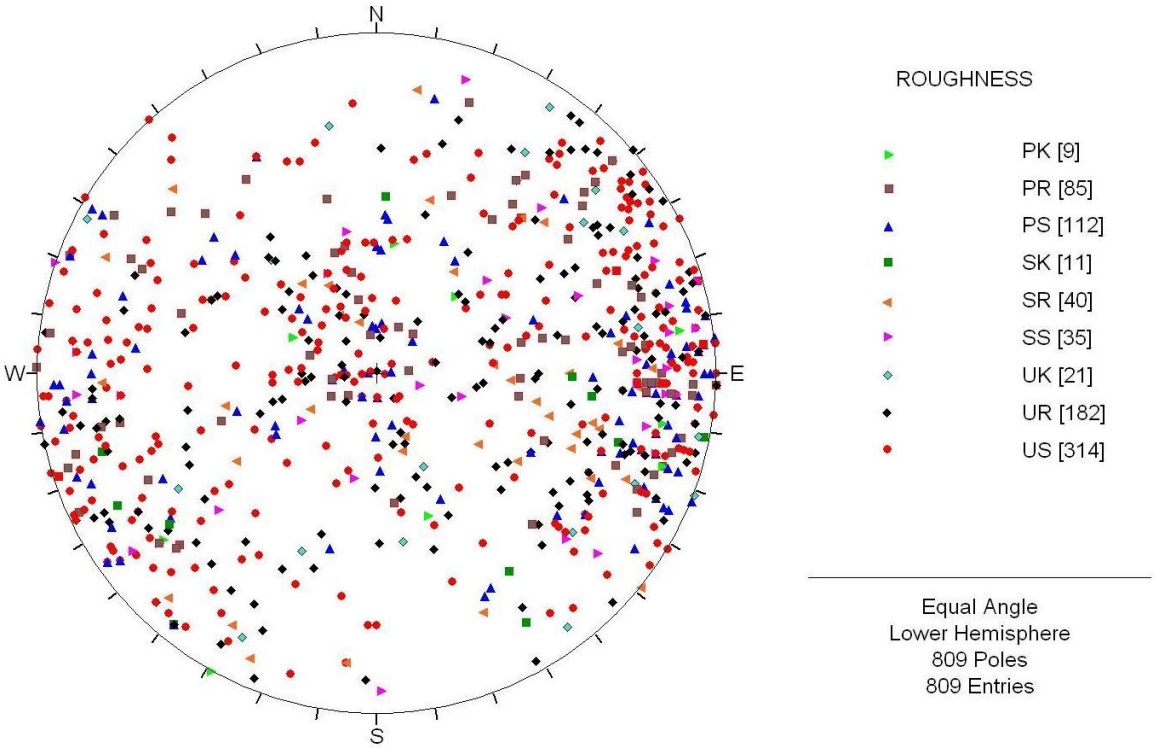

Figure 3.4. Orientation of calcite coated joint classified by roughness profiles for the E Wall.

Of the 36% of joints that contain infill, 5% of these are hematite coated. Within the wide range of orientations, there is a cluster of data at 80°/280° (Figure 3.5). This joint set is of concern in slope stability for the mine as these joints dip towards the pit, threatening berm and crest failure. Further discussion of failure mechanisms will be considered later.

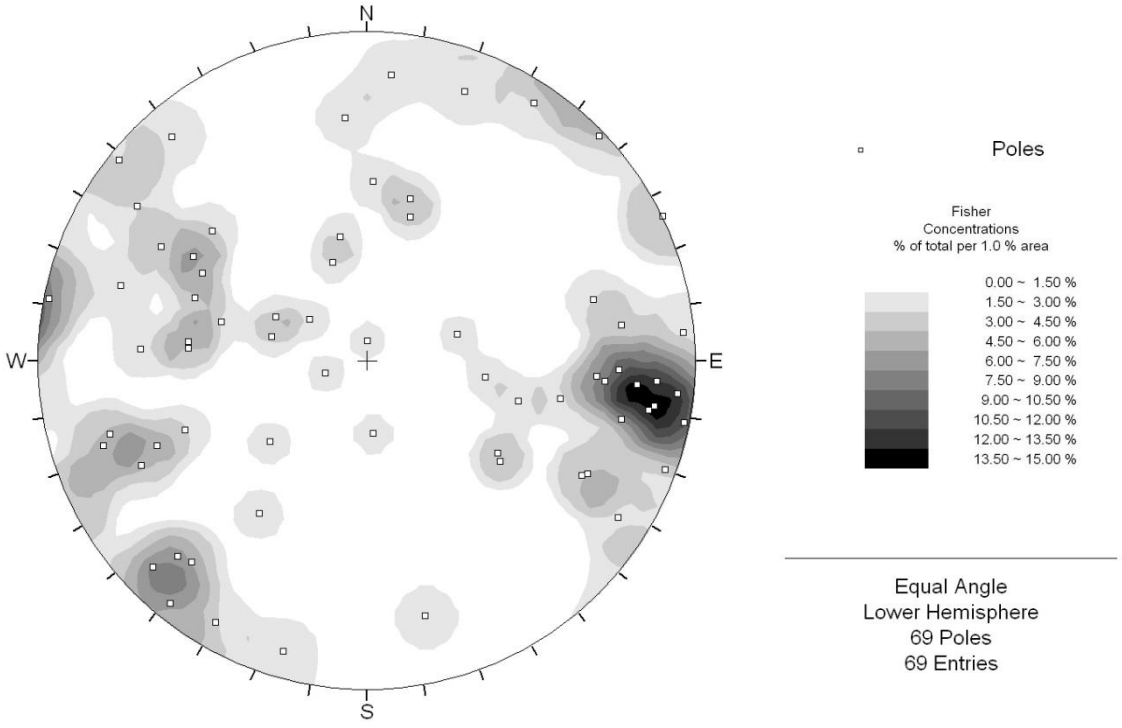

Figure 3.5. Contoured stereographic plot showing orientation of poles to hematite coated joints within the East Wall Assemblage.

The most common roughness profile for hematite coated joints is undulating smooth (36%, Figure 3.6) which is particularly common on the joint set dipping 60°/120°. However, the main set of joints (80°/280°) exhibits a variety of joint roughness profiles including planar smooth, planar rough, undulating slickensided and stepped slickensided. In this joint set, striations and slickenlines decorate the hematite surfaces (Figure 3.7). The surfaces are also highly polished reducing basic friction angles therefore creating a plane of weakness within the rock mass. Oriented unfavourably in regard to the pit wall stability, the joint roughness profile and joint decoration all contribute to these joints being potential release surfaces for rock failure and overall pit wall stability issues.

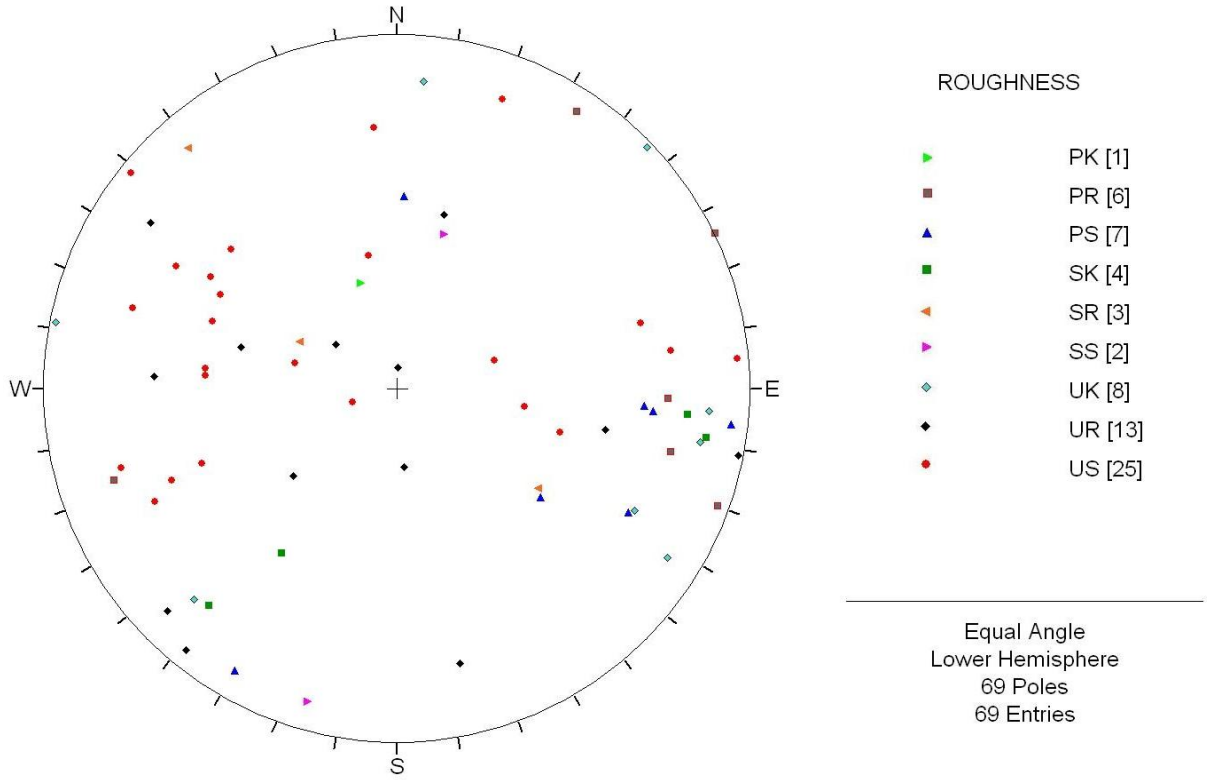

Figure 3.6. Pole plot showing distribution of joint roughness profiles of hematite coated joints of the E Wall.

The E Wall data also includes 2544 joints with no infill, 404 with a chlorite coating, 68 with a carbonate and chlorite coating, 42 with a pyrite coating, 29 with a clay filling, 8 with an epidote infill and 7 with a graphite coating. The dominant orientation of these joints (although the data is scattered) is 85°/265° (Figure 3.8, 3.9).

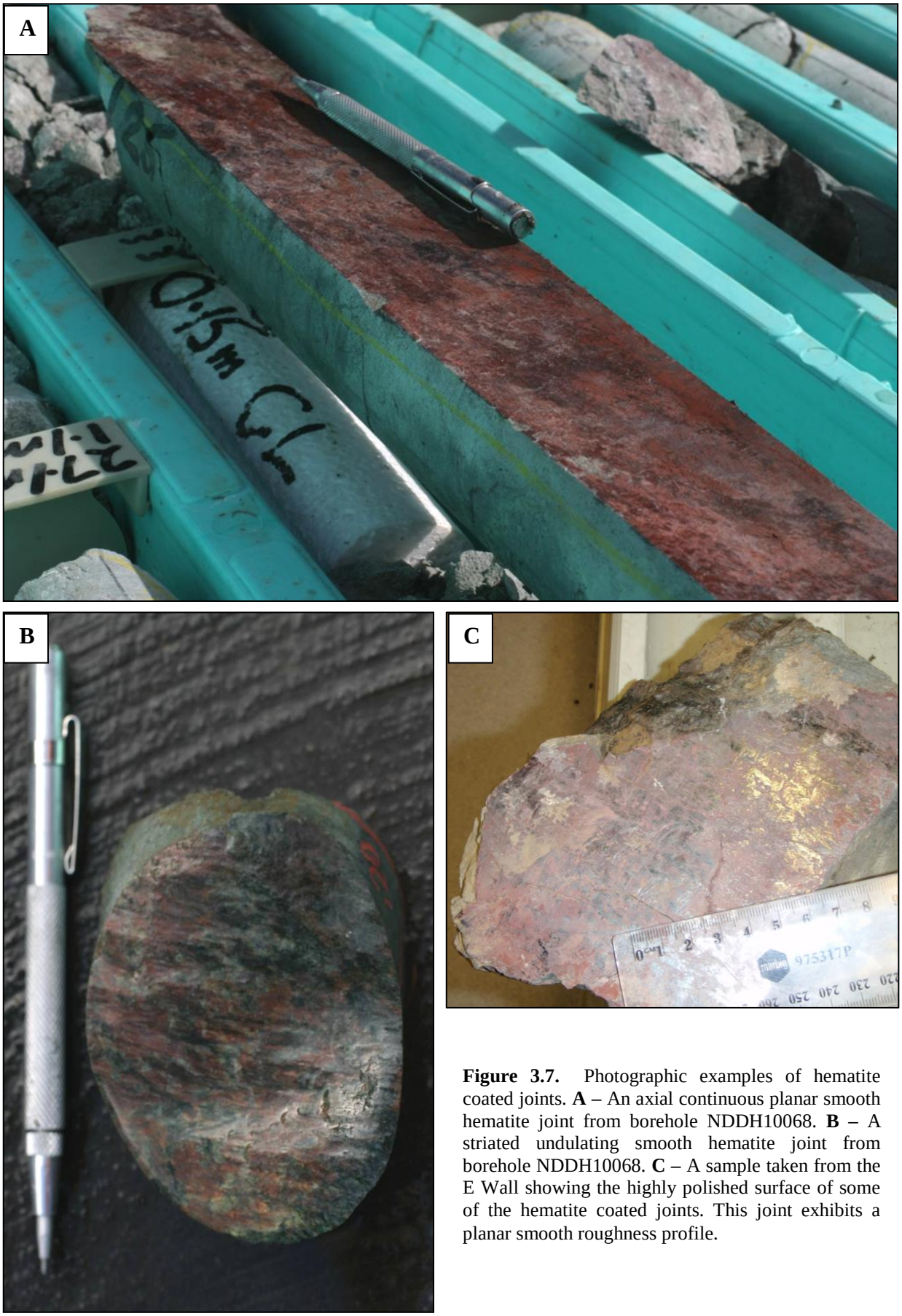

Figure 3.7. Photographic examples of hematite coated joints. **A –** An axial continuous planar smooth hematite joint from borehole NDDH10068. **B –** A striated undulating smooth hematite joint from borehole NDDH10068. **C –** A sample taken from the E Wall showing the highly polished surface of some of the hematite coated joints. This joint exhibits a planar smooth roughness profile.

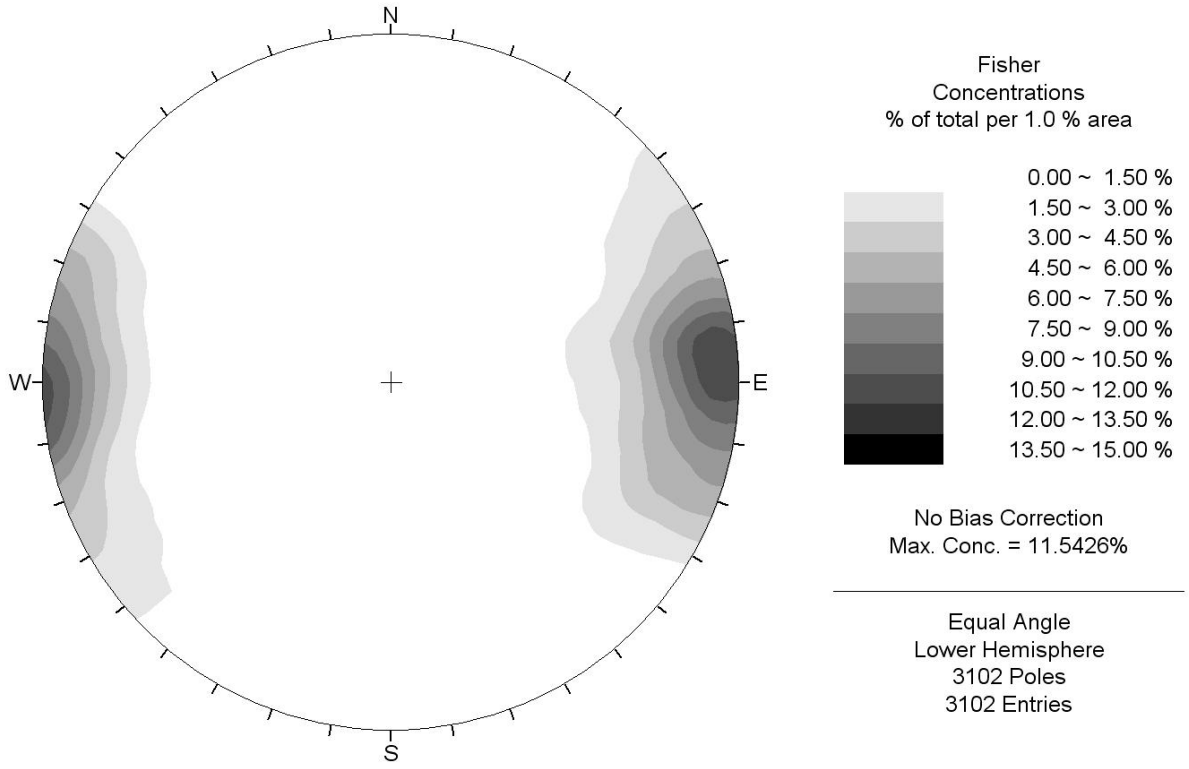

Figure 3.8. Contoured stereographic pole plot showing joints with other types or no infill on the E Wall.

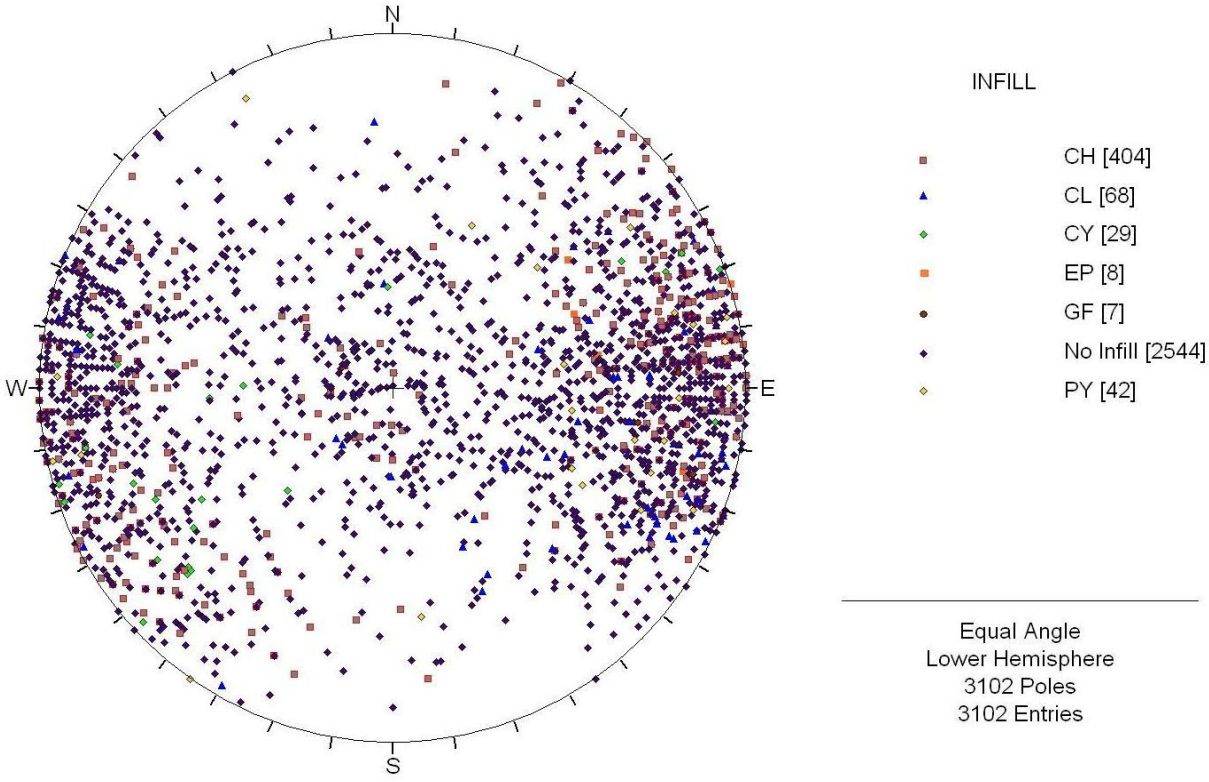

Figure 3.9. Poles to joints with other or no infill, classified by infill type: chlorite (**CH**), chlorite and carbonate (**CL**), clay (**CY**), epidote (**EP**), graphite (**GF**) and pyrite (**PY**).

Approximately 32% of these joints exhibit an undulating smooth roughness profile, 5% are slickensided and the remainder are planar smooth, planar rough, stepped rough, stepped smooth and undulating rough (Figure 3.10).

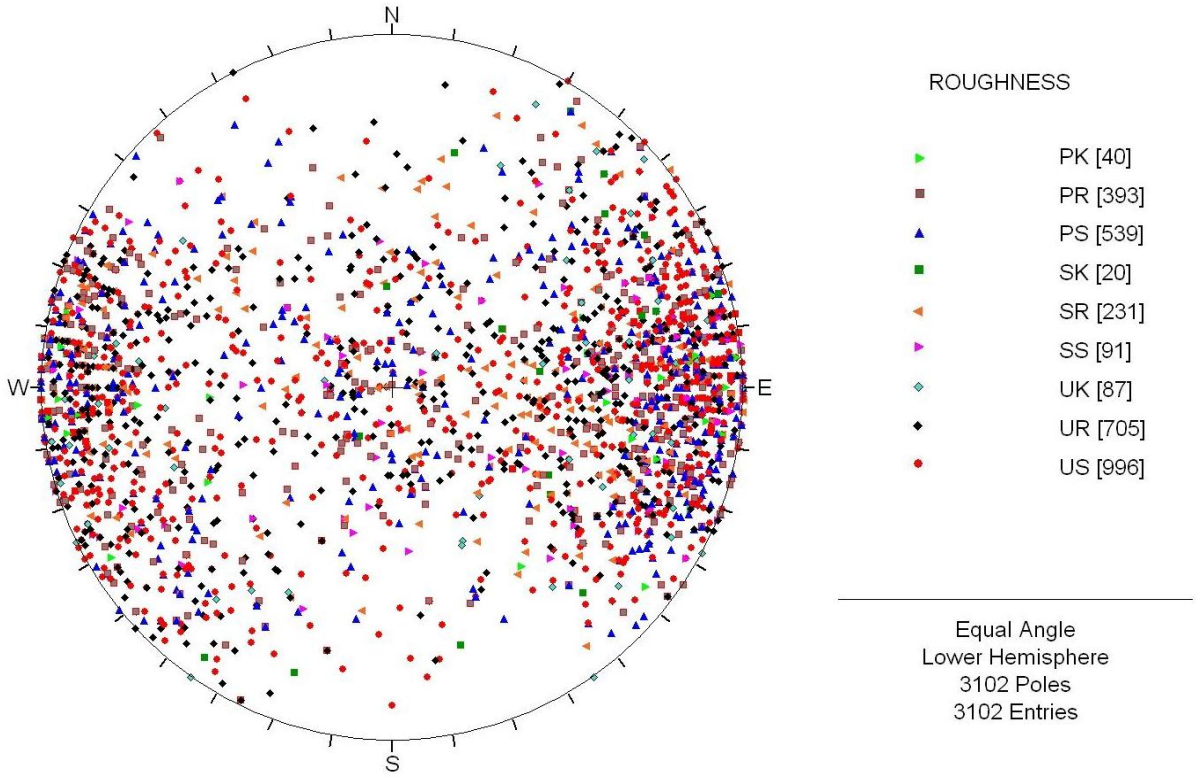

Figure 3.10. Poles to joints by roughness profiles on the E Wall with a variety of infill.

As chlorite is a low friction mineral, the likelihood of instability on one or more of the chlorite coated joints is high. The infill material is softer than the rock mass and the majority of joint roughness profiles are smooth resulting in reduced basic friction angles. A small proportion of joints on the E Wall are infilled with pyrite (Figure 3.11). These joints are steeply dipping mainly to the W, much like the chlorite filled joints (Figure 3.9). The joint roughness profiles are mainly undulating smooth (Figure 3.10). Joints with no infill (Figure 3.11) have a very similar orientation to the dominant foliation. The foliation is weak in some areas and many rocks break readily on the foliation. Many of the joints with no infill could be foliation planes within the rock mass and may not signify a separate joint set sub-parallel to foliation. The roughness profiles for joints with no infill are mainly undulating smooth, undulating rough and planar smooth (Figure 3.10).

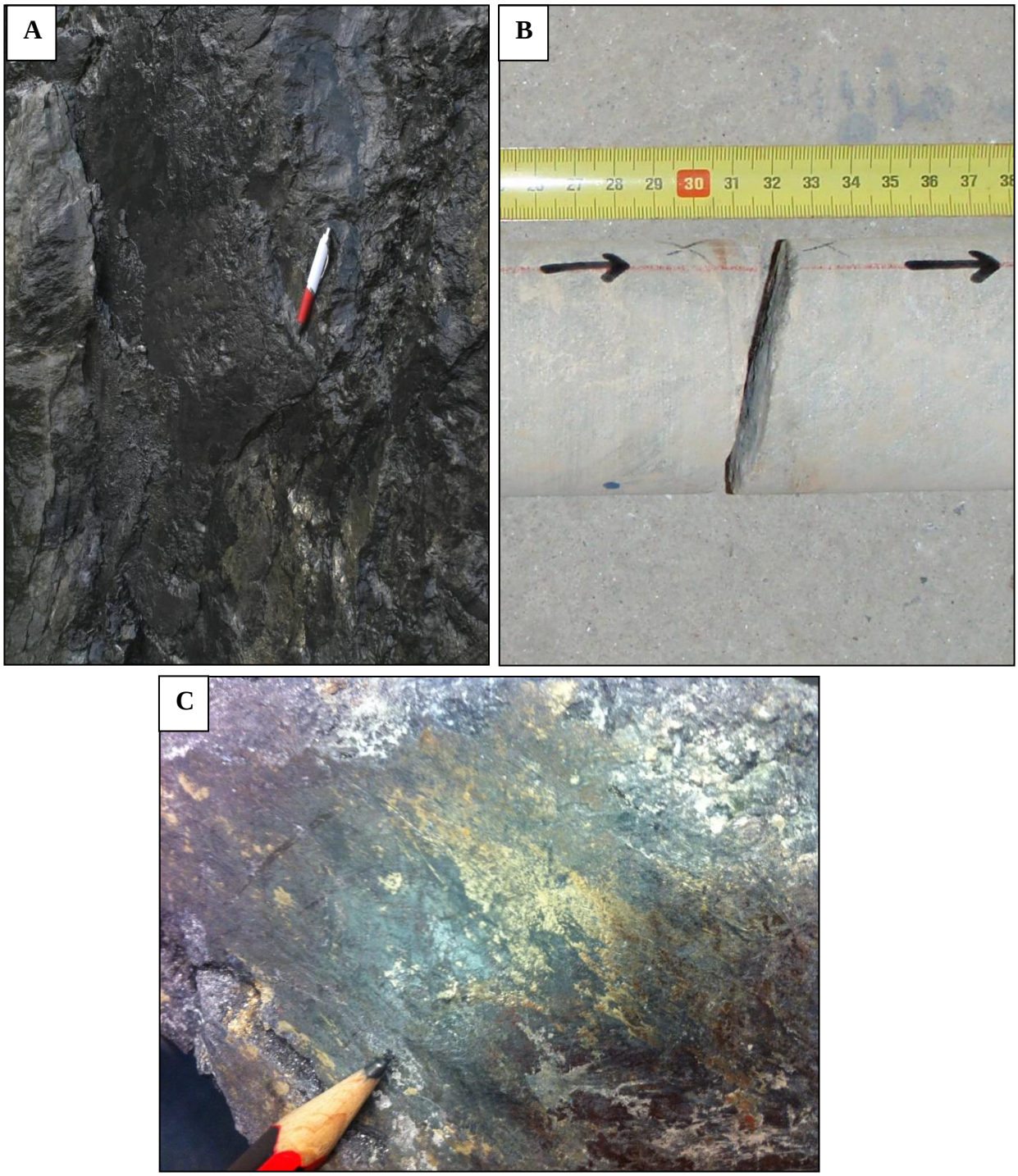

Figure 3.11. Examples of infilling on the E Wall. **A** – Graphitic joint surface. Associated with pyrite. Pen is approximately 12 cm. **B** – A joint with no infill in NDDH08029, arrows denote direction down-hole. Scale in cms. **C** – A pyritic coated joint.

To verify joint infill composition, several samples from the E Wall were analysed by XRD. The samples were all prepared, examined and analysed in the Mineral Resources Tasmania laboratories, Rosny. They were run on an automated Phillips X-Ray diffractometer system: PW 1729 generator, PW 1050 goniometer and PW 1710 microprocessor with nickel-filtered

copper radiation at 40kV/30mA, a graphite monochromator (PW1752), sample spinner and a proportional detector (sealed gas filled PW1711). Sample numbers for the analysis were; 176662, 176663, 176664 and 176665. Each sample was from the surface of joints and the mineralogical analysis was carried out on the infill of each joint (see Appendix 9 - digital). The samples were from Stage 1 and 2 of North Pit. The results confirmed predictions that infill includes calcite, hematite, pyrite and chlorite. Some quartz, plagioclase, mica, tourmaline, rutile, amphibole and K-feldspar were also present within the joint fill.

The E Wall of North Pit strikes N-S and has an overall slope angle of 62°. A set of unfavourably orientated joints namely 'ski-jump joints' (using mine nomenclature) outcrop along the E Wall creating significant stability issues. These joints are oriented within the range of 35-55° dip and 250-290° dip direction. They tend not to be associated with any infill although a small amount of calcite in varying thickness is visible on some surfaces. The joint roughness profile is undulating smooth but the joints have no diagnostic features other than orientation in common. Due to the moderate dip of the structures (relative to other structures on the E Wall) and the westerly dip direction, these structures influence crest and berm failure and were the basal surfaces controlling the pit wall failures in 2009, 2010 and 2012. The release surfaces of these failures were the steeply dipping hematite coated joints. Failure mechanisms of the E Wall will be considered later in this chapter.

3.3.3 Spatial Distribution of Joints

The spatial distribution of joints on the E Wall is of importance for the prediction of future pit wall stability and the prediction of likely failure events. This section includes a number of cross sections produced using the mining software Leapfrog™, a 3D modelling software package. The structural data used for this analysis was retrieved from the 2005-2006 resource drilling programme, the 2008 geotechnical drilling programme and the 2009-2010 resource drilling programme to ensure maximum coverage of the E Wall in North Pit. Figure 3.12

shows a plan view of North Pit with the individual cross-sections highlighted. Unfavourably oriented joints ('ski-jump' joints), hematite coated joints, graphite and pyritic coated joints and calcite coated joints have been highlighted in an attempt to convey their spatial distribution.

The structural data from NDDH0502 was constrained in Leapfrog™ to show only unfavourably dipping joints ('Ski-jump joints'). These joints dip between 35-55° towards 250-290°. Fifty eight joints within this orientation range have been logged within this drillhole (Figure 3.13). They represent 2% of all joints logged. They commonly have an undulating, rough profile (34%) or a stepped, rough profile (31%, Fig. 3.13). Due to the roughness, friction angles will be increased within these areas. Over 95% of these unfavourably oriented joints have no infill associated with them whereas under 5% have a <1 mm calcite coating. These joints are common (0.23 joints/m) near the Eastern Contact Fault and could represent a zone of enhanced brittle fracturing associated with the main fault. They diminish (0.03 joints/m) at about 164m E of the fault, 230 m down-hole.

Drillholes NDDH0602 and NDDH08024 are both visible on section X-6905 and Y-9927. Plunging 42° towards 266° with a maximum depth of 750.10 m and plunging 60° towards 090° with a maximum depth of 225.60 m respectively. 1401 joints were recorded within the East Wall Assemblage within these two drillholes. The average joint orientation is 85°/265°. Eight unfavourably dipping joints are present within these two drillholes, less than 1% of all joints logged.

Drillholes NDDH08029 and NDDH08030 were drilled as part of the geotechnical drilling programme in 2008. They lie on sections X-6941: Y-9446 and X-6723: Y-9633 respectively and are both collared on the E Wall and drilled toward the E. 169 joints were recorded within borehole NDDH08029. Of these, 8 unfavourably oriented joints were logged, just under 5% of the total. Of these unfavourably oriented joints, nearly 40% exhibited a planar rough

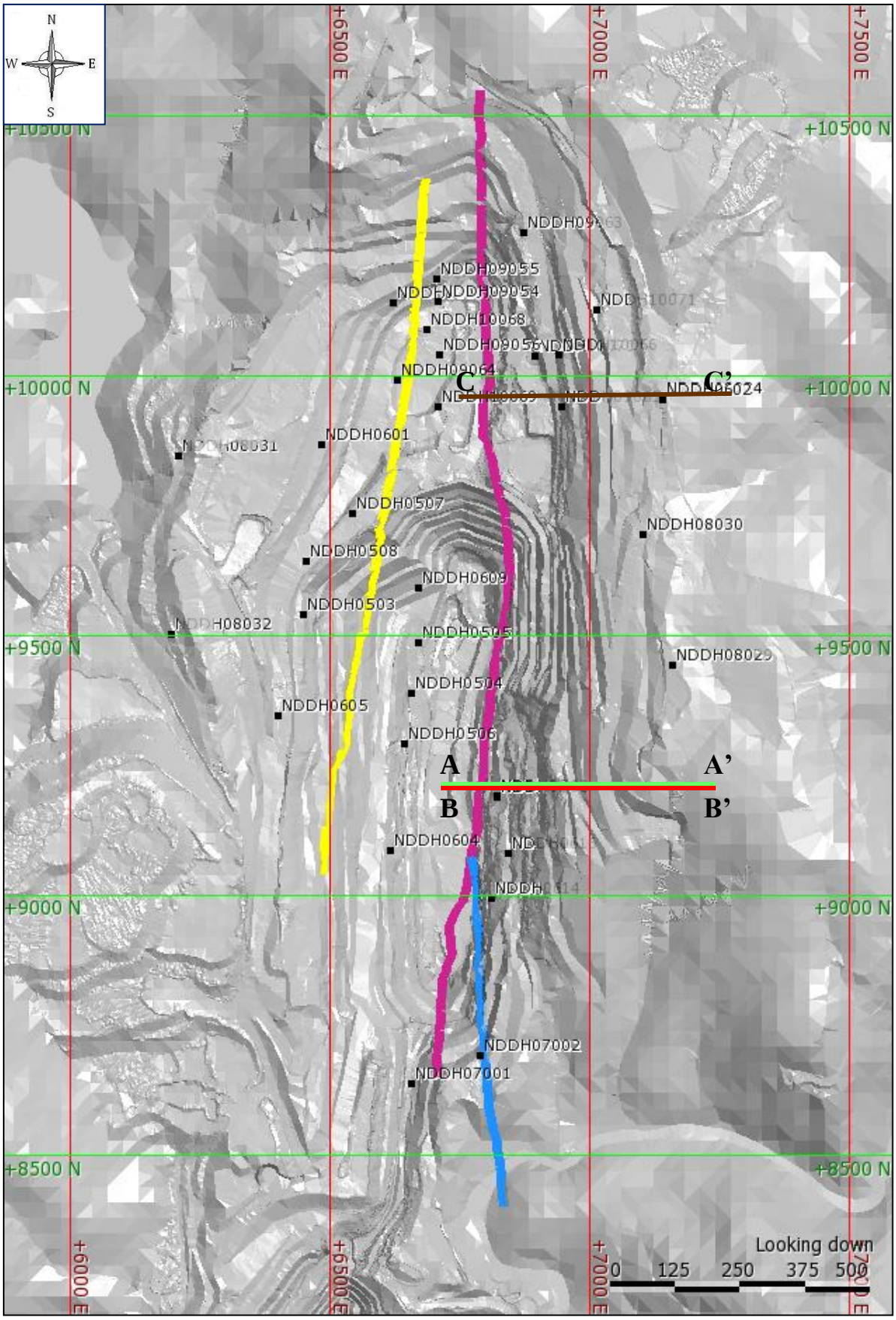

Figure 3.12. Plan view of North Pit showing major faults, drillhole collar locations and location of cross sections.

Figure 3.13

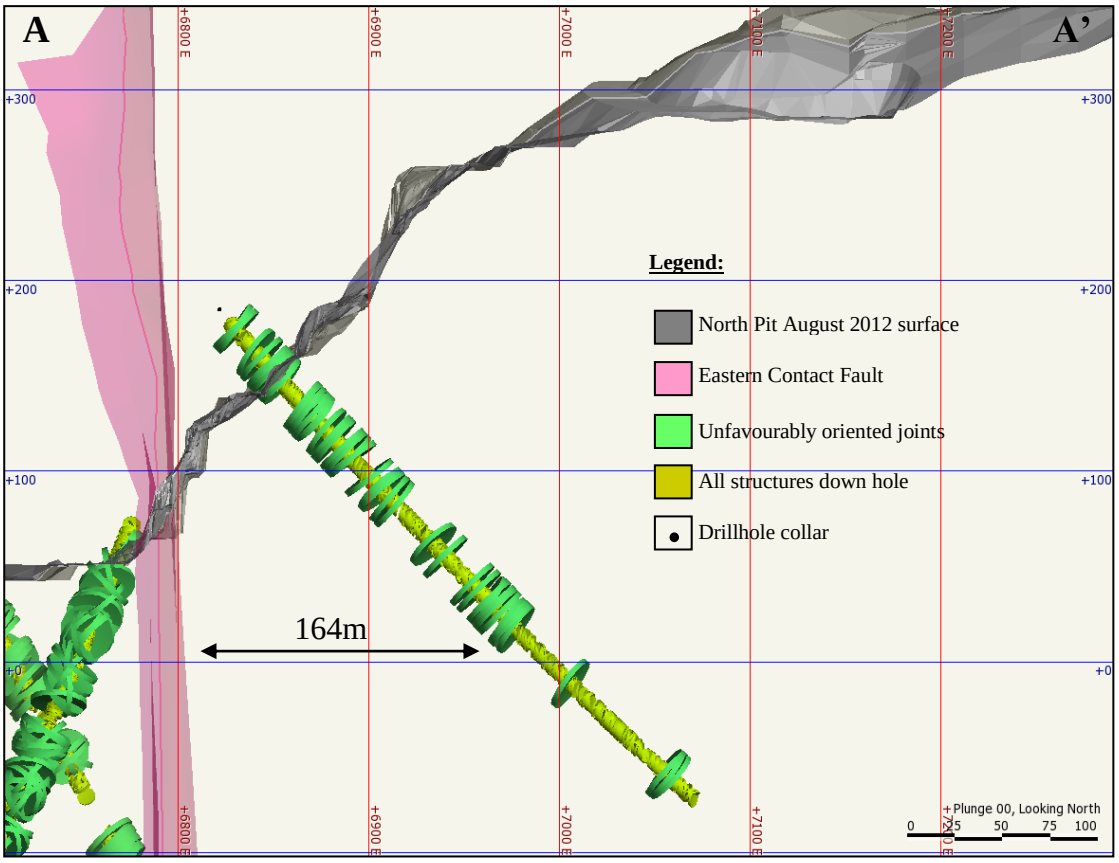

Cross section A-A' showing the position of drillhole NDDH0502 plunging 42-50° and trending 94-99° with a maximum depth of 358.80m. Unfavourably oriented joints are highlighted in green. *Section: 9200 N.*

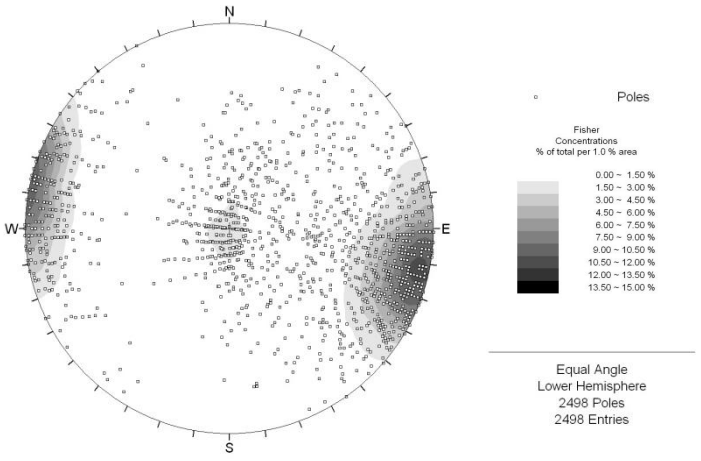

Contoured stereographic projection of all joints logged in drillhole number NDDH0502. 2498 joints were recorded and the modal orientation is approximately 85°/282°.

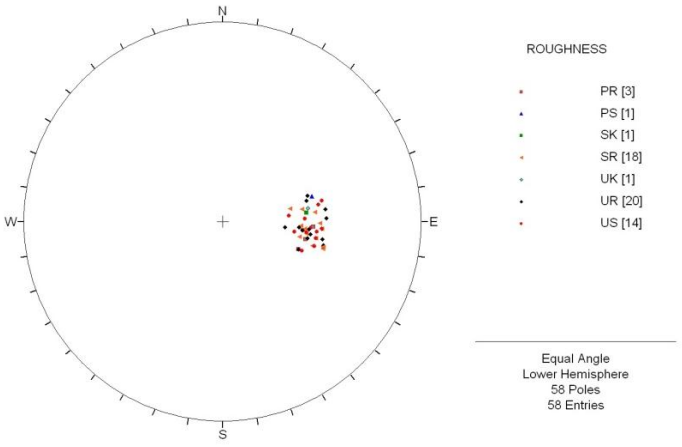

Poles to 58 unfavourably oriented joints within borehole number NDDH0502 classified by the joint roughness profiles.

roughness profile and 40% exhibited an undulating smooth profile. Both instances increase friction angles. 382 joints were recorded within borehole NDDH08030. Of these, 16 unfavourably oriented joints were logged, approximately 4% of the total joint count downhole. Of these unfavourably oriented joints, nearly 65% exhibit an undulating rough roughness profile, increasing friction angles.

Unfavourably oriented joints were not detected in any other borehole through the E Wall. Although some boreholes from the 2009-2010 resource drilling programme in Stage 2, North Pit were collared on the E Wall, the plunge and trend of these boreholes were too similar to the orientation of these joints to adequately sample them. The Leapfrog™ 3D model was constrained to show all joints exhibiting a hematite coating. These joints are of particular interest on the mine due to their specific role in recent failures. The same drillhole was used as Figure 3.13, NDDH0502. This borehole not only trends to the E so the likelihood of structural feature intersection is increased but it is collared close to the Eastern Contact Fault which is paramount when focusing on structural trends on the E Wall. In addition, 23% of all hematite coated joints recorded on the E Wall are contained within this borehole.

Sixteen of the 2498 joints recorded from borehole NDDH0502 have a hematite infill. The hematite coated joints show a spread of roughness profiles (Figure 3.14). Thirty percent of these joints exhibit an undulating, slickensided profile and these joints are steeply dipping to the W (release surfaces of recent failures on the E Wall). The roughness profile and joint decoration is indicative of past movement along these fractures, and have created a lower than normal friction angle for these surfaces. The hematite coated joints are clustered in close proximity to the Eastern Contact Fault with 0.07 joints/m out to 140 m from the fault (Figure 3.14).

Hematite coated joints are present in nine drillholes. Seven are present within borehole NDDH0602. Five of these joints are in close proximity to the Eastern Contact Fault. Three

2008 boreholes drilled to the E show a very low concentration of hematite coated joints; six in total, and they are not clustered near the Eastern Contact Fault. The hematite coated joints tend to be clustered to the S of the Northern Shear and N of Hawkie's Fault (mine nomenclature). The Northern Shear structure is estimated to begin at the ECF at 9450N, projecting into the E wall to approximately 9380N. It is dipping steeply to the SW. Hawkie's Fault is located to the S of North Pit at around 9050N and is dipping at 73° to the SW. There is evidence to indicate that the hematite coated joints are truncated by these structures.

Graphite (0.2%) and pyrite (1.35%) are less common joint fills. Commonly the pyritic and graphitic infilled joints occur together spatially, usually within <5 m of each other. A set of graphite and pyrite coated joints are located within 10m of the Eastern Contact Fault (Figure 3.15). However, pyrite and graphite joints are present within the East Wall Assemblage beyond this bounding fault (Figure 3.15). The graphitic joints are mostly steeply dipping (>68°) to the W with one joint dipping steeply to the E. Pyritic joints have an average orientation of 80°/260° but a spread of orientations is present, from near horizontal to steeply easterly dipping.

Calcite is the most common joint infill mineral on the E Wall and all boreholes transecting the E Wall intersect calcite filled joints. In order to spatially correlate calcite infilled joints, boreholes that display more than 120 m of East Wall Assemblage were used. Starting at the S end, NDDH0502 intersected 179 calcite filled joints at 0.5 joints/m. Other holes were: NDDH08029; 0.08 calcite coated joints/m, NDDH08030; 0.3 calcite filled joints/m, NDDH0602 and NDDH08024 both showed an average of 0.5 calcite coated joints/m, NDDH09065; 0.2 joints/m, NDDH10066; 0.03 joints/m, NDDH10070; 0.04 joints/m and NDDH10071; 0.05 joints/m. Although calcite coated joints are common throughout all boreholes drilled within the E Wall, there is a larger concentration at the S end of North Pit, within the Stage 1 area. No spatial correlation with the Eastern Contact Fault was detected.

Figure 3.14

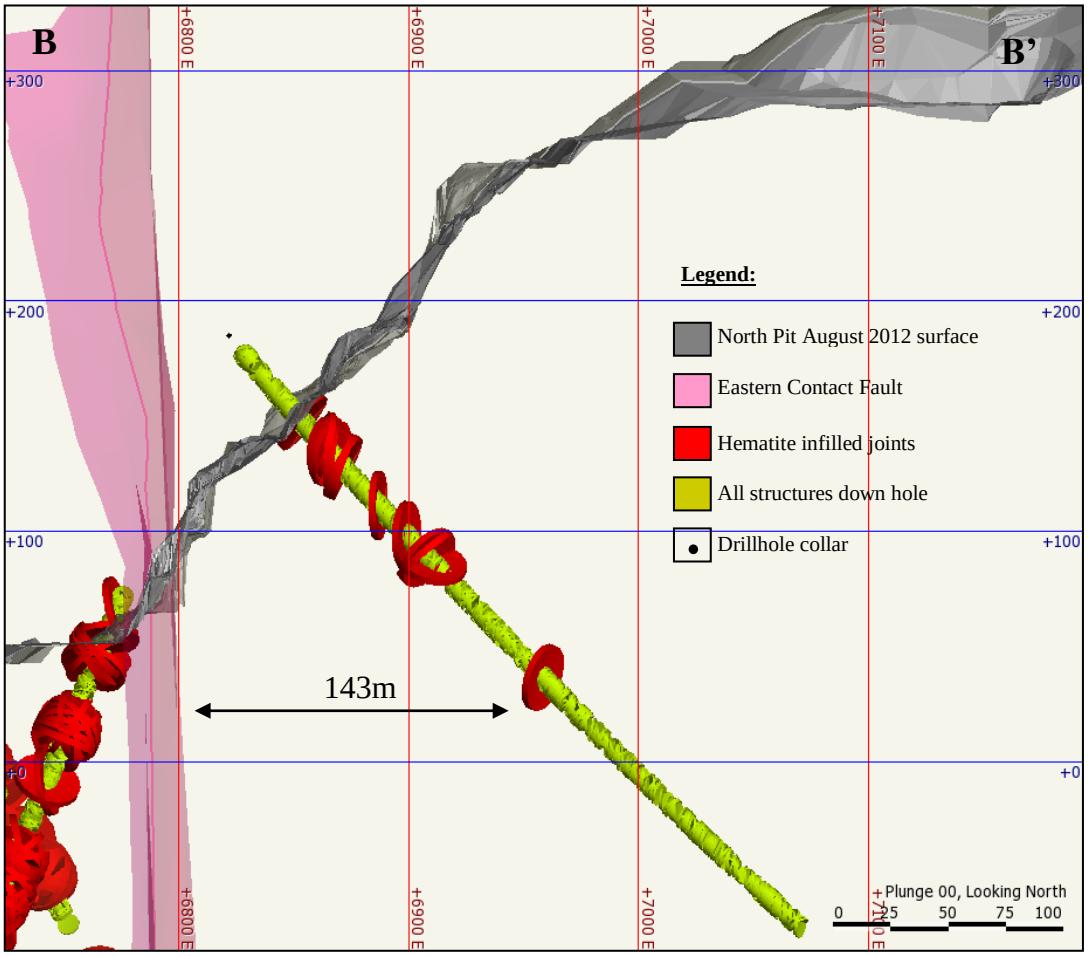

Cross section B-B' showing the position of drillhole NDDH0502 plunging 42-50° and trending 94-99° with a maximum depth of 358.80m. Hematite infilled joints are highlighted in red. *Section: 9200m N.*

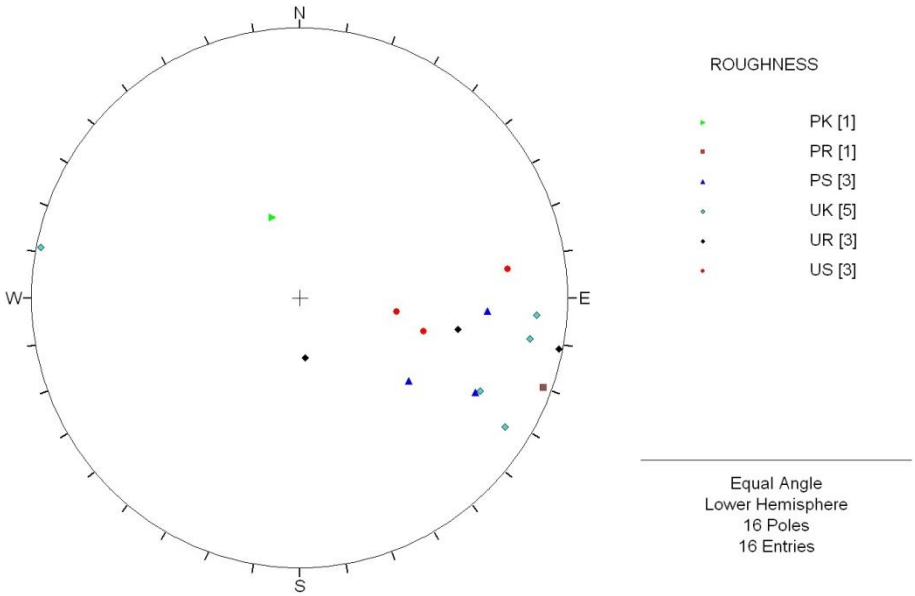

Figure 3.15

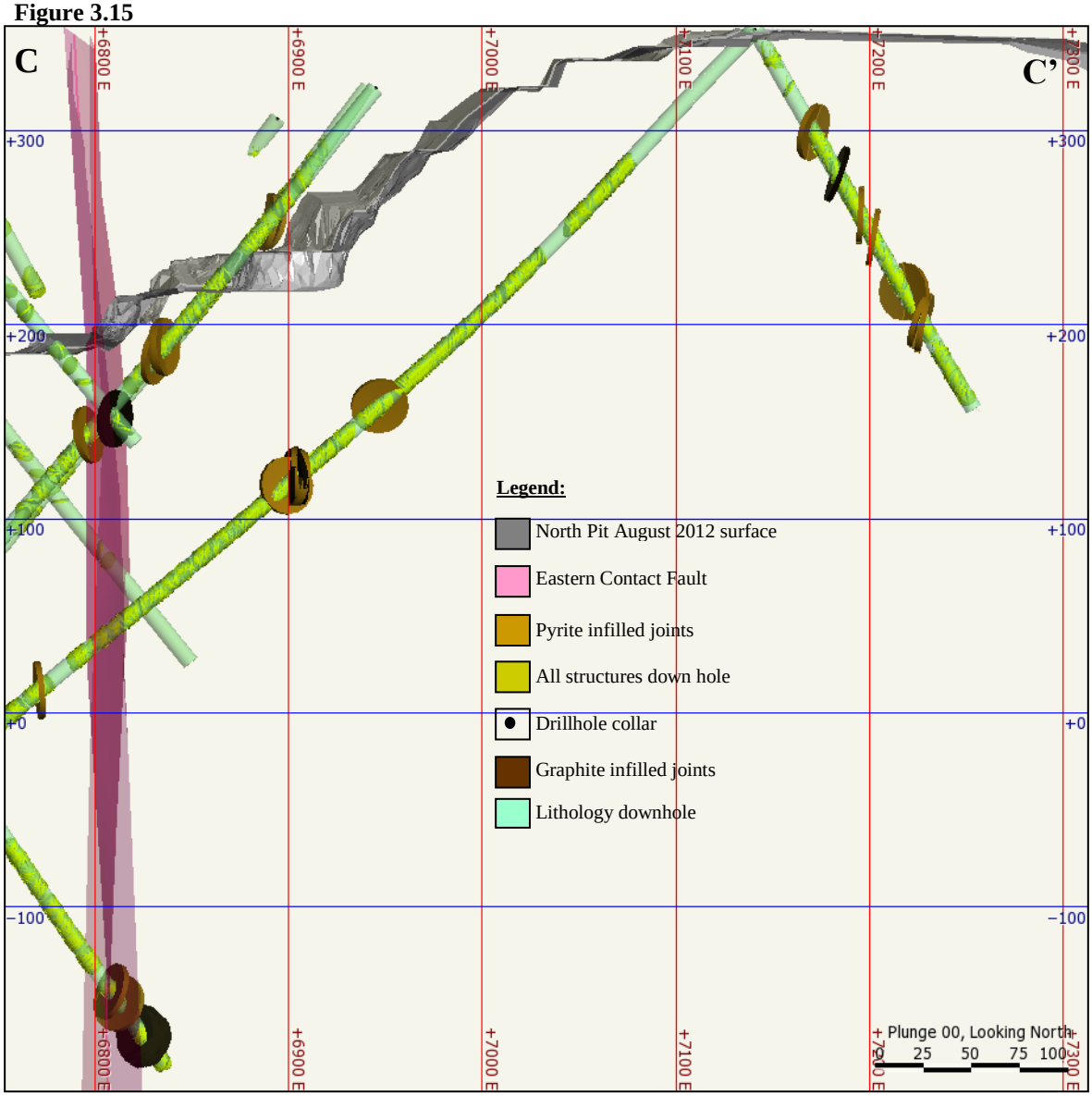

Cross section C-C' showing the spatial distribution of graphitic and pyrite infilled joints. *Section: 9958m N.*

Poles to graphitic coated joints (**GF**) and pyritic (**PY**) coated joints.

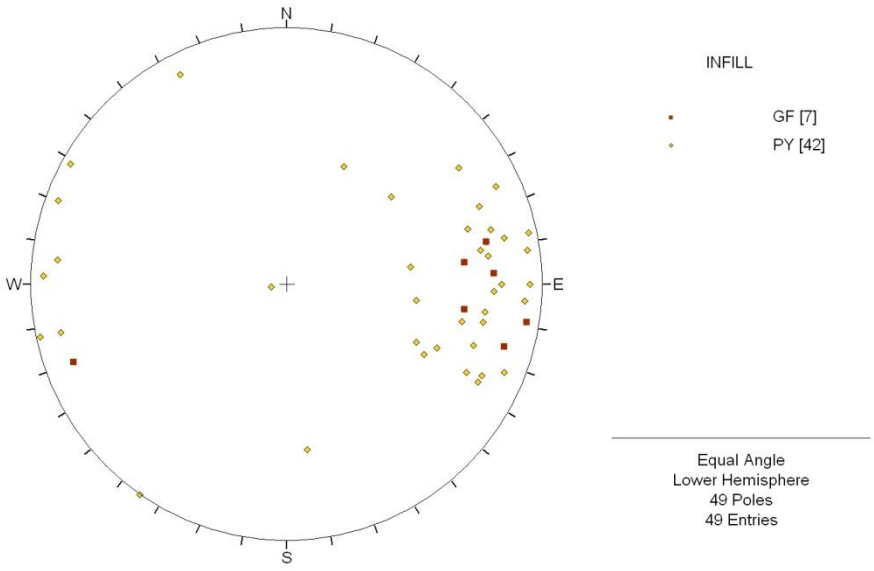

3.3.4 Vein characteristics and spatial distribution

Nearly four thousand individual veins (Figure 3.17) have been logged from drill core since 2005 from the E Wall in North Pit. Ninety percent of these were calcite veins of varying thickness from <1 mm up to 25 mm. Figure 3.16 shows a stereoplot of all 3363 calcite filled veins on the E Wall. Two distinct, opposing orientations are visible; one steeply dipping at approximately 87°/270° and one near horizontal at 08°/090°.

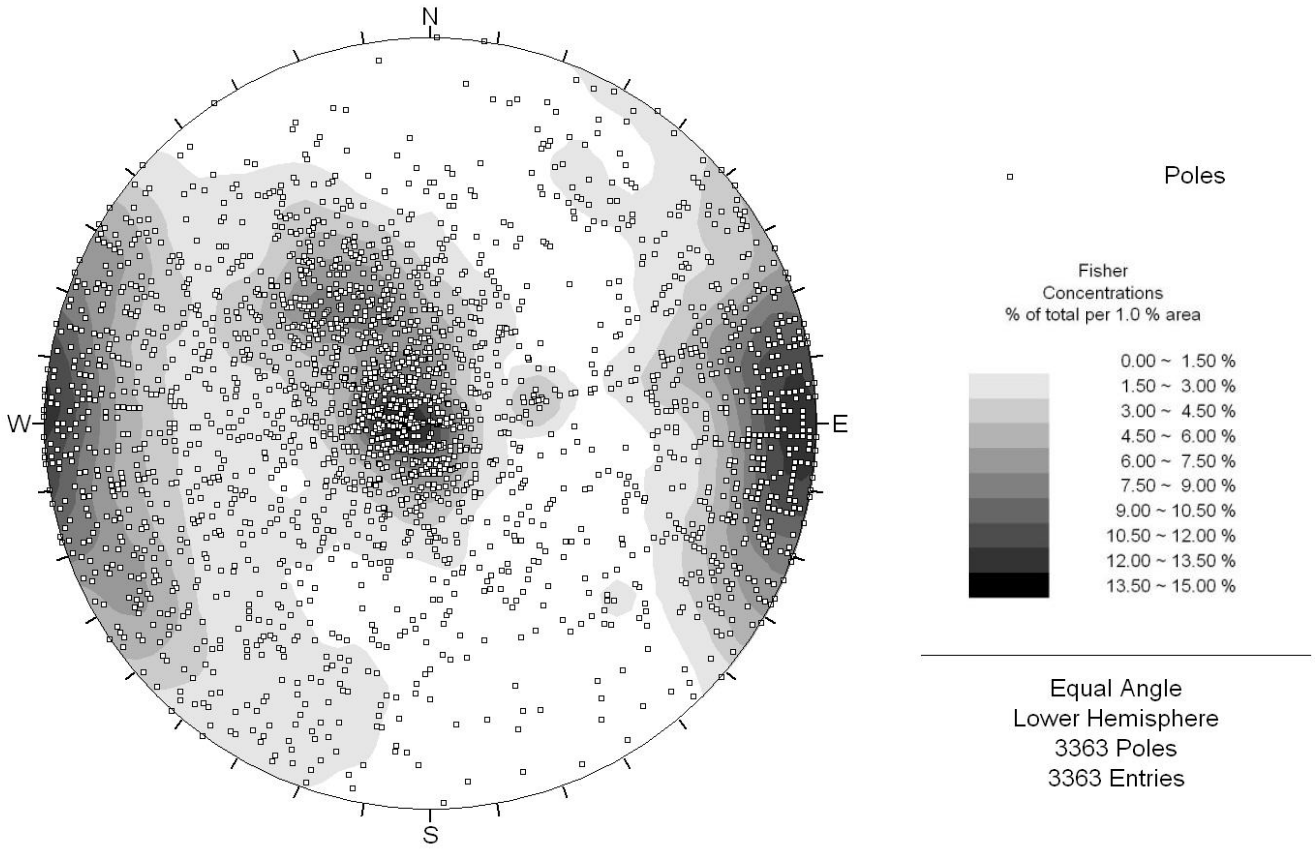

Figure 3.16. Contoured stereographic projection of calcite veins from the E Wall.

Although most calcite veins fit within the two orthogonal orientations, there are less common vein set dipping 30°/259° and 40°/142°. The calcite veins of the E Wall are variable in degree of deformation, planarity and spacing. There are three generations of calcite vein. The oldest of the three generations is oriented parallel to the pervasive foliation (Figure 3.17 – B). These veins are segmented and broken up into elongate, lenticular bodies aligned parallel to one

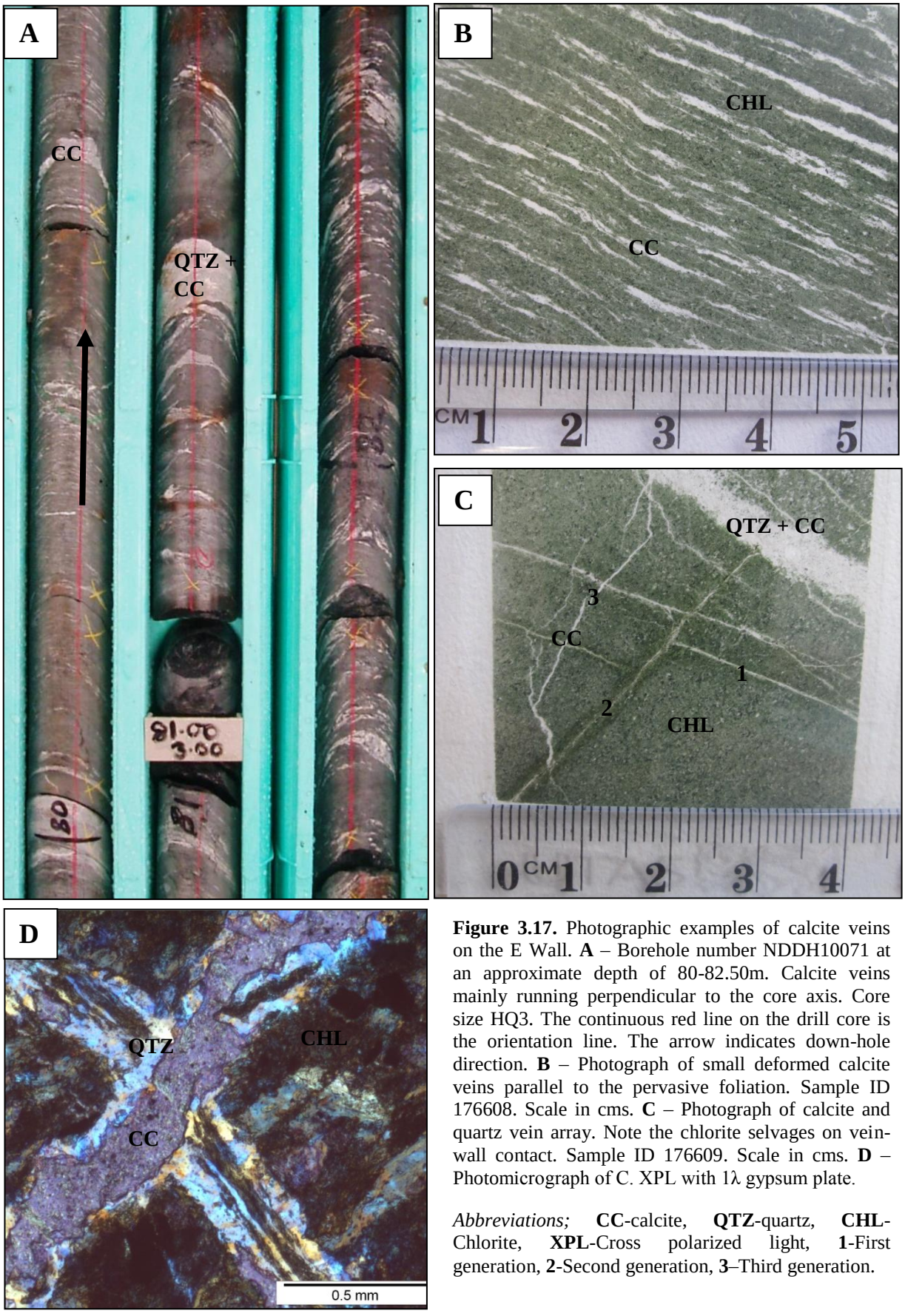

Figure 3.17. Photographic examples of calcite veins on the E Wall. **A** – Borehole number NDDH10071 at an approximate depth of 80-82.50m. Calcite veins mainly running perpendicular to the core axis. Core size HQ3. The continuous red line on the drill core is the orientation line. The arrow indicates down-hole direction. **B** – Photograph of small deformed calcite veins parallel to the pervasive foliation. Sample ID 176608. Scale in cms. **C** – Photograph of calcite and quartz vein array. Note the chlorite selvages on vein-wall contact. Sample ID 176609. Scale in cms. **D** – Photomicrograph of C. XPL with 1λ gypsum plate.

Abbreviations; **CC**-calcite, **QTZ**-quartz, **CHL**-Chlorite, **XPL**-Cross polarized light, **1**-First generation, **2**-Second generation, **3**–Third generation.

another. Originally small calcite veinlets with the wall rock, subsequent extension has stretched and thinned the veinlets. The second generation of calcite veins are less deformed and cross-cut foliation. These veins are also larger in size than the older generation and commonly have quartz associated with them (Figure 3.17 – C). Vein wall rock contact is sharp and there are commonly thin quartz-chlorite selvages along the boundary between the wall rock and vein (Figure 3.17 – C and D). These veins offset the oldest calcite veins. The third generation of calcite veins are of variable thickness. Undeformed and post kinematic, they cross-cut foliation and all other veins. Vein wall rock contact is sharp and no mineral selvages were observed.

Approximately 5% of all veins on the E Wall are quartz filled. One dominant orientation is apparent (Figure 3.18) at 85°/285°. Quartz veins commonly contain other minerals such as calcite and specular hematite and many veins are boudinaged. The orientations of quartz veins are sub-parallel to the dominant cleavage. Figure 3.19 – A, shows an example of smaller siliceous veins as well as larger bands interpreted as boudins or lenses of quartz. In close proximity to the Eastern Contact Fault and the Eastern Splay Fault, which separates the unmineralised East Wall Assemblage from the Main Host Assemblage, the quartz veins are gently dipping at approximately 30° (Figure 3.19 – B) and orthogonal to the pervasive foliation in this area. These shallow dipping veins are off-set by another generation of steeply S dipping quartz veins which are also boudinaged. Narrow quartz veins dextrally and sinistrally offsetting thicker quartz segregations are very common within five metres of both major faults (Figure 3.19 – C). Most vein quartz grains show undulose extinction, with minor subgrain formation. The contacts between the most deformed quartz grains are lobate due to grain-boundary migration. Some grains of quartz have carbonate pressure shadows associated with them (Figure 3.19 – D). The remaining 5% of vein infill includes chlorite, epidote, magnesite, magnetite, pyrite, dolomite and albite (Figure 3.21 - D). Epidote, hematite and magnetite veins are spatially limited to more deformed areas within the E Wall.

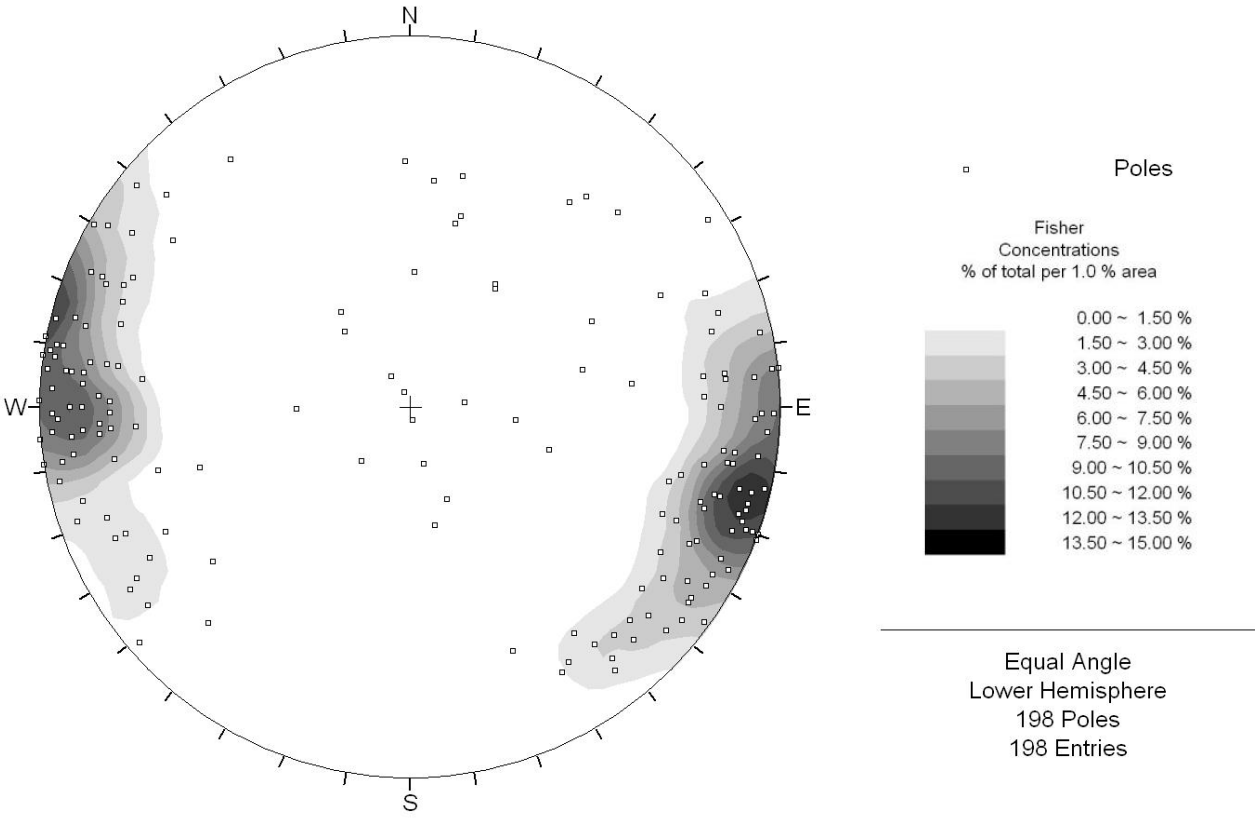

Figure 3.18. Contoured stereographic pole plot showing orientation distribution of quartz veins on the E Wall.

Dolomite, albite and magnesite veins are less common and are mainly located to the S of Stage 1 of North Pit. Dolomite veins are steeply dipping towards the W. Albite veins are gently dipping to near horizontal and dip mainly towards the N and SW. Magnesite veins are predominantly steeply dipping to the W, with 20% of veins dipping <60° (Figure 3.20).

Samples of wall rock and vein infill, exposed on the E Wall at location 6870 m E, 8973 m N and RL 162 m were sent to Mineral Resources Tasmania for mineralogical analysis by XRD (Figure 3.21 – A). Refer to Section 3.3.2. (Page 14) for details on preparation and an analysis technique outline. Three samples were analysed, two variable vein infill type samples (Figure 3.21 – B and C) and one sampled from a 50 cm wide alteration halo bounding the vein. Up to 40 cm in width and up to 20 m in length, the vein displayed a sharp vein-wall rock contact and cross-cut the pervasive foliation in the area. Smaller veins, <5 cm in width, ran parallel to

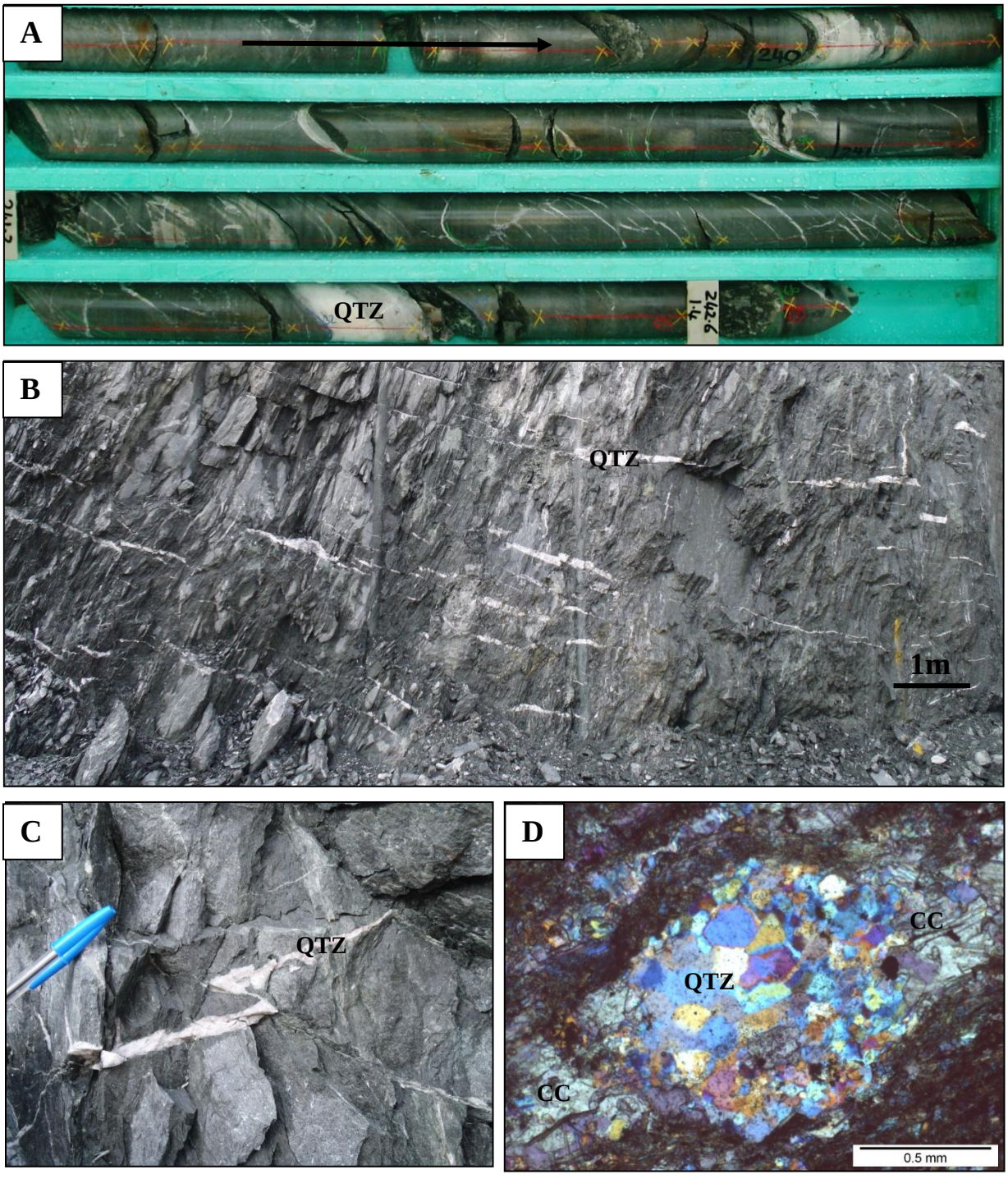

Figure 3.19. Photographs of quartz veins on the E Wall. **A** – Borehole NDDH10071 at 239.30m-242.60m. White coloured siliceous veins and boudins. Arrow denotes the down-hole direction. The red line is the orientation line. **B** – Deformed quartz veins and boudins <5m from the Eastern Contact Fault within a chloritic/carbonate assemblage. **C** – Dextral off-set quartz vein. Off-set fault contains a different narrower quartz vein. The pen lid in this photograph is approximately 3 cm in length. **D** – An example of recrystallised quartz grains with carbonate pressure shadows. Sample ID is 176610. XPL with 1λ gypsum plate.

Abbreviations; **CC**-calcite, **QTZ**-quartz and **XPL**- Cross polarized light.

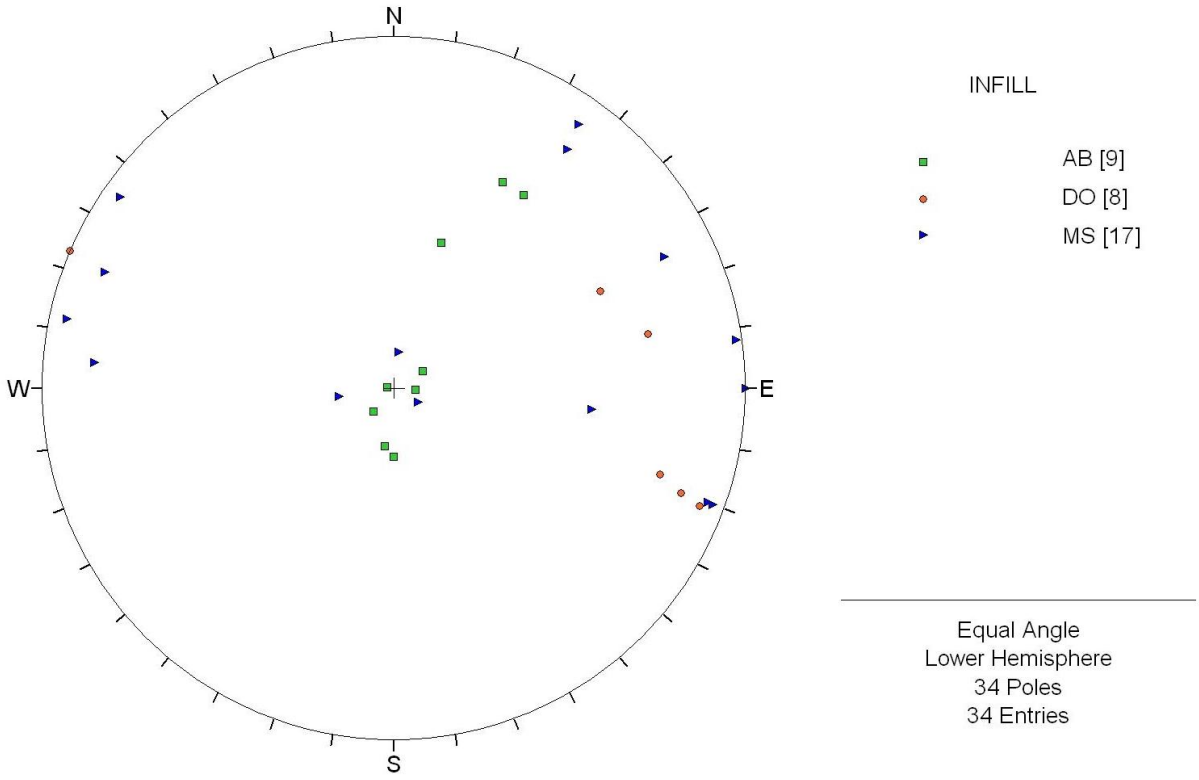

Figure 3.20. A stereographic pole plot showing orientations of albite, dolomite and magnesite veins on the E Wall. *Abbreviations;* **AB**-Albite, **DO**-Dolomite, **MS**-Magnesite.

the vein at a similar orientation. The XRD results confirmed sample ID 176666 vein infill to be ferroan dolomite with minor calcite, quartz and muscovite (Figure 3.21 – B). Sample ID 176667 identified the same minerals but in varying amounts (see Appendix 9 - digital) but with the addition of 25-35% albite and minor chlorite (Figure 3.21 – C).

Within sample ID 176668 (the alteration halo bounding the vein) all minerals above were identified in varying amounts but with the addition of paragonite. Paragonite is rare within the rocks of Savage River Mine but is likely to be related to late-stage albitisation. Fe-dolomite and albite was found in smaller amounts than in sample ID 176667 and an increase in the volume of quartz and chlorite was apparent.

Sample ID 176669, a pink-orange coloured vein approximately 1 cm in width (Figure 3.21 – E) cross-cutting foliation on the E Wall was also analysed by XRD methods in the MRT

laboratory in Rosny. K-feldspar and hematite were identified as the vein infill (Appendix 9 - digital). K-feldspar is rare within the rocks of Savage River Mine. The analysis confirmed a chlorite-amphibole metabasic mineralogy for the host rock.

Calcite veins are distributed throughout the entire E Wall. Domaining based on calcite vein distribution is impossible. However, quartz filled veins occur less frequently, usually clustered in discrete areas of the E Wall. The domain within close proximity of the Eastern Contact Fault has a concentration of non-continuous gently dipping quartz and calcite veins. Hematite veins are mainly observed in close proximity to a concentration of hematite coated joints and epidote and magnetite veins are apparent in these areas of the E Wall. Dolomite, magnesite and albite veins are less common and no spatial concentration was detected.

3.3.5 Foliation Characteristics

A steeply dipping foliation is pervasive. The foliation is logged as FO1: weak, FO2: moderate and FO3: strong. Half of all foliation logged on the E Wall was logged as a weak foliation. 37% as a moderate foliation and 10% was logged as a strong foliation (Figure 3.22). FO1 (weak foliation) strikes 010°, FO2 strikes 000° and FO3 strikes 350° on average.

Geotechnically, the foliation on the E Wall acts as a plane of weakness within the rock and small toppling failures occur in areas of intense foliation (Figure 3.23. – A). Failure surfaces (joints) on the foliation can exhibit <10 mm to >500 mm spacing depending on the lithology (Figure 3.23. – B). Some areas of this assemblage are massive; lacking many veins, joints and foliation. However, distinct foliated areas of rock with increased veins and joints occur alternating between the massive domains.

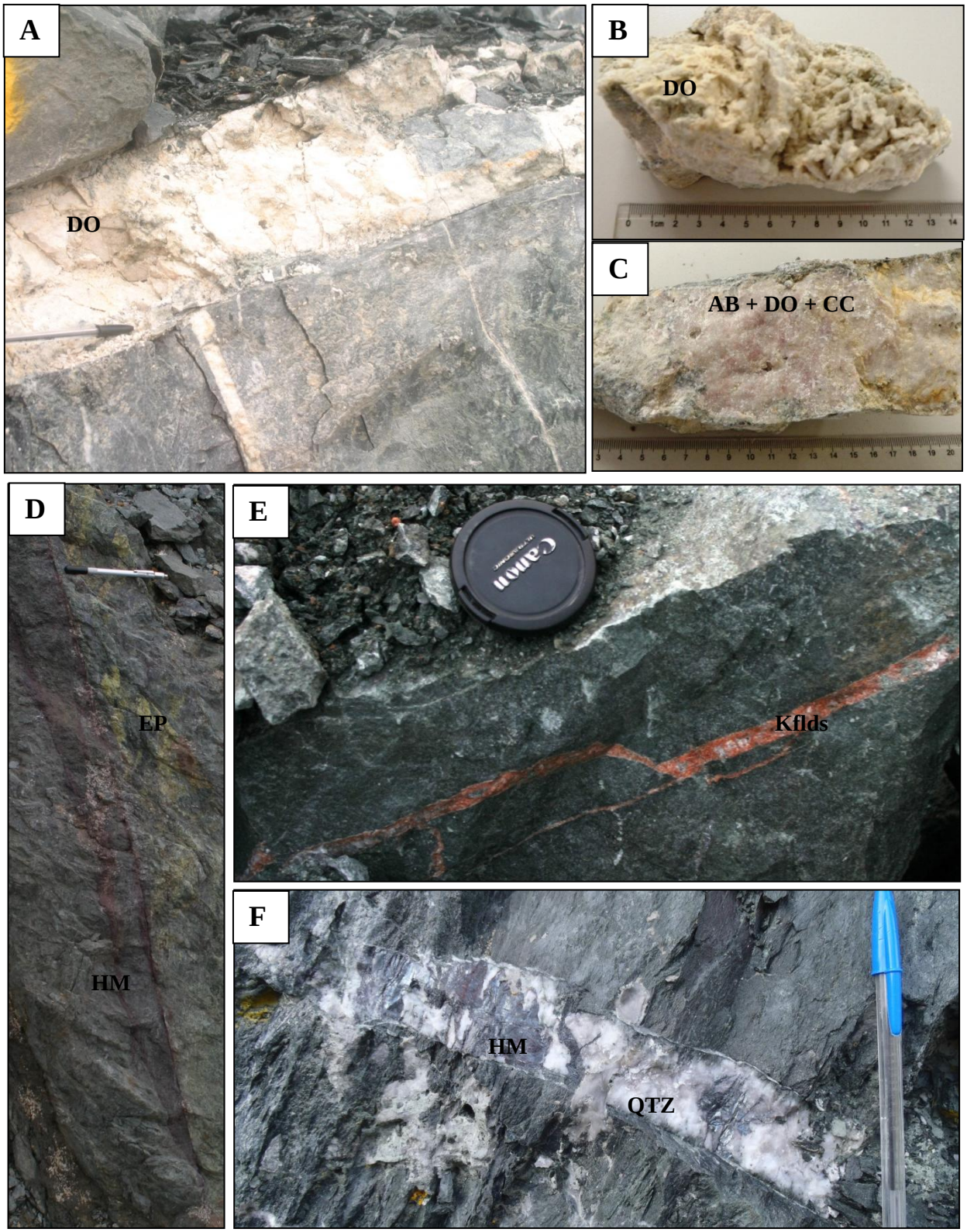

Figure 3.21. Examples of the variety of veins on the E Wall. **A** – Dolomite vein. Pen length approximately 10 cm. **B** – Photograph of the vein infill of **A**. Sample ID 176666. Scale in cms. **C** – Photograph of the vein infill of **A** at a different location within the vein. Sample ID 176667. Scale in cms. **D** – Photograph of hematite and epidote veins steeply dipping. Pen length approximately 14 cm. **E** – Photograph of K-feldspar and hematite veins within chlorite-carbonate schist. Sample ID 176669. Camera lens cap approximately 6 cm in length. **F** – Example of veined specular hematite and quartz. Pen length approximately 13 cm.

Abbreviations; **DO**-Dolomite, **QTZ**-Quartz, **AB**-Albite, **CC**-Calcite, **HM**-Hematite, **Kflds**-K-feldspar and **EP**-Epidote.

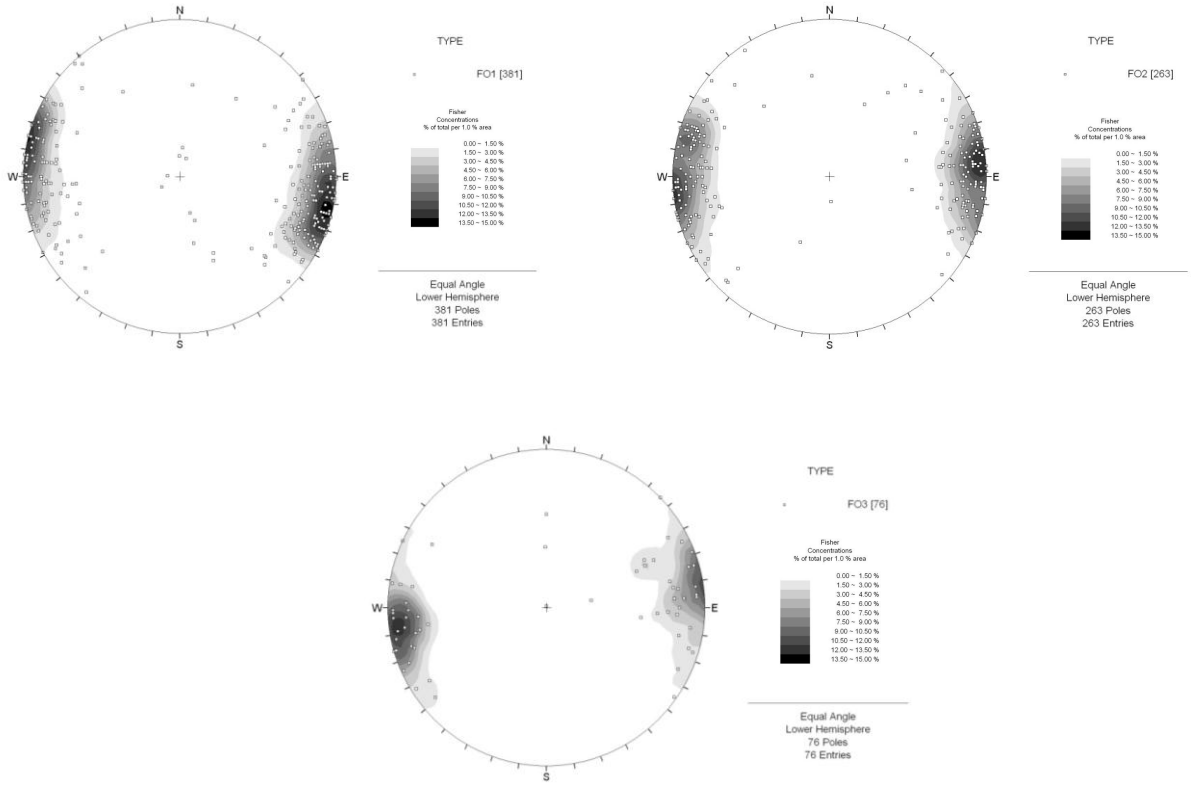

Figure 3.22. Three contoured stereographic pole plots of the orientation trends of **FO1** (top left), **FO2** (top right) and **FO3** (bottom) on the E Wall.

Foliation is continuous and is defined by subparallel chlorite grains (Figure 3.23. – C). Most minerals within this lithology are syn-kinematic. The foliation does not wrap around the grains such as albite (Figure 3.23. –C) or quartz (Figure 3.23 – D). Microscopy revealed the foliated domains of the E Wall have higher quartz content than the massive domains (Figure 3.23. – D). Foliation is generally very steeply dipping. There are however some areas where the dip is shallower. Constraining the structural model on Leapfrog™ of foliation by degrees of dip highlights areas where these areas are (Figure 3.24). Although no foliation domains are apparent spatially, the areas of frequent hematite coated joints and veins lie within areas where foliation commonly has a dip ≥70°. The orientation variation of cleavage on the E wall is of importance when relating the structural aspects of the wall to rock failure. The majority of foliation is steeply dipping to the W but concern occurs when the foliation dip changes to <70°. When moderately dipping, foliation breaks can act as basal surfaces facilitating plane failure.

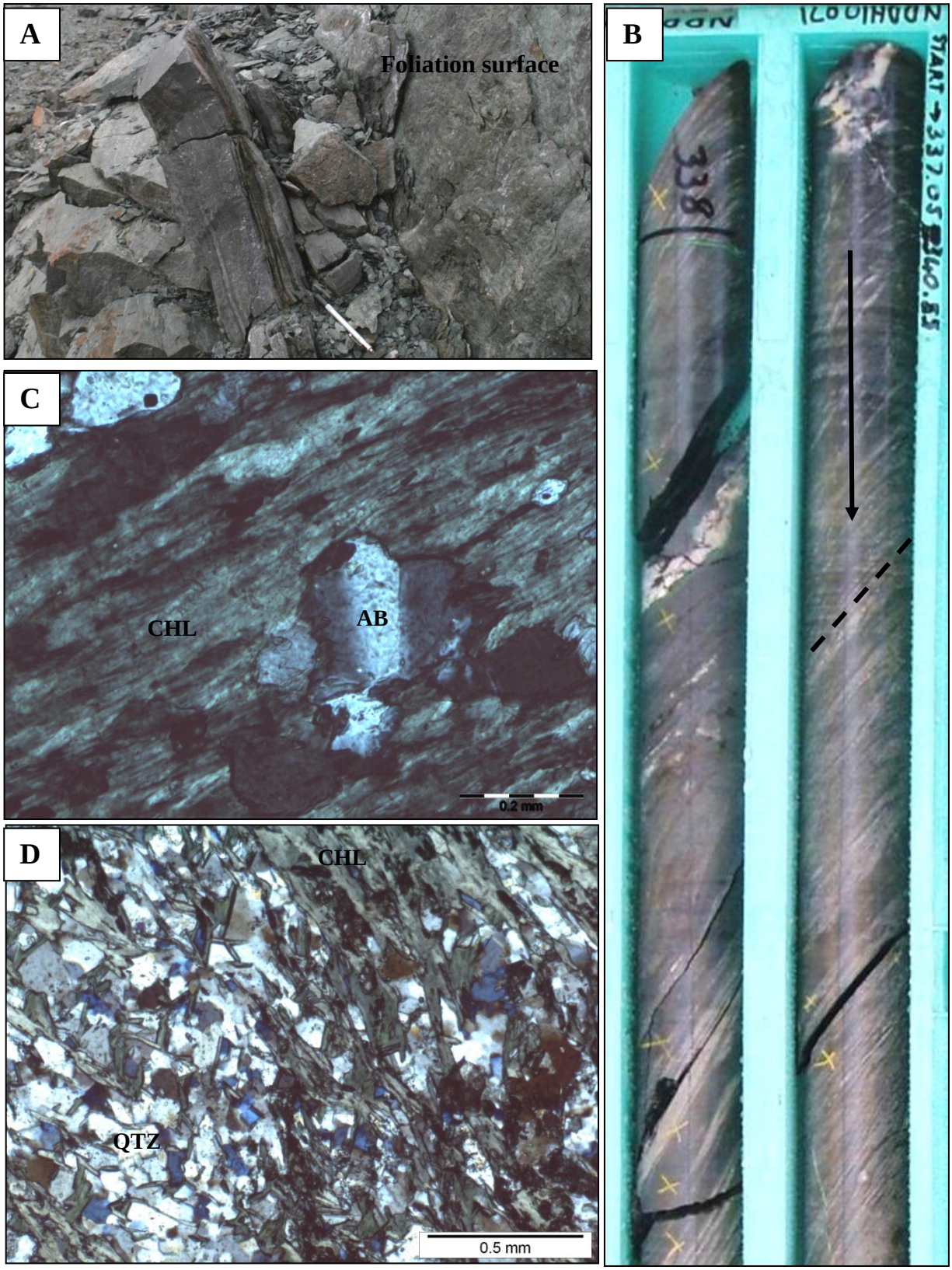

Figure 3.23. Photographic examples of foliation on the E wall. **A** – Annotation depicts the foliation surface. Very steeply dipping in this area. Pen length approximately 14 cm. **B** – Drill core from borehole number NDDH10071 at depth 337.05-338.70 m. Black dotted line denotes foliation orientation. Arrow denotes down-hole direction. Core size is HQ3. **C** – Photomicrograph of sample ID 176611. Chloritic foliation is pervasive. XPL. **D** – Photomicrograph of sample ID 176613. A foliated E wall sample with major quartz. Chloritic foliation observed to the top right of the photomicrograph. XPL.

Abbreviations; **CHL**-Chlorite, **AB**-Albite, **QTZ** – Quartz and **XPL**-Cross polarized light.

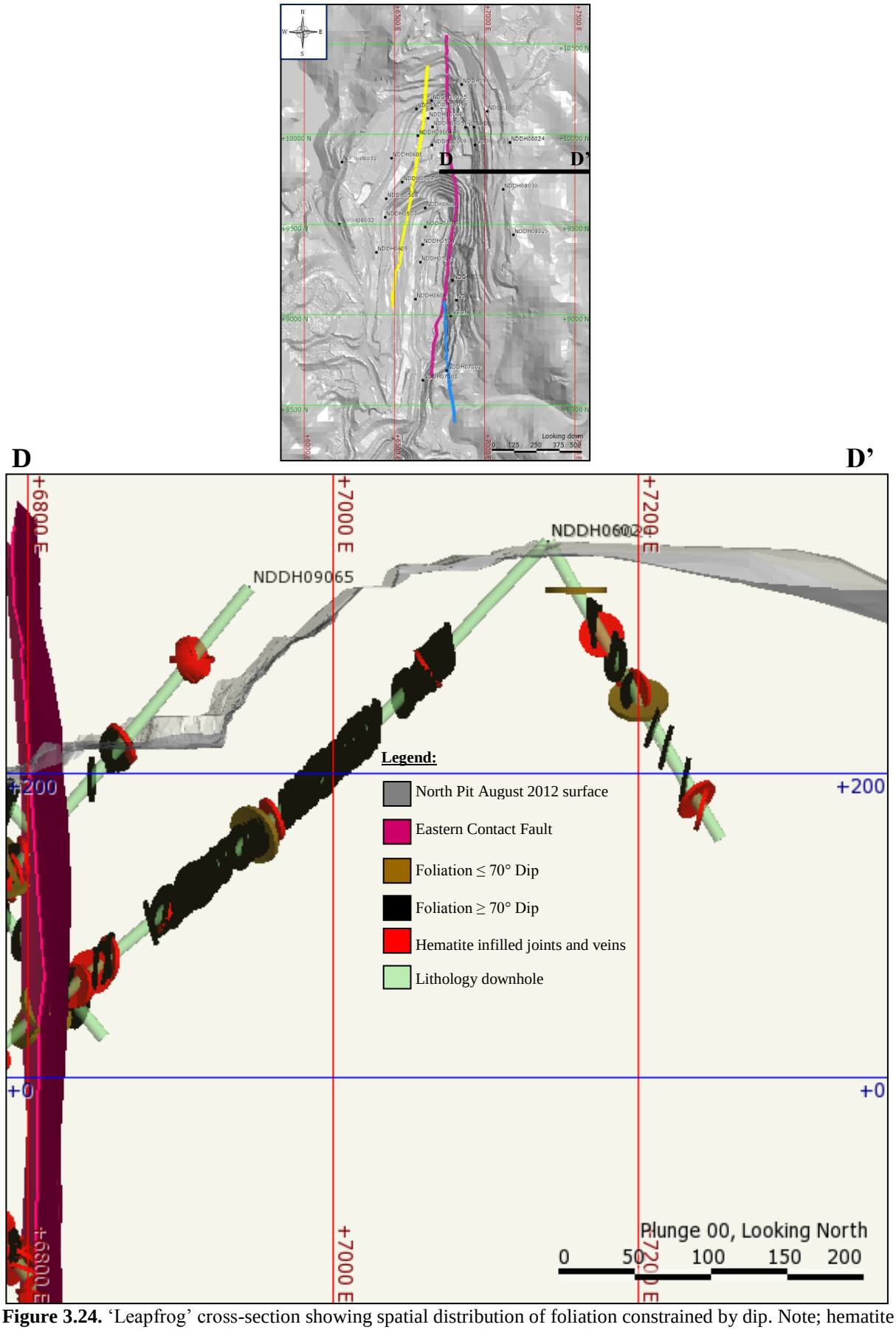

Figure 3.24. 'Leapfrog' cross-section showing spatial distribution of foliation constrained by dip. Note; hematite vein and joint distribution. *Section looking N at 9882 m N*. Plan view map showing location of cross-section.

3.3.6 Failure Modes

Three major failures have occurred on the E Wall of North Pit since the commencement date of this research. The first rock failure in September 2009 occurred towards the S of Stage 1, the second in June 2010 towards the N of Stage 1 and the third in July 2012 in close proximity to the failure in June 2010. Figure 3.25 shows the position of the September 2009 and June 2010 failures.

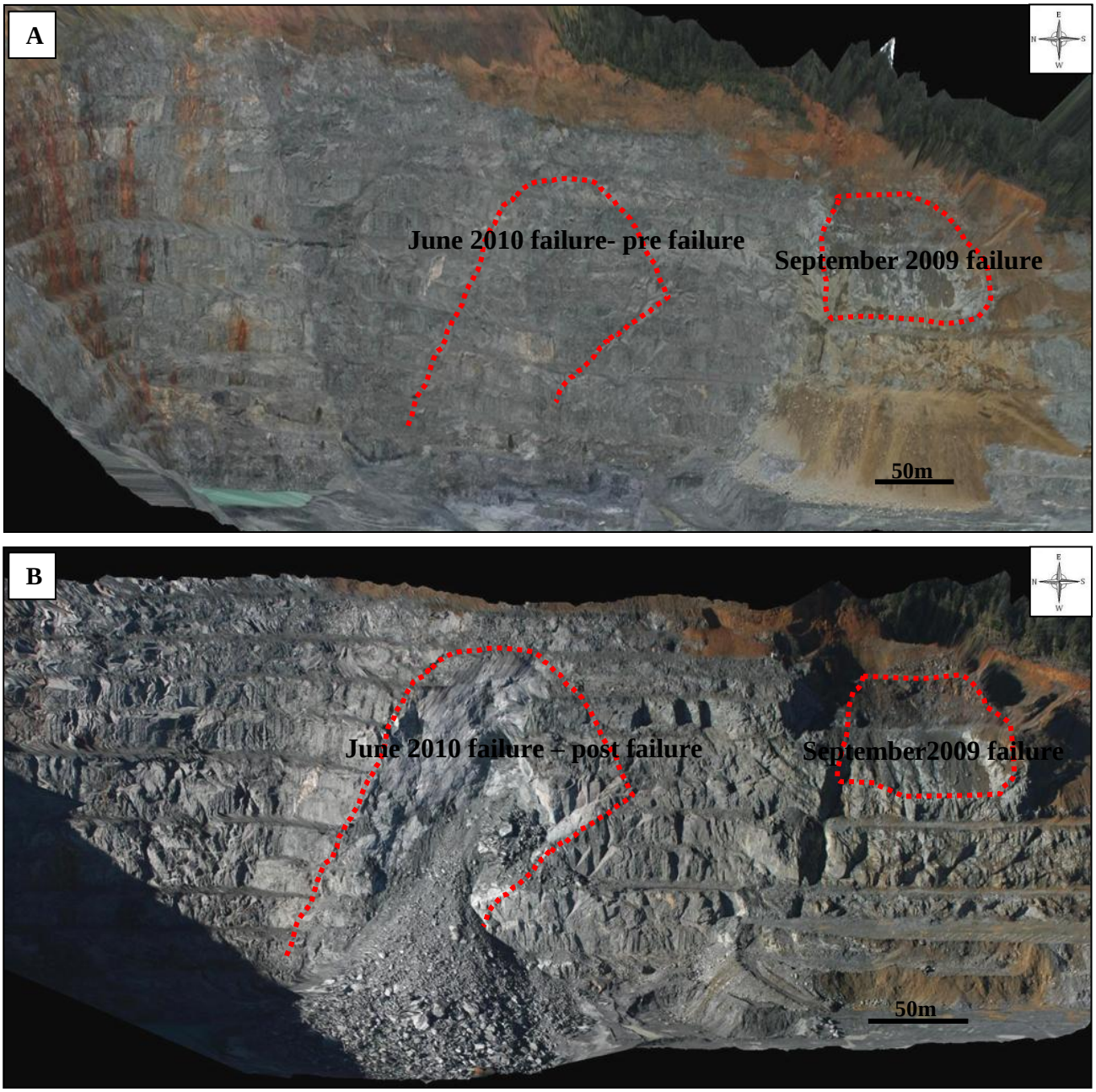

Figure 3.25. Photogrammetry DTM images of the E Wall. **A** – Photographs taken September 2009 rock failure and pre June 2010 rock failure. Positions of failure areas shown with red dotted lines. **B** – Photographs taken in June 2010 after both rock failures. Positions of failure areas denoted with red dotted lines.

Abbreviations; **DTM**-Digital Terrain Model

The September 2009 rock fall involved the failure of a crest of a berm towards the S of the E Wall, Stage 1. This type of failure is referred to as plane failure. Hoek and Bray (1991) outlined the general conditions for plane failure; a). The plane on which sliding occurs must strike parallel or nearly parallel (within ±20°) to the slope face b). The failure plane must 'daylight' in the slope face. This means that its dip must be less than the dip of the slope face c). The dip of the failure plane must be greater than the angle of friction of this plane and d). Release surfaces which provide negligible resistance to sliding must be present in the rock mass to define the lateral boundaries of the slide. Each condition was met during the September 2009 failure. The failure surface was that of a 'ski-jump' joint. This surface daylighted in the face prior to failure (Figure 3.25), dipping at approximately 45° to the W. The pit face at this time was averaging a slope angle of 62° therefore the failure surface was dipping at a smaller angle to that of the slope. The failure surface and the slope face have the same strike. Strength data taken from the 'Mine Life Extension Project' (2006) suggested that the angle of friction (Φ) along an unfilled discontinuity on the E Wall can be expressed as $\Phi = \Phi b + i$; where Φb is the basic friction angle and i is the roughness or the degree of planarity of the discontinuity surface. From data contained within this report in 2006, these values would be Φ = 28° + 12.7° which gives 41° as the value of phi. This value is smaller than the dip of the failure surface, satisfying point c) of the conditions of plane failure. Additional strength could possibly come from cohesion although there was no evidence during core logging and face mapping that these discontinuities were at all cohesive. Although not visible within the pit face in Figure 3.25, a back scarp composed of several discontinuities in the upper surface of the slope acted as the release surface of the failure. These are likely to have been steeply dipping joints at around 77-79°, dipping to the W. Alternatively, the release surface could have been a weak foliation surface as the foliation in this area is also steeply dipping to the W. A volume calculation using photogrammetry techniques before and after the failure confirmed 12,000 tonnes of rock plunged to the pit floor during this failure.

All failures on the E Wall since 2009 have been within the winter months with increased rainfall. In September 2009 and June 2010, monthly rainfall reached 244 mm and 277 mm respectively (courtesy of the Commonwealth of Australia, Bureau of Meteorology). According to Hoek and Bray (1991) the onset of heavy rainfall can result in the rapid build-up of water pressure within the release surface which will offer little resistance to the entry of surface flood water. This scenario was most probably the case for the September 2009 rock failure and heavy rainfall would have had a strong impact on more recent failures.

The June 2010 failure involved a multi-berm rock fall of over 150 m in height. This failure was classified as a wedge failure involving sliding along the line of intersection of discontinuities (Hoek and Bray, 1991). The specific geometry of this failure is given in Figure 3.26a. All orientations were retrieved using photogrammetry techniques due to the size of the failure and the inaccessibility of the pit face at the time. The release surface in this instance was a hematite coated, undulating smooth joint. Striations were visible on the joint surface. This discontinuity was dipping at 70° towards 266°. The basal surfaces were undulating and smooth, exhibiting no infill. The northerly basal surfaces were dipping at an average of 46° with an average dip direction of 298° and the southerly basal surface dipping at 54° to the W. The overall pit slope at the area of this failure was 62°/310°. Figure 3.26b. highlights this scenario on a stereographic projection using a predicted friction angle (phi) as 20°. There are two plane intersections between the hematite and the basal surface orientated at 46°/298° and another between the two basal joints at this phi angle meaning wedge failure is very likely. As the phi angle is not known of the specific joints relating to this failure, the use of a stereonet is paramount in predicting the most probable phi angle in this situation. Modifying the friction cone on the stereonet confirms that the friction angle would have to be ≤35° in order for this wedge failure to have occurred.

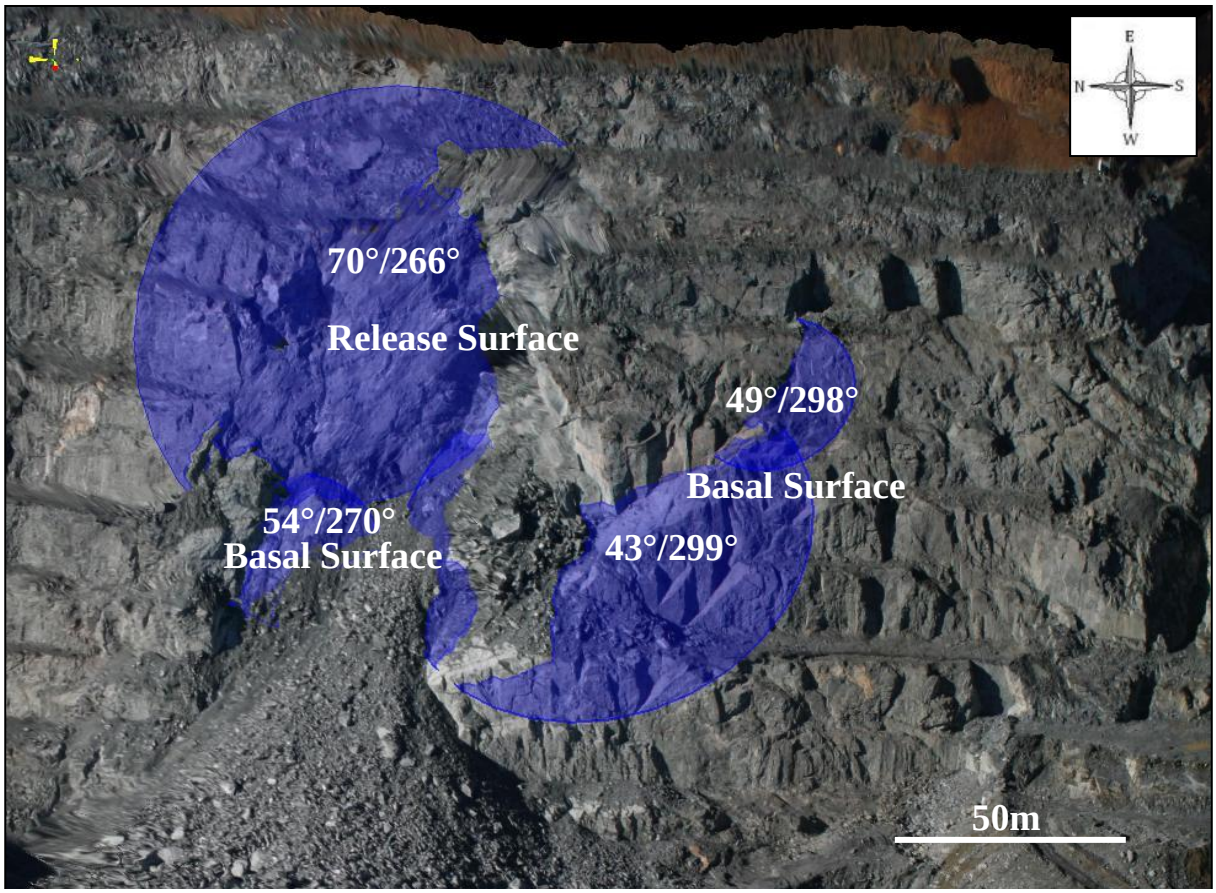

Figure 3.26a. Photogrammetry DTM image of the June 2010 failure. The blue discs denote the extent of each discontinuity responsible for the failure and the text displays orientation data retrieved from the photogrammetry technique.

Abbreviations; **DTM**-Digital Terrain Model

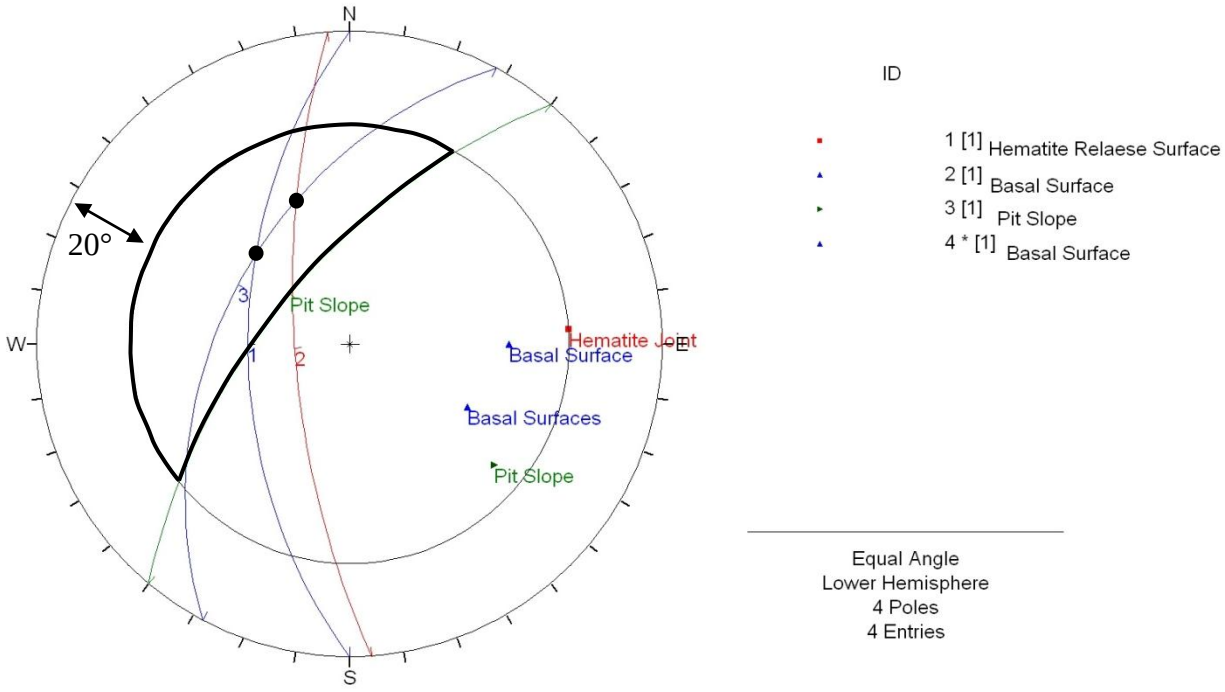

Figure 3.26b. Stereographic projection highlighting the wedge sliding zone (solid black line on stereonet). The phi angle used in this example is 20°. Two plane intersections fall within the wedge sliding zone (black dots on the stereonet) meaning these are potential wedge failures.

The recent failure in July 2012 occurred in the same position as the June 2010 failure. An estimation of 700,000 bulk cubic metres of material fell onto berms below and the pit floor. As before, the release surface was a hematite coated, undulating smooth joint orientated at 78°/271° (striking parallel to the pit wall at 62°/270°). It is predicted that a 'ski-jump' discontinuity is positioned under the failure rill acting as the basal surface. This joint however is not visible. Figure 3.27 shows an estimated cross section of the failure area. The day lighting hematite joint or failure back scarp is shown as well as the predicted location and orientation of the basal 'ski-jump' joint. The known orientation of the hematite coated joint is shown with a predicted orientation of the 'ski-jump' joint. The July 2012 failure mechanism is plane failure (described above). This is similar to the September 2009 failure.

Figure 3.28a shows the geometry of the 2012 failure and the structures of the E Wall in August 2012. All orientations were retrieved using photogrammetry techniques due to inaccessibility to the pit face and the size of the failure area. The data is presented using Leapfrog™ and two separate views; a plan view and an elevation view. A stereonet of the data collected from surface mapping using photogrammetry is also shown characterising the orientations of hematite coated joints, joints displaying minimal infill and 'ski-jump' orientated joints. The hematite coated release surface for the July 2012 failure is also highlighted. The brown line denotes the extent of failure rill. Mine nomenclature is used when naming certain features. Figure 3.28b is an overview of the brittle features within the East Wall Assemblage. It shows three stereonets, outlining overall orientations of all joints, veins and cleavage irrespective of infill, roughness and intensity. Three representative cross sections were also chosen within the E wall of North Pit. These outline the major distribution trends of each structure. Pole plots of the orientation data shown on the cross sections are also presented. All three major failures were hosted in the areas of low GSI (Geological Strength Index) immediately east of the Eastern Contact Fault.

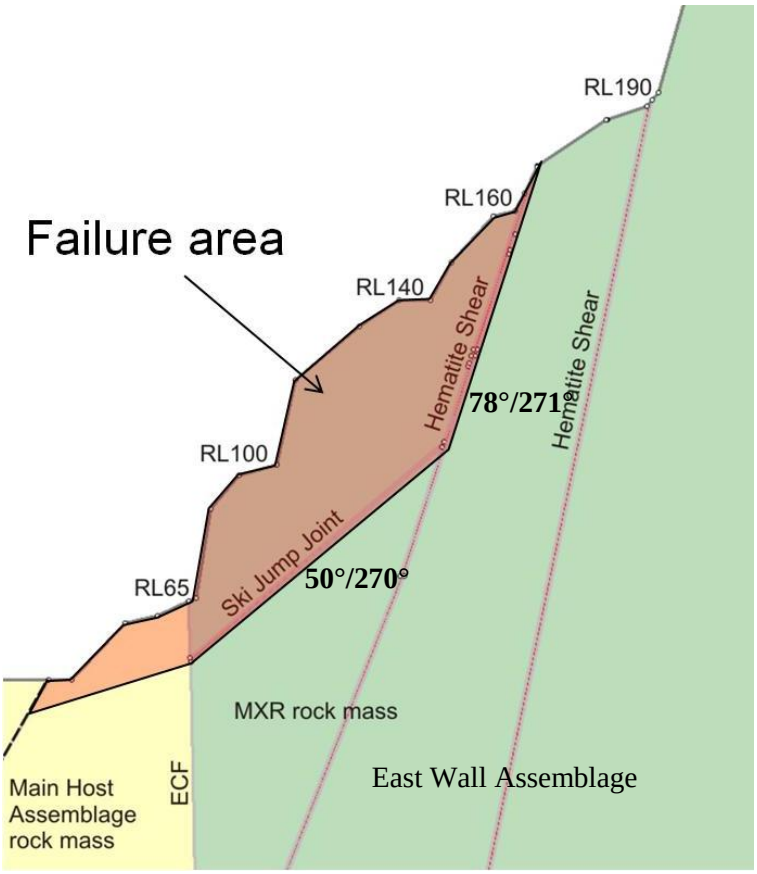

Figure 3.27. A cross section showing the main structures driving the July 2012 failure on the E wall. Looking N. ECF – Eastern Contact Fault. Modified from a Grange Resources unpublished geotechnical report (2012).

Survey Details; August 2012 End of Month mine surface DTM's utilised.

Leapfrog™ Mining Software was used for the generation of these models.

NORTH PIT, EAST WALL ASSEMBLAGE

STRUCTURAL MAP AND INTERPRETATION

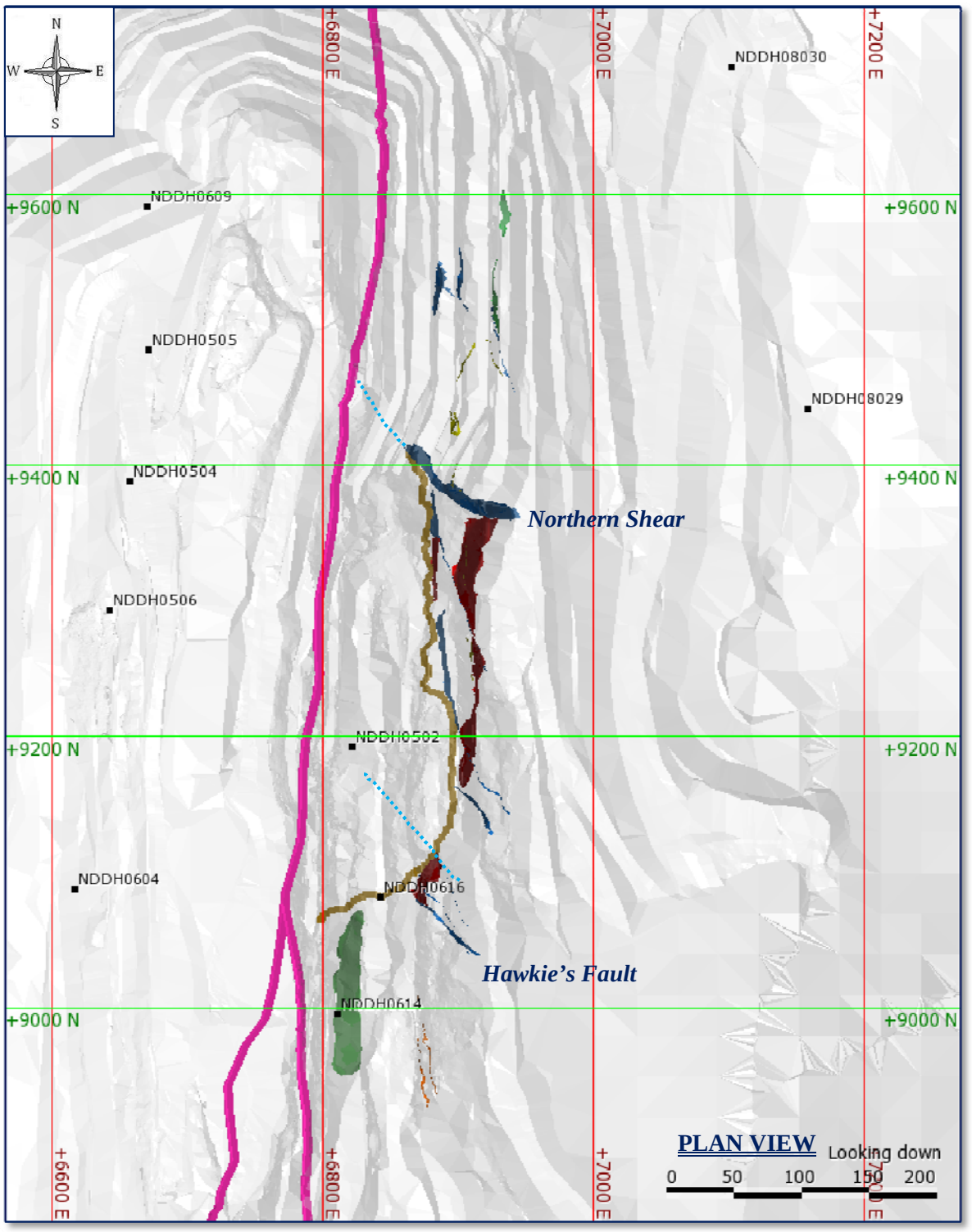

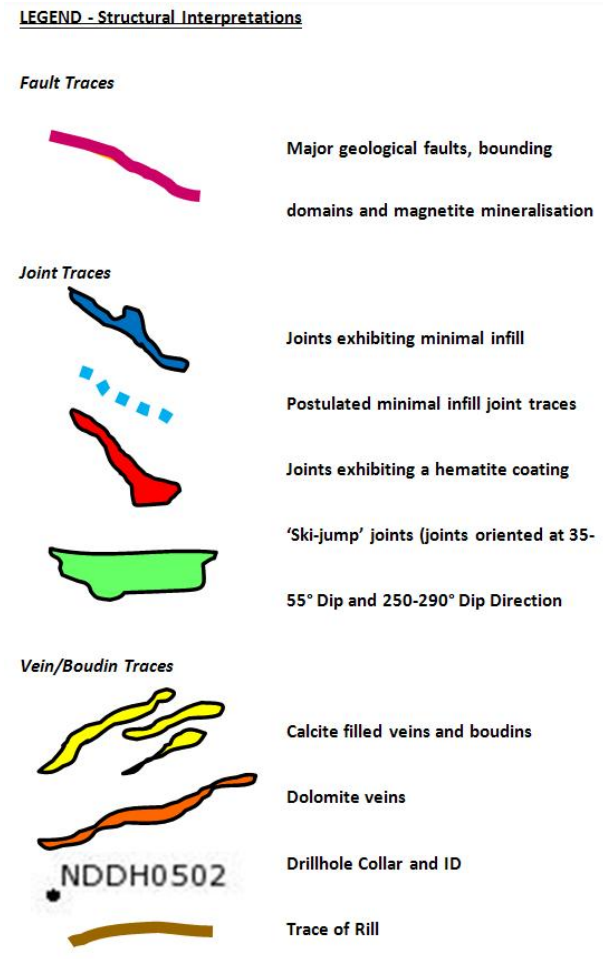

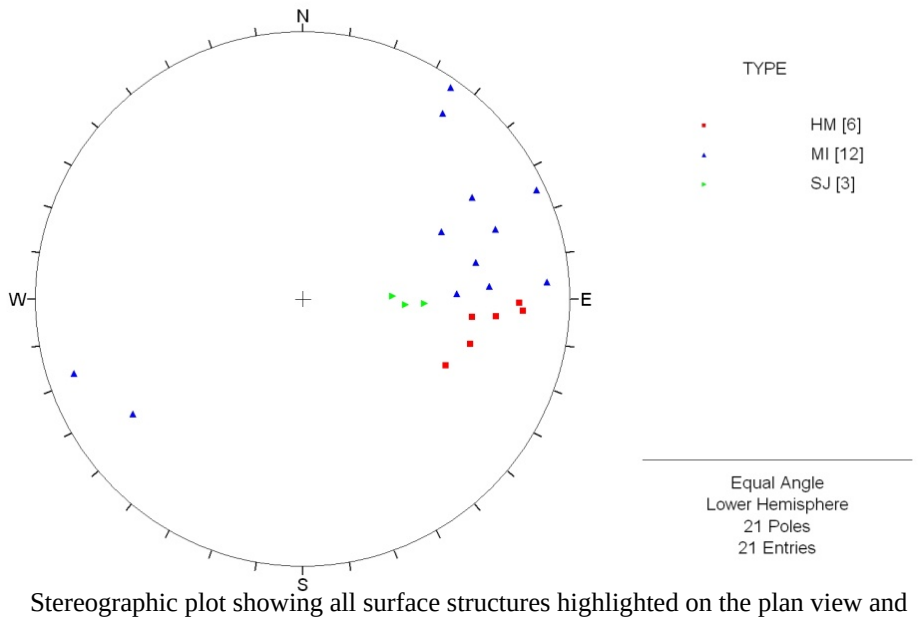

Stereographic plot showing all surface structures highlighted on the plan view and elevation maps of the East Wall. **HM**; Hematite coated Joints, **MI**; Minimal infilled Joints and **SJ**; Ski-Jump Joints.

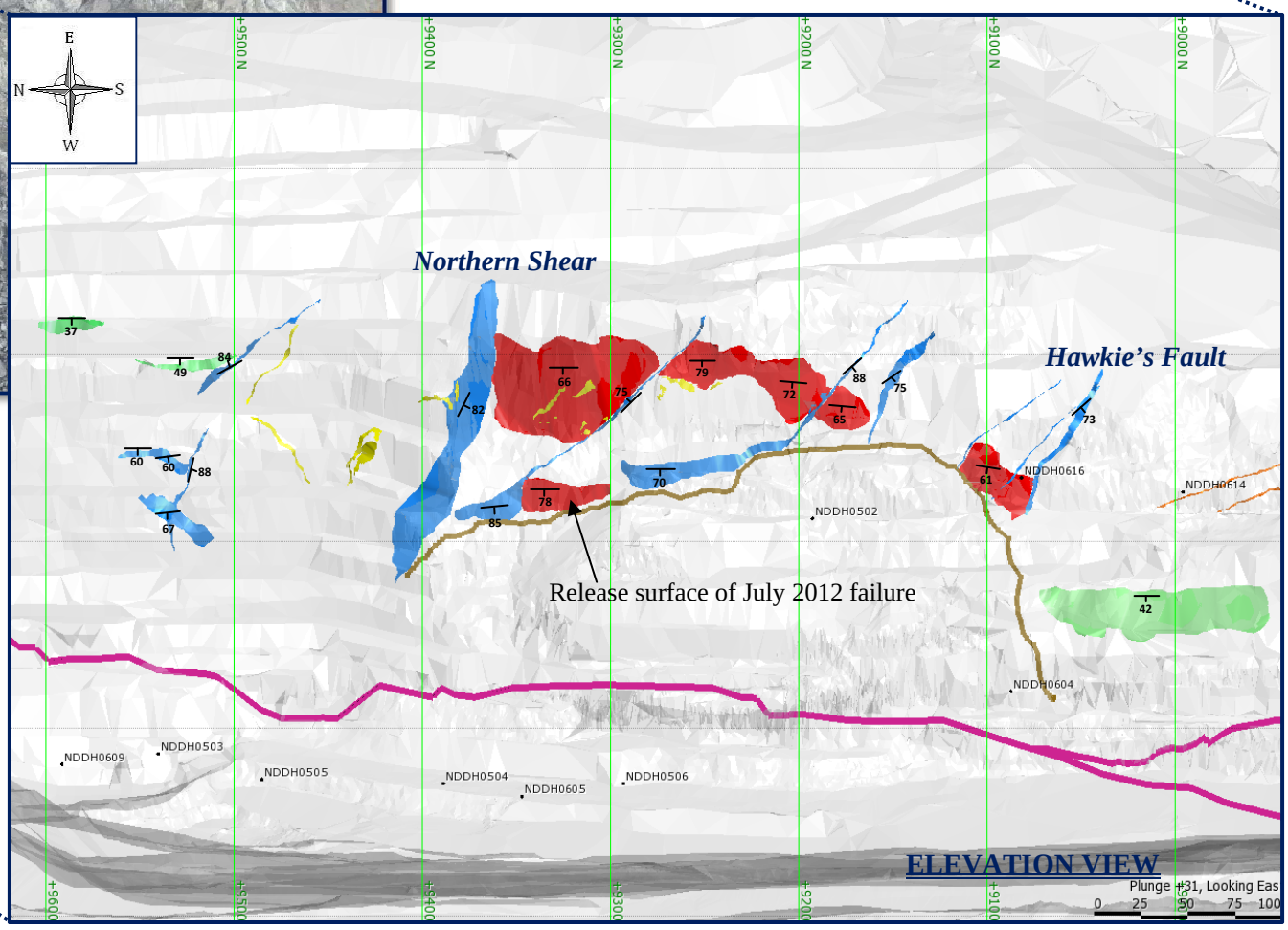

A structural interpretation of the East Wall of North Pit. The elevation map corresponds to the location of the photograph. Structural measurements for each feature are highlighted.

Scale bar is in metres.

Figure 3.28a. Plan view and elevation view showing major features of the east wall and the release surface of the July 2012 failure. Mine nomenclature used for some features (in italics).

NORTH PIT, EAST WALL CROSS SECTIONS

Survey Details; August 2012 End of Month mine surface DTM's utilised.

Leapfrog Mining Software was used for the generation of these sections.

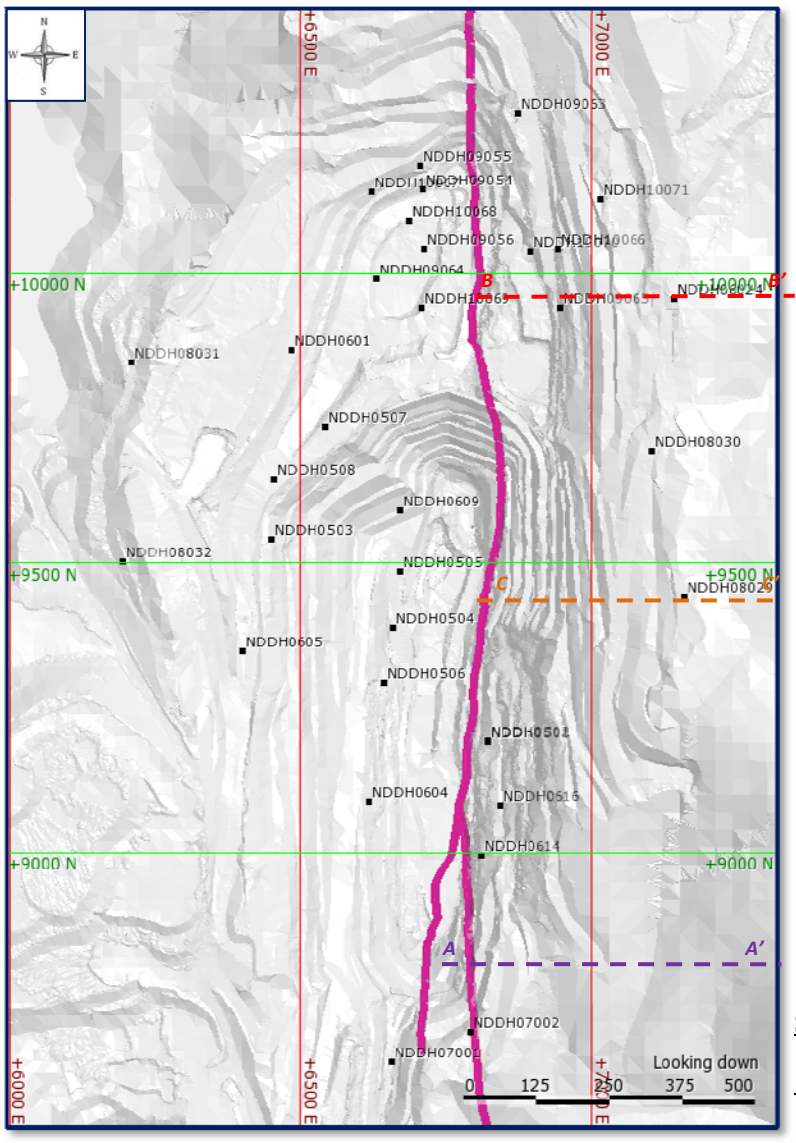

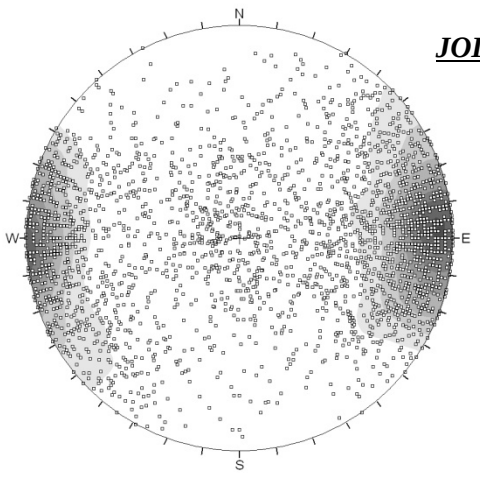

JOINTS

Poles

Equal Angle
Lower Hemisphere
3980 Poles
3980 Entries

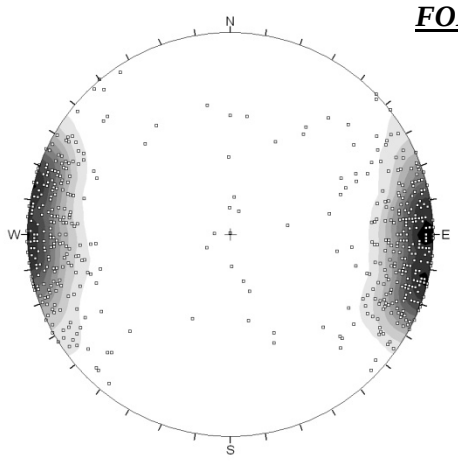

FOLIATION

Poles

Equal Angle
Lower Hemisphere
720 Poles
720 Entries

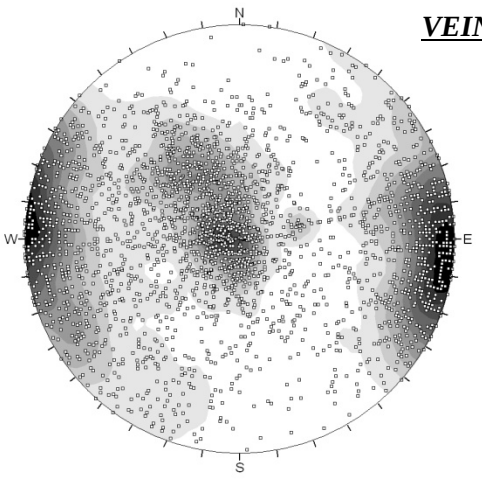

VEINS

Po

Equal Angle
Lower Hemisphere
3740 Poles
3740 Entries

Stereographic projections showing orientation distribution of all joints, veins and foliation on the E Wall. 3DM photogrammetry and the structural results of the 2009-2010 drilling programme borehole logging were used in order to obtain this data.

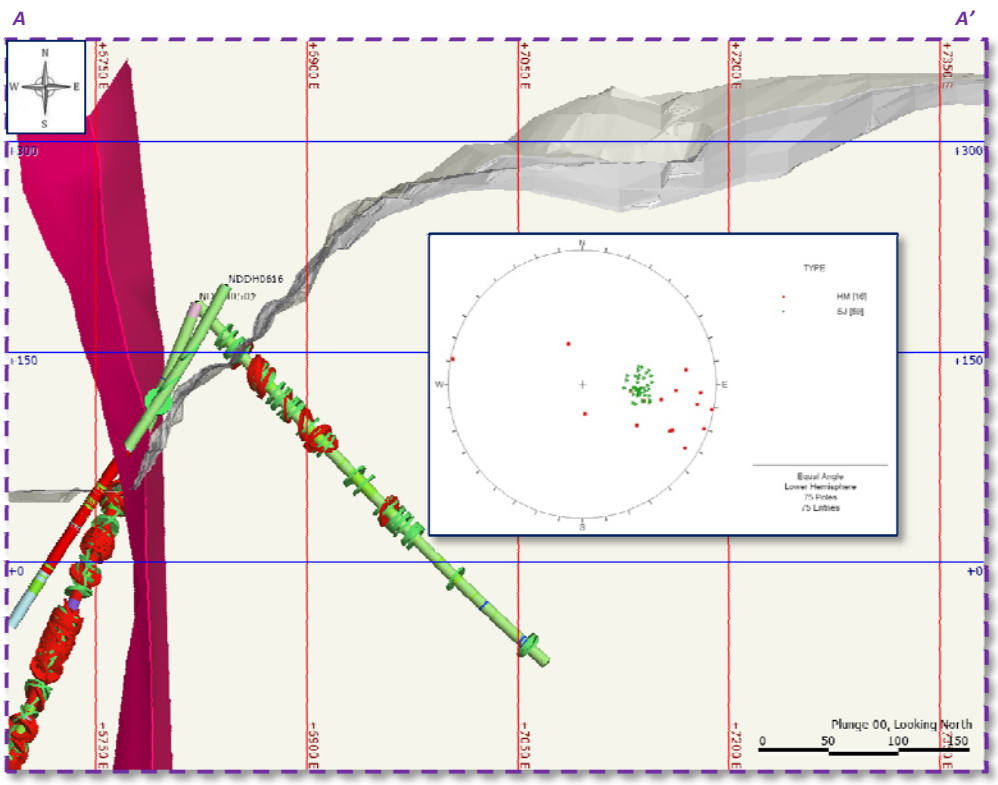

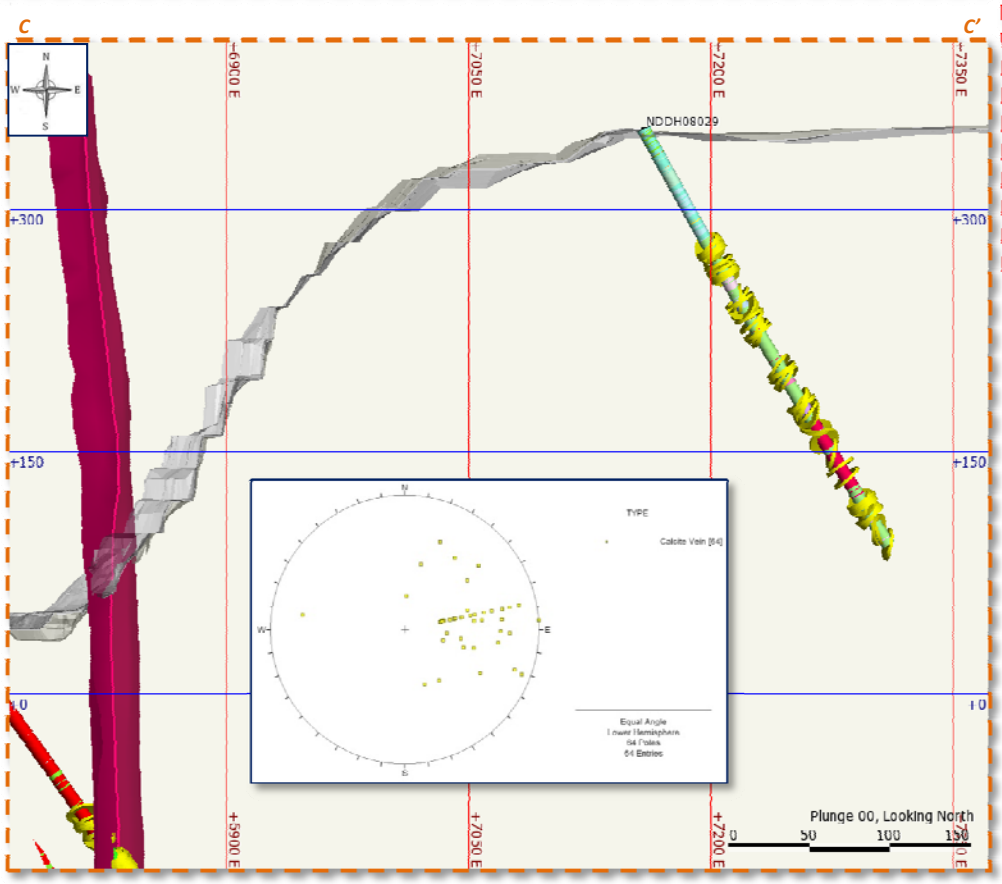

Three cross sections of the E Wall. These sections correspond to the dashed lines on the plan view of North Pit above.

Section ***A-A'*** shows 'ski-jump' joints and hematite joints within drillhole NDDH0502. The corresponding stereonet shows orientation distribution of these joints within this borehole. HM; Hematite coated joints, SJ; 'Ski-jump' joints. Section ***B-B'*** shows foliation trends down-hole in boreholes NDDH0602, NDDH08024, NDDH09065, NDDH10070 and NDDH10071. The corresponding stereonet shows orientation distribution of foliation recorded within these boreholes. Section ***C-C'*** shows calcite vein orientation trend down-hole of borehole NDDH08029. The corresponding stereonet shows calcite vein orientation distribution recorded within this borehole. Scale bars are in metres.

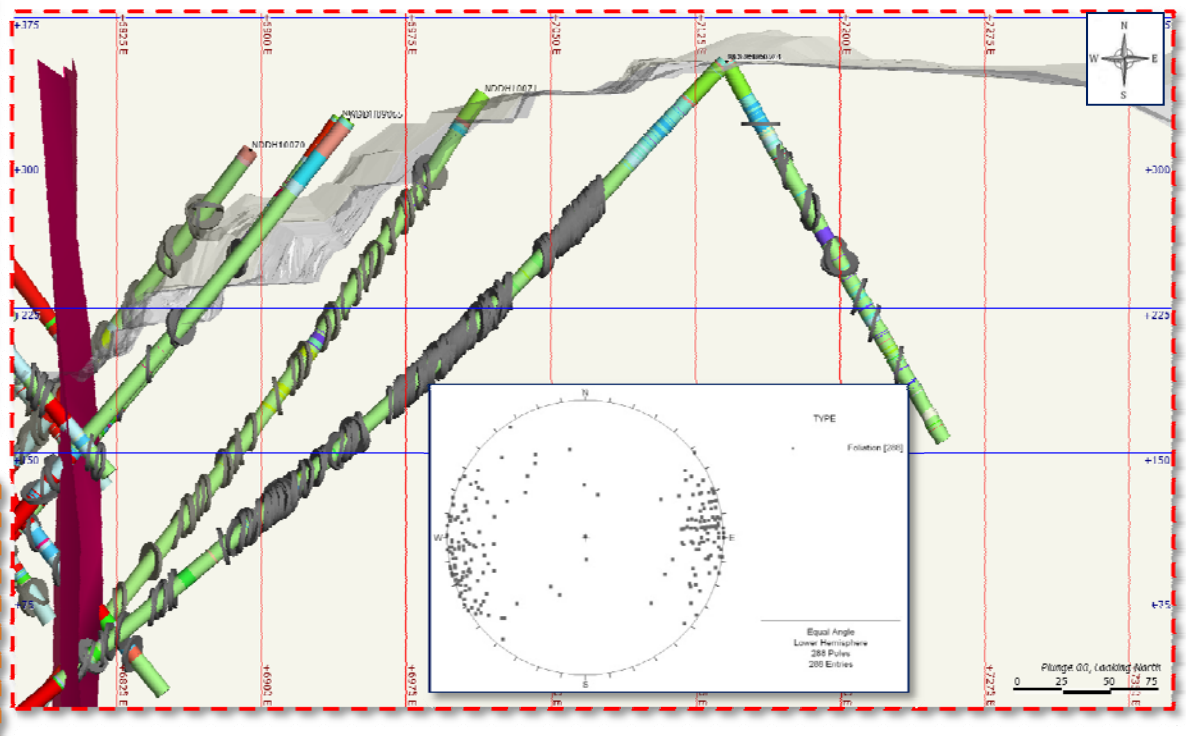

Legend;

- August 2012 Pit Surface
- Eastern Contact Fault
- 'Ski-jump' Joints
- Hematite coated Joints
- Foliation
- Calcite veins/boudins
- NDDH0502 Drillhole collar ID and location

Figure 3.28b. Three stereonets showing all joint, vein and foliation orientations within the East Wall Assemblage and three cross sections showing representative feature distribution throughout the

3.4 Structural Style – Main Host Assemblage

3.4.1 Introduction

The Main Host Assemblage (MHA) hosts the Main Ore Zone (MOZ) and the Western Ore Lens (WOL) in North Pit. Turner (2006) refers to the MHA as being dominated by massive to schistose, fine to coarse grained, mafic, meta-igneous rocks. There are vast compositional variations within what effectively is a fault melange. The deformed, sheared and brecciated nature of this rock mass ensures that the structural and geotechnical properties are spatially variable and complex. This assemblage is continuously excavated for the magnetite it contains, so extensive geological and geotechnical mapping is difficult. A few representative areas of the assemblage have been mapped but drill core information is heavily relied upon for structural and lithological data. Large-scale rock falls and/or multi-berm failures have not occurred within the MHA. The failures that have occurred since 2009 have been smaller than those in the East Wall Assemblage and the failure mechanisms are different. Failure modes of the MHA are discussed in Section 3.4.6.

3.4.2 Joint Characteristics

The key orientation and roughness properties of all joints measured from the MHA are summarised in Table 3.2. Joints are grouped by mineral infill type.

Tremolite and actinolite

Planar, smooth roughness profiles are common on tremolite and actinolite filled joints dipping E at <50°. The orientation data for all other roughness profiles have widely scattered orientations, possibly due to the lack of joints presenting each roughness profile. The undulating and smooth profile is the most common thus meaning the friction angles of these particular joints will be important in some areas of the MHA. Tremolite within the North Pit is soft, fibrous and not compact and therefore is considered to be a low-friction mineral

Infill	% of Joints within the MHA	Orientation Maxima (see Figure 3.29) Dip/Dip Direction (°)	Roughness and %
Tremolite and Actinolite	**5%**	**87/268 60/268 12/084 83/091 (Figure 3.29 – *A*)**	**US – 38% UR – 28% PS – 10% SR – 7% UK – 6% PK – 4% PR – 3% SS - <2.5% SK – 1.5%**
Calcite	**20%**	**84/260 15/265 16/171 (Figure 3.29 – *B*)**	**UR – 33% US – 29% PR – 12% PS – 10% SR – 8% UK – 4% SS – 2% PK - <2% SK - <0.5%**
Chlorite	**11%**	**84/259 (Figure 3.29 – *C*)**	**US – 56% UR – 17% PS – 7% PR – 6% UK – 6% SS – 4% SR – 2% PK – 1% SK – 1%**
Hematite	**10%**	**75/265 12/095 38/183 (Figure 3.29 – *D*)**	**US – 29% UR – 18% UK – 16% PS – 15% PR – 9% PK – 5% SR – 3% SS – 3% SK – 2%**
No Infill	**35%**	**82/266 07/071 (Figure 3.29 – *E*)**	**US – 33% UR – 33% PR – 11% PS – 9% SR – 8% SS – 3% UK – 2% SK – 0.5% PK – 0.5%**

Pyrite	**1.5%**	**75/245** **63/291** **12/090** **(Figure 3.29 – *F*)**	**UR – 34%** **US – 29%** **SR – 12%** **PR – 10%** **PS – 8%** **SS – 2.5%** **UK – 2.5%**
Serpentine	**8%**	**70/261** **87/086** **66/312** **(Figure 3.29 – *G*)**	**US – 52%** **UR – 18%** **UK – 11%** **PS – 7%** **SR – 4.5%** **SS – 3%** **PK – 3%** **PR – 1%** **SK - <0.5%**
Talc	**8%**	**84/266** **82/295** **60/294** **(Figure 3.29 – *H*)**	**US – 51%** **UR – 17%** **PS – 15%** **UK – 5%** **PR – 5%** **SR – 3%** **SS – 3%** **PK – 1%**
Epidote	**0.3%**	**Moderate dips to E and W** **(Figure 3.29 – *I*)**	**UR – 63%** **US – 12.5%** **PR – 12.5%** **SR – 8%** **PS – 4%**
Magnetite	**0.4%**	**Mainly strike NE-SW** **(Figure 3.29 – *J*)**	**UR – 36%** **PR – 17%** **PS – 13%** **SR – 13%** **US – 10%** **UK – 8%** **SS – 3%**
Albite	**0.2%**	**mainly dip NE** **(Figure 3.29 – *K*)**	**PR – 53%** **UR – 24%** **PS – 18%** **US – 5%**
Quartz	**0.07%**	**Only 5 data points** **(Figure 3.29 – *L*)**	**UR – 100%**

Graphite	**0.45%**	**71/250** **45/289** **(Figure 3.29 – *M*)**	**US – 59%** **UR – 14%** **PS – 14%** **UK – 7%** **SR – 3%** **PK – 3%**

Table 3.2 – Summary of the percentage of joints, orientation distribution and joint roughness profile variation of the joints within the MHA.

coating. Actinolite is only differentiated from tremolite by the colour of the mineral in hand specimen; actinolite is dark green within North Pit whereas tremolite occurs as a pale green/white, fibrous infill.

Calcite

The characteristics of calcite filled joints within the MHA are similar to that evident within the East Wall Assemblage. The ratio of calcite coated joints versus all other joints within the MHA is the same as within the East Wall Assemblage. Calcite thickness is variable although the orientation data is more scattered within the MHA compared to the E Wall. However, this could be due to the greater volume of joint data recorded within the MHA. Due to the most common roughness profile being undulating and rough, friction angles will be higher in these areas whereas in areas of planar slickensided joint roughness profiles friction angles will be lower. No trend between joint roughness profiles and orientation distribution was detected.

Chlorite

The orientation of these joints is less variable than all other joint infill mineral type logged within the MHA (Table 3.2). 50% of all the stepped slickensided and planar slickensided joint profiles are dipping ≤57° to the N. The remaining 50% have variable dip, towards the SW. Joints with a planar and smooth profile mainly dip to the W. All other joint roughness profiles have variable orientation. Barton and Bandis failure criterion (1981), originally formulated by

Barton (1973), suggested that first estimates of the peak friction angle of defects can be obtained from the joint roughness and the joint alteration and/or infill. The majority of chlorite filled joints within the MHA are undulating and smooth in profile. Therefore, due to chlorite being a softening or low-friction mineral, the peak friction angle according to this method of estimation will be 25° reducing to 15° on planar, smooth joint roughness profiles. This friction angle is low compared to the estimated friction angle of 45° on undulating and smooth, hematite coated joints of the East Wall Assemblage. Chlorite coated joints of the MHA have high potential for the involvement in failures. Failure mechanisms of the MHA are discussed later in this chapter.

Hematite

Hematite coated joint characteristics of the MHA are very similar to that of the East Wall Assemblage. The most common joint roughness profile is undulating and smooth, with 29% of hematite coated joints of the MHA exhibiting this profile (Table 3.2). This is similar to the East Wall Assemblage (36%). Slickenlines decorate hematite coated joint surfaces of the MHA similar to the same joint type within the East Wall Assemblage. (Kinematic indicators are discussed in Chapter 4, Section 4.2.) Undulating-slickensided roughness profiles of the MHA generally dip to the W. The dip of these structures varies from 03° to 89°. Planar-slickensided joints have a steeper dip, and dip to the SE and NW. All stepped profiles of hematite filled joints dip towards the W, repeating the pattern observed in the East Wall Assemblage. The basic friction angle of decorated joints is decreased due to the polished, undulose nature of the joint surface.

No Infill

Joints exhibiting no infill are the most common within the MHA (35%, Table 3.2). The orientations are most similar to chlorite, and perhaps calcite, filled joints. They exhibit a wide

range of roughness profiles and should not be confused with drilling induced fractures in the drillcore. A variable amount of weathering recognised mainly due to colour variation or the presence of dust/mud is indicative of joints of this type. There is no correlation between joint roughness profile and orientation distribution. According to Barton and Bandis (1981), the friction angle of undulating and smooth joints with unaltered joint walls exhibiting only surface staining is estimated to be 60°. This friction angle will increase if the joints are undulating and rough. These high friction angles reduce the risk of these discontinuities playing a role in stability issues within the MHA.

Pyrite

Pyrite coated joints are relatively uncommon within the MHA (Table 3.2). The planar and smooth joints only dip towards the W. The joints dipping towards the E commonly exhibit undulating, rough and undulating, smooth profiles. The majority of gently dipping joints (<20° dip) exhibit an undulating and rough profile. The pyrite crystals that fill joints within the MHA are up to 2mm in size and cubic, hence the high percentage of undulating and rough joint profiles. There are also smooth pyritic joints, where the pyrite has been smeared along the joint surface, leaving no visible cubic crystals. The smooth pyritic joints are the more common within the East Wall Assemblage and the rough pyritic joints are more common within the MHA. Acid rock drainage is a significant complication for Savage River Mine so characterising different forms of pyrite and their location assists with the long-term acid rock drainage management plan. The majority of pyrite within North Pit is located within the MHA and although a large volume is crushed alongside magnetite, some pyritic coated joints are located outside the ore bodies and become waste rock. The pyrite located within the MHA will probably contribute more to the acid mine drainage than equivalent pyrite in the East Wall Assemblage.

Serpentine

Bottrill and Taheri (2012) state that the serpentine found within the MHA is mostly antigorite and is a common component of mainly medium to high grade ores. There are no trends between joint roughness profile and orientation distribution evident. Due to the serpentine being a softening or low-friction mineral, the basic friction angle of these joints is low; similar to chlorite filled joints of the MHA which were discussed earlier. Although abundant as a mineral in many of the various lithologies of the MHA and also a variety of joint infill and vein, serpentine is not evident within either the East Wall Assemblage or the West Wall Assemblage in lithology, joint infill or vein type.

Talc

Talc infilled joints are also evident within the MHA, with just below 8% of all joints of the MHA exhibiting the mineral as an infill (Table 3.2). There is no trend evident between joint roughness profile and orientation distribution. Similar to chlorite and serpentine coated joints of the MHA, talc is a low-friction mineral and the most common roughness profile is undulating and smooth. Therefore, the basic friction angle of talc infilled joints is estimated at 25° according to Barton and Bandis (1981). Comparable to serpentine, talc is not a mineral evident within the lithologies, joint or vein infill within the East Wall Assemblage and was only found as a joint infill within the MHA and West Wall Assemblage.

Epidote

Only 0.3% of joints within the MHA are infilled with epidote (Table 3.2). Epidote is uncommon within the MHA and the areas of epidote infilled joints and veining occur within mafic lithologies within the MHA. With only 24 measured joints, the orientation is not well defined but only 25% of these have steep W dips which is very different from all the more common joint types discussed above. No joints dip more than 55° to the S; or more than 50°

to the N. The epidote joint infill within North Pit is pistachio green in colour and coarse; usually as prismatic crystals. It is commonly visible near to hematite coated joints. Due to the coarsely crystalline habit of the epidote, 83% of joints have a rough profile with the remainder exhibiting a smooth profile. Rough profiles increase the basic friction angles of these joints. According to Barton and Bandis (1981), the estimated friction angle of joints displaying a non-softening, impermeable filling much like epidote is 70° on rough and undulating joints. This figure reduces to 65° on undulating and smooth joint profiles. However as epidote infilled joints are rare, and the friction angles are relatively high, they do not present potential major instability issues for the mine.

Magnetite

0.4% of all joints within the MHA are magnetite coated (Table 3.2). Although the volume of joints is low compared to other joint data within the MHA, orientation data is anomalous in the high proportion of joints that strike NE-SW and mainly dip to 310° (Figure 3.29). Magnetite coated joints are tightly healed and due to the crystalline nature of the mineral, are impermeable. The planar and smooth joints mainly dip <45° towards the NW. There is no other trend evident between joint roughness profile and joint orientation. The friction angle estimation method devised by Barton and Bandis (1981) states that even with an undulating and slickensided joint profile where some movement has previously occurred, the friction angle of joints exhibiting non-softening infill such as magnetite is only reduced to 60°.

Albite

Only 0.2% of these joints exhibited an albite infill (Table 3.2). Conclusions about orientation distribution are therefore difficult due to the small volume of data available. However, 59% of albite infilled joints were recorded dipping ≤40°. The majority of joints are dipping towards the E or NE. The dip and dip direction of these joints are therefore very different to that of

other mineral infill; which are dominated by steep dips to the W. Similar to epidote and magnetite, albite is a non-softening mineral and with the majority of albite infilled joints being rough, the friction angle of these joints is increased. Although albite is common within joints of the West Wall Assemblage and East Wall Assemblage, it is rare within the MHA. When evident within the MHA, albite is usually found associated with epidote in mafic lithologies.

Quartz

Bottrill and Taheri (2012) state that quartz is absent in most of the MHA, but may locally be a major component (<40%) of some talc rich rocks, dolostones and magnesite-stones, plus some veins. Therefore it is not surprising that only 0.07% of all the joints within the MHA are quartz filled (Table 3.2). All five joints exhibit an undulating and rough profile. Similar to epidote, magnetite and albite, quartz is a hard, impermeable mineral resulting in tightly healed joints. Friction angles of these joints will be close to 70° (Barton and Bandis, 1981).

Graphite

0.45% of all joints within the MHA are graphite coated (Table 3.2). Although evident within all assemblages of the North Pit, the volume of graphite coated joints is low. There is no distinctive orientation features visible in this limited dataset. Spatial distribution of graphite joints will be discussed in the next section in an attempt to compare the distribution of these joints to the distribution of graphite within the East Wall Assemblage (clustered close to the Eastern Contact Fault).

Summary

- Joints exhibiting no infill are the most common within the MHA which is comparable to the East Wall Assemblage. Chlorite and perhaps calcite filled joints have a similar orientation to joints with no infill.
- Actinolite/tremolite, serpentine, talc, pyrite and perhaps hematite filled joints have very similar patterns of joint orientation. These joint fills probably reflect the host rock composition.
- Calcite and hematite filled joints have a much higher proportion of sub-horizontal joints than other groups.
- Epidote, magnetite, albite, quartz and graphite infilled joints are rare within the MHA.
- All joints within the MHA have a common orientation; steeply dipping (≥70°) to the W with the exception of albite filled joints. Due to the small volume of albite coated joint data, sampling bias could be to blame for this potentially ambiguous result.
- Although the orientation of joints within the MHA are more scattered than the East Wall Assemblage, the common orientation is similar.
- The softening, impermeable mineral infills such as talc, graphite and tremolite exhibit the highest ratio of undulating and smooth roughness profiles which decreases friction angles and increases the risk of failure along these discontinuities.
- The tightly healed, hard and non-softening mineral infills such as quartz, pyrite and magnetite exhibit the highest ratio of undulating and rough joint profiles which increases friction angles and decreases the risk of failure along these discontinuities.
- Undulating profiles are the most common for joints within the MHA.

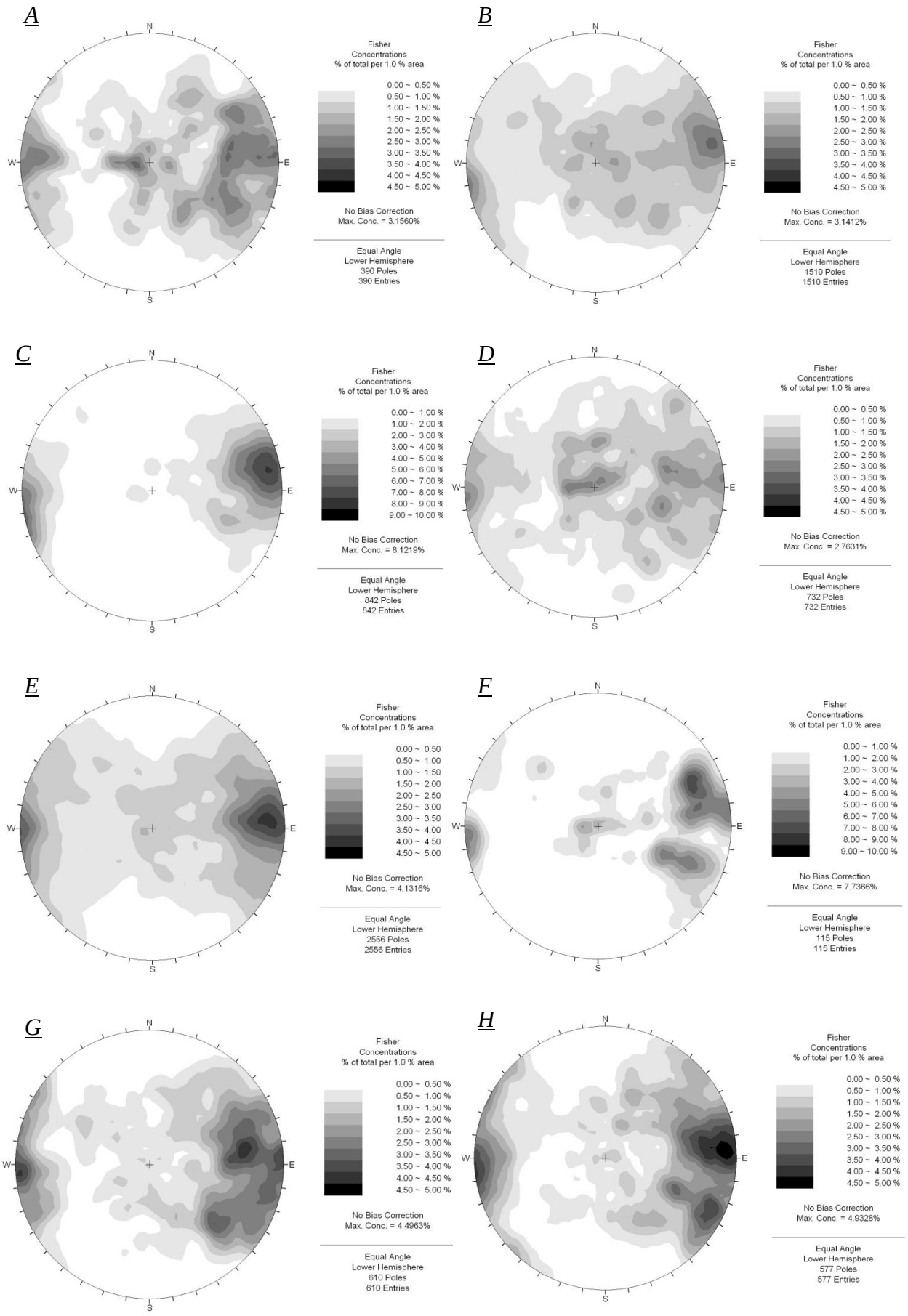
A
N
W
E
S
Fisher
Concentrations
% of total per 1.0 % area
0.00 ~ 0.50 %
0.50 ~ 1.00 %
1.00 ~ 1.50 %
1.50 ~ 2.00 %
2.00 ~ 2.50 %
2.50 ~ 3.00 %
3.00 ~ 3.50 %
3.50 ~ 4.00 %
4.00 ~ 4.50 %
4.50 ~ 5.00 %
No Bias Correction
Max. Conc. = 3.1560%
Equal Angle
Lower Hemisphere
390 Poles
390 Entries
B
N
W
E
S
Fisher
Concentrations
% of total per 1.0 % area
0.00 ~ 0.50 %
0.50 ~ 1.00 %
1.00 ~ 1.50 %
1.50 ~ 2.00 %
2.00 ~ 2.50 %
2.50 ~ 3.00 %
3.00 ~ 3.50 %
3.50 ~ 4.00 %
4.00 ~ 4.50 %
4.50 ~ 5.00 %
No Bias Correction
Max. Conc. = 3.1412%
Equal Angle
Lower Hemisphere
1510 Poles
1510 Entries
C
N
W
E
S
Fisher
Concentrations
% of total per 1.0 % area
0.00 ~ 1.00 %
1.00 ~ 2.00 %
2.00 ~ 3.00 %
3.00 ~ 4.00 %
4.00 ~ 5.00 %
5.00 ~ 6.00 %
6.00 ~ 7.00 %
7.00 ~ 8.00 %
8.00 ~ 9.00 %
9.00 ~ 10.00 %
No Bias Correction
Max. Conc. = 8.1219%
Equal Angle
Lower Hemisphere
842 Poles
842 Entries
D
N
W
E
S
Fisher
Concentrations
% of total per 1.0 % area
0.00 ~ 0.50 %
0.50 ~ 1.00 %
1.00 ~ 1.50 %
1.50 ~ 2.00 %
2.00 ~ 2.50 %
2.50 ~ 3.00 %
3.00 ~ 3.50 %
3.50 ~ 4.00 %
4.00 ~ 4.50 %
4.50 ~ 5.00 %
No Bias Correction
Max. Conc. = 2.7631%
Equal Angle
Lower Hemisphere
732 Poles
732 Entries
E
N
W
E
S
Fisher
Concentrations
% of total per 1.0 % area
0.00 ~ 0.50
0.50 ~ 1.00
1.00 ~ 1.50
1.50 ~ 2.00
2.00 ~ 2.50
2.50 ~ 3.00
3.00 ~ 3.50
3.50 ~ 4.00
4.00 ~ 4.50
4.50 ~ 5.00
No Bias Correction
Max. Conc. = 4.1316%
Equal Angle
Lower Hemisphere
2556 Poles
2556 Entries
F
N
W
E
S
Fisher
Concentrations
% of total per 1.0 % area
0.00 ~ 1.00 %
1.00 ~ 2.00 %
2.00 ~ 3.00 %
3.00 ~ 4.00 %
4.00 ~ 5.00 %
5.00 ~ 6.00 %
6.00 ~ 7.00 %
7.00 ~ 8.00 %
8.00 ~ 9.00 %
9.00 ~ 10.00 %
No Bias Correction
Max. Conc. = 7.7366%
Equal Angle
Lower Hemisphere
115 Poles
115 Entries
G
N
W
E
S
Fisher
Concentrations
% of total per 1.0 % area
0.00 ~ 0.50 %
0.50 ~ 1.00 %
1.00 ~ 1.50 %
1.50 ~ 2.00 %
2.00 ~ 2.50 %
2.50 ~ 3.00 %
3.00 ~ 3.50 %
3.50 ~ 4.00 %
4.00 ~ 4.50 %
4.50 ~ 5.00 %
No Bias Correction
Max. Conc. = 4.4963%
Equal Angle
Lower Hemisphere
610 Poles
610 Entries
H
N
W
E
S
Fisher
Concentrations
% of total per 1.0 % area
0.00 ~ 0.50 %
0.50 ~ 1.00 %
1.00 ~ 1.50 %
1.50 ~ 2.00 %
2.00 ~ 2.50 %
2.50 ~ 3.00 %
3.00 ~ 3.50 %
3.50 ~ 4.00 %
4.00 ~ 4.50 %
4.50 ~ 5.00 %
No Bias Correction
Max. Conc. = 4.9328%
Equal Angle
Lower Hemisphere
577 Poles
577 Entries

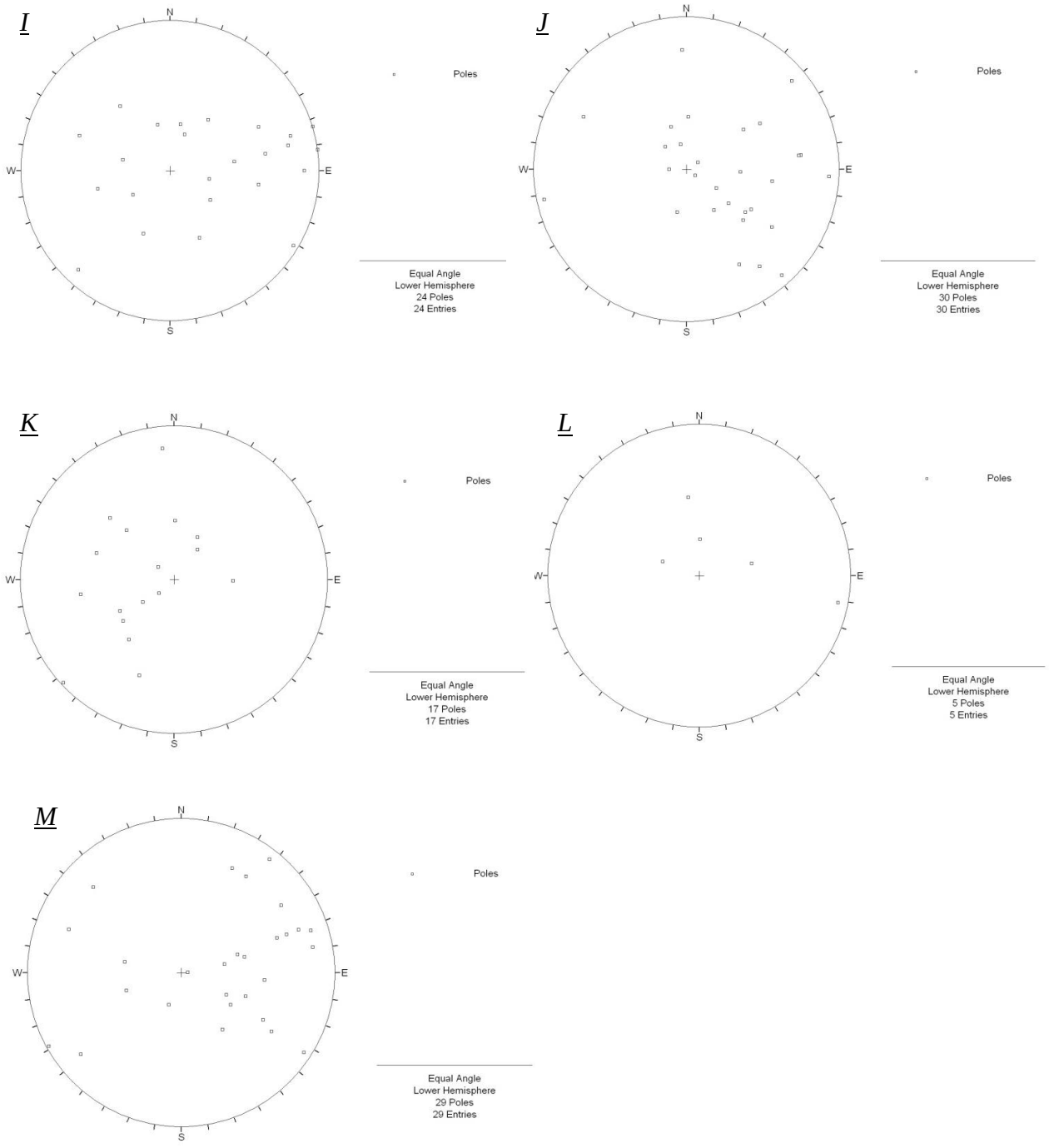

Figure 3.29. Thirteen stereographic projections showing orientation distribution of joints exhibiting different infill minerals within the Main Host Assemblage. Stereonets with more than fifty poles are shown as contoured plots; stereonets with less than fifty poles are shown as pole plots. Mineral infill; *A*- Tremolite and Actinolite; *B*- Calcite; *C*- Chlorite; *D*- Hematite; *E*- No Infill; *F*- Pyrite; *G*- Serpentinite; *H*- Talc; *I*- Epidote; *J*- Magnetite; *K*- Albite, *L*- Quartz and *M* - Graphite.

3.4.3 Spatial Distribution of Joints

Information into the spatial distribution of joints within the MHA is of importance for future mine planning. Although much of the MHA is excavated to liberate the magnetite ore, it is important to understand the structural and geotechnical properties of the assemblage in order to predict rock mass behaviour for final pit wall planning. This section offers a number of cross sections produced using the mining software, Leapfrog™. Figure 3.30 shows a Leapfrog™ model plan view of North Pit indicating the representative cross sections used to highlight spatial distribution trends of the joints within the MHA.

Tremolite and Actinolite

Tremolite and actinolite coated joints are found only within the Main Ore Zone (MOZ). Turner (2006) describes the MOZ within the North Pit as the largest ore body within the mining lease. The boundaries of the MOZ are steeply dipping and the ore body becomes wider with depth. The mineralisation is fairly massive and continuous which contrasts with the Southern part of Centre Pit South where the mineralisation occurs as relatively thin lodes separated by barren silicate rocks (Turner, 2006). Other ore occurrences in the MHA range between these extremes. Within the MOZ and WOL, there are three codes used when describing mineralisation. These are; A-Abundant (DTR 65% to 100%), M-Moderate (DTR 35% to <65%) and S-Sparse (DTR 15% to <35%). DTR stands for Davis Tube Recovery, the method employed at Savage River to test magnetite content. Tremolite and actinolite coated joints are clustered mainly in areas of abundant mineralisation with associated serpentine gangue. They are also evident, albeit to a much lesser extent, in areas of abundant mineralisation with associated talc gangue, moderately mineralised lithology with associated serpentine gangue, barren metabasic lithologies and barren talc-rich lithologies. Tremolite and actinolite coated joints are not evident within mineralised lithologies with associated

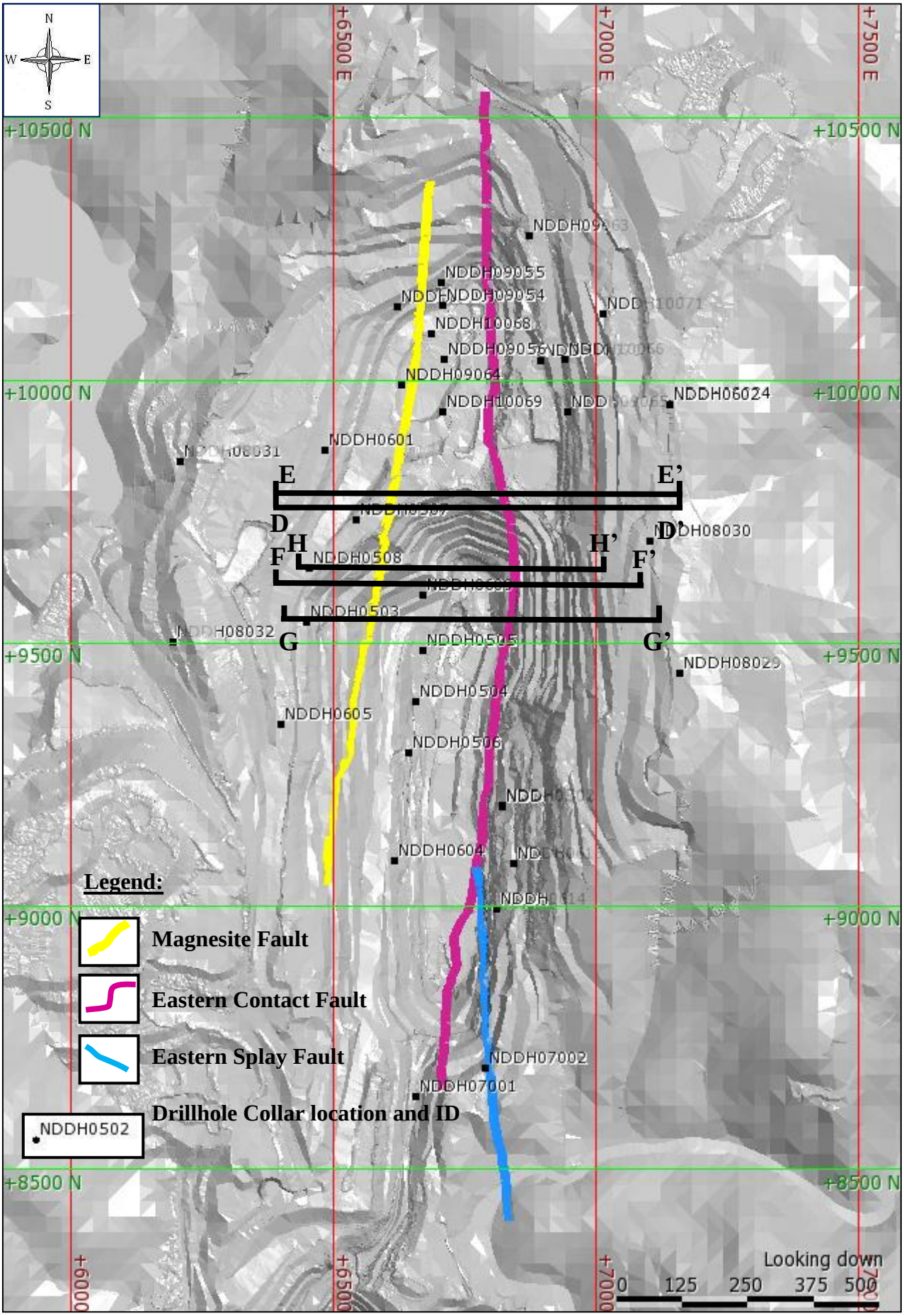

Figure 3.30 – Plan view of North Pit showing major fault traces, drillhole location and cross section locations.

pyrite and chlorite. They only occur within the MOZ and not within the WOL which is proximal to the Magnesite Fault. The distribution of these joints is based on lithology and not proximity to large-scale faults i.e. the joint concentration does not increase near the Eastern Contact Fault or the Magnesite Fault (Figure 3.31).

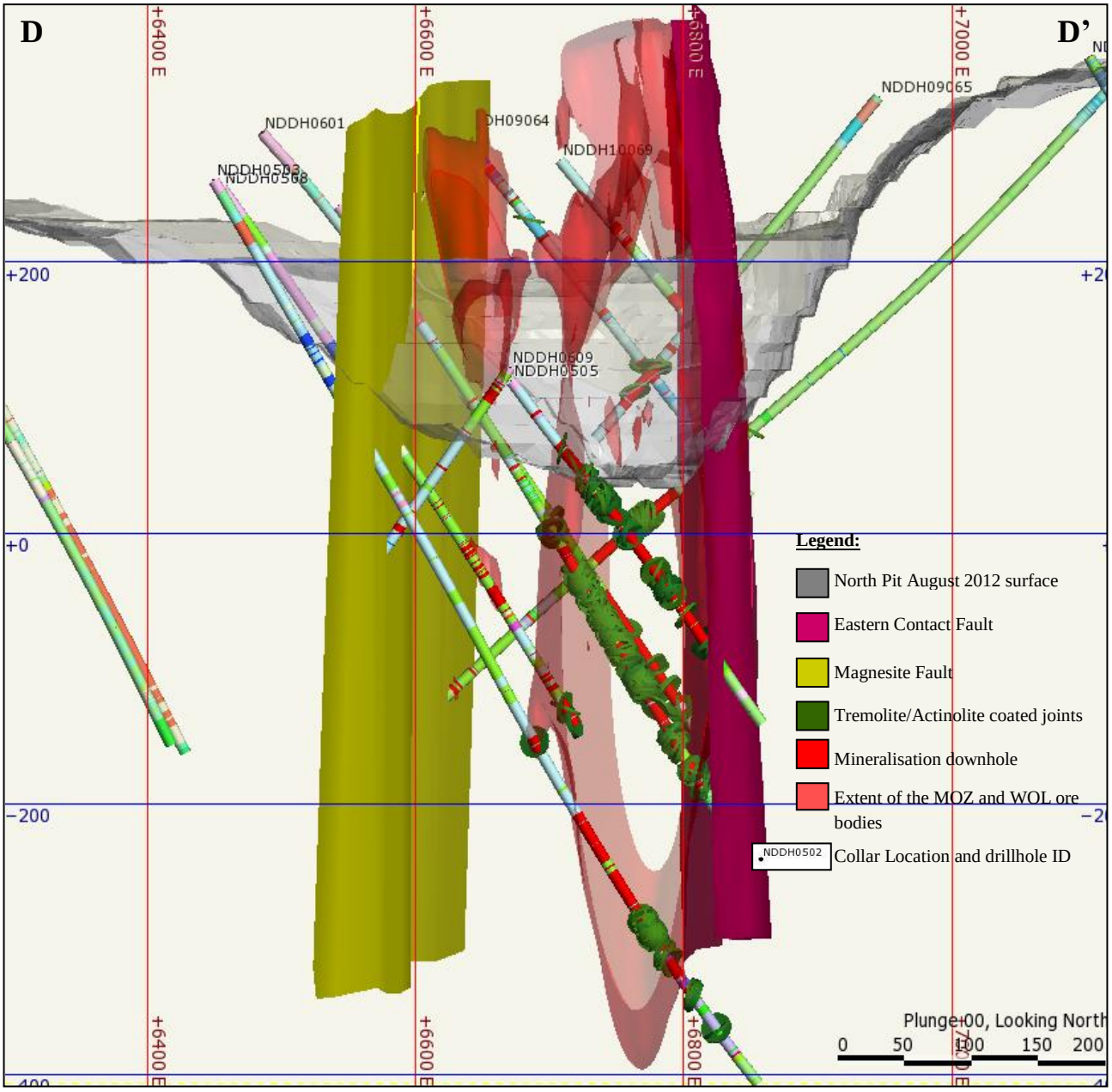

Figure 3.31. Cross Section D-D' showing the position of tremolite/actinolite coated joints as dark green discs down-hole. *Section: 9708 m N (looking N).* Refer to digital Appendix 8 for a complete lithological legend.

Calcite

Calcite coated joints of the MHA are distributed throughout the assemblage. The MOZ and the WOL both contain a large number of calcite coated joints. However, calcite filled joints are very rare within metamafic lithologies of the MHA as well as chlorite and talc rich areas thus suggesting the calcite coated joints are limited to lithologies containing some carbonate. The carbonate is likely to be the most soluble mineral within the lithology therefore the fluid circulating through the joint is probably locally buffered.

Chlorite

Chloritic joints are common within barren metamafic lithologies rich in chlorite. Approximately 20% of chlorite coated joints are found within the MOZ, within areas of abundant mineralisation with associated serpentine gangue. Due to the increase in metamafic lithologies rich in chlorite, the volume of chlorite coated joints increases towards the W of the MOZ and E of the Magnesite Fault (Figure 3.32).

Hematite

Hematite coated joints have the same distribution as calcite coated joints; regularly distributed throughout all lithologies of the MHA regardless of mineralisation. Mafic areas have less frequent hematite coated joints. This is very different to the East Wall Assemblage; where hematite coated joints are prevalent close to the Eastern Contact Fault (≤143 m). The presence of joints with hematite infill in lithologies with no matrix hematite could be due to an influx of an oxidised fluid such as meteoric water. All other elements concentrated in the joints seem to be locally sourced e.g. calcite filled joints are common within carbonate rich rock types.

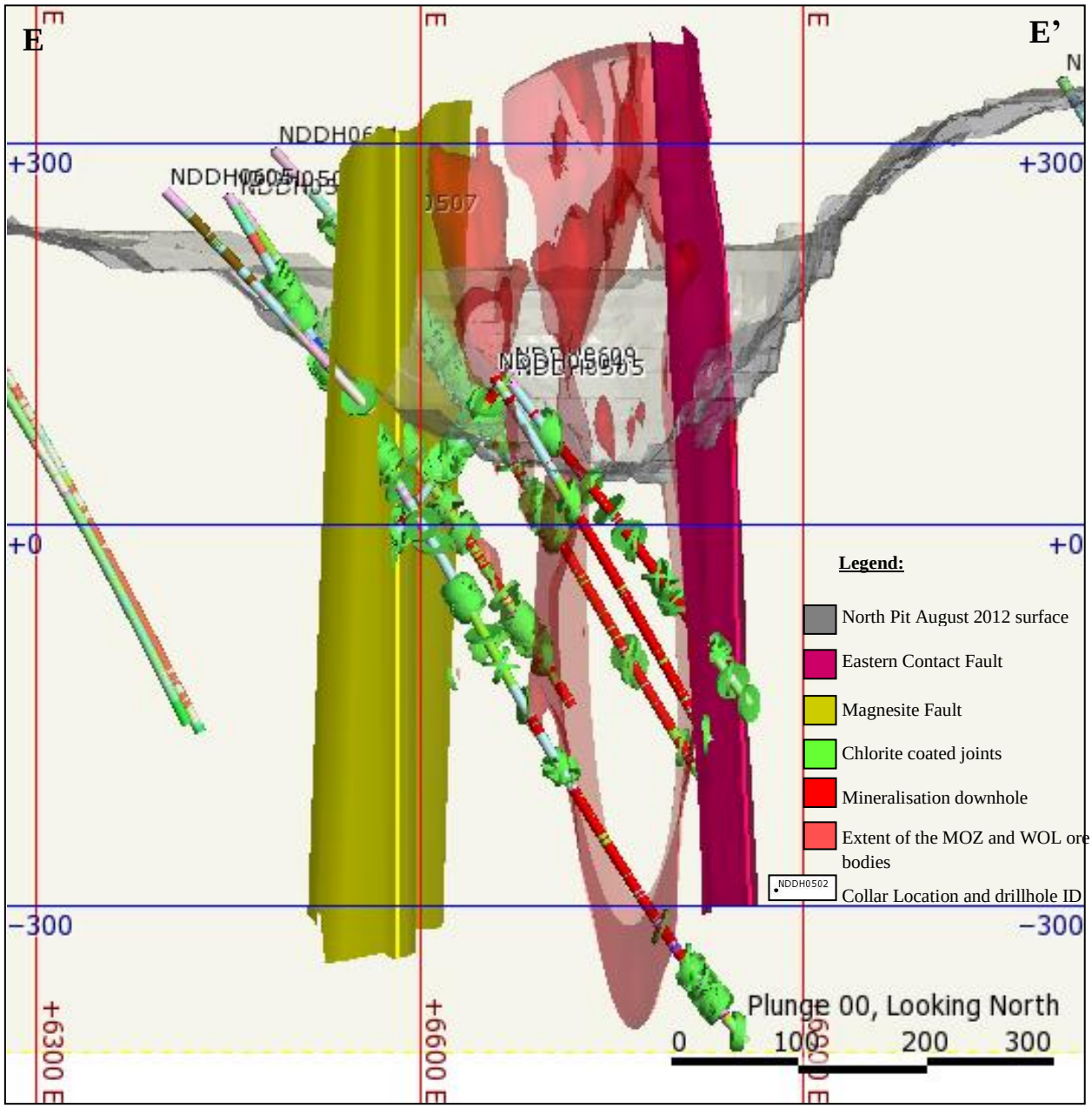

Figure 3.32. Cross Section E-E' showing the position of chlorite coated joints within the MHA; as light green discs down-hole. *Section: 9741 m N (looking N).* Refer to digital Appendix 8 for a complete lithological legend.

No Infill

Joints exhibiting no infill are distributed regularly throughout the MHA and are not lithologically controlled. Down-hole, the joints are regularly spaced regardless to rock type or the proximity to large structural features.

Pyrite

Pyrite coated joints are distributed within both mineralised and barren lithologies (Figure 3.33). More than 50% however are located within the "abundantly mineralised" zones of the MOZ and WOL with associated serpentine and pyrite gangue. Pyrite is disseminated throughout mineralised zones of the MOZ and WOL. The barren lithologies hosting pyrite filled joints include mafic assemblages and chloritic schists; the former have more discontinuities of this nature.

Serpentine

The serpentine coated joints are largely found in the high grade, serpentinitic magnetite ore of the MOZ (Figure 3.33). Less than 10% of these joints occur within barren lithologies such as chloritic schists.

Talc

Talc filled joints of the MHA are concentrated mainly within the MOZ. Within the MOZ, the talc joints are regularly spaced within high grade to low grade, serpentinitic, talcose and tremolitic magnetite ore (Figure 3.34). A few talc filled joints were found within some metamafic lithologies of the MHA.

Epidote

Comparable to the East Wall Assemblage, epidote coated joints of the MHA are spatially correlated with hematite coated joints. Epidote also requires Fe^{3+} and this correlation probably reflects more oxidising conditions. Although common within the MOZ, these joints are also visible within the small (<20 m) intervals of barren metamafic lithologies within small mineralised lenses outside the ore. To the W, epidote coated joints are again visible within mafic assemblages. The mineral is disseminated within the mafic rocks of the MHA.

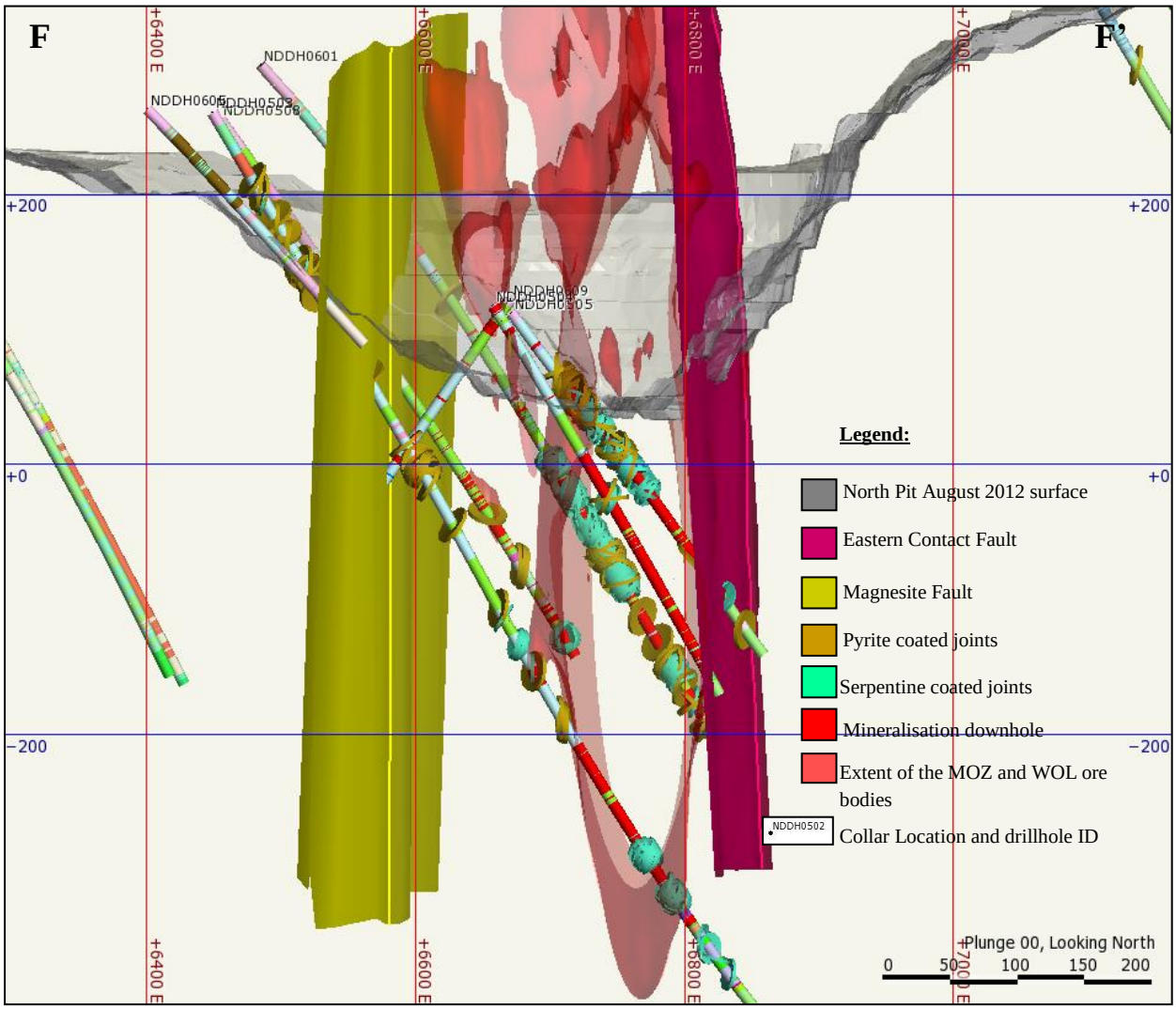

Figure 3.33. Cross Section F-F' showing the position of pyrite and serpentine coated joints within the MHA; as gold and aqua blue discs down-hole respectively. *Section: 9600 m N (looking N).* Refer to digital Appendix 8 for a complete lithological legend.

Magnetite

Although not a common joint infill within any rock packages of North Pit, magnetite coated joints are distributed within the MOZ, within high grade magnetite ore (Figure 3.34). Therefore the fluid responsible for this joint infill is locally buffered, sourced directly from the country rock.

Graphite

The graphite coated joints of the MHA occur proximal to large scale structures (Figure 3.34). A concentration of graphitic joints was found within the MOZ immediately W of the Eastern Contact Fault within Stage 1. Several joints are apparent near the Magnesite Fault to the W within graphitic rich and chlorite rich lithologies of the MHA. There are also several graphitic joints bounding the western edge of the MOZ and the barren lithologies to the W (Figure 3.34).

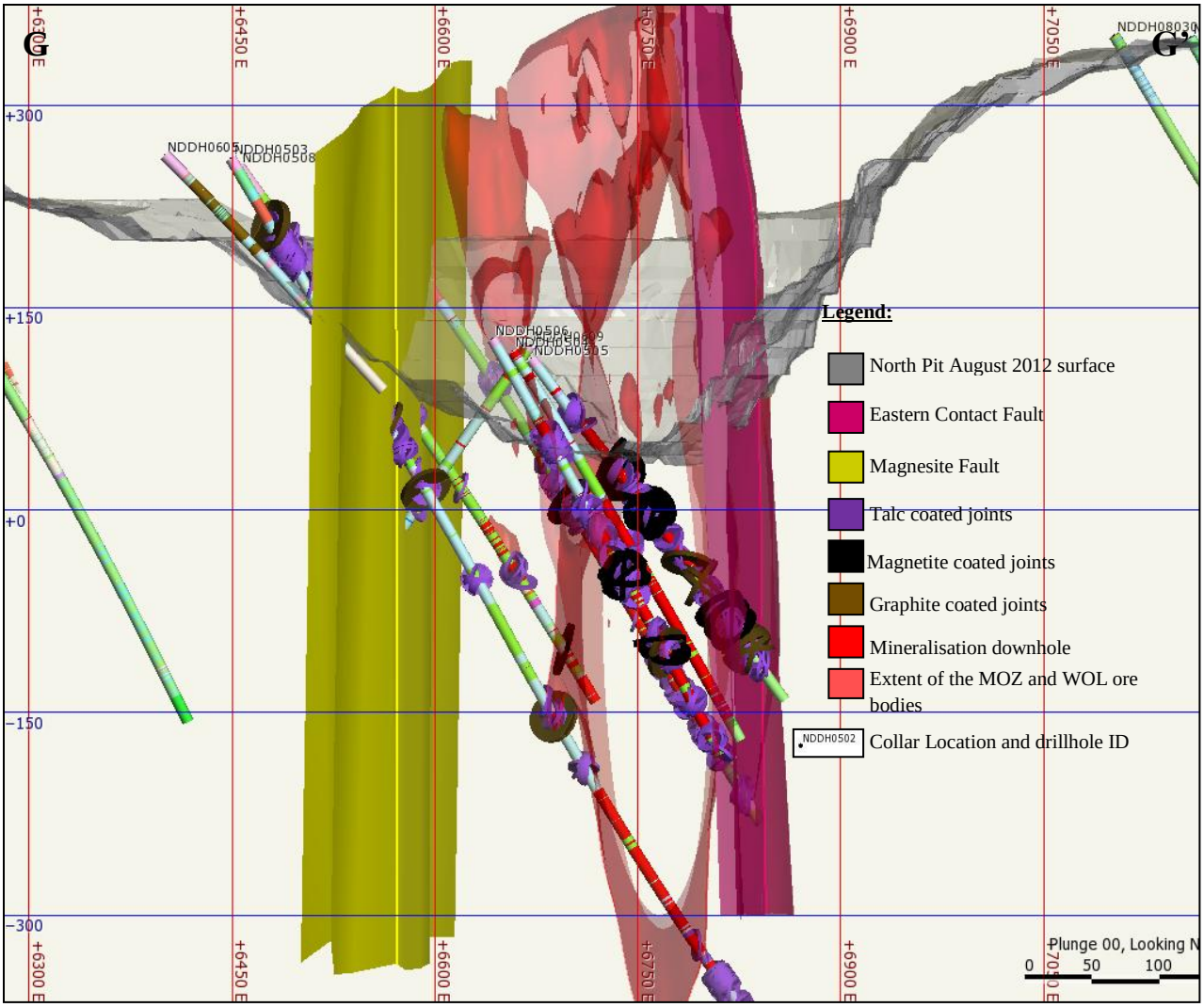

Figure 3.34. Cross Section G-G' showing the position of talc, magnetite and graphite coated joints within the MHA; as purple, black and dark brown discs down-hole respectively. *Section: 9551 m N (looking N).* Refer to digital Appendix 8 for a complete lithological legend.

Albite and Quartz

Joints infilled with quartz or albite are rare within the MHA as described in Section 3.4.2. Spatially, these joints occur within metamafic assemblages of the MHA. They do not occur within mineralised zones, talc rich, chlorite rich, carbonate rich or pyrite rich assemblages.

3.4.4 Vein characteristics and Spatial Distribution

Two thousand individual veins have been logged from drill core since 2005 from the MHA in North Pit. Table 3.3 highlights the percentage of veins within the MHA relating to various infills, orientation and thickness. Figure 3.35 displays a series of stereographic projections of each vein infill type. Figure 3.36 are photographs of the samples sent to MRT laboratories for XRD analysis and Figure 3.38 are photographic examples of vein types within the MHA.

Calcite is the most common vein infill within the MHA, similar to the East Wall Assemblage. Both assemblages are dominated by gently E dipping calcite veins. The East Wall Assemblage however has some calcite veins that dip steeply to the W. Veins with this orientation are rare within the MHA. Calcite veins (and magnesite veins) are the thickest vein type within the MHA. Specular hematite, talc and magnesite commonly occur as accessory minerals with the calcite veins. Calcite veins are regularly spaced throughout all lithologies of the MHA. Evident within the MOZ, WOL and barren lithologies of the MHA, the distribution of calcite veins is similar to the distribution of calcite coated joints within the assemblage. Due to the veins being sub-horizontal, they present little concern for potential slope stability/geotechnical issues on the mine.

A vein sample located within the MHA in Stage 2 was sent to Mineral Resources Tasmania to verify vein infill composition. The sample was pink in colour (Figure 3.36 – **A**) and the

Infill	% of veins within the MHA	Orientation Maxima (see Figure 3.35) Dip/ Dip Direction (°)	Vein Thickness (cm)
Calcite	**62%**	**12/090 (Figure 3.35 – *A* and Figure 3.37 - B)**	**<0.01 – 28**
Chlorite	**3%**	**81/262 (Figure 3.35 – *B*)**	**<0.01 - 4.9**
Epidote	**3%**	**80/274, 55/274 (Figure 3.35 – *C* and Figure 3.37 - A)**	**<0.01 – 3.5**
Hematite	**7%**	**Scattered data – Average; 28/085 and 74/270 (Figure 3.35 – *D* and Figure 3.37 – B and C)**	**<0.01 - 5**
Quartz	**4%**	**52/071 (Figure 3.35 – *E*)**	**0.5 - 5**
Serpentine	**7%**	**Scattered data – Average; 70/312 and 15/012, 30/000 (Figure 3.35 – *F*)**	**0.5 - 10**
Talc	**4%**	**68/235 (Figure 3.35 – *G*)**	**0.5 - 10**
Tremolite	**4%**	**Scattered data – Average; 81/270, 70/115 and 10/255 (Figure 3.35 – *H*)**	**0.5 – 5.2**
Actinolite	**1.4%**	**Broad range – Average; shallow dips (Figure 3.35 – *I* and Figure 3.37 - D)**	**0.5 – 1.2**
Albite	**0.1%**	**2 points only (Figure 3.35 – *J*)**	**0.5 – 2.5**
Magnesite	**1.5%**	**64/271 (Figure 3.35 – *K*)**	**<0.01 - 29**
Magnetite	**1.5%**	**80/259 (Figure 3.35 – *L*)**	**<0.01 – 2.8**

Pyrite	**1.5%**	**83/252 (Figure 3.35 – *M*)**	**<0.01 – 1.3**

Table 3.3 – Summary of the percentage of veins, orientation distribution and vein thickness variation of the diverse range of veins within the MHA.

results confirmed the vein to be calcite possibly with minor Fe or Mn. Another two samples from the MHA were sent for XRD analysis. One sample of the host lithology (Figure 3.36 – **B**) and the other sample from the enclosed vein (Figure 3.36 – **C**). The results confirmed initial predictions that the lithology is chlorite and dolomite rich with minor talc, tourmaline and quartz. Quartz and dolomite are the main vein minerals with lesser amounts of chlorite, talc and pyrite. Refer to digital Appendix 9 for XRD results and Section 3.3.2 for a full description of the XRD analysis.

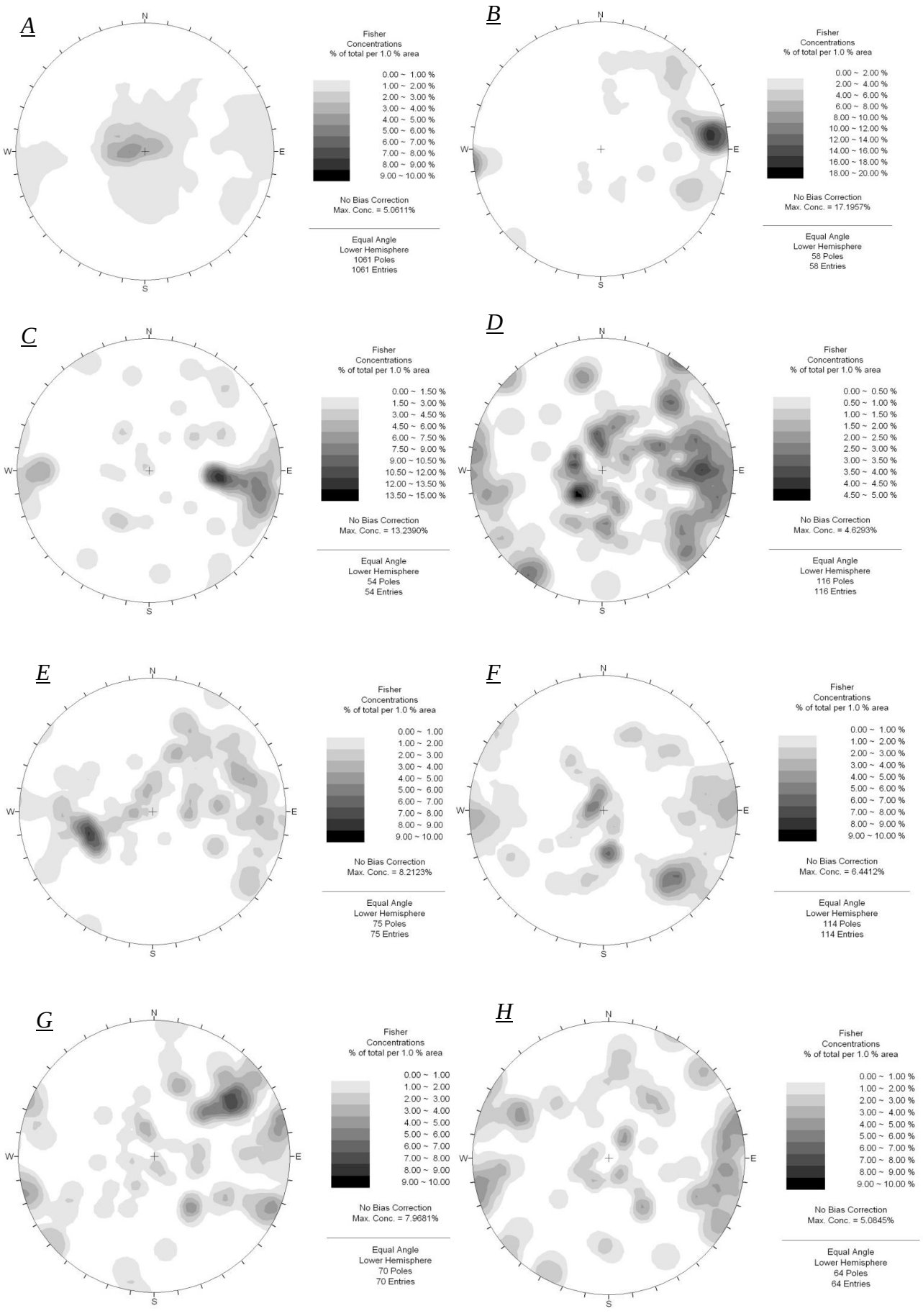
A
N
W
E
S
Fisher
Concentrations
% of total per 1.0 % area
0.00 ~ 1.00 %
1.00 ~ 2.00 %
2.00 ~ 3.00 %
3.00 ~ 4.00 %
4.00 ~ 5.00 %
5.00 ~ 6.00 %
6.00 ~ 7.00 %
7.00 ~ 8.00 %
8.00 ~ 9.00 %
9.00 ~ 10.00 %
No Bias Correction
Max. Conc. = 5.0611%
Equal Angle
Lower Hemisphere
1061 Poles
1061 Entries
B
N
W
E
S
Fisher
Concentrations
% of total per 1.0 % area
0.00 ~ 2.00 %
2.00 ~ 4.00 %
4.00 ~ 6.00 %
6.00 ~ 8.00 %
8.00 ~ 10.00 %
10.00 ~ 12.00 %
12.00 ~ 14.00 %
14.00 ~ 16.00 %
16.00 ~ 18.00 %
18.00 ~ 20.00 %
No Bias Correction
Max. Conc. = 17.1957%
Equal Angle
Lower Hemisphere
58 Poles
58 Entries
C
N
W
E
S
Fisher
Concentrations
% of total per 1.0 % area
0.00 ~ 1.50 %
1.50 ~ 3.00 %
3.00 ~ 4.50 %
4.50 ~ 6.00 %
6.00 ~ 7.50 %
7.50 ~ 9.00 %
9.00 ~ 10.50 %
10.50 ~ 12.00 %
12.00 ~ 13.50 %
13.50 ~ 15.00 %
No Bias Correction
Max. Conc. = 13.2390%
Equal Angle
Lower Hemisphere
54 Poles
54 Entries
D
N
W
E
S
Fisher
Concentrations
% of total per 1.0 % area
0.00 ~ 0.50 %
0.50 ~ 1.00 %
1.00 ~ 1.50 %
1.50 ~ 2.00 %
2.00 ~ 2.50 %
2.50 ~ 3.00 %
3.00 ~ 3.50 %
3.50 ~ 4.00 %
4.00 ~ 4.50 %
4.50 ~ 5.00 %
No Bias Correction
Max. Conc. = 4.6293%
Equal Angle
Lower Hemisphere
116 Poles
116 Entries
E
N
W
E
S
Fisher
Concentrations
% of total per 1.0 % area
0.00 ~ 1.00
1.00 ~ 2.00
2.00 ~ 3.00
3.00 ~ 4.00
4.00 ~ 5.00
5.00 ~ 6.00
6.00 ~ 7.00
7.00 ~ 8.00
8.00 ~ 9.00
9.00 ~ 10.00
No Bias Correction
Max. Conc. = 8.2123%
Equal Angle
Lower Hemisphere
75 Poles
75 Entries
F
N
W
E
S
Fisher
Concentrations
% of total per 1.0 % area
0.00 ~ 1.00 %
1.00 ~ 2.00 %
2.00 ~ 3.00 %
3.00 ~ 4.00 %
4.00 ~ 5.00 %
5.00 ~ 6.00 %
6.00 ~ 7.00 %
7.00 ~ 8.00 %
8.00 ~ 9.00 %
9.00 ~ 10.00 %
No Bias Correction
Max. Conc. = 6.4412%
Equal Angle
Lower Hemisphere
114 Poles
114 Entries
G
N
W
E
S
Fisher
Concentrations
% of total per 1.0 % area
0.00 ~ 1.00
1.00 ~ 2.00
2.00 ~ 3.00
3.00 ~ 4.00
4.00 ~ 5.00
5.00 ~ 6.00
6.00 ~ 7.00
7.00 ~ 8.00
8.00 ~ 9.00
9.00 ~ 10.00
No Bias Correction
Max. Conc. = 7.9681%
Equal Angle
Lower Hemisphere
70 Poles
70 Entries
H
N
W
E
S
Fisher
Concentrations
% of total per 1.0 % area
0.00 ~ 1.00 %
1.00 ~ 2.00 %
2.00 ~ 3.00 %
3.00 ~ 4.00 %
4.00 ~ 5.00 %
5.00 ~ 6.00 %
6.00 ~ 7.00 %
7.00 ~ 8.00 %
8.00 ~ 9.00 %
9.00 ~ 10.00 %
No Bias Correction
Max. Conc. = 5.0845%
Equal Angle
Lower Hemisphere
64 Poles
64 Entries

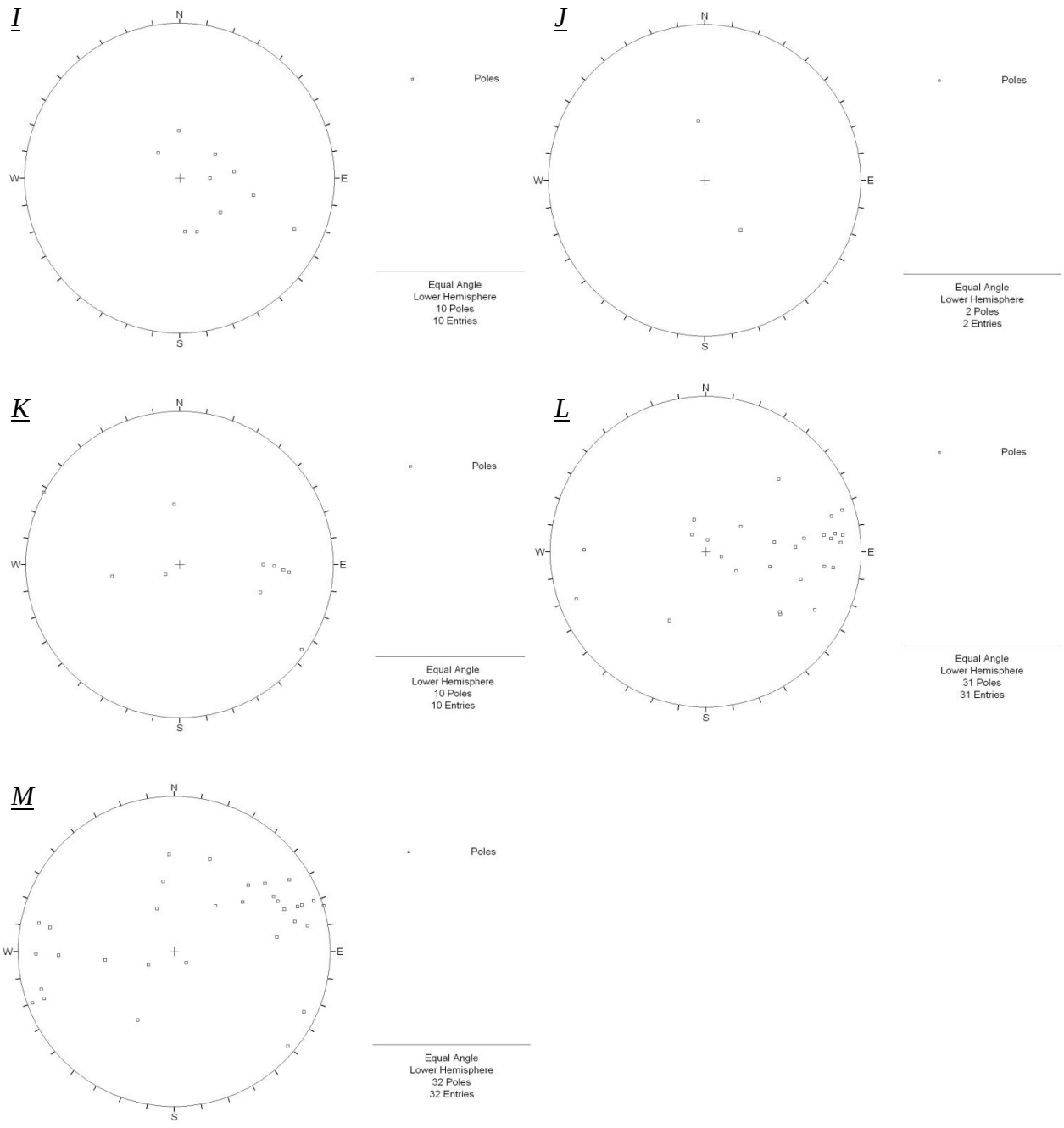

Figure 3.35. Thirteen stereographic projections showing orientation distribution of the variety of veins within the Main Host Assemblage. Stereonets with more than fifty poles are shown on contoured plots; stereonets with less than fifty poles are shown on pole plots. Vein infill; *A*- Calcite; *B*- Chlorite; *C*- Epidote; *D*- Hematite; *E*- Quartz; *F*- Serpentinite; *G*- Talc; *H*- Tremolite; *I*- Actinolite; *J*- Albite; *K*- Magnesite; *L*- Magnetite and *M*- Pyrite.

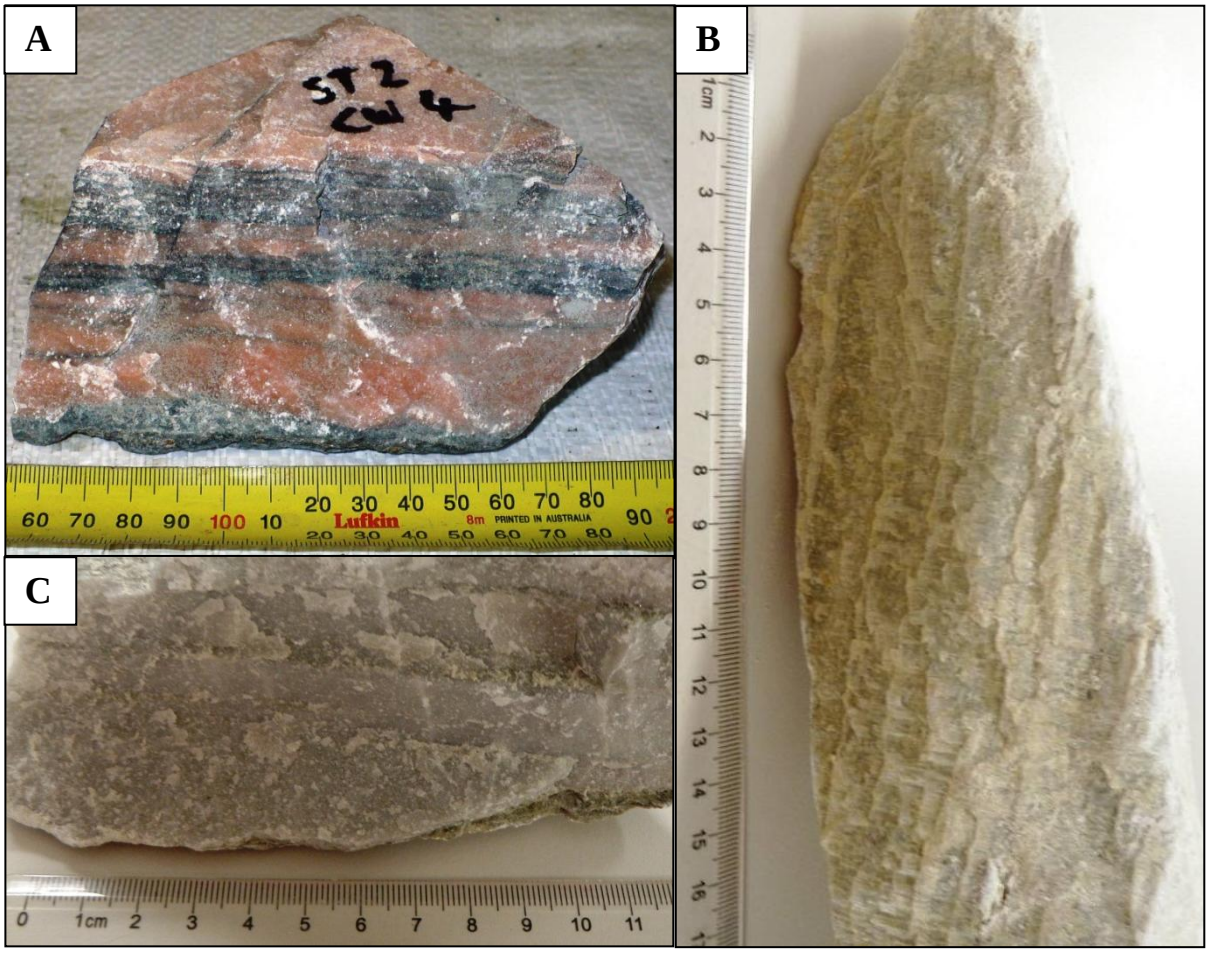

Figure 3.36. Samples sent to MRT laboratories for XRD analysis. **A** – Pink calcite. Sample number 176670. Scale in millimetres. **B** – Chlorite, dolomite and talc rich lithology located <1m W of the Eastern Contact Fault. Sample number 176671. Scale in centimetres. **C** – Quartz, dolomite and chlorite vein located within the dolomitic lithology proximal to **B**. Sample number 176672. Scale in centimetres.

Chlorite and epidote veins mainly dip steeply W but with slightly different strike. Chlorite veins are subparallel to the dominant foliation within the MHA. The epidote veins however include a group dipping 55°W and all strike 010° in contrast to the chlorite veins striking 355°. The moderately W dipping epidote veins are similar in orientation to the 'ski-jump' joints within the East Wall Assemblage and may affect slope stability. The spatial distribution of chlorite and epidote veins within the MHA differs. Chlorite veins mainly occur outside the extent of the MOZ and WOL, within barren lithologies of chloritic composition. Epidote veins occur within mineralised zones and country rock, the latter mainly within mafic

lithologies of meta-basalt. A broad range of hematite vein orientations is very similar to the hematite infill joints. As with the joints, hematite and epidote veins are found close together (Figure 3.37**,** Figure 3.38 - **A**), within mineralised and barren lithologies.

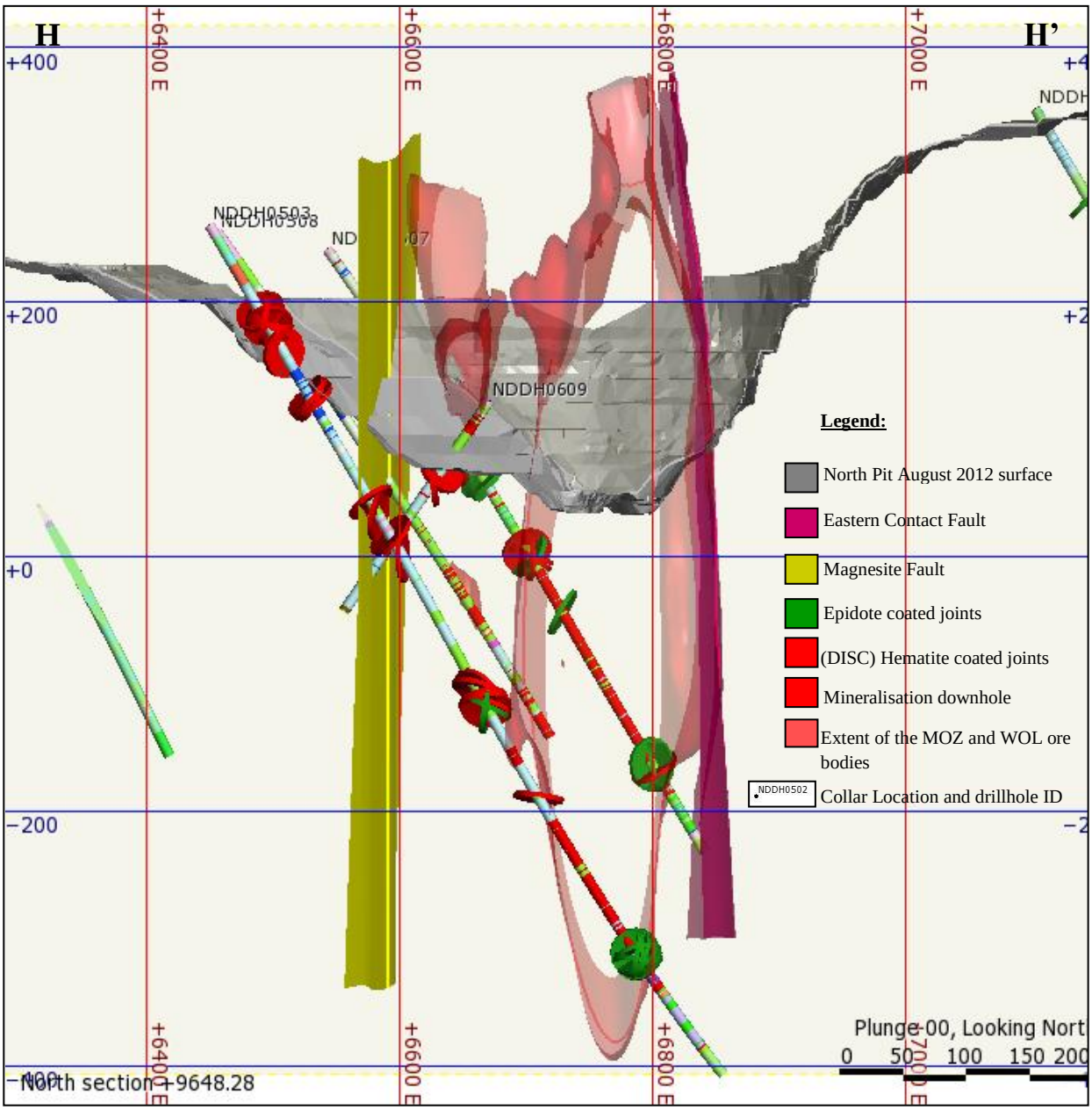

Figure 3.37. Cross Section H-H' shows the position of epidote and hematite veins within the MHA; as green and red discs down-hole respectively. *Section: 9648 m N (looking N).* Refer to digital Appendix 8 for a complete lithological legend.

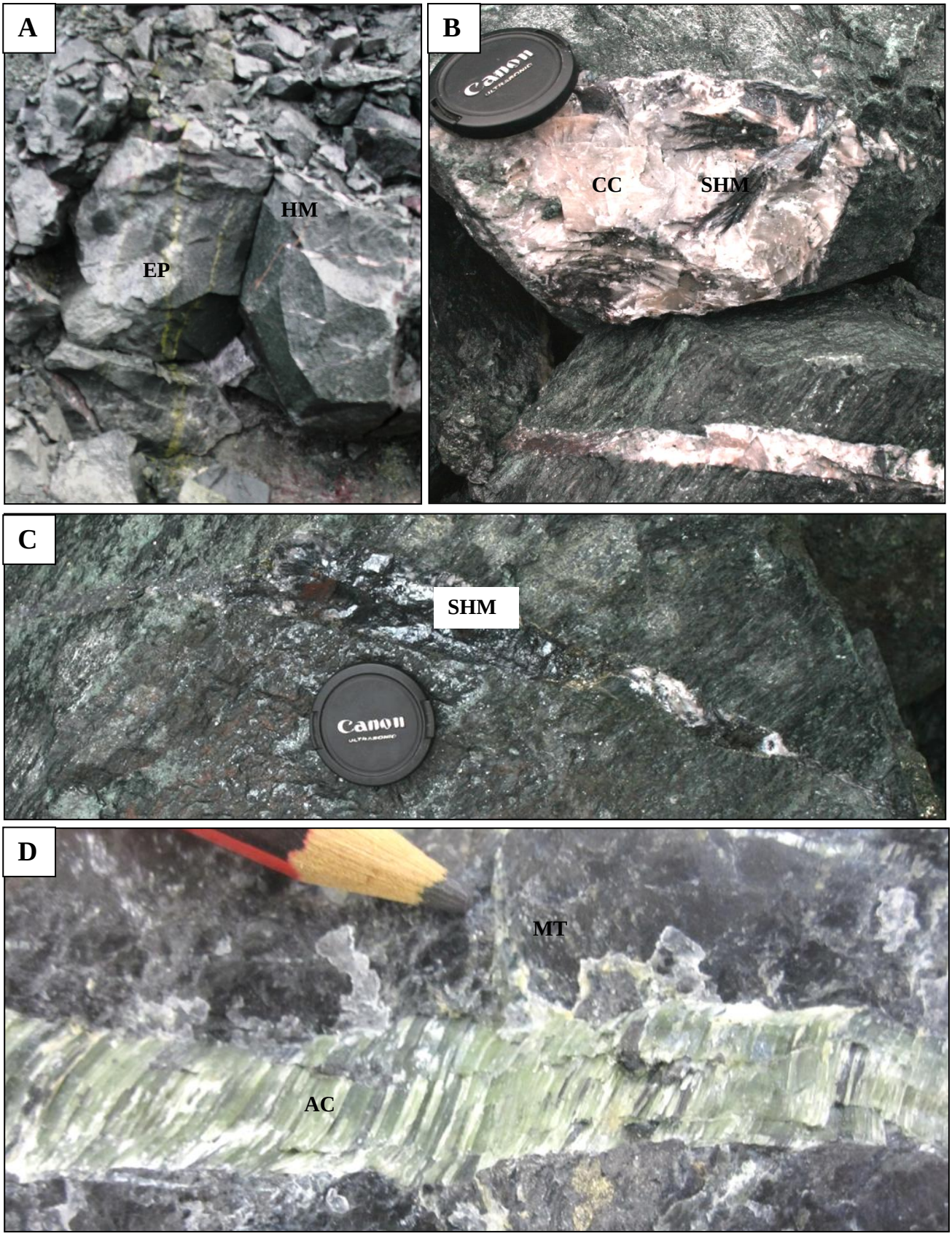

Figure 3.38. Photographic examples of the variety of veins within the MHA. **A** – Epidote and hematite veins within a metamafic host. Located in Stage 2. **B** – Pink calcite (stained with hematite) and specular hematite vein located within chloritic schist in Stage 2. **C** – Specular hematite vein within chloritic schist in Stage 1. Canon camera lens cap approximately 6cm in length. **D** – Actinolite vein within high grade magnetite ore located in Stage 1. The magnetite lacks metallic lustre in this example. Pencil nib approximately 1cm in length. Abbreviations; EP-Epidote, HM-Hematite, SHM-Specular Hematite, CC-Calcite, AC-Actinolite and MT-Magnetite.

The modal orientation of quartz veins is 50°/070° (Table 3.3) which is very different to the modal orientations of all other veins within the assemblage. The quartz veins are only found within barren lithologies of the MHA. The veins are mostly within meta-basaltic rock. Quartz veins are also clustered to the E of the Eastern Contact Fault within the East Wall Assemblage and to the W of the Magnesite Fault within the West Wall Assemblage. These two large scale bounding faults however, have no bearing on the spatial distribution of the quartz veins within the MHA.

Serpentinite, tremolite and actinolite filled veins were only found within mineralised lithologies. They occur together within high-grade and low-grade ore zones with associated serpentine gangue. They have broad ranges of vein orientation. The modal orientation of talc veins is 70°/235° (Table 3.3). These veins are distributed to the E of the MOZ within high-grade talc-rich magnetite ore. The concentration of talc veins increases near the Eastern Contact Fault and then diminish further E into the East Wall Assemblage. The eastern pit wall was designed along the fault contact between the MHA and the East Wall Assemblage. Due to this and the average orientation of the talc veins within the MHA, these discontinuities pose a potential slope stability problem for the mine.

Magnesite veins are not common within the MHA (Table 3.3). The magnesite veins are distributed within talc-rich barren lithologies located within the MOZ and to the W of the MOZ. Along with calcite veins, magnesite veins are thicker than other vein types (Table 3.3). Magnetite and pyrite veins are similarly not very common within the MHA. The modal orientation of both vein types are the same variably dipping with a 340° to 020° strike. In both cases, the veins have a similar orientation to the joints with these mineral infills. Pyrite veins are distributed throughout the MHA, within areas of high-grade mineralisation, as small veinlets within the ore. In contrast to magnetite coated joints, magnetite veins of the MHA are distributed more commonly within barren lithologies such as meta-basalt and chloritic schists.

Both vein types include a significant proportion of veins in geotechnically unfavourable orientations for the pit slope stability.

3.4.5 Foliation Characteristics

A steeply dipping, pervasive foliation is common within the MHA. The same logging parameters used on the E Wall were employed when logging the MHA foliation; FO1, FO2 and FO3 (refer to Section 3.2): 26% of all foliations logged within the MHA are weak foliations, 56% are moderate foliations and 18% are strong foliations. Although foliation orientation varies, there is a clear dominant mode dipping steeply to the W: weak foliation at 87°/260°, moderate foliation at 88°/270° and strong foliation at 85°/265°. The difference between these values is not considered to be statistically significant (Figure 3.39). An example of foliation within NDDH09065 is shown in Figure 3.40.

The foliation planes within the MHA are more prominent within barren lithologies of mafic and chloritic composition. The foliation is not as well developed within the MOZ, and is intermittent down-hole within the mineralisation. This leads to a less prominent cleavage in the eastern section of the MHA. The foliation within the MHA is a slope stability concern for the mine. Due to the variable nature of the foliation depending on lithology, the planes could be strong or weak. This variability ensures planning for rock failure or open pit expansion is difficult. Failure mechanisms, including rock fall due to weak foliation is described in Section 3.4.6.

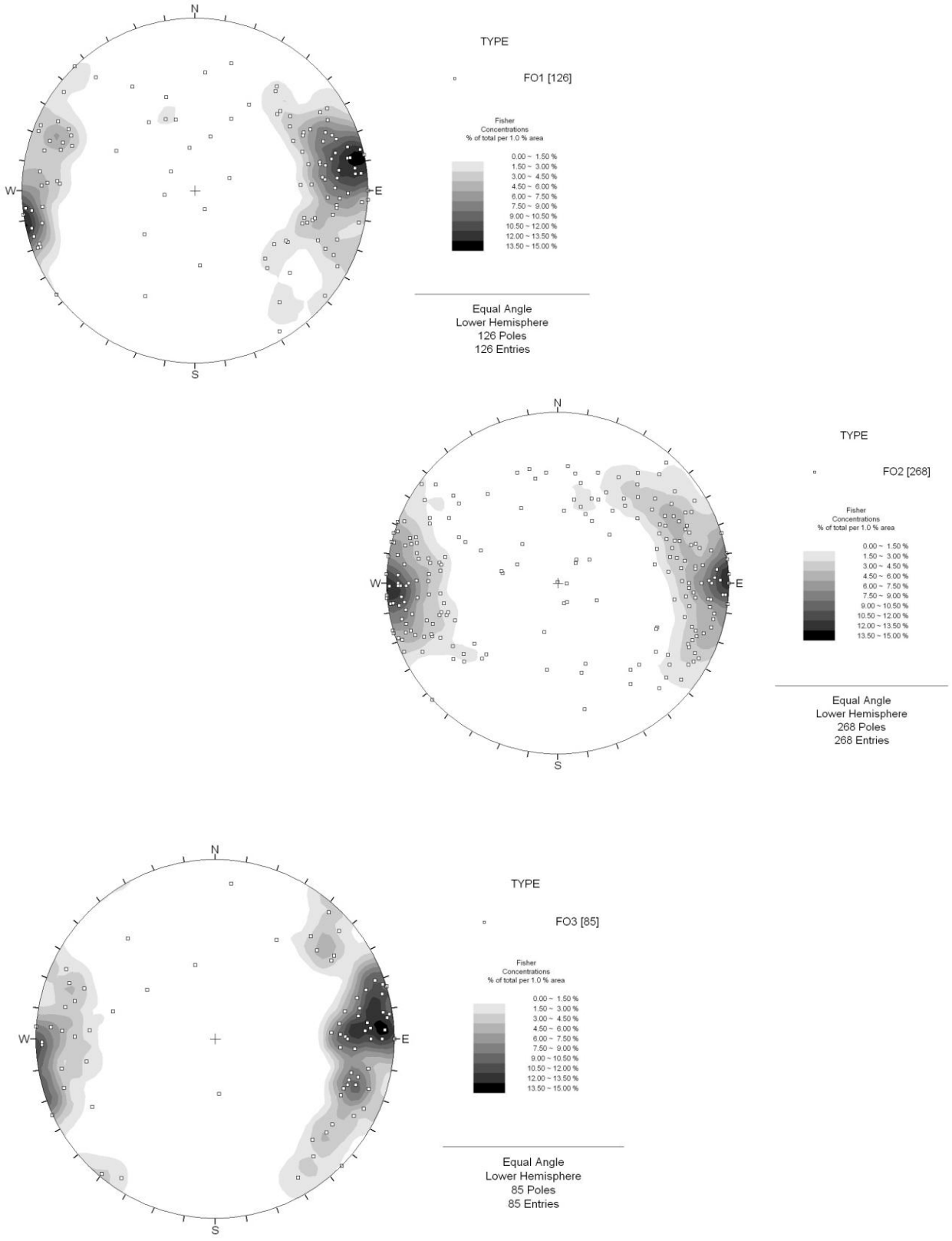

Figure 3.39. Three contoured stereographic pole plots of the orientation trends of FO1 (top left), FO2 (middle right) and FO3 (bottom left) within the MHA.

Figure 3.40. Example of foliation within NDDH09065 at 237.40m to 244.60m. The arrow denotes down-hole direction. Note how the foliation changes down-hole from weakly to strongly foliated. The core is HQ3 sized.

3.4.6 Failure Modes of the Main Host Assemblage

Wedge Failure

Unfavourably oriented joints of the MHA occasionally develop into typical wedge failures, whereby sliding along the line of intersection of two planar discontinuities creates a rock fall (Figure 3.41).

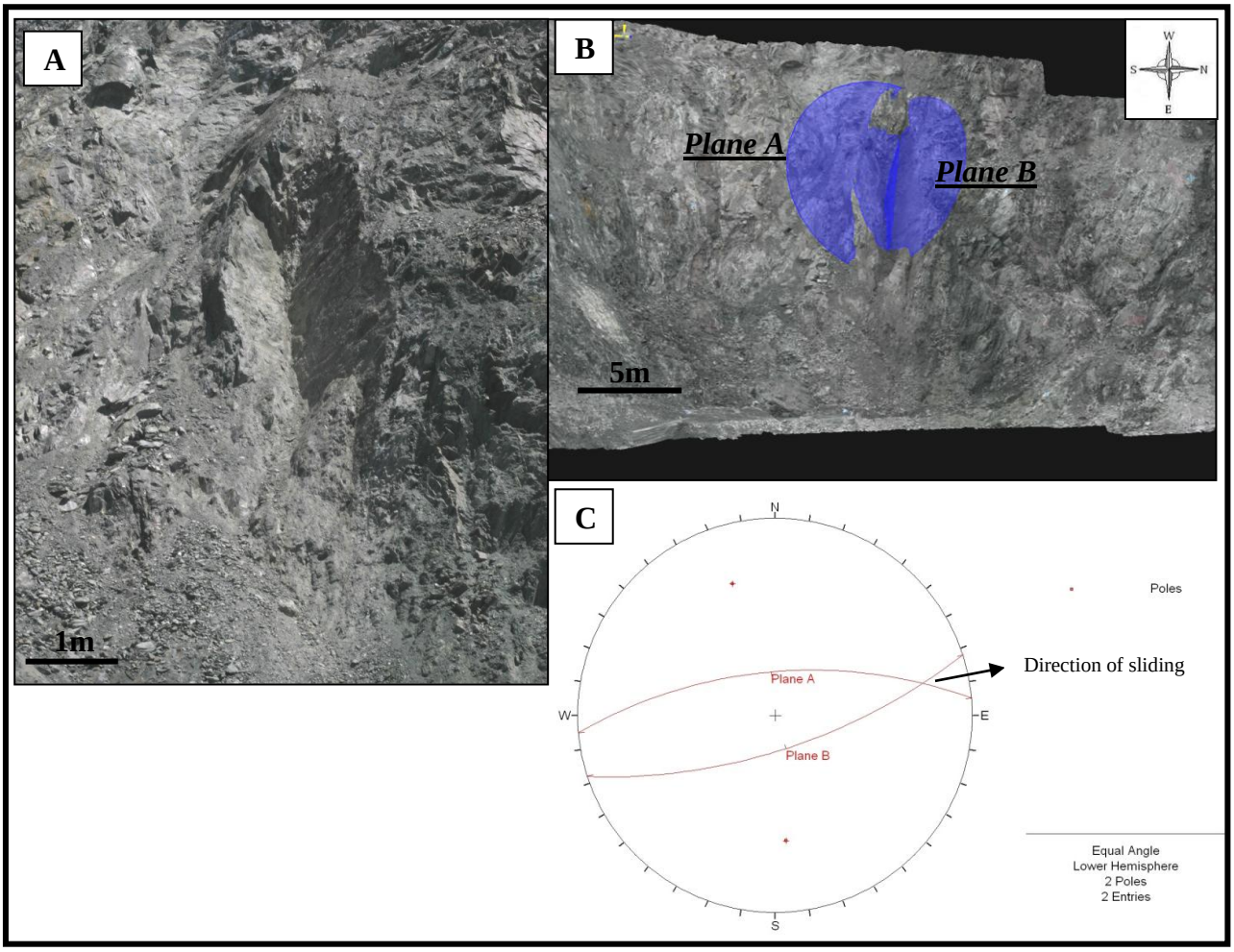

Figure 3.41 A - Wedge failure on the SW pit wall of North Pit. **B** – Digital Terrain Model (DTM) of this pit face, generated from 3DM Analyst™ photogrammetry software. The blue halos indicate the opposing discontinuities of Plane A and Plane B. The orientation of each plane (65°/355° and 70°/162° respectively) was obtained through photogrammetry as the pit face was inaccessible at the time. **C** – A pole/plane stereoplot showing Plane A and Plane B in stereographic projection. The direction of sliding (to the E) is marked.

Discontinuities resulting in wedge failure exhibit a planar and smooth roughness profile. Wedge failures do not occur within mineralised lithologies of the MHA but within the barren mafic or chlorite rich intervals. Although the geometry of the wedge failure differs within the East Wall Assemblage, this mode of rock fall is the most common within the mine. However, the wedge failures of the MHA are much smaller to that of the E Wall and the overall slope height is lower, resulting in a decreased risk of safety to personnel and equipment. Pit faces like the one shown in Figure 3.41 are planned to be temporary unlike the East Wall design.

Lithological control on Failure

The MHA contains a mixture of massive and schistose rocks. Failure mechanisms are therefore lithologically controlled in part due to the structural characteristics of each rock type. Intensely foliated rocks tend to break along foliation which is sometimes characterised by chlorite; thus ensuring low friction angles. Toppling failures can arise due to the breaking along foliation; although this is dependent on the slope geometry. Slumping can also occur in areas where the lithology is puggy or friable; mainly in close proximity to major faults within the mine sequence (refer to Section 3.7 for information regarding major faults and failure mechanisms) or within weathered zones. Slumping is generally a slow process and can be managed once the movement is identified. Due to the variable nature of the rocks within the MHA, overhang of massive rocks can also be a problem. Massive rocks occur as kernels commonly surrounded by very foliated and puggy chloritic rich lithologies. These large massive boudins or lenses of meta-basalt or magnesite (refer to Section 3.7.4 for an example) protrude from pit faces causing rock fall concern. During heavy rainfall, the foliated and puggy material surrounding the lenses is washed away. The massive lenses exhibit hair-line cracks, veins or joints. As the surrounding material is eroded the boudin/lens is undermined causing fragments and falls, or blocks to topple intact. The potential for rock falls to initiate on one of or a mixture of these structures is high.

3.5 Structural Style – West Wall Assemblage

3.5.1 Introduction

The West Wall Assemblage (WWA) encompasses various stratigraphic units. The rocks within this package are mostly unmineralised, chlorite +/- muscovite +/- quartz +/- dolomite +/- graphite schists with strongly banded albite and massive magnesite. For simplicity within this project, these units have been clustered into one group. The WWA contains such units as the Mega Ramp Schist, Box Cut Carbonate, Western Wall Banded Schist (all mine nomenclature) and the Ahrberg Group (refer to Chapter 1; Section 1.3 for a full description of each unit). Twelve drillholes traverse the units of the WWA as opposed to twenty eight traversing the MHA and nineteen in the East Wall Assemblage. For this reason, the volume of geotechnical data available for joint, vein and foliation analysis is lower within the WWA than the other two assemblages discussed in Sections 3.3 and 3.4.

3.5.2 Joint Characteristics

The characteristics of joint infills within the East Wall Assemblage and the MHA have been discussed in Sections 3.3.2 and 3.4.2 respectively. The characteristics of the majority of joints within the WWA fit within the same groups as within these two assemblages. Rather than going through the same descriptions as before, this Section and Section 3.5.4 emphasise the similarities and differences in joint and vein characteristics within the WWA compared to the results discussed within the East Wall Assemblage and the MHA. Table 3.4 is a summary of the percentage of joints, orientation distribution and joint roughness profile variation of the range of joints within the WWA. Figure 3.42 shows nine stereographic projections presenting orientation distribution of joints with specific characteristic infill minerals within the WWA.

Similarities

- Calcite coated joints: orientation is the same; dipping to the W. Joint roughness and infill characteristics are the same in the MHA (Refer to Section 3.4.2).
- Chlorite coated joints: orientation is similar to the foliation, joints with clay and joints with no infill. This unimodal chlorite coated joint orientation was also evident within the East Wall Assemblage and the MHA. Chlorite coated joint roughness profiles are the same within the WWA as for the MHA. Therefore friction angles are similar.
- Joints with no infill are the most common within the WWA as with the other two assemblages.
- Joints with no infill, clay, talc and pyrite coated joints are all orientated similarly to the results shown within the MHA. The mineral characteristics and joint roughness profiles are similar.
- Although not evident within the East Wall Assemblage or MHA, magnesite and gypsum coated joints have a similar orientation to joints with other infill; dipping moderately steeply to the W.
- All joints within the WWA have a common orientation; steeply dipping to the W with the exception of graphite coated joints. The common orientation is comparable to the MHA and East Wall Assemblage but slightly shallower dip W (70° rather than 80°). This may reflect shallower cleavage orientation.
- Undulating roughness profiles are the most common within the WWA; identical to the MHA.
- Although a difference in orientation is evident, the most common roughness profile of graphite coated joints is the same as within the East Wall Assemblage and MHA.

Infill	% of Joints within the WWA	Orientation Maxima (see Figure 3.42) Dip/Dip Direction (°)	Roughness and %
Calcite	**6%**	**31/240** **77/268** **(Figure 3.42 – *A*)**	**UR – 25%** **SR – 22%** **US – 20%** **SS – 14%** **PS – 14%** **PR – 3%** **SK – 1%** **UK – 1%**
Chlorite	**21%**	**71/262** **(Figure 3.42 – *B*)**	**US – 51%** **SR – 13%** **UR – 12%** **PS – 11%** **PR – 5%** **SS – 5%** **UK – 2%** **SK– 0.5%** **PK – 0.5%**
Clay	**4%**	**74/257** **(Figure 3.42 – *C*)**	**US – 45%** **UR – 22%** **PR – 12.5%** **PS – 9.5%** **UK – 5%** **SS – 3%** **SR – 1.5%** **PK – 1.5%**
Magnesite	**3%**	**70/254** **36/226** **20/160** **(Figure 3.42 – *D*)**	**SR – 35%** **UR – 26%** **US – 23%** **PS – 10%** **PR – 2%** **SK – 2%** **SS – 2%**
No Infill	**48%**	**72/258** **(Figure 3.42 – *E*)**	**US – 39%** **UR – 25%** **SR – 12%** **PS – 9%** **PR – 8%** **SS – 6%** **UK – 0.7%** **SK – 0.3%**
Talc	**15%**	**71/265**	**US – 35%** **SR – 24%**

		(Figure 3.42 – *F*)	**PS – 18%** **UR – 10%** **SS – 6%** **PR – 5%** **PK – 1%** **UK – 1%**
Graphite	**1%**	**84/054** **73/234** **(Figure 3.42 – *G*)**	**US – 64%** **UK – 18%** **SR – 9%** **PR – 4.5%** **PK – 4.5%**
Gypsum	**0.2%**	**Only 3 data points** **(Figure 3.42 – *H*)**	**SS – 67%** **UR – 33%**
Pyrite	**1.8%**	**Shallow to steep W dips** **(Figure 3.42 – *I*)**	**UR – 36%** **US – 20%** **SS – 12%** **PS – 12%** **SR – 8%** **PR – 8%** **PK – 4%**

Table 3.4 – Summary of the percentage of joints, orientation distribution and joint roughness profile variation of the diverse range of joints within the WWA.

Differences

- The proportion of calcite coated joints within the WWA is 14% lower than within the East Wall Assemblage and the MHA.
- The mean orientation of chlorite filled joints of the WWA show a decreased dip of 71° as opposed to the 84° dip of chlorite filled joints within the other two assemblages.
- With 15% of all joints within the WWA being talc filled (Table 3.4), this figure is double the proportion of talc filled joints within the MHA.
- Joints infilled with tremolite/actinolite, hematite, serpentine, epidote, magnetite, albite and quartz are not evident within the WWA. The interpretation here is that these infill types are linked to host rock compositions not found in the WWA.

- Magnesite and gypsum infilled joints are only evident within the WWA. Variability in lithology ensures the mineral infill differences. Magnesite infilling increases friction angles to 55° (Barton and Bandis, 1981) due to the tightly healed nature of these joints. Rough joint profiles are the most common in these examples and increase the basic friction angles on these joints. Joint infill ranges from <1 mm to 5 mm in thickness. The gypsum infilled joints within the WWA reduce friction angles due to the softening and low-friction coating. Smooth roughness profiles are the most common due to the soft nature of the mineral.
- The orientation of graphite coated joints within the WWA differs from that of the other two assemblages. The most common orientation is steeply dipping to the NE within the WWA and dipping to the W within the MHA and the East Wall Assemblage. The distribution of the majority of graphite coated joints within North Pit is in close proximity to major bounding faults. The Magnesite Fault is orientated differently to the Eastern Contact Fault (where the majority of graphite coated joint orientations were recorded within the former two assemblages). The change in fault orientation could dictate the change in orientation of the graphite coated joints (refer to Section 3.5.3 for a discussion of the spatial distribution of joints within the WWA).

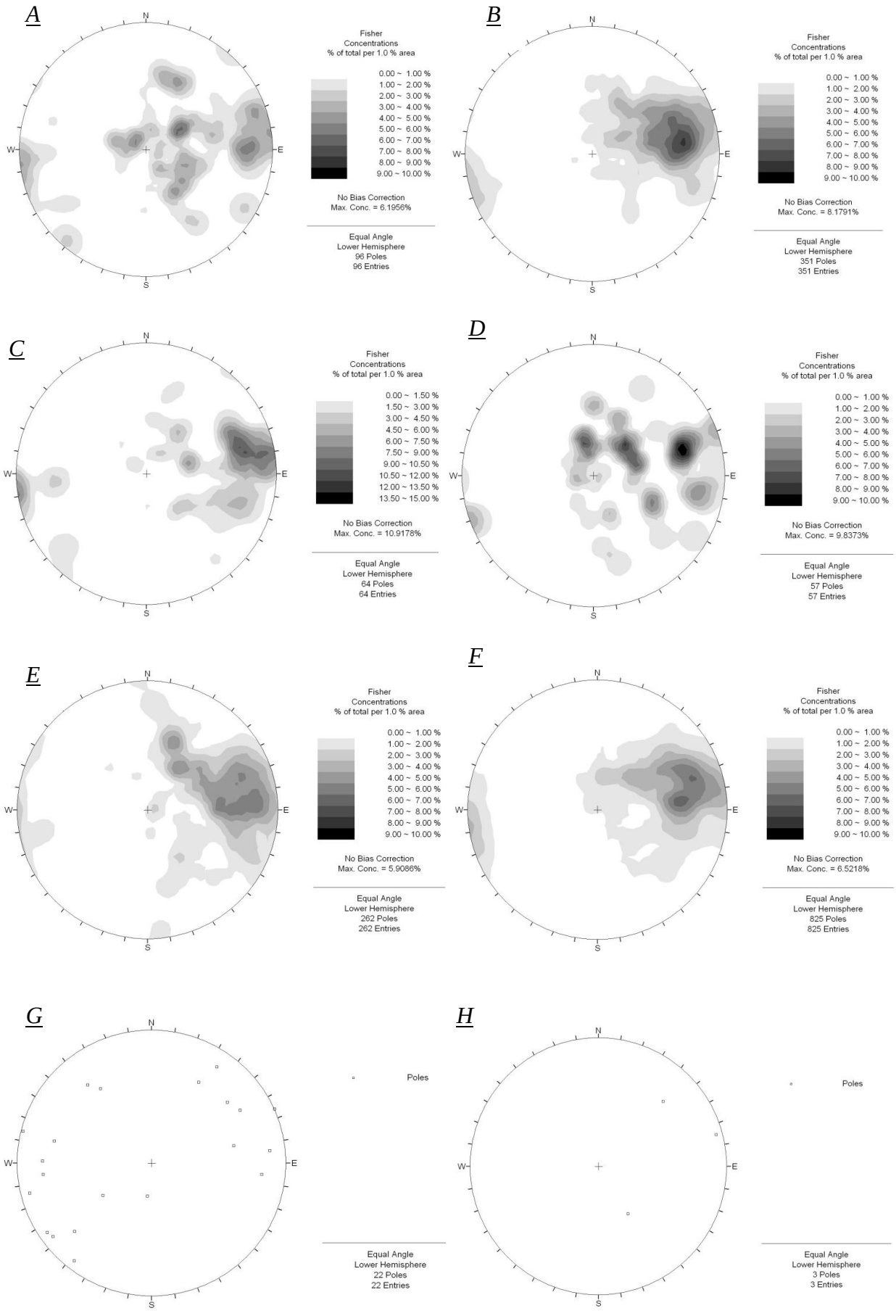
A
N
W
E
S
Fisher
Concentrations
% of total per 1.0 % area
0.00 ~ 1.00 %
1.00 ~ 2.00 %
2.00 ~ 3.00 %
3.00 ~ 4.00 %
4.00 ~ 5.00 %
5.00 ~ 6.00 %
6.00 ~ 7.00 %
7.00 ~ 8.00 %
8.00 ~ 9.00 %
9.00 ~ 10.00 %
No Bias Correction
Max. Conc. = 6.1956%
Equal Angle
Lower Hemisphere
96 Poles
96 Entries
B
N
W
E
S
Fisher
Concentrations
% of total per 1.0 % area
0.00 ~ 1.00 %
1.00 ~ 2.00 %
2.00 ~ 3.00 %
3.00 ~ 4.00 %
4.00 ~ 5.00 %
5.00 ~ 6.00 %
6.00 ~ 7.00 %
7.00 ~ 8.00 %
8.00 ~ 9.00 %
9.00 ~ 10.00 %
No Bias Correction
Max. Conc. = 8.1791%
Equal Angle
Lower Hemisphere
351 Poles
351 Entries
C
N
W
E
S
Fisher
Concentrations
% of total per 1.0 % area
0.00 ~ 1.50 %
1.50 ~ 3.00 %
3.00 ~ 4.50 %
4.50 ~ 6.00 %
6.00 ~ 7.50 %
7.50 ~ 9.00 %
9.00 ~ 10.50 %
10.50 ~ 12.00 %
12.00 ~ 13.50 %
13.50 ~ 15.00 %
No Bias Correction
Max. Conc. = 10.9178%
Equal Angle
Lower Hemisphere
64 Poles
64 Entries
D
N
W
E
S
Fisher
Concentrations
% of total per 1.0 % area
0.00 ~ 1.00 %
1.00 ~ 2.00 %
2.00 ~ 3.00 %
3.00 ~ 4.00 %
4.00 ~ 5.00 %
5.00 ~ 6.00 %
6.00 ~ 7.00 %
7.00 ~ 8.00 %
8.00 ~ 9.00 %
9.00 ~ 10.00 %
No Bias Correction
Max. Conc. = 9.8373%
Equal Angle
Lower Hemisphere
57 Poles
57 Entries
E
N
W
E
S
Fisher
Concentrations
% of total per 1.0 % area
0.00 ~ 1.00 %
1.00 ~ 2.00 %
2.00 ~ 3.00 %
3.00 ~ 4.00 %
4.00 ~ 5.00 %
5.00 ~ 6.00 %
6.00 ~ 7.00 %
7.00 ~ 8.00 %
8.00 ~ 9.00 %
9.00 ~ 10.00 %
No Bias Correction
Max. Conc. = 5.9086%
Equal Angle
Lower Hemisphere
262 Poles
262 Entries
F
N
W
E
S
Fisher
Concentrations
% of total per 1.0 % area
0.00 ~ 1.00 %
1.00 ~ 2.00 %
2.00 ~ 3.00 %
3.00 ~ 4.00 %
4.00 ~ 5.00 %
5.00 ~ 6.00 %
6.00 ~ 7.00 %
7.00 ~ 8.00 %
8.00 ~ 9.00 %
9.00 ~ 10.00 %
No Bias Correction
Max. Conc. = 6.5218%
Equal Angle
Lower Hemisphere
825 Poles
825 Entries
G
N
W
E
S
Poles
Equal Angle
Lower Hemisphere
22 Poles
22 Entries
H
N
W
E
S
Poles
Equal Angle
Lower Hemisphere
3 Poles
3 Entries

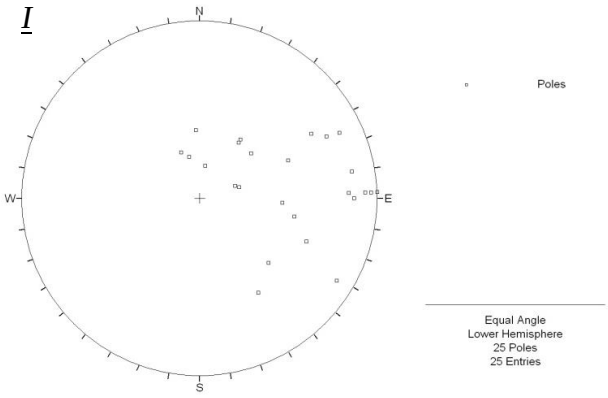

Figure 3.42. Nine stereographic projections presenting orientation distribution of joints showing different infill minerals within the West Wall Assemblage. Stereonets with more than fifty poles are shown on contoured plots; stereonets with less than fifty poles are shown on pole plots. Mineral Infill; *A*- Calcite; *B*- Chlorite; *C*- Clay/gouge; *D*- Magnesite; *E*- No Infill; *F*- Talc; *G*- Graphite; *H*- Gypsum and *I*- Pyrite.

3.5.3 Spatial Distribution of Joints

Information into the spatial distribution of joints within the WWA is important for future mine planning. The current W Wall of Stage 1 in North Pit has not changed since this research commenced. The planned position of the W Wall in Stage 2 however has undergone many cutbacks commencing in 2010. This wall will be cutback in the future to ensure maximum pit depth and therefore the spatial distribution of joints is significant in understanding how the rock mass of the WWA will behave from a geotechnical point of view. As in the previous sections, this section offers cross sections produced using Leapfrog ™. Figure 3.43 shows a Leapfrog™ model plan view of North Pit indicating the representative cross sections used to highlight the spatial distribution of the joints within the WWA.

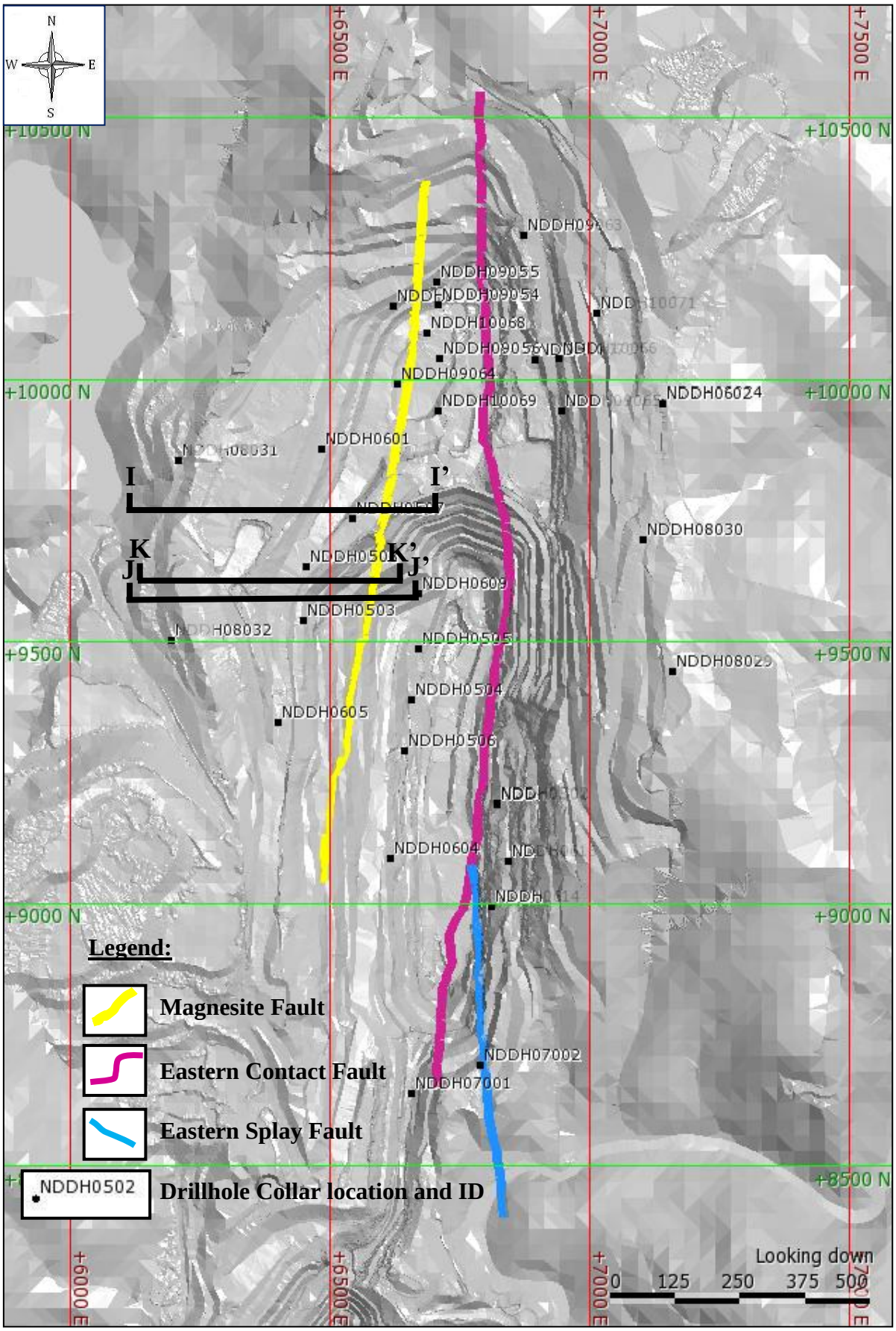

Figure 3.43 – Plan view of North Pit showing major fault traces, drillhole location and cross section locations.

Calcite

All calcite coated joints within the WWA (with the exception of one) are located within a zone within 120 m W of the Magnesite Fault. Mine geologists at Savage River call the stratigraphic unit here the Box Cut Carbonate Assemblage. One calcite coated joint is located within micaceous schist within the Fulfords Creek unit. No calcite joints are located within the Mega Ramp Schist, Western Wall Banded Schists or Ahrberg Group. Due to the Box Cut Carbonate Assemblage containing a high percentage of disseminated carbonate, this mineral is likely to be the most soluble within the package resulting in a locally buffered fluid regime in the production of this specific joint infill.

Chlorite

The percentage of chlorite filled joints diminishes from 100 m W of the Magnesite Fault (Figure 3.44).

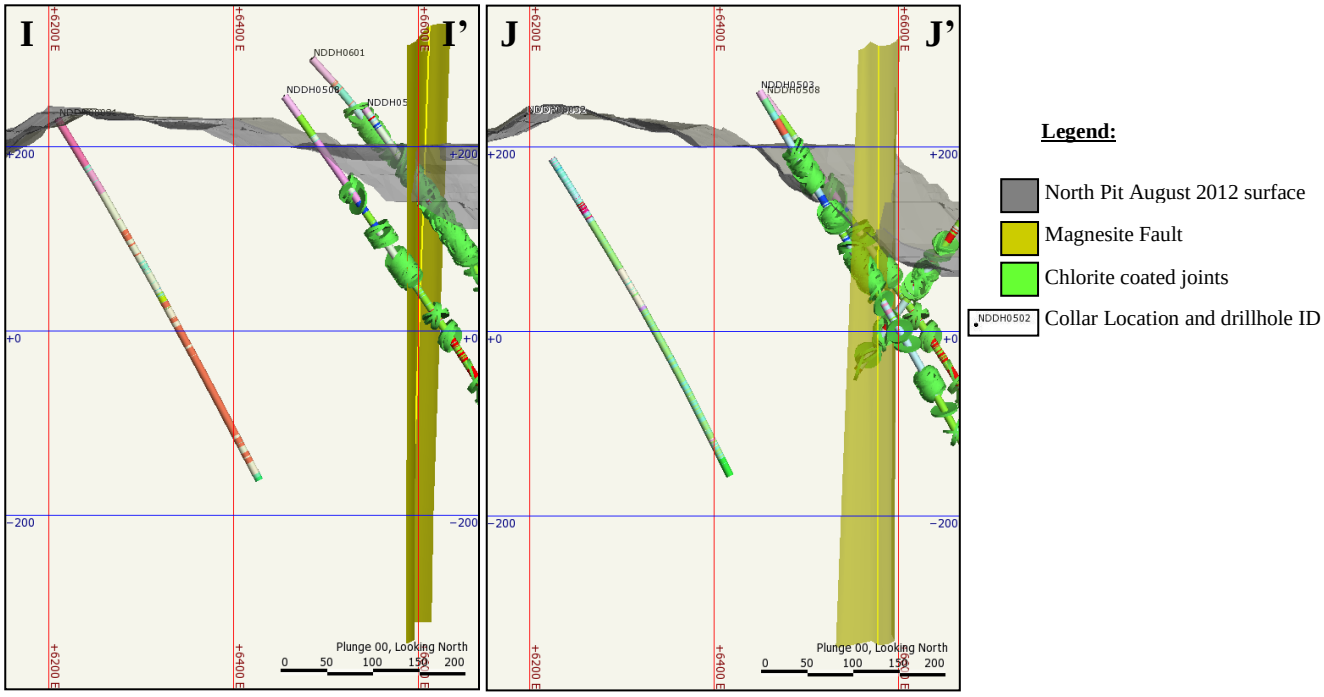

Figure 3.44. Cross section I-I' and J-J' showing the position of chlorite coated joints within the WWA; as light green discs down-hole. *Sections: X-6696 Y-9755 and X-6694 Y-9583 respectively (looking N).* Refer to digital Appendix 8 for a complete lithological legend.

Chlorite infilled joints are distributed throughout the Box Cut Carbonate and Mega Ramp Schist Assemblages. They are not evident within the Fulfords Creek Schist or the westerly Ahrberg Group.

Clay

Clay coated joints were found within 150 m W of the Magnesite Fault with the concentration diminishing to the west. The majority of clay infilled joints are in the Box Cut Carbonate. Similar to the Eastern Contact Fault, the Magnesite Fault has a damage zone surrounding the main planar fault line. The clay coated joints are distributed within this zone. Also, thin seams of puggy fine-grained clay are indicative of the magnesite rich areas of the Box Cut Carbonate.

Magnesite

The distribution of magnesite coated joints is concentrated within the Box Cut Carbonate (Figure 3.45).

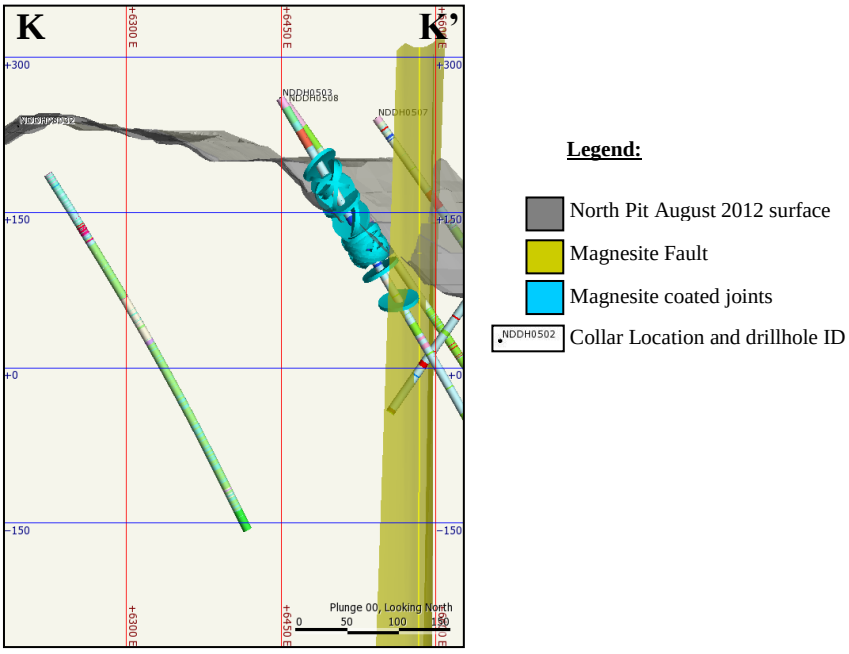

Figure 3.45. Cross section K-K' showing the position of magnesite coated joints within the WWA; as cyan coloured discs down-hole. *Section: X-6694 Y-9610(looking N).* Refer to digital Appendix 8 for a complete lithological legend.

As magnesite coated joints are only distributed within magnesite rich areas of the Box Cut Carbonate, this would suggest that the magnesite was sourced locally within the lithology.

No Infill

Joints with no infill are distributed throughout all lithologies within the WWA, although the majority are within the Magnesite Fault damage zone. The Ahrberg Group (the most westerly unit within North Pit) contains the least joints/m with no infill and the Box Cut Carbonate Assemblage the most.

Talc

The Box Cut Carbonate is the only unit that contains talc infilled joints on the west wall. They are distributed in, and close to, magnesite and dolomite rich areas. The Mega Ramp Schist, Fulfords Creek Schist, Western Wall Banded Schist and Ahrberg Group do not contain any talc filled joints.

Graphite

Graphite coated joints are distributed in close proximity (≤20 m) to the Magnesite Fault. This is a similar observation to that found within the East Wall Assemblage where graphitic joints were only found close to the Eastern Contact Fault. There is a relationship between major faults and graphitic lithology and joints (refer to Chapter 4 , for a structural discussion of this subject). Graphite coated joints were also found within the magnesite rich areas of the Box Cut Carbonate. A 10 m wide graphite-rich member lies on the contact between the Box Cut Carbonate and the Mega Ramp Schist. Some graphite coated joints are distributed throughout this lithology although the majority of these joints are also near the Magnesite Fault.

Gypsum

Although only three gypsum coated joints were recorded, they were all within the Fulfords Creek Schist, to the W of the Box Cut Carbonate and Mega Ramp Schist. It is difficult to draw any conclusions of the spatial distribution of these joints due to the small number of data points. It may indicate that gypsum is a minor component of the Fulfords Creek Schist.

Pyrite

Pyrite coated joints within the WWA are spatially related to graphite coated joints (as was observed in the East Wall Assemblage). They occur within <5 m of each other. Therefore pyrite filled joints are common in close proximity to the Magnesite Fault, within magnesite and dolomite rich areas of the Box Cut Carbonate and within graphite rich lithologies in close proximity to unit contacts.

3.5.4 Vein Characteristics and Spatial Distribution

In North Pit, 335 veins have been logged from drillcore from within the WWA. This number is considerably smaller than the four thousand and two thousand veins logged within the East Wall Assemblage and the MHA respectively. Table 3.5 highlights the percentage of veins within the WWA relating to dominant vein minerals, orientation and thickness. Figure 3.46 displays a series of stereographic projections of each vein type. Figure 3.47 shows a number of photographic examples of vein types within the WWA. Refer to Chapter 4, Section 4.3 for a structural geology synopsis of the orientation and distribution of joints and veins within the WWA as well as micro-faults and folding within the assemblage.

Infill	% of veins within the WWA	Orientation Maxima (see Figure 3.46) Dip/ Dip Direction (°)	Vein Thickness (cm)
Calcite	**27%**	**Sub-horizontal** **70/261** **(Figure 3.46 – *A*)**	**<0.01 - 2**
Magnesite	**28%**	**79/246** **80/283** **(Figure 3.46 – *B*)**	**0.5 – 29**
Quartz	**29%**	**70/295** **60/258** **06/090** **(Figure 3.46 – *C*)**	**0.5 – 1.8**
Albite	**3%**	**Variable – 9 only** **(Figure 3.46 – *D*)**	**<0.01 - 1**
Chlorite	**2%**	**W to SW moderate dips** **8 only** **(Figure 3.46 – *E*)**	**<0.01 - 2**
Gypsum	**6%**	**27/262** **61/251** **(Figure 3.46 – *F*)**	**<0.01 – 0.6**
Hematite	**5%**	**Horizontal to steep WSW dips** **80/270** **(Figure 3.46 – *G*)**	**<0.01 - 4**

Table 3.5 – Summary of the percentage of veins, orientation distribution and vein thickness variation of the range of veins within the WWA.

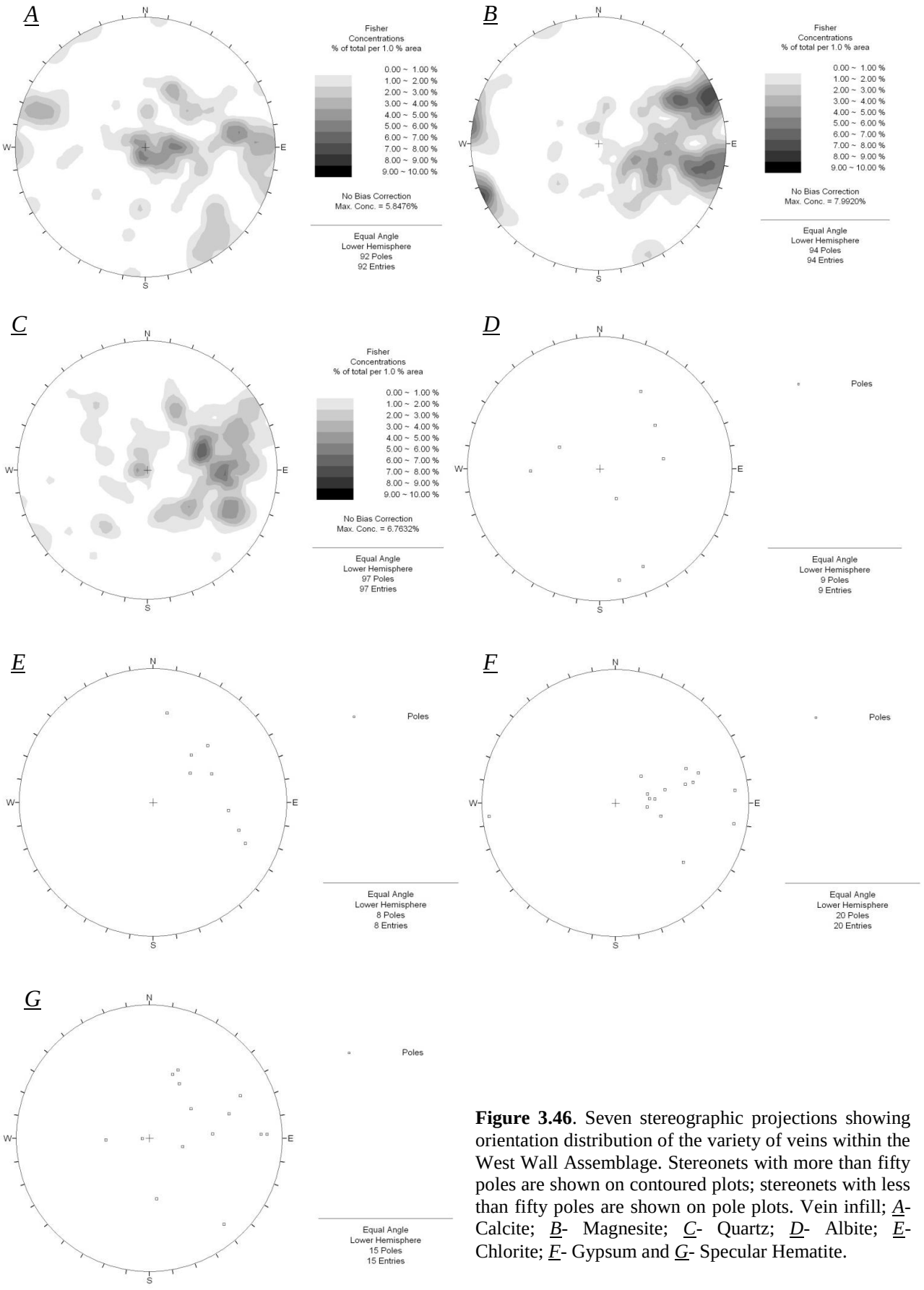

Figure 3.46. Seven stereographic projections showing orientation distribution of the variety of veins within the West Wall Assemblage. Stereonets with more than fifty poles are shown on contoured plots; stereonets with less than fifty poles are shown on pole plots. Vein infill; *A*- Calcite; *B*- Magnesite; *C*- Quartz; *D*- Albite; *E*- Chlorite; *F*- Gypsum and *G*- Specular Hematite.

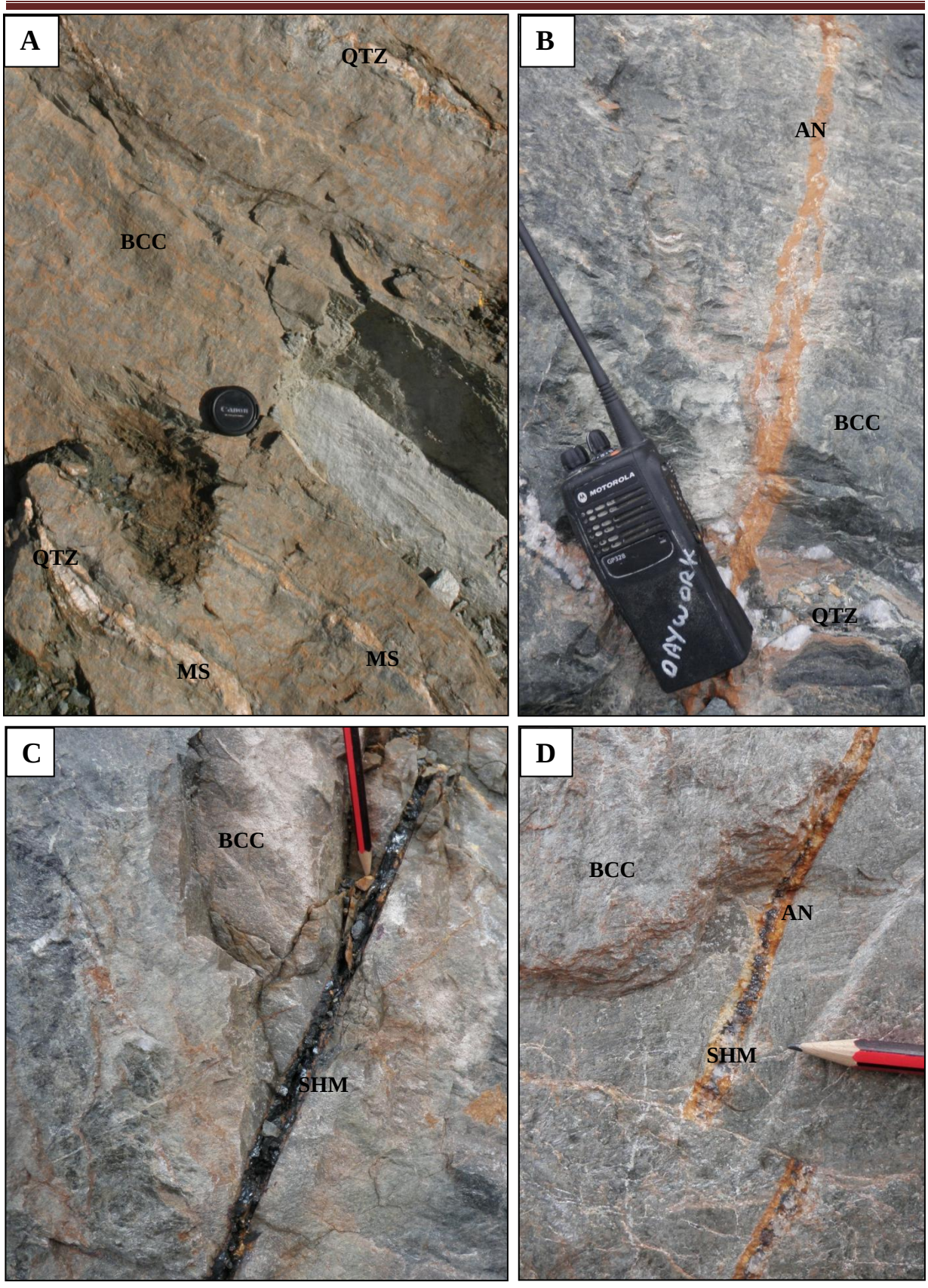

Figure 3.47. Photographic examples of the variety of veins within the WWA. **A** – Magnesite and quartz veins within the BCC. Canon camera lens cap approximately 6cm in length. **B** – Ankerite vein and quartz boudins located within the BCC. Two-way radio body approximately 15cm in length. **C** – Specular hematite vein within the same unit as **A** and **B**. Pencil approximately 5 cm in length. **D** – Displaced specular hematite vein with ankerite selvage located in close proximity to **C**. Visible part of pencil approximately 2 cm in length. Abbreviations; BCC-Box Cut Carbonate, MS-Magnesite, QTZ-Quartz, AN-Ankerite, SHM-Specular Hematite.

A quarter of all veins within the WWA are calcite which is much lower than the percentage within the East Wall Assemblage and the MHA. The orientation of calcite veins is dominated by two sets; one sub-horizontal and the second set steeply W dipping. Both sets are also evident within the East Wall Assemblage and MHA although the steeply W dipping veins are rare within the MHA. As with the calcite coated joints, calcite veins are distributed throughout all lithologies of the WWA but are more common within the Box Cut Carbonate. This unit lies along the west side of the Magnesite Fault and therefore calcite veins are more common within a 120 m wide zone west of the fault. Less than 10% of calcite veins were found in the other lithologies of the WWA. The veins are also much thinner in the WWA than in the East Wall Assemblage and the MHA. They only reach 2cm in thickness within the WWA as opposed to up to 28cm in thickness within the MHA. Both orientation sets present little concern for potential slope stability/geotechnical issues on the mine due to one set being sub-horizontal and the other dipping W, into the pit wall.

Another quarter of all veins within the WWA are dominated by magnesite and these are much less common in the East Wall Assemblage and MHA. Magnesite veins are mainly subparallel to the dominant foliation within the WWA which is steeply dipping to the W (refer to Section 3.5.5 for foliation characteristics) but there are several magnesite veins that dip shallowly. These vein orientations are not a slope stability concern for the mine. Magnesite veins are the thickest within the WWA (Table 3.5). The thickness is similar to magnesite veins within the MHA. The veins are distributed within magnesite and dolomite rich lithologies of the Box Cut Carbonate, similar to the distribution of magnesite coated joints. No magnesite veins were found within the other units of the WWA. Although there are fewer data points recorded within the East Wall Assemblage and MHA, vein orientation and thickness is similar.

Quartz is the most common vein infill within the WWA. In contrast, only 4% of all veins within the MHA and 5% of all veins within the East Wall Assemblage are quartz veins. The

orientation of the quartz veins within the WWA, the East Wall Assemblage and MHA are very different. Within the WWA, the veins dip moderately to the W and shallowly to the E. Within the East Wall Assemblage, the veins dip steeply to the W, subparallel to foliation. Within the MHA, the veins dip moderately to the E. The quartz veins within the WWA are deformed and boudinaged (Figure 3.47 – B) and are distributed in close proximity to magnesite veins (Figure 3.47 – A). Due to this, quartz veins are mainly distributed within the Box Cut Carbonate and are concentrated immediately W of the Magnesite Fault. The Ahrberg Group contains less than 2% of the quartz veins and these are concentrated within a graphitic rich area within the unit. The orientation of the veins within the WWA is not a slope stability concern for the mine due to the flat lying nature of one set and the westerly dip of the other.

Albite veins account for 3% of all veins within the WWA (Table 3.5). Albite veins are rare within the East Wall Assemblage and MHA (0.1%). The veins are thin, undeformed and are distributed only within the Western Wall Banded Schist, which is in very close proximity to the Magnesite Fault. Chlorite veins are also rare within the WWA, the East Wall Assemblage and the MHA. They are distributed within the same stratigraphic unit within the WWA as the albite veins. This unit contains common chlorite and albite. The orientation of the chlorite veins are moderately dipping W. Although dipping in the same direction, the foliation is steeper.

Gypsum veins are only evident within the WWA in close proximity (<10 m) to gypsum coated joints of the Fulfords Creek Schist. They are the thinnest of all veins within the assemblage (Table 3.5) and mainly dip moderately to shallowly (65° to 20°) to the W. Specular hematite veins account for 5% of all veins within the WWA (Table 3.5). This percentage is similar to that found in the East Wall Assemblage and the MHA. Specularite veins are friable within the WWA and the veins that daylight on current pit walls are vuggy (Figure 3.47 – C). They are commonly associated with ankerite; specularite usually forming

the core of veins with ankerite forming a rim or selvage (Figure 3.47 – D). These varieties of vein are displaced by micro-faults within the Box Cut Carbonate (Figure 3.47 – D). They have the same distribution as the magnesite and quartz veins. Hematite veins are regularly spaced down-hole so clustering behaviour (such as quartz veins clustering closer to the Magnesite Fault) is not evident.

A vein sample (ID; 176673) located within the WWA in Stage 1 was sent to Mineral Resources Tasmania to verify vein infill composition. Originally mapped as siderite or weathered dolomite/magnesite, the XRD analysis confirmed vein infill as ankerite. Refer to digital Appendix 9 for XRD results and Section 3.3.2 for a full description of the XRD analysis. The most recent significant drilling within the WWA was in 2008 and this result was not available when the logging was in progress. Distinguishing between magnesite and dolomite within the North Pit is difficult and most magnesite veins are described as being associated with 'weathered' dolomite showing orange staining. These could be ankerite veins so caution is advised when using the magnesite vein data.

3.5.5 Foliation Characteristics

A steeply dipping, pervasive foliation is common within the WWA. The same logging parameters used on the E wall and MHA were employed when logging the WWA foliation; FO1, FO2 and FO3 (see Section 3.2). 73% of all foliations logged within the WWA are weak foliations, 23% are moderate foliations and 4% are strong foliations (Figure 3.48). The number of foliations recorded within the WWA is considerably lower than within the East Wall Assemblage and the MHA suggesting that the rocks of the WWA are not as strongly foliated as the other assemblages within North Pit. Although foliation orientation varies as within the MHA, there is a clear dominant mode dipping steeply to the W; weak foliation is

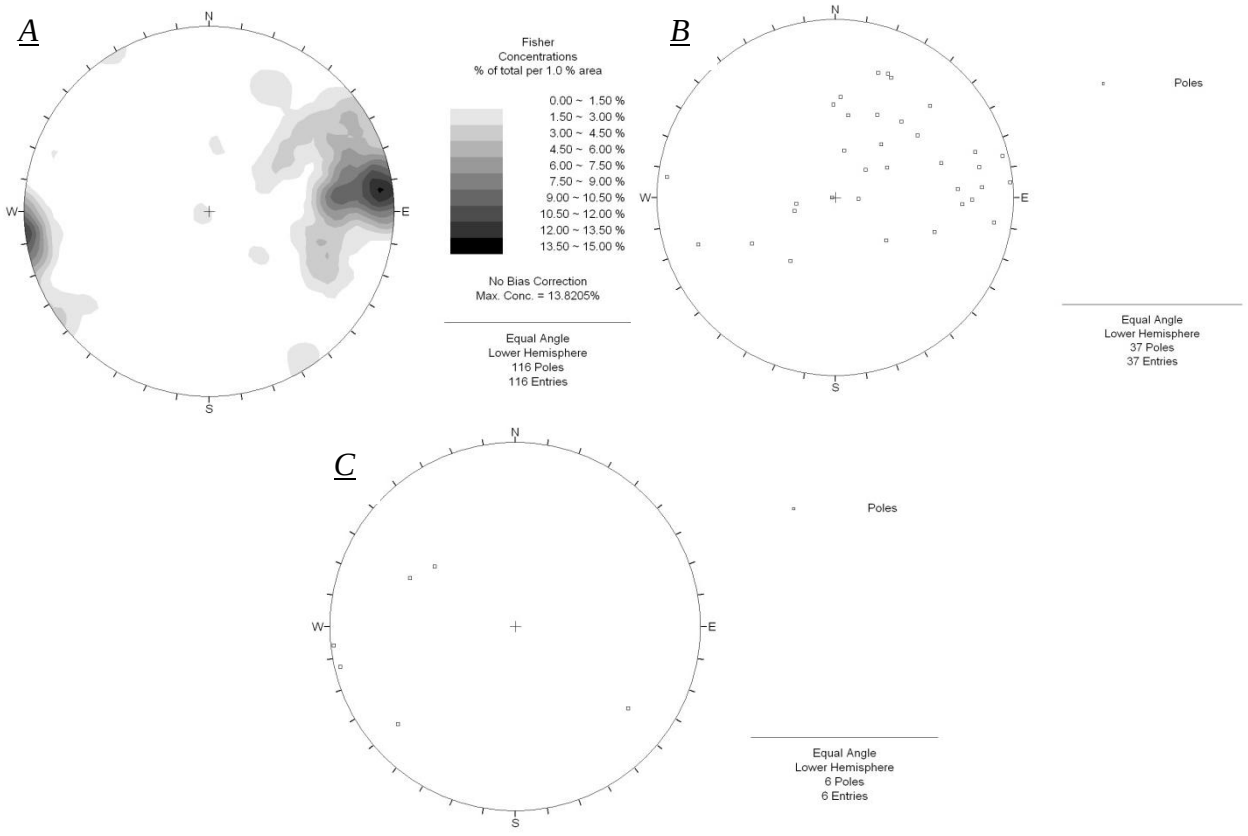

Figure 3.48 – Three stereographic projections of the orientation trends of foliation within the WWA. A - FO1. B – FO2. C – FO3. Plots with ≥ 50 data points are contoured.

85°/263° but measurements are more variable than in the area east of the Magnesite Fault. Examples of medium and strong foliation are much more variable in orientation. Moderate foliation has on average a shallower dip to the W. No pattern can be detected in the small sample of strong foliation. FO2 measurements are concentrated within the Western Wall Banded Schist and Box Cut Carbonate units of the WWA, within 150 m of the Magnesite Fault. FO3 measurements are recorded within 20 m of the Magnesite Fault. Only a small number of foliations were recorded within the Mega Ramp Schist and no foliations were recorded within the Fulfords Creek Schist or the Ahrberg Group of the WWA. The rocks are more intensely foliated closer to the Magnesite Fault. The foliation within the WWA in North Pit is generally not a slope stability concern for the mine. This is due to the majority of foliation planes dipping steeply into the pit face. However, the few foliation planes recorded

that dip steeply to the E is of a geotechnical/slope stability concern for the mine and historically has resulted in the flexural toppling of the W wall in Centre Pit (refer to Section 1.6.2 for a description of historical failure modes of the WWA).

3.5.6 Failure Modes of the West Wall Assemblage

The overall pit slope angle of the W wall in Stage 1 of North Pit is 37°. This is considerably lower than the angle of the E wall due to historical failures within the WWA located in other Savage River open-cut pits. The slope angle of individual benches is approximately 60°. Foliation planes and joints that dip steeply into the pit wall and strike parallel to the pit face facilitate the development of small-scale toppling failures in North Pit (Figure 3.49). Flexural toppling, the type of toppling evident on the W wall, involves continuous columns of rock, which are separated by well developed steeply dipping planes (foliation/joint planes), breaking in flexure as they bend forward. Undermining or erosion of the toe of the slope starts the toppling process and results in the formation of tension cracks, as the failure migrates backwards into the rock mass. Back facing scarps or reverse scarps (Figure 3.49 - B) are produced due to the outward movement of each rock column. This type of toppling failure is difficult to see from the bottom of the slope so the tension cracks along the W wall berms are closely monitored by the geotechnical team on the mine.

Although flexural toppling failures occur on the W wall, they are small-scale and each berm is wide enough to capture the failing rock (Figure 3.49 - C). Joints within the WWA are generally steeply dipping to the W. This is also the dominant orientation of foliation planes and veins. This orientation could potentially facilitate the development of toppling failures if the foliation plane, joint or vein are persistent structures. The veins are not likely to be persistent, joints more likely but foliation planes are very likely to be. The rock however is

more foliated closer to the Magnesite Fault meaning any future cut-backs to the W will decrease the intensity/number of foliation planes affecting the pit wall and thus decreasing the slope stability risk.

Slumping is another failure mechanism evident within the weathering profile of the W wall. An extensive amount of clay and weathered rock is seen outcropping on the benches closest to natural ground level. This clay is unstable and time dependent slumps are common. This was not seen within the East Wall Assemblage or the MHA. The weathering profile of the mine dips to the W thus it is thicker to the W, and the higher benches of the W wall are composed of clay and weathered rock causing slumping problems. Due to the variable nature of some rocks within the WWA, similar to the MHA, the overhang of massive rocks can also be a problem. This is especially the case within the Box Cut Carbonate on the W wall. After heavy rainfall, the foliated and puggy material surrounding massive lenses within the unit is washed away. This leaves large massive boudins of magnesite protruding from the pit face. Due to the erosion of the material surrounding the boudins they fall either in fragments or intact, onto the berm below. This happens within magnesite rich areas (Box Cut Carbonate) and in areas with mafic intrusions (Mega Ramp Schist). Coulthard et al. (2000) state that the overall uniaxial compressive strength of the rock bounding the Magnesite Fault to the W is 25 MPa which is much lower to the 125 MPa of the E wall. Due to the low rock strength and the unfavourable orientation of some joints and foliation, the overall pit slope angle of 37° was considered necessary to ensure stable pit faces.

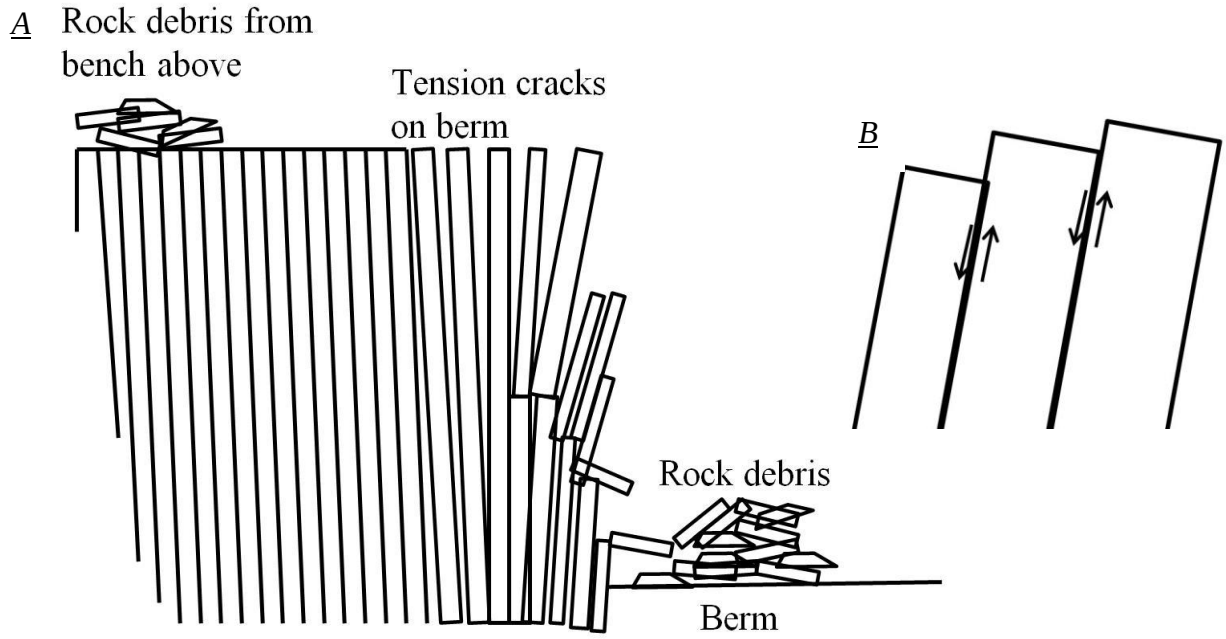

Figure 3.49 – Flexural toppling within the WWA. A – A cartoon drawing of the mechanism of flexural toppling. The bench slope angle is exaggerated. In reality, the inter-berm slope angle is approximately 60 °. B – Interlayer sliding between rock columns resulting in a series of reverse scarps developing. C – Photograph of the 140RL berm, W wall of North Pit looking N. Dotted black lines denote tension cracks within the berm. Note that the berm is wide enough to catch the rock debris of the bench above. The berm is approximately 4m wide at this point.

3.6 Structural Style – Eastern Splay Assemblage

3.6.1 Introduction

The Eastern Contact Fault and the Eastern Splay Fault first daylighted in the S/SSE of North Pit on the 140RL. These two faults created a barren wedge of material on the S/SSE pit wall approximately 100m in length. A total of twenty reverse circulation and diamond boreholes, and mapping traverses were drilled and mapped between 1979 and 2010 in this area. This assemblage is highly variable within the boreholes/mapping traverses. The area was revisited in the present project due to the increased exposure of the section within the pit. Mapping was carried out in November and December of 2010 and the structure in the drillholes was validated. The focus was on lithology and structure. Photogrammetry was used in the Pit for structural mapping. Turner (2006) originally described this area as a continuation of the East Wall Assemblage, although the area was not exposed in the Pit at the time of his mapping.

The results of this work suggest that this wedge is not typical East Wall Assemblage, both lithologically and structurally. This section gives an overview of the Eastern Splay Assemblage from a geotechnical point of view. Figure 3.50 shows a plan view of North Pit. The assemblage is highlighted and the locations of cross sections referred to later within the section are shown. Refer to Section 1.6.1 for a lithological overview of this assemblage. Refer to Section 3.7 for a geotechnical review of the faults in North Pit. Also refer to Chapter 4, Section 4.4.4 for a structural geology review of this assemblage and the faults that bound it.

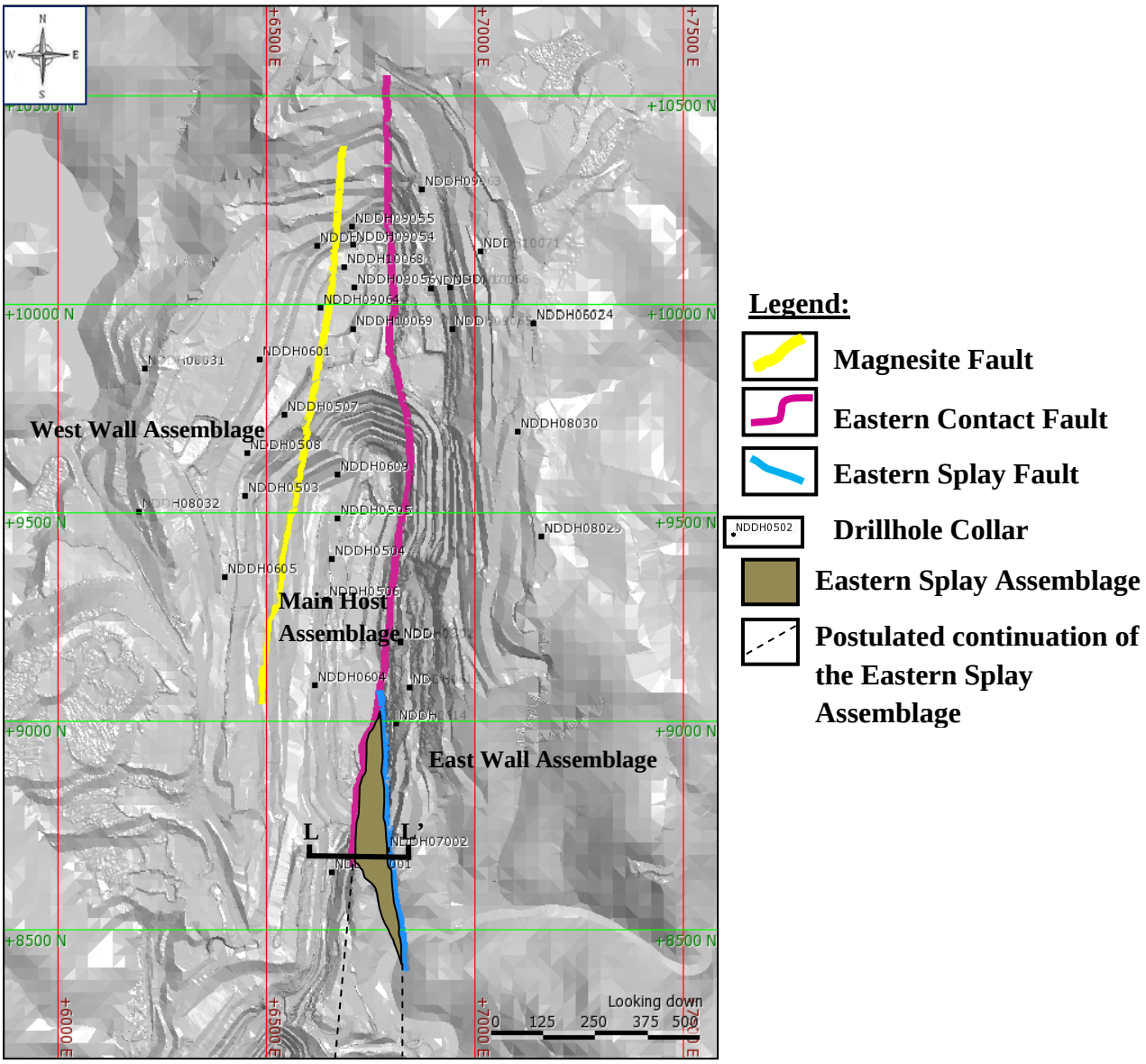

Figure 3.50. Plan view of North Pit showing major fault traces, drillhole location, cross section locations and the Eastern Splay Assemblage.

3.6.2 Joint Characteristics and Spatial Distribution

Of the diamond boreholes drilled within this assemblage, the only orientated holes are NDDH0614, NDDH07001 and NDDH07002. Within these boreholes; 46% of all joints were recorded to contain no infill or mineral coating on the joint plane. 23% were calcite coated joints, 15% chlorite coated, 14% quartz coated and 2% talc coated. The mean orientation of joints with no infill is dipping 06° to the E. Another set is dipping 85° to the NE (Figure 3.51). Calcite coated joints are scattered but are mostly shallowly dipping (Figure 3.51). Other minor sets are dipping 60° to the ENE and dipping 52° to the NNW. Although scattered,

chlorite coated joints are orientated at a mean orientation of 18°/080° (Figure 3.51). Quartz coated joints are mostly dipping to the NE or shallowly dipping. There is only one data point for talc coated joints; this is dipping 10° to the E (Figure 3.51).

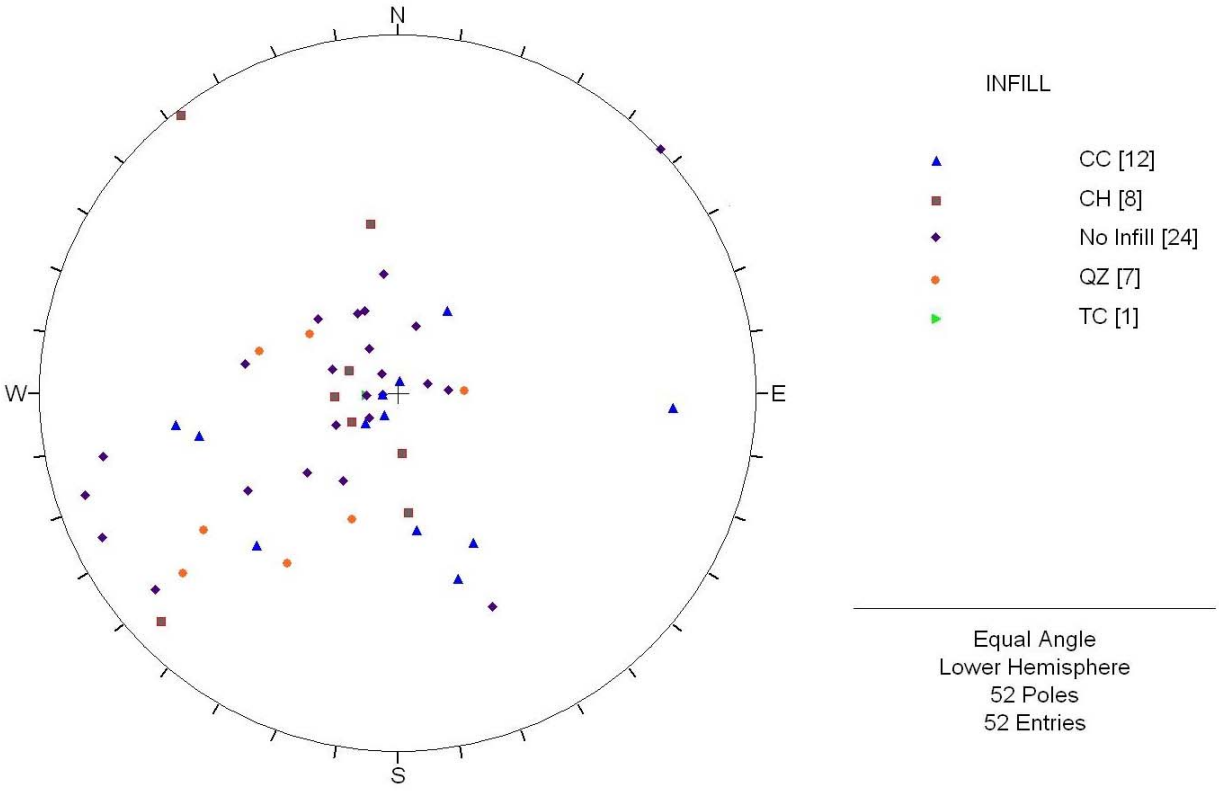

Figure 3.51. Pole plot showing orientation data of joints with no infill, calcite (CC), chlorite (CH), quartz (QZ) and talc (TC) within the Eastern Splay Assemblage.

A three dimensional terrain model (DTM) was generated of the 15m high pit face on the 80RL looking SE using photogrammetry. An additional twelve joints were selected and their orientations were generated by photogrammetry (Figure 3.52). Although many of the joints were too high up the face to see infill type and joint roughness profiles, the majority of these joints had no infill. The additional joint orientation data were plotted on a stereonet (Figure 3.52) using the Adam Technology 3DM™ Photogrammetry in-built stereonet generator.

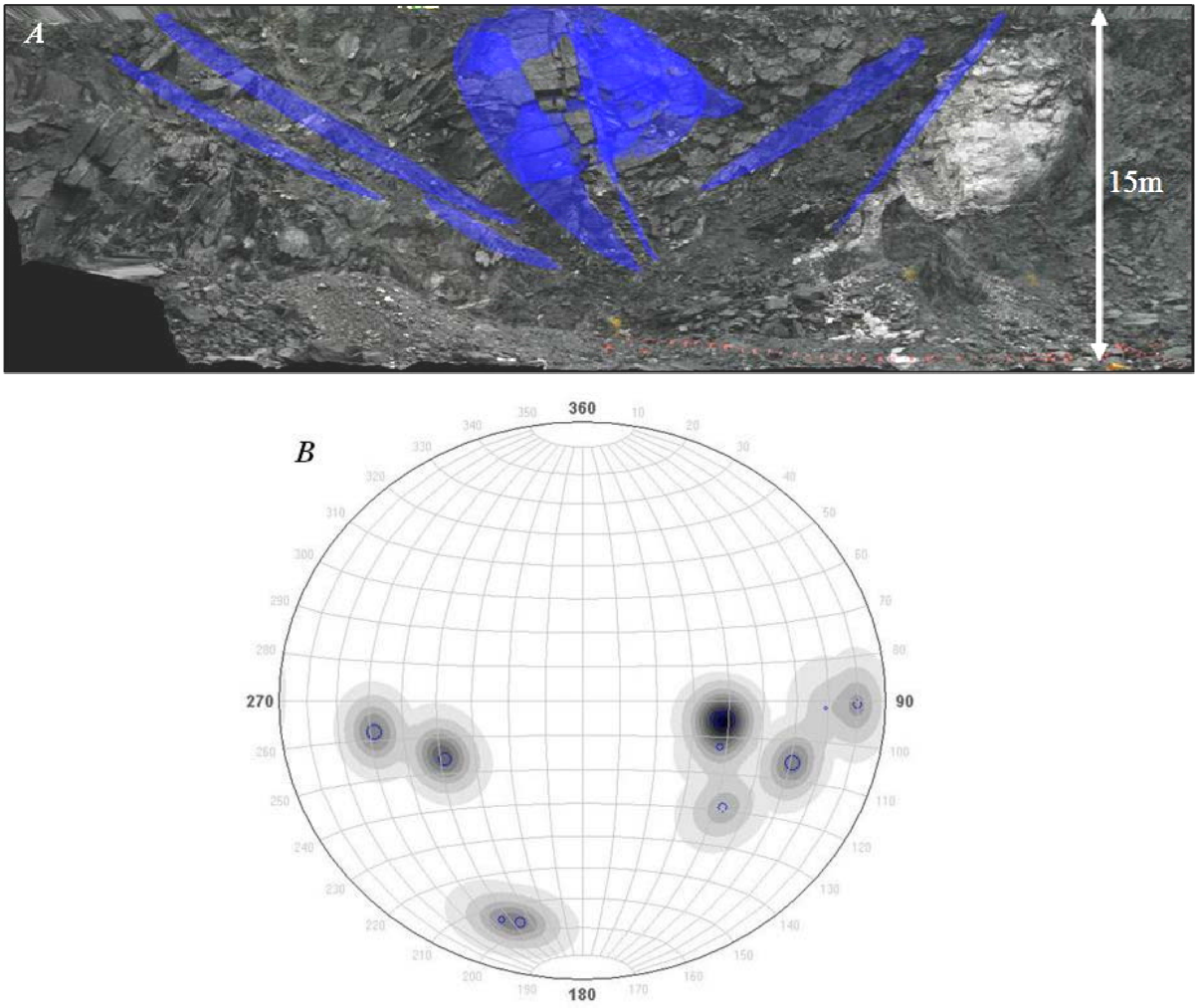

Figure 3.52. ***A***- DTM of the 80RL. Blue halos denote joints. Looking SE. ***B*** – Pole/contour plot showing joint orientation from ***A***. The more persistent the joint in the model above, the larger the pole within the stereonet below.

Many of the joints recognised using the photogrammetry technique are dipping 40° to the W. This is the orientation of a common set of unfavourably dipping joints seen within the East Wall Assemblage ('Ski-jump joints'). These joints are of particular slope stability concern for the mine, acting as basal slip planes for recent failures on the E wall (refer to Section 3.3.2). Although remaining a slope stability concern within the Eastern Splay Assemblage, the difference in the strike of the pit face reduces the risk of failure on these discontinuities. The unfavourably oriented joints are on the eastern end of the face. A damage zone of intensely jointed rock is visible to the E of the Eastern Contact Fault within the Eastern Wall

Assemblage. This damage zone extends N-S along the strike length of the Eastern Contact Fault in some areas such as within the Eastern Splay Assemblage. The unfavourably orientated joints are located within this damage zone.

Comparatively, the orientations of joints logged within boreholes (Figure 3.51) and the joints captured with photogrammetry (Figure 3.52) are different. For all other assemblages within North Pit, many more joint recordings were taken so a general orientation trend is noticeable within a large data set. For the Eastern Splay Assemblage, <70 joint recordings were taken making it more difficult for major joint orientation trends to be visible. Sampling bias also has to be taken into account when using two methods to retrieve joint data. Two boreholes were drilled E to W (NDDH0614 and NDDH07002) and one was drilled W to E (NDDH07001). The trend and plunge of the borehole presents bias within drilling and the geometry of the pit wall presents bias within photogrammetry. This could account for some of the difference in joint orientation between the two methods. The west dipping joints should have been detected in NDDH07001 but this drillhole did not penetrate through to the Eastern Splay Fault (Fig. 3.53) and was 100 m higher where it approaches the fault.

Calcite coated joints were only found within the mafic carbonate rich schist of the Eastern Splay Assemblage. No calcite coated joints were recorded within the dolomitic rich mylonitised rock types within this assemblage. The majority of calcite filled joints have an undulating and rough joint profile. This roughness profile is the most common within the MHA and WWA but an undulating and smooth profile dominates within the East Wall Assemblage. Due to the roughness, friction angles are increased along these discontinuities within the assemblage.

Chlorite coated joints were found within NDDH07001 AND NDDH07002. They are distributed throughout mafic and mylonitised dolomitic lithologies of the assemblage. The orientations of these joints differ from the foliation orientation in the assemblage. Therefore it

is clear that foliation has not been mistaken for chlorite coated joints. Planar and smooth joint roughness profiles are the most common within this assemblage, reducing basic friction angles on the joints. This profile is the same as for chlorite filled joints in all other assemblages of North Pit.

Joints with no infill are the most common within this assemblage. This is a common trend for all assemblages. These joints, although evident at regular intervals down-hole, are concentrated close to the Eastern Contact Fault (Figure 3.53). Undulating and rough joint profiles are the most common, which is different to the undulating and smooth profiles which dominate joints with no infill within the other assemblages.

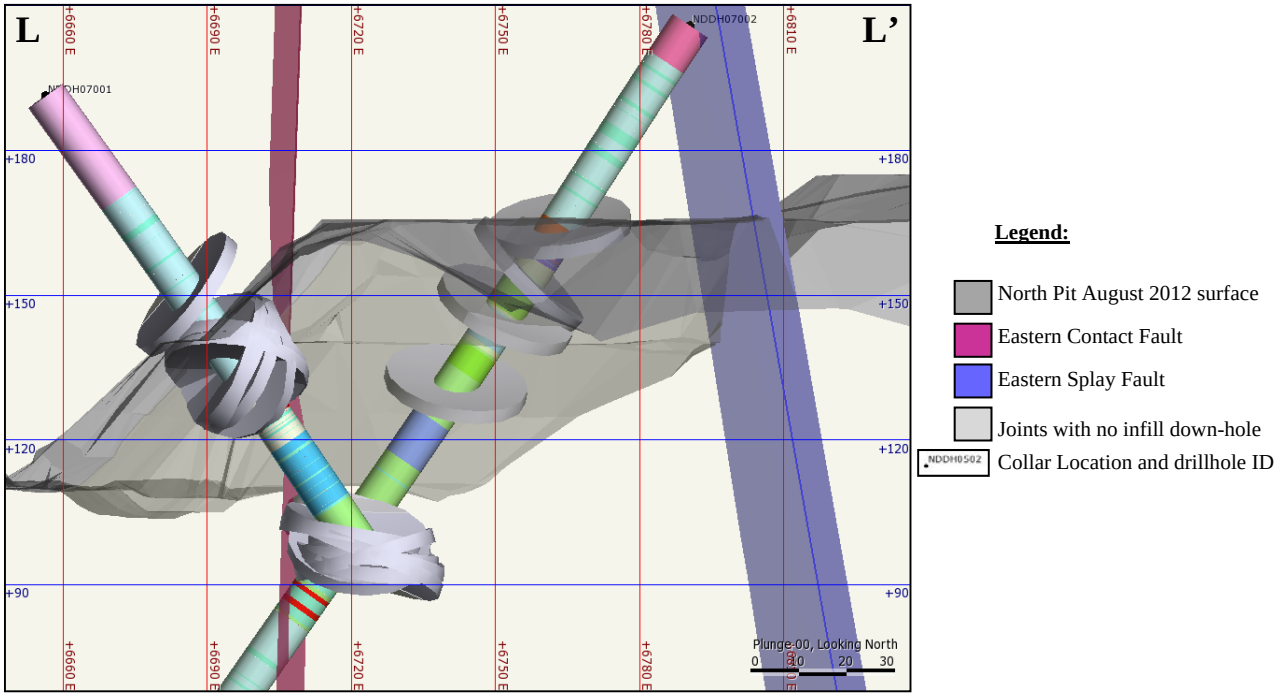

Figure 3.53. Cross Section L-L' showing the distribution of joints with no infill within the Eastern Splay Assemblage; as light grey discs down-hole. Section: 8649 m N (looking N). Refer to digital Appendix 8 for a complete lithological legend.

Quartz coated joints are only distributed within one 10m interval in NDDH07002. The joints are in both mafic and dolomitic lithologies. The proportion of quartz coated joints within the Eastern Splay Assemblage is higher than within other assemblages but with the small sample set this is probably not significant. Undulating and rough joint profiles are the most common,

increasing basic friction angles of these discontinuities.

3.6.3 Vein Characteristics and Spatial Distribution

A small volume of veins were recorded within the Eastern Splay Assemblage. 86% were calcite veins and only one quartz vein was recorded. The calcite vein orientation, although scattered, were shallow and or dipping to the E. Dips range from 10° to 75° (Figure 3.54).

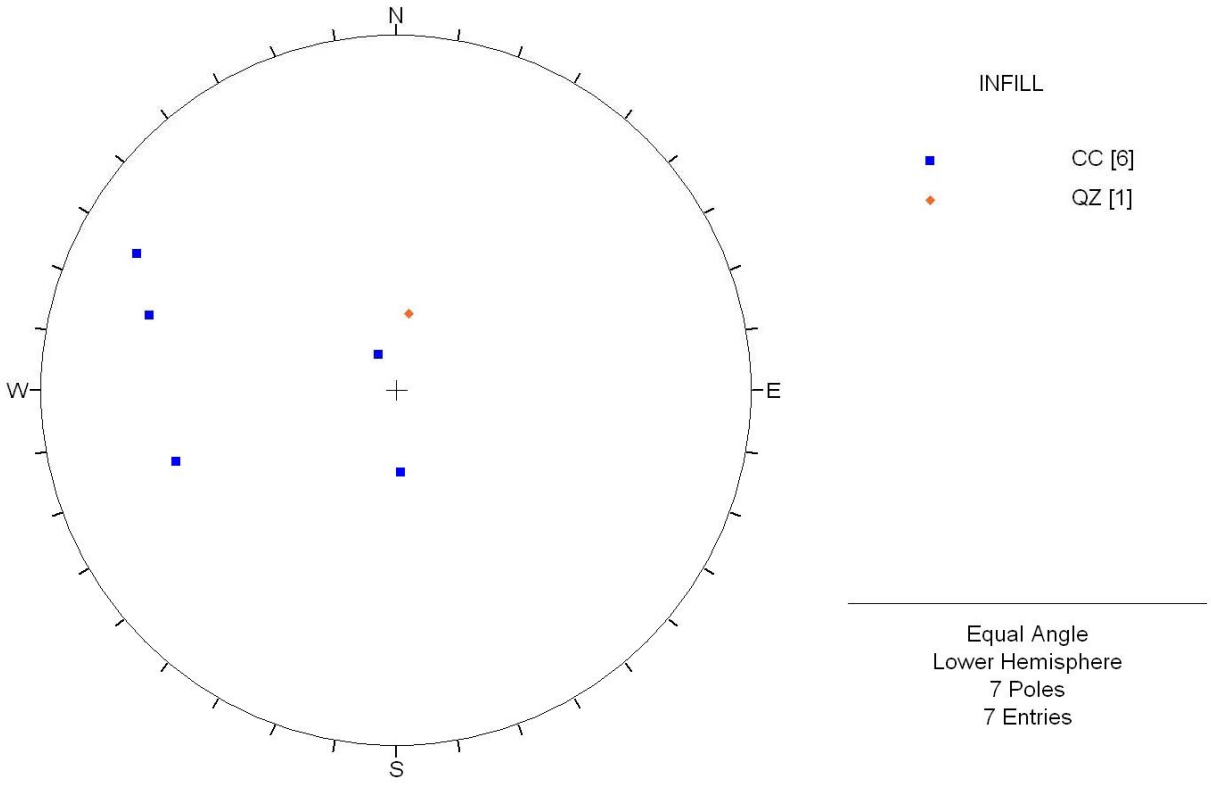

Figure 3.54. Pole plot showing orientation data of calcite (CC) veins and quartz (QZ) veins within the Eastern Splay Assemblage.

Calcite veins occur within carbonate-bearing mafic assemblages of the Eastern Splay Assemblage. The veins are concentrated within a zone 25 m W of the Eastern Splay Fault. The quartz vein was detected within a mafic lithology next to the quartz coated joints described in Section 3.6.2. The quartz veins are strongly deformed, boudinaged and brecciated within this assemblage (Figure 3.55). Calcite veins are not as thick, not deformed and generally are orthogonal to the quartz veins; overprinting them.

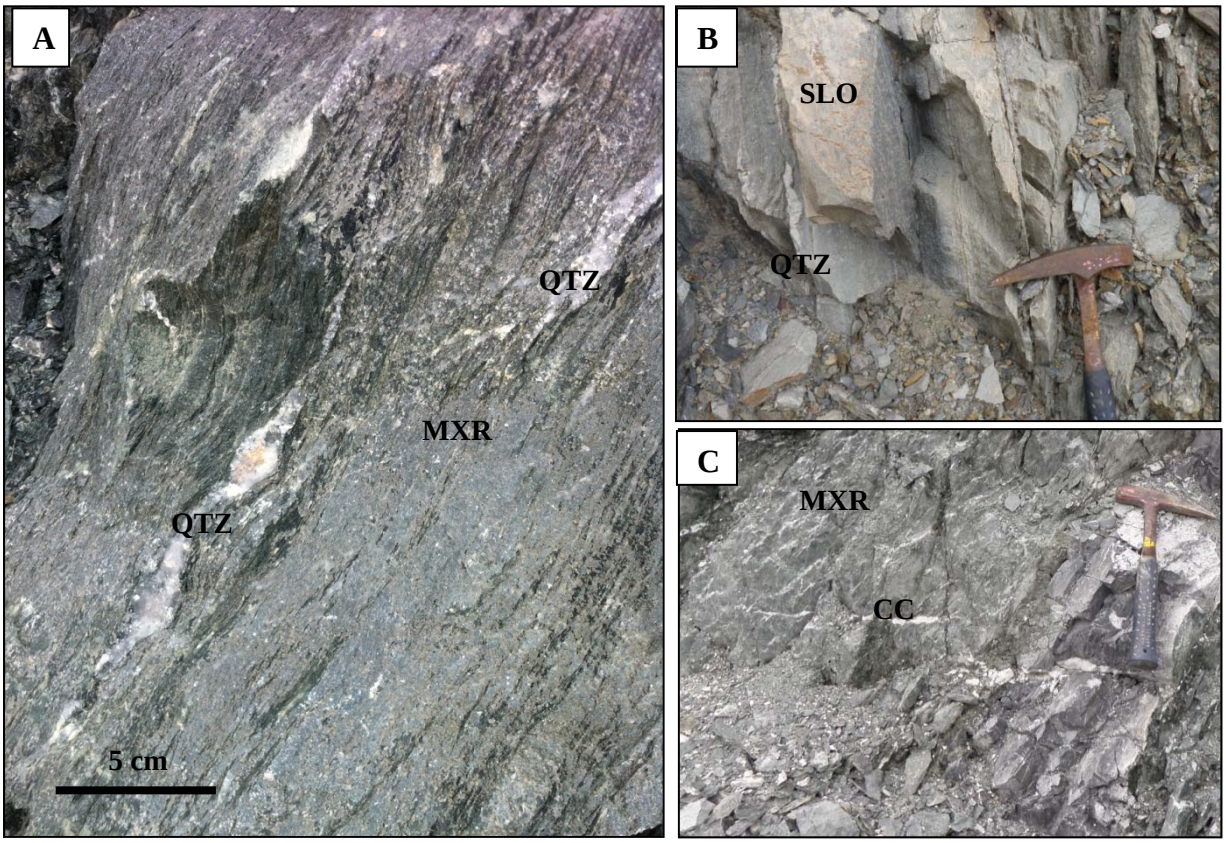

Figure 3.55. Vein types within the Eastern Splay Assemblage. **A** – Boudinaged quartz veins within mafic schist. **B** – Deformed quartz vein within a dolomite rich lithology. **C** – Flat lying undeformed calcite vein within mafic schist. Geological hammer is approximately 35 cm in length.

Abbreviations: QTZ- Quartz, CC- Calcite, MXR- Mafic carbonate schist and SLO- Dolomitic lithology.

3.6.4 Foliation Characteristics

Only a small number of foliations were recorded within the Eastern Splay Assemblage. All the foliations within the boreholes were FO2 (moderate foliation). Refer to Section 3.2 for an overview of foliation logging parameters. There are two main sets of foliation orientation; steeply dipping to the W and moderately dipping to the SE (Figure 3.56).

3.6.5 Failure Modes of the Eastern Splay Assemblage

Failure mechanisms within the Eastern Splay Assemblage are lithologically controlled, similar to the MHA and WWA. Due to the variable structural and strength characteristics of the rocks within the Eastern Splay Assemblage, overhang of massive rocks is a geotechnical

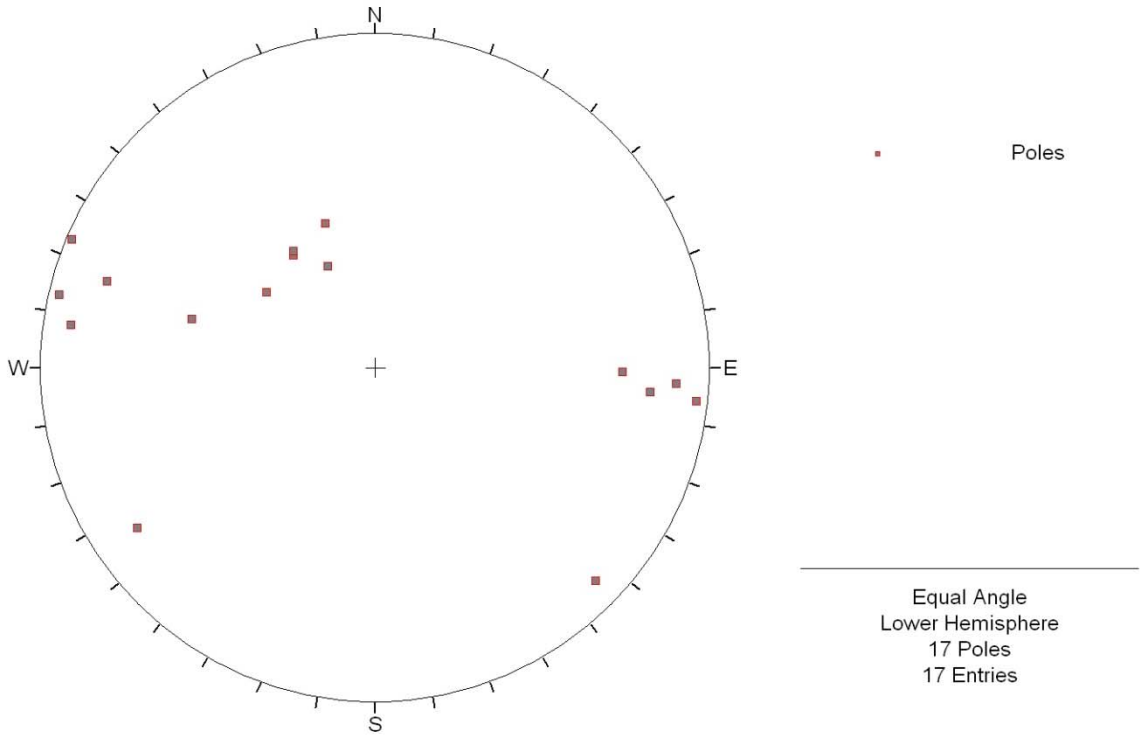

Figure 3.56. Pole plot showing orientation data of foliations recorded within the Eastern Splay Assemblage.

problem. Massive magnesite lenses outcrop within the assemblage (Figure 3.57 – A) in a similar manner to those within the WWA. The kernels of massive magnesite are surrounded by intensely foliated, puggy chlorite rich lithologies which falls down the face after heavy rainfall, leaving the magnesite block protruding and at risk of failure. Similar to the MHA and WWA, weak foliation planes or joints facilitate toppling failures on benches. Figure 3.57 – B and C show how the 140 RL within this assemblage is presenting tension cracks, a sign that there is movement on the wall below. Lithologically, structurally and geotechnically the Eastern Splay Assemblage is very different from the East Wall Assemblage. The East Wall rocks are strong, joint dominated with areas of intense foliation. Puggy, chloritic seams are not observed in these rocks neither are magnesite lenses or variable foliation orientation. The Eastern Splay Assemblage are softer and more schistose than the East Wall rocks, but the failure mechanisms and rock mass behaviour are similar to the MHA and WWA. Persistent hematite coated joints were not found and therefore planar failure is not as much a slope stability concern for this assemblage as for the East Wall. Due to the area originally being

mapped as part of the East Wall Assemblage, caution is advised for future planning in this area.

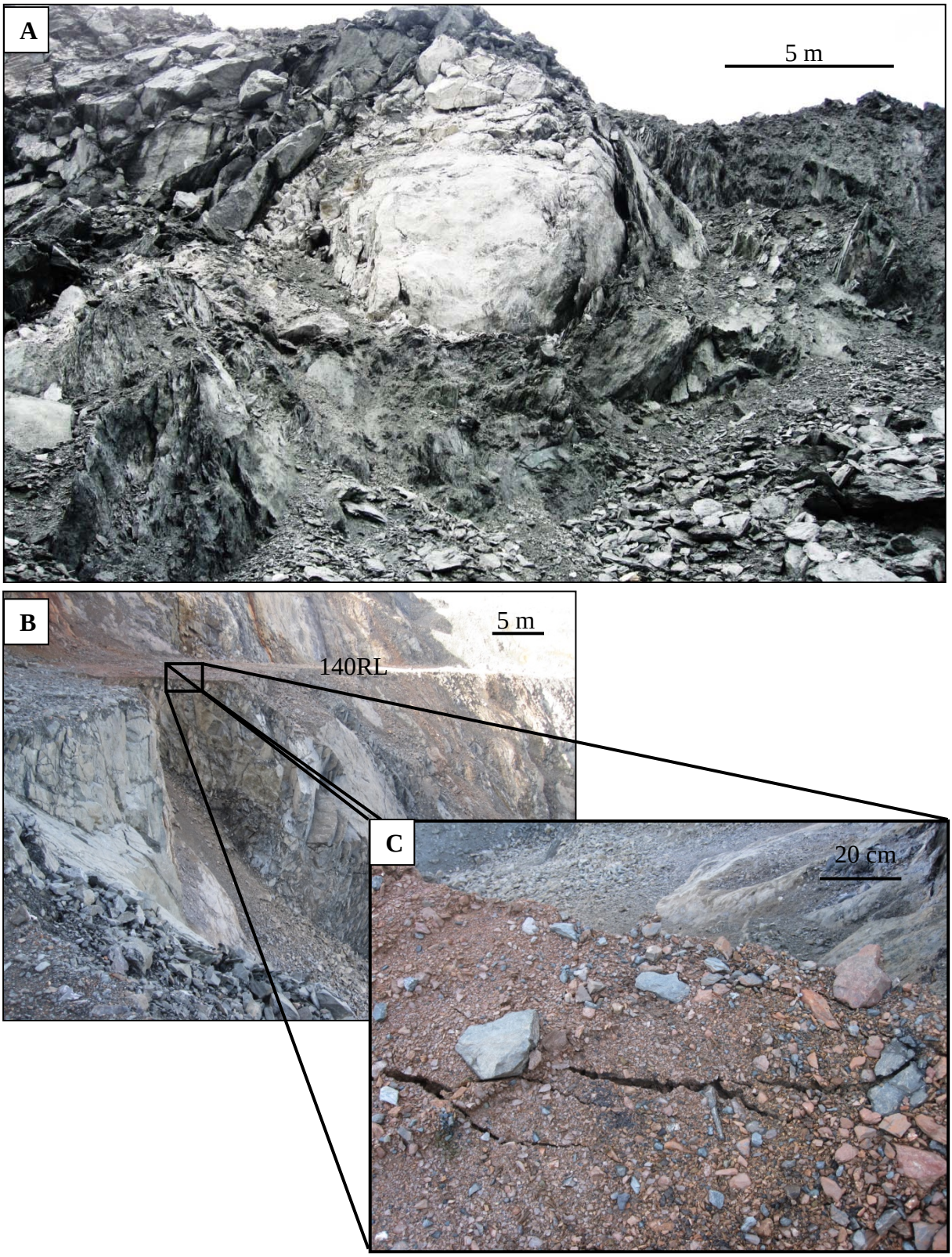

Figure 3.57. A – Magnesite lens within the Eastern Splay Assemblage on the 80RL. Looking SE. **B** – The 140RL berm within the Eastern Splay Assemblage. Looking SW. **C** – Tension cracks on the 140RL berm.

3.7 Major faults in North Pit and associated failure mechanisms

3.7.1 Introduction

Three major faults are recognised within North Pit. The Eastern Contact Fault (ECF) which separates the East Wall Assemblage to the E from the Main Host Assemblage (MHA) to the W. This structure runs parallel to the eastern limit of the Main Ore Zone (MOZ) within Stage 1 and 2 of North Pit. The Magnesite Fault which bounds the MHA to the W is named due to the presence of magnesite to the W of the fault. The Eastern Splay Fault which splays off the Eastern Contact Fault to the E creates an unmineralised wedge of rock in between the two faults. The Eastern Splay Fault daylighted within North Pit in 2009. This section describes each fault from a geotechnical perspective and outlines past failure mechanisms relating to each (refer to Chapter 4, Sections 4.4.3 to 4.4.6 for a description of the faults from a structural geology perspective).

3.7.2 Eastern Contact Fault

The ECF consistently dips steeply to the E and strikes N-S. A damage zone of variable thickness is evident along the strike length of the ECF in North Pit. This is characterised by a graphite rich zone and/or a dolomite rich zone bounding the fault plane to the W commonly transitioning into a zone of talc alteration, an increased number of sub-horizontal calcite veins, hematite coated joints and unfavourably orientated joints (ski-jump joints) directly to the E of the fault. The N-S strike and weak rock strength of the graphite and/or dolomite rich zones ensures slope stability issues in these areas along the fault. Due to the nature of the alteration W of the fault, rocks within this zone fail onto capture berms below (Figure 3.58 – A and B). The MHA to the W of the fault is generally weak so the excavation of the fault zone further to the E is advised. Benches displaying the graphite/dolomite rich zones are a slope stability risk for the mine.

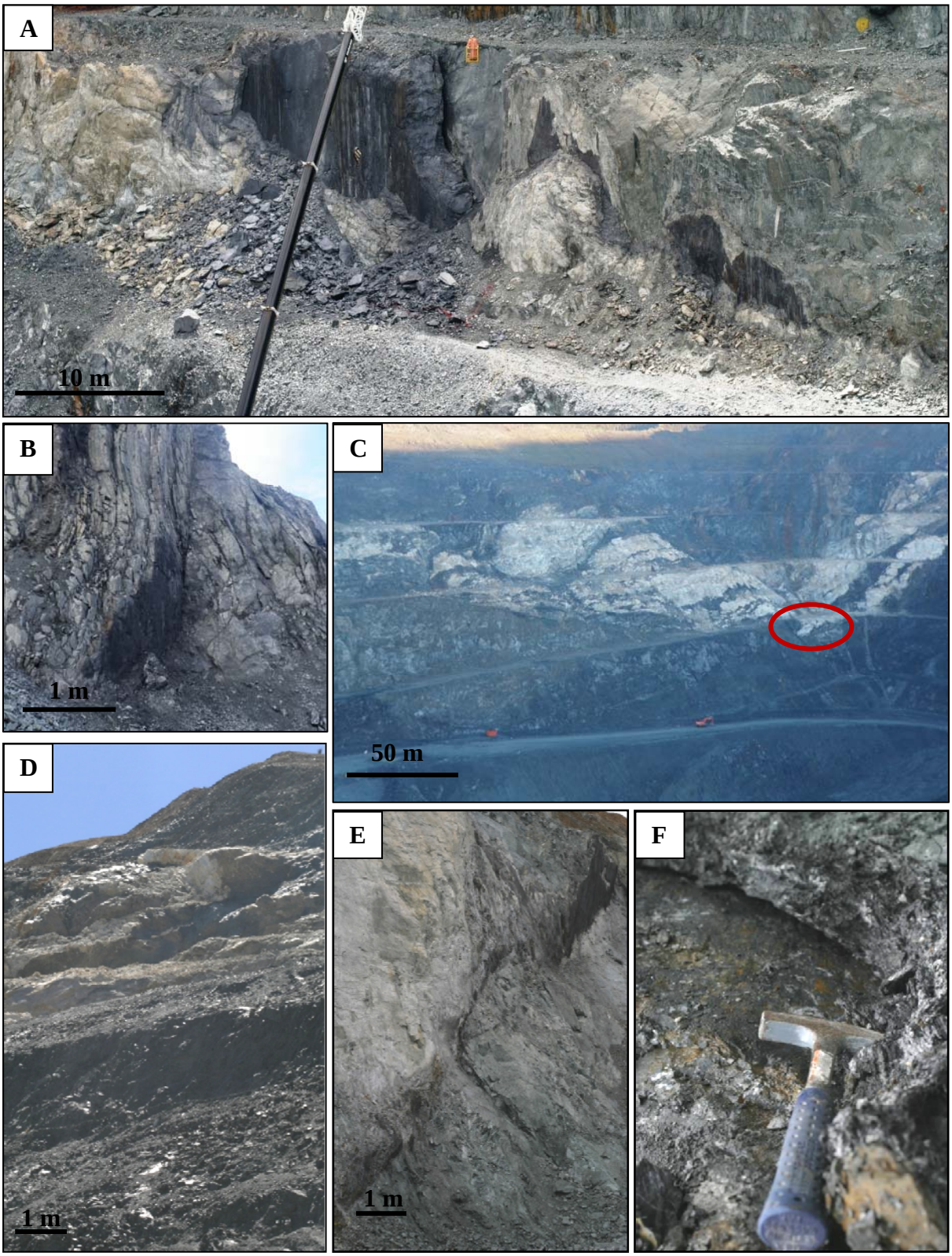

Figure 3.58. A – ECF in Stage 1. Graphite zone defining the fault is exposed on the E wall pit face. Looking NE. **B** - Another example of graphitic area on the ECF trace in Stage 2. Looking SE. **C** – WWA and the MHA, showing the Magnesite Fault. Berm failure is highlighted in red. Looking NW. **D** – An example of magnesite overhang within the Magnesite Fault zone. Looking W. **E** – Graphitic trace of the Eastern Splay Fault. Looking SE. **F** – Puggy zone on the Eastern Splay Fault. Geological Hammer length is approximately 35 cm in length.

3.7.3 Magnesite Fault

The Magnesite Fault is planar, dips steeply to the W, and contains graphitic puggy gouge. Directly to the W of the feature is the Box Cut Carbonate. This W wall unit contains a high volume of magnesite with variable amounts of soft, chloritic schist. The fault was intersected when the 140 RL on the W wall was excavated (Figure 3.58 – C). The crest of the berm eventually failed due to the soft, puggy nature of the rock surrounding the fault plane. Therefore caution is advised when designing a bench to be excavated on or within 5 m from this fault plane. The area directly to the W of the Magnesite Fault contains large lenses of magnesite. As with the MHA, WWA and Eastern Splay Assemblage, the overhang and potential failure of more massive rocks within a puggy chloritic matrix is likely near the Magnesite Fault (Figure 3.58 – D).

3.7.4 Eastern Splay Fault

The Eastern Splay Fault dips steeply to the E, splaying off the ECF to the E at the S end of North Pit. The fault plane is characterised by graphitic gouge (Figure 3.58 – E and 3.59) and has >20 mm gaps along the fault boundary in the present exposure (Figure 3.58 – F and Figure 3.59). When first day lighted in 2009, water was seeping from the fault plane but this has since dried up due to horizontal dewatering/depressurising boreholes being drilled in the area. At least in part due to the water, a plane failure occurred in October 2009 on the area directly to the W of the fault, exposing the fault plane (Figure 3.59). The failure was small in comparison to other failures in North Pit both before and after October 2009. Failures seen near to or directly on the fault planes are lithologically controlled. Damage zones occur from <1 m to tens of metres thick and are associated with all major faults of North Pit. Future pit planning must take the geotechnical properties of fault damage zones into consideration and not necessarily focus on the fault as a 2 dimensional feature.

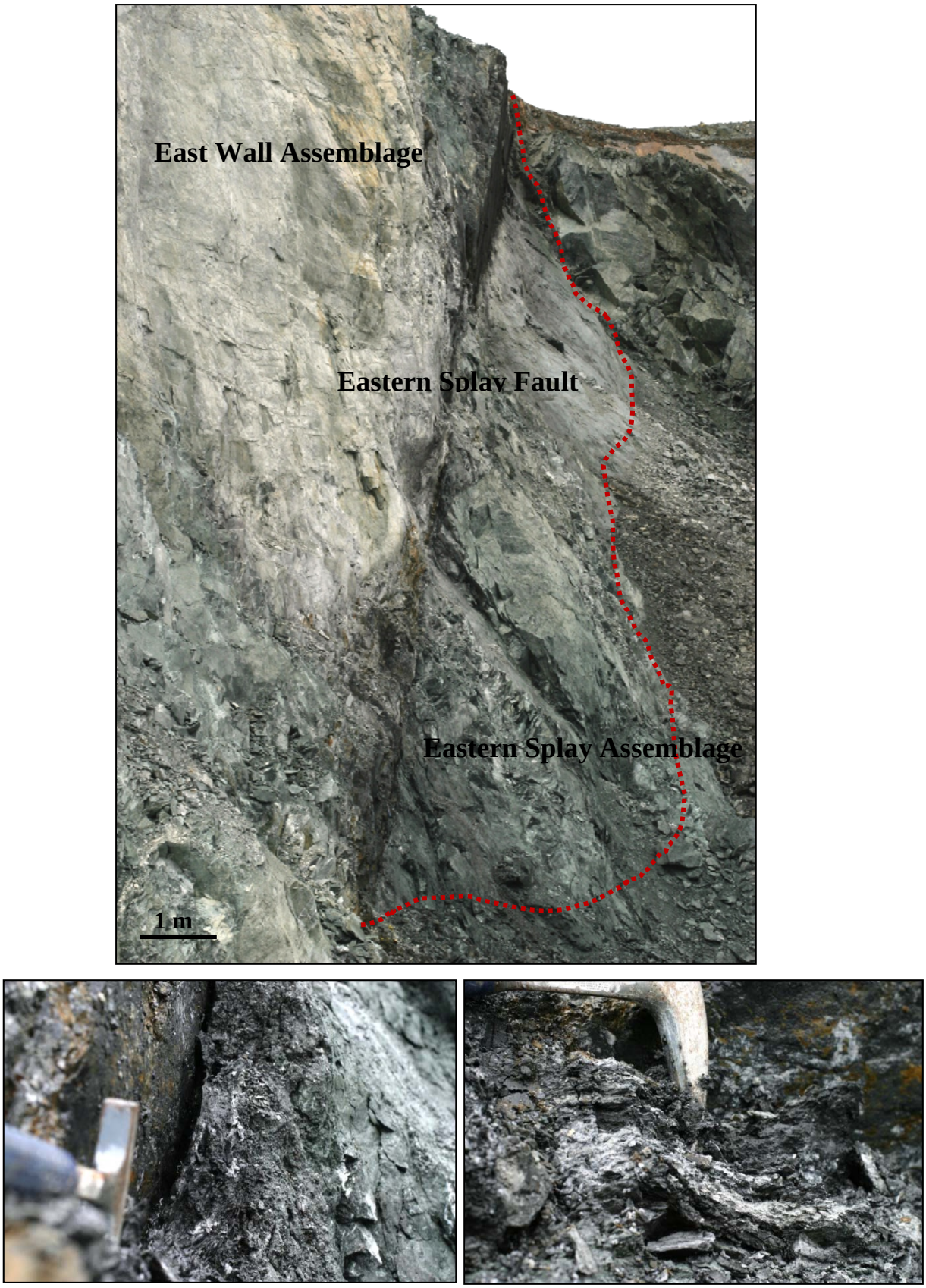

Figure 3.59. A –The Eastern Splay Fault highlighting the October 2009 rock fall area (dashed red line). Looking SE. **B** – The aperture along the fault plane. **C** – Puggy gouge at the fault plane.

3.8 Discussion and conclusions

3.8.1 Geotechnical Significance

From a future mine planning perspective, several major conclusions of the geotechnical properties of each assemblage should be considered. The orientation of hematite infilled joints and 'ski-jump' joints of the E wall facilitate plane and wedge failure. This research has confirmed that hematite coated joint and 'ski-jump' joint frequency per metre diminishes 140 m and 160 m E of the ECF respectively. This is due to the ECF damage zone which varies in composition and thickness along strike (refer to Chapter 4). The hematite coated joints display clustering behaviour and mainly occur within the southern area of North Pit (where historic failures have occurred). 'Ski-jump' joints also follow this pattern. Structures that steeply dip to the SW cut-off the hematite coated joints. Three major structures with this orientation are the 'Northern Shear', 'Hawkie's Fault' and the 'Waterfall Fault' in Stage 2 (mine nomenclature), the Northern Shear being the most northerly structure cutting off the cluster of hematite coated joints to the S. If the E wall at the southern extent of North Pit is excavated further to the E (E of the fault damage zone) large multi-berm failures will be minimised. The failures that occur within the East Wall Assemblage are structurally controlled and primarily joint dominated.

Since the commencement of this research and the subsequent rock failures from the east wall since 2009, future plans have been extensively changed in regard to the east wall. Original plan parameters included; bench heights at 30 m, batter angles at 90°, the berm width at 12 m and the inter-ramp slope angle (the angle which is measured from toe to toe or crest to crest exclusive of any ramps) at 74.6°. The proposed revised east wall design comprises the following; bench heights at 30 m, batter angles at 60°, the berm width at 12 m and the inter-ramp slope angle of 45.7°. The inter-ramp slope angle would be less than the average dip of the ski-jump joints which is 47°. This research has confirmed that the ski-jump structures act

as basal surfaces facilitating failure. This plan ensures that due to the lower slope angle less ski-jump structures will be intersected thus minimising large wall failures to small batter scale failures.

Comparatively, many more joint infill minerals and veins are observed within the MHA than within the East Wall Assemblage; reflecting the variability in lithology within this assemblage. Failures within the MHA are structurally controlled (small-scale wedge failure and slumping) and lithologically controlled (massive lenses within an intensely foliated matrix). The consistent and regular mapping of different rock types within the MHA is paramount in ensuring decreased risk of rock failure of temporary and final pit walls. The modal orientation of all joints (steeply dipping to the W) and cleavage (sub-vertical) should be taken into account when predicting the geotechnical performance of planned and future open pit designs.

Historically, the major failure modes of the WWA are flexural toppling (structurally controlled) and slumping (lithologically controlled). The discontinuities facilitating the development of toppling failures on this wall are weak cleavage planes. A steeply W dipping foliation is present within the Box Cut Carbonate and Western Wall Banded Schist. The small number of cleavage planes recorded in the Mega Ramp Schist and none recorded within the Fulfords Creek Schist or the Ahrberg Group suggests that if the W wall was cutback a further 175 m to the W, to these non-foliated rock units, failures will be minimised. However, gypsum coated joints are present within the Fulfords Creek Schist, reducing basic friction angles considerably. This has to be taken into account when planning W wall cut backs. The proposed end of mine-life North Pit model is presented in Figure 3.60. The orebody is highlighted; low grade ore and high grade ore are coloured blue and red respectively. The position of the west wall of this design is a further 200-300 m W of the current west wall in North Pit, thus intersecting the units and brittle features discussed in this research.

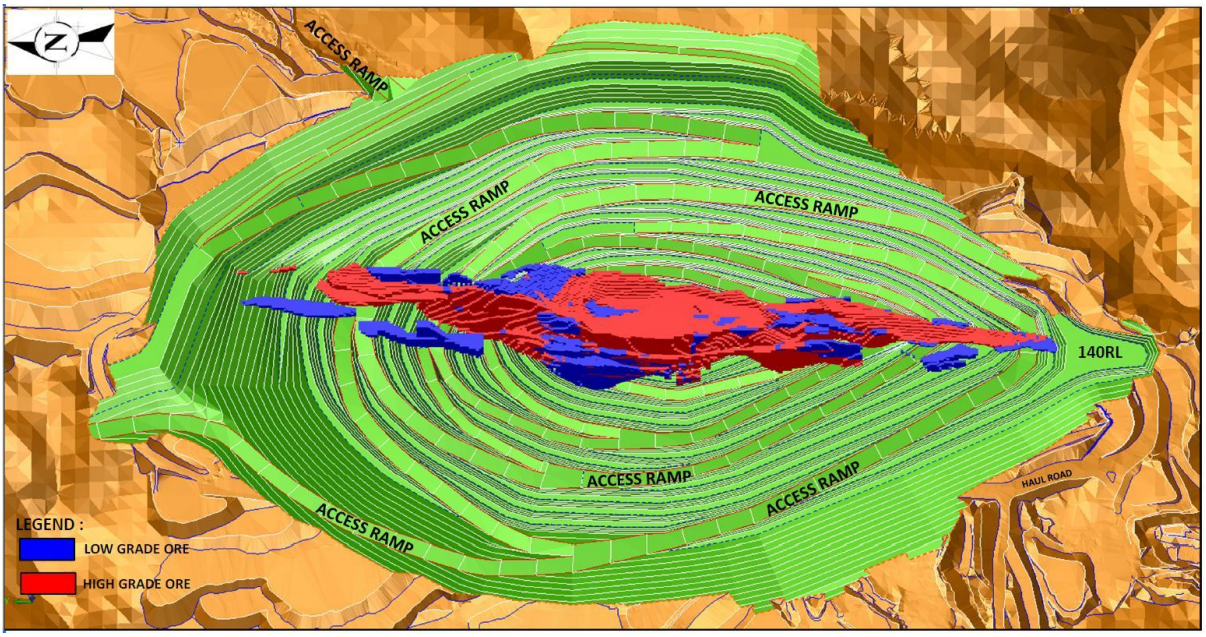

Figure 3.60. Plan-view of North Pit showing the end of mine-life design and orebody. Modified after Grange Resources, 2012.

Due to its location at an intersection of two large scale faults, the Eastern Splay Assemblage is not a typical East Wall Assemblage as previously mapped but a variable, barren melange of massive and foliated rock. Additional folding is common. It would be more realistic for the mine to treat this package of rocks as geotechnically similar to the MHA as the rock mass is has similar geotechnical characteristics to the MHA as opposed to the East Wall Assemblage. The geotechnical mapping of major faults is also paramount in the minimisation of failure on these structures along strike. It is recommended that soft graphite and dolomite rich lithologies, present at some areas of the fault damage zones, are excavated and mined until the rock is hard enough to withstand periods of exposure in the pit without the risk of failure. Table 3.6 summarises the failure modes apparent within each rock package in North Pit.

Failure Mode	Rock Assemblage(s)	Comments
Toppling	MHA, WWA	Requires foliation plane shears to dip steeply into the wall and be spaced at 1-10m apart
Rotational Wedge	MHA	Related to transverse faults dipping at 40^{o}-80^{o}. rock gradually rips through intact or jointed rock due to lack of second continuous discontinuity to form classic wedge.
Circular	MHA, WWA, highly weathered rock	Generally through weak rock but occasionally structurally controlled by foliation
Large Scale Slumps	MHA	Several slumps in weak ore or along undulating hematite coated discontinuities in MHA.
Complex	MHA	Usually controlled by weak rock and structural features
Planar	East Wall Assemblage	Controlled by unfavourably dipping 40^{o}-60^{o} "ski-jump" discontinuities

Table 3.6. Failure modes and rock assemblage relationships. Modified after Grange Management Plan Ground Control- The Geotechnical Domain Model, 2013.

3.8.2 Methods and Protocols Development

The measurement procedures employed to carry out this research utilised a metal pivoting arm protractor to measure alpha angles of discontinuities. This method is very precise and is much easier to use than flexible wrap-around protractors. To measure the beta angle, the wrap-around protractor method was employed. The protractor has to be printed on transparent film as it is easier to see any lines drawn on the core. The wrap-around protractor template was taken from http:/www.holcombecoughlinoliver.com/, structural geology consultants. For this research, the logging system was modified to include measurements of lines (striations) on discontinuity surfaces. The alpha and beta were measured on the plane and the gamma (γ) angle of the line within the plane measured using the same wrap-around protractor as was

used to obtain the beta angle. This method is quick and easy compared to the 'rocket launcher' technique. Due to the large volume of discontinuities in the rock core needing to be measured, the time it takes to measure orientation is very important. However, core orientations, core integrity and the confidence in orientation marks need to be checked from the start of each drilling program to identify any problems early.

A detailed geotechnical drill core logging protocol (refer to Section 3.2) is essential in obtaining the maximum amount of useful data from each structure within the rock core. The defect infilling, thickness and roughness of joints is very important in categorising joint sets and estimating friction angles. Measuring rock strength is an important parameter in slope stability analysis. Measuring the orientation of joint surface decoration such as slickensides and slickenlines (the γ angle) proved to be useful in this research. Although discontinuities with striations present on the plane are referred to as 'joints' within the geotechnical logging, from a structural geology point of view, they are micro-faults. Within the logging dictionary employed at Savage River Mine at the time of this research, there was no option to log these defects as micro-faults. Subsequently the logging dictionary was changed in October 2011 to include 'MF' – Micro-fault. As a gamma angle was recorded of striations on micro-faults for the duration of this research, this did not present a major problem. However, pre 2009, micro-faults or gamma angles were not recorded, ensuring difficulty in locating micro-faults throughout the assemblages. Kinematic indicators are discussed in Chapter 4. Foliation breaks and larger scale faults also could not be logged at the time of the research due to the logging dictionary. Subsequently these have been added to the current Savage River Mine geotechnical logging dictionary.

The information on discontinuity infilling is not only useful in the estimation of friction angles but in the purely geological prediction of the type of circulating fluids within the rock packages. Hematite coated joints of the East Wall Assemblage and MHA are present within

lithologies with no matrix hematite. This could be due to an influx of an oxidised fluid such as meteoric water. All other joint infill types of all assemblages in North Pit are limited to lithologies containing some of the infill mineral in the matrix. Therefore, the fluid circulating through the joint is probably locally buffered. From using the geotechnical data alone it is clear to see that a damage zone is present surrounding the major faults of North Pit. Lithology is different within these zones as well as vein orientation and joint distribution. The damage zone is variable along strike. Refer to Chapter 4 for a description of fault damage zones from a geological perspective.

The orientation data collected from joints, veins and foliations do not include many measurements dipping N or S. It is important to acknowledge possible sampling bias as a potential cause. All drillholes used for this research trend E (70° to 98°) or W (251° to 295°) so the identification of N or S dipping structures is more difficult. Much of the data obtained from the WWA is from E trending drillholes, introducing increased sampling bias in this area. The East Wall Assemblage structural data is mainly obtained from W trending drillholes apart from 4 drillholes that were drilled to the E. The MHA data is obtained from both W and E trending boreholes. The plunge of the drillholes (40° to 68°) also adds to the bias, meaning structures that dip similarly to the plunge as the drillholes are more difficult to detect. The alpha, beta and gamma angle measurements in the core are also measured to the nearest 5° which needs to be taken into account when commenting on sampling bias. To help minimise sampling bias, photogrammetry was used to obtain structural information of pit faces. Although sampling bias occurs with this method as well (due to the slope geometry and the orientation of the pit wall) the method was used to combat sampling bias in drillcore. As well as photogrammetry, a trial investigation with an Unmanned Aerial Vehicle (UAV) was carried out in North Pit in 2012. Although this method is not currently used on site, a comparative analysis between this technique and the current mine photogrammetry technique was documented (refer to Appendix 1).

CHAPTER 4
FAULT STYLES

4.1. Introduction

This chapter describes the style of small and large-scale faults exposed in North Pit, Savage River Mine. Kinematic indicators present on microfaults of the East Wall Assemblage and MHA are discussed first. Structural and geological drill core logging and in-pit mapping techniques have provided the data used in this chapter. The drill core used was a product of the 2005-2007 resource drilling campaign, the 2008 geotechnical drilling programme and the 2009-2010 resource drilling programme. 18 drillholes intersect the Eastern Contact Fault (ECF) along a 1700 m N/S strike length. 10 drillholes intersect the Magnesite Fault along a 1050 m NNE/SSW strike length. 2 geotechnical drillholes intersect the Eastern Splay Fault along a 375 m NNW/SSE strike length.

4.2. Kinematic Indicators

In order to gain additional information into the direction of latest movement within the brittle rocks of the east wall and Main Host Assemblage, minor structures such as slickenlines and striations on microfault planes were described and the orientation recorded. The method used involved measuring the gamma angle of the lineation. This involved firstly measuring the alpha and beta angles of the plane containing the lineation. Then measuring the lineation anticlockwise, looking down-hole, from the down-hole end of the long axis of the elliptical trace of this plane. The results were entered into the Microsoft Excel™ based program, *CoreSolutions* (Scott et al., 2005). This program determines the 'real-space' orientations of structures in axially-oriented drill core (Scott, 2005). The orientations of both planar and linear structures are determined from their angular relationships to the core axis and a bottom-of-core orientation line (Scott, 2005). A software package, 'Stereonet for Fault-Striation

Analysis' (Yamaji, 2001) was used to show fault-slip data although due to the nature of the striations logged, the shear sense was not determined.

Pre 2009, kinematic indicators such as slickenlines and striations were not a geotechnical or geological core logging parameter integrated at Savage River Mine. Therefore there are fewer resulting lineation orientations compared to joint, vein and foliation orientations for each assemblage. The resulting stereoplot for the east wall is shown in Figure 4.2. The great circles of the microfaults are plotted as well as the lineation direction. Due to the polished nature of the striations, the sense of shear was not clear and therefore not plotted. All striations and slickenlines are quite shallowly plunging (≤45°) trending to the N and S. Joint decoration lineations on chlorite filled structures are plunging at a shallow angle (≤36°) to the south (4) and north (2). Lineations on calcite filled structures are plunging at a shallow angle of ≤20° to the N and S. A conjugate fault system is likely given the orientations shown on the stereonet with the faults dipping shallowly (17° to 36°) to the S, SE and NE. The chlorite and calcite coated faults on the E wall are probably of the same age. Although no striated hematite coated faults within the East Wall Assemblage were intersected by any of the post 2009 drillholes, they are visible on the high benches of the east wall (Figure 4.6 – A). On these same planes, discontinuous polishing of the infill mineral is visible (Figure 4.6 – B and D).

Movement indicators are also evident within the MHA (Figures 4.3 to 4.5). Lineations on hematite coated faults (Figure 4.3, 4.6 – C) are moderately plunging (≤54°) mainly towards the N with 15% of lineation readings trending S. The fault planes are moderately to gently dipping (≤79°) to the NW, NE and SE. The kinematics of the NE dipping faults (Figure 4.2) indicates oblique movement and the SE dipping faults a dip/slip movement. Two possible transfer faults dip to the NW. Hematite coated joints day-lighting on the pit faces of North Pit cut across many other structural features on the pit wall, indicating that these faults are late in the fault history (Figure 4.1). No faults are known to offset these surfaces. The presence of

hematite coating indicates the influx of oxidised water into these structures. This circumstantial information supports correlation of these structures with the Tertiary extensional event in Tasmania (c.f. Stacey and Berry. 2004). The Southern Rift System developed south of Australia in the Jurassic (e.g. Veevers et al. 1991). The Sorell, Bass and Durroon rift basins were initiated in the latest Jurassic–Early Cretaceous by a NE-SW oriented, extension. Regional NW-SE shortening in the Cenomanian (Miller et al. 2002) resulted in folding of the Otway Ranges and uplift over most of SE Australia (e.g. Kohn et al. 2002). A phase of strike slip faulting is prominent in western and southern Tasmania. These faults are widespread but largely minor in nature. The faults affect rocks as young as 100 Ma and are probably caused by this Cenomanian inversion.

In the Late Cretaceous (at about 90 Ma), the Bass Basin extended onshore with the opening of the Tamar Graben. The Devonport-Port Sorell Sub-basin formed in the Early Paleocene, and the Longford Sub-basin in the Late Paleocene. On the west coast, the Sorell Basin extended onshore with the development of the Macquarie Harbour Graben in the Late Paleocene. During the Eocene the major southern rift basins were opened (Derwent Graben, Coal River Graben).

The large-scale topographic depressions produced by the Tamar Graben, the Devonport-Port Sorell and the Longford Sub-basins, are easily observed on the DEM, as are the main boundary faults of these structures (Stacey and Berry 2004). In western Tasmania, there is a discrete break in topography that runs north south just west of Rosebery. The unconformity at the base of the Permian is offset 1000 m along this zone. Late ?Tertiary normal faults dipping SW were reported near Tullah by Berry (1989). Low temperature, sometimes clay filled normal faults are common in NW Tasmania and at least in part these are younger than the Cretaceous strike slip faults. In Western Tasmanian the latest normal faults strike generally N-S but vary over a large range and commonly reactivate older faults.

Mio-Pliocene compressional tectonics is widely recognized in Victoria and measurements of the modern stress field indicate that Tasmania is also affected by a NNW compressional stress. However there is very little evidence for neotectonic structures in Tasmania. The only active fault scarp is the Lake Edgar Fault (Stacey and Berry 2004).

Figure 4.1. An example of a late hematite coated fault with striations cutting off other features.

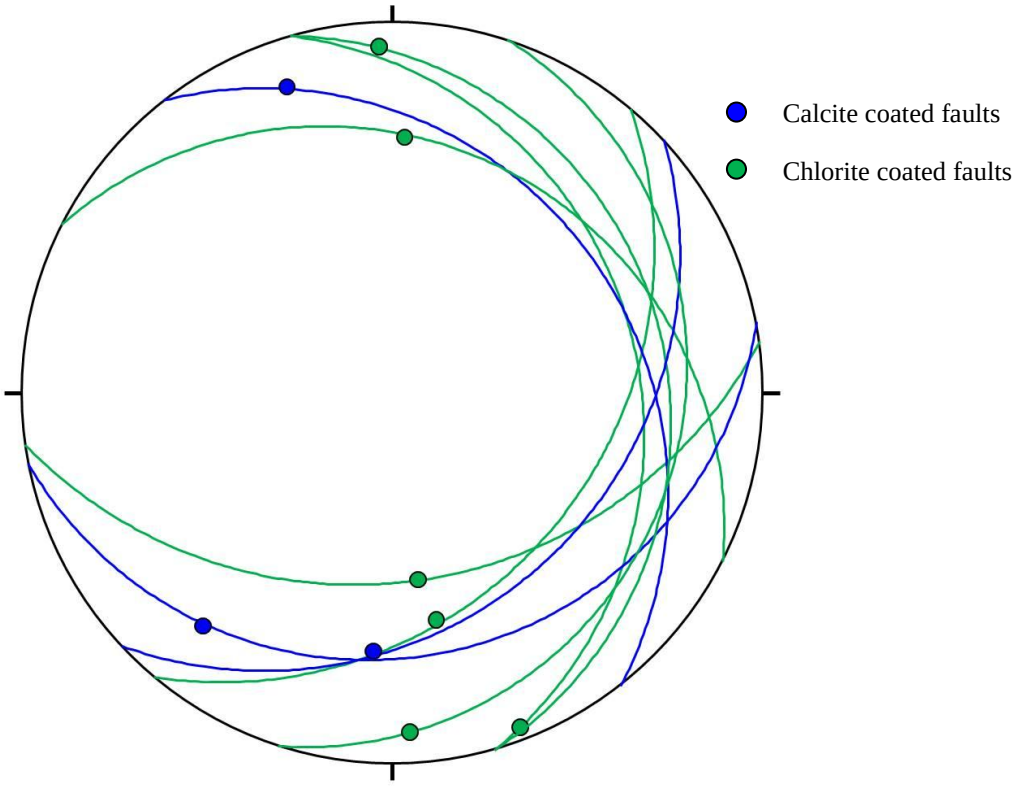

Figure 4.2 Stereographic plot showing the great circles of microfaults and the point of intersection of lineation (striation and slickenlines) on the plane within the East Wall Assemblage. The two mineral infills of the planar structures are shown. Chlorite coated faults, N=6. Calcite coated faults, N=3.

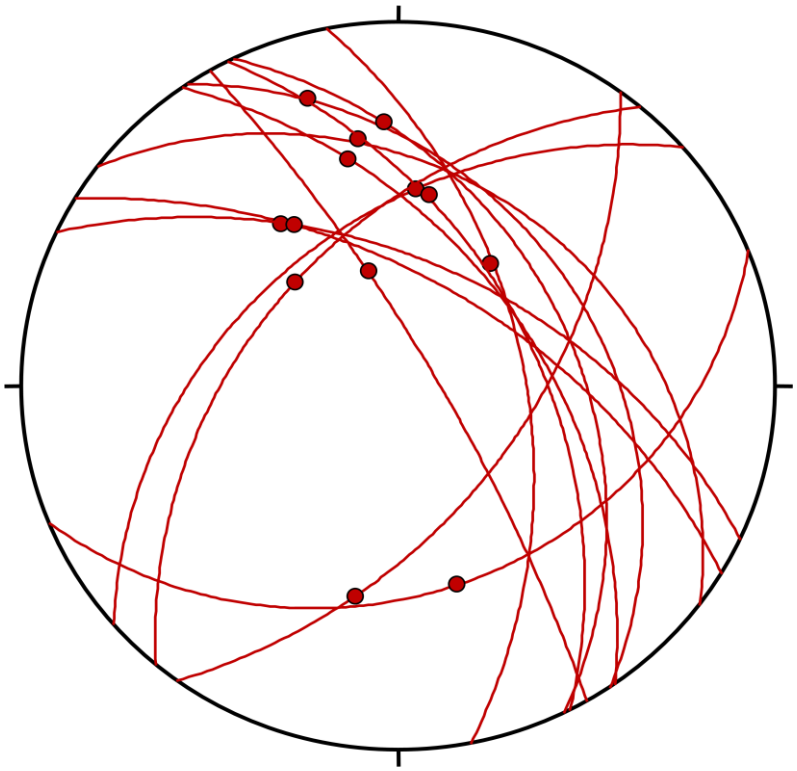

Figure 4.3 Stereographic plot showing the great circles of hematite coated microfaults and the lineation point of intersection (striation and slickenlines) on the plane within the MHA. N=13.

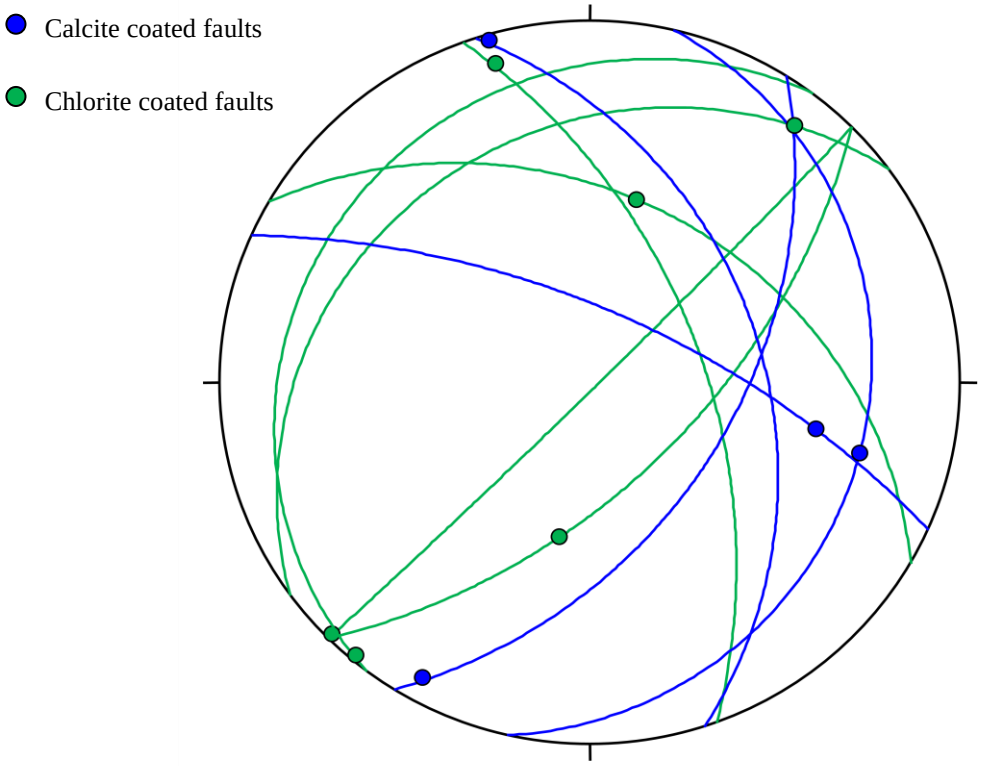

Figure 4.4. Stereographic plot showing the great circles of chlorite and calcite coated microfaults and the lineation point of intersection (striation and slickenlines) on the plane within the MHA. Chlorite coated faults, N=6. Calcite coated faults, N=4.

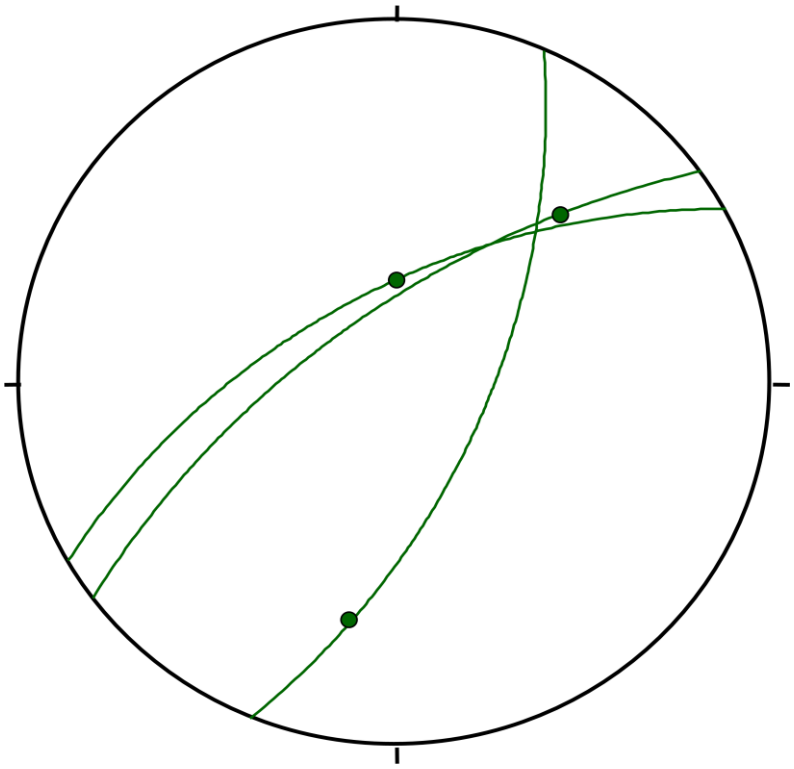

Figure 4.5 Stereographic plot showing the great circles of serpentine coated microfaults and the lineation point of intersection (striation and slickenlines) on the plane within the MHA. N=3.

Chlorite and calcite coated faults in the MHA (Figure 4.4) are variable in orientation. Comparatively, the calcite and chlorite coated faults of the E wall are more coherent as opposed to a more random set of orientation data of the MHA. Four lineations on chlorite coated faults and two lineations on calcite coated surface (Figure 4.4) suggest strike slip movement possibly with a NE and NNW striking conjugate pair. These orientations are more like the late stage Devonian pattern recognised in the Mt Read Volcanics (Berry, 1988) than the Mesozoic strike slip faults (Stacey and Berry, 2004).

Lineations on serpentine coated faults (Figure 4.5) plunge moderately (≤58°) on fault planes striking NE. The NW dipping serpentine coated faults are similar in orientation to the some of the hematite coated faults. This suggests that either the serpentine lineations are late features or that they have been reactivated when the late stage hematite lineations were produced. Due to the very low temperatures needed to reactivate serpentine (Hirth and Guillot, 2013), the latter of the two suggestions is the most likely.

The geotechnical description of faults on the east wall and MHA indicate they all have a lineation. The structure profile however varies. Of all lineations recorded on the E wall, two thirds of these were contained on faults with an undulating profile with the remainder being planar, stepped. 74% of all lineations recorded within the MHA were on undulating fault surfaces. 22% were on faults with a stepped profile and the remainder on planar faults.

4.3. Small-scale faulting of the WWA

Mapping on the west wall of Stage 1, North Pit has shown that there is extensive small-scale faulting within the Box Cut Carbonate (Figure 4.7). No faulting was evident within the Mega Ramp Schist or Western Wall Banded Schist which are both exposed towards the N and S of Stage 1 respectively. All but one of the faults mapped have normal/dextral offsets. Kinematic indicators on these features were not visible so the sense of movement could not be obtained from the tectoglyphs.

The brittle faults typically off-set ankerite and quartz veins. The recognition of these faults would be very difficult if the rocks did not contain veins. No alteration halo or lithological differences is apparent surrounding the features although schistose, puggy material is locally present. The relative timing of features can be estimated through the overprinting relationships in the rock. The timing of small-scale faults is later than the formation of ankerite veins; which are later than the quartz veins. The quartz veins are often strongly deformed and boudinaged, indicating that they were an early feature (pre- to syn-cleavage) of the protolith. The ankerite veins cross-cut the quartz veins (Figure 4.7 – A and B). The ankerite veins are thinner than the quartz veins and specular hematite is occasionally associated with them (Figure 4.7 – C).

The orientations of some faults were obtained by photogrammetry techniques (Figure 4.7 – D). The measured faults were dipping ≥70° to the NE. Many of the faults however are visible

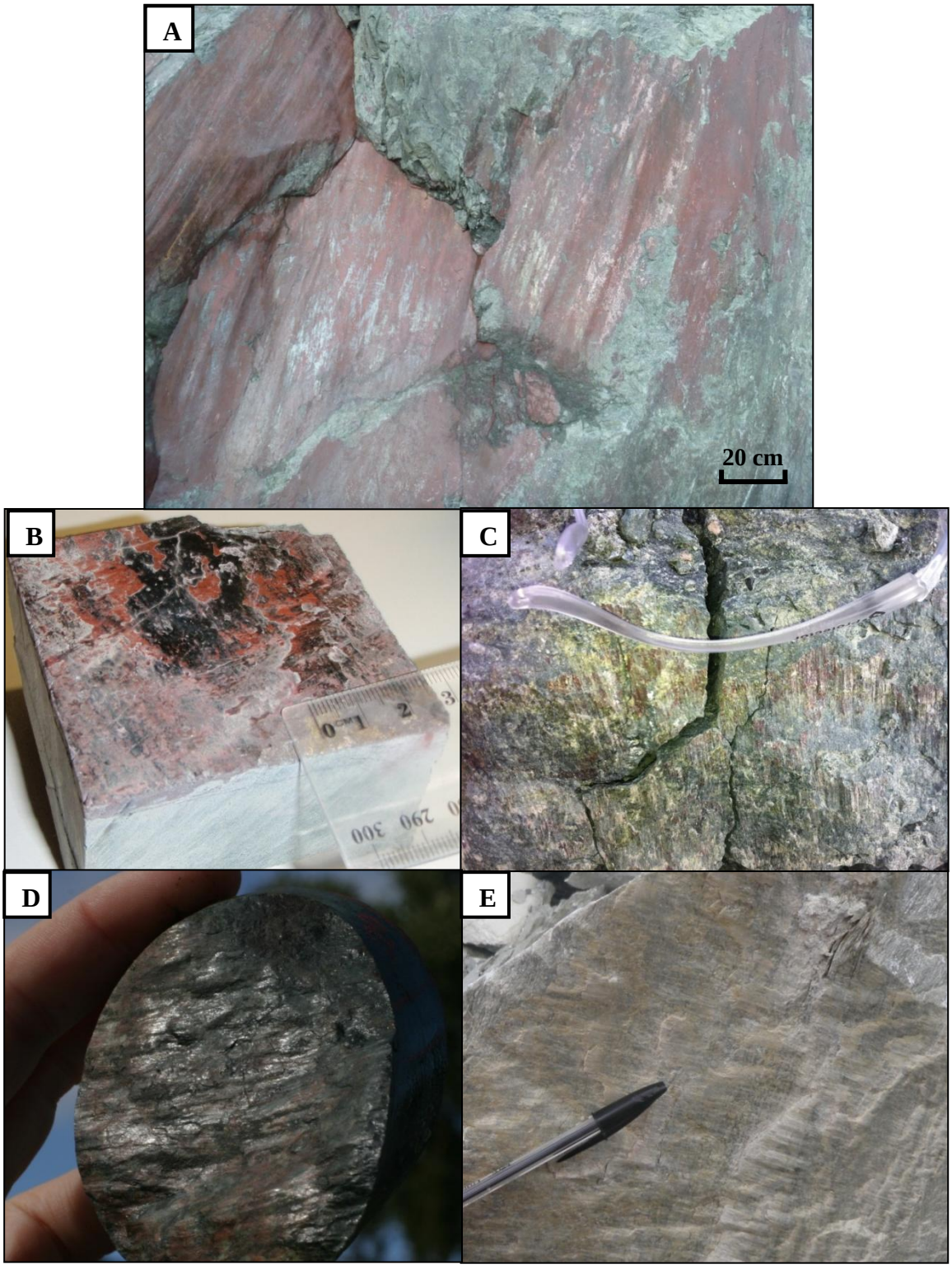

Figure 4.6 – **A** – examples of striated hematite coated microfaults on the east wall. There are some areas of polishing on the structure surface. **B** – An example of a polished hematite coated fault on the east wall. Scale in cms. **C** – Slickenlines on a structure within the Main Host Assemblage. Formed within an infilling of hematite and epidote (hematite creating lineation). Safety glasses arm approximately 10cm in length. **D** – Planar drill core structure showing lineation contained within the plane. From drill hole NDDH10068. **E**- Calcite slickenfibres within a dolomite rich lithology in the Eastern Wall Assemblage, in close proximity to the Eastern Contact Fault. Pen length approximately 11cm.

only as a trace on the pit wall so the orientation of the fault plane could not be obtained (Figure 4.7 – A, B and C). The fault in Figure 4.7 – C has a reverse/sinistral displacement. No overprinting relationship between normal and thrust faulting could be established. The individual normal faults incur <300 mm of displacement whereas the thrust fault has <100 mm of displacement.

4.4 Macro-scale faults of North Pit

4.4.1 Introduction

This section describes the three main faults; ECF, Magnesite Fault and the Eastern Splay Fault in North Pit from a structural geology perspective. Chapter 3 indicates that from a geotechnical perspective, a damage zone is present around the ECF and Magnesite Fault. This is indicated from the increase or decrease of specific brittle features near to the faults. This section characterises the fault damage zones further and provides possible predictions of the structural history of the features.

Chapter 3, Section 3.2 describes geotechnical drillcore logging parameters. The domaining of drillcore was also carried out by the author of this research. There was no parameter within the logging system at the time to record domains of drillcore. Therefore, the Hoek-Brown Geological Strength Index (GSI) was employed for this purpose and described in the next section.

4.4.2 Geological Strength Index (GSI)

The GSI is a classification scheme used in domaining rock masses. It stresses the importance of fundamental geological observations about the blockiness of the rock mass and the condition of the joint surfaces. Although numerously modified since 1980, the GSI table used for this research (Table 4.1) is the most used in practice (Karzulovic and Read, 2009).

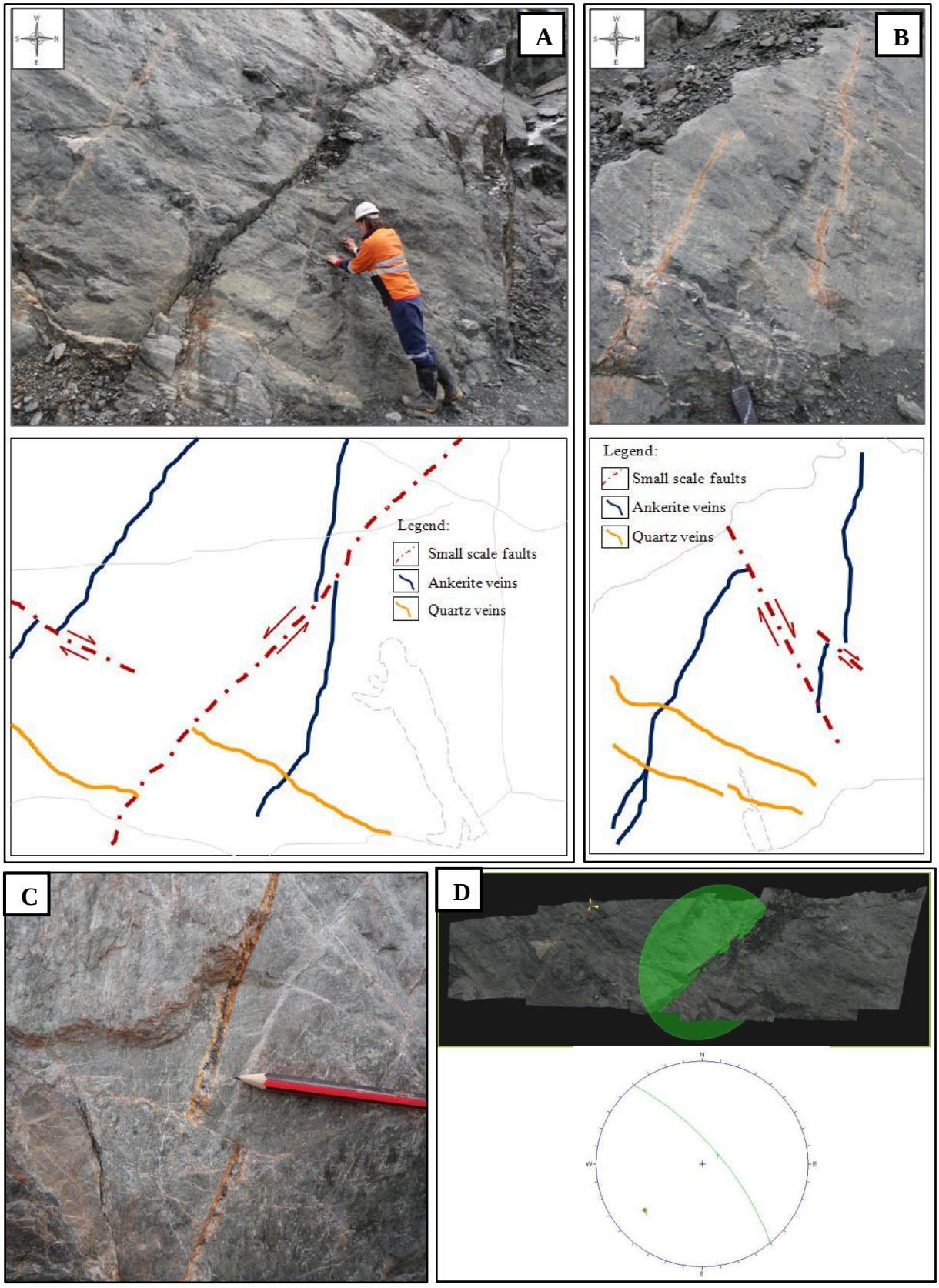

Figure 4.7. A and **B** - Photographs and interpretation of areas of the 120 RL Box Cut Carbonate, W wall. Looking W. Scales; researcher pictured in **A** and hand-held radio 20cm in length in **B**. **C**- Offset ankerite and specularite vein. Looking W. A common feature of the W wall. **D** – Photogrammetry DTM of the area shown in **A.** Looking W**.** The photogrammetry technique is necessary to obtain fault orientation which is presented on the stereographic projection below. Both the pole and plane of the fault is shown. The green halo on the DTM denotes the fault plane.

This method of domaining is subjective. An average GSI number is only estimated so quoting a range is more realistic (GSI ≥35≤45 instead of GSI=40). For this reason, each structure category was assigned a letter and each surface condition a number (Table 4.1). This makes domaining more precise for quantitative modelling. The mine planning software employed on Savage River Mine handles values well but not ranges of values. Using this method of only assigning a letter and number instead of a GSI range increases the compatibility of this parameter with the software, ensuring the domaining can be integrated into future mine planning. Figure 4.8 shows an example of domaining within drillcore.

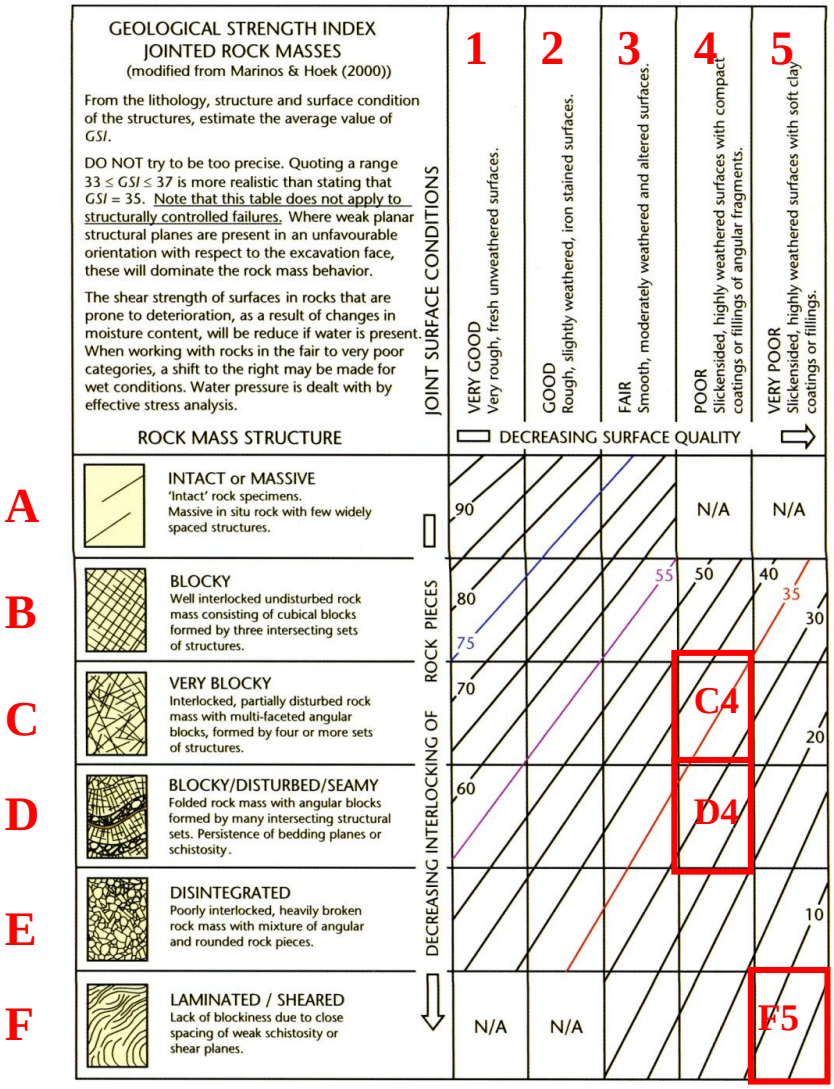

Table 4.1. Modified Hoek-Brown rock mass classification system, 2000. The red letters and numbers are assigned to rock mass structure and joint surface conditions respectively. The red boxes shown within the chart are examples of how the letters and numbers were assigned e.g. **A1**- intact or massive rock mass with very good joint surface condition, **F5** – laminated/sheared rock mass with very poor joint surface condition. This method proved quicker and easier than quoting a GSI number range. Source of chart; Karzulovic and Read, 2009.

GRANGE RESOURCES

DOMAIN CORE LOGGING

Borehole ID:	NDDH09057
Date:	
Logger:	VB

Depth from (m)	Depth to (m)	GSI Number	Code	Comments
0.00	32.70	10 - 20	E5	Weathered profile. Some areas of basalt, puggy clay and heavily orange stained schist. Associated core loss.
32.70	45.10	5 - 10	F5	Non-intact core. Rubble and distintegrated. Areas of gravel. Associated core loss.
45.10	64.70	25 - 35	D4	Persistence of schistosity, veins and some joints. Mainly weak on foliation planes.
64.70	69.40	5 - 15	F5	A lot of associated core loss. Fault? Very disintegrated rock mass around core loss.
69.40	80.10	30 - 40	C4	Very blocky but with many calcite/quartz veins, vugs and joints.
80.10	92.30	10 - 20	E5	Much associated core loss.
92.30	102.80	5 - 10	F5	Disintegrated rock mass around core loss. Non - intact core.
102.80	111.10	30 - 40	D3	Stockwork of calcite and quartz veins. Moderately weathered defect surfaces.
111.10	116.20	5 - 10	F5	Much associated core loss. Very disintegrated rock mass. Non intact. Fault?
116.20	123.85	30 - 40	D3	Stockwork of calcite and quartz veins.
123.85	126.70	5 - 10	E5	Associated core loss. Weaker rock mass. Many defects in core.
126.70	140.70	40 - 50	C3	Some calcite/dolomite veins, some pervasive foliation but strong rock mass.
140.70	146.00	50 - 60	B3	Strong, intact core. Could be due possibly to lithological variation in core (quartz rich domain).
146.00	159.00	30 - 40	C4	Very blocky but with many calcite/quartz veins, vugs and joints.
159.00	171.20	50 - 60	B3	Strong, intact core.
171.20	177.60	25 - 35	D4	Persistence of schistosity, veins and some joints. Mainly weak on foliation planes.

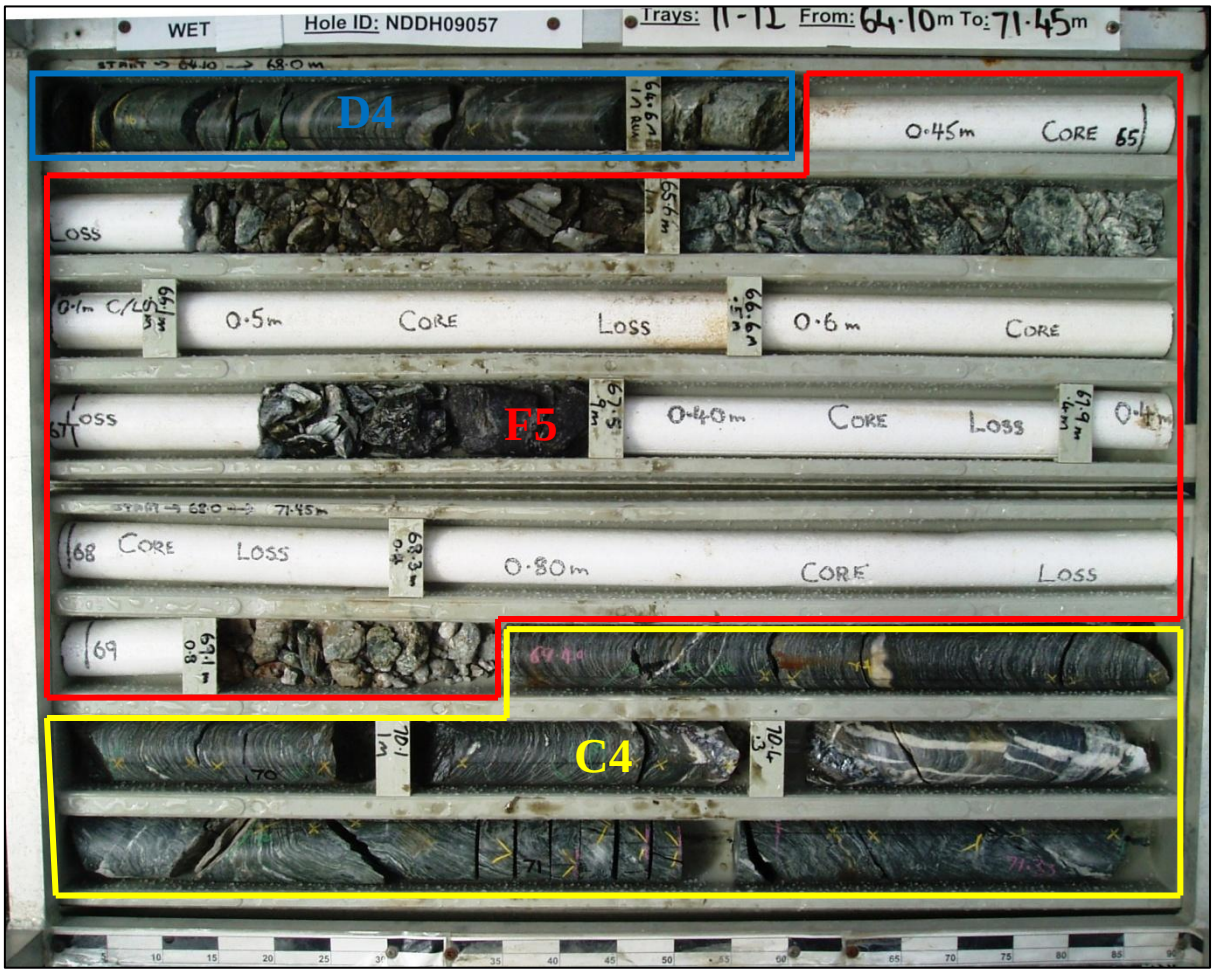

Figure 4.8. An example of domaining drillcore. **A** – An example of the parameter logging sheet implemented by the author of this research. **B** – Corresponding drillcore domains to **A**.

4.4.3 Eastern Contact Fault

Along the length of the Eastern Contact Fault (ECF) a damage zone has been identified by the change in lithology and structural features. Table 4.2 presents each of the 18 drillholes that intersect the fault along the 1700m strike length. The estimated co-ordinates of the damage zone, the apparent width of the zone, the lithology, GSI number and brittle features are presented from each drillhole. Each damage zone has been classified by width into groups as follows; minimum damage zone (≤20 m), moderate damage zone (≤40 m) and maximum damage zone (>40 m). This section discusses the characteristics of each group and how they differ.

Minimum Damage Zones

41% of drillholes intersecting the ECF present a minimum damage zone (≤ 20 m wide). These are characterised by a high percentage of serpentine schist (UXS), talc schist (UXT), chloritic schist (MXC) and chloritic-carbonate schist (MXR). The chloritic +/- carbonate schist is intensely foliated with major quartz boudins and calcite veins. Disseminated pyrite is also visible within these areas as well as minor magnetite bands. Other lithologies include graphite rich rocks (OXG) which are a common feature throughout all damage zones. Large veins or bands of quartz, calcite and dolomite are also present. All lithologies are associated with core loss due to the condition of the rock mass but puggy shears tend to be associated with talc and graphite rich zones (Figure 4.9). Friable shear zones are minor within the minimum damage zones and are categorised by weathered non-intact core usually proximal to core loss. The rocks within the damage zones are heavily jointed. MXC and MXR lithologies present more joints than talc, serpentine and graphite rich lithologies. All lithologies contain many calcite veins and boudins. Figure 4.9 shows examples of minimum damage zones within drillcore and Leapfrog™ models.

GSI values range from B3 to E5; with the highest percentage of rock being within category E4 (or GSI number ≥15≤28). E4 is disintegrated (poorly interlocked, heavily broken rock mass with mixture of angular and rounded rock pieces) with poor (slickensided, highly weathered surfaces with compact coatings or fillings or angular fragments) surface conditions.

Moderate Damage Zones

41% of drillholes intersecting the ECF present a moderate damage zone (>20 to ≤40 m wide). These are characterised by a higher percentage of talc rich (UXT), serpentine rich (UXS, URS and ORS), dolomite rich (OLQ and OXL), quartz rich (OOQ, ORK and OXK) and graphite rich (SXG and UXG) lithologies than those found in minimum damage zones. A lower percentage of chloritic-carbonate schist (MXR) and chloritic schist (MXC) are found within the moderate damage zones but these are intensely foliated with major calcite veining and quartz boudins. Minor epidote and albite veining is present along with disseminated magnetite. Joints dominate the brittle features of moderate damage zones and intense veining is common. Puggy and friable shears with associated core loss are a common feature of all damage zones. Figure 4.10 shows examples of lithologies within moderate damage zones and the extent of the damage zone shown with Leapfrog™ software. The only noticeable difference between the moderate and minimum damage zones is the width of damage zone and the increase of dolomitic, talcose, siliceous and graphitic lithologies within the moderate damage zones. GSI values range from C3 to F4. The C3 value is assigned to less than 5% of all rock within all the damage zones within this classification. The blockiness of the rock mass and the condition of the joint surfaces is generally poorer than that of the rock present in minimum damage zones. This is likely to be due to the difference in lithology in these areas.

Borehole Number (N drillholes to S drillholes)	*Coordinates of damage zone (X,Y,Z From_to)*	*Apparent width of damage zone*	*Lithology % within damage zone*	*GSI number (% of classification within zone)*	*Brittle features*	*Classification Maximum/ moderate or minimum damage*
NDDH09063			**Anomalous drillhole (refer to Section 4.4.3, page 187)**			
NDDH09055	From: X 6792.02 Y 10189.95 Z 216.65 To: X 6798.30 Y 10190.22 Z 208.37	**≥10.4 m** (Drillhole is terminated within damage zone)	**Talc Schist** - 6% (talc shear zone) **Serpentine Schist** - 77% (associated core loss, fine-grained. Minor magnetite) **Chlorite schist** - 17% (foliated with disseminated pyrite and talc) Six clay puggy shears up to 80 mm in thickness.	**E4** - 84% **B3** - 16% (Refer to Section 4.4.2 for description)	Quartz veins – 7% Calcite boudin – 4% Joints – 37% Shears – 27% Fracture zone – 8% Sharp contact between lithologies – 17%	**Minimum (estimated to be ≤20 m)**
NDDH09054	From: X 6794.91 Y 10135.86 Z 212.56 To: X 6803.41 Y 10135.07 Z 200.95	**15.1 m**	**Chlorite Schist** – 56% (intensely foliated fine-grained chlorite schist. Increasing in calcite veining with depth and deformed quartz veins) **Talc Schist** – 3% **Chlorite Schist** – 18% (brecciated. Serpentine +/- quartz +/- albite +/- calcite). **Talc Schist**- 10% (associated core loss, highly sheared) **Chlorite-carbonate Schist** – 13% (strongly foliated)	**C3** – 56% (strong rock mass dominated by siliceous and/or calcite banding and veins. **E5** – 44% (associated core loss, areas of non-intact core).	Quartz and calcite veins – 25% Joints – 54% Shears – 6% Sharp contacts between lithologies – 15% Intensely veined within the fault damage zone. Minor shears with associated clay pug.	**Minimum**
NDDH10068	From: X 6795.52 Y 10093.70 Z 160.73	**≥37.34 m** (Drillhole is terminated within damage	**Chlorite Schist** – 2.5% **Talcose ore** – 1.5% (foliated puggy talc schist with magnetite clasts)	**E4** – 44% (weak shear strength on foliation planes, associated core loss)	Calcite veins – 32% Quartz boudins – 6% Joints – 52% Shears – 10%	**Maximum (estimated to be ≥40 m)**

	To: X 6819.50 Y 10094.92 Z 132.19	zone)	**Chlorite Schist** – 6% (heavily foliated with many calcite veins) **Chlorite-carbonate Schist** – 6% (puggy shears in areas, albite and quartz veining) **Serpentine Schist** – 13% (major calcite and quartz veining) **Talc Schist** – 18% (major talc pug in areas, dolomite veining apparent) **Dolomite** - 18% (dolomite/calcite rich lithology with quartz veining) **Chlorite Schist** – 35% (strongly foliated, pyrite and quartz rich banding and very schistose)	**C2** – 11% **B2** – 3% **C4** – 42% (strongly foliated, minor friable shear zones throughout)	Minimal core loss. Strongly foliated and veined rock mass with massive siliceous and dolomitic banding.	
NDDH10070	From: X 6807.28 Y 10077.82 Z 192.62 To: X 6825.51 Y 10069.22 Z 216.40	**31.1 m**	**Chlorite Schist** – 41% (strongly foliated, minor magnetite banding and major siliceous banding with major quartz veining) **Chlorite-quartz rich rock** - 48% (strongly foliated siliceous chlorite rich lithology) **Chlorite-carbonate Schist** – 5% (major quartz and calcite veins) **Quartz** – 6% (massive quartz zone)	**D4** – 51% (rock strength variation from R1 – R4 – refer to Chapter 3 Section 3.2.4. Locally strongly foliated. **E4** – 49% (friable and locally puggy with interbanded competent blocky material)	Calcite veins – 21% Magnesite veins – 4% Friable shears – 10% Puggy shears – 8% Fractured shears – 7% Joints – 50% (of these joints, 5% are hematite coated)	**Moderate**
NDDH10071	From: X 6815.61 Y 10069.37 Z 59.38 To: X 6798.17 Y 10064.38 Z 37.54	**28.4 m**	**Dolomite and quartz** – 6% (interbanded dolomite and quartz) **Chlorite-quartz rich rock** – 17% (strongly foliated with minor albite) **Talc Schist** – 22% (moderate to strongly foliated, major puggy and fractured shear zones) **Graphite Schist** – 5% (strongly foliated graphitic schist, major	**E4** – 100% (associated core loss, persistent strong localised foliation and defects)	Calcite veins – 30% Joints – 40% Sharp contact between lithologies – 10% Friable shears – 10% Puggy shears – 5% Fractured zones – 5%	**Moderate**

			quartz boudins) **Chlorite Schist** – 26% (strongly foliated, major quartz boudins, minor talc rich zones and minor disseminated pyrite) **Chlorite-quartz rich rock** – 8% (siliceous unit, minor magnetite boudins, major calcite veins and minor disseminated chalcopyrite) **Serpentine Schist** – 16% (serpentine schist with quartz boudins)			
NDDH10066	From: X 6801.83 Y 10029.12 Z 146.27 To: X 6826.73 Y 10030.88 Z 175.73	**38.64 m**	**Talc Schist** – 19% (strongly foliated, major calcite veins) **Talc Schist** – 1% (talc rich puggy shear) **Graphitic Schist** – 2% **Magnesite** – 13% (strongly foliated and talc rich) **Serpentine Schist** – 11% **Serpentine Schist** – 4% (puggy shear) **Quartz** – 6% (siliceous zones) **Chlorite-carbonate Schist** – 24% (strongly foliated, major disseminated pyrite) **Serpentine ore** – 8% (magnetite and talc veining) **CORE LOSS** – 12%	**D4** – 55% **C3** – 10% **E4** – 35%	Calcite veins – 35% Joints – 54% (7% hematite coated) Fractured zones – 4% Puggy shears – 4% Friable shears – 3%	**Moderate**

NDDH09064	From: X 6818.25 Y 9982.68 Z 64.27 To: X 6834.93 Y 9982.05 Z 43.73	**26.50 m**	**Talc Schist** – 19% (puggy unconsolidated, disseminated pyrite with associated core loss) **Chlorite Schist** – 36% (epidote and pyrite rich) **Serpentine Schist** – 26% (strongly foliated, calcite rich) **Graphitic Schist** – 19% (areas of puggy graphite, strongly foliated, major calcite and quartz veins)	**F4** – 20% **D3** – 66% **E4** – 14%	Fractured zones – 67% Foliation breaks – 15% (graphitic unit) Quartz veins – 9% Calcite veins – 9%	**Moderate**
NDDH0601	From: X 6813.28 Y 9978.09 Z -150.57 To: X 6826.43 Y 9982.91 Z -168.99	**23.20 m**	**Serpentine-rich rock** – 5% (minor magnetite and puggy zones) **Serpentine-rich rock** – 7% **Talc Schist** – 50% (strongly deformed with major quartz boudins) **Dolomite** – 14% (altered dolomite rich unit with strong localised foliation) **Graphitic Schist** – 12% (strongly deformed graphite unit with abundant quartz veins and boudins). **CORE LOSS** – 12%	GSI domaining was not a logging parameter in 2006	Joints – 60% Calcite veins – 14% Quartz boudins – 4% Puggy shears – 3% Friable shears – 2% Fractured zones – 17%	**Moderate**
NDDH09065	From: X 6801.40 Y 9937.18 Z 149.10 To: X 6807.77 Y 9937.29	**9.75 m**	**Serpentine Schist** – 67% (strongly foliated, major quartz and albite veins and minor magnetite banding) **Chlorite-carbonate Schist** – 31% (strongly foliated with associated core loss)	**D4** – 100%	Joints – 56% Foliation breaks – 24% Fractured zones – 20%	**Minimum**

	Z 156.49		**Talc Schist** – 2% (Puggy talc shear zone)			
NDDH10069	From: X 6798.41 Y 9934.40 Z 165.79 To: X 6810.79 Y 9933.44 Z 151.01	**19.35 m**	**Chlorite Schist** – 75% (with disseminated pyrite, major calcite veins, siliceous zones and puggy shears in areas) **Calcite and quartz** – 2% (large calcite and quartz vein) **Serpentine Schist** – 20% (trace pyrite, major quartz +/- albite +/- calcite veins) **Quartz** – 2% (large quartz boudin) **Graphite Schist** – 1% (graphitic puggy shear)	**E4** – 100% (some puggy and graphitic zones. Areas of strong foliation with a tendency to break on foliation. Associated core loss. Rock of variable strength)	Calcite veins – 26% Quartz boudins – 13% Joints – 32% Puggy shears – 19% Friable shears – 11%	**Minimum**
NDDH0602	From: X 6794.19 Y 9930.28 Z 30.59 To: X 6818.39 Y 9931.86 Z 50.22	**31.30 m**	**Dolomite** – 4% (weakly foliated schistose unit with some silicification) **Chlorite-carbonate Schist** – 71% (strongly deformed, minor disseminated magnetite, some quartz boudins and albite veins) **Graphitic Schist** – 1% (crenulated graphite schist) **Talc Schist** – 17% (strongly deformed with quartz and calcite veins) **Serpentine-rich rock** – 3% (massive serpentinite, abundant calcite and talc fracture fill) **CORE LOSS** – 4%	GSI domaining was not a logging parameter in 2006	Joints – 73% Puggy shears – 11% Fractured zones – 8% Calcite veins – 8%	**Moderate**
NDDH0507	From: X 6813.58 Y 9727.06 Z -186.95	**46 m**	**Meta-basalt** – 7% (heavily fractured with occasional veining) **Talc Schist** – 43% (variable rock strength, heavily fractured,	GSI domaining was not a logging parameter in 2005	Joints – 70% Puggy shears – 15% Calcite veins – 15%	**Maximum**

	To: X 6837.31 Y 9726.56 Z -226.20		abundant calcite veining, locally soft and puggy) **Chlorite-carbonate Schist** – 7% (strongly deformed, weakly foliated) **Magnesite** – 4% (massive magnesite with minor quartz boudins) **Dolomite** – 15% (quartz and calcite veining) **Graphitic Schist** – 10% (erratic frequent calcite veining) **CORE LOSS** – 14%			
NDDH0503	From: X 6805.59 Y 9572.85 Z -340.14 To: X 6841.56 Y 9576.70 Z -389.26	**61.05 m**	**Talc Schist** – 31% (variably altered, erratic veining and foliation with siliceous and sheared areas) **Mafic rock** – 7% (massive fine-grained rock with calcite veins and siliceous areas) **Serpentine-rich rock** – 52% (massive serpentinite with major calcite +/- albite veining. **Chlorite-rich rock** – 3% (Chlorite rich rock with erratic foliation and minor pyrite and albite) **Graphitic Schist** – 7% (dolomitic rich with minor calcite veining)	GSI domaining was not a logging parameter in 2005	Joints – 55% Calcite veins – 10% Quartz veins – 5% Albite veins – 2% Chlorite veins – 4% Fractured shears – 24%	**Maximum**
NDDH0505	From: X 6826.50 Y 9487.03 Z -96.18 To: X 6845.03 Y 9488.09	**32.25 m**	**Talc Schist** – 22% (sheared talc schist, soft and puggy in areas, strongly deformed) **Graphitic Schist** – 8% (strongly deformed with abundant calcite veins) **Chlorite-carbonate Schist** – 48%	GSI domaining was not a logging parameter in 2005	Calcite veins – 35% Joints – 45% Puggy shears – 10% Fractured zones – 20%	**Moderate**

	Z -122.52		(strongly foliated with frequent erratic calcite veining) **Dolomite** – 23% (strongly foliated with abundant calcite veining)	GSI domaining was not a logging parameter in 2005	Calcite veins – 18% Joints – 56% (3% hematite coated joints) Quartz boudins – 4% Shears – 22%d	**Minimum**
NDDH0504	From: X 6816.92 Y 9395.75 Z -154.08 To: X 6820.49 Y 9395.81 Z -160.64	**7.62 m**	**Talc Schist** – 78% (strongly sheared and deformed, moderately to strongly foliated, variable rock strength and localised puggy clay and talcose zones) **Graphitic Schist** – 4% (strongly foliated, alternating bands of carbonate, graphite and pyrite with quartz veining) **CORE LOSS** – 18%			
NDDH0501	From: X 6784.09 Y 9188.92 Z 91.50 To: X 6787.37 Y 9188.98 Z 99.28	**8.5 m**	**Chlorite-carbonate Schist** – 68% (strongly foliated, possibly mylonitic with calcite veins and quartz boudins) **Talc Schist** – 32% (talc and clay rich, soft and friable, puggy in areas with disseminated pyrite)	GSI domaining was not a logging parameter in 2005	Calcite veins – 52% Joints – 35% Quartz boudins – 6% Fractured zones – 7%	**Minimum**
NDDH0616	From: X 6771.86 Y 9086.70 Z 80.65 To: X 6776.27 Y 9086.38 Z 87.19	**8 m**	**Chlorite-carbonate Schist** – 81% (strongly foliated, major quartz boudins and calcite veins) **Chlorite Schist** – 19% (soft, friable, strongly deformed with disseminated magnetite)	GSI domaining was not a logging parameter in 2005	Joints – 85% Calcite veins – 15%	**Minimum**

Table 4.2. Extraction of data from the Savage 2010 drillhole database defining the extent of the ECF damage zone from drillhole intersections in 2005, 2006, 2009 and 2010. The size of damage zone, lithology, GSI number (where possible) and number of brittle features are outlined. A damage zone classification of minimum (blue), moderate (light blue) and maximum (grey) has been assigned to each drillhole intersection. **X** – Easting, **Y** – Northing and **Z** – Relative Level.

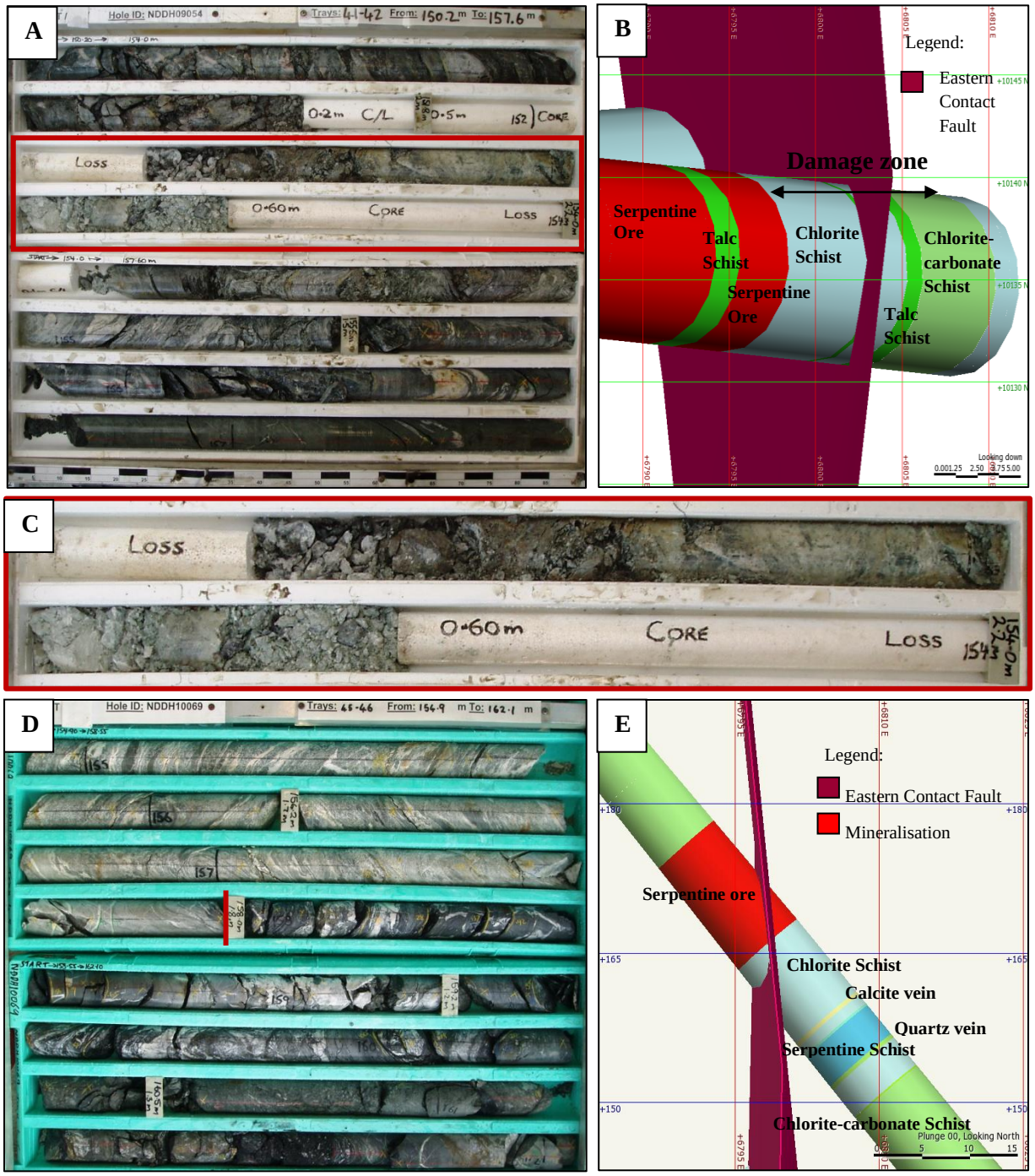

Figure 4.9. Examples of minimum damage zones. **A** – NDDH09054 fault damage zone from 150.2 to 157.6 m. The last metre is not categorised as damaged. Note the core loss. **B** – Plan view Leapfrog™ model of NDDH09054 showing the intersecting ECF, the extent of the damage zone and lithologies downhole. The red coloured lithology denotes mineralisation. **C** – NDDH09054 from 152.20 to 154 m. Puggy and friable sheared zone with associated core loss. This is an example of a domain that was assigned GSI code 'E5'. **D** – NDDH10069 fault damage zone from 154.9 to 162.1 m. Talc rich lithology with major quartz, talc and calcite veins. The contact between the talc rich lithology and graphitic rich lithology is shown. The graphite includes major quartz veins. The talc rich lithology is assigned GSI code 'B3' and the graphitic rich lithology 'D4'. **E** – Leapfrog™ cross-section of NDDH10069, looking N showing the ECF, extent of damage zone and lithologies downhole.

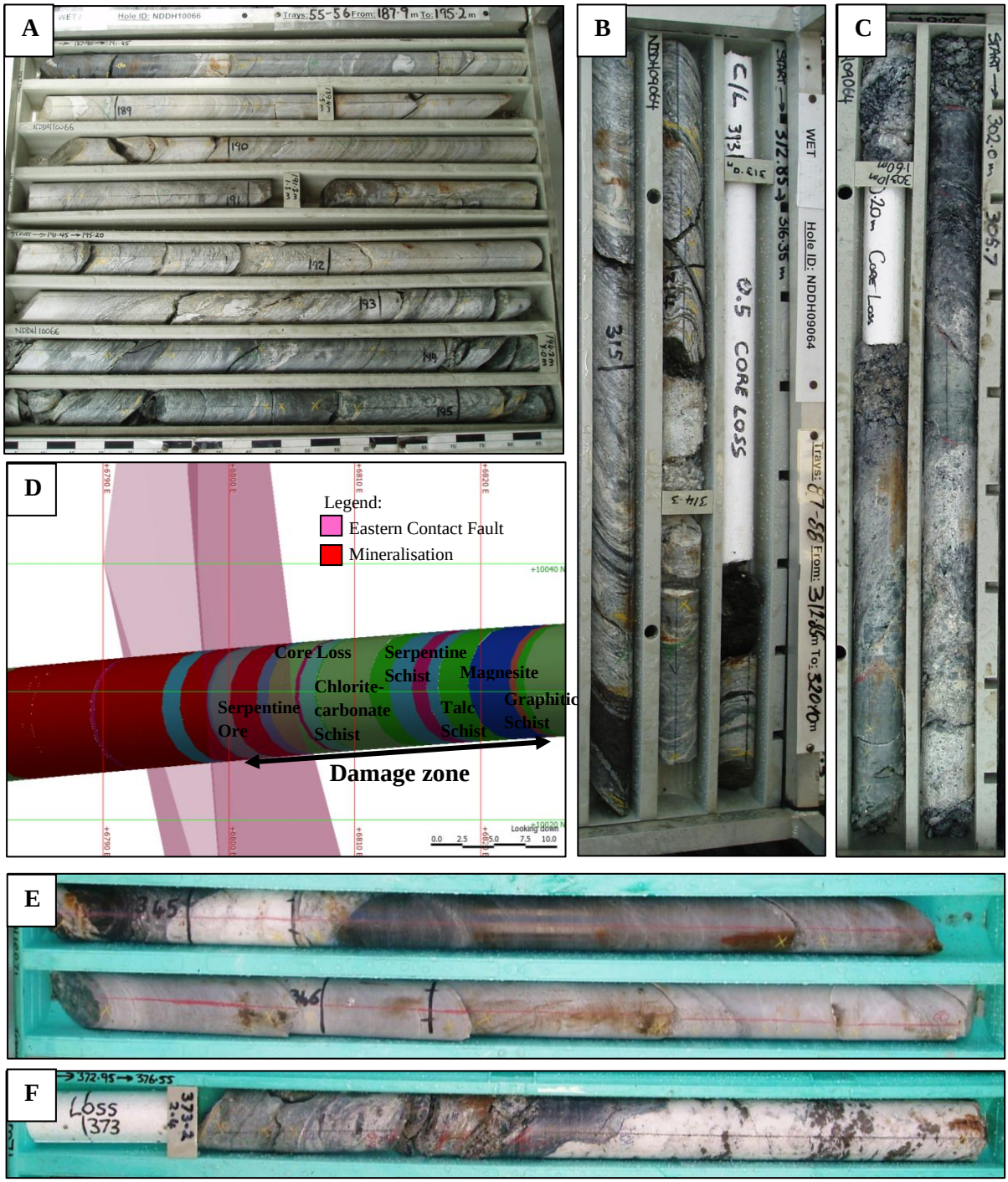

Figure 4.10. Examples of moderate damage zones. **A** – NDDH10066, 187.9 m to 195.2 m. A magnesite rich unit with calcite and quartz veining. Assigned GSI code 'C3'. **B** – NDDH09064, 312.85 m to 315.70 m. A talc rich unit with some graphite rich zones. Associated core loss. Assigned GSI code 'D3'. **C** – Puggy shear zone in NDDH09064, 302 m to 303.90 m. Assigned GSI code 'F4'. **D** – Plan view Leapfrog™ model of NDDH10066 showing the ECF, extent of the damage zone and lithologies downhole. **E** – Siliceous graphitic unit in NDDH10071 at 344.90 m to 346.80 m. Assigned GSI code 'C3'. **F** – NDDH10071, 372.95 m to 373.80 m. It shows a large quartz vein within the fault damage zone. Assigned GSI code 'D4'.

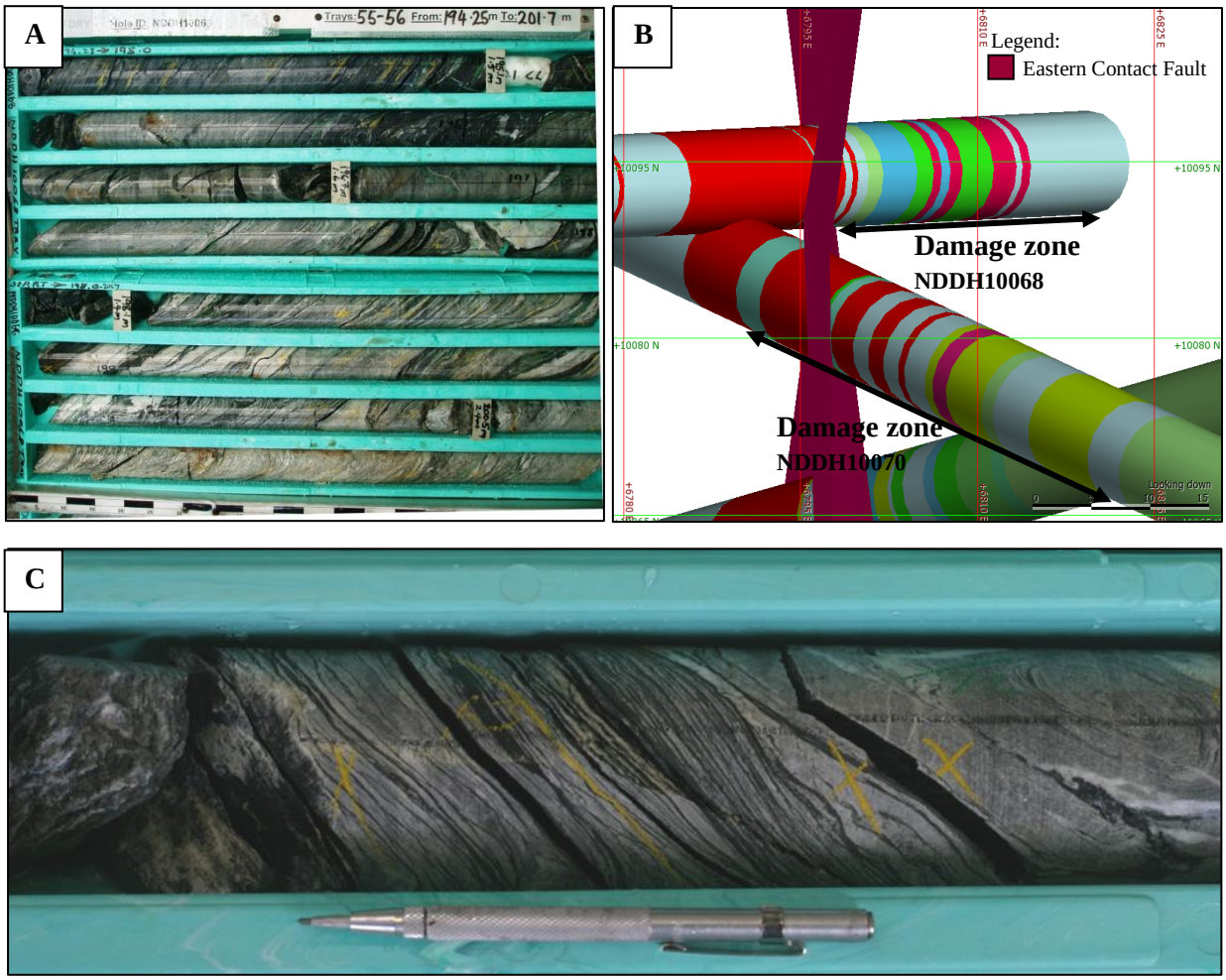

Figure 4.11. Examples of maximum fault damage zones. **A** – NDDH10068, 194.25 m to 201.7m. Strongly foliated and banded rock with graphitic areas and quartz veins. **B** – Plan view Leapfrog™ model of NDDH10068 and NDDH10070, showing the extent of the fault damage zone. **C** – NDDH10068 205.70 m to 205.95 m. Strongly foliated and banded rock. Assigned GSI code 'C4'. **D** – NDDH10068, crenulated quartz veins and banded pyrite within siliceous lithology. Assigned GSI code 'C2'. **E** – NDDH10068, puggy lithology with brecciated disseminated magnetite. Serpentinite and tremolite rich. Assigned GSI code 'E4'. **F** – NDDH10068, siliceous lithology with banding of dolomite and pyrite. Assigned GSI code 'C4'.

Maximum Damage Zones

18% of drillholes intersecting the ECF present a maximum damage zone (>40m). The lithologies within the maximum damage zones are very similar to lithologies found within moderate damage zones. Maximum damage zones are richer in dolomitic lithologies and siliceous zones are wider. Figure 4.11 shows examples of lithologies within maximum damage zones and damage zone extent using Leapfrog™ software. GSI numbers range from B2 to E4. The B2 value is only assigned to a very small percentage of rock within one borehole intersecting the maximum damage zone. The blockiness of the rock mass and the condition of the joint surfaces is very similar to that of moderate damage zones. Due to the higher percentage of siliceous areas, the core is not assigned as low a value as F4. Generally, intact siliceous areas of core score a high GSI value (Figure 4.11).

Brittle Features

The orientations of all brittle features of the rock logged within the damage zone are shown in Figure 4.12. A total of 754 features were measured. Although the damage zone is small relative to the other assemblages of North Pit, the number of measured structures is less than the records of other assemblages due to ground conditions in puggy and sheared areas of the damage zone. In some areas of the damage zone, non-intact core was recovered meaning orientating the core was difficult and unreliable. Of the measured structures 59% were joints, 32% were veins, 5% foliation, 3% rock contacts and 1% shears. The joints display a modal orientation distribution of 70°/258°, with a smaller sub-horizontal joint set. Veins are commonly sub-horizontal and steeply dipping to the W. Foliation is steeply dipping to the E and W. The rock contacts are dipping steeply to the E and W, with some dipping gently to the N and S. Shears dip steeply to the W and NW.

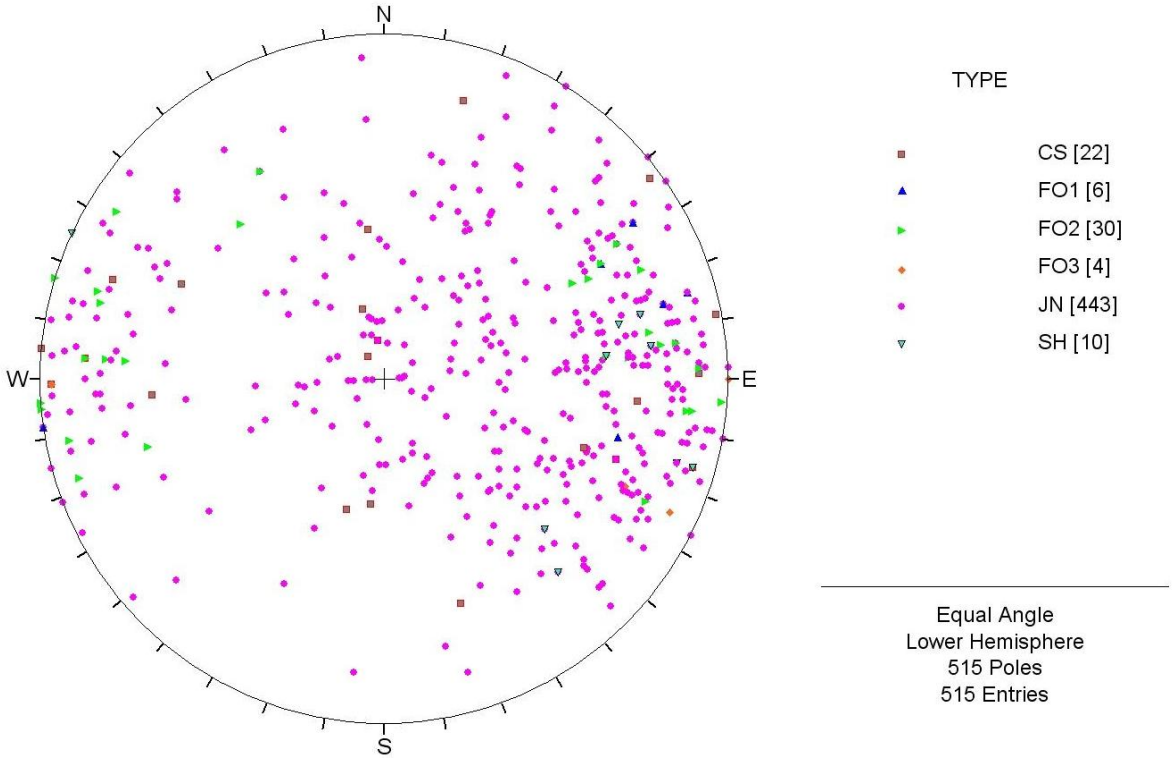

Figure 4.12. Poles to all brittle features within the ECF damage zone. Abbreviations; CS; Sharp contact, FO; Foliation (1-weak, 2-moderate, 3-strong), JN; Joints and SH; Shears.

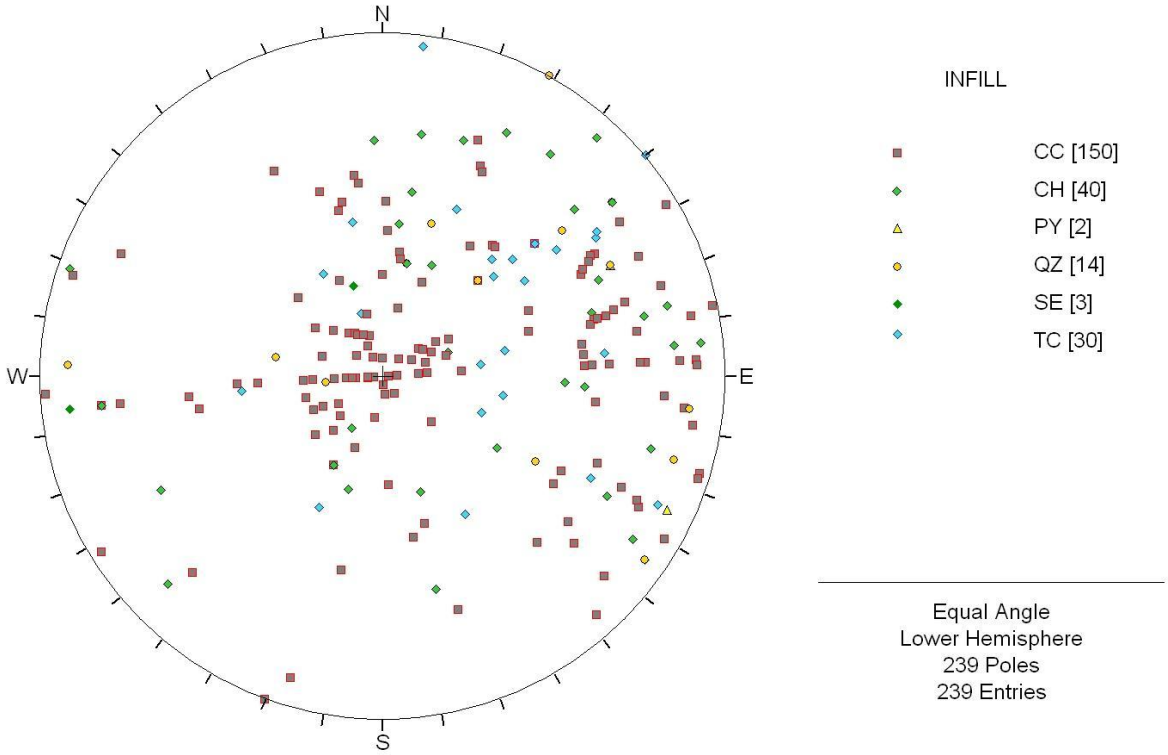

Figure 4.13. Poles to all veins within the ECF damage zone, separated by infill. Abbreviations; CC; Calcite, CH; Chlorite, PY; Pyrite, QZ; Quartz, SE; Serpentine and TC; Talc.

Figure 4.13 shows the orientation distribution of different vein infills within the damage zone of the ECF. Of the 239 veins, 63% are calcite, 17% are chlorite, 12% are talc, 6% are quartz, 1% are serpentine and 1% are pyrite veins. Due to the small volume of serpentine and pyrite veins, an average orientation distribution could not be established. There are two sets of calcite veining; sub-horizontal and steeply dipping to the W. The sub-horizontal set is recognised on the E wall of North Pit. Chlorite veins have a scattered orientation but many are steeply to moderately dipping to the S and W. The dip of talc veins is gentle to steep, dipping to the S and W and quartz veins also have variable dip to the W, E and NW. The orientations of structural features within the ECF damage zone are similar to that of the features present within the E wall and the MHA of North Pit. There is no dramatic difference between orientations within the damage zone versus the host rock on the E and W of the fault.

NDDH09063 – anomalous fault damage zone

This borehole is the most northerly in North Pit. The review of the drillcore suggests that a splay fault is present in this area, similar to the Eastern Splay Fault. Talc schist is present to the E with graphitic banding. Serpentine rich lithologies are present between bands of competent chlorite and carbonate schist further to the W. A 3 m band of intensely foliated (potentially mylonitic) rock separates the splay fault assemblage from mineralisation on the W. The apparent width of the zone between the ECF and the splay fault is 145.85m. The GSI number in this zone ranges from F5 (puggy and friable areas with associated core loss) to B3 (areas of competent MXR and MXC). Ranges in between these two include E5 and D4. Hematite coated joints are a common feature within this lithology. Figure 4.14 shows the drillcore characteristics of NDDH09063 and the lithology using Leapfrog™ software.

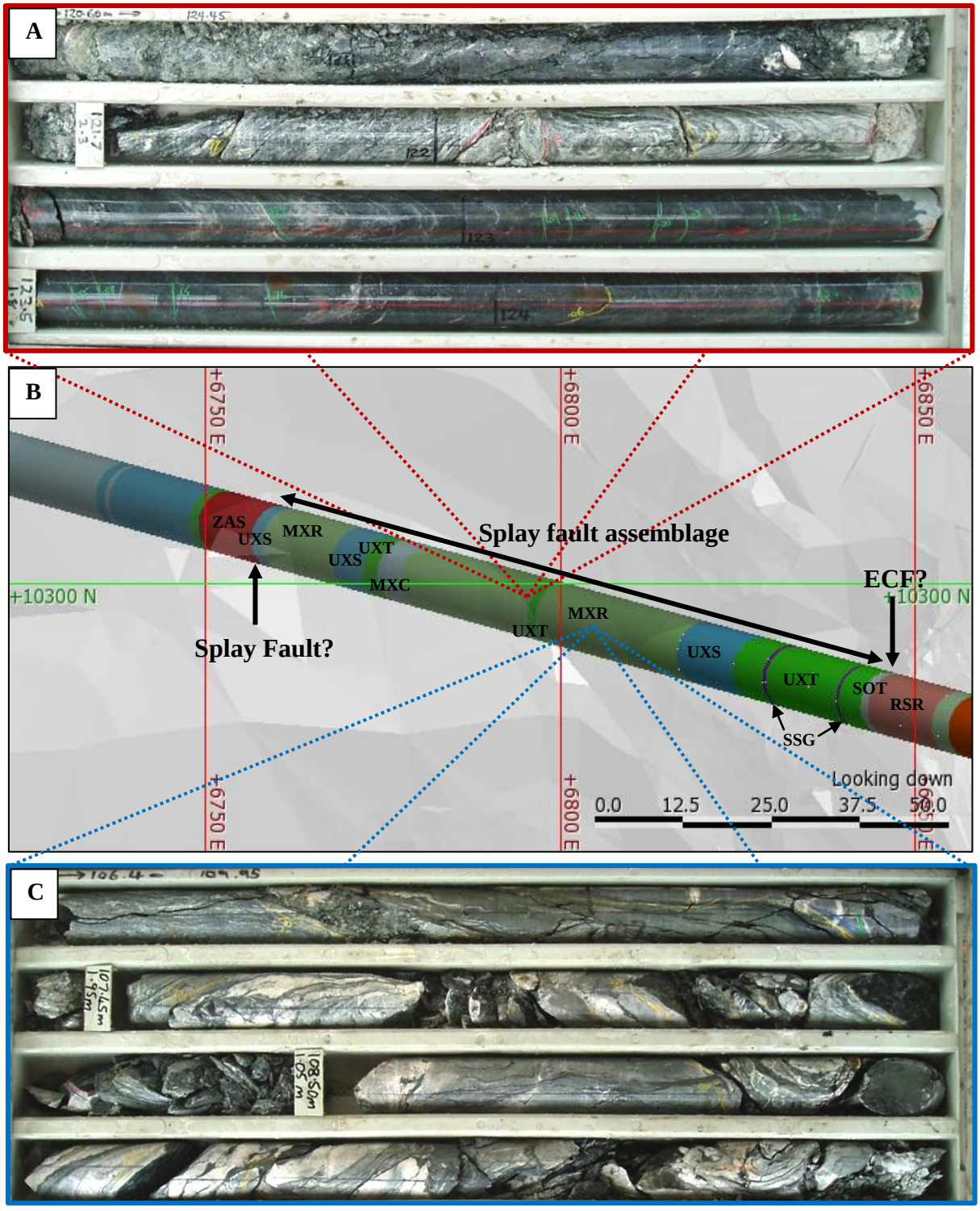

Figure 4.14. Examples of drillcore and lithologies in NDDH09063. **A** – 120.60 to 124 m. A friable non-intact sheared talcose lithology (GSI code 'E5') abruptly changing to a competent chlorite-carbonate schist lithology (GSI code 'B3'). This is an example where the change in lithology governs the GSI number range designation. **B** – A plan-view of the borehole in Leapfrog™ showing the location of **A** and **C**, the extent and variable lithologies of the splay fault assemblage and the estimated location of the Eastern Contact Fault and splay fault. Lithology legend: **ZAS** – Serpentine ore, **UXS** – Serpentine schist, **MXR** – Chlorite-carbonate schist, **UXT** – Talc schist, **MXC** – Chlorite schist, **SSG** – Graphite-rich sedimentary rock, **SOT** – Talc-rich rock and **RSR** – Residual soil. **C** – 106.4 to 109.95 m. Foliated chlorite schist with siliceous banding and veins. Disseminated pyrite is present throughout. Assigned GSI code 'D4'.

4.4.4 Eastern Splay Fault

Chapter 3, Section 3.7.4 describes the Eastern Splay Fault from a geotechnical perspective. The Eastern Splay Assemblage which forms a wedge between the Eastern Splay Fault and the ECF contains lithologies of similar composition to the lithologies within the ECF damage zones to the N (Figure 4.15). Therefore it is possible that this assemblage should be considered a maximum damage zone of the ECF. The mine has termed the fault to the E the Eastern Splay and the contact between barren lithologies and mineralisation to the W the ECF. This research suggests that it is more likely that the most easterly contact is the main strand of the fault (continuation of the ECF) and the contact to the W, is a splay fault. This section describes the evidence for this.

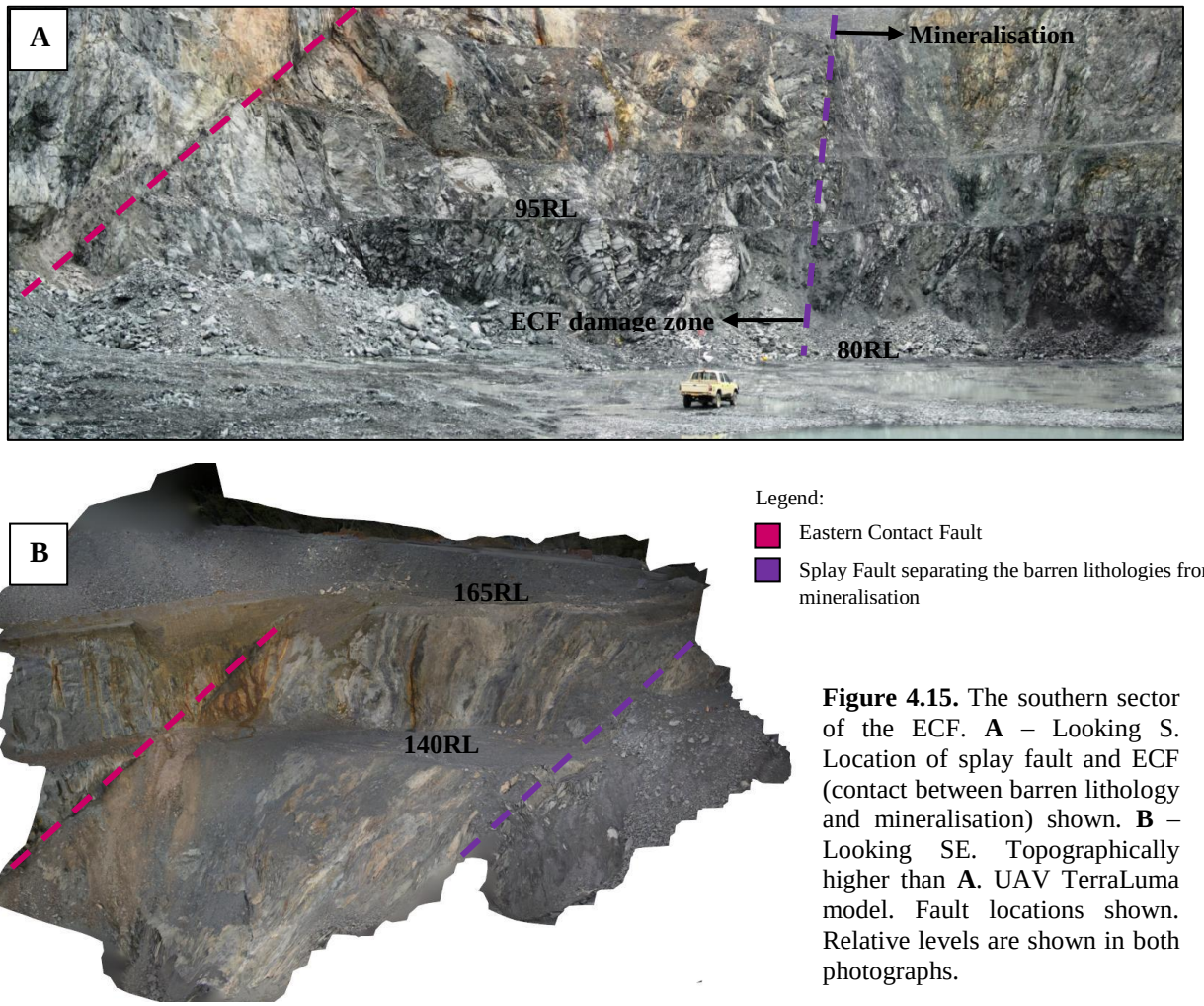

Figure 4.15. The southern sector of the ECF. **A** – Looking S. Location of splay fault and ECF (contact between barren lithology and mineralisation) shown. **B** – Looking SE. Topographically higher than **A**. UAV TerraLuma model. Fault locations shown. Relative levels are shown in both photographs.

Although only two geotechnically logged boreholes (NDDH0614 and NDDH07002) have been drilled through the Eastern Splay Assemblage, another eighteen reverse circulation boreholes, diamond boreholes (not orientated) and mapping traverses were drilled and mapped between 1979 and 2010 in this area. These are outlined in Table 4.3. Analysis of the lithologies and minerals of these boreholes and mapping traverses from the Savage River Database (2010) indicates similarities to the damage zones analysed to the N of this southern sector of the ECF. Major dolomite and graphite are present; common lithologies of the ECF damage zones. Siliceous zones and talcose and albite rich rocks are present. Heavily foliated rocks are recorded and are potentially mylonitic (MYF, FYL). Ductile deformation is commonly present within damage zone rocks but not common within the east wall rocks. For example, an open synform plunging NE is identified within the southern sector of the ECF (Figure 4.16). The fold is of mesoscopic scale with many parasitic folds and quartz, calcite and magnesite veins and boudins observed on the limbs.

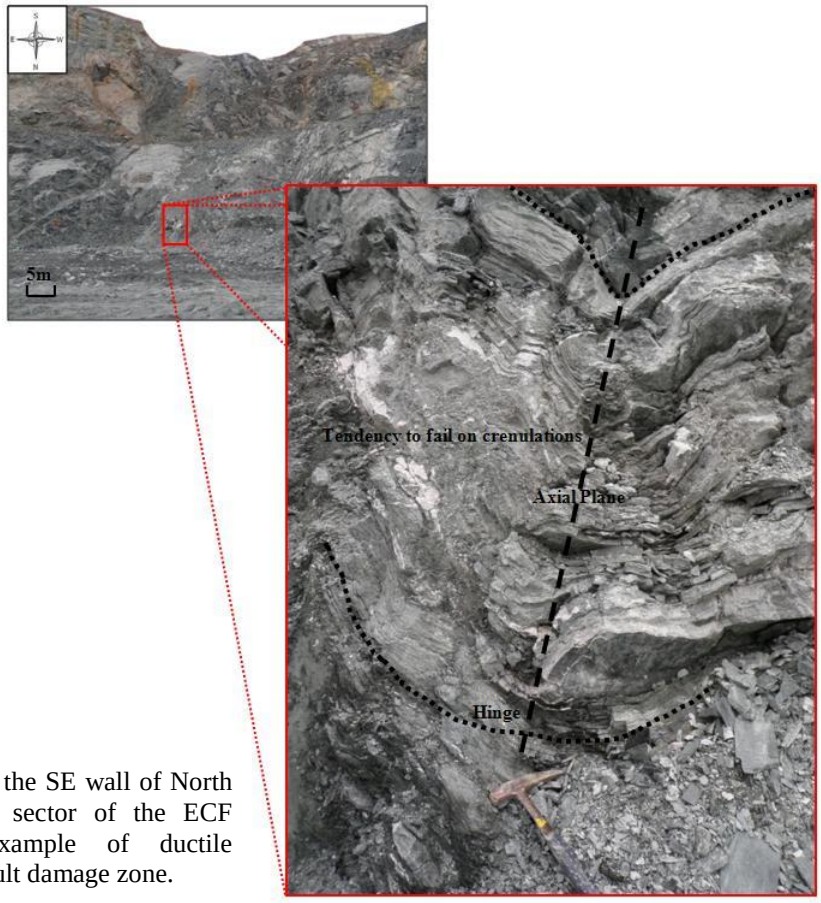

Figure 4.16. Synform on the SE wall of North Pit within the southern sector of the ECF damage zone. An example of ductile deformation within the fault damage zone.

Hole ID, average Plunge and Trend	Depth From_	Depth To_	Rock Type	Minerals	Comments
NPRC07021 Plunge 60° Trend 266°	90m	160m	MXR	ab/cb	
NDDH07022 Plunge 60° Trend 265°	1.4m	25m	MXR	ch/qz/cb	Banded and weathered.
	25m	54.1m	MXR	ch	Minimal carbonate. Foliation 20-30° alpha.
	54.1m	57m	MXR	ch/cb/qz	Weakly banded and foliated.
	57m	95.2m	MXR	qz/fs/cb	Stronger carbonate, local contortion of foliation.
	95.2m	95.5m	VQ		Brecciated vein, irregular contacts approx parallel to foliation.
	95.5m	103m	MXR	cb/ch	Weaker foliation, less defined carbonate veins, more local contortion of foliation 50-60° alpha.
				ch/cb/qz	Banded, strong fine foliation 60° alpha.
	103m	105.9m	MXR		Dark grey band of tourmaline (?) rich MXR.
				ch/cb/tl	
	105.9m	106.5m	MXR	ch/cb	Soft, puggy, sheared MXR, local intensely sheared zone (FAULT).
	106.5m	111.4m	MXR		
NDDH07002 Plunge 56° Trend 269°	9m	49.3m	MXC	ch/py/cc	Variable foliation. Sheared areas and core loss.
	49.3m	54.2m	MYF	ch/fs/py	Possible intervals of magnesite.
	54.2m	54.5m	MYF	ch/fs/fe	As above but leached and fe-stained.
	54.5m	56.3m	MDO	ch/mt/py	Becoming foliated towards end of interval
	56.3m	56.5m	MYF	ch/fs/py	Sheared and fractured.
	56.5m	58.2m	MDO	ch/ms/py	Possible dolerite intrusion; magnesite is brecciated. Associated core loss here.
	58.2m	61m	MYL	ch/do/py	Foliation change.
	61m	64.5m	SLO	do/ch/py	Brecciated, layered and foliated.
	64.5m	70.7m	MBO	hb/py/fs	Mafic (basaltic) interval, some foliation throughout and some calcite veins.
	70.7m	71.4m	SLO	do/py	Brecciated, layered and foliated. Foliated and slightly mylonitic.
	71.4m	78.8m	MXO	hb/ch/py	Mylonitic and folded.
	78.8m	79.9m	SLO	do/ch/py	Richly chloritised; large quartz veins.
	79.9m	80.5m	MXR	ch/cc/qz	Foliated MBO; calcite may be dolomitic.
	80.5m	86m	MBO	ch/cc/py	Banding of weak to strong foliation. Phlogopite. Minor chlorite
	86m	97.7m	MXR	ch/cc/py	intervals. Variable foliation. Large fs vein.
	97.7m	108.1m	FYL	ch/qz/py	Alternating between competent to more sheared areas. Associated
	108.1m	136m	MXR	ch/cc/py	core loss. Much core loss. Shear zone with
	136m	140.2m	MXR	ch/cc/tc/py	some talc. (FAULT).

NPRC10089 Plunge 60° Trend 227°	0m 14m	14m 18m	MXR UXS	ch/cb/qz tc/se/ab	Rich in quartz veins. Talc-serpentine-chlorite schist, puggy shear? Albite and quartz veins present. (FAULT).
NPRC07020 Dip 54° Trend 279°	28m 30m 33m 34m 110m	30m 33m 34m 110m 111m	MXR MXR MXR MXR VQ	ab/cb ch/cb cb/ch ch/ab/cb qz	Albite-rich zone with mod carbonate. Sparse carbonate. Abundant carbonate. Local concentration of albite and carbonate. Quartz vein. (FAULT).
NDDH0614 Plunge 51° Trend 252°	102.5m 102.8m 123.5m	102.8m 123.5m 125.5m	MXR MXR UXT	cc/ch ch/cc/mt ch/cc/tc	Minor friable MXR; sheared core. Moderately foliated MXR. Soft and friable talc-carbonate schist. Transitional into ore zone. (FAULT).
NDDH07023 Plunge 52° Trend 274°	86.65m 88.90m 101m 102.1m 105.4m 110.5m 115.5m 119.5m	88.90m 101m 102.1m 105.4m 110.5m 115.5m 119.5m 120m	MXR MXR MBO MXR MXR OFO MXR OFO	cb/qz/ch cb/ch cb/ch cb/cc/ch cb/qz/ch cb cb se	Up to 20cm thick veins of quartz and calcite, minor pyrite and chalcopyrite. Carbonate mainly follows foliation also some veins. Minor pyrite. Pyrite and hematite traces in fine veins. Pyrite disseminated throughout. Trace pyrite, weakly foliated with some hematite coated joints. Erratic foliation, trace serpentinite. Faulted friable MXR, contorted foliation. Typical MXR. Intensely sheared/puggy, sharp contact at 60deg alpha. (FAULT).
NRC200614 Plunge 50° Trend 269°	75m 104m	104m 108m	MXR ZSS	ch/se/cc mt/se/ch/py	Contact between MXR and ore at 104m. (FAULT).
NRC200615 Plunge 55° Trend 280°	0.00m 82m 86m	82m 86m 90m	MXR MXR ZMS	ch/se/cc ch/se/mt/py mt/se/ch/py	Change of lithology. From unmineralised to mineralised. (FAULT).
ND099 Plunge 65° Trend 270°	0.00m 61.7m 63.6m	61.7m 63.6m 81.3m	SLO OFO ZSS	do se/mt	 (FAULT).
ND098 Plunge 55° Trend 270°	0.00m 80m	80m 92m	SLO ZMS	do mt/se	Mineralised assemblage. (FAULT).
ND097 Plunge 63° Trend 270°	0.00m 83.3m 84.7m	83.3m 84.7m 87.8m	SLO VMO OXC	do/py ch/se/py	 Mineralised next assemblage. (FAULT).
NMAP08004 Trend 91.3°	0.00m	25m	MXR		Unweathered MXR.

NMAP08011 Trend 44° - 351°	0.00m 31m 60m 70m 85m 104m 116m 121.5m 130m 131.5m	31m 60m 70m 85m 104m 116m 121.5m 130m 131.5m 150m	MXR OXNcy MXR MXR MXR MDA MXR MXR SXG MGR	gh/lm ms/cy gh/lm gh/lm gh/lm ch ch ch gf ch	No fault feature due to mapping being carried out in between the two faults.
NMAP08005 Trend 89°	0.00m	20m	MXR		Mapped from photographs
ND094 Plunge 40° Trend 270°	0.00m 20.5m 55.5m 56.3m 58.3m 60.7m	20.5m 55.5m 56.3m 58.3m 60.7m 65m	MXR SLO URT VMO URS MDO	ch/cc/se/ep do tc/se ms se/qz se/ep/mt	Next assemblage is mineralised. (FAULT).
ND088 Plunge 67° Trend 137°	1.0m 12.3m 38.9m 60.5m 67.8m 71.1m 111.6m 115.6m 138.7m 175.5m 179.4m 182.3m 242.6m 259.6m 261.6m	12.3m 38.9m 60.5m 67.8m 71.1m 111.6m 115.6m 138.7m 175.5m 179.4m 182.3m 242.6m 259.6m 261.6m 271.6m (EOH)	VMO MXR VMO OXQ VMO MXR OXH UXS VMO URS SLO VMO SLO SQO SLO	Ms cc/ch/qz/py ms/py/se qz/do/ch/py ms/py/se cc/ch/qz/hm qz/py se/do/ms/mt ms/py se/qz/py do/qz ms/py do/qz/tc/se/py qz/hm/do do/cc/qz/se/hm	
ND087 Plunge 60° Trend 90°	1.5m 169m 177m	169m 177m 181.2m	SLO MXR SLO	do/cc/py/qz/se cc/ch/py/qz/hm do/cc/py/qz/se	
DH050 Plunge 45° Trend 94°	158.5m 160m 160.6m 161.8m 164.6m	160m 160.6m 161.8m 164.6m 209.1	MXC SLO MXC SLO MXR	ch/cb do ch do ch/hb/cb/qz	
ND061 Plunge 51° Trend 270°	3m 26m 36.5m	26m 36.5m 42.5m	MXR UXT MXR	hb/ch/cb tc/ch hb/ch/cb/py	Next assemblage mineralised. (FAULT).

Table 4.3. The lithologies and major minerals of the Eastern Splay Assemblage indicating the corresponding boreholes and mapping traverses carried out from 1979 to 2011. Refer to Chapter 1, Section 1.5 for rock type and mineral abbreviations.

The technical team at Savage River Mine named the easterly fault of the southern sector of the ECF zone the Eastern Splay Fault, and the fault bounding the mineralisation the ECF. From mapping campaigns in this area in 2010 and 2011, the characteristics of these faults indicate the reverse of the applied mine nomenclature. The easterly fault in the southern sector of the ECF damage zone is characterised by graphitic clay pug and disseminated pyrite on the fault boundary (Figure 4.17). This is an indicative feature of the ECF to the N.

Magnesite is evident along the contact of the westerly fault of the southern part of the ECF (Figure 4.17). Magnesite is not generally seen in large quantities in close proximity to the ECF to the north. Siliceous banding and dolomite was also found near the southern splay segment boundary with local areas of fault breccia (Figure 4.17) which is not evident on the ECF to the north. The contact between the magnesite and magnetite mineralisation is gradational (Figure 4.17) along the southern splay segment suggesting magnesite metasomatism. Gradational contacts from barren lithologies to mineralisation are not commonly evident along the ECF, where contacts tend to be sharp. There is no graphite banding evident proximal to the southern section of the Eastern Splay Fault, south of the intersection with the ECF.

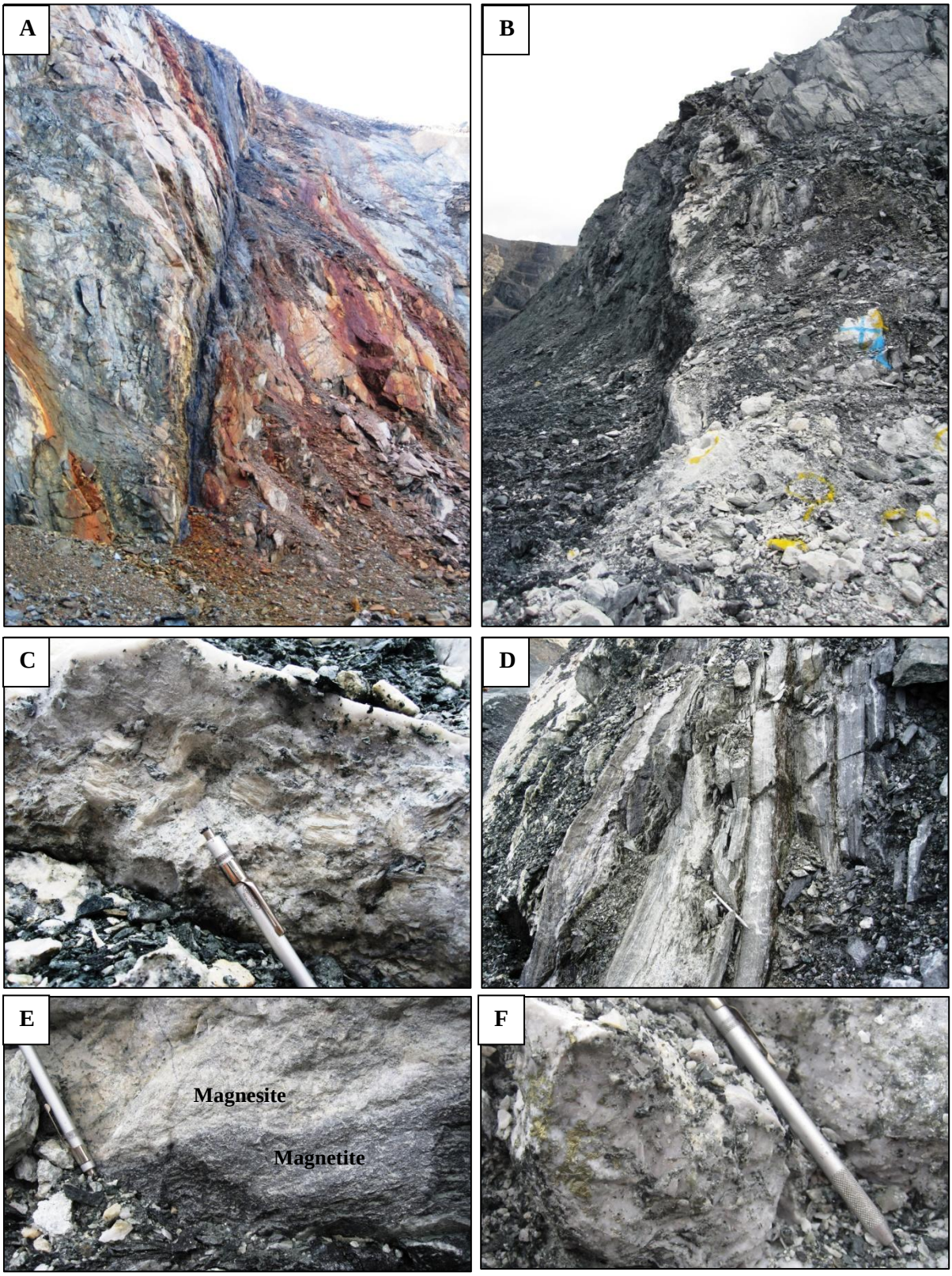

Figure 4.17. A – ECF in the southern sector. The water associated with the fault has weathered the rock around the feature an orange colour. Looking SE. **B** - The Eastern Splay Fault of the southern sector. Looking N. Mineralisation outcrops to the W and magnesite to the E. The fault separates the two lithologies. **C** – Feldspathic quartz fault breccia evident proximal to the Eastern Splay Fault. **D** – Dolomitic and siliceous banding outcropping to the E of the Eastern Splay Fault. **E** – Gradational contact between weakly mineralised magnesite and magnetite. **F** – An example of quartz with disseminated pyrite from the Eastern Splay Fault boundary.

4.4.5 Proposed Eastern Contact Fault Model

Due to twenty recent (2005-2010) drillholes intersecting the ECF and related splay faults, a model of the ECF damage zone can be produced. Figure 4.18 shows the eastern boundary of the ECF damage recognised within drillcore plotted against the Northing and Relative Level (RL). The width of damage (m) is represented next to each eastern boundary position on the plot. The N and S sectors of the fault show wide damage zones, 145.85 m, 142.2 m and 44 m respectively. These indicate the Splay Fault positions discussed in Sections 4.4.2 and 4.4.3. There is an area of thicker ECF damage zones from Northing 10150 to 9500 (Figure 4.18). The RL of the eastern boundary of the thicker damage zones vary from 215 RL to -390 RL.

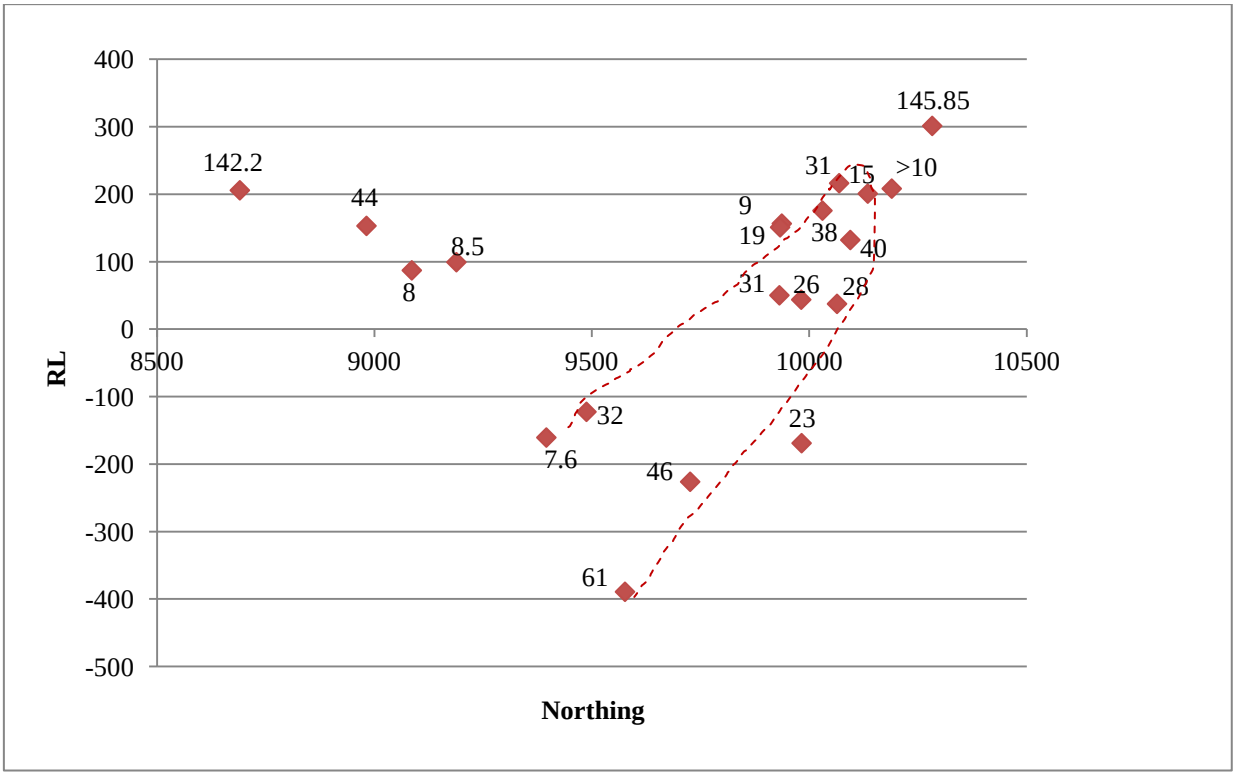

Figure 4.18. A long-section showing Northing and Relative Levels (RL) of the eastern boundaries of the ECF damage zone. The red diamonds denote the location of the eastern boundary at each drillhole and the number denotes the thickness (m) of the damage zone at that location. The red dotted line denotes a block of thicker damage zones within the fault system. The 25 m contour is drawn as a broken line.

Figure 4.19 is a model of the ECF damage zone and relating splay structures. A North Pit surface from August 2012 was used in order to provide context. Northing, Easting and RL are shown. The western and eastern boundaries of the damage zone along the ECF are shown separately with green and orange spots respectively. The splay fault in the N sector of the ECF zone is shown by a dark blue spot denoting the W boundary and a yellow spot denoting the E boundary. It is likely that the E boundary in this area is the ECF and the W boundary a splay fault. The splay fault in the S sector of the ECF zone is shown by a light blue spot denoting the W boundary and a light purple spot denoting the E boundary. It is likely that, similar to the N sector, the E boundary is the "true" ECF and the W boundary a splay fault as discussed in Section 4.4.3. The extent of the fault damage zone is coloured in pale yellow.

Discrete blocks of damaged rock are located where the fault trace is slightly curved (Figure 4.19). A smaller scale later fault is suggested at Northing 9950, offsetting the ECF. A structure called the 'Waterfall Fault' (mine nomenclature) has been observed in this location in Stage 2, steeply dipping to the SW. The western boundary of the fault model indicates the eastern boundary of the MHA and the eastern boundary forms the western boundary of the East Wall Assemblage.

The lithology within the damage zone is different from the wall rocks and is probably para-autochthonous correlates of the large magnesite/dolomite lens outcropping to the W of the South Lens Pit, approximately 500 m south of North Pit.

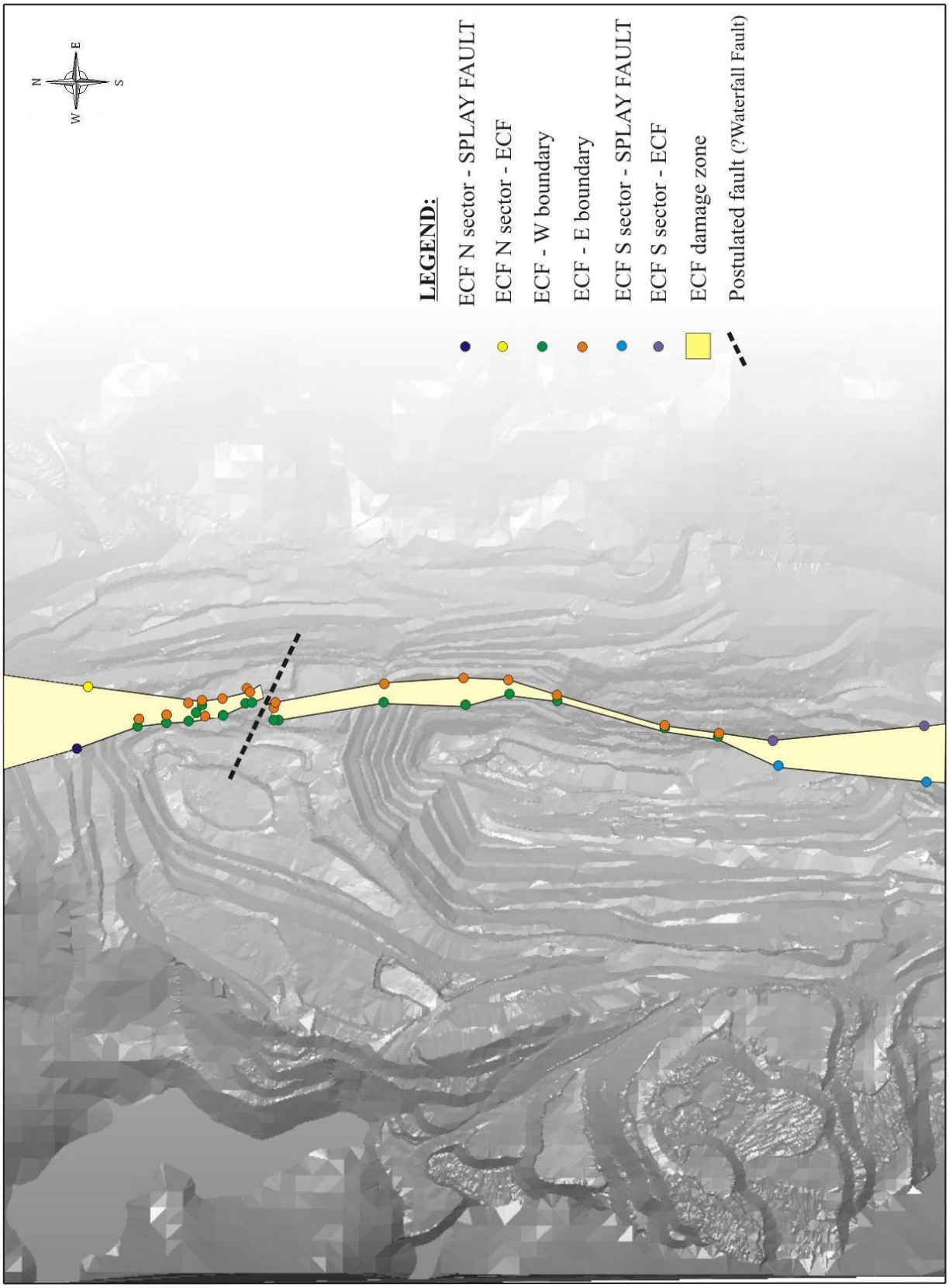

Figure 4.19. Proposed ECF model over an end of month survey of North Pit in August 2012. The data is from twenty drillholes that intersect the ECF. The coloured spots relate to ECF boundaries along strike. The Eastern Wall Assemblage outcrops to the E of the ECF and the MHA to the W. This is not exactly a plan view but has been rotated to make the fault appear vertical.

4.4.6 Magnesite Fault

The Magnesite Fault dips steeply to the W. Turner (2005) suggests a west block down (normal) sense of movement with the younger and lower grade Fulfords Creek Muscovite Schist in the hanging wall and the MHA in the footwall. The fault separates the MHA from the metasediments of the west wall. Due to the variable lithologies of the west wall, it is more difficult to recognise the boundaries of a discrete fault damage zone.

Figure 4.20 shows examples of the Magnesite Fault within drillcore and the various lithologies of the W wall through a Leapfrog™ model of NDDH10067 which intersects the fault. Large magnesite lenses are evident directly to the W of the fault (Figure 4.20 – A) adjacent to highly sheared (puggy in areas) graphite rich lithologies on the fault plane. Cataclasite is observed in drillcore (Figure 4.20 – C) between the contact of the magnesite rich lithology and graphite. Cataclasite is not evident within the ECF damage zone. Quartz and dolomite rich lithologies and potential mylonitic lithologies are common up to 30m W of the fault, similar to the ECF.

The GSI numbers assigned to the rock mass within 1 m of the Magnesite Fault are low (E4 to F5) due to the puggy, foliated and sheared nature of the rock at the fault. However, GSI numbers of the rock >1 m from the fault are on average higher (C3 to D3) than the numbers assigned to the ECF damage zone. The volume of intact siliceous and/or dolomitic drillcore is high. To an extent, lithology controls GSI designation therefore areas of stronger lithology (e.g. stronger rock mass) results in a higher GSI number range.

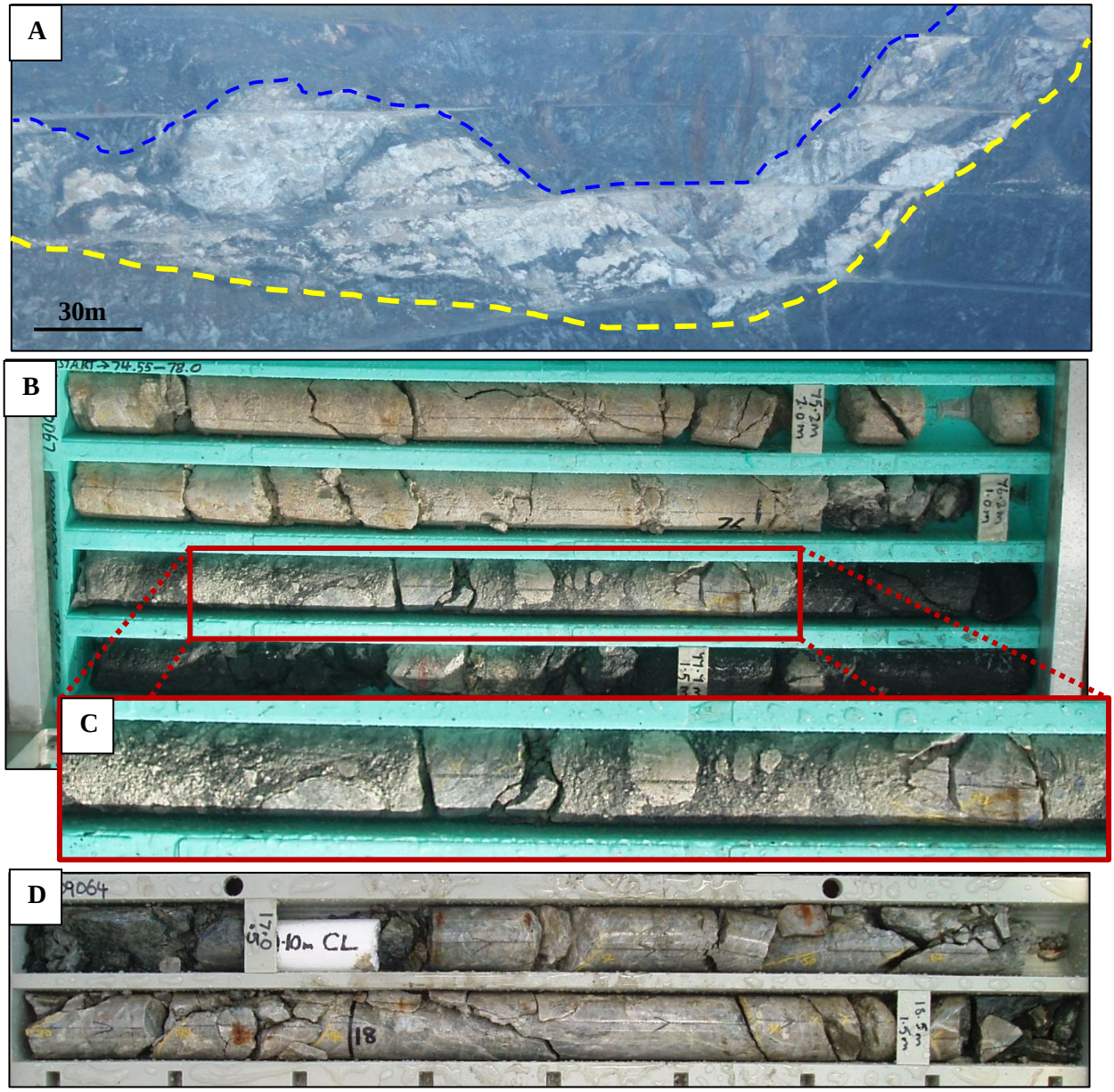

Figure 4.20. Examples of the Magnesite Fault. **A** – Magnesite Fault, North Pit, looking NW. The blue dotted line denotes the contact between the Mega Ramp Schist (above line) and the Box Cut Carbonate (below line) on the W wall. The yellow dotted line denotes the Magnesite Fault location. **B** – NDDH10067, 74.55 TO 78 m. Magnesite to puggy graphite. **C** – 0.60 m of cataclasite from **B**. Located in between the magnesite and graphitic rich lithologies. **D** – NDDH09064, 16.80 to 18.65 m. Brecciated siliceous zone approximately 20 m W of the Magnesite Fault. E – Annotated plan view Leapfrog™ model of NDDH10067 showing Magnesite Fault location and lithologies to the W. **LOS** – Core loss, **OXC** – Chloritic Schist, **VMO** – Magnesite and **SXG** – Graphitic Schist.

4.5 Summary

Measurements of striations on fault surfaces present in drillcore proved to be a useful addition to the core logging method employed at Savage River Mine. Striations and slickenfibres were measured from the E wall and the MHA. Although more coherent on the E wall, calcite and chlorite coated faults present a conjugate fault system, dipping gently to the N and S. It is likely these faults formed at similar times. Striated hematite coated faults of the MHA recognised in drillcore are dominated by steeply east dipping faults with oblique NE trending striations. Hematite coated faults are the youngest faults recognised at the mine and possibly could be related to Tertiary extension of Tasmania. Small-scale normal and thrust faulting is evident on the W wall. This faulting is likely to be late in the relative timing of faulting events in Savage River Mine (refer to Section 4.3).

The extent of the ECF damage zone is variable along strike in North Pit (ranging from 7 m to 61 m). The damage zones are commonly associated with quartz, dolomite, talc and graphite rich lithologies. Hydrothermal water-rich fluids have altered the dolomite and quartz to talc (c.f. Spear, 1993) suggesting that at one time through the ECF history, externally derived fluids have passed through the fault. The ECF is a major controlling factor in fluid transport. The thickest damage zones of the ECF are presented as discrete blocks adjacent to bends on the fault geometry. The Magnesite Fault damage zone is difficult to constrain due to the variability of lithologies on the west wall. Graphite, dolomite, magnesite and quartz rich lithologies are common up to 30 m W of the fault.

The GSI domaining method proved a useful addition to the core logging system employed at Savage River Mine. The GSI numbers of the ECF damage zones relate to the volume of disintegrated and sheared rock in the area. In most cases, the GSI numbers alone, without lithological description can be used to determine the apparent width of the ECF fault damage zone. However, although the GSI method is effective at highlighting areas of poor rock mass

condition, the method only takes brittle deformation into account. Areas of high ductile strain (?mylonite) (Figure 4.21) and cataclasite (Figure 4.20 – C) are not designated low GSI numbers due to the core being intact with few joints and veins. Ductile deformation is essentially ignored in the GSI classification method and this could potentially result in the large shear zones or faults not being recognised.

Figure 4.21. NDDH09063, 173.45 m to 183.30 m. An example of possible mylonitic fabric ignored by the GSI method. This drillcore was designated a B3 GSI rating although it is an indicator of a ductile fault in the area.

CHAPTER 5

DUCTILE DEFORMATION

5.1 Introduction

This chapter describes the composition, foliation characteristics and ductile deformation of the three rock packages of North Pit in Savage River Mine. The foliation development is described first then the general mineralogy, petrography and microstructure of the East Wall Assemblage, Main Host Assemblage (MHA) and West Wall Assemblage (WWA) are discussed respectively. Representative samples of each assemblage were chosen from drill core and from North Pit to assist with this task. There are several unpublished company reports including Thornett (1999), the Mine Life Extension Plan Vol 1 and 2, Australian Bulk Minerals (2006), Turner (2006) and Bottrill (2006) which outline the composition of each assemblage. Also published reports such as Bottrill and Taheri (2007), Taheri and Bottrill (2013), Turner and Bottrill (1993) and Turner and Bottrill (2001) discuss petrological aspects of the assemblages. In-pit mapping and the microstructural results from mylonitic rocks in North Pit determined the presence of two generations of shear zone; a strike-slip generation and dip-slip generation. The sampling technique, mylonitic characteristics, amphibole compositions, the lattice-preferred orientation of quartz, and monazite geochronology is discussed in this chapter.

5.2 Foliation development and folding in North Pit

The foliation within the Savage River Mine North Pit rocks is pervasive throughout the three assemblages. The foliation of the East Wall Assemblage, MHA and WWA steeply dips to the west. The modal foliation orientation of the East Wall Assemblage is striking 005° and sub-vertical (Figure 5.1 – ***A***). The MHA modal foliation orientation is 88°/267° (Figure 5.1 – ***B***)

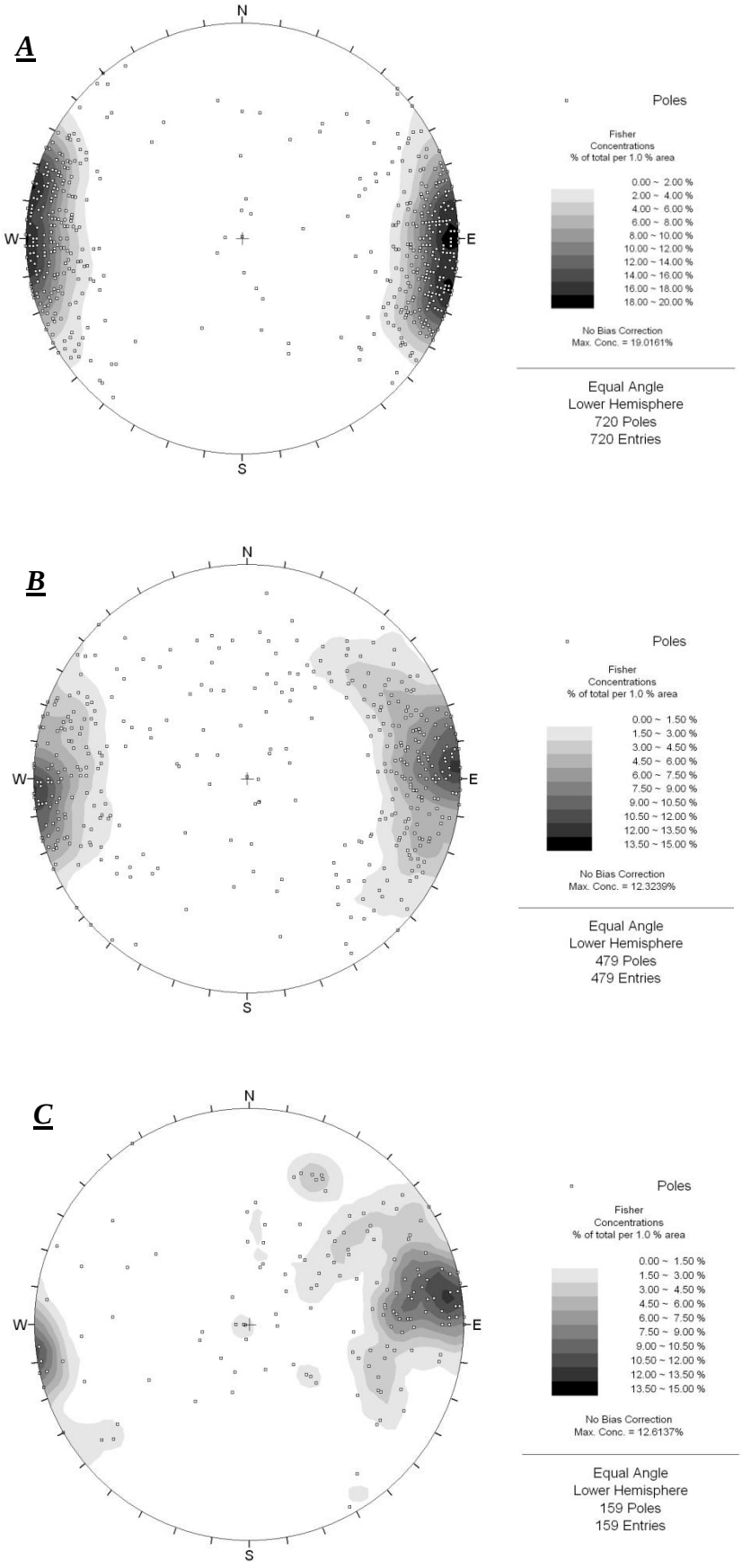

Figure 5.1. Pole and contour plots of foliation orientation data from North Pit. ***A*** – East Wall Assemblage. ***B*** – Main Host Assemblage. ***C*** – West Wall Assemblage.

and the WWA is 85°/261° (Figure 5.1 – ***C***). The modal foliation changes very slightly between the domains with the WWA striking about 15° clockwise of the East Wall Assemblage. The East Wall Assemblage has a foliation very close to the major faults while the WWA has the lowest overall strain, weakest foliation and has the highest angle between the major faults and the modal foliation. The foliation orientation variation of the East Wall Assemblage is the least variable of all rock packages in North Pit. This is visible in Figure 5.1 - ***A*** with the small volume of poles outside the calculated contours. Within the MHA, variation is greater.

The number of data points could have a significant effect on the stereonet data (over four times the volume of foliation data was recorded within the East Wall Assemblage than in the WWA). Post-foliation folding within the rocks would have a significant effect on the foliation orientations but in-pit mapping has confirmed folding is not common within any of the rocks in North Pit. No mesoscopic folds have been identified within the East Wall Assemblage or MHA during this research. The only significant mesoscopic fold within the sequence were visible on the SE wall of North Pit, within the southern sector of the ECF damage zone (refer to Chapter 4, Section 4.4.3). Mesoscopic synforms are exposed within Western Wall Banded Schist, within the WWA. The fold plunges gently to the SE (Figure 5.2). The lack of visible folding may be partly due to the orientation of the pit face. This mesoscopic fold is the only example identified within North Pit which is surprising. Rocks exposed 1.5 km to the east of the pit (Oonah Formation) are intensely folded on all scales.

Turner et al., (1991) described the "high strain" Oonah Formation as a micaceous quartz schist with interbeds of grey, green and pelitic phyllite and fine-grained schist. The "high strain" Oonah Formation differs from the Oonah Formation further east in having more intense foliation development and tighter folding (Holm, 2002). Both rocks have a locally recognisable isoclinal $\boldsymbol{Ca}F_1$ folds strongly overprinted and refolded by $\boldsymbol{Ca}F_2$. In most rocks

CaS2 is the dominant foliation.

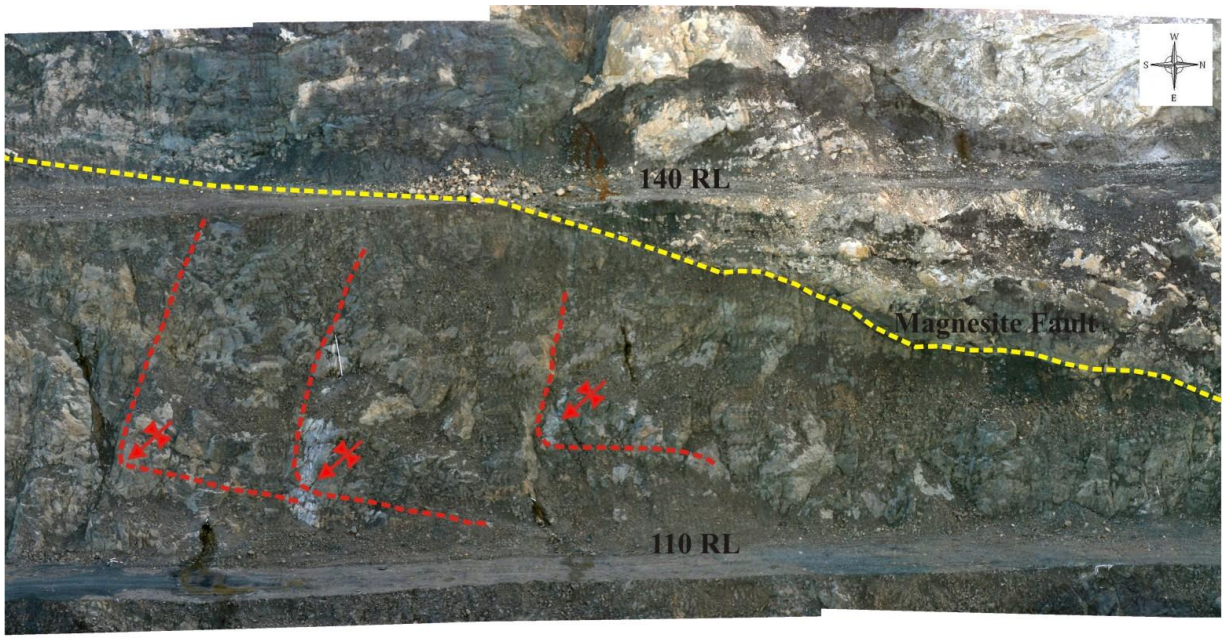

Figure 5.2. Gently plunging synform within a 30 m high bench of the Western Wall Banded Schist. The Magnesite Fault crossing the bench to the N is denoted with a broken yellow line and the synforms shown as broken red lines including the plunge direction.

Webster (2009) reported tight folding within the "high strain" Oonah Formation along the Mine Access Road, 1 km E of North Pit. A major fault separates these rocks from a major amphibolite unit east of the East Wall Assemblage but the nature of the transition is not exposed in the vicinity of the North Pit. Holm and Berry (2002) reported this transition 25 km to the south in the spillway of the Reece Dam.

The East Wall Assemblage and MHA are generally interpreted as allochthonous units (e.g. Holm and Berry, 2002) and were probably far from the Oonah Formation during CaD_1 and possibly still distant during CaD2.

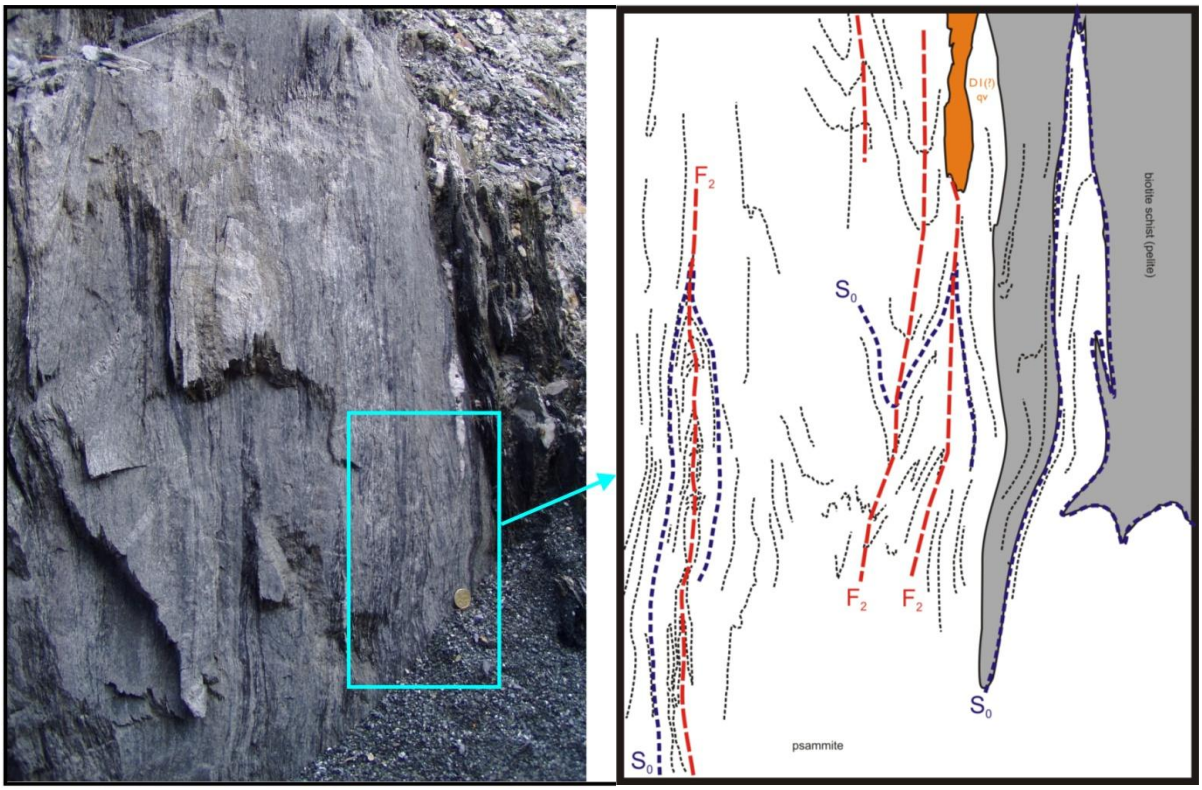

Figure 5.3. Well-preserved bedding in Oonah Formation psammite. Folded by CaF_2. Modified after Webster, 2009.

5.2.1 Foliation development, massive amphibolite and strain localisation

Post-cleavage folding has little effect on the foliation orientation of the rock packages in North Pit. The main reason for the variation in foliation orientation, especially within the MHA, is strain partitioning between various lithologies. Boudins and lenses of magnetite/ mafic rocks/ carbonates are commonly observed within the MHA and WWA. The rocks surrounding the boudins and lenses are usually highly schistose and/or puggy and the foliation wraps around the lenses, locally changing the foliation orientation. As previously discussed (refer to Chapter 3, Sections 3.4.6 and 3.5.6) this causes minor geotechnical problems in North Pit. Although strain localisation is common within the MHA and the WWA, it is difficult to observe within the East Wall Assemblage. In hand specimen, the mineralogy is uniform throughout the rock package. Seemingly the only characteristic for recognition of strain localisation is the apparent intensity of foliation. Some areas through this assemblage,

exposed in drillcore, are massive amphibolite interleaved with areas of intensely foliated material. The foliated domains are rich in quartz and carbonate veins. The amphibolite zones were analysed to determine whether the foliation development reflects protolith composition or alteration within the assemblage.

In order to detect changes in composition that may affect the development in foliation of these rocks a series of 22 samples across a small foliated zone were analysed by handheld XRF (Appendix 2). The samples all have a similar Ti/Zr ratio averaging 120 which is typical of basaltic compositions (Figure 5.4). For the massive samples there are two groups, a high Ti composition and a low Ti composition. It is assumed here these groups reflect original bulk composition and are not a result of alteration. The Neoproterozoic rift tholeiites from western Tasmania have similar Ti/Zr ratios and include rocks with a similar range in Ti content (e.g. Crawford and Berry, 1992). The foliated rocks have a similar Ti/Zr ratio and this is accepted here as evidence that they were also basaltic in composition before alteration.

The foliated rocks cluster close to, and trend away from, the low Ti basaltic group and therefore the change in composition of this group is discussed based on the assumption that the unaltered composition for the foliated rocks lies close to the average of the low Ti massive amphibolites.

All the foliated samples have lower Ti and Zr than the massive rocks, suggesting that in all cases there has been a net mass addition to the foliated samples (Gresen, 1967). Most of the foliated samples show strong increases in Ca (Figure 5.5) and this is interpreted as calcite addition possibly in veins but the high strain makes the recognition of veins in these zones difficult. These six samples show a similar depletion in Si to Ti suggesting there is limited SiO_2 mobility (Figure 5.6). Two foliated samples do not show enrichment in Ca. One foliated sample shows strong Mg and Fe enrichment along with Si depletion compatible with chloritic alteration. This sample has similar Ca and Ti content to the massive samples.

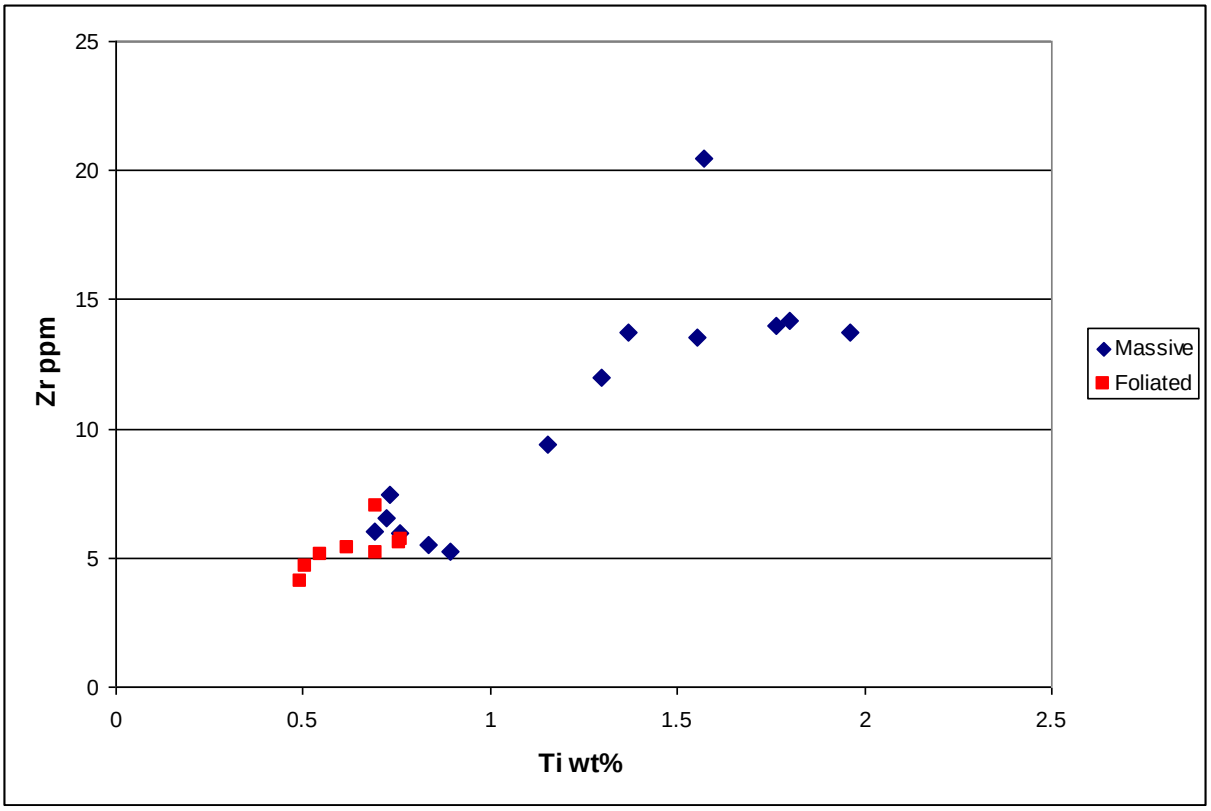

Figure 5.4. Plot showing the Zr (ppm) and Ti (wt %) ratio of massive and foliated samples of the E wall.

Foliation development in these rocks has a strongly spatial correlation with calcite addition. Calcite addition during deformation would provide a strong feedback mechanism to enhance strain localisation but it is also possible that the calcite addition predated the foliation. Evidence from the spatial concentration of veins near faults (Chapter 4) supports the conclusion that this was a syn-deformational alteration process.

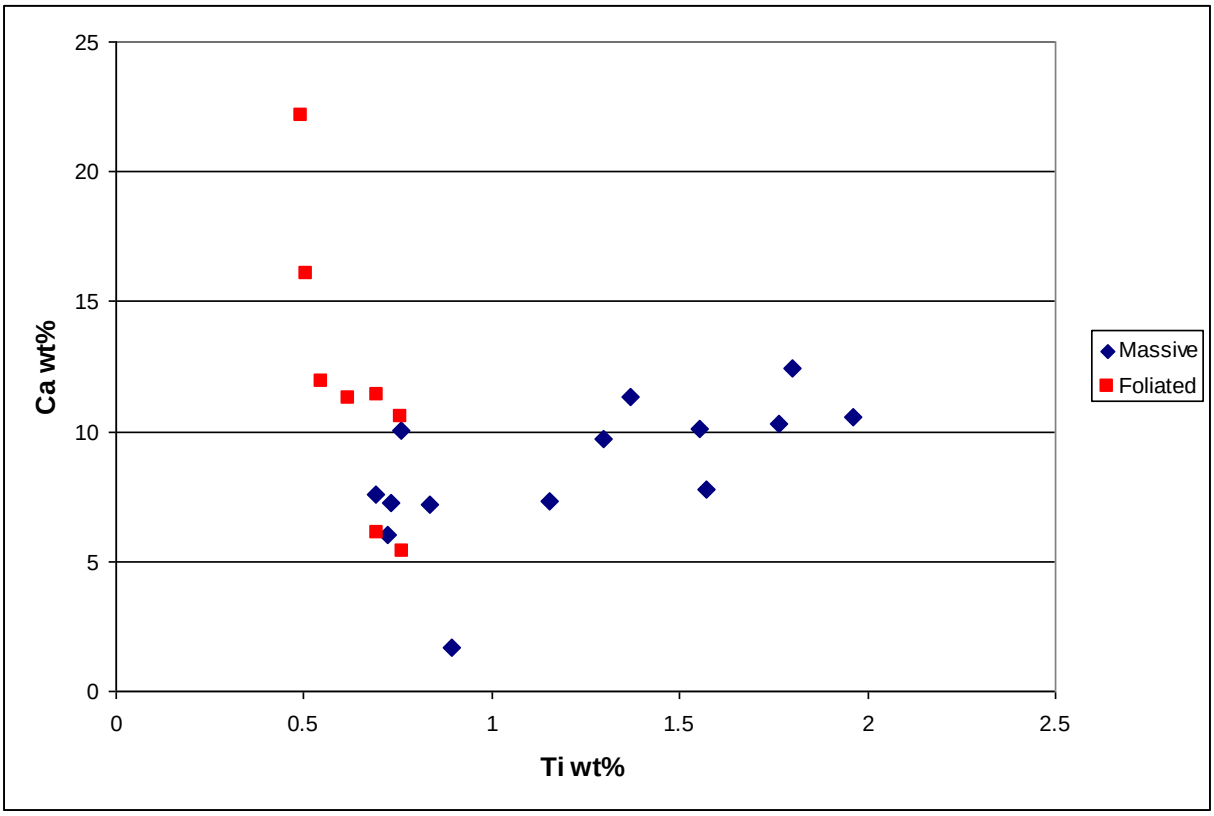

Figure 5.5. Compositional variation in Ca for the mafic rocks at Savage River Mine.

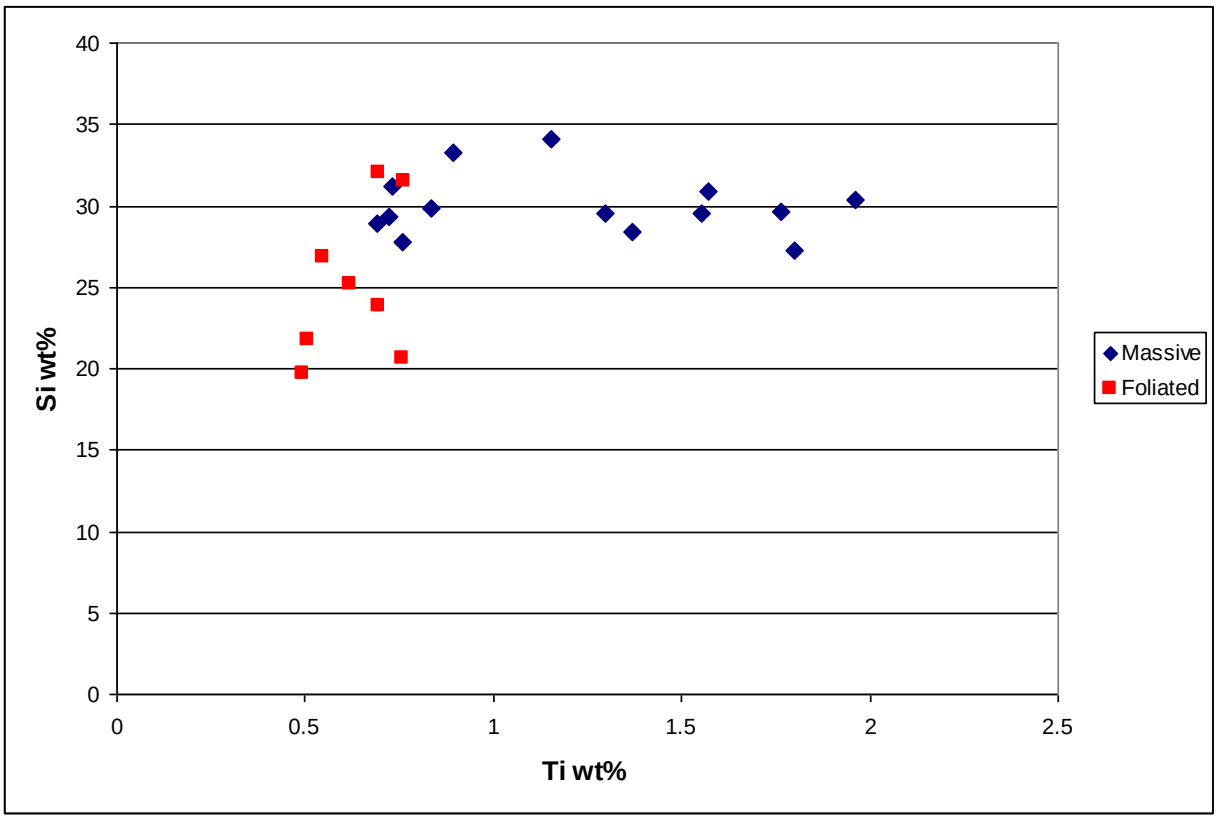

Figure 5.6. Compositional variation in Si for the mafic rocks at Savage River Mine.

5.3. General mineralogy, petrography and microstructure

5.3.1. East Wall Assemblage

In hand specimen, the east wall rocks are fine-grained, green-grey, massive to finely schistose rocks with weak to moderate foliation, some lamination, and little or no obvious mineralisation (Bottrill and Taheri, 2007). Discontinuous and boudinaged calcite veins are common portraying three generations; the oldest oriented parallel to the pervasive foliation, another generation cross-cutting foliation and the youngest and least deformed vein set cross-cutting all veins and foliation (refer to Chapter 3, Section 3.3.4). Quartz boudins, segregations and veinlets are also common.

The mineralogy of the East Wall Assemblage is dominated by chlorite and albite (Table 5.1). Calcite, quartz, muscovite and epidote are locally abundant. Relict green amphiboles are present in some samples. Minor biotite is apparent in some samples and is typically partly chloritised. Minor disseminated anhedral fine-grained pyrite, magnetite and minor hematite are present in some samples (Figure 5.7) but Fe oxides never approach ore grade. Taheri and Bottrill (2013) state that some zones of the Eastern Wall Assemblage contain very abundant carbonate (calcite and/or dolomite) and quartz, grading into massive dolostone beds to about 1m thick, but thinner in the east.

The albite grains have post-kinematic textures (Figure 5.7) over-printing the pervasive foliation. The quartz present is very deformed indicating strain was strong at temperatures in the ductile field for quartz (? $\geq$ 300°C). Discrete fractures and shear bands in the foliation are apparent. Extensional crenulations are common within chlorite rich zones. Compositional banding is also present, usually alternating between albite and calcite rich bands. An East Wall Assemblage mineralogy summary (Bottrill and Taheri, 2007) is shown in Table 5.1.

The East Wall Assemblage alternates between massive and intensely foliated rock. In order to

detect possible composition changes that may affect the development in foliation of these rocks, a series of samples were analysed by handheld XRF. Refer to Section 5.2.1 for the results. Petrographically, the difference between the massive rock and the foliated rock is the ratio of mafic minerals and calcite. The massive samples have a mafic composition with minor calcite whilst the foliated samples contain a chlorite, quartz, epidote and carbonate rich mineralogy. The calcite addition has a strong spatial correlation with foliation development in these rocks (Section 5.2.1).

Bottrill and Taheri (2007) state that this unit is probably dominantly an altered and metamorphosed mafic tuff and/or tuffaceous sandstone sequence with a minor component of clastic rocks of a more quartzose, micaceous and/or feldspathic composition. They state that the biotite and muscovite probably indicate early potassic alteration and the albite-rich zones some sodic alteration. Taheri and Bottrill (2013) suggest that the East Wall Assemblage is generally significantly richer in quartz, carbonates and chlorite and poorer in albite, amphibole and epidote than the Main Host Assemblage mafic rocks.

Wt%	**Max**	**Min**
Mg-Ca-Fe carbonate	5	0
Calcite	10	0
Quartz	25	0
K-Feldspar	5	0
Albite	55	10
Epidote	25	0
Amphibole	40	0
Chlorite	35	10
Biotite	20	0
Muscovite	10	0
Tourmaline	1	0
Leucoxene	5	0
Magnetite	4	0
Hematite	1	0
Pyrite	2	0

Table 5.1. Mineralogy summary of the East Wall Assemblage, taken from 7 samples (Bottrill and Taheri, 2007).

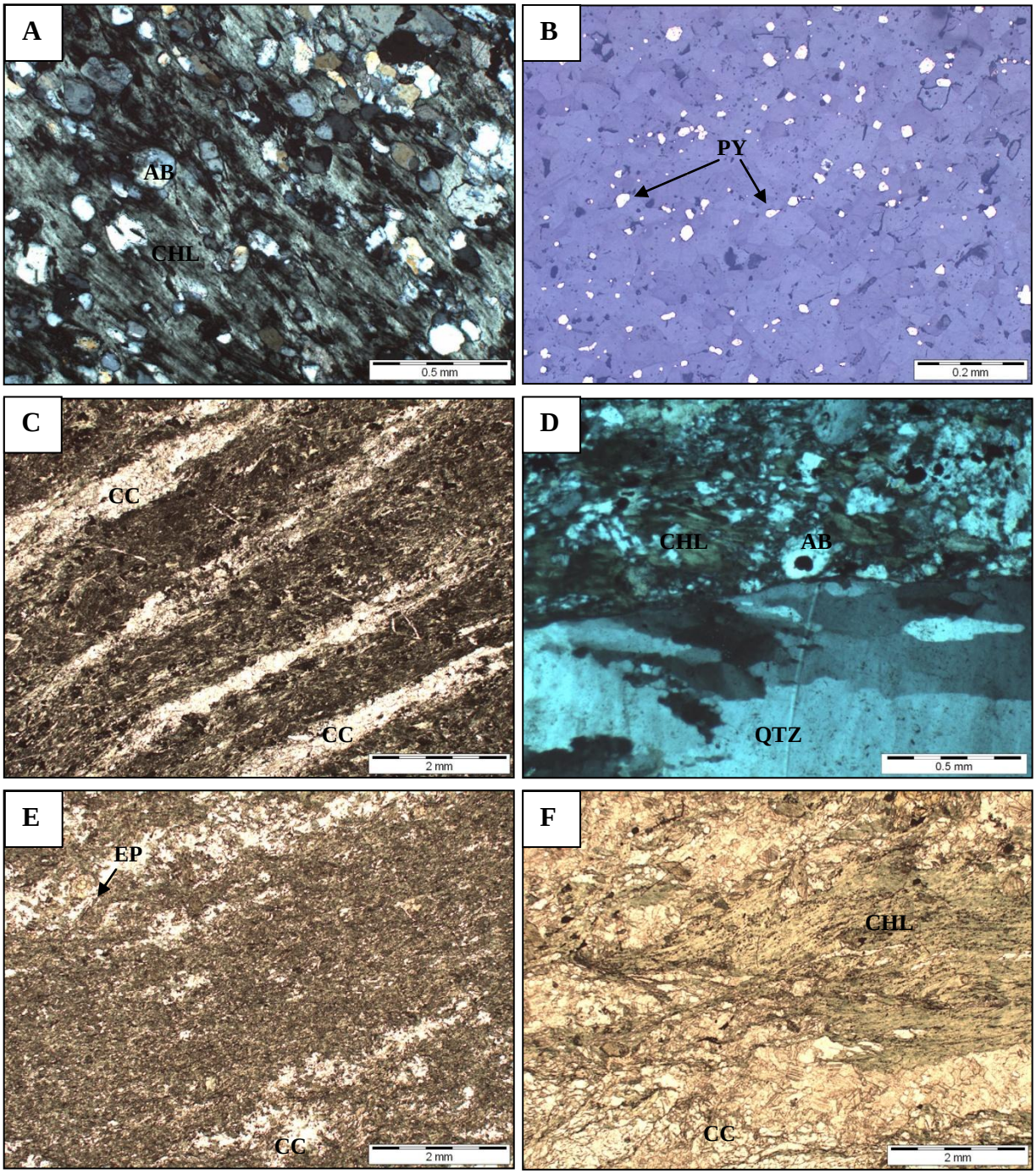

Figure 5.7. Photomicrographs of the East Wall Assemblage. **A** – 176616. XPL. Pervasive chloritic foliation with post-kinematic, undeformed albite porphyroblasts. **B** – 176614. Reflected light. Disseminated fine-grained anhedral pyrite grains. **C** – 176608. PPL. Common fabric of rocks from this package. A matrix of mafic minerals with discontinuous lenticular veins or boudins of calcite preserving high twinning. **D** – 176615. XPL. Chlorite, albite and carbonate rich sample. Quartz with new sub-grains. Limited nucleation. The host rock is chlorite and albite. **E** - 176612. PPL. Massive sample, mafic composition. Minor quartz with a pervasive chloritic foliation. Minor epidote. Carbonate veins within sample following the orientation trend of the foliation. **F** – 176613. PPL. Chlorite, carbonate, quartz and epidote. Strongly foliated in hand specimen.

Abbreviations: **XPL** – Cross polarised light, **PPL** – Plane polarised light, **CHL** – Chlorite, **AB** – Albite, **QTZ** – Quartz, **PY** – Pyrite, **EP** - Epidote and **CC** – Calcite.

5.3.2. Main Host Assemblage

As the name suggests, this assemblage hosts the magnetite ore in North Pit. The unit is rich in Mg-rich lithologies, including carbonate, amphibole, pyroxene, chlorite, serpentine and talc-rich rocks (Bottrill and Taheri, 2007). According to Bottrill and Taheri (2007) the unit includes the following subunits; amphibolite and pyroxenite, mineralised units, serpentinite, talc-chlorite-quartz-dolomite rocks, dolostones, magnesite marble and mafic rocks. The mafics of the MHA are similar to the Eastern and Western Wall mafics, but are generally slightly mineralised, with minor magnetite and pyrite (Taheri and Bottrill, 2013). The carbonate units include magnesite and dolomite-rich to sparry sedimentary rocks and grade into dolomitic quartzites and mafic schists. These occur to the W of the MHA in North Pit (Taheri and Bottrill, 2013). The magnesite marbles are generally unfoliated. Intense foliation is apparent within talc, tremolite and chlorite-rich lithologies of the MHA (Figure 5.8 – **C** and **D**). A spaced cleavage is locally apparent and crenulations are common. Epidote is common within the rocks of the MHA. The epidote is pre- or syn-kinematic (Figure 5.8 – **A** and **B**) based on the porphyroblast matrix relationships. Calcite is common, showing extensive twinning (Figure 5.8 – **E**). Albite is common in all assemblages of North Pit. Within the MHA, the albite porphyroblasts show a slight domino-type fragmentation (Trouw et al., 2010) which can be used to identify shear sense in the matrix (Figure 5.8 – **F**).

The rocks of the MHA grade from 0-95% magnetite. The Savage River Mine defines mineralised rocks as being >15% of combined magnetite, pyrite, hematite, apatite and chalcopyrite (Bottrill and Taheri, 2007). The host rock is variable, but is mostly very dark metallic grey or black, coarse-grained, disseminated to massive magnetite, with grey-green-white flecks and bands and patches of unfoliated silicates and disseminated coarse-grained pyrite (Bottrill and Taheri, 2007). Taheri and Bottrill (2013) suggest that based on principal gangue minerals, the magnetite ore bodies can be divided into four main groups; serpentinitic,

amphibolitic (mainly tremolite – actinolite), talcose, chloritic and dolomitic ores (Table 5.2). Reflected light microscopy has confirmed there are two generations of magnetite growth; an early, pre-/syn-kinematic (Figure 5.9 – **A**, **B, C** and **D**). In some rocks these early grains have the appearance of σ porphyroclasts with a tremolite foliation with asymmetric form wrapped around the magnetite grains. Late, post-kinematic disseminated euhedral magnetite grains with hematite rims (Figure 5.9 – **E**) were found in one sample that also has specular hematite veins (Figure 5.9 – **F**). Pyrite is commonly associated with magnetite and is locally abundant. LA-ICPMS analyses of pyrite grains from the MHA were undertaken to determine trace metal concentrations and to highlight element zonation if present (Appendix 3). The pyrite was typically fractured and elements such as Ni, Co, Mg and Al are concentrated along fractured edges indicating probable local remobilisation along fractures. The only systematic element zonation detected was closely linked to brittle fractures within the grains.

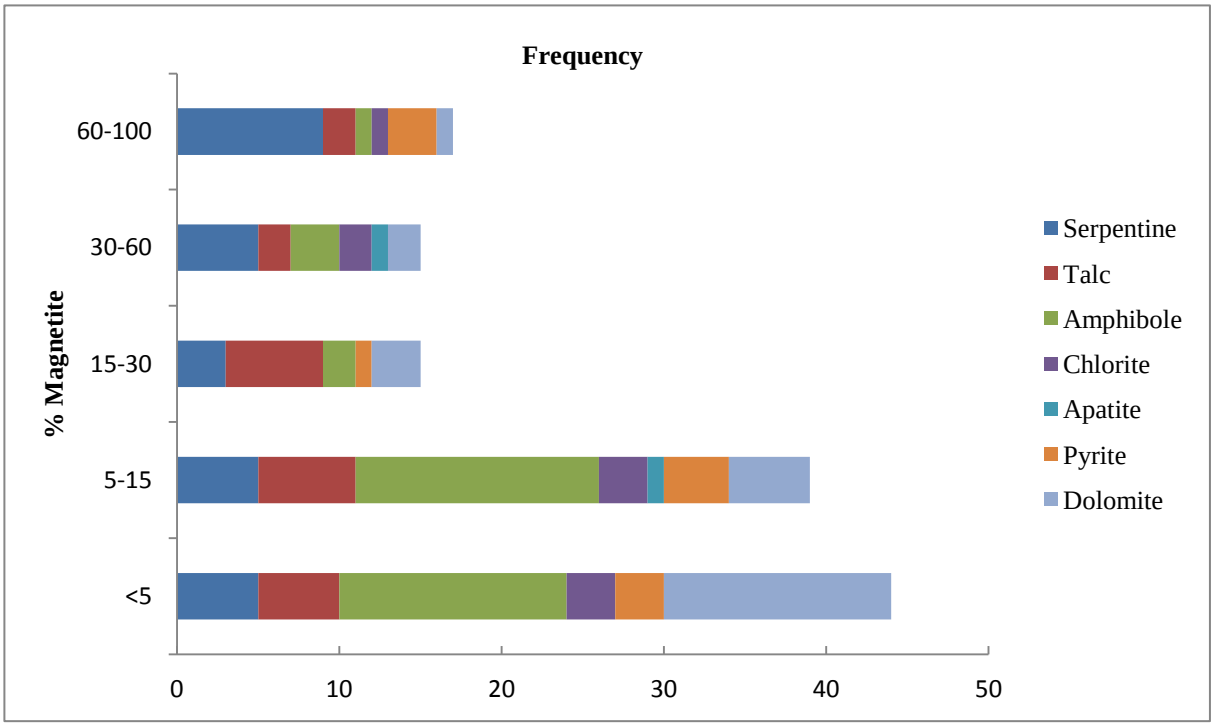

Table 5.2. Frequency distribution of magnetite over different dominant gangue mineral associations in Savage River Mine ores and host rocks of the MHA, excluding the veins and felsic mafic rocks (Taheri and Bottrill, 2013).

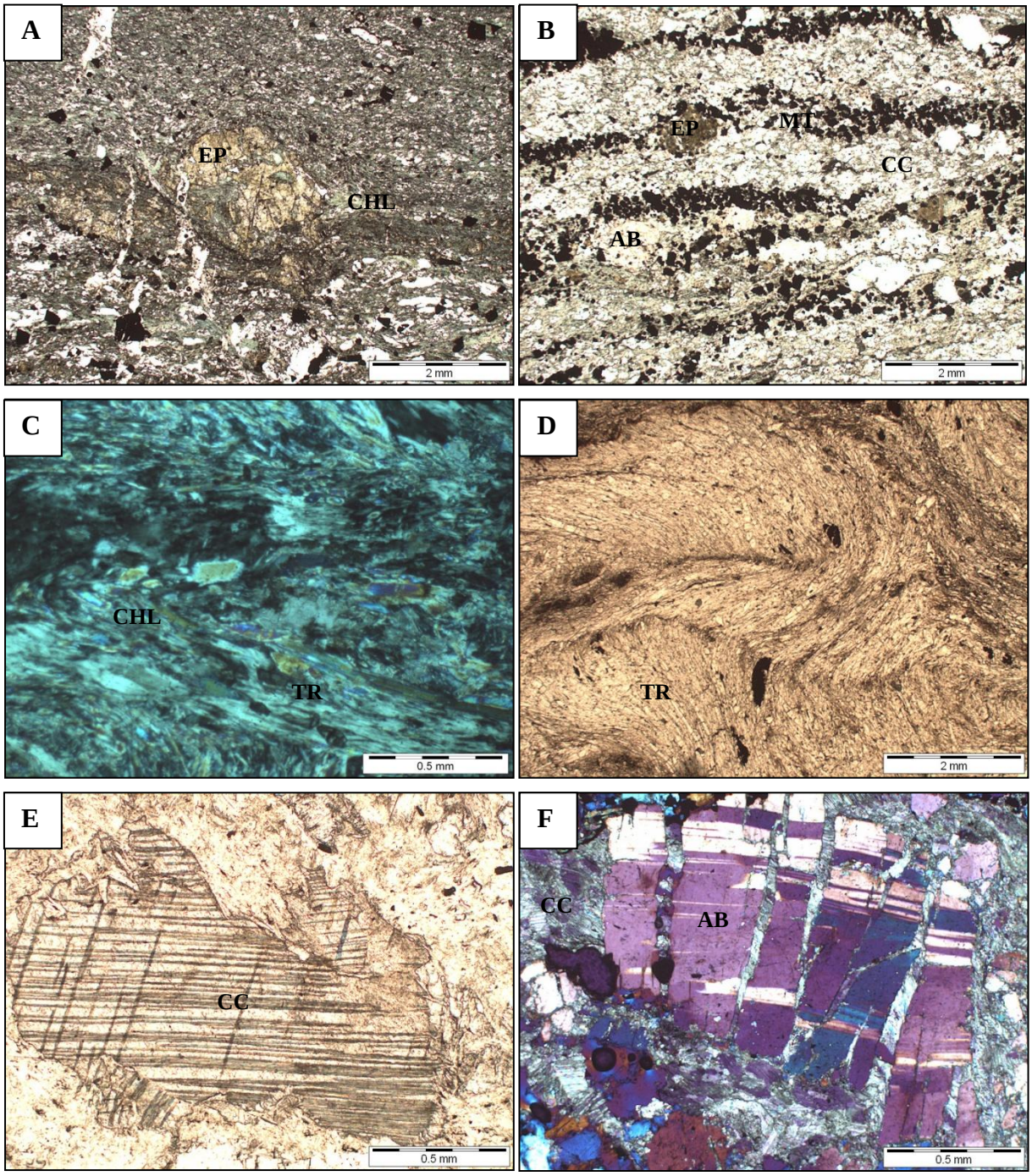

Figure 5.8. Photomicrographs of the MHA. **A** – 176622. PPL. Pre-kinematic epidote with chlorite pressure shadows. **B** – 176623. PPL. Fabric within low grade magnetite ore. Magnetite rich bands with minor pyrite. Epidote occurs within the mineralised bands. Gangue rich bands are calcite, albite and chlorite. **C** – 176617. XPL with gypsum plate. An example of a spaced cleavage composed of tremolite and chlorite. **D** – 176618. PPL. Crenulations in tremolite resulting in a spaced cleavage within the sample. **E** – 176619. PPL. Highly twinned calcite. **F** – 176623. XPL with gypsum plate. Fractured albite in calcite rich matrix.

Abbreviations: **XPL** – Cross polarised light, **PPL** – Plane polarised light, **EP** – Epidote, **CHL** – Chlorite, **AB** – Albite, **MT** – Magnetite, **CC** – Calcite and **TR** – Tremolite.

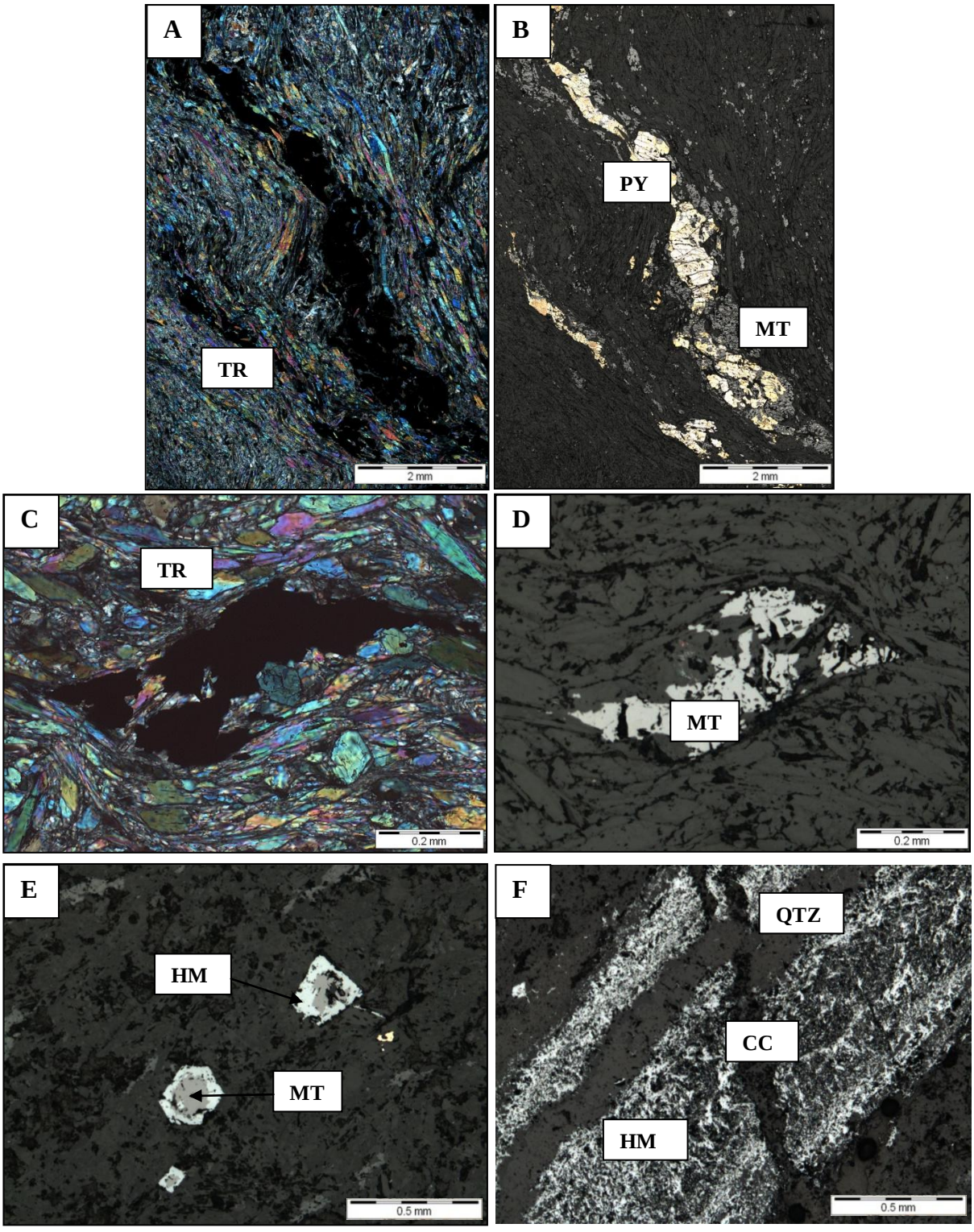

Figure 5.9. Photomicrographs of ore minerals within the MHA. **A** – 176618. XPL. Opaque vein with tremolite/actinolite matrix. **B** – 176618. Reflected light view of **A**. The opaque vein is composed of pyrite and magnetite. **C** – 176620. XPL. A porphyroclastic opaque grain surrounded by tremolitic foliation. This grain has an σ porphyroclast habit. In this view, the sense of shear is dextral. **D** – 176620. Reflected light view of **C**, confirming a deformed magnetite grain. **E** – 176635. Reflected light. Post kinematic euhedral magnetite grains. The cores of the grains are magnetite with hematite rims. **F** – 176635. Reflected light. Post kinematic hematite veins, occurring as needle-like (specular), radiating aggregates. Hematite is concentrated in the centre of the vein. Hematite vein offset by a younger calcite vein.

Abbreviations: **XPL** – Cross polarised light, **PPL** – Plane polarised light, **TR** – Tremolite, **MT** – Magnetite, **HM** – Hematite, **QTZ** – Quartz and **CC** – Calcite.

5.3.3. West Wall Assemblage

The West Wall Assemblage (WWA) contains interbedded albitites, metamafites (possibly mafic sandstone +/- volcaniclastics), quartzites, mica schists, rare pyroxene hornfels and quartz-amphibolites with local mylonitised rocks of mixed composition (Taheri and Bottrill, 2013). The Western Wall Banded Schist is relatively unmineralised, typically banded albite-chlorite-amphibole-quartz schist along the western side of the Bowry Formation (Figure 5.10 – **A**). The fabric is attributed to metamorphic differentiation during deformation, probably preceded or accompanied by albite alteration (MLEP, vol 2, 2006). Other rock types within the Western Wall Banded Schists include boudins and lenses of meta-dolerite, chlorite schist, magnetite ore and fine-grained ultra-mylonite. Bottrill and Taheri (2007) divided the Western Wall Banded Schists into five sub-units; Albitite (fine-grained), Albitite (coarse-grained), Western Wall mafics, Quartzite and Quartz-amphibolite/pyroxenite. Only the Albitite (fine-grained) is evident within the west wall of North Pit. Fine-grained albitite (greater than 50% albite) varies from granoblastic to schistose texture. These rocks are moderately rich in amphibole and/or micas (Figure 5.10 – **C** and **D**) but locally are mainly albite and quartz. The chlorite and mica layering may be inherited from bedding. A strong foliation is locally present. Biotite is also locally present, partially chloritised (Figure 5.10 – **B**). Opaque minerals are pyrite (up to 10%) and magnetite (up to 5%) and locally there are traces of hematite (Bottrill and Taheri, 2007). Bottrill and Taheri (2007) suggest the albitite probably represents a highly albite-metasomatised and deformed sandstone sequence. It may be a more albitised version of the Mega Ramp Schist. The Mega Ramp Schist is composed of chlorite, albite and muscovite and locally quartz. The albite grains have textures indicate pre-/syn-kinematic formation with respect to the dominant foliation. Minor tourmaline and biotite is present within the rock type. Late-stage calcite veins are common (Figure 5.10 – **E** and **F**). Only minor disseminated pyrite is present and no mineralisation. Bottrill and Taheri (2007) suggest this is a chlorite-muscovite-albite schist (refer to Table 5.3 for a mineralogy

summary), probably representing a highly altered, brecciated and deformed pelitic and mafic-rich metasediment, partly albitised and locally carbonate altered.

Wt%	**Max**	**Min**
Dolomite	15	0
Quartz	20	0
Albite	30	15
Chlorite	25	0
Biotite	20	0
Muscovite	50	20
Tourmaline	0.5	0
Leucoxene	5	0
Pyrite	5	0

Table 5.3. Mineralogy summary of the Mega Ramp Schist, taken from 4 samples (Bottrill and Taheri, 2007).

The Box-Cut Carbonate Assemblage is also described on the west wall of North Pit. There is no equivalent unit to this on the western walls of South Lens, Centre or South Deposit pits (MLEP, vol 2, 2006). In North Pit, the Mega Ramp Schist passes eastwards with structural conformity into interbanded chlorite schist and massive cream magnesite marble of the Box Cut Carbonate Assemblage (MLEP, vol 2, 2006). This carbonate assemblage also contains massive grey dolomite, thinly banded dolomite-chlorite-muscovite schist, and subordinate lenses of muscovite schist, micaceous quartz schist and graphite schist. The latter lithologies are probably meta-sedimentary (MLEP, vol 2, 2006).

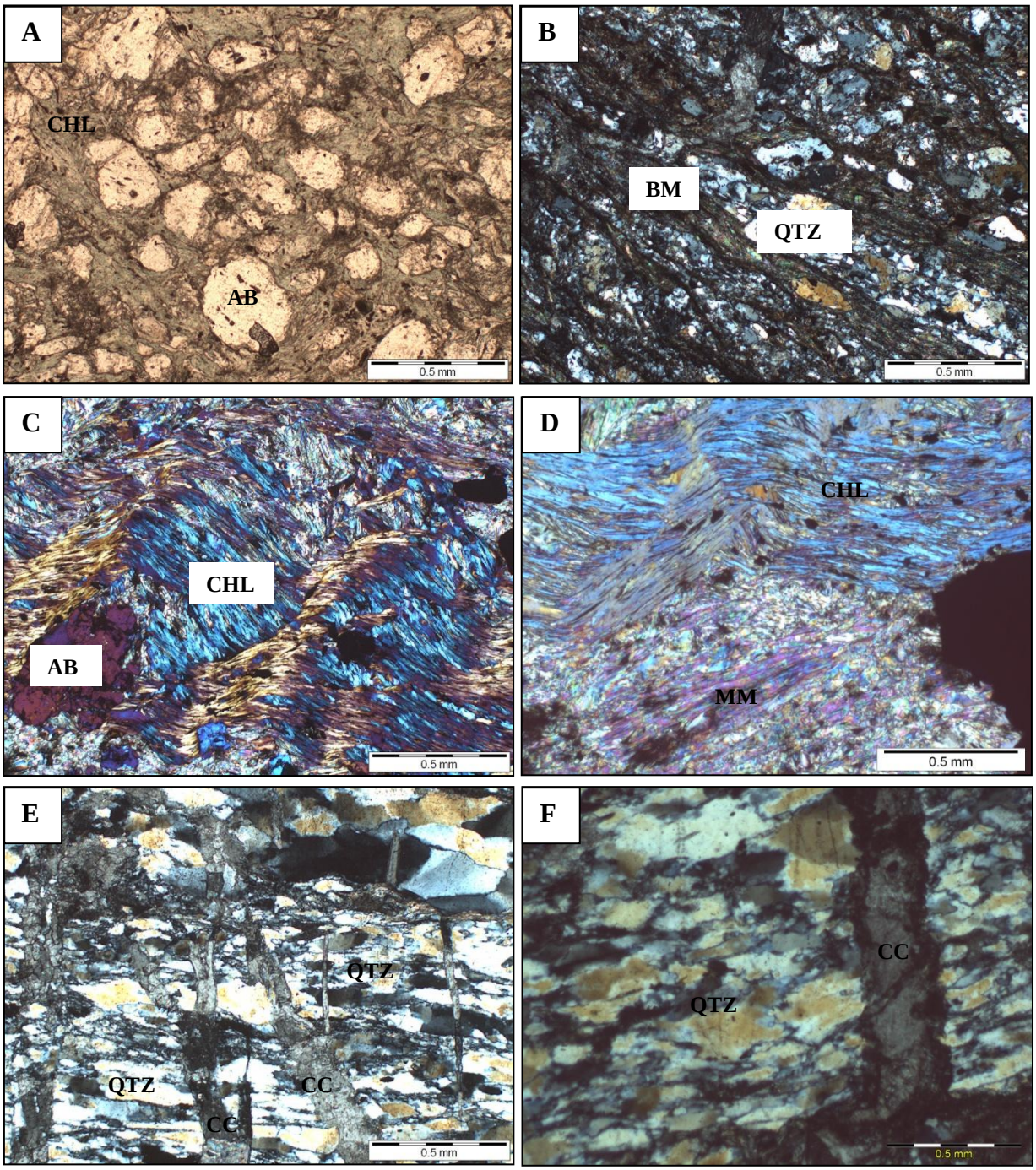

Figure 5.10. Photomicrographs of the WWA. **A** – 176624. PPL. Western Wall Banded Schist. Unmineralised banded albite +/- chlorite +/- amphibole +/- quartz schist. Fine-grained rock and albite rich. **B** – 176625. XPL. Sample located close to the MHA contact. Albite schist. Albite, quartz, muscovite, chlorite and biotite mineralogy. Biotite is heavily retrogressed, generally chloritised. A crenulation cleavage wraps around the albite porphyroblasts. **C** and **D** – 176626. XPL. Chlorite and muscovite foliation that is crenulated. The crenulation axial plane deviates around an albite porphyroblast. **E** and **F** – 176621. XPL. Quartz rich sample located within the Mega Ramp Schist assemblage in Stage 2. A shear sense can be identified by using the quartz sub-grain fabric. This sample is very deformed with calcite veins oriented 90° to the dominant foliation.

Abbreviations: **PPL**– Plane polarised light, **XPL**- Cross polarised light, **AB**– Albite, **CHL**- Chlorite, **QTZ**- Quartz, **MM**- Muscovite mica, **BM**- Biotite and **CC**- Calcite.

5.4 Savage River Mine – North Pit Mylonites

5.4.1 Introduction

Snoke and Tullis (1998) produced a photographic atlas which provides a discussion of fault rock texture and the evolution of the word mylonite. According to Trouw et al. (2010) the term mylonite refers to rocks with specific (micro) structure that, in most cases, can be qualified as follows;

- Presence of a strong LS fabric
- Presence of a fine-grained matrix with porphyroclasts. Minerals like quartz, chlorite, biotite and muscovite are usually present in the matrix, either highly strained at low grade, or recrystallised at higher grades. Minerals like feldspar, garnet, hornblende and pyroxenes may form porphyroclasts, commonly showing evidence of crystal-plastic deformation by undulose extinction and/or partial recrystallisation.
- Presence of a certain asymmetry, especially in low-grade mylonites, in the form of C/S fabric or C' shear bands, mineral fish, stair stepping, oblique foliation etc.

Trouw et al. (2010) suggest that the definition of mylonites can be described as rocks of any composition, usually associated with shear zones, with a specific structure indicative of stronger ductile deformation than adjacent rocks. Trouw et al. (2010) argue that the formation of mylonites and related rocks is mainly controlled by the following variables; intensity (and/or rate) of deformation, metamorphic conditions during and after mylonitisation including temperature, pressure and the presence and composition of fluids and the mineralogical composition of the parent rock. The first of these variables is expressed in the classification of protomylonites, mylonites and ultramylonites. The second variable can be understood as depth of formation (Figure 5.11). The third variable controls mineralogical composition of the mylonites.

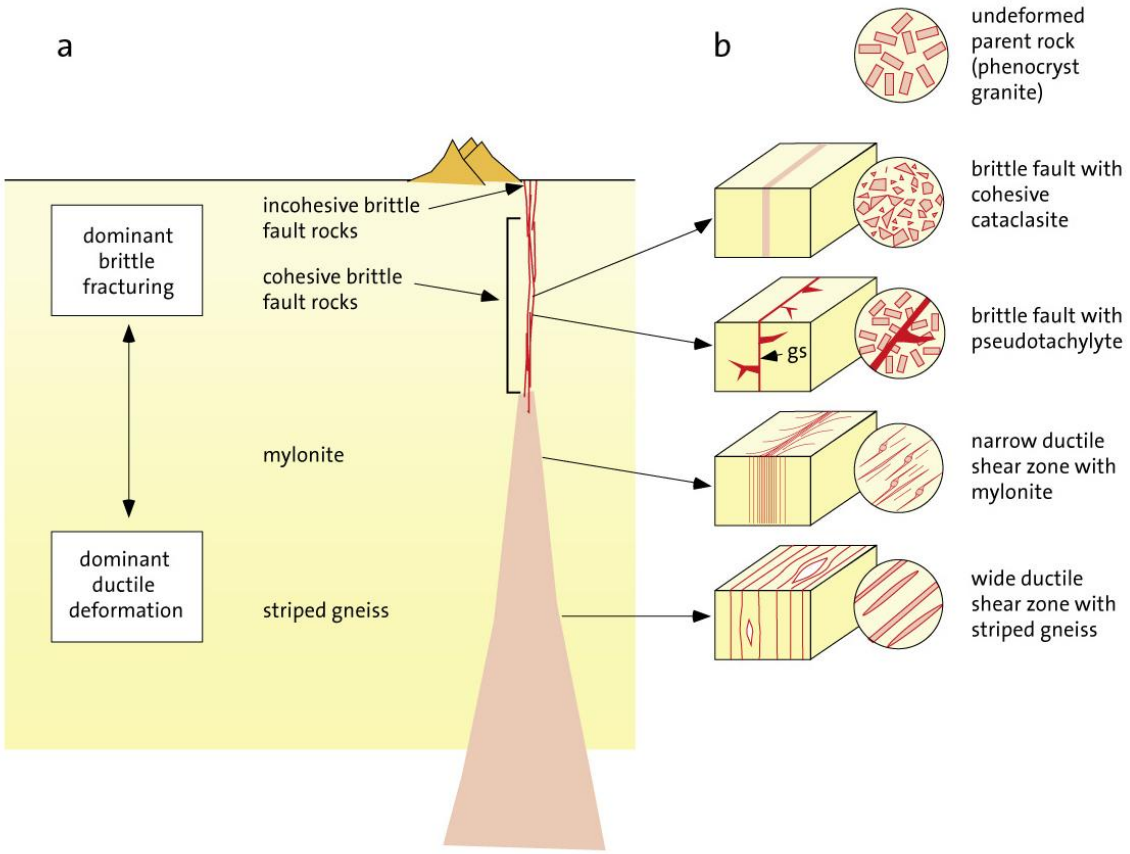

Figure 5.11 – Distribution of the main types of fault rocks with depth in the crust (after Trouw et al., 2010). **a** Schematic cross-section through a transcurrent shear zone. The zone may widen and changes in geometry and dominant type of fault rock occur with increasing depth and metamorphic grade. **b** Schematic representation of four typical fault rocks (out of scale) and the local geometry of the shear zone in a one metre wide block, such as would develop from a phenocryst granite.

The presence of mylonites was confirmed in North Pit using microstructural and petrographic work. This section focuses on the mylonitic microtextures of the rocks from North Pit. Conventional oriented sample retrieval could not be carried out on the mine due to rock magnetism so the sampling method and sample locations are discussed. Examples of shear sense indicators and crystal-plastic deformation evident in the Savage River Mine mylonites are presented.

5.4.2 Sample collection, location and preparation

Conventional oriented sample collection based on a magnetic compass could not be carried out in North Pit. The method employed for the extraction of oriented samples involved survey equipment namely the *Trimble R8 GPS Rover* to get specific orientations for the samples. In other respects the collection and marking of samples followed the protocol in McClay (1994

pp 41-44). The mylonites in North Pit are difficult to recognise in outcrop. During the first set of sampling, 35 oriented samples were taken. Of these, only 6 had typical mylonitic micro-texture. The appearances of the mylonitic samples were studied in hand specimen and the locations noted prior to the second set of sampling. More foliated and lineated rocks were targeted as well as assemblages rich in albite, muscovite, biotite, chlorite and quartz. Only some walls of North Pit are safe to approach and this introduced a sampling bias. As much as OHS restrictions allowed, effort was made to target as many different assemblages and different areas as possible. The second set of sampling resulted in 14 oriented samples being taken with 9 of these having micro-textures typical of mylonite. The locations of the samples chosen for further microstructural analysis (8 samples) are presented in Figure 5.12. These samples present stronger mylonitic textures and have shear sense indicators not seen in the other samples.

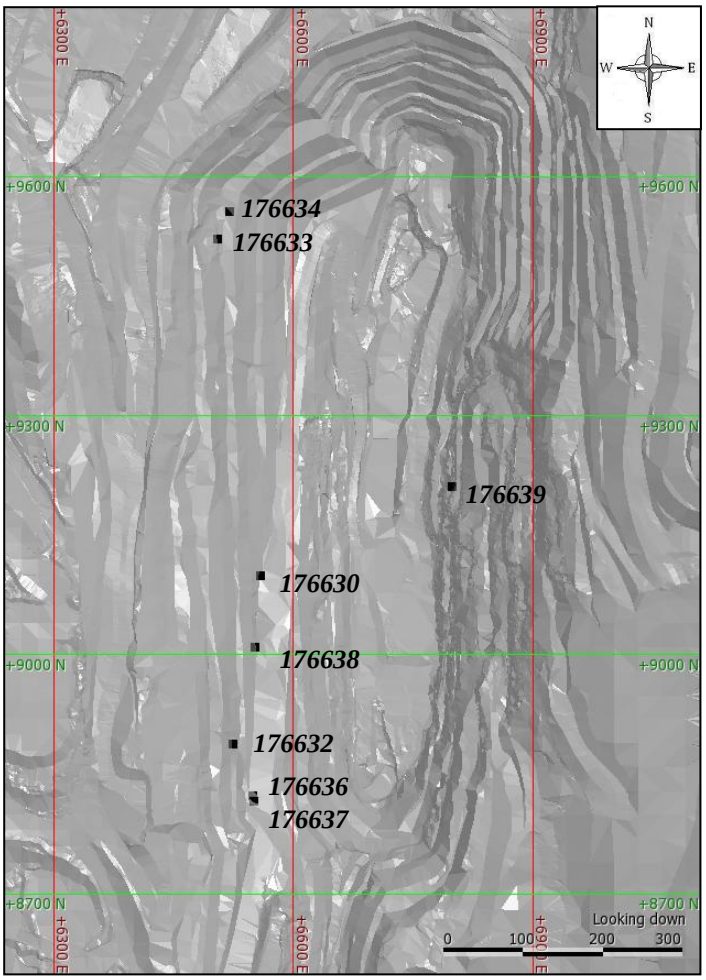

Figure 5.12 – Plan-view Leapfrog™ model showing Stage 1 of North Pit and the mylonite sample locations.

All oriented samples were cut perpendicular to the mylonitic foliation and parallel to the stretching lineation and also parallel to the mylonitic foliation and normal to the stretching lineation (Figure 5.13). The thin sections cut parallel proved suitable to determine shear sense (Figure 5.14). Additional mineralogy information of the matrix and porphyroblasts composition was gained using the thin sections cut normal to the stretching lineation.

Figure 5.13 – Hand specimen of oriented sample 176637 and corresponding thin section cuts. This presents a strong (micro) mylonitic fabric and interpretable shear sense indicators. Scale in cms.

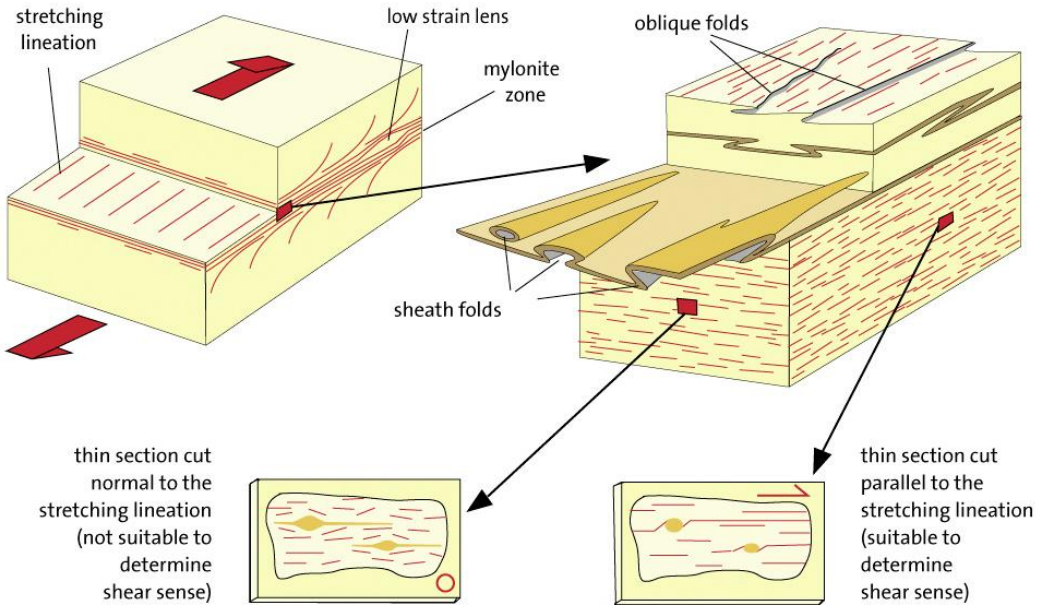

Figure 5.14 – Schematic diagram showing the geometry of a mylonite zone and the nomenclature used. Notice that shear sense indicators can only be judged correctly in sections parallel to the aggregate or stretching lineation and perpendicular to the mylonitic foliation (modified after Trouw et al. 2010).

5.4.3 Microstructural Results

All the mylonitic rocks have a steeply dipping foliation striking N-S. The majority of oriented samples collected are associated with dip-slip stretching lineations. However, two oriented samples retrieved from near to the geological contact of the MHA and the WWA have a strike-slip stretching lineation. Both sets of mylonites will be discussed respectively. Abbreviations in the figure captions include; PPL – Plane polarised light and XPL – cross polarised light.

Chlorite, muscovite, biotite, albite, fine-grained quartz, amphibole (actinolite) and carbonate are common minerals of the dip-slip mylonite samples from North Pit. There is a presence of a strong LS fabric in most of the rocks however there are varying degrees of fabric strength. Shear sense indicators include asymmetrical sigmoidal boudins up to 1 cm in length (Figure 5.15). The boudins are generally quartz rich with muscovite defining the foliation. Mica fish are present within mica-rich samples (Figure 5.16) indicating shear sense. This is especially the case if the mica is surrounded by quartz. C'-type shear bands are present within quartz-rich samples (Figure 5.17). The shear bands are dark, straight and spaced. Rotated opaque porphyroclasts in a stair stepping arrangement also support the shear sense interpretation. The quartz within the samples is deformed by crystal-plastic processes as shown by its change in shape and by undulose extinction (Figure 5.18). Bulge nucleation and recrystallisation is apparent (Figure 5.19). These rocks are probably low-temperature mylonites where deformation occurred roughly between 250 and 500°C (Trouw et al., 2010). Recrystallised quartz is fine-grained (<50 μm), muscovite fish are common and shear sense indicators are well developed, all characteristics common in low-grade mylonites. The dip-slip mylonite generation indicates dextral sense of movement in all thin sections, equating to a west-block-up movement regime.

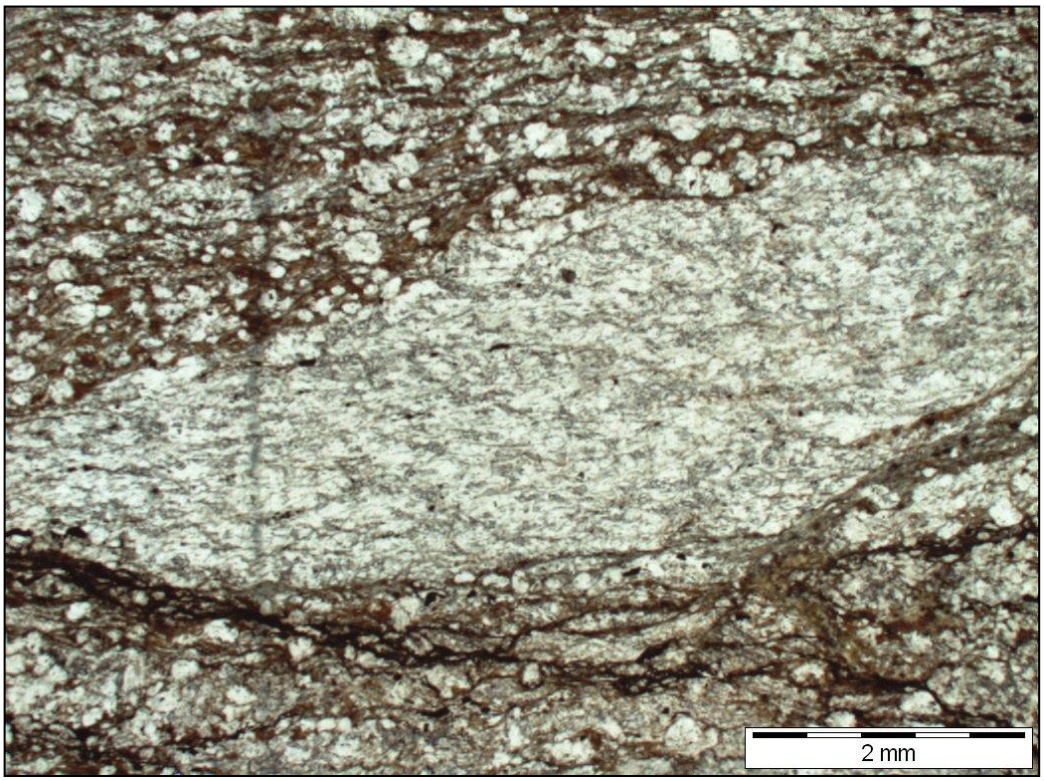

Figure 5.15 – 176630. PPL. A boudin of quartz and muscovite. The orientation of the muscovite is defining a weak horizontal foliation. The matrix is mainly biotite and carbonate with albite micro-porphyroblasts. The asymmetric boudin presents stair stepping to the right indicating dextral shear in this view. Sample is looking N, W side up.

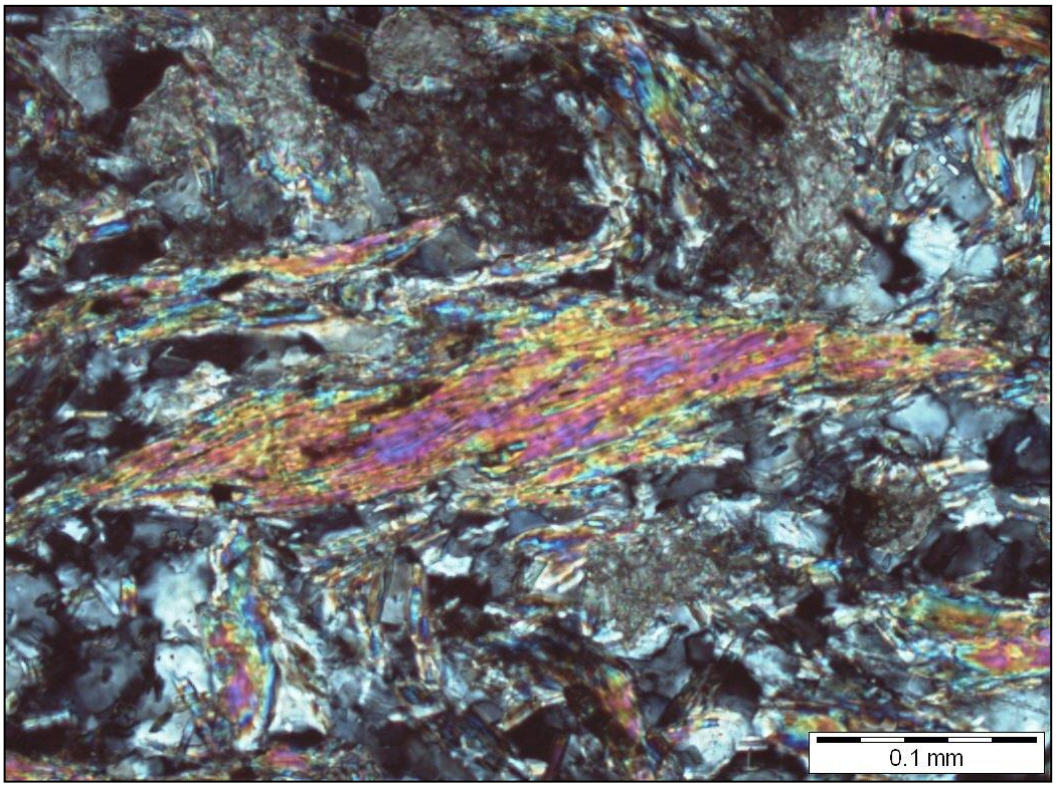

Figure 5.16 – 176632. XPL. Mica fish within a quartz, muscovite and carbonate matrix. The shear sense is dextral in this view, as is evident from the inclined position of the fish and the stair stepping. Sample is looking N, W side up.

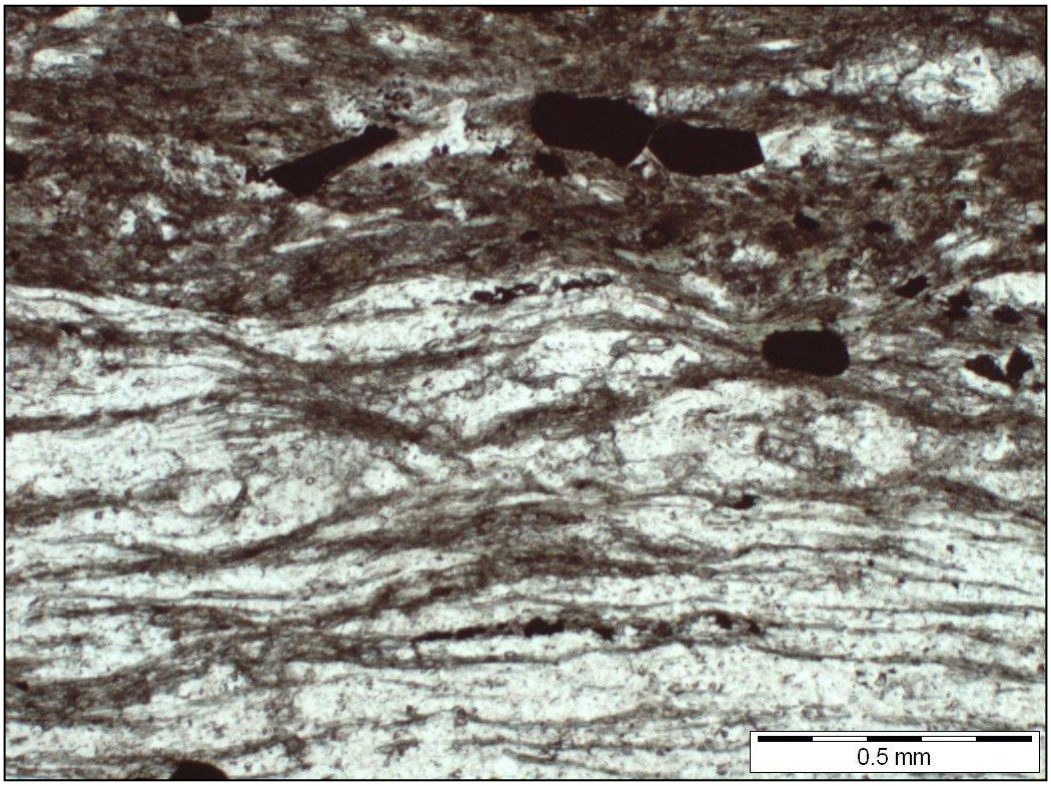

Figure 5.17 – 176633. PPL. Two shear bands (C') are developed from upper left in the chlorite rich part to lower right. The sense of shear is dextral in this view. Sample is looking N, W side up.

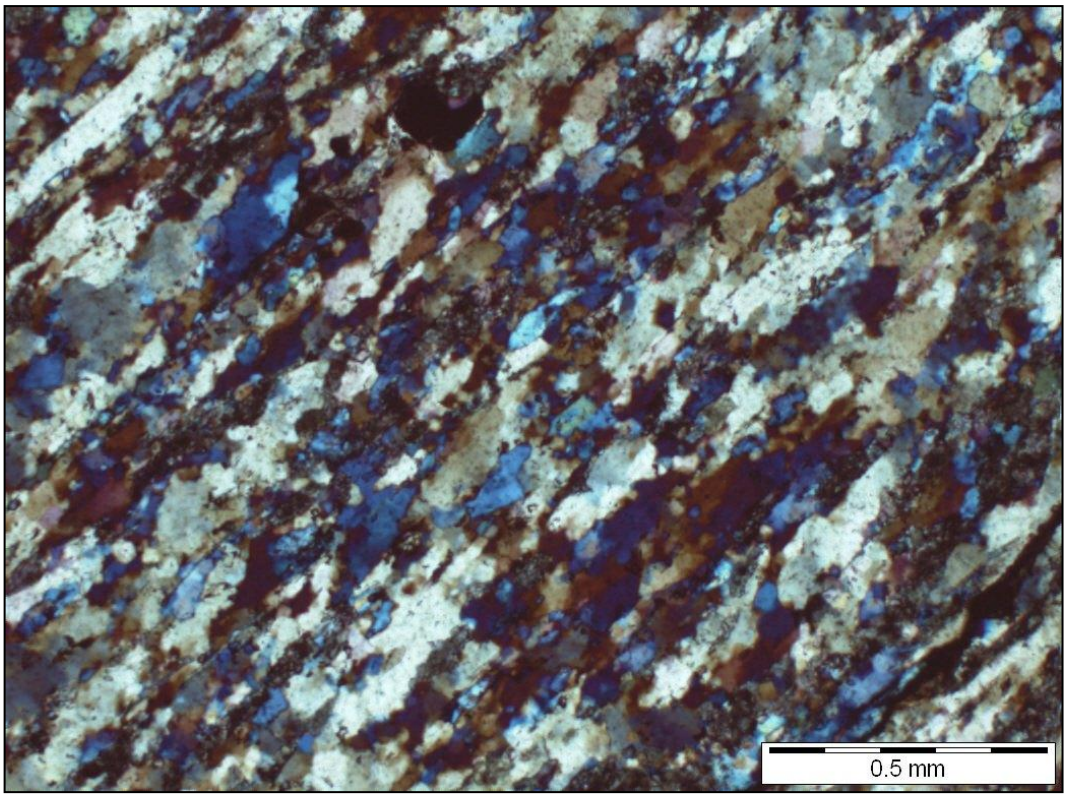

Figure 5.18 – 176634. XPL with gypsum plate inserted. Quartz grains showing undulose extinction, with some sub grain formation. Quartz grain boundaries lobate due to grain-boundary migration.

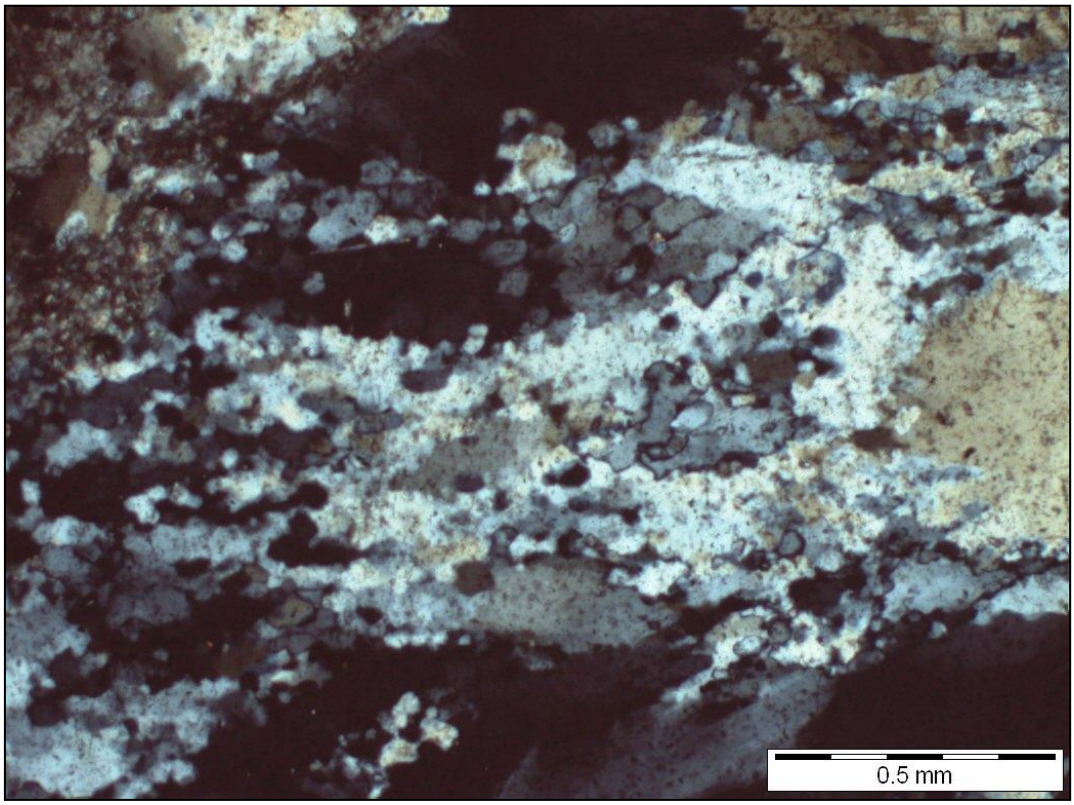

Figure 5.19 – 176639. XPL. Quartz showing patchy undulose extinction and partial recrystallisation into new small grains. The mechanism of recrystallisation is probably bulge nucleation.

Fine-grained quartz, albite, amphiboles, chlorite and biotite are common minerals of the strike-slip generation of mylonites from North Pit. The biotite is typically chloritised. Minor rutile and tourmaline are also present. Minor anhedral magnetite grains are present within the samples showing hematite cores. Disseminated anhedral post-kinematic pyrite and pre/syn-kinematic rutile is also present. The fabric shows higher strain to that of the dip-slip mylonites (Figures 5.20 and 5.21). There is the presence of a very strong LS fabric within both samples which is typically offset by brittle features. 176636 presents a dark band (Figure 5.20, centre of photomicrograph) that is likely to be ultramylonite with a strong horizontal foliation. Kinematic indicators such as asymmetric amphibole porphyroclasts (Figure 5.22), sigmoidal deformed amphiboles (Figure 5.23) and C'-type shear bands (Figure 5.24) indicate sinistral shear sense. Brittle features cross-cut the mylonitic foliation and displaces some kinematic indicators (Figure 5.22). The quartz shows undulose extinction and lobate contacts (Figure 5.25) with sub-grain orientation typical of sinistral sense of shear.

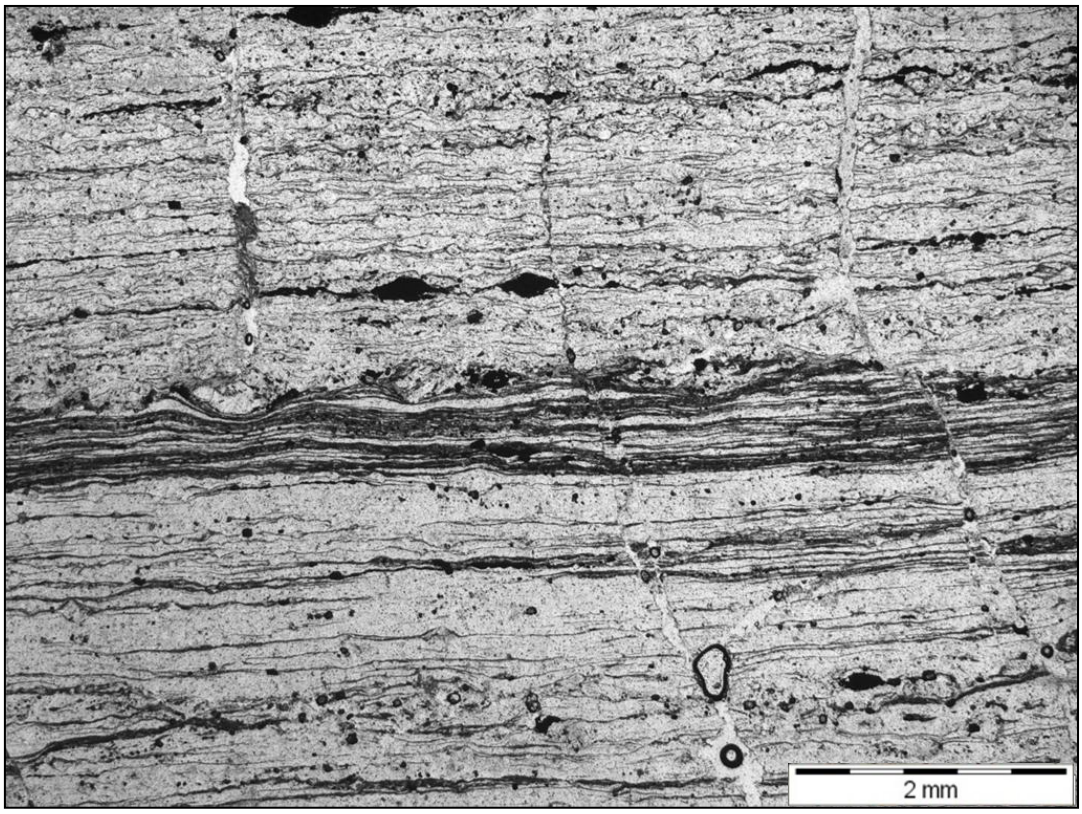

Figure 5.20 - 176636. PPL. Presence of strong LS fabric. Porphyroblasts within the sub-horizontal linear fabric. The darker, more lineated area in the centre of the photomicrograph is probably ultramylonite.

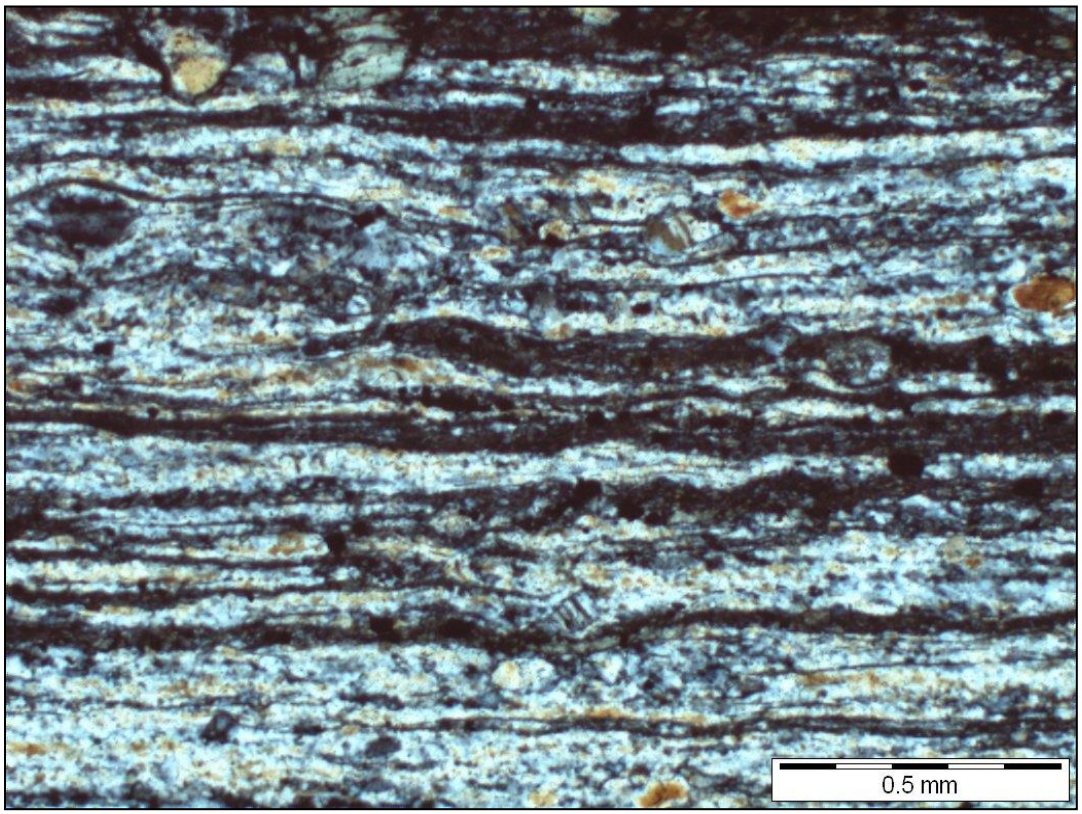

Figure 5.21 – 176637. XPL. Presence of strong LS fabric within this sample.

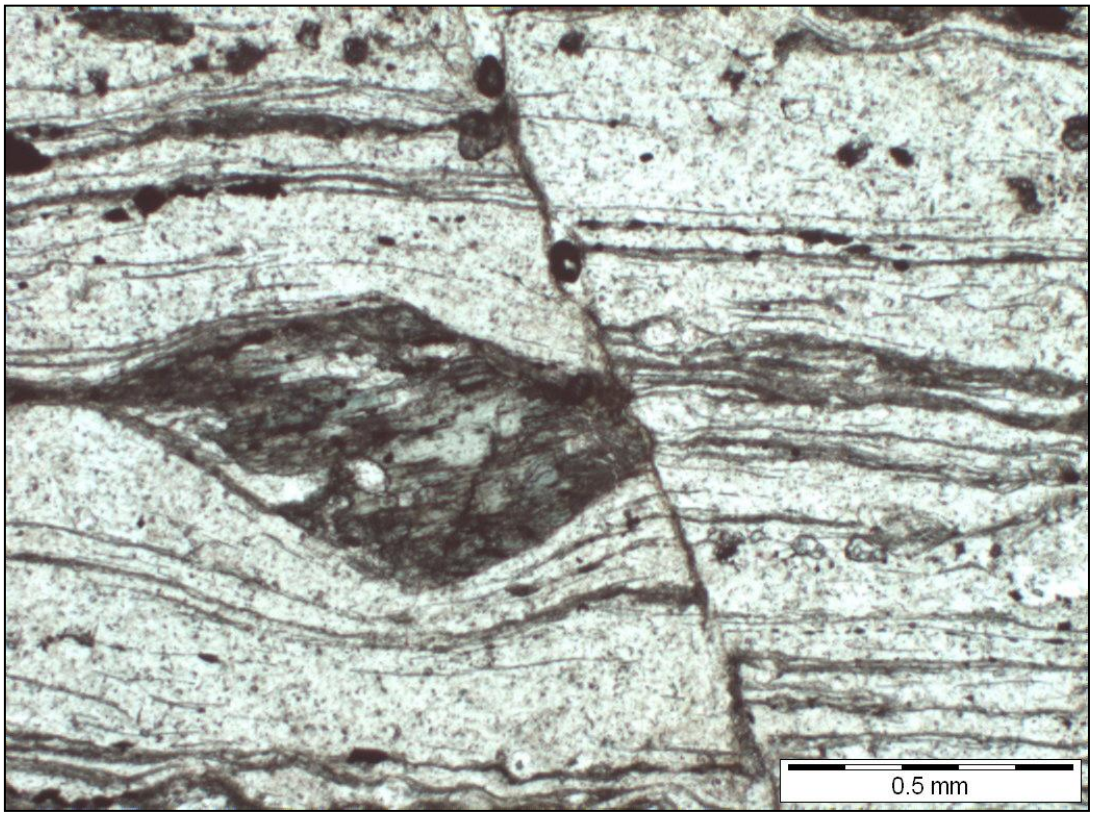

Figure 5.22 – 176636. PPL. Amphibole porphyroblast showing stair stepping indicative of a sinistral shear sense. A later brittle fault off-sets the lineation.

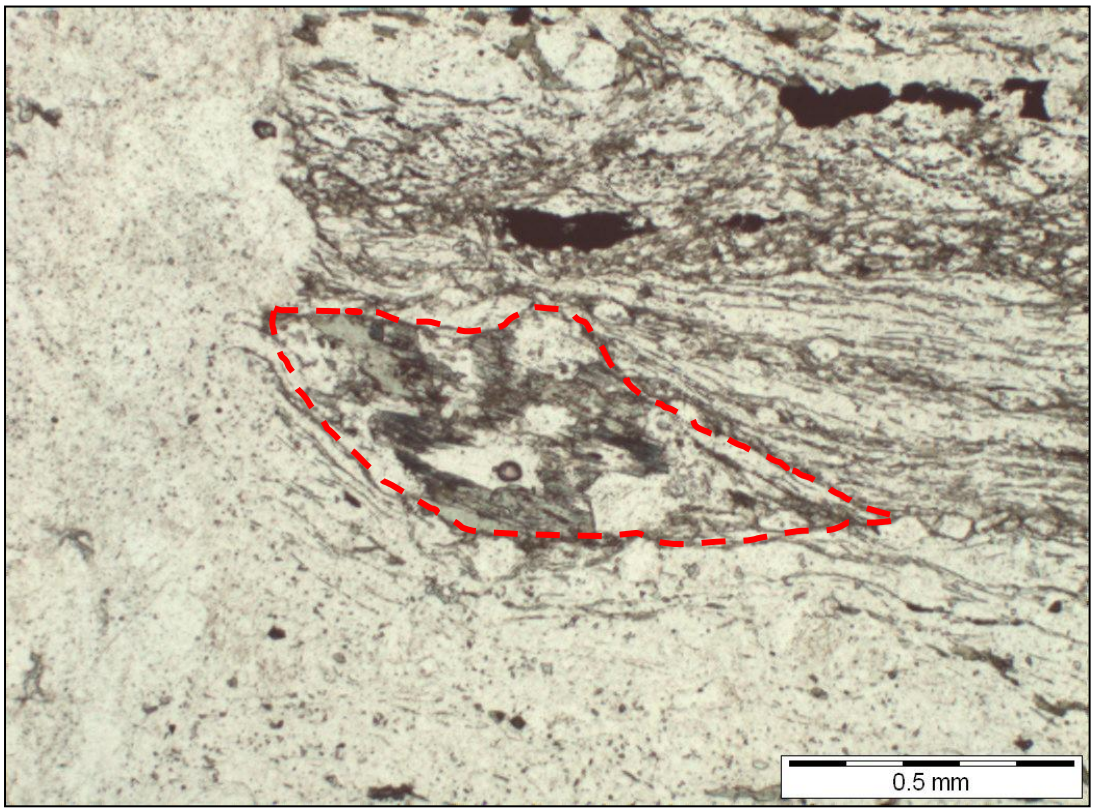

Figure 5.23 – 176637. PPL. Deformed amphibole (denoted by a red dotted line) indicating a sinistral sense of shear in this view.

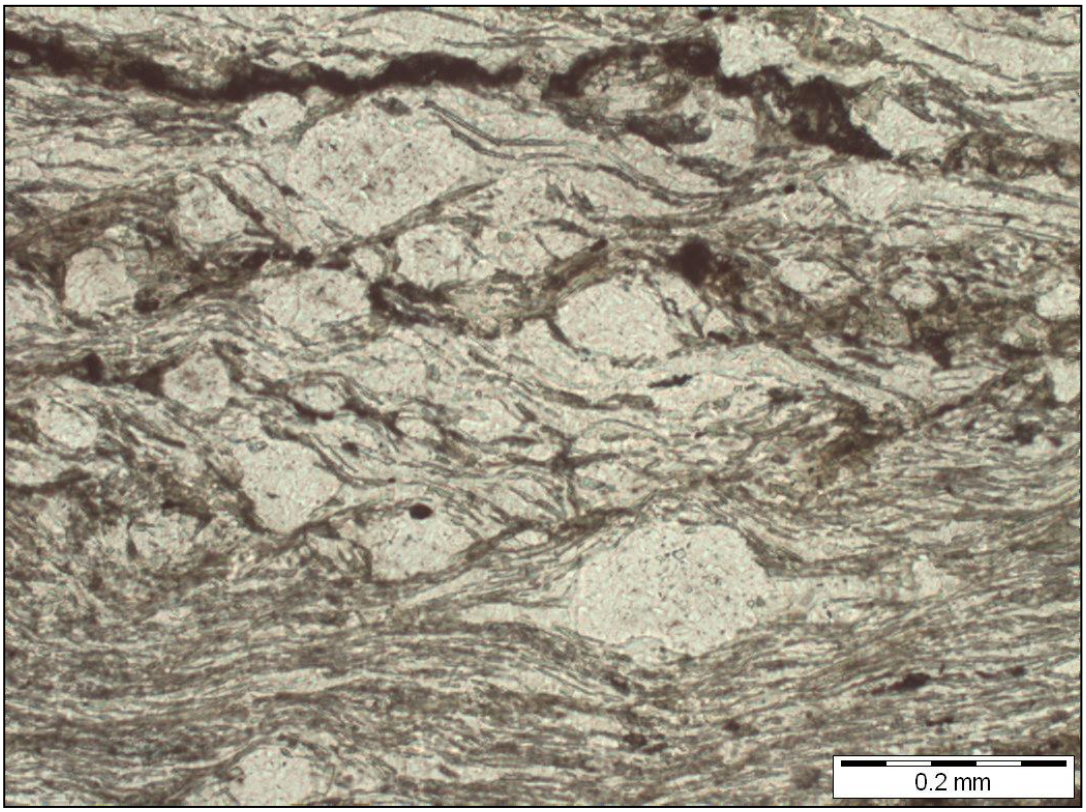

Figure 5.24 – 176637. PPL. C' type shear bands inclined to the left indicating a sinistral sense of shear in this view.

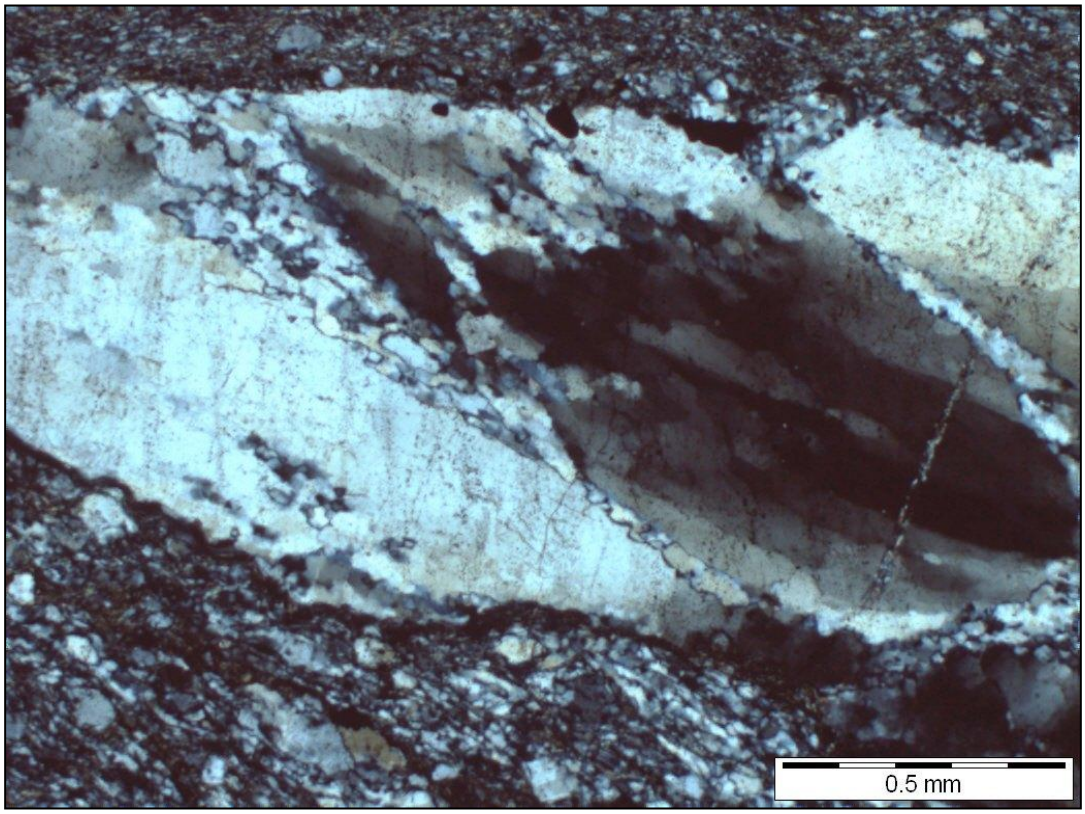

Figure 5.25 – 176637. XPL. Quartz showing patchy undulose extinction and partial recrystallisation into sub-grains. Sub-grain orientation indicates sinistral sense of shear.

The strike-slip mylonites present evidence for higher strain than the dip-slip samples. Kinematic indicators are common. Carbonate and chlorite retrograde alteration which is common in the former mylonites is not apparent within these samples. The occurrence of pre/syn- kinematic amphibole porphyroblasts within the fabric indicates that these samples have deformed at a higher grade of metamorphism than the dip-slip samples. To confirm this interpretation the composition of the amphiboles were measured by EPMA.

Within both sets of mylonites, the fine-grained quartz have a lattice-preferred orientation. To determine the nature of the crystallographic preferred orientation a Microfabric Analyser was used to determine the nature of the quartz c-axis fabric (see Section 5.6).

The microstructural results show that there is two generations of mylonite in North Pit; one showing a dip-slip, west-block-up movement regime and the other a strike-slip, sinistral movement regime. Although the strike-slip samples show a stronger mylonitic fabric and includes the presence of ultramylonite, shear sense could also be determined within the dip-slip samples. It is likely that both generations are mylonites were active at low metamorphic grade.

5.5 Amphibole Compositions

5.5.1 Introduction

Blue amphiboles in the Arthur Lineament were reported by Spry (1964) from near Reece Dam and by Green and Spiller (1977) from the Savage River Mine. More recent discoveries include blue amphibole minerals found in the southern part of the Arthur Metamorphic Complex (Seymour and Calver, 1995), within the Bowry Formation and the northern part of the complex, outside of the Bowry Formation (Everard, 1999). Turner and Bottrill (2001) reported glaucophane -winchite compositions within the Bowry Formation.

The compositions of amphiboles present in the strike slip mylonite samples from North Pit

were analysed by electron microprobe analysis (EPMA) using a Cameca SX100 microprobe at the Central Science Laboratory, University of Tasmania.

5.5.2 Amphibole Compositions – Results

Actinolite and tremolite are commonly recognised in hand specimen and under the microscope within the samples relating to dip-slip movement. Of more direct interest was that blue amphibole grains are visible in the strike slip samples; 176636 and 176637. The microprobe analyses of amphiboles in these samples (Table 5.4) confirmed the presence of calcic amphibole compositions (actinolite and hornblende) and sodic-calcic amphibole compositions (winchite and barroisite) within the strike-slip samples (nomenclature of Leake et al., 1997). Glaucophane and magnesioriebeckite were not detected. According to Taheri and Bottrill (2013), the only true glaucophane found to date in the Savage River mine area are in dolerites from the Eastern Wall Assemblage in Centre Pit. Of the 14 microprobe analyses, 3 are in the winchite/ferrowinchite compositional field, 1 in the barroisite field, 1 in the hornblende field and 9 in the actinolite compositional field. The cation contents were calculated using the program 'AX' (https://www.esc.cam.ac.uk/research/research-groups/holland/ax) which accepts microprobe data in the form of oxide weight percents and performs standard mineral recalculations. The ferric/ferrous ratio for amphibole is based on Holland and Blundy (1994). The sodium in B sites (Na(B)) is the minimum of (2-Ca) and total Na cations. The aluminium in tetrahedral (T) sites (Al(iv)) was calculated as the minimum of (8- Si) and total Al cations.

Figure 5.26 compares the compositional data from this research with the amphibole compositions from Green and Spiller (1977) and Turner and Bottrill (2001). Green and Spiller (1977) used samples of mafic schists and metabasalts from Savage River Mine. The results confirmed the presence of winchite within the host rocks at the mine. Turner and Bottrill carried out microprobe analyses on amphiboles present within mafic schist interbanded with

magnesite and dolomite approximately 20 km north of Reece Dam at Main Creek. Main Creek lies approximately 7 km SW of Savage River Mine. These amphiboles (NC118 in Figure 5.26) range in composition from winchite to glaucophane. Amphiboles from the west of Reece Dam (approximately 25 km SSW of Savage River Mine) ranged in composition from barroisite to winchite-glaucophane (NC493 in Figure 5.26). These samples were amphibolites consisting of 50 vol% of amphiboles in a finer grained matrix of mainly epidote, albite, chlorite and quartz (Turner and Bottrill, 2001). At another locality near Reece Dam, a medium-grained amphibolite was sampled (NC3 in Figure 5.26). The amphiboles ranged in composition from actinolite, hornblende, barroisite, winchite and glaucophane. The amphibole grains were predominantly green, but there were patches of blue to mauve amphibole present in the grains. According to Turner and Bottrill (2001), the calcic and sodic-calcic amphiboles comprise the green component, while glaucophane-winchite comprises the blue to mauve component.

High pressure, sodic-calcic amphiboles of barroisite and winchite were not detected within the dip-slip mylonites of North Pit. They are present however in the strike-slip mylonites of North Pit. Actinolite-tremolite amphiboles are present in both shear zone generations. Petrographically, the higher pressure amphiboles have a distinctive blue/green colour (Figure 5.27). An amphibole grain located in sample 176636 presents a core of barroisite with a rim of actinolite (Figure 5.28). The fabric of the strike-slip mylonites of North Pit has higher grain size reduction and more intense foliation suggesting higher strain than the dip-slip generation. Sodic calcic amphiboles in Tasmania are correlated with the Middle Cambrian ophiolite obduction event (e.g. Turner and Bottrill, 2001) and therefore the strike slip movement reported here is probably a Middle Cambrian event. The areas of the mine showing strike-slip movement are very limited and probably represent isolated relicts of an early texture. Monazite geochronology was carried out to try to confirm the age of mylonite in North Pit (refer to Section 5.7).

	Amph 1	Amph 2	Amph 3	Amph 4	Amph 5	Amph 6	Amph 7	Amph 8	Amph 9	Amph 10	Amph 11	Amph 12	Amph 13	Amph 14
SiO_2	54.16	55.2	54.15	55.48	55.04	54.03	53.72	53.97	49.1	49.67	52.76	52.33	54.06	54.50
TiO_2	0.21	0.18	0.18	0.17	0.3	0.53	0.23	0.53	0.12	0.16	0.12	0.07	0.06	0.44
Al_2O_3	1.56	1.08	0.46	1.21	1.21	1.85	0.6	1.73	6.04	5.34	2.97	3.05	1.69	1.63
Cr_2O_3	0	0.02	0.02	0	0.02	0.09	0.06	0.11	0.15	0.08	0.06	0.03	0	0.11
Fe_2O_3	0	3.97	6.14	0	0	0.38	10.61	0.25	3.64	5.62	3.36	3.04	1.54	0
FeO	7.49	11.04	11.44	7.11	6.08	6.74	9.78	7.37	10.72	10.8	7.97	8.25	9.32	6.31
MnO	0.09	0.12	0.13	0.11	0.11	0.11	0.12	0.15	0.23	0.17	0.22	0.24	0.18	0.12
MgO	20.02	15.23	13.66	20.23	20.8	19.95	11.55	19.49	13.73	13.39	16.75	16.86	17.83	20.72
CaO	12.42	7.63	6.19	12.86	12.31	11.68	3.4	11.75	10.13	8.41	10.28	11.4	11.53	11.89
Na_2O	0.32	2.81	3.52	0.28	0.45	0.77	4.8	0.75	1.83	2.4	1.47	0.89	0.76	0.74
K_2O	0.07	0.05	0.05	0.05	0.1	0.11	0.05	0.12	0.16	0.15	0.08	0.08	0.05	0.11
Totals	96.35	96.93	95.32	97.5	96.41	96.2	93.86	96.19	95.5	95.63	95.7	95.94	96.86	96.58
Si	7.725	7.932	7.961	7.798	7.788	7.696	7.986	7.713	7.253	7.322	7.626	7.571	7.743	7.715
Ti	0.023	0.019	0.02	0.018	0.032	0.057	0.025	0.057	0.013	0.018	0.013	0.007	0.006	0.047
Al	0.263	0.183	0.079	0.201	0.202	0.311	0.106	0.291	1.052	0.928	0.506	0.52	0.286	0.272
Cr	0	0.002	0.003	0	0.002	0.01	0.007	0.012	0.017	0.01	0.007	0.003	0	0.012
Fe_3	0	0.429	0.679	0	0	0.041	1.186	0.027	0.405	0.623	0.366	0.331	0.166	0
Fe_2	0.894	1.327	1.407	0.836	0.719	0.802	1.216	0.881	1.324	1.332	0.964	0.999	1.117	0.747
Mn	0.011	0.015	0.016	0.014	0.013	0.013	0.015	0.018	0.029	0.021	0.027	0.029	0.022	0.015
Mg	4.257	3.263	2.993	4.238	4.385	4.236	2.559	4.151	3.023	2.941	3.608	3.635	3.806	4.371
Ca	1.898	1.175	0.975	1.937	1.867	1.783	0.542	1.799	1.603	1.328	1.593	1.767	1.77	1.804
Na	0.089	0.784	1.004	0.076	0.123	0.213	1.384	0.208	0.524	0.687	0.413	0.25	0.21	0.204
K	0.013	0.009	0.01	0.009	0.017	0.019	0.009	0.022	0.03	0.028	0.014	0.016	0.008	0.02
Sum	15.172	15.28	15.373	15.126	15.149	15.196	15.434	15.188	15.41	15.446	15.257	15.237	15.189	15.207
Al(iv)	0.263	0.068	0.039	0.201	0.202	0.304	0.014	0.287	0.747	0.678	0.374	0.429	0.257	0.272
Na(B)	0.089	0.784	1.004	0.063	0.123	0.213	1.384	0.201	0.397	0.672	0.407	0.233	0.21	0.196
Classification	act	win	win	act	act	act	win	act	hbd	bar	act	act	act	act

Table 5.4 – Microprobe analyses of fourteen amphiboles within mylonitic rocks within North Pit, Savage River Mine. Classification abbreviations: **act** – actinolite, **win** - winchite, **hbd** – hornblende and **bar** – barroisite. Cations calculated using AX program (using the ferric scheme of Holland and Blundy, 1994).

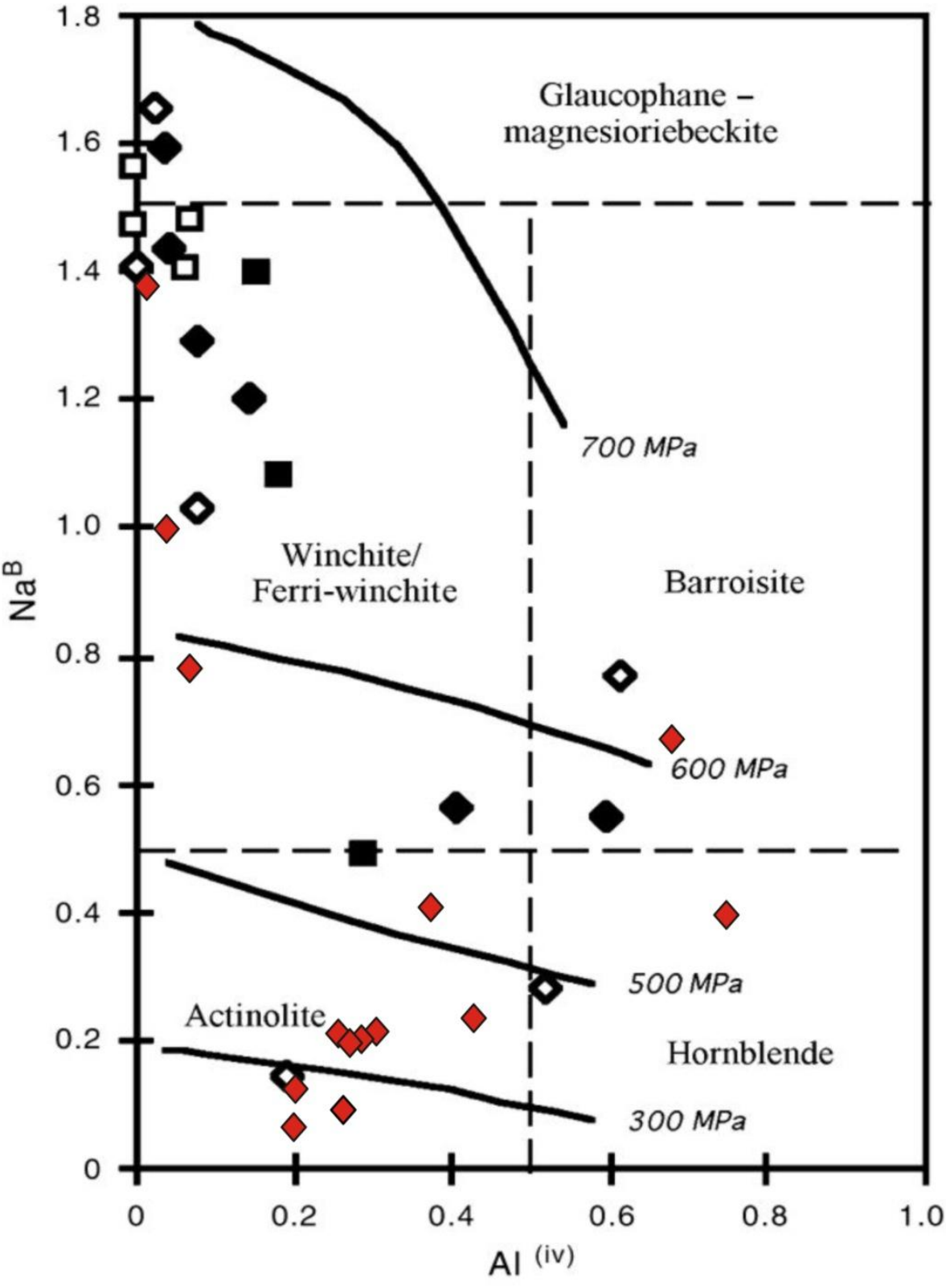

Figure 5.26 – Amphiboles of the Bowry Formation: Na(B) vs. Al(iv). Modified from Turner and Bottrill, 2001. The compositional fields are from Leake et al (1997) and the isobars from Brown (1977). ■ – Data from Green and Spiller, 1977 at the Savage River Mine. □ – Data from Turner and Bottrill, 2001. NC118 location. Retrogressed assemblage. ◆ – Data from Turner and Bottrill, 2001. NC493 location. Western amphibolite, prograde assemblage. ◇ – Data from Turner and Bottrill, 2001. NC3 location. Retrogressed assemblage. ◆ – Data from this research. Strike-slip mylonites from North Pit. Samples 176636 and 176637.

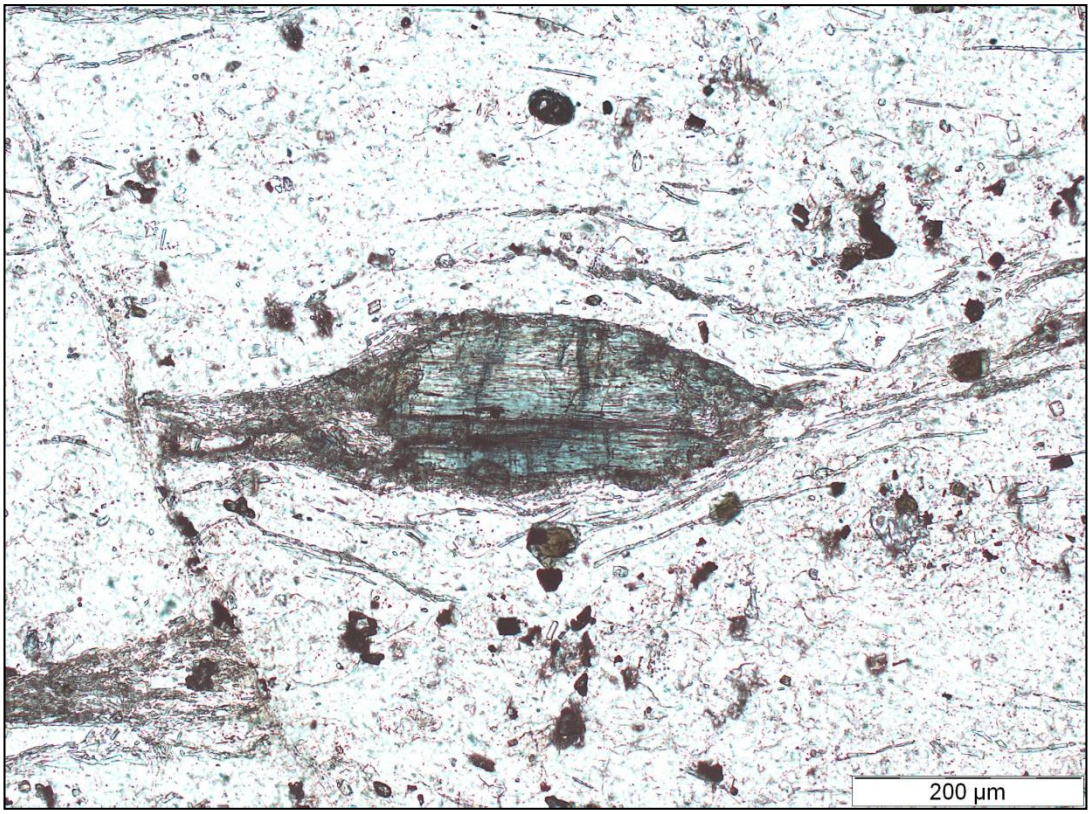

Figure 5.27 – 176636. PPL. Blue/green winchite grain within fine-grained matrix of quartz, chlorite and albite.

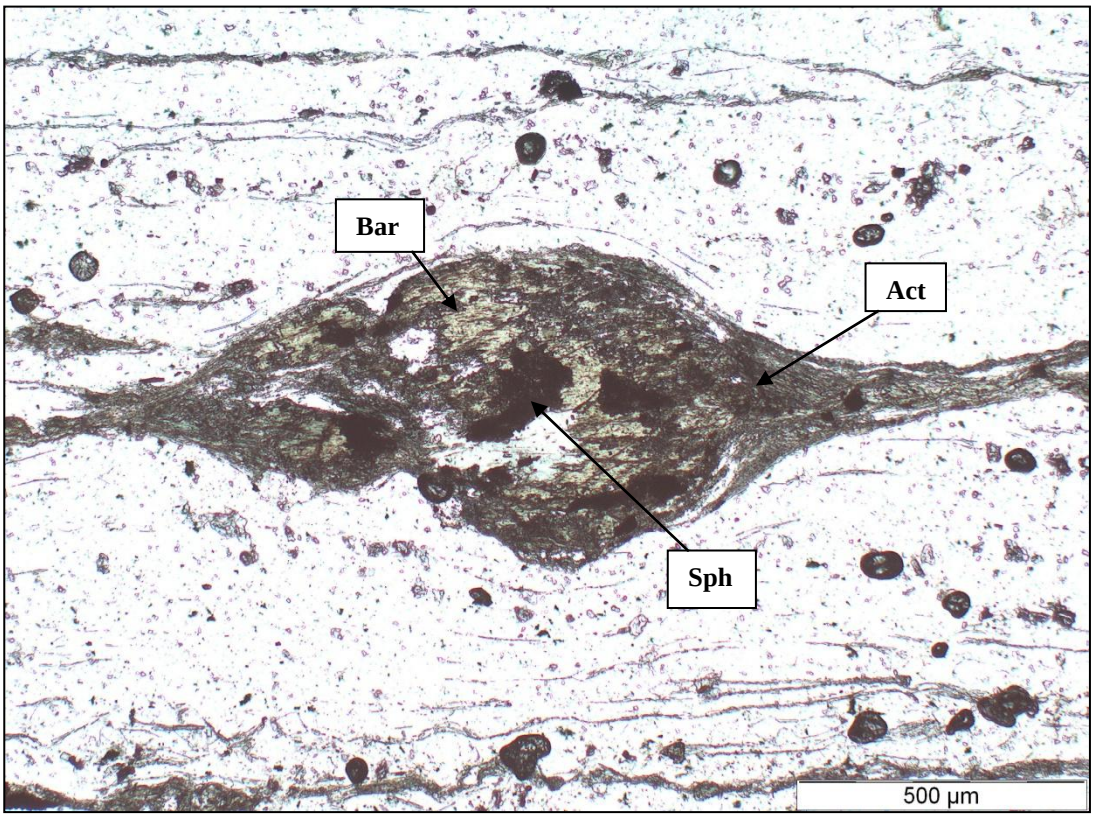

Figure 5.28 – 176636. PPL. Porphyroclast of amphibole. Light green barroisite core with actinolite rim within a fine-grained quartz matrix. Sub-opaques within the grain are sphene. *Abbreviations;* **PPL** – Plane polarised light, **Bar** – Barroisite, **Sph** - Sphene and **Act** – Actinolite.

5.6 Microfabric Analyser (MiFa)

5.6.1 Introduction

In rocks deformed in the crystal plastic field (dislocation creep and dislocation glide), the lattice orientation of crystals is not randomly distributed but arranged in a systematic way during the strain. Such rocks have a lattice-preferred orientation (LPO) for a specific mineral (Passchier and Trouw, 2005). Whilst using a petrographic microscope with cross polars and a gypsum plate and by rotating the stage, it became apparent that the quartz rich areas of some thin sections showed crystallographic preferred orientations. These features were detected in rocks that were suspected to be mylonitic based on textures. The Microfabric Analyser (MiFa) method was used in order to analyse the quartz c-axis fabrics within seven thin sections of possible mylonite from the Savage River Mine. The work was carried out in 2012 at Monash University, Melbourne under the supervision of Professor Christopher Wilson.

5.6.2 Methodology and Results

Wilson et al. (2007) concludes that the MiFa can be used for the fast collection of high-resolution spatial c-axis orientation data from a set of digital polarized light images. Wilson et al. (2003, 2007) gave a complete outline of the methods, principles and comparative analysis of this method. Although quartz rich mylonites are present at Savage River Mine, the dip-slip mylonites have more calcite, muscovite, albite and chlorite in some areas (Figure 5.29) and it was difficult to select only quartz rich areas to scan on each thin section. The strike-slip samples are more quartz rich and less affected by post-kinematic alteration (Figure 5.33). Individual c-axis orientations of the selected areas were recorded using the highest resolution of 2.8 µm. Individual tiles are scanned and then stitched together to produce a digital colour map where gradational shades of colour represent orientations of the c-axes (Wilson et al., 2009). After the thin section is scanned, the data is loaded into analysis software called

INVESTIGATOR (http://www.earthsci.unimelb.edu.au/facilities/analyser/downloads.html) for data investigation.

The dip-slip samples analysed using the MiFa technique included; 176632, 176633, 176639, 1776631 and 176634. The strike-slip samples included; 176636 and 176637. Only quartz rich areas were selected on each thin section and some proved difficult to isolate the quartz rich areas from other minerals. For many of the dip slip samples c-axis patterns did not match typical mylonitic patterns. The most interesting contoured stereographic projections are shown in Figures 5.30, 5.31, 5.32, 5.34 and 5.35 respectively. Each is based on more than 2000 C-axis orientations. Each point represents the orientation of one quartz grain. The trace of the foliation is oriented along the equator with the stretching lineation at the horizontal for this great circle.

Two of the dip-slip mylonites resulted in an interpretable quartz c-axis pattern (Figures 5.30 and 5.31). There is an internal asymmetry with respect to the foliation, indicating a dextral (in section) or W side up (in geographic coordinates) shear sense. This supports the results from microstructure and shear sense indicator analyses (refer to Section 5.4.3). The remaining samples resulted in non-interpretable quartz c-axis patterns (e.g. Figure 5.32). Both strike-slip samples produced strong quartz c-axis patterns (Figures 5.34 and 5.35) indicating a sinistral (in section and in true coordinates) shear sense. This supports the results from microstructure and shear sense indicator analyses (refer to Section 5.4.3). The resulting patterns of the strike-slip samples (particularly sample 176637) follow an asymmetric Type I crossed girdle (Lister, 1977) where small circle girdles are connected by a central girdle in plane strain (Passchier and Trouw., 2005). This pattern is most common in the case of non-coaxial progressive plane strain deformation (Burg and Laurent, 1978; Lister and Hobbs, 1980; Schmid and Casey, 1986).

Although the results of the MiFa technique support the microscopy analysis of the mylonite samples, it could not be used alone, in this case, for the determination of shear sense. The dip-slip samples had poorly developed C axis fabrics which could indicate lower total strain and/or a fault zones with complex movement history. The presence of a mixed fabric could be evidence that originally these samples had a strike-slip fabric that has been partially reset during a dip-slip movement. The strike-slip samples have a simpler c-axis pattern typical of low-temperature mylonites.

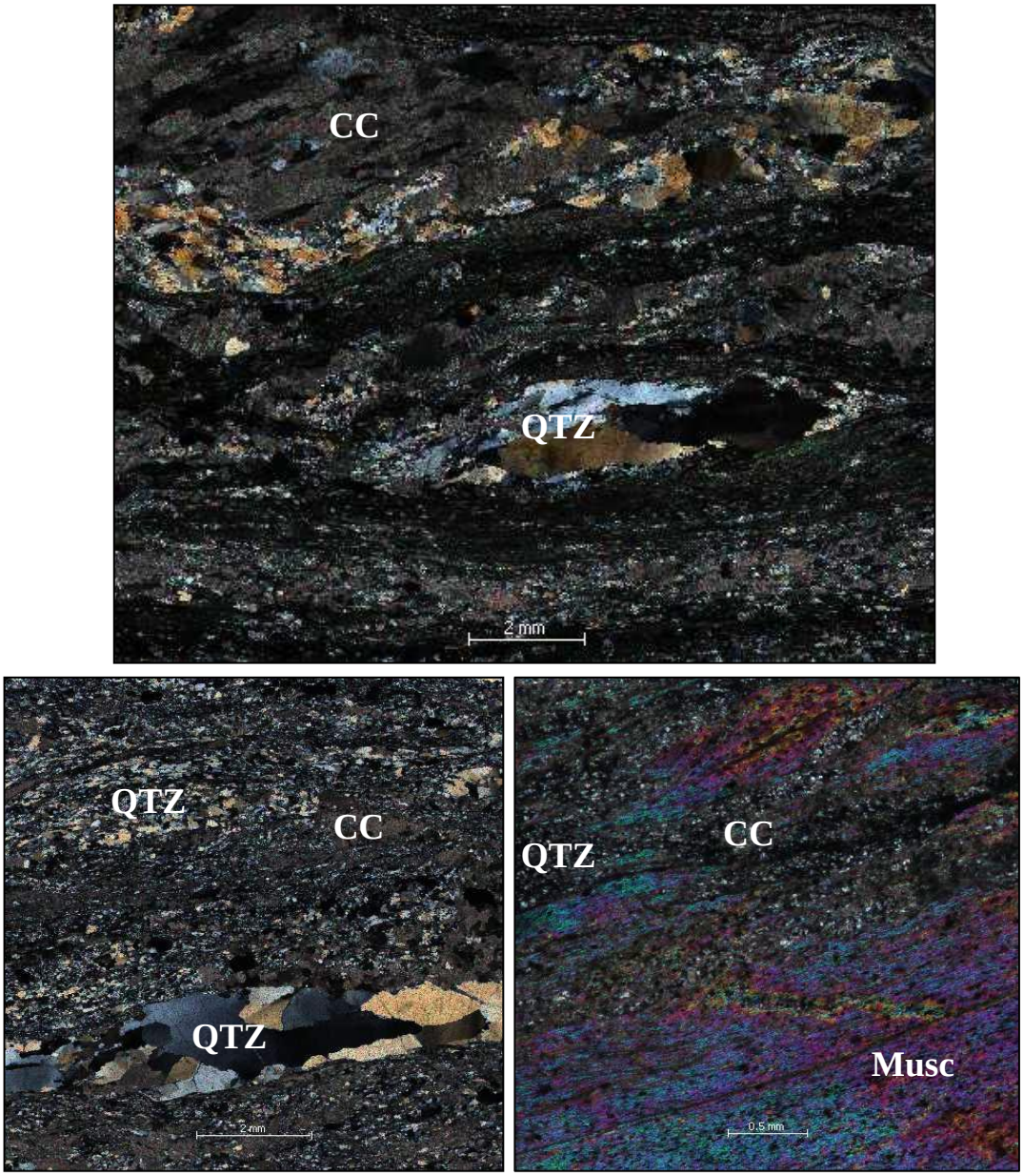

Figure 5.29 – XPL photomicrographs of the dip-slip shear zone samples 176639 (top), 176634 (bottom left) and 176632 (bottom right). It was difficult to find areas of pure quartz due to high contents of carbonate, muscovite and chlorite. Abbreviations; **XPL** – Cross Polarised Light, **QTZ**- Quartz, **CC**- Carbonate and **Musc** – Muscovite Mica.

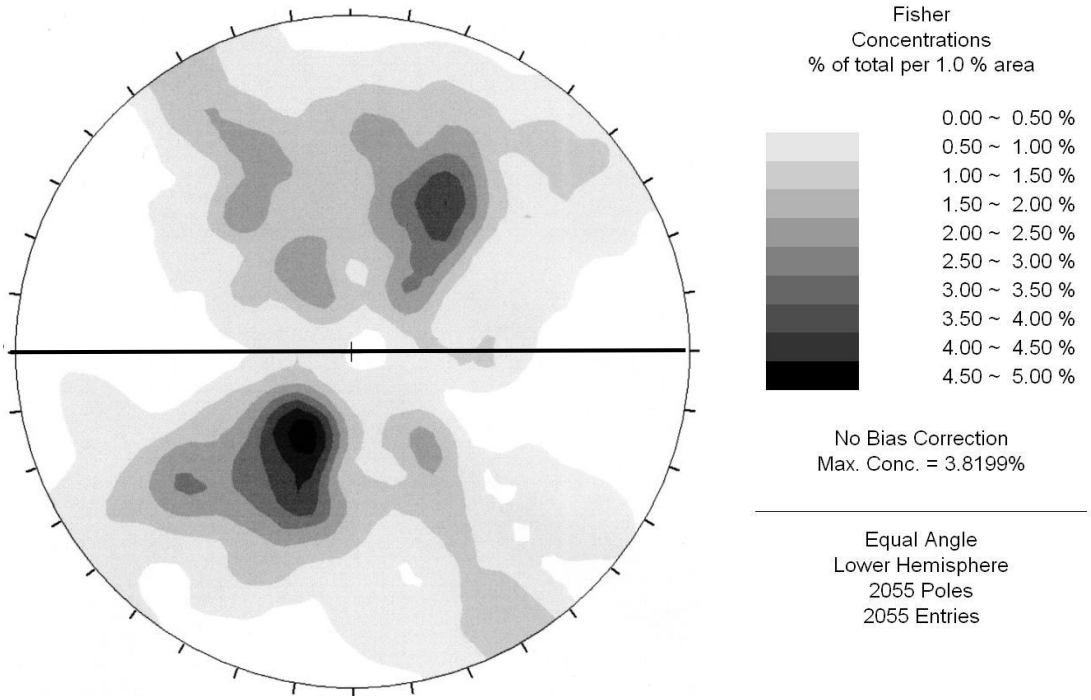

Figure 5.30 - Stereonet showing the LPO of quartz measured within sample 176639; dip-slip mylonite sample, looking N. The solid black line oriented through the equator denotes the trace of the foliation.

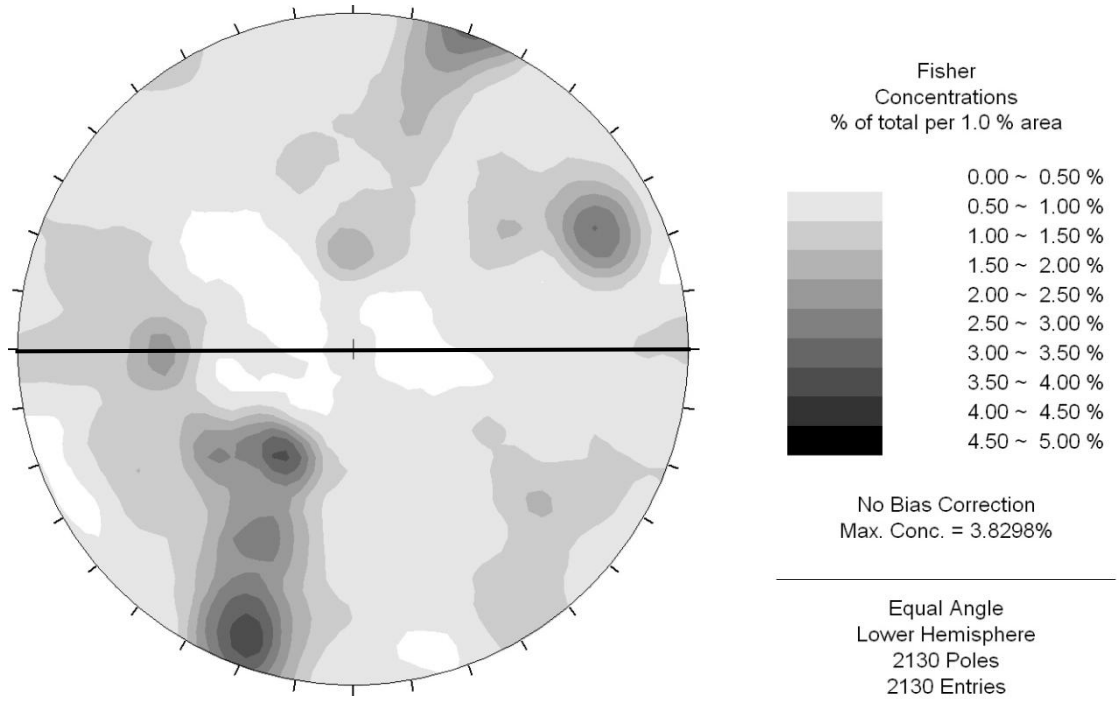

Figure 5.31 – Stereonet showing the LPO of quartz measured within sample 176634; dip-slip mylonite sample, looking N. The solid black line oriented through the equator denotes the trace of the foliation.

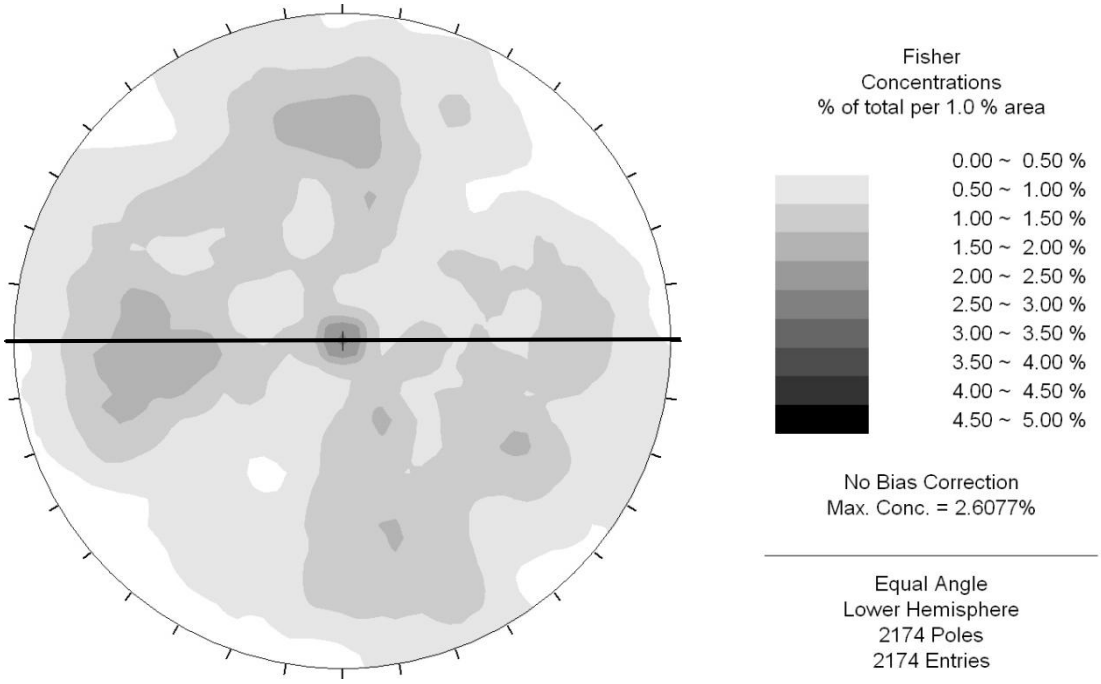

Figure 5.32 – Stereonet showing the LPO of quartz measured within sample 176632; dip-slip mylonite sample, looking N. The solid black line oriented through the equator denotes the trace of the foliation. This is an example of a c-axis pattern that does not match published patterns for mylonites.

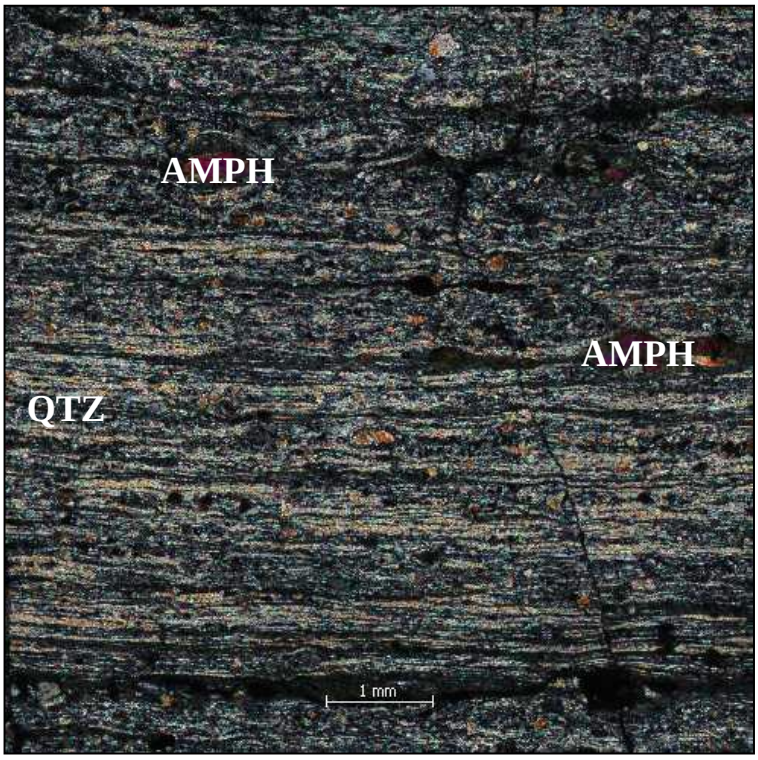

Figure 5.33 – XPL photomicrograph of strike-slip sample 176636 showing the location of quartz. The fabric is notably different to the dip-slip samples (Figure 1) with fewer and smaller porphyroclasts. Abbreviations; **XPL** – Cross Polarised Light, **QTZ**- Quartz and **AMPH**- Amphiboles. It was easier to select quartz rich areas for measurement within the strike-slip samples.

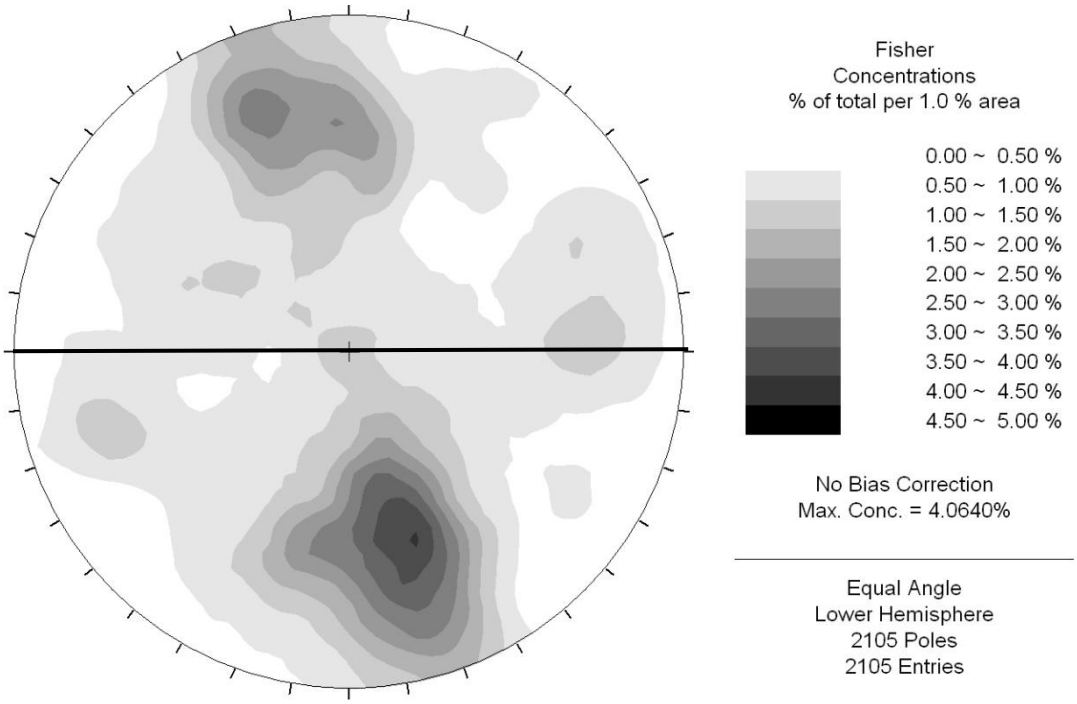

Figure 5.34 – Stereonet showing the LPO of quartz measured within sample 176636; strike-slip mylonite sample, looking down. The solid black line oriented through the equator denotes the trace of foliation.

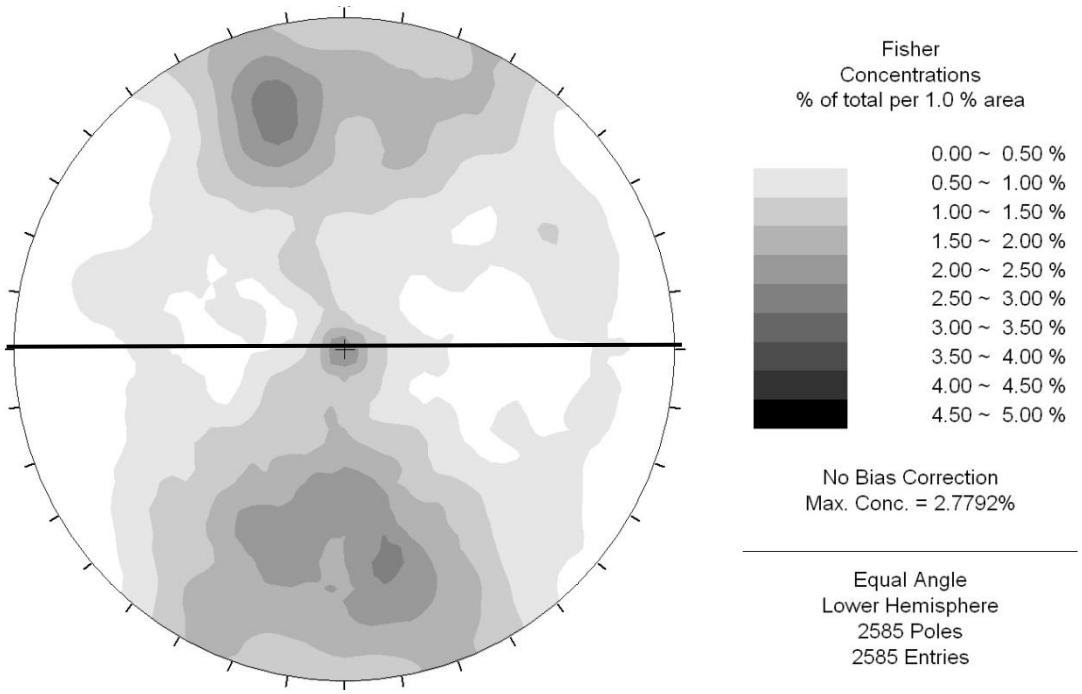

Figure 5.35 - Stereonet showing the LPO of quartz measured within sample 176637; strike-slip mylonite sample, looking down. The solid black line oriented through the equator denotes the trace of foliation.

5.7 Monazite Geochronology

5.7.1 Introduction

Monazite is a Th, U, REE-bearing phosphate mineral that has been historically considered to crystallise mainly from magma or form during medium- to high-grade metamorphism, and from hydrothermal fluids (Overstreet, 1967). Monazite has also been found in unmetamorphosed and low-grade metamorphic rocks of sedimentary origin, having formed during diagenesis to low-grade metamorphism (Rasmussen and Fletcher, 2002).

Taheri and Bottrill (2013) dated monazites at Savage River by U/Pb methods using the LA-ICPMS method. Two pyrite-rich ore samples were selected for study to determine the age of the monazites (mostly occurring as fine inclusions enclosed in pyrite). The resulting monazite dates were 501+/-13Ma and 500+/-9Ma. They also looked at the distribution of Pb isotopes and other elements in pyrite to determine the degree of isotopic equilibrium and recrystallisation in these samples. The common Pb composition in the pyrite is compatible with the radiogenic age of the monazite. Thus the monazite dates of about 500 +/- 9Ma indicate a Cambrian age for the pyrite and monazite. This monazite occurred in massive unfoliated ore from the western ore lens, South Pit.

The objective of this analysis was to date monazites located within the shear zones in North Pit.

5.7.2 Methodology

Mylonitic samples from both shear zone generations were prepared as 25 mm round polished blocks. These were mapped using SEM/EDS methods at the Central Science Laboratory, University of Tasmania using MLA (Mineral Liberation Analyser) software (Gu, 2003). The software was tuned to search for monazite grains larger than 5 microns on the polished blocks (cf. Sack et al., 2011). Once located, the position of the monazite grains was recorded and the

blocks were transferred to a LA-ICPMS (Laser sourced, induction coupled plasma, quadrupole mass spectrometer, under the supervision of Sebastian Meffre and Jay Thompson, University of Tasmania. Refer to Appendix 4 for a full method description. The probability plots shown here were calculated using ISOPLOT version 3 (Ludwig, 2001).

5.7.3 Results

No monazites were located within the high pressure, strike-slip mylonitic rocks of North Pit. However, monazite grains varying in size from 10 – 50 µm were located within three samples (176632, 176638 and 176639) of the dip-slip mylonitic rocks. The grains found have low U and low Th which is typical for low T monazite. The monazite grains analysed from 176632 had high common Pb and very low U and no useful age data was obtained. Monazite grains analysed in 176638 and 176639 gave better analytical results (Figures 5.36, 5.37). The peak in the probability distribution for U^{238}/Pb^{206} and Th^{232}/Pb^{208} ages of monazites from 176638 are 464 Ma and 458 Ma respectively. The most likely U and Th ages of monazites within the 176639 are 425 Ma and 435 Ma respectively. There is however a small peak at 520 Ma within the 176639 Th age data (Figure 5.37).

Three significant deformation events of the Arthur Metamorphic Complex have been identified (Holm and Berry, 2002; Holm et al., 2003). The first event was during the early part (514-510 Ma) of the Middle to Late Cambrian; Tyennan Orogeny (514-490 Ma, which is equivalent to the Delamerian Orogeny in Western Victoria and South Australia). The Bowry Formation was thrust-emplaced as an allochthonous fault-bounded block during this time (Holm and Berry, 2002). It was subsequently affected by less intense phases of deformation during the Middle Devonian; Tabberabberan Orogeny (Holm and Berry, 2002) and geological relationships suggest further fault movement post Devonian. The dominant metamorphic assemblage at Savage River Mine is probably due to the Cambrian event but some deformation and recrystallisation occurred in the Devonian (~400 Ma). No evidence of

deformation in Western Tasmania has been reported between the Middle Ordovician and the Early Devonian (470-410 Ma).

The results of the monazite geochronology in this research indicate that the age of the dip-slip shear zone deformation within North Pit is younger than Cambrian age. It is likely that the strike-slip deformation occurred during the Cambrian Tyennan Orogeny based on the high pressure mineral assemblages associated with these rocks. The best available interpretation for the monazite data is that Cambrian monazites in these dip-slip shear zones have been partially reset during Devonian deformation. The dip-slip movement on these zones could record a Devonian event. However more data is required to see what level of resetting has occurred in monazite grains outside the dip slip shear zones before this can be considered a reliable conclusion.

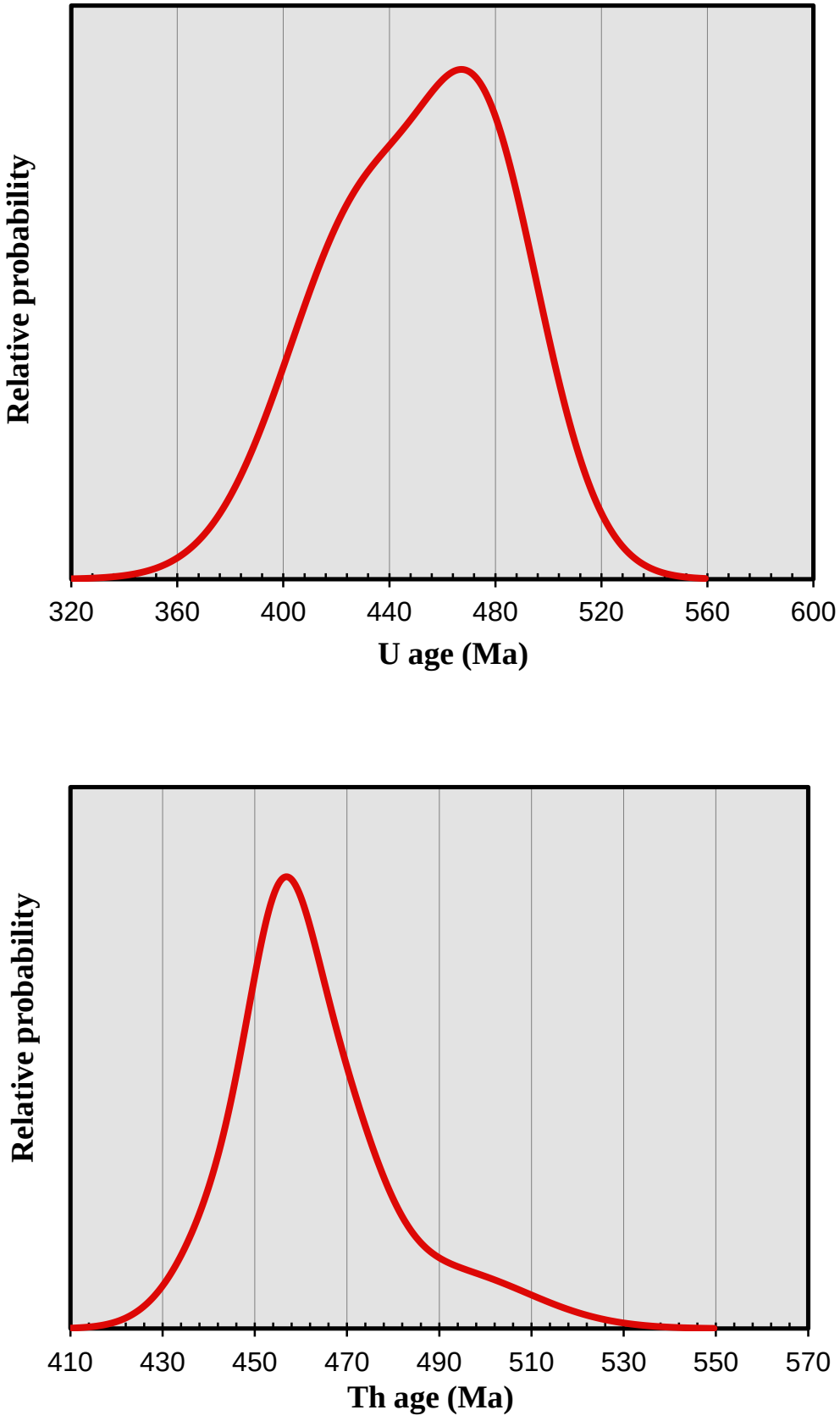

Figure 5.36. Relative probability plots of sample 176638. The U^{238} age is at the top with the Th age below. The peak U age is 464Ma as opposed to the peak Th age of 458Ma.

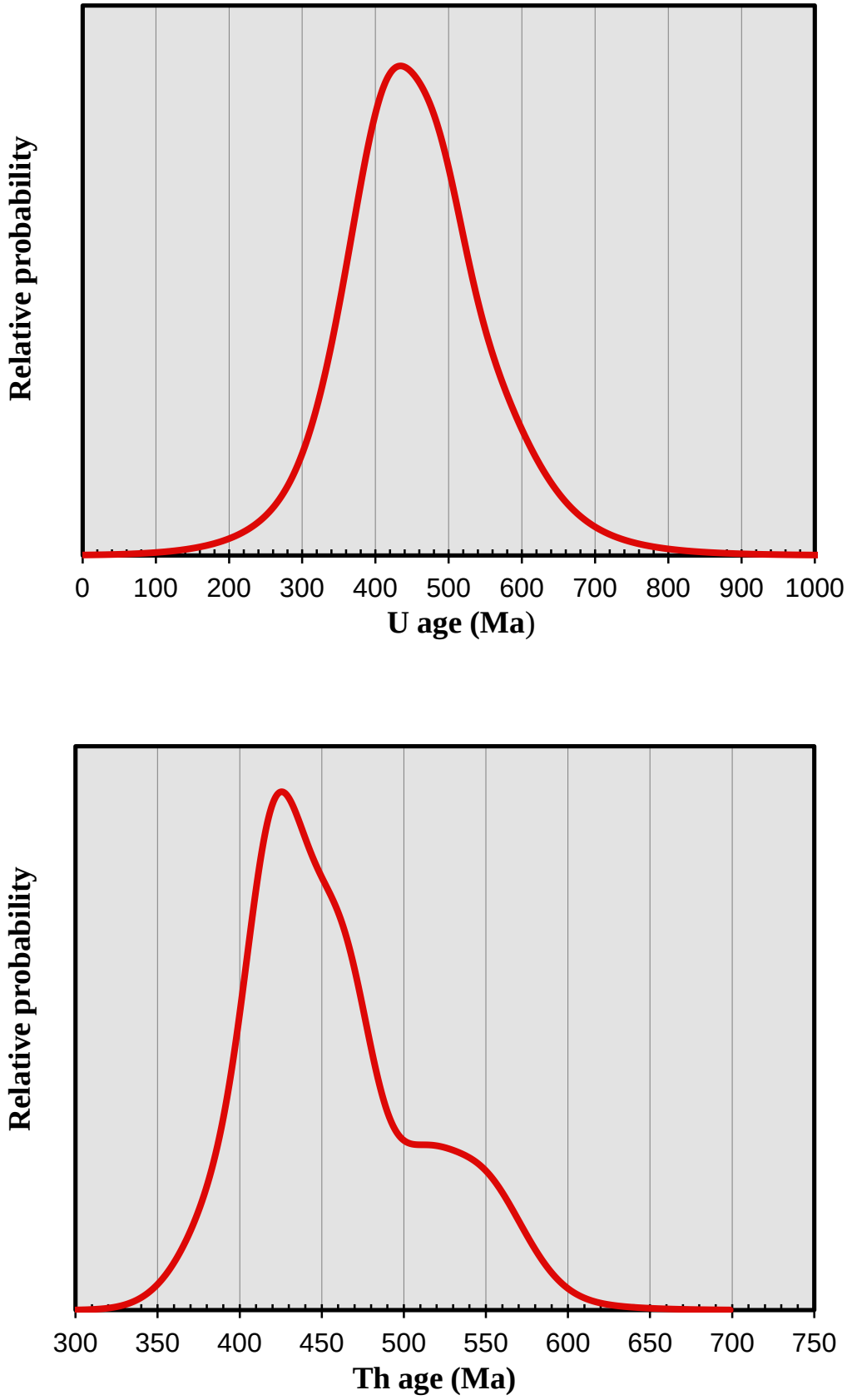

Figure 5.37. Relative probability plots of sample 176639. The U^{238} age is at the top with the Th age below. The peak U age is 435Ma. The main Th peak is at 425Ma with a small peak at approximately 520Ma.

5.8 Summary

A single foliation dominates the structure of the three large fault blocks in North Pit. The foliation is sub-vertical and varies in strike from 350° in the West Wall Assemblage to 005° in the East Wall Assemblage. There is very limited folding of the dominant foliation in the study area in contrast to rocks 2 km to the east Strain partitioning during the formation of the dominant foliation leads to outcrop scale variation in foliation intensity that cause face instability, especially within the MHA. The variation of foliation intensity with amphibolites correlates with calcite addition possibly as syn-kinematic veins, into the high strain rocks.

The mineralogy of the East Wall Assemblage includes major chlorite and albite with locally abundant calcite, quartz, muscovite and epidote. Crenulations are common within chlorite rich zones and compositional banding is present. Quartz within the assemblage shows ductile deformation features whilst albite is rarely deformed and commonly occurs as post-kinematic porphyroblasts. Three generations of calcite vein have been identified.

The mineralogy of the MHA is complex, grading from 0-95% magnetite. The assemblage is variably rich in Mg-rich lithologies including carbonate, amphibole, pyroxene, serpentine and talc-rich rocks. Intense foliation is present within talc, tremolite and chlorite-rich lithologies. Two generations of magnetite growth has been identified; an early pre/syn kinematic and a later, post kinematic euhedral phase, locally with hematite rims. Post-kinematic hematite veins, occurring as needle-like, radiating aggregates are common; indicating the influx of an oxidised fluid late in the sequence of events.

The mineralogy of the WWA contains muscovite, albite and chlorite with locally abundant quartz, biotite and dolomite. Compositional banding is prevalent as well as strong crenulations. Biotite is commonly partly chloritised. Disseminated pyrite, magnetite and hematite are rare. A strong mylonitic foliation was recognised at several sites.

Oriented mylonitic samples were chosen from North Pit after two sampling campaigns. Mylonitic textures in hand specimen proved difficult to recognise so lineated rocks rich in albite, muscovite, biotite, chlorite and quartz were targeted. Eight samples were chosen for microstructural analysis, due to their stronger mylonitic textures and shear sense indicators. A variety of shear sense indicators were used to determine shear sense. These included; asymmetrical sigmoidal boudins, mica mineral fish, C'-type shear bands and magnetite σ porphyroclasts. Two generations of shear zone were apparent; a west-block-up, dip-slip generation and a sinistral, strike-slip generation.

Of the two generations of shear zone, the strike-slip samples showed a stronger mylonitic foliation with porphyroclasts of Na-Ca amphibole not present within the mylonitic samples of the dip-slip fault zone. The amphibole compositions in the strike-slip mylonites included winchite, barroisite, hornblende and actinolite. Only actinolite was recognised within the mylonitic dip-slip samples. The strike-slip mylonites have quartz c-axis orientations typical of low temperature quartz-rich mylonites. The association with "high pressure" amphiboles indicate the strike-slip mylonites were active in the Cambrian. It is likely that the dip-slip mylonites subsequently overprinted and retrogressed these rocks.

The Microfabric Analyser (MiFa) method was used to analyse the quartz c-axis fabrics within the mylonitic samples from North Pit. The results supported the microstructural results, indicating a west-block-up, dip-slip generation and a sinistral, strike-slip generation. The strike-slip samples have c-axis patterns typical of low-grade mylonites. The quartz c-axis patterns in the dip-slip samples were less useful. This is interpreted as indicating lower strain, an observation that is also compatible with the hand specimen and microscopic textures of the samples. The monazite dating of the dip-slip shear zone generation resulted in U^{238}/Pb^{206} and Th^{232}/Pb^{208} ages younger than the Cambrian. This suggests that the dip-slip mylonites were active in the Devonian.

CHAPTER 6

SUMMARY, DISCUSSION AND CONCLUSIONS

6.1 Summary against objectives

The plan for this research program was outlined in Chapter 1 in the form of 8 objectives. Each objective was met and the summaries are as follows:

Objective 1 was to *'establish the geotechnical properties of each lithology'*. In-pit mapping with the addition of photogrammetry and core logging enabled this objective to be met. Data from the 2009-2010 drilling programme was gathered and existing data from the 2005-2007 and 2008 drilling programmes was included after validation. Standard geotechnical core logging procedures were reviewed and parameters were added for the use in this research. Due to the high variability in lithology and the existence of two major faults, North Pit was separated into three assemblages. The East Wall Assemblage which contains infilled, decorated and barren joint sets, generally steeply dipping to the west and displaying various roughness profiles. The joint sets display clustering behaviour within 150 m of the Eastern Contact Fault (ECF). Calcite veins are the most common within the assemblage, with sets dipping steeply to the east and west and sub-horizontal. As with all the assemblages of North Pit, foliation is pervasive throughout and acts as a weak surface. The Main Host Assemblage contains differing joint infill compositions to that of the East Wall Assemblage, reflecting the host rock composition. Although the orientations of joints within the MHA are more scattered than the joints within the East Wall Assemblage, the common orientations are similar. Joint distribution within the MHA is generally lithologically controlled. Vein infill is varied but calcite veins are the most common. The West Wall Assemblage (WWA) is the least drilled rock package within North Pit and contains the only gypsum and magnesite filled joints in the rock sequence. Talc filled joints are more common within this assemblage than further east.

Foliated units within the WWA are common near the Magnesite Fault. Less foliated domains are present 175 m west of the fault.

Objective 2 was to *'develop a classification scheme for the various forms of discontinuities seen in the rock masses at Savage River Mine based on the identification of various infilling in discontinuities. Furthermore define if joint infilling impacts on wall failure and how'.* The recording of joint infill composition, thickness, strength and joint roughness profile assisted with this task. The presence of infillings has a direct impact on the strength of defects. Joint infill composition affects friction angles relating to wall failure. Tightly healed, hard, non-softening and impermeable infills such as quartz or epidote typically present high friction angles and the likelihood of failure along these infilled joints is reduced. Softening or low-friction mineral coatings such as mica, chlorite, talc, gypsum and graphite reduce the friction angle greatly thus failure on these surfaces, especially if the orientation of the structures is steeper than the friction angle, is likely. The joint roughness profile is an important variable in the estimation of friction angles. The smoother and more planar the joint surface, the lower the friction angle.

Objective 3 was to '*identify the structures that have the greatest influence on pit wall stability'.* Three major failures on the east wall of North Pit have occurred since the commencement of this research. These failures were analysed with the assistance of photogrammetry and the structures that have the greatest influence on pit wall stability identified. Hematite coated joints displaying surface striations and polishing act as the release surface for all the rock failures. 'Ski-jump' joints dipping at 35-55° towards 250-290° act as a basal surface facilitating wedge type failure mechanisms on the east wall. These joint types appear to be spatially concentrated within 150 m of the Eastern Contact Fault (ECF) and mostly within the southern area of North Pit (Stage 1). Historically, weak foliation planes within the units of the WWA have facilitated rock failure. In-pit mapping and core logging

has confirmed that foliation intensity decreases away from the Magnesite Fault. Although monitored, the west wall in North Pit is not currently a geotechnical problem due to a considerably lower overall pit slope angle for the west wall compared to that of the east wall.

Objective 4 was to *'establish the types of rock failure in North Pit. If rock failure modes are different within each assemblage define how and why'.* Historical rock failures of the Savage River Mine were studied. The major and minor rock falls that developed in the time period of this research were analysed. The structure and/or lithology of each assemblage facilitate different failure modes. The rock failures within the East Wall Assemblage are commonly structurally controlled and joint dominated. They are typically wedge and plane failure. Failures within the MHA are structurally controlled (small-scale wedge failure and slumping) and lithologically controlled (massive lenses within an intensely foliated matrix). The major failure modes of the WWA are flexural toppling (structurally controlled) and slumping (lithologically controlled).

Objective 5 was to *'design and implement new parameters within the current database system in the mine technical services department for the geotechnical logging of recent core and geotechnical in-pit mapping'.* The orientation measurements of lineations on joint surfaces such as slickensides and slickenlines (the γ angle) were added as a new parameter within the current core logging database system. Previously ignored, the information obtained from such kinematic indicators proved useful. Recently added to the database, the domaining of rock core using the GSI method proved effective particularly close to large-scale faults in order to determine the existent of fault damage zones. A GSI range was assigned to outcrops whilst in-pit mapping. The technique of photogrammetry was not integrated into standard geotechnical and geological mapping procedures when this research commenced. A standard operating procedure was written and the method was integrated and is currently a very powerful mapping tool in Savage River Mine.

Objective 6 was to *'modify the existing fault models in North Pit and comment on if the presence of the faults affects pit wall stability'.* Three major faults occur within North Pit, the ECF, Magnesite Fault and the Eastern Splay Fault. Minor failures are common on or close to the fault planes due to the nature of the rock within the fault zone. Quartz, dolomite, talc and graphite rich lithologies are indicative of the ECF damage zone which varies along strike from 7 m to 61 m wide. Failures along the ECF are lithologically controlled, with the softer, intensely foliated and sometimes puggy nature of the rocks facilitating failure. The use of the GSI method helped to constrain the fault zone. In the southern area of the fault damage zone is a large discrete block of intensely faulted, folded and sheared material inferred to be part of the chaotic fault breccia. To the west of this block is a faulted contact with the MHA. This is the southern segment of the ECF. Although more difficult to constrain, similar lithologies are common near to the Magnesite Fault.

Objective 7 was to *'document the sequence of ductile structural events that may have impacted on the ore bodies and wall rocks. Undertake mapping and microscopy to determine whether any overprinting relationships exist'.* Core logging and in-pit mapping assisted with this objective. Folding is not common in the rocks in North Pit so structural events relating to folding could not be established. A sampling campaign to retrieve samples from all assemblages of the pit was undertaken and mineralogy and microstructures, including over-printing relationships were identified using a standard petrological microscope. Oriented samples were then retrieved, prepared correctly and studied. A higher strain, strike-slip Cambrian generation of mylonite was recognised along with younger lower strain, dip-slip mylonite zones. The strike-slip mylonite outcropped on a discrete ductile faulted contact between the MHA and Western Wall Banded Schist. High pressure Na-Ca amphibole compositions were found in the strike-slip mylonites. Only actinolite-tremolite assemblages were apparent within the dip-slip mylonite samples.

Objective 8 was to *'confirm whether there are any advantages and/or disadvantages to overlapping the two usually separate disciplines of geotechnical engineering and structural geology'.* This objective was met and is discussed in Section 6.4.

6.2 Discussion - Methods

Photogrammetry software from Adam Technology™ was used in order to measure the orientation of structures on dangerous or inaccessible pit walls. The digital terrain models created from this method can record aspects of mining progression and track geological and geotechnical features such as faults, joints and geological contacts. The geological and structural information provided can subsequently be exported into other programmes such as mine planning software suites (e.g. Surpac™ and Leapfrog™) and stereographic projection analysis software (e.g. DIPS™). A trial investigation of the TerraLuma Unmanned Aerial Vehicle (UAV) technique was undertaken at Savage River Mine. This method utilises photogrammetry techniques for high-precision mapping applications. Comparative analyses were carried out of the photogrammetry technique employed on the mine and the UAV technique (Appendix 1). This study revealed that although the UAV technique generates a true model of reality at a much higher resolution to that of the Adam Technology photogrammetry method, it is not compatible with mine planning software due to the large files it generates at such a high resolution. The number of triangles creating the wireframes for each model would need to be decimated in order for them to operate in mine planning software which in turn, decreases the resolution to a level that the standard photogrammetry employed at the mine produces anyway. The photogrammetry method has proven to be a very powerful mapping tool at Savage River Mine. Due to geotechnical safety issues, past multi-berm failure events and the lack of accurate compass bearings due to rock magnetism, the use of this method is paramount for ensuring accurate structural mapping. The technique however, should be used in conjunction with face mapping and core logging to gain data of all

scales; from large persistent joints visible in a >150 m high wall to <1 mm thick veins.

The Geological Strength Index (GSI) method was employed in the domaining of drillcore and in-pit mapping when this research commenced. Although subjective, this proved to be a quick method of domaining and produces effective results. Lower GSI values highlight areas of weaker rock masses vital in the prediction of failure areas. The rock core was domained and the method was employed whilst in-pit mapping. The technique was especially effective in the determination of the extent of the ECF damage zone. Although the fault damage zone is lithologically and structurally varied, the lower GSI values indicated significantly weaker rock masses to that of the surrounding rock. Therefore the domaining acted as another variable to constrain the extent of fault damage zones. Although this method is effective at highlighting areas of poor rock mass condition, the method only takes brittle deformation into account. Areas of high ductile strain are not recognised by this method resulting in large shear zones or ductile faults not being recognised. Despite this drawback, the GSI method of domaining in drillcore has been subsequently added as a separate parameter to the geotechnical logging dictionary.

In an attempt to gain more geotechnical data in North Pit, the method of scanline surveys (Priest and Hudson, 1981) was employed. This is a basic technique involving a line set on the surface of a rock mass. The survey consists of recording data for all discontinuities that intersect the scanline along its length. A trial investigation commenced in order to verify if this method was effective for the rock masses of North Pit. The nature of the rocks within the MHA and WWA (e.g. intensely foliated, schistose in areas) resulted in arduous data collection. 50 m scanline surveys were carried out. The process was lengthy and not as accurate as core logging. Due to compass interference, the dip direction of each defect was estimated. Scanline surveys on the joint dominated East Wall Assemblage however proved easier and took less time compared to within the MHA and WWA. The volume of structures

that intersected the line was reduced but core logging proved more accurate. The major problem with the scanline survey technique is the time spent working near high pit-walls (20 m). There are major safety concerns employing such a method and the process had to be modified prior to execution. A 50 m line was drawn onto the pit wall using spray paint. A measuring tape was set up on the ground a safe distance from the pit face (20 m). The scanline survey was completed by using three people, one at the pit face recording discontinuities and parameters, one at the tape measure recording the measurements and one person for safety reasons, 'spotting' any change, rilling or noises from the high wall indicative of rock failure. Although the scanline survey resulted in increased geotechnical knowledge of an area, the dip directions of features were not accurate. Highlighting each structure measured using spray paint and then using photogrammetry to define accurate orientations was tested. This method took a long time to carry out but produced effective data. If drillcore is available, core logging is recommended to be the more accurate technique and has no safety concerns.

6.3 General Discussion and Future Recommendations

The Eastern Contact Fault strikes 1.7 km N/S in North Pit. Due to the large volume of drillholes intersecting the fault, the internal structure of the fault could be analysed in detail, which is generally not the case in many mines. This research confirms that the fault is made up of small segments which differ in character and orientation. Thicker damage zones relating to discrete blocks of rock occur adjacent to bends in the fault. The large volume of alteration of dolomite and quartz to talc within the fault damage zone suggests that externally derived hydrothermal water-rich fluids have passed through the fault system.

Probably the most significant and persistent structure in North Pit throughout all assemblages is the foliation. Although a ductile feature, the weak foliation planes facilitate failure within all assemblages; plane failure on the east wall, slumping and plane failure within the MHA and flexural toppling within the WWA. It is treated as a brittle feature in the mine and is

measured and characterised within the geotechnical logging procedure. Inferred as the regional S2 fabric (Holm, 2002), the inability to recognise an S1 generation probably indicates the likelihood of a composite S1 and S2 fabric. The lack of post-cleavage folding is a surprising and unique characteristic of the structural environment. It is likely that the foliation orientation has dictated the joint pattern within the assemblages. A foliation parallel joint array is evident throughout North Pit regardless of lithology.

Mineralogy, over-printing relationships and joint and vein infill compositions has indicated a transition over time from an early quartz rich system to the later introduction of calcite. The latest or youngest vein event is associated with the introduction of oxidised fluids creating hematite coated joints and veins. The oxidised fluid may be meteoric in origin. The age of this last event could relate to the Tertiary extensional event in Tasmania, when Savage River was near the surface (Kohn et al., 2002). Joint and vein infill is an indication of the types of circulating fluids in the rock packages. Hematite joint and vein infill are present within lithologies with no matrix hematite suggesting the fluid is probably externally buffered and with the oxidised character perhaps meteoric water. The graphitic zones along the ECF may indicate the influx of a reduced (?methane bearing) fluid along the fault at an earlier stage. All other joint and vein infill are limited to lithologies containing some of the infill mineral in the matrix suggesting locally buffered fluids.

Higher strain strike-slip Cambrian movement and a younger lower strain dip-slip reactivation have been confirmed through this research. It is recommended that the ages of the faults be analysed in more detail to determine the actual age of the dip-slip movement. Mylonitic samples in North Pit are difficult to distinguish in hand specimen so more sampling in the pit is required to find the critical samples for geochronology purposes.

It is recommended that the modifications to the logging procedure should become permanent. The gamma (γ) angle of the striations on fault planes should be routinely measured. This

measurement has proved to be quick to acquire and adds invaluable information to the movement of faults within the rock packages. GSI domaining should be carried out habitually within drillcore and a range should be quoted when in-pit mapping. On-site geologists, if not already aware, should be taught the GSI technique and it should be expected they use it whilst mapping. Geotechnical engineers, if not already aware, should be taught the geology of all packages of rocks within the North Pit. They should know at least the basic mineralogy and structural characteristics of each assemblage. This is to ensure that the maximum knowledge of each assemblage is obtained and utilised in the predictions of future rock failure.

A drilling programme is commencing in Centre Pit South in 2013. Centre Pit South forms part of Savage River Ore Reserve and is scheduled to be mined as part of the 2013 budget. It is vital the drillhole location and orientation is optimised for not only ore body definition but for geotechnical purposes. Drillholes located on the east wall especially have to be oriented correctly so features that have been demonstrated to affect stability in North Pit are intersected. For example, 'ski-jump' joints, dipping 35°-55° towards 250°-290° were not commonly intersected within North Pit due to the drillholes plunging on average 50°-60° to the west. Core logging without in-pit mapping and photogrammetry would not have highlighted these features as potential basal surfaces facilitating wedge failure.

6.4 Conclusions

This research has confirmed that there are many advantages in combining the geotechnical and structural geology data in a mining environment such as Savage River Mine. The structure is complex and it is essential that the two disciplines work together in obtaining a comprehensive data set to capable of accurate prediction of future failure events based on proposed mine plans.

Data can be shared between the two disciplines and there is a distinct overlap. For example,

foliation intensity, orientation and characteristics are logged as geotechnical features on the Savage River Mine. Although generally weak surfaces which facilitate plane failure, foliation is also the dominant structural feature. Foliation information can be used to predict future failure events (geotechnical) and as a strain guide portraying strain localisation (structural geology). Techniques used by geotechnical engineers can contribute to knowledge of the structural environment. For example, the internal structure of faults. Although the extent of the fault damage zone can be obtained through only geological methods i.e. mapping and core logging or only by geotechnical methods i.e. core logging and domaining, the combination of the two provides increased understanding into the extent of damage zone and the predicted behaviour of the rock mass.

Understanding the structural geology of a deposit is critical to fully understanding the geotechnical behaviour of a rock mass. Safety is paramount in all mines and with the combination of knowledge from both disciplines, rock failures will be better understood, predicted and prevented.

REFERENCES

Adam Technology, 3DM, 1995. Photogrammetry software. http://www.adamtech.com.au.

Adams, C.J., Black, L.P., Corbett, K.D. and Green, G.R., 1985. Reconnaissance isotopic studies bearing on the tectonothermal history of Early Palaeozoic and Late Proterozoic sequences in western Tasmania. *Australian Journal of Earth Sciences*, v. 32, no. 1, p. 7-36.

Australian Bulk Minerals, 1996. Feasibility Study for the Resumption of Operations at Savage River and Port Latta, dated December 1996. Unpublished report.

Australian Bulk Minerals, 2006. Mine Life Extension Project – Volumes 1 to 3. Unpublished report to Australian Bulk Minerals, September, 2006.

Australian Rock Engineering Consultants, 1972. Report on Consultation – Preliminary Pit Slope Design, Savage River Mine, dated 21 August 1972. Unpublished report.

Australian Rock Engineering Consultants, 1973. Progress Report – Slope Design Studies, Savage River Mine, dated 31 October 1973. Unpublished report.

Australian Rock Engineering Consultants, 1974. First Stage of Open Pit Design Review, Savage River, Tasmania – Volume 1 Report, dated 24 April 1974. Unpublished report.

Australian Rock Engineering Consultants, 1974. First Stage of Open Pit Design Review, Savage River, Tasmania – Volume 2 Appendices, dated 24 April 1974. Unpublished report.

Australian Rock Engineering Consultants, 1974. First Stage of Open Pit Design Review, Savage River, Tasmania – Supplementary Report, dated 27 June 1974. Unpublished report.

Australian Rock Engineering Consultants, 1974. Progress Report on Phase 11 Open Pit Design Investigations, Savage River Mine, Tasmania, dated November 1974. Unpublished report.

Australian Rock Engineering Consultants, 1975. Review of Results of Slope Monitoring – Rock Slide at North End of the East Wall, Savage River Mine, Tasmania, dated April 1975. Unpublished report.

Barrett, Fuller and Partners, 1988a. Slope Stability and Savage River Mines, Letter report 10-1079, dated 16 September 1988. Unpublished report.

Barrett, Fuller and Partners, 1988b. Site Visit October 11 1998, Letter report, dated 12 October 1988. Unpublished report.

Barrett, Fuller and Partners, 1988c. Letter report to Savage River Mines on Slope Wall Instability, dated 23 December 1988. Unpublished report.

Barrett, Fuller and Partners, 1988d. Letter report to Savage River Mines Remedial Works, East Wall Central Pit, dated 29 December 1988. Unpublished report.

Barrett, Fuller and Partners, 1989a. Geotechnical Studies Central and North Pits, Letter report to Savage River Mines, dated 1 November 1989. Unpublished report.

Barrett, Fuller and Partners, 1989b. Savage River Mines - Geotechnical Review of West and East Walls – Central Pit, Report 10-1460/61, dated November 1989. Unpublished report.

Barrett, Fuller and Partners, 1990a. Savage River Mines – Geotechnical Assessment of the Proposed North Pit Deepening, Report 10-1507 Volumes I and II, dated January 1990. Unpublished report.

Barrett, Fuller and Partners, 1990b. Review of West Wall Remedial Work (Central Pit) – Site Visit on 5 June 1990, Letter report 10-11681, dated 13 June 1990. Unpublished report.

Barrett, Fuller and Partners, 1990c. Stability Analyses of West Wall Remedial Work, Letter report 11709, dated 25 September 1990. Unpublished report.

Barrett, Fuller and Partners, 1991a. Review of West Wall Remedial Work (Central Pit) – Site Visit on 3 April 1991, Letter report 11906, dated 7 May 1991. Unpublished report.

Barrett, Fuller and Partners, 1991b. Result of Site Inspection – West Wall – Central Pit – Site Visit on 10 May 1991, Letter report 11939, dated 21 May 1991. Unpublished report.

Barrett, Fuller and Partners, 1991c. West wall instability untitled letter 11939 JRB0378, dated 21 May 1991. Unpublished report.

Barrett, Fuller and Partners, 1991d. Current West Wall Stability, Letter 11939 JRB00404, dated 31 May 1991. Unpublished report.

Barrett, Fuller and Partners, 1991e. Savage River Mines – West Wall Central Pit, Letter report 11955, dated 31 July 1991. Unpublished report.

Barrett, Fuller and Partners, 1992a. Conceptual Underground Mine Study – Savage River Mines, Letter Report 12103, dated April 1992. Unpublished report.

Barrett, Fuller and Partners, 1992b. North Pit Conceptual Underground Study – Savage River Mines, Letter Report 12144, dated May 1992. Unpublished report.

Barrett, Fuller and Partners, 1992c. Savage River Mines – Site Visit and North Pit Review, Letter Report 12187, dated 5 August 1992. Unpublished report.

Barton, N., 1973. Review of a new shear strength criterion for rock joints. *Engineering Geology 7*, 287-332.

Barton, N. and Choubrey, V., 1977. The shear strength of rock joints in theory and practice. *Rock Mechanics 12(1),* 1-54.

Berry, R.F., 1989. The history of movement on the Henty Fault Zone, western Tasmania: an analysis of fault striations. *Australian Journal of Earth Sciences*, 36, 189-205.

Berry, R.F. and Banks, M.R., 1985. Striations on minor faults and the structure of the Parmeener Supergroup near Hobart, Tasmania. Pap. Proc. Roy. Soc.Tas., 119, 23-30.

Berry, R.F. and Crawford, A.J., 1988. The tectonic significance of Cambrian allochthonous mafic-ultramafic complexes in Tasmania. *Australian Journal of Earth Sciences*, v.35, no.4, pp.523-533.

BFP Consultants Pty. Ltd., 1999a. Savage River Mine – Site Visit Report of 22/23 April 1999. Unpublished report.

BFP Consultants Pty. Ltd., 1999b. Savage River Mine – UDEC Modelling – North Pit, 27 page fax, dated 15 October 1999. Unpublished report.

BFP Consultants Pty. Ltd., 1999c. Savage River Mine – UDEC Modelling – North Pit, 5 page fax, dated 27 October 1999. Unpublished.

BFP Consultants Pty. Ltd., 2000. UDEC Stability Analysis Results – North Pit Extensions 1 and 2 for Australian Bulk Minerals Savage River Mine, Letter report dated March 2000. Unpublished.

Bieniawski, Z.T., 1979. The geomechanics classification in rock engineering applications. Proceedings of 4th Congress of International Society of Rock Mechanics, Montreux, vol.2, pp.41-48. Balkema, Rotterdam.

Black, L.P., Calver, C.R., Seymour, D.B. and Reed, A., 2004. SHRIMP U-Pb detrital zircon ages from Proterozoic and Early Palaeozoic sandstones and their bearing on the early geological evolution of Tasmania. *Australian Journal of Earth Sciences*, v.51, no.6, pp.885-900.

Black, L.P., Seymour, D.B., Corbett, K.D., Cox, S.E., Streit, J.E., Bottrill, R.S., Calver, C.R., Everard, J.L., Green, G.R., McClenaghan, M.P., Pemberton, J., Taheri, J. and Turner, N.J., 1997. Dating Tasmania's oldest geological events. Record – Australian Geological Survey Organisation.

Bottrill, R.S. and Baker, W.E., 2008. A Catalogue of the Minerals of Tasmania. Bulletin Geological Survey Tasmania 73.

Bottrill, R.S. 2006. Petrological examination of rock samples from the Savage River Mine. Unpublished Report for Australian Bulk Minerals.

Bottrill, R.S. and Taheri, J., 2007. Petrology of the host rocks, including mineralisation and adjacent rock sequences, from the Savage River Mine. Tasmanian Geological Survey Record 2007/05.

Brady, B.H.G and Brown, E.T., 2004. Rock Mechanics for Underground Mining, 3rd edn. Kluwer, Dordrecht.

Brown, E.H., 1977. The crossite content of Ca-amphibole as a guide to pressure of metamorphism. *Journal of Petrology* 18, 53-72.

Brown, A.V., 1986. Geology of the Dundas-Mt Lindsay-Mt Youngbuck region. Rosny Park, Tasmania, Department. Of Mines.

Burg, J.P. and Laurent, P., 1978. Strain analysis of a shear zone in a granodiorite. *Tectonophysics* 47: 15-42.

Calver, C.R. and Walter, M.R., 2000. The Late Neoproterozoic Grassy Group of King Island, Tasmania: correlation and palaeogeographic significance. Precambrian research, 100, pp.299-312.

Centre for Tasmanian Historical Surveys, 2006. http://www.utas.edu.au/library/companion_to_tasmanian_history/S/Savage%20river.htm.

Coleman, R.J., 1975. Savage River magnetite deposit. In: Knight, C.L., (ed.) Economic Geology of Australia and Papua New Guinea. Australas. *Inst. Min. Metall. Monog*. 5, vol.1 (Metals), pp.598-604.

Collins, P.L.F. and Williams, E., 1986. Metallogeny and Tectonic Development of the Tasman Fold Belt in Tasmania. *Ore Geology Reviews* 1: 153-201.

Commonwealth of Australia, Bureau of Meteorology, 2012. http://www.bom.gov.au/tas/.

Coulthard, M.A., Dugan K.J., and Hutchison, B.J., 2001. Numerical Modelling of complex slope movements at Savage River Mine, Tasmania. In Desai, C.S. et al. (eds), *Computer Methods and Advances in Geomechanics:1673-79*. Rotterdam: Balkema.

Crawford, A.J. and Berry, R.F., 1992. Tectonic implications of Late Proterozoic-early Palaeozoic igneous rock associations in western Tasmania. *Tectonophysics* 214, 37-56.

Dight, P., 1982. *Improvements to the Stability of Rock Walls in Open Pit Mines*, PhD Thesis, Civil Engineering, Monash University, Melbourne.

DIPS™. Graphical and Statistical Analysis of Orientation Data. http://www.rocscience.com/products/1/Dips

Duncan, D.McP. and Weatherstone, N., 1990. Exploration history of the Savage River iron ore deposits. In: Glasson, K.R., and Rattigan, J.H. (eds.). *Geological aspects of the discovery of some important mineral deposits in Australia*. AusIMM. Monograph Series. 17, pp287-292.

Etheridge, M.A., Branson, J.C. and Stuart-Smith, P.G., 1985. Extensional basin-forming structures in Bass Strait and their importance for hydrocarbon exploration. *APEA Journal*. 25, 344-361.

Everard, J.L., 1999. A blue amphibole locality from the northern Arthur Lineament. Geological Survey of Tasmania Record 1999/5.

Gee, R.D., 1967. *The tectonic evolution of the Rocky Cape Geanticline in NW Tasmania*. PhD thesis, Unpub. University of Tasmania.

Grange Management Plan Ground Control- The Geotechnical Domain Model, 2013. Unpublished report.

Grange Resources, 2012. Unpublished Geotechnical report.

Green, T.H. and Spiller, A.R., 1977. Blue amphibole from Precambrian metabasalts, Savage River, Tasmania. *American Mineralogist 62*, pp.164-166.

Gresen, R.L., 1967. Composition-volume relationships of metasomatism. *Chemical Geology* 2, pp.47-65.

Gu, Y., 2003. Automated scanning electron microscope based mineral liberation analysis. *Journal of Minerals and Materials Characterization and Engineering* 2, pp.33–41.

Hall, G. and Solomon, M., 1962. Metallic mineral deposits. In: Spry, A.H. and Banks, M.R. (eds). The geology of Tasmania. *J. Geol. Soc. Aust*., 9, pp.285-309.

Hill, K.C., Hill, K.A., Cooper, G.T., O'Sullivan, A.J.,O'Sullivan, P.B. and Richardson, M.J., 1995. Inversion around the Bass Basin, SE Australia. In: Buchanan, J.G. and Buchanan, P.G. (Eds), *Basin Inversion, Geological Society*, Special Publication 88, pp.525–547.

Hirth, G. and Guillot, S., 2013. Rheology and tectonic significance of serpentine. *Elements 9*, pp.107-113.

Hoek, E and Bray, J.W., 1991. *Rock Slope Engineering*, revised 3rd edn. Elsevier applied science.

Holcombe, R., 2012. http://www.holcombecoughlinoliver.com.

Holland, T. and Blundy, J., 1994. Non-ideal interactions in calcic amphiboles and their bearing on amphibole-plagioclase thermometry. *Contributions to Mineralogy and Petrology.* 116, pp.433-447.

Holm, O.H., 2002. *Structural and Metamorphic Evolution of the Arthur Lineament, NW Tasmania.* PhD thesis. University of Tasmania.

Holm, O.H. and Berry, R.F., 2002. Structural History of the Arthur Lineament, NW Tasmania: An analysis of critical outcrops. *Australian Journal of Earth Sciences, v.49*, pp.167-185.

Hughes, T.D. 1958. Savage River Iron Ore Deposits. Tas Geol Survey Tech Rept 2, pp.33-41.

Hutchison, B.J., 2000. Geotechnical Aspects of the Savage River Iron Ore Mine, Tasmania. *Journal and news of the Australian Geomechanics Society*, vol 35, no 2.

Hutchison, B.J., Dugan, K. and Coulthard, M., 2000. *Analysis of flexural toppling at Australian Bulk Minerals Savage River Mine*. GeoEng2000, Melbourne, Australia.

INVESTIGATOR, software. http://www.earthsci.unimelb.edu.au/facilities/analyser/downloads.html

ISRM, 2007. *The complete ISRM suggested methods for rock characterisation, testing and monitoring: 1974-2006* (Eds Ulusay, R. and Hudson, J.A.). ISRM Turkish National Group, Ankara, Turkey.

Karzulovic, A. and Read, J.R.L., 2009. *Guidelines for open pit slope stability*, 1st edn. CSIRO.

Kohn, B.P., Gleadow, A.J.W., Brown, R.W., Galagher, K., O'Sullivan, P.B. and Foster, D.A., 2002. Shaping the Australian crust over the last 300 million years: insights from fission track thermotectonic imaging and denudation studies of key terranes. *Australian Journal of Earth Sciences,* Volume 49, Issue: 4, pp. 697-717.

Leake, B.E., Woolley, A.R., Arps, C.E.S., Birch, W.D., Gilbert, M.C., Grice, J.D., Hawthorne, F.C., Kato. A., Kisch, H.J., Krivovichev, V.G., Linthout, K., Laird, J., Mandarino, J.A., Maresch, W.V., Nickel, E.H., Rock, N.M.S., Schumacher, J.C., Smith, D.C., Stephenson, N.C.N., Ungaretti, L., Whittaker, E.J.W. and Youzhi, G., 1997. Nomenclature of Amphiboles: Report of the subcommittee on amphiboles of the International Mineralogical Association, commission on new minerals and mineral names. *The Canadian Mineralogist*, vol.35, pp. 219-246.

Leapfrog™ mining software. http://www.leapfrog3d.com/products/leapfrog-mining.

Lister, G.S. and Hobbs, B.E., 1980. The simulation of fabric development during plastic deformation and its application to quartzite: the influence of deformation history. *J Struct Geol*, vol.2, pp. 355-371.

Lister, G.S., 1977. Discussion: crossed-girdle c-axis fabrics in quartzites plastically deformed by plane strain and progressive simple shear. *Tectonophysics*, vol.39, pp. 51-54.

Marinos, P. and Hoek, E., 2000. GSI: a geologically friendly tool for rock mass strength estimation. *Proceedings of GeoEng2000 Conference*, Melbourne, vol.1, pp.1422-1440. Technomic, Lancaster, PA.

McClay, K., 1994. *The Mapping of Geological Structures.* Geological Society of London Handbook. Handbook series editor – Keith Cox. pp. 41-44.

McPhee, E., 2011. Report on the Lithological and Structural Mapping of Extension 4, Stage 2, Savage River. Unpublished internal report, Grange Resources.

Miller, J.McL., Norvick, M.S. and Wilson, C.J.L., 2002. Basement controls on rifting and the associated formation of ocean transform faults - Cretaceous continental extension of the southern margin of Australia. *Tectonophysics*, 359, 131-155.

Morris, E., 2012. *Structural relationship of the Oonah Formation near the Arthur Lineament, Savage River, NW Tasmania.* Honours thesis, University of Tasmania.

Mueller, A.M., 1998. *Sedimentology of the Oonah Formation, western Tasmania.* Honours thesis. University of Tasmania.

Overstreet, W.C., 1967. *The geological occurrence of monazite.* United States Geological Survey, Professional Paper 530.

Parks and Wildlife Service Tasmania. http://www.parks.tas.gov.au/

Passchier, C.W. and Trouw, R.A.J., 2005. *Microtectonics*, 2nd edn. Springer, Berlin.p 104 – 109.

Patton, F.D. 1966. Multiple modes of shear failure in rock. *Proceedings of 1st Congress of International Society of Rock Mechanics*, Lisbon, 1, 509-513.

Piteau and Associates, 1979. Savage River Mine – Report on Slope Stability Analysis and Design of the Open Pit Slopes, Project 78-148. Unpublished report.

Priest, S.D. and Hudson, J.A., 1981. Estimation of discontinuity spacing and trace length using scanline surveys. *Int. J. Rock Mech. Min. Sci. And Geomech*. Abstr., 18 (3): 183-97.

Reid, A.M., 1919. Iron Ore in the Long Plains and Zeehan districts. In: Reid, A.M.; Twelvetrees, W.H., Eds. *The Iron Ore Deposits of Tasmania*. Tas Geol Survey Mineral Resources, 6, p.67-88.

RocScience; software tools for rock and soil. DIPS v5.0. Toronto, Ontario.

Sack, P.J., Berry, R.F., Meffre, S., Falloon, T.J., Gemmell, J.B. and Friedman, R.M., 2011. In situ location and U-Pb dating of small zircon grains in igneous rocks using laser ablation–inductively coupled plasma–quadrupole mass spectrometry, *Geochem. Geophys. Geosyst.*, 12, Q0AA14, doi:10.1029/2010GC003405.

Savage River Mine drillhole database, 2010. Access file. Unpublished.

Schmid, S.M. and Casey, M., 1986. Complete fabric analysis of some commonly observed quartz C-axis patterns. *Geophys Monogr* 36: 263-286.

Scott, R.J., Berry, R. F. and Selley, D., 2005. *CoreSolutions*: a *Microsoft Excel*™-based program for determining the real-space orientations of planar and linear fabrics in axially-oriented drill core: Centre for Ore Deposit Research, University of Tasmania, Hobart, Australia.

Seymour, D.B. and Calver C.R., 1995. Explanatory notes for the time-space diagram and stratotectonic elements map of Tasmania. Geological Survey of Tasmania Record 1995/01.

Snoke, A., Tullis, J., 1998. An overview of fault rocks. In: Snoke, A., Tullis, J. and Todd, V.R. (Eds) *Fault related rocks – a photographic atlas*. Princeton University Press, New Jersey. pp.3-18.

Spiller, A.R., 1974. *The petrology of the Savage River iron ore deposit, Tasmania*. Unpub. B.A. Hons. Thesis, Macquarie Uni.

Spry, A.H., 1964. *Precambrian rocks of Tasmania, Part IV, the Zeehan-Corinna area*. Papers and Proceedings of the Royal Society of Tasmania 98, 23-48.

Spry, A.H., Blissett, A.H., Burns, K.L., Jennings, I.B. and Scott, B., 1962. The geology of Tasmania: the Precambrian rocks: *Journal of the Geological Society of Australia*, v.9, no.2, p. 107-126.

Spry, A.H. and Ford, R., 1957. A reconnaissance of the Corinna-Pieman Heads area-Geology. *Papers and Proceedings of the Royal Society of Tasmania*, 91. pp. 1-10.

Stacey, A.R., and Berry, R.F., 2004. The structural history of Tasmania: a review for petroleum explorers. In: Boult, P.J., Johns, D.R. and Lang, S.C. (Eds), *Eastern Australasian Basins Symposium II*, Petroleum Exploration Society of Australia, Special Publication, 151–162.

Surpac™ mining software. http://www.gemcomsoftware.com/products/Surpac.

Taheri, J. and Bottrill, R. S., 2005. *The nature and origins of copper and tin-tungsten deposits in the Balfour - Temma area, northwest Tasmania*, Mineral Resources Tasmania, Record 2004_05.

Taheri, J. and Bottrill, R., (2013) in press. *The nature and origin of magnetite ore bodies in the Savage River Mine*.

Thornett, J.R., 1999. Report on the structural and lithological mapping of North Pit and South Lens Pit, Savage River magnetite mine. Unpublished internal report, Australian Bulk Minerals.

Trouw, R.A.J., Passchier, C.W. and Wiersma, D.J., 2010. *Atlas of Mylonites and related microstructures*. Springer-Verlag Berlin Heidelberg.

Turner, N.J. and Crawford, A.J. 1993. *General features and chemical analyses of mafic and other rocks, Corinna geological map quadrangle*. Report Mineral Resources Tasmania 1993/23.

Turner, N.J. and Bottrill, R.S., 1993. *Blue amphibole in the Proterozoic to Cambrian Arthur Metamorphic Complex, northwest Tasmania*. Mineral Resources Tasmania Report. 1993/26.

Turner, N.J. and Bottrill, R.S., 2001. Blue amphibole, Arthur Metamorphic Complex, Tasmania: composition and regional tectonic setting. *Australian Journal of Earth Sciences*, 48, pp.167-181.

Turner, N.J., 1989. The Precambrian. In: Burrett C.F. and Martin. E.L. eds. *Geology and Mineral Resources of Tasmania*. Geological Society of Australia. Special Publication, 15, pp.5-46.

Turner, N. J., 1992. *Corinna 1:50 000 geological map. Field guide to selected rock exposures*. Tas Geol Survey UR1992_06.

Turner, N.J., 2006. North Pit regional geology map, 1:5000. Unpublished.

Turner, N.J., 2006. North Pit geology map. 1:1000. Unpublished.

Turner, N.J., 2009. Faults at Savage River Mine. Unpublished.

Turner, N.J., Black, L.P. and Kamperman, M., 1998. Dating of Neoproterozoic and Cambrian orogenies in Tasmania. *Australian Journal of Earth Sciences*, v.45, no.5, p.789-806.

Turner, N.J., Brown, A.V., McClenaghan, M.P. and Soetrisno, I.R., 1991. Geological Atlas 1:50000 series. Sheet 43 (7914N). Corinna. Department of Resources and Energy, Tasmania.

Twelvetrees, W. H., 1900. *Report on the mineral fields between Waratah and Corinna*. Rep. Secr. Mines Tasm. 1899- 1900: cxi -ccviii. O.S. Rept.

Urquhart, G., 1966. Magnetite Deposits of the Savage River-Rocky River Region. *Tasmanian Geological Survey Bulletin* No 48. Mines Department, Hobart.

Veevers, J.J., Powell C, McA., and Roots, S.R., 1991. Review of seafloor spreading around Australia. I Synthesis of the patterns of spreading. *Australian Journal of Earth Sciences*, 38, 391-408.

Webster, A., 2009. The Savage River Magnetite Deposits: Structural and textural clues to the formation of Tasmania's largest metal deposits. An unpublished report to Grange Resources, Tasmania.

Williams, B., 2011. Savage River lithology mapping and modelling project. Unpublished consultancy report, Grange Resources.

Williams, E., McClenaghan, M.P., Collins, P.L.F., Brown, S.G., Camacho, A., Dronseika, E.V., Higgins, N.C., Morland, R., Reid, E.J. and Seymour, D.B., 1989. *Mid-Palaeozoic deformation, granitoids and ore deposits*. Special Publication – Geological Society of Australia, v.15, p. 238-292.

Wilson, C.J.L., Robinson, J.A. and Dugdale, A.L., 2009. Quartz vein fabrics coupled to elevated fluid pressures in the Stawell gold deposit, South-Eastern Australia. *Mineral Deposita* 44, 245-263.

Wilson, C.J.L., Russell-Head, D.S. and Sim, H.M., 2003. The application of an automated FA system to the textural evolution of folded ice layers in shear zones. *Annals of Glaciology* 37, 7-17.

Wilson, C.J.L., Russell-Head, D.S., Kunze, K. and Viola. G., 2007. The analysis of quartz c-axis fabrics using a modified optical microscope. *Journal of Microscopy* 227, 30-41.

Yamaji, A., 2001. A stereonet program for fault-striation analysis. *Geoinformatics*, 12, 167-182

Young, I.M., Trupp, M.A. and Gidding, M.J., 1991. Tectonic Evolution of Bass Strait-Origins of Tertiary Inversion. *Exploration Geophysics*, v. 22, 465–468.

Young, M.K., Rawlinson, N., Arroucau, P., Reading, A.M., and Tkalcic, H., 2011. High frequency ambient noise tomography of southeast Australia: New constraints on Tasmania's tectonic past. *Geophysical Research Letters*, v.38, no.13.

APPENDIX 1

A COMPARATIVE ANALYSIS OF THE 3DM ANALYST (ADAM TECHNOLOGY) PHOTOGRAMMETRY AND THE TERRALUMA UNMANNED AERIAL VEHICLE (UAV) TECHNIQUE AT SAVAGE RIVER MINE, NW TASMANIA

Introduction

3DM Analyst software created by Adam Technology is a 3D data extraction package for use with digital imagery. The software integrates 3D spatial data with 2D visual data to create spatially accurate representations of the surface topology of the rock. It does this by using pairs of overlapping or convergent aerial or terrestrial digital images. This photogrammetry technique has been used on Savage River Mine since 2008.

In April 2012, Dr Arko Lucieer and Mr Darren Turner from the University of Tasmania (School of Geography and Environmental Studies) visited Savage River Mine to undertake a trial investigation using their 'OktoKopter'. They had developed an Unmanned Aerial Vehicle (UAV) for environmental and agricultural high-precision mapping applications and visited Savage River Mine in the hope that the technique would be advantageous in a mining environment.

This report aims to compare the two techniques (3DM Analyst and the UAV) from a geological/geotechnical mapping viewpoint.

The Advantages of using 3DM Analyst - Photogrammetry Technique

Geological and geotechnical mapping is challenging to undertake in this environment due to the effect the magnetite rich ore has on compasses used when mapping faces. 3DM Analyst has been used on Savage River Mine to collect structural information from dangerous and inaccessible open pit faces in a safe manner. The DTM's (Digital Terrain Model) created from the photogrammetry can record aspects of mining progression and track geological and geotechnical features such as faults, joints and contacts. Structures can be traced through a succession of mine faces and predictive models tested on new exposures as they become available in the mine. The programme produces a stereographic projection of the structures that the user has identified and these can be analysed and interpreted. All of the geological and structural information from the program can be exported into other programmes such as Surpac and DIPS for further analysis and interpretation.

The technique is a very powerful tool aiding Geologists and Geotechnical Engineers in their in-pit and regional mapping.

A comparative analysis of 3DM Analyst and TerraLuma UAV methods

Grange Resources invests money annually for the use of 3DM Analyst software. The technique is used in-house with some of the Geologists, Geotechnical Engineers and Structural Geologist (past and present) participating in the collection of the raw data, processing the data and the ultimate analysis and interpretation. The TerraLuma UAV technique requires the Consultant being on site, controlling the vehicle and creating the end result which subsequently is handed back to Grange Resources for the analysis and interpretation. Comment can only be made on the method to produce a 3DM Analyst DTM and not a TerraLuma UAV 3D model, as this has never been attempted in-house. Some observations of the TerraLuma UAV technique will be discussed but please note that these are subjective comments with the primary goal being to attempt to compare the two.

The overall concept of 3DM Analyst has to be fully understood by the operator prior to attempting to take any photographs for processing. There are two ways the photographs can be taken in an in-pit environment; a strip and a fan configuration of photographs. The strip photographs involve setting up the tripod and camera directly in front of the wall/structure of interest. The operator takes a photograph and moves to the next position either directly to the left or right of the photograph just taken. There has to be at least a 40% overlap of the two photographs. This is then repeated until the wall/structure of interest is entirely photographed from left to right or right to left in what essentially is a number of photographs making up a 'strip'. A fan configuration involves taking a number of different photographs with overlap by just moving the angle of the camera up and down; left to right on the tripod but not moving the actual ground position of the tripod. Approximately three tripod locations need to be used photographing the wall/structure of interest.

In order for the created DTM's to be within the Savage River Mining Grid Control Network (for gaining orientation data, Surpac application etc) control points are painted onto the wall/structure of interest. The spray-painted dots are painted along the face at regular intervals when taking strip photographs and subsequently surveyed. The tripod locations are surveyed when using the fan configuration and at least three control points should be spray painted on the wall for extra control.

Strip photographs are useful on Savage River Mine for bench (10 – 50m) scale mapping and fan photographs for entire pit wall scale (>50m). The method is relatively easy to use and not as cumbersome as Sirovision but there are still some problems. Firstly, if there is machinery working on the floor where ideally the tripod should be set up the photographs cannot be taken until the machinery leaves that area. The floor in front of a face may be too muddy/uneven to keep the tripod steady. There have been a few occasions when using the fan configuration that too many photographs have been taken and subsequently 'crashes' the computer and a DTM cannot be generated.

From observations, the TerraLuma UAV technique was very quick in gathering the raw data. A safe place out of the way of machinery and potential areas of rock failure can be sought prior to flying the

UAV to the area of interest. Control needs to be set up and surveyed much like the 3DM Analyst technique but these are not spray-painted dots on the surface of a wall but orange coloured plates that can be dotted around the floor of the face. This minimises the operator's time at a potentially dangerous pit wall. Also, enforced restricted zones on the mine (access to the face is prohibited) can still be photographed with ease. These could not be photographed using 3DM Analyst unless control points were previously on the face or features of known coordinates on the face can be used.

There is no doubt that the method surrounding raw data collection using the TerraLuma UAV technique is safer for the operator compared to 3DM Analyst. Inclement weather affects both techniques and the type of natural light on the day gives a variable result. The TerraLuma UAV technique is also quicker and there are fewer variables regarding the success of the technique. In a geotechnically challenging environment such as Savage River Mine, safety is paramount.

Test Areas for the Trial

Three test areas were chosen in April 2012 for the TerraLuma UAV Savage River Mine trial. The first in Stage 2 of North Pit, the second to the south of North Pit and the third to the East of Stage 1 of North Pit. The first and third test areas were within the same rock package – a carbonate mafic assemblage. This rock package is joint and vein dominated and is photographed using 3DM Analyst in-house more frequently than all three main rock packages on the mine. The second test area, to the south of North Pit is a geologically interesting area being a wedge bounded by two major faults. A melange of dolomite, chlorite schist and mafic boudins dominate this area. This test area is the only area that the control was changed from a common datum to the Savage River Mine Grid control datum in order to check the capabilities with Surpac.

Results

The following results from both the TerraLuma UAV and 3DM Analyst utilises screen shots in collaboration with descriptions.

The results of the TerraLuma UAV technique presented in this report are of a Pdf format. The original models were decimated from 10+ million triangles to around 200,000 triangles in order to view the results by using a manageable file format. The 3DM Analyst images are not decimated and the screen shots shown are directly from the programme used for structural/geological analysis and interpretation.

Comparisons have been made difficult due to some of the images from the TerraLuma UAV being different to the images from 3DM Analyst. In the dynamic, evolving mining environment, unless areas are photographed without delay, they become quickly unavailable. 3DM Analyst was not used to photograph the same areas at the same time as the TerraLuma UAV technique, although care has been

made to only compare the results of areas that were proximate to each other and within the same rock package.

- ***Stage 2, North Pit***

In September 2011, the East Wall of Stage 2 in North Pit was photographed for the generation of a DTM for the subsequent analysis of the structures exposed on the pit wall. The tripod and camera was set up on the pit floor which was 215RL and the camera used was a Canon EOS 10D with a 24mm fixed lens. In April 2012, the same face was photographed using the TerraLuma UAV technique. The pit floor at this time was 185RL so the pit had increased in depth by 30m in that time period. **Figure 1** (page 5 of this report) shows the comparison between the techniques using the DTM (Digital Terrain Model) created by 3DM Analyst in September 2011 and the Pdf of the TerraLuma UAV model created in April 2012.

The comparative analysis shows that both techniques can be effectively used when analysing structures. Joint sets are visible using both techniques; although the 3DM Analyst DTM shows approximately double the amount of less persistent, closed joint sets (although the model it is being compared to has been highly decimated). This can be seen on the last two photographs of **Figure 1**; non-persistent, horizontal joints or factures can be seen on the rock mass from the 3DM Analyst DTM whereas they are not so visible in the TerraLuma UAV technique. This could possibly be due to the photographs being taken after heavy rainfall in September 2011, thus saturating the pit face causing the smaller joints/fractures to be highlighted in the photographs. The rock has also been subject to weathering since the first sets of photographs were taken. Dust may have concentrated within these areas making them less visible to the naked eye. The overall rock mass condition of the face can be categorised using both techniques. GSI (Geological Strength Index) domaining can be carried out in conjunction with geological mapping from the images using both techniques.

Geological variation can be observed generally by colour and/or structure. The TerraLuma UAV technique has a greater colour variation within the photographs meaning geological contacts are more visible to the operator. This could just be due to the type of natural light on the day of the collection of the photographs. Colour variation is also important when analysing joint decoration or infill. The East Wall rock mass has a range of joint infill which impacts directly on the geotechnical performance of the pit wall. Although the majority of joints have no infill, some have hematite and/or calcite usually <100mm thick. Some structures show decoration such as slickensides and striations on the joint surfaces as well as mineral fibres which give an indication of movement direction. Comparative analysis of Stage 2 of North Pit shows that both techniques ensure joint infill visibility (**Figure 2**).

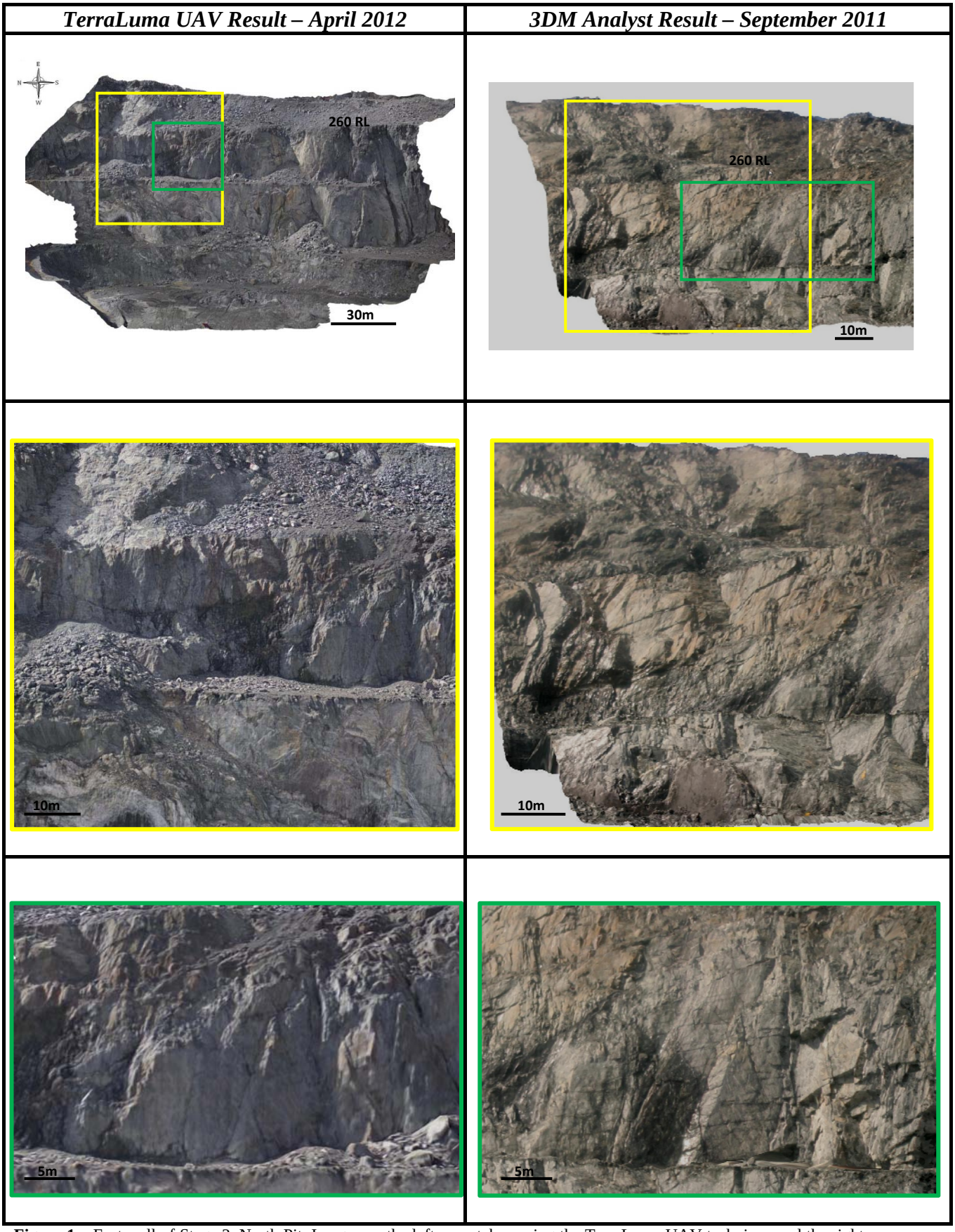

Figure 1 – East wall of Stage 2, North Pit. Images on the left were taken using the TerraLuma UAV technique and the right images were taken using 3DM Analyst. The scale reduces respectively through the images and the yellow and green boxes within the first image denote the lower image location.

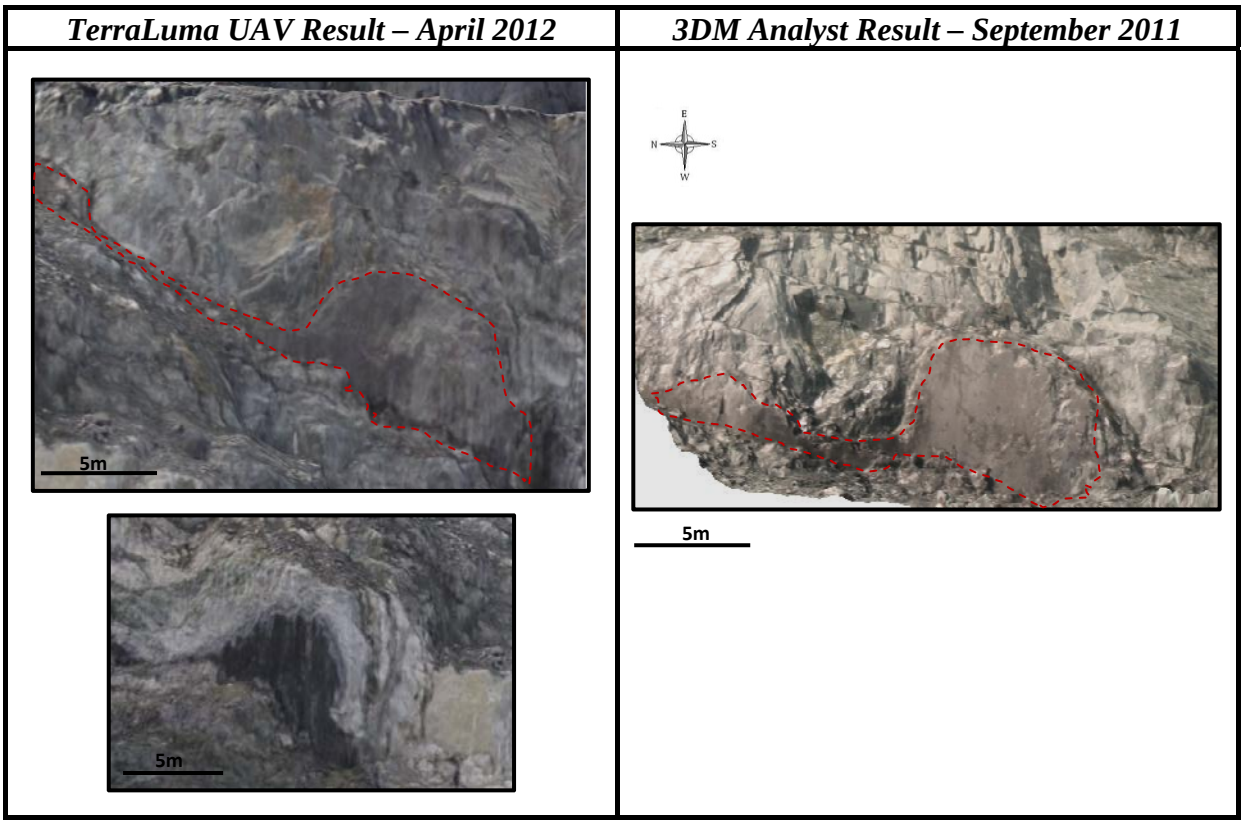

Figure 2 – East wall of Stage 2, North Pit. Images on the left were taken using the TerraLuma UAV technique and the right images were taken using 3DM Analyst. The red dotted line on both upper photographs denotes the area of graphite/hematite infill on the same smooth, planar structure photographed in September 2011 and April 2012. The lower image shows how colour variation can be used to determine infill (in this case graphite) and geological variation (the white areas being dolomite as opposed to carbonate mafic schist).

- ***South Wall, North Pit***

The South wall of North Pit was another test area photographed in April 2012. This area is of high geological importance on the mine. The area forms a wedge between two large faults (the Eastern Contact Fault and Eastern Splay Fault). Its structural and mineralogical characteristics are different to the other rock assemblages on the mine thus this area being a separate domain to accompany the other four domains on the mine. The rock is not as heavily jointed nor as veined as the East wall but mapping lithological variation along this wall is paramount.

The biggest problem with this face is that there has not been an opportunity to photograph it properly using 3DM Analyst. The berm itself is too narrow so when the tripod is set up as far from the face as possible, it is still too close to the face to capture the full height of the wall. The face is 25m in height from the 165RL to the 140RL. The floor of North Pit now stands at 50RL. **Figure 3** shows a 3DM Analyst DTM of this area taken in March 2011. The image has been cropped to only show this particular area. The tripod and camera were set up on the floor of the pit (50RL) and a Canon EOS 10D camera with a 24mm fixed lens was used. Theoretically the tripod should have been set up nearer to the face but this was not possible. The current pit floor is too low to capture a realistic image of this

face at present. The TerraLuma UAV technique reaches complex, inaccessible areas with ease and flexibility and the model produced is a true representation for use in geological mapping. This is definitely one of the most important advantages of this technique compared to 3DM Analyst.

- ***East wall, North Pit***

The East Wall of North Pit was another test area photographed in April 2012. This wall has been subject to a mining cut-back due to two large rock failures occurring in 2010. In order to track mining activity, the wall has been photographed and analysed using 3DM Analyst every three months. **Figure 5** (page 9) shows a table comparing the two DTM's created by the TerraLuma UAV technique and the 3DM Analyst technique.

Due to the UAV camera trigger failing the 3D model was generated from low resolution video frames. In this instance, the 3DM Analyst technique is clearer meaning structures, infill and decoration and roughness of the surfaces of structures can be seen easier. Approximately three times more structures are visible using this technique. The last two photographs of **Figure 5** shows a hematite filled joint. It is visible here that the 3DM Analyst DTM is a clearer model than the TerraLuma UAV DTM. The infill (hematite – maroon colour coated the joint) is visible on both models but striations and the shine created from the surface effectively being 'polished' is only visible from the 3DM Analyst DTM. As well as infill, structure type, position and orientation, the visible roughness of structures is also important when analysing these 3D models. Friction angles change according to roughness i.e. the angle increases with increasing roughness so this parameter is paramount when mapping areas of potential rock failure. Roughness is visible using both techniques but again, as the 3DM Analyst DTM is clearer, the increase in the confidence of this parameter is heightened. In this instance (the lower hematite coated joint photograph) the joint can be seen clearly to be smooth and slickensided.

- ***General East Wall Assemblage, North Pit***

Figure 6 (page 10) shows an area from Stage 2, East wall of North Pit which was produced using the TerraLuma UAV technique and an area on the East wall, Stage 1 of North Pit on the 260RL which was produced using the 3DM Analyst technique. These two areas have been used for a comparison due to the scale of image being similar (although location differs). Both are heavily jointed rock masses within the same mafic carbonate schist package of the East wall.

In this particular example, the original TerraLuma UAV 3D model of the East wall, Stage 2 of North Pit was cropped to give an impression of the full detail that can be provided if the full resolution model is used (as opposed to the decimated Pdf models used in this report). The 3D model created using the TerraLuma UAV technique is much clearer at this resolution than the 3DM Analyst DTM. Less persistent joints are visible and the small areas of joint surface day lighting in the face can be analysed for the presence of joint infill and/or joint decoration. Veins are common within this rock mass but no veins are visible within either 3D model at these locations.

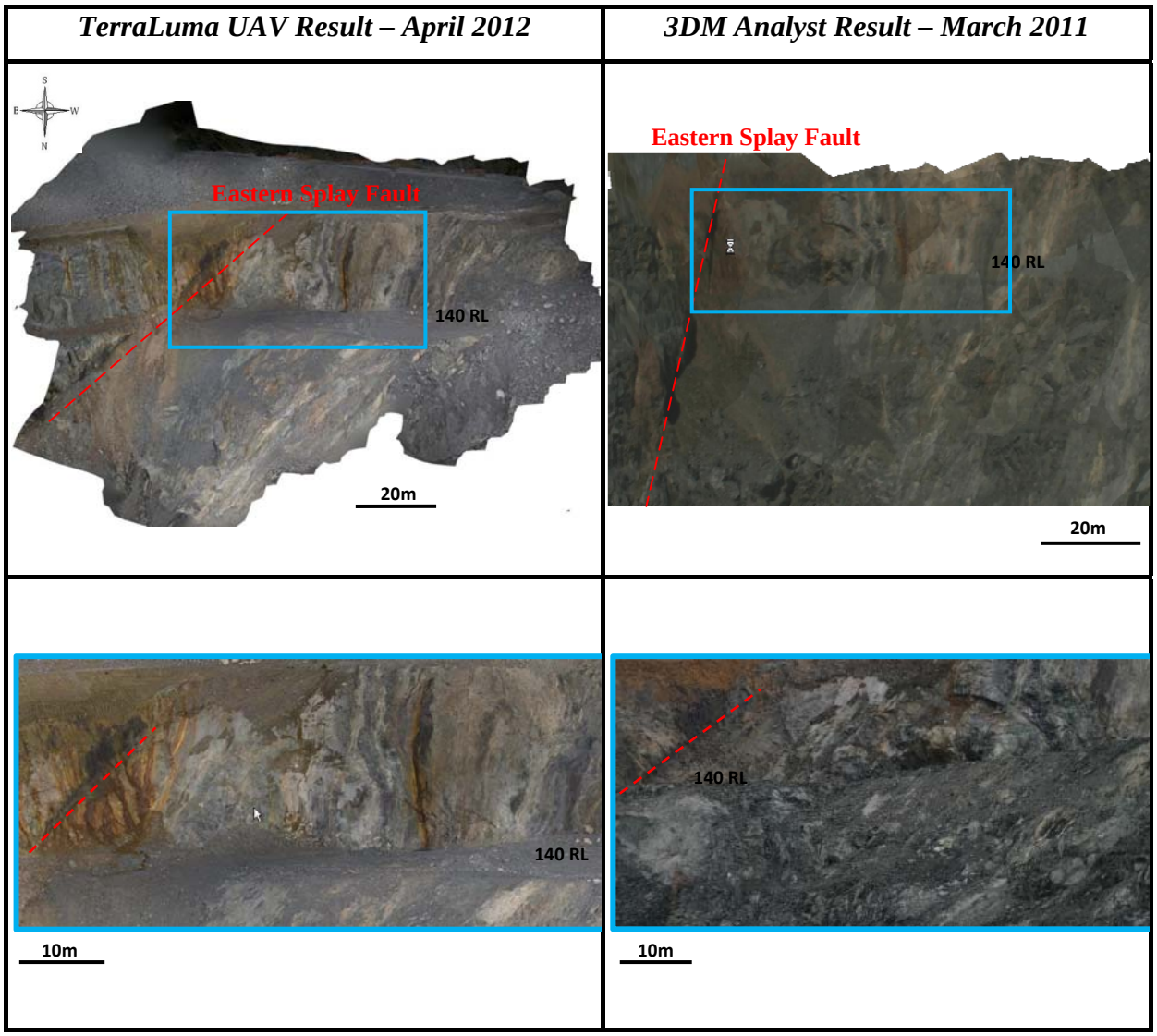

Figure 3 – South Wall of Stage 2, North Pit. Images on the left were taken using the TerraLuma UAV technique and the right images were taken using 3DM Analyst. The scale reduces respectively through the images and the blue box within the first image denotes the lower image location. The Eastern Splay Fault trace is drawn to assist the reader with the comparison.

The comparative analysis shows that in this instance, the TerraLuma UAV is the more precise technique when mapping this variation of lithology. The rock types and associated colours are more visible. The minimal joints can be seen and mapped as well as some veins. Mafic boudins are distributed throughout this rock type and lithologies can be mapped wrapping around the boudin (**Figure 4**).

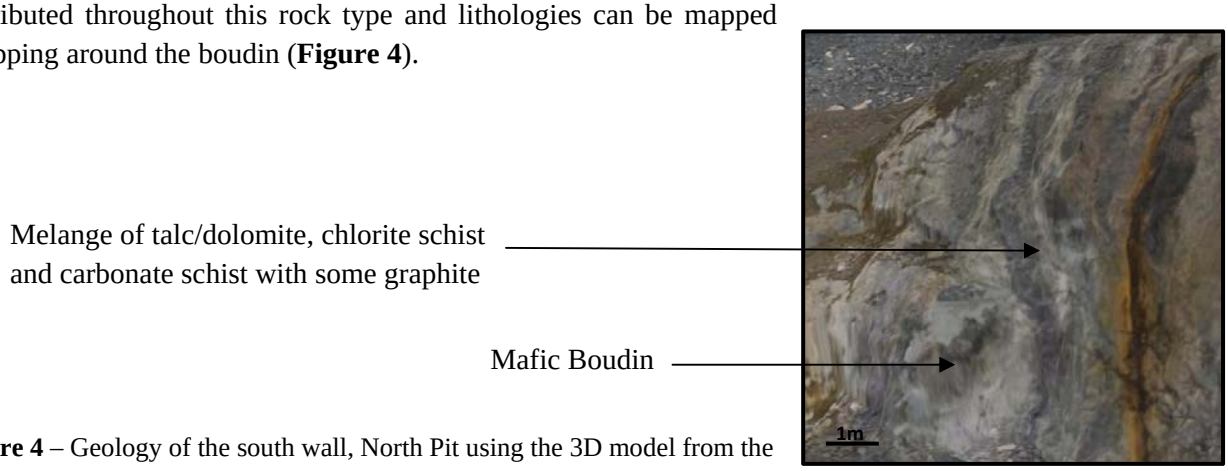

Figure 4 – Geology of the south wall, North Pit using the 3D model from the TerraLuma UAV

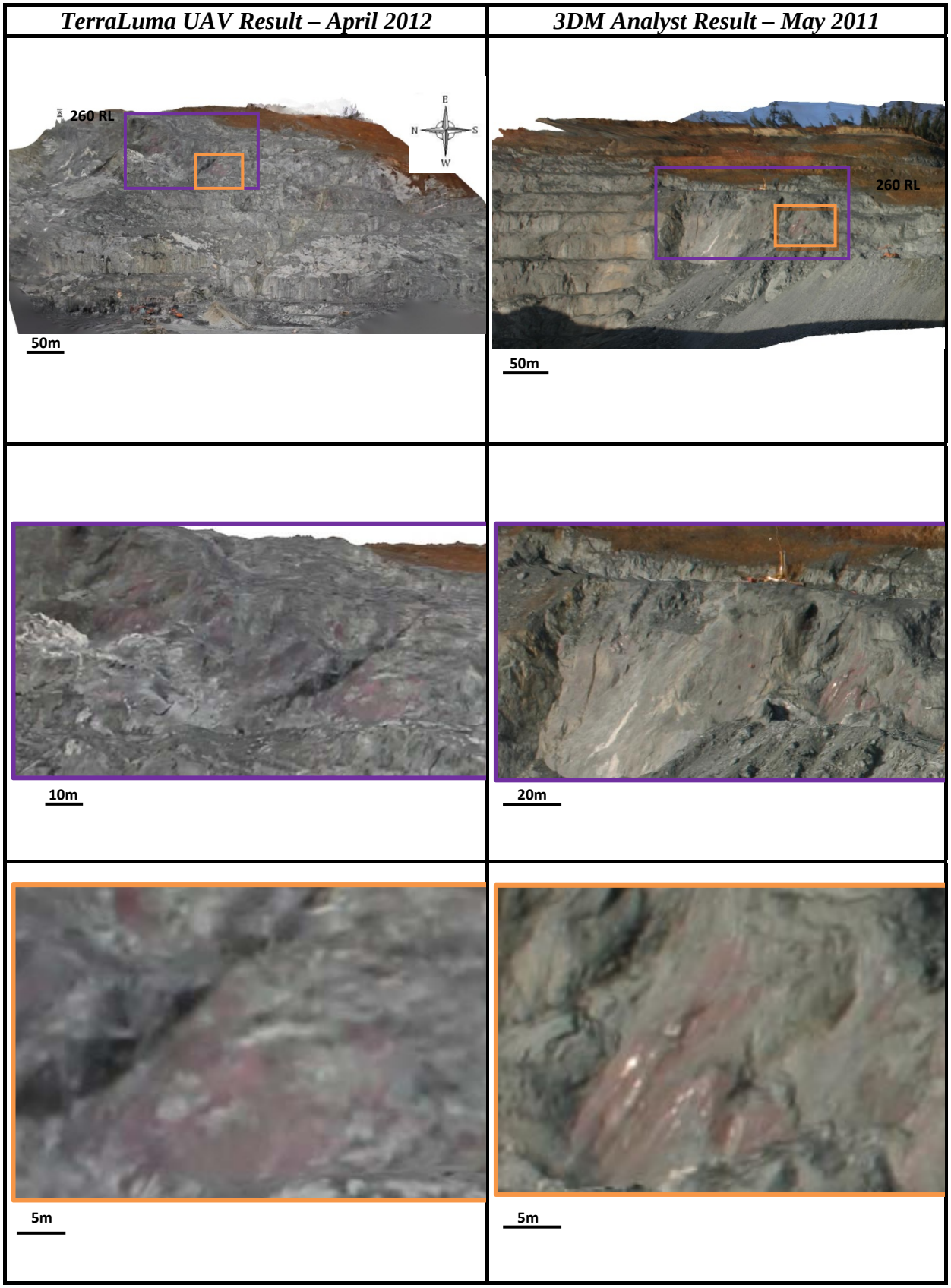

Figure 5 – East Wall of Stage 1, North Pit. Images on the left were taken using the TerraLuma UAV technique and the right images were taken using 3DM Analyst. The scale reduces respectively through the images and the purple and orange coloured boxes within the first image denote the lower image locations.

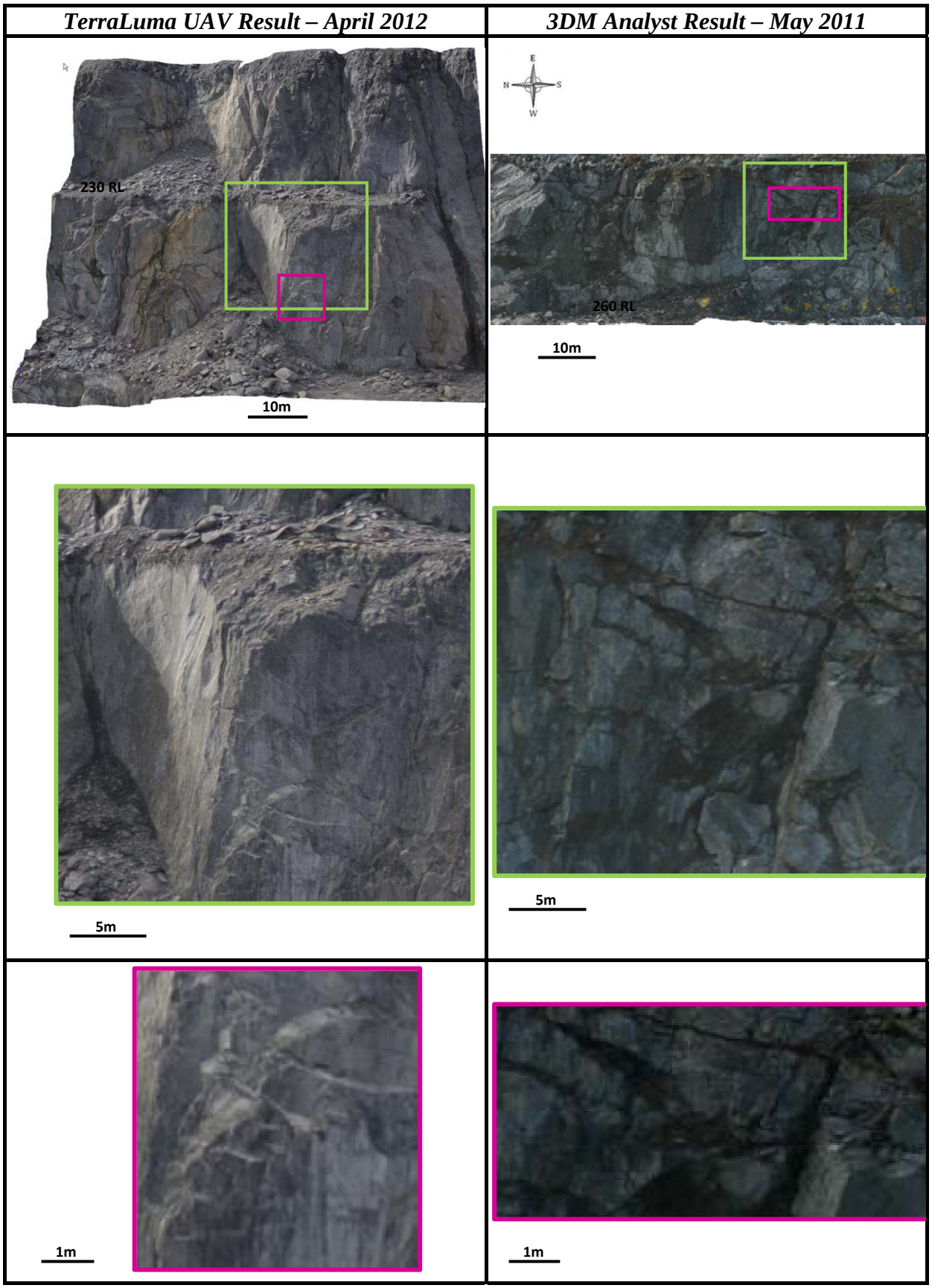

Figure 6 – Images on the left were taken using the TerraLuma UAV technique and are from a section of the East wall, Stage 2. The right images were taken using 3DM Analyst and are from a section of the East wall, Stage 1 at the 260RL. The scale reduces respectively through the images and the green and magenta coloured boxes within the first image denote the lower image locations.

Having compared the TerraLuma UAV results to the 3DM Analyst results, it is clear to state that although the TerraLuma UAV 3D models are sometimes not as clear as the 3DM Analyst DTM's, this is the more effective technique when analysing/interpreting structures on pit walls only if the models are used at a higher resolution than the Pdf's supplied. One advantage that will be described next in this report (page 11) is the level of distortion of the 3D models created by each technique which impacts heavily on the structural/geological analysis and interpretation.

Distortion variability

The method of obtaining photographs using the 3DM Analyst technique (as described on page 2) involves the operator to set the tripod and camera up directly in front of a face. Therefore the DTM is only 3D on areas that the camera has taken a photograph of. Areas that are not visible on the photograph are not visible on the DTM such as berms and joint surfaces. As the method of obtaining photographs using the TerraLuma UAV technique uses an 'OktoKopter', this captures the pit walls from different angles and locations thus creating a truly 3D model. Not only creating a more engaging and interesting model, the model is a true representation of a pit wall. Berm debris such as rock fall rill can be analysed in more detail and volume calculations may be possible. Also the geometry of pit walls can be analysed and interpreted easier as well as any joint/structure infill and decoration can be more easily seen. **Figure 7** shows an example of two models in Plan view from each technique. The clarity of the TerraLuma UAV model when the orientation of the view is altered stays the same whereas the 3DM Analyst model becomes increasingly distorted when changing the DTMs' orientation. This is a great advantage for the TerraLuma UAV technique.

TerraLuma UAV Result – April 2012	***3DM Analyst Result – May 2011***
	

Figure 7 – Plan view of Stage 2, East wall, North Pit using the TerraLuma UAV technique (left image) and a plan view of Stage 1, East wall, North Pit using the 3DM Analyst technique (right image). Note the distortion in the right image.

Conclusion

The comparative analysis has concluded that, if used at a higher resolution to that of the supplied Pdf's, the TerraLuma UAV technique will be more beneficial in the geotechnical and geological mapping of pit walls than that of the 3DM Analyst technique already employed on the mine (the actual

final models are approximately five times the resolution of the Pdf's analysed here). Not only are the 3D models clearer for analysis but inaccessible areas can be reached with relative ease and the technique will be safer for the operator. More information can be gained such as structure infill/decoration and roughness which is very beneficial on a mine with restricted access to pit walls. Berms are visible so there is potential for volume calculations of rock fall. Also cracks or other signs of berm failure can be mapped from the model itself, minimising exposure time at dangerous areas by on-site Geotechnical Engineers and Geologists.

Orientation (dip and dip direction) information can be gained from the 3DM Analyst software. This is very important for Savage River Mine due to the magnetite ore affecting mapping compasses. Any dip direction data whilst mapping on the mine by Geologists or Geotechnical Engineers who have not employed the photogrammetry technique has to be estimated therefore could be inaccurate. It would be very useful to gain this level of information from the TerraLuma UAV technique.

The 3DM Analyst technique also creates a stereographic plot of all structures. The operator can click on a particular joint set, colour all structures within that set and the programme will highlight all of these structures on the 3D model this same colour. This is very useful to correlate joint sets spatially in an area. Geological contacts can also be drawn onto the model. These 'polyline' contacts and the structural data can be exported into Surpac (the mine planning software used on Savage River Mine) in order to integrate this information into mine planning and production.

It will be very important to make the wireframe 3D model created by the TerraLuma UAV technique compatible with Surpac. The 'texture' or photographs of the wireframe are not so important at this stage but there needs to be an opportunity to extract the structural/geological data from the model into Surpac. Subjectively, the TerraLuma UAV technique creates a true model of reality. The 3DM Analyst is not a true model just a 3D DTM from a 2D image. An increased amount of geological and structural information can be gained from using the TerraLuma UAV technique but this may or may not be useful in the level of mapping that is required to be carried out on Savage River Mine. If only persistent, large structures are of interest either technique would suffice.

APPENDIX 2

XRF METHODOLOGY AND RAW DATA

The instrument used was called the Innovx Delta premium handheld XRF in the Mining Plus mode. 2 minute analyses were carried out and 27 elements were tested for, including: Mg (dl 1%), Al (dl 0.1%), Si (dl 0.1%), P (dl 0.02%), S (dl 0.01%), K (dl 0.01%), Ca (dl 0.02%), Ti (dl 0.02%), Mn (dl 0.01%) and Fe (dl 0.02%). The analyses shown in Table 1 are the result of averaging 2-4 analyses for each sample. The Mg is close to the detection limit and is not considered reliable. This method of analysis is much more accurate for elements with higher energy characteristic X-rays. The absorption corrections for Al and Si are inaccurate. The absolute value reported for Si is too high considering the mineralogy of these rocks. The relative abundance of Si in the rocks is discussed in the thesis but the absolute value should not be relied on.

Sample	Texture	Mg	Al	Si	S	K	Ca	Ti	V	Mn	Fe	Zr
176649	Massive	0.6	7.0	30.4	0.21	0.54	10.58	1.96	0.06	0.23	11.4	0.014
176643	Massive	0.4	6.4	27.3	0.27	0.13	12.46	1.80	0.06	0.26	8.7	0.014
176647	Massive	0.5	7.1	29.7	0.25	0.21	10.29	1.77	0.07	0.20	8.6	0.014
176644	Massive	0.6	6.7	30.9	0.23	0.47	7.79	1.57	0.05	0.22	12.3	0.020
176648	Massive	0.5	7.1	29.6	0.15	0.21	10.08	1.55	0.08	0.16	10.3	0.014
176642	Massive	0.6	6.7	28.4	0.09	0.01	11.32	1.37	0.06	0.24	10.3	0.014
176645	Massive	0.5	6.7	29.5	0.10	0.68	9.70	1.30	0.05	0.20	10.4	0.012
176646	Massive	0.5	5.4	34.1	0.36	0.12	7.32	1.16	0.07	0.16	8.3	0.009
176650	Massive	2.9	8.0	33.2	0.09	0.14	1.71	0.89	0.04	0.09	13.6	0.005
176651	Massive	0.6	7.7	29.9	0.11	0.27	7.17	0.84	0.05	0.11	9.5	0.006
176659	Massive	0.6	7.3	27.8	0.36	0.71	10.06	0.76	0.05	0.22	9.6	0.006
176658	Massive	1.1	8.4	31.2	0.06	0.27	7.25	0.73	0.04	0.21	10.2	0.007
176640	Massive	1.5	8.5	29.3	0.10	0.94	6.03	0.72	0.05	0.11	9.0	0.007
176641	Massive	1.3	7.7	28.9	0.14	0.38	7.60	0.69	0.05	0.14	9.9	0.006
176652	Foliated	2.2	8.2	31.5	0.07	0.22	5.37	0.76	0.05	0.13	9.7	0.006
176653	Foliated	6.5	8.6	20.6	0.14	0.02	10.57	0.76	0.05	0.28	15.7	0.006
176654	Foliated	0.6	8.1	23.8	0.14	0.36	11.42	0.70	0.05	0.13	7.1	0.007
176655	Foliated	0.6	6.8	26.8	0.06	0.01	11.94	0.55	0.04	0.16	8.6	0.005
176656	Foliated	2.2	5.3	21.8	0.04	0.31	16.07	0.51	0.03	0.25	8.9	0.005
176657	Foliated	2.8	7.9	25.2	0.01	0.01	11.30	0.62	0.04	0.26	10.7	0.005
176660	Foliated	0.4	4.6	19.6	0.02	0.23	22.17	0.49	0.03	0.34	5.7	0.004
176661	Foliated	0.9	7.5	32.0	0.09	0.10	6.12	0.70	0.04	0.17	9.4	0.005

Table 1. Weight % element compositions of samples of mafic rocks with variable foliation development

APPENDIX 3

PYRITE CHEMISTRY

Laser ablation inductively coupled plasma mass spectrometry (LA-ICPMS) analyses of pyrite grains from the Main Host Assemblage have been undertaken to determine trace metal concentrations and to highlight element zonation if present. Three pyrite grains from three separate samples within the Main Host Assemblage in North Pit Stage 1 and 2 were chosen and prepared for the analysis. Sample numbers are 176627, 176628 and 176629. The location in mine grid coordinates are as follows respectively; X-6676.009 Y-9573.523 Z-67.171, X-6648.23 Y-9561.975 Z-67.657 and X-6807.195 Y-9933.627 Z-232.215. 176627 and 176628 were taken from the north wall of North Pit Stage 1(Figure 1) and were from the main ore zone. 176629 (Figure 1) was taken from the south wall of North Pit Stage 2; immediately west of the Eastern Contact Fault which bounds the main ore zone to the east.

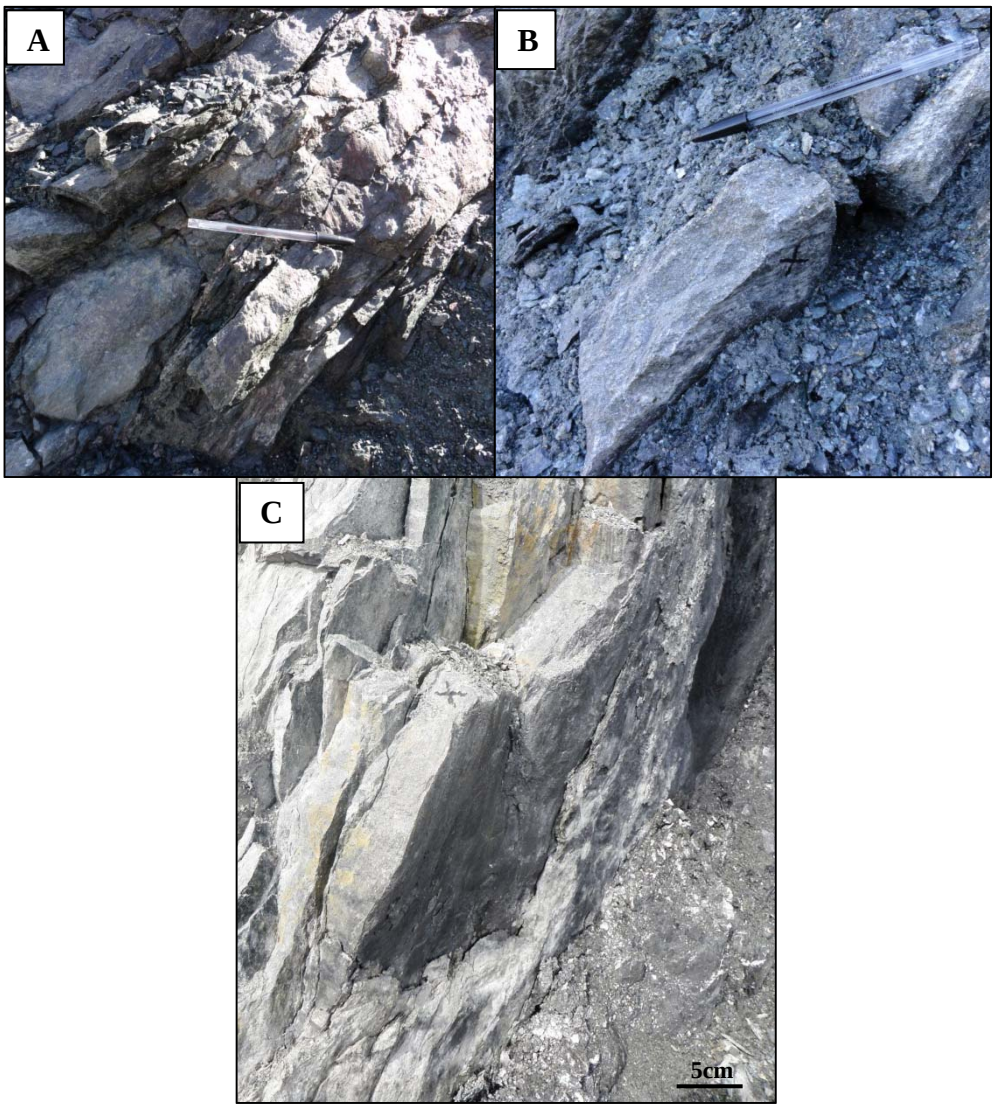

Figure 1. A. In situ photograph of sample 176627. Pyrite was disseminated within magnetite, wrapping around a mafic boudin. (Pen; 14cm in length) **B**. In situ photograph of sample 176628. Pyrite was located within magnetite ore on the North Wall. (Pen; 14cm in length) **C**. In situ photograph of sample 176629. Pyrite was disseminated on a joint surface with graphite.

Methodology

The LA- ICPMS analyses were carried out at CODES, University of Tasmania, under the supervision of Sebastien Meffre and Jay Thompson. The technique utilises a UP213 laser coupled with an Agilent 7500a ICPMS. Danyushevsky et al. (2011) provides a detailed description of the methodology.

The imaging was performed by ablating sets of parallel lines in a grid across the samples. Lines were ablated with a beam size at 15µm for sample numbers NP NW 4 and 5 and beam size set at 35µm for sample number ST2 CW 8. Spacing between the lines was kept constant and the same size as the laser beam for each separate sample. The lines were ablated with a repetition rate at 10 Hz. Thirty six elements were measured for in each of the pyrite samples. Every line sweep recorded in the mass spectrometer forms a separate pixel in the element maps shown in Figures 2 to 4. Background levels were measured before, after and two times during each analysis and the primary sulphide standard (Danyushevsky et al. 2011) were measured before and after each element map was generated.

Results

A comment on the results is provided below each element map (Figures 2 to 4). High concentrations of Co and Ni are common in each sample. Although 176627 and 176628 have higher concentrations (exhibit hotter colours) of these elements, 176629 does have sporadic higher concentrations of these elements within the grain. These elements seem to be closely linked to brittle fractures within 176628. In sample 176627, these elements form some zonation within the grain; the core of the pyrite being Co and Ni enriched.

176627 exhibits lower concentrations of arsenic than the other samples. Arsenic zonation is exhibited in sample number 176629; with the rim of the grain higher in As concentration than the core. In sample number 176628, the arsenic concentration is higher in close proximity to the brittle fractures on the grain. This could suggest that the fluid that created these brittle structures was Co, Ni and As rich.

Common to all samples analysed was the low concentrations of metals; Ag, Au, Cu, Zn, V and Ti.

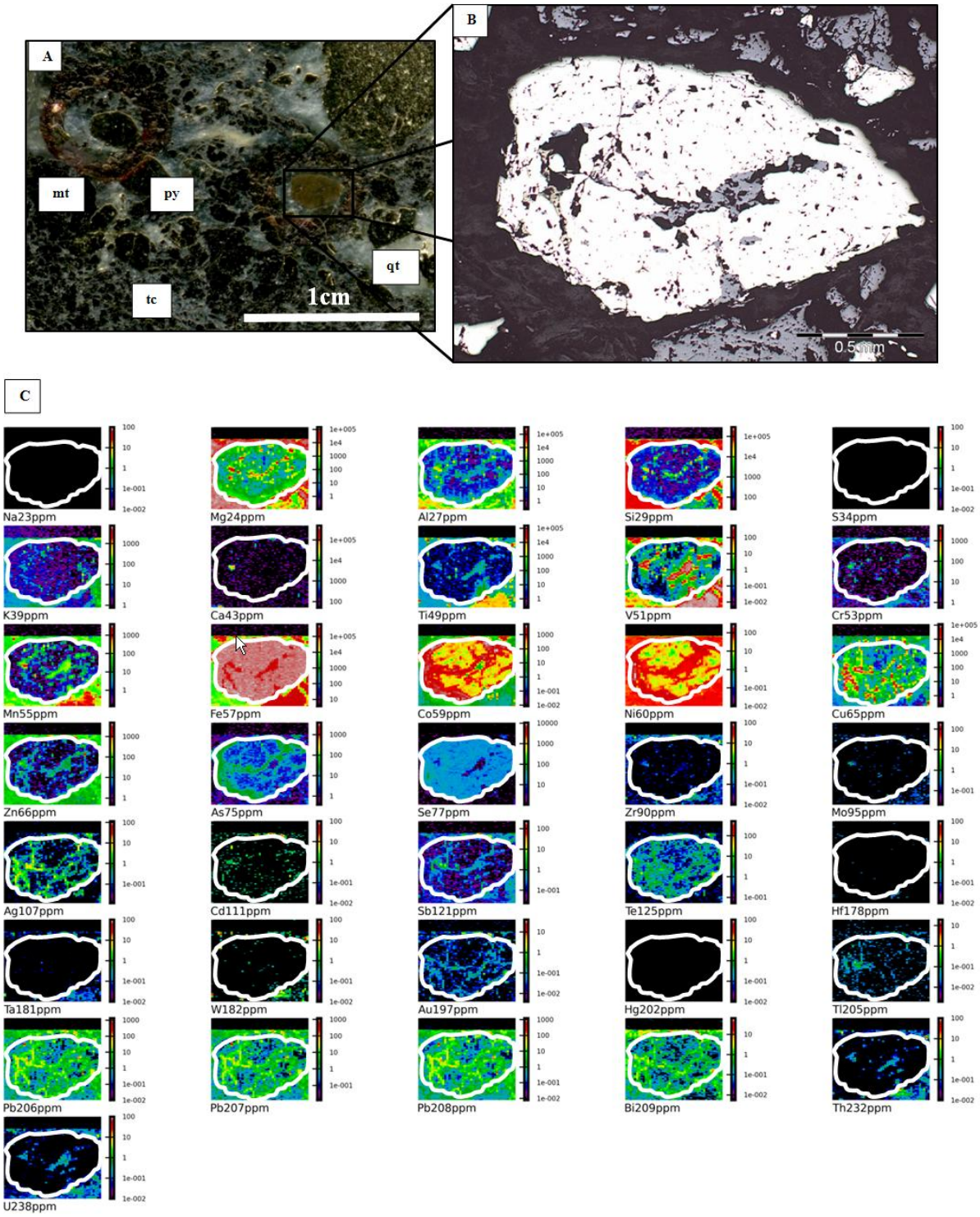

Figure 2. A. Sample number 176628. A section of a 1" epoxy mount with the ablated pyrite grain highlighted. Abbreviations: qt=quartz, py=pyrite, mt=magnetite, tc=talc. **B**. Photomicrograph (reflected light) of the pyrite grain. The pyrite is heterogenous and subhedral. Pyrite is in close proximity to magnetite. Magnetite inclusions within the grain. **C**. LA-ICPMS trace element maps of sample 176628. The element maps show high (hot colours) and low concentrations (cool colours) of various elements. The maps show element distribution in ppm across the pyrite grain. The white line shows the outline of the grain boundary. The grain possibly formed later in the sequence of events due to the brittle fracturing it exhibits. There is a higher concentration of Arsenic associated with these fractures along with Pb, Bi, Ni, Co and Sb. There is no observable zonation within the grain. Low concentrations of Au, Ag, Cu and Zn are present within the sample.

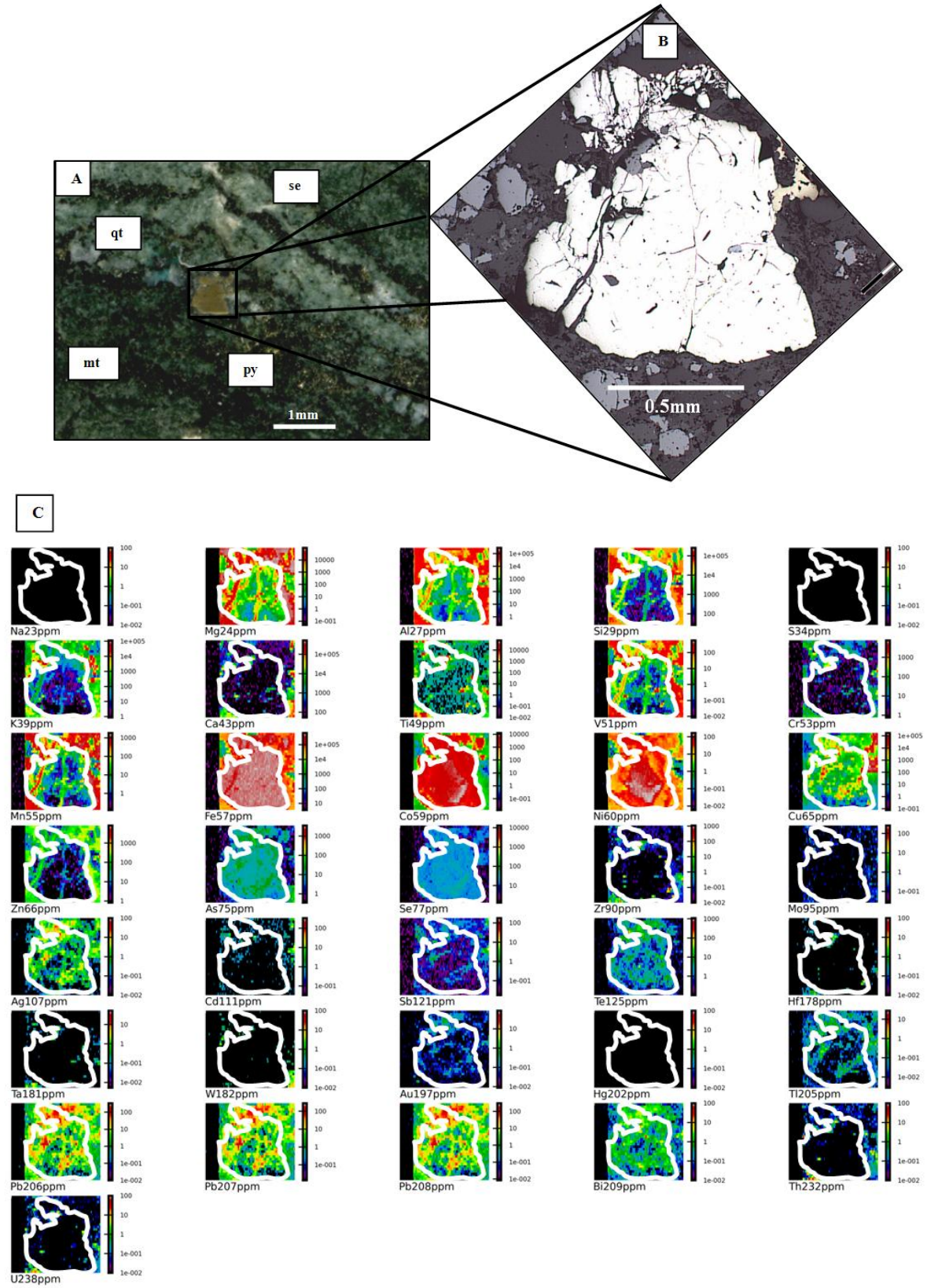

Figure 3. A. Sample number 176627. A section of a 1" epoxy mount with the ablated pyrite grain highlighted. Abbreviations: qt=quartz, py=pyrite, mt=magnetite, se=serpentinite. **B**. Photomicrograph (reflected light) of the pyrite grain. The pyrite is heterogenous and subhedral. Pyrite is heavily fractured. **C**. LA-ICPMS trace element maps of sample 176627. The element maps show high (hot colours) and low concentrations (cool colours) of various elements. The maps show element distribution in ppm across the pyrite grain. The white line shows the outline of the grain boundary. The pyrite is enriched with Co and Ni. These elements are concentrated within the core of the grain. There are small areas within the grain that are rich in Ti and V. Low concentrations of Au, Ag, Pb and Cu are detectable.

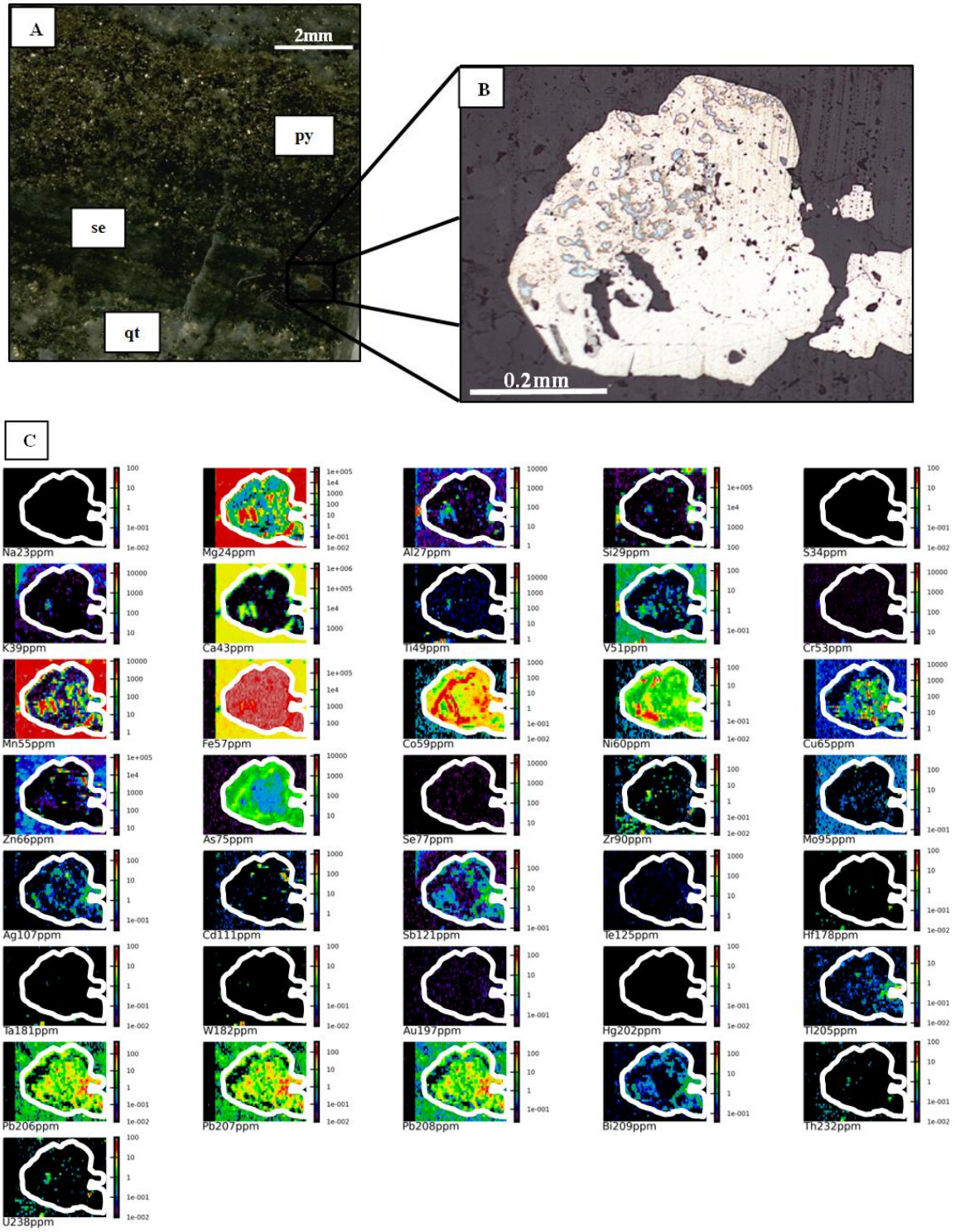

Figure 4. A. Sample number 176629. A section of a 1" epoxy mount with the ablated pyrite grain highlighted. Abbreviations: qt=quartz, py=pyrite, se=serpentinite. **B**. Photomicrograph (reflected light) of the pyrite grain. The pyrite is heterogenous and subhedral. Pyrite is heavily fractured. **C**. LA-ICPMS trace element maps of sample 176629. The element maps show high (hot colours) and low concentrations (cool colours) of various elements. The maps show element distribution in ppm across the pyrite grain. The white line shows the outline of the grain boundary. Arsenic concentration is higher on the rim of the grain and lower within the core exhibiting some As zonation. Co concentration is sporadic throughout the grain but has areas of high concentration within the core of the pyrite. High concentrations of Cu and Zn are disseminated throughout the grain along with low concentrations of Au, Ag, V and Ti.

APPENDIX 4

MONAZITE DATING METHODOLOGY

LA-ICPMS monazite geochronology at the University of Tasmania

Sebastien Meffre & Jay Thompson, April 2013

The LA-ICPMS method is now widely used for measuring U, Th and Pb isotopic data in mineral phases(e.g. Fryer et al. 1993; Compston 1999; Black et al. 2003; Kosler & Sylvester 2003, Black et al. 2004; Jackson et al. 2004, Chang et al. 2006 Harley & Kelly 2007). Monazite grains within polished blocks were located using the MLA (Mineral Liberation Analyser) which integrates Scanning Electron Microscopy and EDS analysis technologies.

The analyses in this study were performed on an Agilent 7500cs quadrupole ICPMS with a 193 nm Coherent Ar-F gas laser and the Resonetics S155 ablation cell at the University of Tasmania in Hobart. The downhole fractionation, instrument drift and mass bias correction factors for Pb/U & Pb/Th ratios on monazites were calculated using 2 analyses on the primary (RGL4B standard of Rubatto et al. 2001) and 1 analysis on each of the secondary standard monazites (MB35 standard of Berry et al. 2008 & BH2310 of Page et al. 2005) analysed at the beginning of the session and every 15 unknown monazites (roughly every 1/2 hour) using the same spot size and conditions as used on the samples. The correction factor for the 207Pb/206Pb ratio was calculated using large spots (32 microns) of NIST610 analysed every 30 unknowns and corrected using the values recommended by Baker et al. (2004).

Each analysis on the monazites began with a 30 second blank gas measurement followed by a further 30 seconds of analysis time when the laser was switched on. Monazites were ablated using 13 micron spots at 5 Hz and an energy density of approximately 2 J/cm2. A small spot size was used to keep U and Th in analog mode of detection. A flow of He carrier gas at a rate of 0.35 litres/minute carried particles ablated by the laser out of the chamber to be mixed with Ar gas and carried to the plasma torch. Isotopes measured were 27Al, 31P, 43Ca, 140Ce,172Yb, 202Hg, 204Pb, 206Pb, 207Pb, 208Pb, 232Th and 238U with each element being measured every 0.17 s with longer counting time on the Pb isotopes compared to the other elements. The data reduction used was based on the method outlined in detail in Meffre et al. 2008 and Sack et al. 2011 similar to that outlined in Black et al. (2004) and Paton et al (2010).

Element abundances on monazites were calculated using the method outlined by Kosler (2001) using 140Ce as the internal standard element, assuming stoichiometric proportions and using the NIST610 to standard correct for mass bias and drift.

References

Baker, J., Peate, D., Waight, T. and Meyzen, C., 2004. Pb isotopic analysis of standards and samples using a Pb-207-Pb-204 double spike and thallium to correct for mass bias with a double-focusing MC-ICP-MS. Chemical Geology, 211, 275-303.

Compston, W., 1999, Geological age by instrumental analysis: the 29th Hallimond Lecture. Mineralogical Magazine 63, 297-311.

Fryer, B.J., Jackson, S.E., Longerich, H.P., 1993, The Application of Laser Ablation Microprobe-Inductively Coupled Plasma-Mass Spectrometry (Lam-Icp-Ms) to in situ (U)-Pb Geochronology. Chemical Geology 109, 1-8.

Harley, S.L. and Kelly, N.M., 2007. Zircon: Tiny but timely. Elements, 3(1): 13-18.

Jackson, S.E., Pearson, N.J., Griffin, W.L., Belousova, E.A., 2004, The application of laser ablation-inductively coupled plasma-mass spectrometry to in situ U–Pb zircon geochronology. Chemical Geology 211, 47-69.

Kosler, J., 2001, Laser-ablation ICPMS study of metamorphic minerals and processes. In: Sylvester P. J. ed. Laser-ablation-ICPMS in the earth sciences; principles and applications Mineralogical Association of Canada Short Course Handbook 29, 185-202.

Kosler J.& Sylvester P.J. ,2003 Present trends and the future of zircon in geochronology; laser ablation ICPMS. Reviews in Mineralogy and Geochemistry 53, 243-275.

Meffre, S., Large, R. R., Scott, R., Woodhead, J., Chang, Z., Gilbert, S. E., Danyushevsky, L. V., Maslennikov, V., and Hergt, J. M., 2008, Age and pyrite Pb-isotopic composition of the giant Sukhoi Log sediment-hosted gold deposit, Russia: Geochimica et Cosmochimica Acta, v. 72, p. 2377-2391.

Sack, P.J., Berry, R.F., Meffre, S., Falloon, T.J., Gemmell, J.B., Friedman, R.M., 2011. In situ location and U-Pb dating of small zircon grains in igneous rocks using laser ablation-inductively coupled plasma-quadrupole mass spectrometry. Geochemistry, Geophysics, Geosystems 12.

Berry et al. 2008, Precambrian Research. 166, 387-398.

Page et al. 2005, Economic Geology, 100, 633-661.

Rubatto D., Williams I.S. & Buik I.S. Zircon and Monazite response to prograde metamorphism in the Reynolds Range, central Australia. 2001 Contributions to Mineralogy and Petrology 140: 458-468.